

INTERNATIONAL COUNCIL FOR BUILDING RESEARCH STUDIES AND DOCUMENTATION

WORKING COMMISSION W18 - TIMBER STRUCTURES

CIB - W18

MEETING THIRTY

VANCOUVER

CANADA

AUGUST 1997

INTERNATIONAL COUNCIL FOR BUILDING RESEARCH STUDIES AND DOCUMENTATION

WORKING COMMISSION W18 - TIMBER STRUCTURES

CIB - W18

MEETING THIRTY

VANCOUVER

CANADA

AUGUST 1997

Lehrstuhl für Ingenieurholzbau und Baukonstruktionen
Universität Karlsruhe
Germany
Compiled by Rainer Görlacher
1997

ISSN 0945-6996

CONTENTS

0	List of Participants
1	Chairman's Introduction
2	Co-operation With Other Organisations
3	Timber Columns
4	Stresses for Solid Timber
5	Timber Joints and Fasteners
6	Duration of Load
7	Timber Beams
8	Environmental Conditions
9	Laminated Members
10	Trussed Rafters
11	Structural Stability
12	Statistics and Data Analysis
13	Fracture Mechanics
14	Serviceability
15	Structural Design Codes
16	Any other Business
17	Venue for Next Meeting
18	Close
19	List of CIB W18 Papers/Vancouver, Canada 1997
20	Current List of CIB W18 Papers
	CIB-W18 Papers 30-2-1 up to 30-102-1

1. **Chairman's Introduction**
2. **Co-operation With Other Organisations**
3. **Timber Columns**
4. **Stresses for Solid Timber**
5. **Timber Joints and Fasteners**
6. **Duration of Load**
7. **Timber Beams**
8. **Environmental Conditions**
9. **Laminated Members**
10. **Trussed Rafters**
11. **Structural Stability**
12. **Statistics and Data Analysis**
13. **Fracture Mechanics**
14. **Serviceability**
15. **Structural Design Codes**
16. **Any other Business**
17. **Venue for Next Meeting**
18. **Close**

**INTERNATIONAL COUNCIL FOR BUILDING RESEARCH,
STUDIES AND DOCUMENTATION**

WORKING COMMISSION W18 - TIMBER STRUCTURES

MEETING THIRTY

VANCOUVER, B.C. 25 - 28 AUGUST 1997

MINUTES

1. CHAIRMAN'S INTRODUCTION

The chairman H. Blaß opened the meeting and welcomed everybody. He reiterated the importance of Timber Engineering Research at UBC, with researchers such as Dr. Borg Madsen and Dr. Ricardo Foschi leading the field in areas of in-grade testing and reliability.

Dean Michael Isaacson, Faculty of Applied Science, University of BC gave the introductory speech and welcomed everybody to Vancouver. He stressed the importance of the Forest Products sector to the well-being of British Columbians and the increasing need for university education, continuing education, research and code development. In this regard the researchers involved in the CIB group play an important role. He gave a brief overview of the different departments and faculties involved in wood related teaching and research at UBC. New programs are being introduced in the areas of Wood Processing and Wood Building Design, and the aim is to establish a Centre for Wood Building Design and Construction. He also recognised important linkages to other organisations such as Forintek Canada Corp., CSIRO in Australia, BRE in Britain, BRI in Japan and various forest products industries.

Mr Chris Pollington, Deputy Secretary of CIB gave an overview of the history and activities of the CIB. Currently more than 5000 experts from 500 organisations are active members. Their professional background is: 35% from universities, 25% are practitioners or from industry, 30% from research organisations and 15% are from elsewhere. Big companies are also members, especially in Japan and Europe. Geographical distribution: 60% from Europe, 15% from North America, 15% from Asia and 15% elsewhere. A recent policy is to reduce inactive commissions or merge with partner organisations. Future perspectives are on Integrated approach to innovative themes and international information exchange. The organisation will become more member oriented and membership fees will be an important income to sustain the organisation.

H. Blaß commented:

- Only papers sent in ahead will be incorporated in proceedings
- Internet distribution of papers from server in Karlsruhe considered in the future. Papers will be downloadable with password; therefore electronic submissions will be required.
- Next meeting to be in Helsinki in August 1998.

2. CO-OPERATION WITH OTHER ORGANISATIONS

(a) CIB - W18B

B. Leicester reported on the CIB-W18B group

(b) ISO TC165

E. Karacabeyli reported on the ISO TC 165 activities

(c) RILEM

S. Thelandersson reported on RILEM: 40 technical committees, mostly in concrete. New task groups are welcome. Very few in timber presently, for example J. Ehlbeck's group on "Test methods for transferring metal work"

J. Ehlbeck reported on the activities of the TCMTE. An attempt is made to harmonise test methods for metal connectors in timber engineering since results were found to be highly dependent on the test and evaluation procedure.

(d) CEN

H. Larsen reported on the progress of the CEN TC 124. Much effort is concentrated on the evaluation of panel products and several standards are currently being updated.

H. Blaß reported on the status of Eurocode 5. Three parts are being worked on currently: General design and buildings part - the ENV is complete, the trial period has passed and it is awaiting decision for adoption as an EN; the Fire code is complete as a pre-standard ENV and is awaiting comments; the Bridge code is in progress.

(e) IABSE

No report

(f) IUFRO

No report

(g) CIB - W85

No report

3. TIMBER COLUMNS

*Paper 30-2-1 Beam-Column Formula for Specific Truss Applications -
W Lau, F Lam and J D Barrett*

R.Leicester : Studies on beam-columns have shown that linear interaction works better for major axis bending while a square interaction formula is more appropriate for minor axis bending.

W.Lau : In a truss the lateral support of the decking prevents lateral buckling

R.Leicester : Minor axis buckling not always prevented

H.Larsen: Since a truss is a beam-column member, amplification due to axial loads need to be considered too. Moment shape factors are questionable, however. Verification is needed (See Fig. 4)

S.Theandersson: Concerned about K_M factor (Weibull) since it does not consider variability between members. It might be very low in certain cases.

B.Källsner: Calculate K_M for entire member, not only for one panel

W.Lau: The Truss Plate Institute (TPIC) considers one panel at a time in their analysis method.

A.Buchanan: Moment amplification factor is recommended (not required) in the code. From tests it was shown that the P- Δ amplification is important. The P- Δ effect can be ignored, however, when a linear interaction formula is used. Does Canadian Standard (CSA) require moment magnification and how is it calculated?

W.Lau: Yes, except when using truss design rules. An estimation is used.

Recommendation: Don't mix non-linear cross-sectional strength with linear moment interaction. Need to use second order analysis with cross-sectional strength formula.

4. STRESSES FOR SOLID TIMBERS

*Paper 30-6-1 Strength Relationships in Structural Timber Subjected to Bending
and Tension - N Burger and P Glos*

E.Gehri: f_t/f_m relationship complex and no single figure available for all cases. Separate grading required for bending and tension - e.g. glulam requires tension grades, for transverse bending need bending strength. Cannot derive f_m/f_t from f_t/f_m . South African results show poor bending results for tension graded lumber. New generation of grading should also include density variations.

N.Burger: MSR grade more correlated to tension (flat-wise MOE) while visual grades more to bending.

B.Madsen: Different failure modes occur at different locations. Cannot mix these.

A.Buchanan: Test method also has an influence, e.g. testing length.

*Paper 30-6-2 Characteristic Design Stresses in Tension for Radiata Pine Grown
in Canterbury - A Tsehaye, J C F Walker and A H Buchanan*

H.Blaß: Stiffness values low in comparison with European values. How were they determined?

A.Buchanan: Tension tests over 2m. Stiffness values were checked with bending over 2m span.

G.Schickhofer: What grading machine was used; COV values seem high.

A.Buchanan: Metriguard machine from sawmill. There were differences in stiffness measurements.

R.Leicester: Should also check different ratios of f_t/E for different locations of wood in log.

R.Marsh: Should also check what LRTB researchers have done (paper in PTEC'94 conf.)

Paper 30-6-3 Timber as a Natural Composite: Explanation of Some Peculiarities in the Mechanical Behaviour - E Gehri

H.Larsen: Other studies by IUFRO similar

E.Gehri: Those studies on clear material, not structural wood.

C.Mettem: Should select material according to application.

F.Rouger: Grading is a problem in glulam applications.

5. TIMBER JOINTS AND FASTENERS

Paper 30-7-1 Flexural Behaviour of GLT Beams End-Jointed by Glued-in Hardwood Dowels - K Komatsu, A Koizumi, J Lauritzen Jensen, T Sasaki and Y Iijima

H.Blaß: Were the dowels graded?

K.Komatsu: Yes, they were tested

G.Schickhofer: Why not use one length of beam, fingerjointed?

K.Komatsu: Dowel connection can be applied on site with predrilled holes

A.Ceccotti: Brittle shear failure at joint could be a problem.

K.Komatsu: Did shear tests. The predictions were not very good. Excessive embedment.

F.Lam: Under load control (real situation) compression dowels might not be of much use.

K.Komatsu: Agree. Shear keys were added to help carry the load.

U.Meierhofer: How was adequate glue coverage assured?

K.Komatsu: It was assumed that the coverage was adequate. No checks were performed.

H.Blaß: Were the beam faces glued together?

K.Komatsu: No. Paper was used to separate beam faces.

Paper 30-7-2 Modelling of the Block Tearing Failure in Nailed Steel-to-Timber Joints - J Kangas, K Aalto and A Kevarinmäki

H.Blaß: Is the addition of tension and shear capacity appropriate? Load sharing?

J.Kangas: Yes. Test results compare well with model predictions. Nail ductility will permit redistribution of load.

H.Blaß: Characteristic tension strength values seem much higher than known values. Shear values comparable.

J.Kangas: "Clear specimen" values were chosen assuming no major defects in connection area. Also small volume.

E.Gehri: Should also consider realistic characteristic strength for net section failures.

H.Larsen, J.Ehlbeck: "Block-shear" a better expression instead of "peeling".

J.Ehlbeck: Cannot assume two failure modes will occur simultaneously. Have to calculate 3 different failure modes and use critical (highest) value. Could also adjust shear values and ignore tension strength.

Paper 30-7-3 Cyclic Testing of Joints with Dowels and Slotted-in Steel Plates - E Aasheim

H.Larsen: Not advisable to test at 25Hz. Heating and impact load may change test results.

F.Lam: What was the variability and the no. of test?

E.Aasheim: 5 per series, low variability (<10%)

Paper 30-7-6 Influence of Ductility on Load-Carrying Capacity of Joints with Dowel-Type Fasteners - A Mischler

C.Mettem: Are equations proposed for all dowel fasteners? (Yes) May not be generally applicable. Nobody else has been able to reproduce R_u vs. λ relationship. Exclude single fasteners? Be careful not to extrapolate results from BSB connection.

A.Mischler: It depends on fabrication tolerances. BSB is an automated fabrication process. Similar reductions are experienced for wood-wood connections.

H.Blaß: What were the failure modes? Any plastic hinges?

A.Mischler: Plastic hinges were observed in ductile connections.

H.Blaß: Fig.17 - no reduction for more than 3 dowels in line?

A.Mischler: They should not be in the same figure. Total no. of dowels and rows also a factor.

A.Jorissen: Why is the spacing effect not in the formula? Tolerances not important?

A.Mischler: There are different definitions of tolerance.

Paper 30-7-5 Multiple Fastener Timber Connections with Dowel Type Fasteners - A Jorissen

C.Mettem: No apparent effect from λ on n_{ef} .

A.Mischler: Reductions are not consistent with European yield moment values.

A.Jorissen used values approx. 23% lower. A.M. used EC5 values and found significant reductions.

H.Larsen: Results need explanation. Should be careful with selection of material properties for EC5 predictions. Very large scatter of results need explanation. Is there a set of t, d, \dots values that give EC5 values when $n=1$?

E.Gehri: Large discrepancies: tested values are 30% lower than EC5 values. Need to be careful to conclude reduction factors as long as such large differences exist in calculating single dowel loads.

J.D.Barrett: Does this mean that the Canadian code is unnecessarily conservative? (Yes)

Paper 30-7-4 A Steel-to-Timber Dowelled Joint of High Performance in Combination with a High Strength Wood Composite (Parallam) - E Gehri

No questions or comments

6. DURATION OF LOAD

Paper 30-9-1 DOL Effect in Tension Perpendicular to the Grain of Glulam Depending on Service Classes and Volume - S Aicher and G Dill-Langer

- R.Leicester: Why not use pre-damage model calculations due to moisture for DOL effect?
- S.Aicher: Too much difference for different service class conditions. Eigen-stresses not only dependent on climate but also on dimensions. Can also calculate other eigen-stress distributions. Failure mechanisms are complicated: fracture can be initiated internally or externally. Can use simplified code rules or calculated approach. Climate test conditions also open to discussion.
- E.Gehri: What was the moisture level? Were the ramp tests done with high moisture content?
- S.Aicher: No difference was expected since the average m.c. was not much different from start value. Moisture gradient through the section was more pronounced: the outside 1-4mm were at about 19% m.c. while the inside was dry. No high m.c. ramp test were done.
- J.D.Barrett: Did you test survived specimens?
- S.Aicher: Yes. Lower values than ramp test due to eigen-stresses.
- J.D.Barrett: What was the DOL effect for the surviving specimens? Was there a strength reduction?
- S.Aicher: Was calculated using Weibull stress levels.
- F.Lam: Were the test results based on ranking?
- S.Aicher: The calculations were very close, thus chosen rate was close too.
- U.Meierhofer: Were there cracks prior to failure? (No) One should include the effect of cracks.
- S.Aicher: Yes, they are important. Specimens were conditioned to 12% - one could dry them out to impose cracks, or concentrate on "wetting". This would be beyond the scope of damage model approach.
- E.Karacabeyli: 0.5 threshold stress? Some failed at 0.35 range.
- S.Aicher: This was the start value for numerical fitting procedure. Low failures due to damage accumulation. Load history also important.

Paper 30-9-2 Damage Modelling of Glulam in Tension Perpendicular to Grain in Variable Climate - G Dill-Langer and S Aicher

- F.Rouger: How was the calibration of parameters done? Over the entire σ - ϵ curve?
- G.Dill-Langer: Parameter set was calibrated to only one time to failure.
- F.Rouger: There are 5 parameters, but only one point? Choice of 2 sets of parameters from 2 different points?
- G.Dill-Langer: There was a careful consideration of parameter sensitivity using linear and exponential methods.
- R.Leicester: Have to differentiate between damage and stress-related failures. Damage model is an empirical fit only. A stress model is more rigorous and can predict creep. Have compared this with creep of glulam specimens.
- G.Dill-Langer: Yes, this was checked: small vs large specimens, loaded and unloaded (4 ways). Material parameters were calibrated with creep behaviour.
- S.Thelandersson: Be careful with calibration in moisture induced stress fields.
- G.Dill-Langer: There are many different creep models
- S.Aicher(response to R.Leicester): Regarding the question of damage definition: constant- Weibull stress from external loads; varying- incremental Weibull stress. They produce the same damage.
- E.Karacabeyli: $k_{mod}=0.5$, tension perpendicular more severe. Are threshold values absolute? Have seen failure at lower stress levels.

G.Dill-Langer: It depends on the definition of the stress level, which is the nominal stress level. The real stress level = Weibull, which is much higher (~2x). The model is meant for short/medium term loading only.

7. TIMBER BEAMS

Paper 30-10-1 Non-destructive Evaluation of Wood-based Members and Structures with the Help of Modal Analysis - P Kuklik

A.Buchanan: Have you compared modal and ultrasonic methods?

P.Kuklik: Obtained good comparison; tested 100x150mm members.

Paper 30-10-2 Measurement of Modulus of Elasticity in Bending - L Boström

H.Blaß: Are you proposing using global MOE instead of local? (Yes)

F.Rouger: This was discussed in European Forum and adopted. Will be proposed

B.Madsen: It is a question of finding the worst defect and the placement of the specimen is important.

E.Gehri: Should randomise defect location; separate E and G.

Paper 30-10-3 A Weak Zone Model for Timber in Bending - B Källsner, K Salmela and O Ditlevsen

J.D.Barrett: Any results to improve the finger joint strength?

B.Källsner: Would prefer to do tests in another way, but don't know how.

R.Leicester: Could one reduce the data in Fig. 6 and 7 to the original length of the beam?

S.Theandersson: When comparing long and short beams: long beams store more energy which favours crack propagation. In small specimens the cracks may be arrested.

E.Gehri: Why not test short elements within long lengths to avoid stored energy discrepancy? Then all are on the same basis.

B.Källsner: Had considered that. Did the short tests first - to be followed by long tests.

W.Lau: What is the difference between series 1 and 2? Different size factors?

B.Källsner: Both are from the same source.

W.Lau: For k in equation 8, was a Poisson distribution assumed?

B.Källsner: No, we used a normal distribution.

Paper 30-10-4 Load Carrying Capacity of Timber Beams with Narrow Moment Peaks - T Isaksson and J Freysoldt

A.Buchanan: Concerned about the large number of steps in the simulations. Are there any other tests to confirm the results?

T.Isaksson: No. Simulations were just completed. Good correlation was achieved with some test results.

R.Leicester: Was this a realistic representation of timber strength?

T.Isaksson: For the lumber the knots were evenly distributed

F.Lam: The parameters in the model are specific to the results. In order to extrapolate, one needs to consider other species as well.

S.Theandersson: The results are species related but they show that commonly believed length effects and configuration effects are not always applicable.

8. ENVIRONMENTAL CONDITIONS

Paper 30-11-1 Probabilistic Design Models for the Durability of Timber Constructions - R H Leicester

K.Oiger: How do you determine front of decay?

R.Leicester: Fit it to general context of field studies. Permeability of timber very variable.

C.Mettem: Non-classical parameters, asymmetrical statistical assumptions?

R.Leicester: This is part of uncertainty. Model is based on simple assumptions. Another approach is to ask people for opinions (e.g. expert system). Parametric model is easier to adapt.

H.J.Larsen: There is no need to have a probabilistic model related to failure. Interim maintenance will prevent total decay.

R.Leicester: Agree. Some aspects can be modelled successfully e.g. power lines in remote areas: treated vs. untreated; inspection intervals.

9. LAMINATED MEMBERS

Paper 30-12-1 Experimental Investigation and Analysis of Reinforced Glulam Beams - K Oiger

H.Blaß: Are beams with curved glued-in bars used in buildings?

K.Oiger: No, but used in arches to reinforce the cantilever.

E.Gehri: Why is there a 50% loss in prestress?

K.Oiger: Because of creep of timber and crushing of anchor plate. 50% is maybe somewhat high, but comparable to stress-lam bridges (up to 60% loss)

A.Jorissen: Did you use strength instead of deflection considerations for predicted reduction in timber?

K.Oiger: Deflection was governing

10. TRUSSED RAFTERS

Paper 30-14-1 The Stability Behavior of Timber Trussed Rafter Roofs - Studies Based on Eurocode 5 and Full Scale Testing - R J Bainbridge, C J Mettern, A Reffold and T Studer

H.Blaß: Why concerned about directional bias?

R.Bainbridge: This is only an observation. There is also a bias at the node points in construction.

H.Blaß: How is the stiffness and load distribution?

R.Bainbridge: Unequal load distributions are caused by stiff elements e.g. ceilings. Too strong connections attract more force.

H.Larsen: There should be no bias regarding the roof slope (hand calc's) since the sign of the bias can change. Could there be a simplified model? (p.8 eq 1) Don't agree about overstrength in connections.

C.Mettem: Construction bias is commonplace.

S.Thelandersson: R_1 = contribution of unbraced roof.

H.Larsen: No.

R.Bainbridge: Will check and correct for final version of paper.

11. STRUCTURAL STABILITY

Paper 30-15-1 Cyclic Performance of Perforated Wood Shear Walls with Oversize Oriented Strand Board Panels - Ming He, H Magnusson, F Lam, H G L Prion

- A.Buchanan: Different conclusions: since the engineer has no influence on openings, regular boards are more reliable
- H.Prion: Should keep in mind that oversized panel walls have higher stiffness and ductility.
- C.Mettem: Engineers nowadays have greater influence on lay-out. In future should also consider walls with semi-rigid inter-storey connections, not only walls connected to rigid base beams.
- A.Jorissen: Why is the no. of nails similar? Could avoid nail failure in small panels by adding nails.
- M.He: It is an economical consideration.
- A.Buchanan: For seismic design need well established hierarchy of failure, thus have to know how structure fails - nail failures preferable. Need to apply capacity design concept.
- S.Thelandersson: Are there any other advantages?
- F.Lam: Benefits for pre-fabricated construction and tilt-up walls, also for smaller prefabricated panels.
- E.Karacabeyli: What are the energy dissipation characteristics?
- M.He: Conventional walls have a slightly higher energy dissipation
- M.Yasumura: The new cyclic protocol does not properly represent the energy dissipation characteristics. Figs. 8 & 9 have similar loads but no large cycles.
- H.Prion: The new protocol is based on realistic expectations of energy dissipation.

Paper 30-15-2 A Numerical Analysis of Shear Walls Structural Performances - L Davenne, L Daudeville, N Kawai and M Yasumura

- F.Lam: Did you observe any nail fatigue failures? (No) Will model predict wall performance under all protocols?
- L.Davenne: Will consider other protocols in future.
- A.Buchanan: Should be careful with nails - poor specifications. Nail withdrawal is important. Coatings, ringed-shank will change behaviour. Model should consider different pull-out modes.
- K.Oiger: How were spring stiffnesses calculated? Tests?
- L.Davenne: Fitted to single nail test results.
- E.Karacabeyli: Panels overlapped in the analysis. Does the program have gap control?
- L.Davenne: The program allows overlap. No-overlap analysis was tried - not much difference.
- S.Aiger: When working with contact elements one will also get overlap if elements not infinitely stiff.
- H.Blaß: Was there a gap between the panels?
- N.Kawai: No gap. Contact and buckling of plywood were observed.

Paper 30-15-3 Seismic Force Modification Factors for the Design of Multi-Storey Wood-Frame Platform Construction - E Karacabeyli and A Ceccotti

- H.Prion: Do the results warrant an increase in R values?

- E.Karacabeyli: Eventually yes, but for now have to monitor changes in the code which may affect the overall behaviour of structures.
- A.Ceccotti: The model is not perfect. Need more verification to increase R values.
- A.Buchanan: For higher R values need also higher ductility demand. Also consider wind loads which often govern. Did you compare wind loads?
- A.Ceccotti: In Europe wind is more important.
- C.Mettem: How is the compatibility when using gypsum wall board (GWB) and plywood on the same frame?
- E.Karacabeyli: Tests were done on plywood/GWB, GWB only and plywood only. Up to ~50mm displacements were compatible. Dual system walls were not as ductile, therefore R=2 recommended. Considerable damage was observed on GWB.
- F.Lam: Why are the results for the artificial earthquake records so different. Maybe these records are not appropriate.
- A.Ceccotti: These records were provided by geophysicists - they are meant to be expected earthquakes for Vancouver. There is still controversy about the expected damage. Rather than pondering on the R values, should consider design details and load path - much more critical is the conceptual design.
- F.Lam: Real walls also have much worse construction details than laboratory specimens.

*Paper 30-15-4 Evaluation of Wood Framed Shear Walls Subjected to Lateral Load
- M Yasumura and N Kawai*

- A.Ceccotti: The CEN standard is not intended to calculate yield load, but for calculating ductility. Have you done any ductility comparisons? (No)
- H.Blaß: Have you considered strength degradation? (No)
- A.Buchanan: Strength impairment not a good term since earthquake will follow displacement until resistance is reached. Displacement capacity more important. Gypsum board performance is very dependent on quality of board. Should specify the type of board.
- M.Yasumura: Used type X board according to GIS Standard.
- F.Lam: Not all earthquakes break a wall. Critical earthquakes often have much lower energy dissipation than in laboratory tests.
- M.Yasumura: Have not compared with dynamic results.
- E.Karacabeyli: Difference between apparent and true deformation will be smaller with different standard, for longer walls and with vertical load added. ASTM E465 might be more suitable.
- C.Mettem: Agree with E.K. about difference in test procedures. Move more away from analytical to design approach.
- M.He: How can one have rotation with vertical displacement of wall at foundation.
- M.Yasumura: Embedding of studs in bottom plate.

12. STATISTICS AND DATA ANALYSIS

*Paper 30-17-1 A New Statistical Method for the Establishment of Machine Settings
- F Rouger*

- H.Blaß: Was the machine rejected or was it the settings?
- F.Rouger: Combination of machine and settings.
- N.Burger: Where did you obtain the cost of upgrading from? It is dependent on machine settings.
- F.Rouger: Yes. Will change. Was used as a basis assumption to calculate global cost

matrix.

N.Burger: Calculation of costs in eqn. 4.4 and 4.5: Same result?

F.Rouger: No. Different concept for up(safety) and downgrading (loss of material).
Upgrading ~ 2-3 times cost of downgrading.

H.Larsen: One could also multiply cost factors with constant.

N.Burger: How was the population chosen?

F.Rouger: Have to use one population to approve machine.

B.Madsen: Were "real" machines used?

F.Rouger: Tested on at least 4 different machines.

B.Madsen: Did you verify if 5th percentile values were correct?

F.Rouger: Yes, tested population and it worked.

L.Boström: Have also approved machine and compared with test results. I question procedure for determining repeatability - don't use first pass but most frequent grade.

A.Jorissen: In the global cost matrix, what is the meaning of the negative values?

F.Rouger: It means : too safe.

13. FRACTURE MECHANICS

Paper 30-19-1 Failure Analysis of Single-Bolt Joints - L Daudeville, L Davenne and M Yasumura

A.Jorissen: Was the energy release rate based on the assumption of one crack (load parallel to grain)?

L.Daudeville: Yes, gives best comparison. One crack 30% and two cracks somewhat lower, but not much different.

A.Jorissen: Other researchers (Gustafsson, Petterson) found 2-crack model more appropriate. At the beginning there are always two cracks, while the failure usually involves only one crack.

L.Daudeville: For the critical energy release value, assumed linear elastic behaviour. Maybe the assumption is wrong, but good comparisons.

A.Jorissen: It is a matter of model calibration and initial assumptions. Observation: at max. load 2 cracks; friction is important. Energy release rate should be a material property and should not vary according to fracture assumptions.

H.Larsen: Agree with A.J. May need re-evaluation of experimental methods to determine energy release rate for material. Code rules are little theory and lots of interpretation. EC5 more theoretical ; with limitations. When doing research, distinguish between theory based on tests and code rules which may have other assumptions. One tends to lean too much on code rules, e.g. embedding values should be based on basic material properties.

J.D.Barrett: Tension perpendicular test - is this a fracture mechanics problem? What about scale effects - different size specimens and bolts? Have you done any such tests?

L.Daudeville: Tension parallel: Yielding and fracture. Tension perpendicular: clearly visible crack propagation ; tested under displacement control.

J.D.Barrett: Was the ultimate load governed by fracture mechanics theory?

M.Yasumura: Perpendicular to grain tension - development of crack stable. Maximum load not at beginning of crack formation, thus fracture mechanics problem.

R.Leicester: Fracture initiation should be dependent on the stress field around bolt. Not shown in paper.

L.Daudeville: Applied stress criteria to determine location of crack. Not always good

results.

14. SERVICEABILITY

Paper 30-20-1 Design Principles for Timber in Compression Perpendicular to Grain - S Thelandersson and A Mårtensson

R.Leicester: Australian tests were done on 5 configurations of floor joists in platform construction. It keeps deforming, some also failed. Cannot ignore ultimate limit states design.

B.Madsen: Creep important for acceptance of timber structures. Consequences devastating for industry.

E.Karacabeyli: Important when using stucco on the outside - water penetration. Canadian code (O86) has two-level design philosophy. Research by C.Lum relevant (2 month tests).

Paper 30-20-2 Serviceability Performance of Timber Floors - Eurocode 5 and Full Scale Testing R J Bainbridge and C J Mettem

S.Thelandersson: Personal perceptions are an important aspect of research.

15. STRUCTURAL DESIGN CODES

Paper 30-102-1 Concepts for Drafting International Codes and Standards for Timber Constructions - R H Leicester

C.Mettem: What was the basis for design: LSD? Complicated for some.

R.Leicester: Have to keep to a very low level.

B.Madsen: Cost of in-grade testing about \$100,000 per species. Canada produces ~13 billion board-feet. In situ grading 0.03c / board in Canada.

16. ANY OTHER BUSINESS

A.Buchanan: PTEC99 Conference March 1999 in Rotorua, NZ. Similar to PTEC84, 88 and 94. Call for papers is out.

S.Thelandersson: COST E5 Symposium: Cardington, June 10-12, 1998.

17. VENUE AND PROGRAMME OF THE NEXT MEETING

H.Blaß: Next CIB Meeting in Helsinki, 12-14 August 1998 (close to Lausanne conference).

Invitation for 1999 meeting from Graz, Austria (End of August)

2000 meeting - tentatively in Delft.

18. CLOSE

**19. List of CIB-W18 Papers,
Vancouver, Canada 1997**

List of CIB-W18 Papers, Vancouver, Canada 1997

- 30 - 2 - 1 Beam-Column Formula for Specific Truss Applications - W Lau, F Lam and J D Barrett
- 30 - 6 - 1 Strength Relationships in Structural Timber Subjected to Bending and Tension - N Burger and P Glos
- 30 - 6 - 2 Characteristic Design Stresses in Tension for Radiata Pine Grown in Canterbury - A Tsehaye, J C F Walker and A H Buchanan
- 30 - 6 - 3 Timber as a Natural Composite: Explanation of Some Peculiarities in the Mechanical Behaviour - E Gehri
- 30 - 7 - 1 Flexural Behaviour of GLT Beams End-Jointed by Glued-in Hardwood Dowels - K Komatsu, A Koizumi, J Jensen, T Sasaki and Y Iijima
- 30 - 7 - 2 Modelling of the Block Tearing Failure in Nailed Steel-to-Timber Joints - J Kangas, K Aalto and A Kevarinmäki
- 30 - 7 - 3 Cyclic Testing of Joints with Dowels and Slotted-in Steel Plates - E Aasheim
- 30 - 7 - 4 A Steel-to-Timber Dowelled Joint of High Performance in Combination with a High Strength Wood Composite (Parallam) - E Gehri
- 30 - 7 - 5 Multiple Fastener Timber Connections with Dowel Type Fasteners - A Jorissen
- 30 - 7 - 6 Influence of Ductility on Load-Carrying Capacity of Joints with Dowel-Type Fasteners - A Mischler
- 30 - 9 - 1 DOL Effect in Tension Perpendicular to the Grain of Glulam Depending on Service Classes and Volume - S Aicher and G Dill-Langer
- 30 - 9 - 2 Damage Modelling of Glulam in Tension Perpendicular to Grain in Variable Climate - G Dill-Langer and S Aicher
- 30 - 10 - 1 Nondestructive Evaluation of Wood-based Members and Structures with the Help of Modal Analysis - P Kuklik
- 30 - 10 - 2 Measurement of Modulus of Elasticity in Bending - L Boström

- 30 - 10 - 3 A Weak Zone Model for Timber in Bending - B Källsner, K Salmela and O Ditlevsen
- 30 - 10 - 4 Load Carrying Capacity of Timber Beams with Narrow Moment Peaks
T Isaksson and J Freysoldt
- 30 - 11 - 1 Probabilistic Design Models for the Durability of Timber Constructions -
R H Leicester
- 30 - 12 - 1 Experimental Investigation and Analysis of Reinforced Glulam Beams -
K Oiger
- 30 - 14 - 1 The Stability Behaviour of Timber Trussed Rafter Roofs - Studies Based on
Eurocode 5 and Full Scale Testing - R J Bainbridge, C J Mettern, A Reffold
and T Studer
- 30 - 15 - 1 Cyclic Performance of Perforated Wood Shear Walls with Oversize
Oriented Strand Board Panels - Ming He, H Magnusson, F Lam, and
H G L Prion
- 30 - 15 - 2 A Numerical Analysis of Shear Walls Structural Performances - L Davenne,
L Daudeville, N Kawai and M Yasumura
- 30 - 15 - 3 Seismic Force Modification Factors for the Design of Multi-Storey Wood-
Frame Platform Construction - E Karacabeyli and A Ceccotti
- 30 - 15 - 4 Evaluation of Wood Framed Shear Walls Subjected to Lateral Load -
M Yasumura and N Kawai
- 30 - 17 - 1 A New Statistical Method for the Establishment of Machine Settings -
F Rouger
- 30 - 19 - 1 Failure Analysis of Single-Bolt Joints - L Daudeville, L Davenne and
M Yasumura
- 30 - 20 - 1 Design Principles for Timber in Compression Perpendicular to Grain -
S Thelandersson and A Mårtensson
- 30 - 20 - 2 Serviceability Performance of Timber Floors - Eurocode 5 and Full Scale
Testing - R J Bainbridge and C J Mettem
- 30 - 102 - 1 Concepts for Drafting International Codes and Standards for Timber
Constructions - R H Leicester

20. Current List of CIB-W18(A) Papers

CURRENT LIST OF CIB-W18(A) PAPERS

Technical papers presented to CIB-W18(A) are identified by a code CIB-W18(A)/a-b-c, where:

a denotes the meeting at which the paper was presented. Meetings are classified in chronological order:

- 1 Princes Risborough, England; March 1973
- 2 Copenhagen, Denmark; October 1973
- 3 Delft, Netherlands; June 1974
- 4 Paris, France; February 1975
- 5 Karlsruhe, Federal Republic of Germany; October 1975
- 6 Aalborg, Denmark; June 1976
- 7 Stockholm, Sweden; February/March 1977
- 8 Brussels, Belgium; October 1977
- 9 Perth, Scotland; June 1978
- 10 Vancouver, Canada; August 1978
- 11 Vienna, Austria; March 1979
- 12 Bordeaux, France; October 1979
- 13 Otaniemi, Finland; June 1980
- 14 Warsaw, Poland; May 1981
- 15 Karlsruhe, Federal Republic of Germany; June 1982
- 16 Lillehammer, Norway; May/June 1983
- 17 Rapperswil, Switzerland; May 1984
- 18 Beit Oren, Israel; June 1985
- 19 Florence, Italy; September 1986
- 20 Dublin, Ireland; September 1987
- 21 Parksville, Canada; September 1988
- 22 Berlin, German Democratic Republic; September 1989
- 23 Lisbon, Portugal; September 1990
- 24 Oxford, United Kingdom; September 1991
- 25 Åhus, Sweden; August 1992
- 26 Athens, USA; August 1993
- 27 Sydney, Australia; July 1994
- 28 Copenhagen, Denmark, April 1995
- 29 Bordeaux, France, August 1996
- 30 Vancouver, Canada, August 1997

b denotes the subject:

- 1 Limit State Design
- 2 Timber Columns
- 3 Symbols
- 4 Plywood
- 5 Stress Grading
- 6 Stresses for Solid Timber
- 7 Timber Joints and Fasteners
- 8 Load Sharing
- 9 Duration of Load
- 10 Timber Beams
- 11 Environmental Conditions
- 12 Laminated Members
- 13 Particle and Fibre Building Boards
- 14 Trussed Rafters
- 15 Structural Stability
- 16 Fire
- 17 Statistics and Data Analysis
- 18 Glued Joints
- 19 Fracture Mechanics
- 20 Serviceability
- 100 CIB Timber Code
- 101 Loading Codes
- 102 Structural Design Codes
- 103 International Standards Organisation
- 104 Joint Committee on Structural Safety
- 105 CIB Programme, Policy and Meetings
- 106 International Union of Forestry Research Organisations

c is simply a number given to the papers in the order in which they appear:

Example: CIB-W18/4-102-5 refers to paper 5 on subject 102 presented at the fourth meeting of W18.

Listed below, by subjects, are all papers that have to date been presented to W18. When appropriate some papers are listed under more than one subject heading.

LIMIT STATE DESIGN

- 1-1-1 Limit State Design - H J Larsen
- 1-1-2 The Use of Partial Safety Factors in the New Norwegian Design Code for Timber Structures - O Brynildsen
- 1-1-3 Swedish Code Revision Concerning Timber Structures - B Noren
- 1-1-4 Working Stresses Report to British Standards Institution Committee BLCP/17/2
- 6-1-1 On the Application of the Uncertainty Theoretical Methods for the Definition of the Fundamental Concepts of Structural Safety - K Skov and O Ditlevsen
- 11-1-1 Safety Design of Timber Structures - H J Larsen
- 18-1-1 Notes on the Development of a UK Limit States Design Code for Timber - A R Fewell and C B Pierce
- 18-1-2 Eurocode 5, Timber Structures - H J Larsen
- 19-1-1 Duration of Load Effects and Reliability Based Design (Single Member) - R O Foschi and Z C Yao
- 21-102-1 Research Activities Towards a New GDR Timber Design Code Based on Limit States Design - W Rug and M Badstube
- 22-1-1 Reliability-Theoretical Investigation into Timber Components Proposal for a Supplement of the Design Concept - M Badstube, W Rug and R Plessow
- 23-1-1 Some Remarks about the Safety of Timber Structures - J Kuipers
- 23-1-2 Reliability of Wood Structural Elements: A Probabilistic Method to Eurocode 5 Calibration - F Rouger, N Lheritier, P Racher and M Fogli

TIMBER COLUMNS

- 2-2-1 The Design of Solid Timber Columns - H J Larsen
- 3-2-1 The Design of Built-Up Timber Columns - H J Larsen
- 4-2-1 Tests with Centrally Loaded Timber Columns - H J Larsen and S S Pedersen
- 4-2-2 Lateral-Torsional Buckling of Eccentrically Loaded Timber Columns - B Johansson
- 5-9-1 Strength of a Wood Column in Combined Compression and Bending with Respect to Creep - B Källsner and B Norén
- 5-100-1 Design of Solid Timber Columns (First Draft) - H J Larsen
- 6-100-1 Comments on Document 5-100-1, Design of Solid Timber Columns - H J Larsen and E Theilgaard
- 6-2-1 Lattice Columns - H J Larsen
- 6-2-2 A Mathematical Basis for Design Aids for Timber Columns - H J Burgess
- 6-2-3 Comparison of Larsen and Perry Formulas for Solid Timber Columns - H J Burgess
- 7-2-1 Lateral Bracing of Timber Struts - J A Simon
- 8-15-1 Laterally Loaded Timber Columns: Tests and Theory - H J Larsen
- 17-2-1 Model for Timber Strength under Axial Load and Moment - T Poutanen
- 18-2-1 Column Design Methods for Timber Engineering - A H Buchanan, K C Johns, B Madsen
- 19-2-1 Creep Buckling Strength of Timber Beams and Columns - R H Leicester

- 19-12-2 Strength Model for Glulam Columns - H J Blaß
- 20-2-1 Lateral Buckling Theory for Rectangular Section Deep Beam-Columns-
H J Burgess
- 20-2-2 Design of Timber Columns - H J Blaß
- 21-2-1 Format for Buckling Strength - R H Leicester
- 21-2-2 Beam-Column Formulae for Design Codes - R H Leicester
- 21-15-1 Rectangular Section Deep Beam - Columns with Continuous Lateral Restraint -
H J Burgess
- 21-15-2 Buckling Modes and Permissible Axial Loads for Continuously Braced Columns -
H J Burgess
- 21-15-3 Simple Approaches for Column Bracing Calculations - H J Burgess
- 21-15-4 Calculations for Discrete Column Restraints - H J Burgess
- 22-2-1 Buckling and Reliability Checking of Timber Columns - S Huang, P M Yu and
J Y Hong
- 22-2-2 Proposal for the Design of Compressed Timber Members by Adopting the
Second-Order Stress Theory - P Kaiser
- 30-2-1 Beam-Column Formula for Specific Truss Applications - W Lau, F Lam and J D
Barrett

SYMBOLS

- 3-3-1 Symbols for Structural Timber Design - J Kuipers and B Norén
- 4-3-1 Symbols for Timber Structure Design - J Kuipers and B Norén
- 28-3-1 Symbols for Timber and Wood-Based Materials - J Kuipers and B Noren
- i Symbols for Use in Structural Timber Design

PLYWOOD

- 2-4-1 The Presentation of Structural Design Data for Plywood - L G Booth
- 3-4-1 Standard Methods of Testing for the Determination of Mechanical Properties of
Plywood - J Kuipers
- 3-4-2 Bending Strength and Stiffness of Multiple Species Plywood - C K A Stieda
- 4-4-4 Standard Methods of Testing for the Determination of Mechanical Properties of
Plywood - Council of Forest Industries, B.C.
- 5-4-1 The Determination of Design Stresses for Plywood in the Revision of CP 112 -
L G Booth
- 5-4-2 Veneer Plywood for Construction - Quality Specifications - ISO/TC 139.
Plywood, Working Group 6
- 6-4-1 The Determination of the Mechanical Properties of Plywood Containing Defects -
L G Booth
- 6-4-2 Comparison of the Size and Type of Specimen and Type of Test on Plywood
Bending Strength and Stiffness - C R Wilson and P Eng
- 6-4-3 Buckling Strength of Plywood: Results of Tests and Recommendations for
Calculations - J Kuipers and H Ploos van Amstel

- 7-4-1 Methods of Test for the Determination of Mechanical Properties of Plywood - L G Booth, J Kuipers, B Norén, C R Wilson
- 7-4-2 Comments Received on Paper 7-4-1
- 7-4-3 The Effect of Rate of Testing Speed on the Ultimate Tensile Stress of Plywood - C R Wilson and A V Parasin
- 7-4-4 Comparison of the Effect of Specimen Size on the Flexural Properties of Plywood Using the Pure Moment Test - C R Wilson and A V Parasin
- 8-4-1 Sampling Plywood and the Evaluation of Test Results - B Norén
- 9-4-1 Shear and Torsional Rigidity of Plywood - H J Larsen
- 9-4-2 The Evaluation of Test Data on the Strength Properties of Plywood - L G Booth
- 9-4-3 The Sampling of Plywood and the Derivation of Strength Values (Second Draft) - B Norén
- 9-4-4 On the Use of the CIB/RILEM Plywood Plate Twisting Test: a progress report - L G Booth
- 10-4-1 Buckling Strength of Plywood - J Dekker, J Kuipers and H Ploos van Amstel
- 11-4-1 Analysis of Plywood Stressed Skin Panels with Rigid or Semi-Rigid Connections - I Smith
- 11-4-2 A Comparison of Plywood Modulus of Rigidity Determined by the ASTM and RILEM CIB/3-TT Test Methods - C R Wilson and A V Parasin
- 11-4-3 Sampling of Plywood for Testing Strength - B Norén
- 12-4-1 Procedures for Analysis of Plywood Test Data and Determination of Characteristic Values Suitable for Code Presentation - C R Wilson
- 14-4-1 An Introduction to Performance Standards for Wood-base Panel Products - D H Brown
- 14-4-2 Proposal for Presenting Data on the Properties of Structural Panels - T Schmidt
- 16-4-1 Planar Shear Capacity of Plywood in Bending - C K A Stieda
- 17-4-1 Determination of Panel Shear Strength and Panel Shear Modulus of Beech-Plywood in Structural Sizes - J Ehlbeck and F Colling
- 17-4-2 Ultimate Strength of Plywood Webs - R H Leicester and L Pham
- 20-4-1 Considerations of Reliability - Based Design for Structural Composite Products - M R O'Halloran, J A Johnson, E G Elias and T P Cunningham
- 21-4-1 Modelling for Prediction of Strength of Veneer Having Knots - Y Hirashima
- 22-4-1 Scientific Research into Plywood and Plywood Building Constructions the Results and Findings of which are Incorporated into Construction Standard Specifications of the USSR - I M Guskov
- 22-4-2 Evaluation of Characteristic values for Wood-Based Sheet Materials - E G Elias
- 24-4-1 APA Structural-Use Design Values: An Update to Panel Design Capacities - A L Kuchar, E G Elias, B Yeh and M R O'Halloran

STRESS GRADING

- 1-5-1 Quality Specifications for Sawn Timber and Precision Timber - Norwegian Standard NS 3080
- 1-5-2 Specification for Timber Grades for Structural Use - British Standard BS 4978

- 4-5-1 Draft Proposal for an International Standard for Stress Grading Coniferous Sawn Softwood - ECE Timber Committee
- 16-5-1 Grading Errors in Practice - B Thunell
- 16-5-2 On the Effect of Measurement Errors when Grading Structural Timber- L Nordberg and B Thunell
- 19-5-1 Stress-Grading by ECE Standards of Italian-Grown Douglas-Fir Dimension Lumber from Young Thinnings - L Uzielli
- 19-5-2 Structural Softwood from Afforestation Regions in Western Norway - R Lackner
- 21-5-1 Non-Destructive Test by Frequency of Full Size Timber for Grading - T Nakai
- 22-5-1 Fundamental Vibration Frequency as a Parameter for Grading Sawn Timber - T Nakai, T Tanaka and H Nagao
- 24-5-1 Influence of Stress Grading System on Length Effect Factors for Lumber Loaded in Compression - A Campos and I Smith
- 26-5-1 Structural Properties of French Grown Timber According to Various Grading Methods - F Rouger, C De Lafond and A El Quadrani
- 28-5-1 Grading Methods for Structural Timber - Principles for Approval - S Ohlsson
- 28-5-2 Relationship of Moduli of Elasticity in Tension and in Bending of Solid Timber - N Burger and P Glos
- 29-5-1 The Effect of Edge Knots on the Strength of SPF MSR Lumber - T Courchene, F Lam and J D Barrett
- 29-5-2 Determination of Moment Configuration Factors using Grading Machine Readings - T D G Canisius and T Isaksson

STRESSES FOR SOLID TIMBER

- 4-6-1 Derivation of Grade Stresses for Timber in the UK - W T Curry
- 5-6-1 Standard Methods of Test for Determining some Physical and Mechanical Properties of Timber in Structural Sizes - W T Curry
- 5-6-2 The Description of Timber Strength Data - J R Tory
- 5-6-3 Stresses for EC1 and EC2 Stress Grades - J R Tory
- 6-6-1 Standard Methods of Test for the Determination of some Physical and Mechanical Properties of Timber in Structural Sizes (third draft) - W T Curry
- 7-6-1 Strength and Long-term Behaviour of Lumber and Glued Laminated Timber under Torsion Loads - K Möhler
- 9-6-1 Classification of Structural Timber - H J Larsen
- 9-6-2 Code Rules for Tension Perpendicular to Grain - H J Larsen
- 9-6-3 Tension at an Angle to the Grain - K Möhler
- 9-6-4 Consideration of Combined Stresses for Lumber and Glued Laminated Timber - K Möhler
- 11-6-1 Evaluation of Lumber Properties in the United States - W L Galligan and J H Haskell
- 11-6-2 Stresses Perpendicular to Grain - K Möhler
- 11-6-3 Consideration of Combined Stresses for Lumber and Glued Laminated Timber (addition to Paper CIB-W18/9-6-4) - K Möhler

- 12-6-1 Strength Classifications for Timber Engineering Codes - R H Leicester and W G Keating
- 12-6-2 Strength Classes for British Standard BS 5268 - J R Tory
- 13-6-1 Strength Classes for the CIB Code - J R Tory
- 13-6-2 Consideration of Size Effects and Longitudinal Shear Strength for Uncracked Beams - R O Foschi and J D Barrett
- 13-6-3 Consideration of Shear Strength on End-Cracked Beams - J D Barrett and R O Foschi
- 15-6-1 Characteristic Strength Values for the ECE Standard for Timber - J G Sunley
- 16-6-1 Size Factors for Timber Bending and Tension Stresses - A R Fewell
- 16-6-2 Strength Classes for International Codes - A R Fewell and J G Sunley
- 17-6-1 The Determination of Grade Stresses from Characteristic Stresses for BS 5268: Part 2 - A R Fewell
- 17-6-2 The Determination of Softwood Strength Properties for Grades, Strength Classes and Laminated Timber for BS 5268: Part 2 - A R Fewell
- 18-6-1 Comment on Papers: 18-6-2 and 18-6-3 - R H Leicester
- 18-6-2 Configuration Factors for the Bending Strength of Timber - R H Leicester
- 18-6-3 Notes on Sampling Factors for Characteristic Values - R H Leicester
- 18-6-4 Size Effects in Timber Explained by a Modified Weakest Link Theory- B Madsen and A H Buchanan
- 18-6-5 Placement and Selection of Growth Defects in Test Specimens - H Riberholt
- 18-6-6 Partial Safety-Coefficients for the Load-Carrying Capacity of Timber Structures - B Norén and J-O Nylander
- 19-6-1 Effect of Age and/or Load on Timber Strength - J Kuipers
- 19-6-2 Confidence in Estimates of Characteristic Values - R H Leicester
- 19-6-3 Fracture Toughness of Wood - Mode I - K Wright and M Fonselius
- 19-6-4 Fracture Toughness of Pine - Mode II - K Wright
- 19-6-5 Drying Stresses in Round Timber - A Ranta-Maunus
- 19-6-6 A Dynamic Method for Determining Elastic Properties of Wood - R Görlacher
- 20-6-1 A Comparative Investigation of the Engineering Properties of "Whitewoods" Imported to Israel from Various Origins - U Korin
- 20-6-2 Effects of Yield Class, Tree Section, Forest and Size on Strength of Home Grown Sitka Spruce - V Picardo
- 20-6-3 Determination of Shear Strength and Strength Perpendicular to Grain - H J Larsen
- 21-6-1 Draft Australian Standard: Methods for Evaluation of Strength and Stiffness of Graded Timber - R H Leicester
- 21-6-2 The Determination of Characteristic Strength Values for Stress Grades of Structural Timber. Part 1 - A R Fewell and P Glos
- 21-6-3 Shear Strength in Bending of Timber - U Korin
- 22-6-1 Size Effects and Property Relationships for Canadian 2-inch Dimension Lumber - J D Barrett and H Griffin
- 22-6-2 Moisture Content Adjustments for In-Grade Data - J D Barrett and W Lau

- 22-6-3 A Discussion of Lumber Property Relationships in Eurocode 5 - D W Green and D E Kretschmann
- 22-6-4 Effect of Wood Preservatives on the Strength Properties of Wood - F Ronai
- 23-6-1 Timber in Compression Perpendicular to Grain - U Korin
- 24-6-1 Discussion of the Failure Criterion for Combined Bending and Compression - T A C M van der Put
- 24-6-3 Effect of Within Member Variability on Bending Strength of Structural Timber - I Czmocho, S Thelandersson and H J Larsen
- 24-6-4 Protection of Structural Timber Against Fungal Attack Requirements and Testing - K Jaworska, M Rylko and W Nozynski
- 24-6-5 Derivation of the Characteristic Bending Strength of Solid Timber According to CEN-Document prEN 384 - A J M Leijten
- 25-6-1 Moment Configuration Factors for Simple Beams - T D G Canisius
- 25-6-3 Bearing Capacity of Timber - U Korin
- 25-6-4 On Design Criteria for Tension Perpendicular to Grain - H Petersson
- 25-6-5 Size Effects in Visually Graded Softwood Structural Lumber - J D Barrett, F Lam and W Lau
- 26-6-1 Discussion and Proposal of a General Failure Criterion for Wood - T A C M van der Put
- 27-6-1 Development of the "Critical Bearing": Design Clause in CSA-086.1 - C Lum and E Karacabeyli
- 27-6-2 Size Effects in Timber: Novelty Never Ends - F Rouger and T Fewell
- 27-6-3 Comparison of Full-Size Sugi (*Cryptomeria japonica* D. Don) Structural Performance in Bending of Round Timber, Two Surfaces Sawn Timber and Square Sawn Timber - T Nakai, H Nagao and T Tanaka
- 28-6-1 Shear Strength of Canadian Softwood Structural Lumber - F Lam, H Yee and J D Barrett
- 28-6-2 Shear Strength of Douglas Fir Timbers - B Madsen
- 28-6-3 On the Influence of the Loading Head Profiles on Determined Bending Strength - L Muszyński and R Szukala
- 28-6-4 Effect of Test Standard, Length and Load Configuration on Bending Strength of Structural Timber - T Isaksson and S Thelandersson
- 28-6-5 Grading Machine Readings and their Use in the Calculation of Moment Configuration Factors - T Canisius, T Isaksson and S Thelandersson
- 28-6-6 End Conditions for Tension Testing of Solid Timber Perpendicular to Grain - T Canisius
- 29-6-1 Effect of Size on Tensile Strength of Timber - N Burger and P Glos
- 29-6-2 Equivalence of In-Grade Testing Standards - R H Leicester, H O Breitingner and H F Fordham
- 30-6-1 Strength Relationships in Structural Timber Subjected to Bending and Tension - N Burger and P Glos
- 30-6-2 Characteristic Design Stresses in Tension for Radiata Pine Grown in Canterbury - A Tsehaye, J C F Walker and A H Buchanan
- 30-6-3 Timber as a Natural Composite: Explanation of Some Peculiarities in the Mechanical Behaviour - E Gehri

TIMBER JOINTS AND FASTENERS

- 1-7-1 Mechanical Fasteners and Fastenings in Timber Structures - E G Stern
- 4-7-1 Proposal for a Basic Test Method for the Evaluation of Structural Timber Joints with Mechanical Fasteners and Connectors - RILEM 3TT Committee
- 4-7-2 Test Methods for Wood Fasteners - K Möhler
- 5-7-1 Influence of Loading Procedure on Strength and Slip-Behaviour in Testing Timber Joints - K Möhler
- 5-7-2 Recommendations for Testing Methods for Joints with Mechanical Fasteners and Connectors in Load-Bearing Timber Structures - RILEM 3 TT Committee
- 5-7-3 CIB-Recommendations for the Evaluation of Results of Tests on Joints with Mechanical Fasteners and Connectors used in Load-Bearing Timber Structures - J Kuipers
- 6-7-1 Recommendations for Testing Methods for Joints with Mechanical Fasteners and Connectors in Load-Bearing Timber Structures (seventh draft) - RILEM 3 TT Committee
- 6-7-2 Proposal for Testing Integral Nail Plates as Timber Joints - K Möhler
- 6-7-3 Rules for Evaluation of Values of Strength and Deformation from Test Results - Mechanical Timber Joints - M Johansen, J Kuipers, B Norén
- 6-7-4 Comments to Rules for Testing Timber Joints and Derivation of Characteristic Values for Rigidity and Strength - B Norén
- 7-7-1 Testing of Integral Nail Plates as Timber Joints - K Möhler
- 7-7-2 Long Duration Tests on Timber Joints - J Kuipers
- 7-7-3 Tests with Mechanically Jointed Beams with a Varying Spacing of Fasteners - K Möhler
- 7-100-1 CIB-Timber Code Chapter 5.3 Mechanical Fasteners; CIB-Timber Standard 06 and 07 - H J Larsen
- 9-7-1 Design of Truss Plate Joints - F J Keenan
- 9-7-2 Staples - K Möhler
- 11-7-1 A Draft Proposal for International Standard: ISO Document ISO/TC 165N 38E
- 12-7-1 Load-Carrying Capacity and Deformation Characteristics of Nailed Joints - J Ehlbeck
- 12-7-2 Design of Bolted Joints - H J Larsen
- 12-7-3 Design of Joints with Nail Plates - B Norén
- 13-7-1 Polish Standard BN-80/7159-04: Parts 00-01-02-03-04-05. "Structures from Wood and Wood-based Materials. Methods of Test and Strength Criteria for Joints with Mechanical Fasteners"
- 13-7-2 Investigation of the Effect of Number of Nails in a Joint on its Load Carrying Ability - W Nozynski
- 13-7-3 International Acceptance of Manufacture, Marking and Control of Finger-jointed Structural Timber - B Norén
- 13-7-4 Design of Joints with Nail Plates - Calculation of Slip - B Norén
- 13-7-5 Design of Joints with Nail Plates - The Heel Joint - B Källsner
- 13-7-6 Nail Deflection Data for Design - H J Burgess
- 13-7-7 Test on Bolted Joints - P Vermeijden

- 13-7-8 Comments to paper CIB-W18/12-7-3 "Design of Joints with Nail Plates"-
B Norén
- 13-7-9 Strength of Finger Joints - H J Larsen
- 13-100-4 CIB Structural Timber Design Code. Proposal for Section 6.1.5 Nail Plates -
N I Bovim
- 14-7-1 Design of Joints with Nail Plates (second edition) - B Norén
- 14-7-2 Method of Testing Nails in Wood (second draft, August 1980) - B Norén
- 14-7-3 Load-Slip Relationship of Nailed Joints - J Ehlbeck and H J Larsen
- 14-7-4 Wood Failure in Joints with Nail Plates - B Norén
- 14-7-5 The Effect of Support Eccentricity on the Design of W- and WW-Trussed with
Nail Plate Connectors - B Källsner
- 14-7-6 Derivation of the Allowable Load in Case of Nail Plate Joints Perpendicular to
Grain - K Möhler
- 14-7-7 Comments on CIB-W18/14-7-1 - T A C M van der Put
- 15-7-1 Final Recommendation TT-1A: Testing Methods for Joints with Mechanical
Fasteners in Load-Bearing Timber Structures. Annex A Punched Metal Plate
Fasteners - Joint Committee RILEM/CIB-3TT
- 16-7-1 Load Carrying Capacity of Dowels - E Gehri
- 16-7-2 Bolted Timber Joints: A Literature Survey - N Harding
- 16-7-3 Bolted Timber Joints: Practical Aspects of Construction and Design; a Survey -
N Harding
- 16-7-4 Bolted Timber Joints: Draft Experimental Work Plan - Building Research
Association of New Zealand
- 17-7-1 Mechanical Properties of Nails and their Influence on Mechanical Properties of
Nailed Timber Joints Subjected to Lateral Loads - I Smith, L R J Whale,
C Anderson and L Held
- 17-7-2 Notes on the Effective Number of Dowels and Nails in Timber Joints - G Steck
- 18-7-1 Model Specification for Driven Fasteners for Assembly of Pallets and Related
Structures - E G Stern and W B Wallin
- 18-7-2 The Influence of the Orientation of Mechanical Joints on their Mechanical
Properties - I Smith and L R J Whale
- 18-7-3 Influence of Number of Rows of Fasteners or Connectors upon the Ultimate
Capacity of Axially Loaded Timber Joints - I Smith and G Steck
- 18-7-4 A Detailed Testing Method for Nailplate Joints - J Kangas
- 18-7-5 Principles for Design Values of Nailplates in Finland - J Kangas
- 18-7-6 The Strength of Nailplates - N I Bovim and E Aasheim
- 19-7-1 Behaviour of Nailed and Bolted Joints under Short-Term Lateral Load -
Conclusions from Some Recent Research - L R J Whale, I Smith and B O Hilson
- 19-7-2 Glued Bolts in Glulam - H Riberholt
- 19-7-3 Effectiveness of Multiple Fastener Joints According to National Codes and
Eurocode 5 (Draft) - G Steck
- 19-7-4 The Prediction of the Long-Term Load Carrying Capacity of Joints in Wood
Structures - Y M Ivanov and Y Y Slavic
- 19-7-5 Slip in Joints under Long-Term Loading - T Feldborg and M Johansen

- 19-7-6 The Derivation of Design Clauses for Nailed and Bolted Joints in Eurocode 5 - L R J Whale and I Smith
- 19-7-7 Design of Joints with Nail Plates - Principles - B Norén
- 19-7-8 Shear Tests for Nail Plates - B Norén
- 19-7-9 Advances in Technology of Joints for Laminated Timber - Analyses of the Structural Behaviour - M Piazza and G Turrini
- 19-15-1 Connections Deformability in Timber Structures: A Theoretical Evaluation of its Influence on Seismic Effects - A Ceccotti and A Vignoli
- 20-7-1 Design of Nailed and Bolted Joints-Proposals for the Revision of Existing Formulae in Draft Eurocode 5 and the CIB Code - L R J Whale, I Smith and H J Larsen
- 20-7-2 Slip in Joints under Long Term Loading - T Feldborg and M Johansen
- 20-7-3 Ultimate Properties of Bolted Joints in Glued-Laminated Timber - M Yasumura, T Murota and H Sakai
- 20-7-4 Modelling the Load-Deformation Behaviour of Connections with Pin-Type Fasteners under Combined Moment, Thrust and Shear Forces - I Smith
- 21-7-1 Nails under Long-Term Withdrawal Loading - T Feldborg and M Johansen
- 21-7-2 Glued Bolts in Glulam-Proposals for CIB Code - H Riberholt
- 21-7-3 Nail Plate Joint Behaviour under Shear Loading - T Poutanen
- 21-7-4 Design of Joints with Laterally Loaded Dowels. Proposals for Improving the Design Rules in the CIB Code and the Draft Eurocode 5 - J Ehlbeck and H Werner
- 21-7-5 Axially Loaded Nails: Proposals for a Supplement to the CIB Code - J Ehlbeck and W Siebert
- 22-7-1 End Grain Connections with Laterally Loaded Steel Bolts A draft proposal for design rules in the CIB Code - J Ehlbeck and M Gerold
- 22-7-2 Determination of Perpendicular-to-Grain Tensile Stresses in Joints with Dowel-Type Fasteners - A draft proposal for design rules - J Ehlbeck, R Görlacher and H Werner
- 22-7-3 Design of Double-Shear Joints with Non-Metallic Dowels A proposal for a supplement of the design concept - J Ehlbeck and O Eberhart
- 22-7-4 The Effect of Load on Strength of Timber Joints at high Working Load Level - A J M Leijten
- 22-7-5 Plasticity Requirements for Portal Frame Corners - R Gunnewijk and A J M Leijten
- 22-7-6 Background Information on Design of Glulam Rivet Connections in CSA/CAN3-086.1-M89 - A proposal for a supplement of the design concept - E Karacabeyli and D P Janssens
- 22-7-7 Mechanical Properties of Joints in Glued-Laminated Beams under Reversed Cyclic Loading - M Yasumura
- 22-7-8 Strength of Glued Lap Timber Joints - P Glos and H Horstmann
- 22-7-9 Toothed Rings Type Bistyp 075 at the Joints of Fir Wood - J Kerste
- 22-7-10 Calculation of Joints and Fastenings as Compared with the International State - K Zimmer and K Lissner

- 22-7-11 Joints on Glued-in Steel Bars Present Relatively New and Progressive Solution in Terms of Timber Structure Design - G N Zubarev, F A Boitemirov and V M Golovina
- 22-7-12 The Development of Design Codes for Timber Structures made of Compositive Bars with Plate Joints based on Cylindrical Nails - Y V Piskunov
- 22-7-13 Designing of Glued Wood Structures Joints on Glued-in Bars - S B Turkovsky
- 23-7-1 Proposal for a Design Code for Nail Plates - E Aasheim and K H Solli
- 23-7-2 Load Distribution in Nailed Joints - H J Blass
- 24-7-1 Theoretical and Experimental Tension and Shear Capacity of Nail Plate Connections - B Källsner and J Kangas
- 24-7-2 Testing Method and Determination of Basic Working Loads for Timber Joints with Mechanical Fasteners - Y Hirashima and F Kamiya
- 24-7-3 Anchorage Capacity of Nail Plate - J Kangas
- 25-7-2 Softwood and Hardwood Embedding Strength for Dowel type Fasteners - J Ehlbeck and H Werner
- 25-7-4 A Guide for Application of Quality Indexes for Driven Fasteners Used in Connections in Wood Structures - E G Stern
- 25-7-5 35 Years of Experience with Certain Types of Connectors and Connector Plates Used for the Assembly of Wood Structures and their Components- E G Stern
- 25-7-6 Characteristic Strength of Split-ring and Shear-plate Connections - H J Blass, J Ehlbeck and M Schlager
- 25-7-7 Characteristic Strength of Tooth-plate Connector Joints - H J Blass, J Ehlbeck and M Schlager
- 25-7-8 Extending Yield Theory to Screw Connections - T E McLain
- 25-7-9 Determination of k_{def} for Nailed Joints - J W G van de Kuilen
- 25-7-10 Characteristic Strength of UK Timber Connectors - A V Page and C J Mettem
- 25-7-11 Multiple-fastener Dowel-type Joints, a Selected Review of Research and Codes - C J Mettem and A V Page
- 25-7-12 Load Distributions in Multiple-fastener Bolted Joints in European Whitewood Glulam, with Steel Side Plates - C J Mettem and A V Page
- 26-7-1 Proposed Test Method for Dynamic Properties of Connections Assembled with Mechanical Fasteners - J D Dolan
- 26-7-2 Validatory Tests and Proposed Design Formulae for the Load-Carrying Capacity of Toothed-Plate Connected Joints - C J Mettem, A V Page and G Davis
- 26-7-3 Definitions of Terms and Multi-Language Terminology Pertaining to Metal Connector Plates - E G Stern
- 26-7-4 Design of Joints Based on in V-Shape Glued-in Rods - J Kangas
- 26-7-5 Tests on Timber Concrete Composite Structural Elements (TCCs) - A U Meierhofer
- 27-7-1 Glulam Arch Bridge and Design of it's Moment-Resisting Joints - K Komatsu and S Usuku
- 27-7-2 Characteristic Load - Carrying Capacity of Joints with Dowel - type Fasteners in Regard to the System Properties - H Werner
- 27-7-3 Steel Failure Design in Truss Plate Joints - T Poutanen

- 28-7-1 Expanded Tube Joint in Locally DP Reinforced Timber - A J M Leijten, P Ragupathy and K S Virdi
- 28-7-2 A Strength and Stiffness Model for the Expanded Tube Joint - A J M Leijten
- 28-7-3 Load-carrying Capacity of Steel-to Timber Joints with Annular Ring Shanked Nails. A Comparison with the EC5 Design Method - R Görlacher
- 28-7-4 Dynamic Effects on Metal-Plate Connected Wood Truss Joints - S Kent, R Gupta and T Miller
- 28-7-5 Failure of the Timber Bolted Joints Subjected to Lateral Load Perpendicular to Grain - M Yasumura and L Daudeville
- 28-7-6 Design Procedure for Locally Reinforced Joints with Dowel-type Fasteners - H Werner
- 28-7-7 Variability and Effects of Moisture Content on the Withdrawal Characteristics for Lumber as Opposed to Clear Wood - J D Dolan and J W Stelmokas
- 28-7-8 Nail Plate Capacity in Joint Line - A Kevarinmäki and J Kangas
- 28-7-9 Axial Strength of Glued-In Bolts - Calculation Model Based on Non-Linear Fracture Mechanics - A Preliminary Study - C J Johansson, E Serrano, P J Gustafsson and B Enquist
- 28-7-10 Cyclic Lateral Dowel Connection Tests for seismic and Wind Evaluation - J D Dolan
- 29-7-1 A Simple Method for Lateral Load-Carrying Capacity of Dowel-Type Fasteners - J Kangas and J Kurkela
- 29-7-2 Nail Plate Joint Behaviour at Low Versus High Load Level - T Poutanen
- 29-7-3 The Moment Resistance of Tee and Butt - Joint Nail Plate Test Specimens - A Comparison with Current Design Methods - A Reffold, L R J Whale and B S Choo
- 29-7-4 A Critical Review of the Moment Rotation Test Method Proposed in prEN 1075 - M Bettison, B S Choo and L R J Whale
- 29-7-5 Explanation of the Translation and Rotation Behaviour of Prestressed Moment Timber Joints - A J M Leijten
- 29-7-6 Design of Joints and Frame Corners using Dowel-Type Fasteners - E Gehri
- 29-7-7 Quasi-Static Reversed-Cyclic Testing of Nailed Joints - E Karacabeyli and A Ceccotti
- 29-7-8 Failure of Bolted Joints Loaded Parallel to the Grain: Experiment and Simulation - L Davenne, L Daudeville and M Yasumura
- 30-7-1 Flexural Behaviour of GLT Beams End-Jointed by Glued-in Hardwood Dowels - K Komatsu, A Koizumi, J Jensen, T Sasaki and Y Iijima
- 30-7-2 Modelling of the Block Tearing Failure in Nailed Steel-to-Timber Joints - J Kangas, K Aalto and A Kevarinmäki
- 30-7-3 Cyclic Testing of Joints with Dowels and Slotted-in Steel Plates - E Aasheim
- 30-7-4 A Steel-to-Timber Dowelled Joint of High Performance in Combination with a High Strength Wood Composite (Parallam) - E Gehri
- 30-7-5 Multiple Fastener Timber Connections with Dowel Type Fasteners - A Jorissen
- 30-7-6 Influence of Ductility on Load-Carrying Capacity of Joints with Dowel-Type Fasteners - A Mischler

LOAD SHARING

- 3-8-1 Load Sharing - An Investigation on the State of Research and Development of Design Criteria - E Levin
- 4-8-1 A Review of Load-Sharing in Theory and Practice - E Levin
- 4-8-2 Load Sharing - B Norén
- 19-8-1 Predicting the Natural Frequencies of Light-Weight Wooden Floors - I Smith and Y H Chui
- 20-8-1 Proposed Code Requirements for Vibrational Serviceability of Timber Floors - Y H Chui and I Smith
- 21-8-1 An Addendum to Paper 20-8-1 - Proposed Code Requirements for Vibrational Serviceability of Timber Floors - Y H Chui and I Smith
- 21-8-2 Floor Vibrational Serviceability and the CIB Model Code - S Ohlsson
- 22-8-1 Reliability Analysis of Viscoelastic Floors - F Rouger, J D Barrett and R O Foschi
- 24-8-1 On the Possibility of Applying Neutral Vibrational Serviceability Criteria to Joisted Wood Floors - I Smith and Y H Chui
- 25-8-1 Analysis of Glulam Semi-rigid Portal Frames under Long-term Load - K Komatsu and N Kawamoto

DURATION OF LOAD

- 3-9-1 Definitions of Long Term Loading for the Code of Practice - B Norén
- 4-9-1 Long Term Loading of Trussed Rafters with Different Connection Systems - T Feldborg and M Johansen
- 5-9-1 Strength of a Wood Column in Combined Compression and Bending with Respect to Creep - B Källsner and B Norén
- 6-9-1 Long Term Loading for the Code of Practice (Part 2) - B Norén
- 6-9-2 Long Term Loading - K Möhler
- 6-9-3 Deflection of Trussed Rafters under Alternating Loading during a Year - T Feldborg and M Johansen
- 7-6-1 Strength and Long Term Behaviour of Lumber and Glued-Laminated Timber under Torsion Loads - K Möhler
- 7-9-1 Code Rules Concerning Strength and Loading Time - H J Larsen and E Theilgaard
- 17-9-1 On the Long-Term Carrying Capacity of Wood Structures - Y M Ivanov and Y Y Slavic
- 18-9-1 Prediction of Creep Deformations of Joints - J Kuipers
- 19-9-1 Another Look at Three Duration of Load Models - R O Foschi and Z C Yao
- 19-9-2 Duration of Load Effects for Spruce Timber with Special Reference to Moisture Influence - A Status Report - P Hoffmeyer
- 19-9-3 A Model of Deformation and Damage Processes Based on the Reaction Kinetics of Bond Exchange - T A C M van der Put
- 19-9-4 Non-Linear Creep Superposition - U Korin
- 19-9-5 Determination of Creep Data for the Component Parts of Stressed-Skin Panels - R Klinger
- 19-9-6 Creep an Lifetime of Timber Loaded in Tension and Compression - P Glos

- 19-1-1 Duration of Load Effects and Reliability Based Design (Single Member) - R O Foschi and Z C Yao
- 19-6-1 Effect of Age and/or Load on Timber Strength - J Kuipers
- 19-7-4 The Prediction of the Long-Term Load Carrying Capacity of Joints in Wood Structures - Y M Ivanov and Y Y Slavic
- 19-7-5 Slip in Joints under Long-Term Loading - T Feldborg and M Johansen
- 20-7-2 Slip in Joints under Long-Term Loading - T Feldborg and M Johansen
- 22-9-1 Long-Term Tests with Glued Laminated Timber Girders - M Badstube, W Rug and W Schöne
- 22-9-2 Strength of One-Layer solid and Lengthways Glued Elements of Wood Structures and its Alteration from Sustained Load - L M Kovaltchuk, I N Boitemirova and G B Uspenskaya
- 24-9-1 Long Term Bending Creep of Wood - T Toratti
- 24-9-2 Collection of Creep Data of Timber - A Ranta-Maunus
- 24-9-3 Deformation Modification Factors for Calculating Built-up Wood-Based Structures - I R Kliger
- 25-9-2 DVM Analysis of Wood. Lifetime, Residual Strength and Quality - L F Nielsen
- 26-9-1 Long Term Deformations in Wood Based Panels under Natural Climate Conditions. A Comparative Study - S Thelandersson, J Nordh, T Nordh and S Sandahl
- 28-9-1 Evaluation of Creep Behavior of Structural Lumber in Natural Environment - R Gupta and R Shen
- 30-9-1 DOL Effect in Tension Perpendicular to the Grain of Glulam Depending on Service Classes and Volume - S Aicher and G Dill-Langer
- 30-9-2 Damage Modelling of Glulam in Tension Perpendicular to Grain in Variable Climate - G Dill-Langer and S Aicher

TIMBER BEAMS

- 4-10-1 The Design of Simple Beams - H J Burgess
- 4-10-2 Calculation of Timber Beams Subjected to Bending and Normal Force - H J Larsen
- 5-10-1 The Design of Timber Beams - H J Larsen
- 9-10-1 The Distribution of Shear Stresses in Timber Beams - F J Keenan
- 9-10-2 Beams Notched at the Ends - K Möhler
- 11-10-1 Tapered Timber Beams - H Riberholt
- 13-6-2 Consideration of Size Effects in Longitudinal Shear Strength for Uncracked Beams - R O Foschi and J D Barrett
- 13-6-3 Consideration of Shear Strength on End-Cracked Beams - J D Barrett and R O Foschi
- 18-10-1 Submission to the CIB-W18 Committee on the Design of Ply Web Beams by Consideration of the Type of Stress in the Flanges - J A Baird
- 18-10-2 Longitudinal Shear Design of Glued Laminated Beams - R O Foschi
- 19-10-1 Possible Code Approaches to Lateral Buckling in Beams - H J Burgess
- 19-2-1 Creep Buckling Strength of Timber Beams and Columns - R H Leicester

- 20-2-1 Lateral Buckling Theory for Rectangular Section Deep Beam-Columns - H J Burgess
- 20-10-1 Draft Clause for CIB Code for Beams with Initial Imperfections - H J Burgess
- 20-10-2 Space Joists in Irish Timber - W J Robinson
- 20-10-3 Composite Structure of Timber Joists and Concrete Slab - T Poutanen
- 21-10-1 A Study of Strength of Notched Beams - P J Gustafsson
- 22-10-1 Design of Endnotched Beams - H J Larsen and P J Gustafsson
- 22-10-2 Dimensions of Wooden Flexural Members under Constant Loads - A Pozgai
- 22-10-3 Thin-Walled Wood-Based Flanges in Composite Beams - J König
- 22-10-4 The Calculation of Wooden Bars with flexible Joints in Accordance with the Polish Standard Code and Strict Theoretical Methods - Z Mielczarek
- 23-10-1 Tension Perpendicular to the Grain at Notches and Joints - T A C M van der Put
- 23-10-2 Dimensioning of Beams with Cracks, Notches and Holes. An Application of Fracture Mechanics - K Riipola
- 23-10-3 Size Factors for the Bending and Tension Strength of Structural Timber - J D Barret and A R Fewell
- 23-12-1 Bending Strength of Glulam Beams, a Design Proposal - J Ehlbeck and F Colling
- 23-12-3 Glulam Beams, Bending Strength in Relation to the Bending Strength of the Finger Joints - H Riberholt
- 24-10-1 Shear Strength of Continuous Beams - R H Leicester and F G Young
- 25-10-1 The Strength of Norwegian Glued Laminated Beams - K Solli, E Aasheim and R H Falk
- 25-10-2 The Influence of the Elastic Modulus on the Simulated Bending Strength of Hyperstatic Timber Beams - T D G Canisius
- 27-10-1 Determination of Shear Modulus - R Görlacher and J Kürth
- 29-10-1 Time Dependent Lateral Buckling of Timber Beams - F Rouger
- 29-10-2 Determination of Modulus of Elasticity in Bending According to EN 408 - K H Solli
- 29-10-3 On Determination of Modulus of Elasticity in Bending - L Boström, S Ormarsson and O Dahlblom
- 29-10-4 Relation of Moduli of Elasticity in Flatwise and Edgewise Bending of Solid Timber - C J Johansson, A Steffen and E W Wormuth
- 30-10-1 Nondestructive Evaluation of Wood-based Members and Structures with the Help of Modal Analysis - P Kuklik
- 30-10-2 Measurement of Modulus of Elasticity in Bending - L Boström
- 30-10-3 A Weak Zone Model for Timber in Bending - B Källsner, K Salmela and O Ditlevsen
- 30-10-4 Load Carrying Capacity of Timber Beams with Narrow Moment Peaks - T Isaksson and J Freysoldt

ENVIRONMENTAL CONDITIONS

- 5-11-1 Climate Grading for the Code of Practice - B Norén
- 6-11-1 Climate Grading (2) - B Norén

- 9-11-1 Climate Classes for Timber Design - F J Keenan
- 19-11-1 Experimental Analysis on Ancient Downgraded Timber Structures - B Leggeri and L Paolini
- 19-6-5 Drying Stresses in Round Timber - A Ranta-Maunus
- 22-11-1 Corrosion and Adaptation Factors for Chemically Aggressive Media with Timber Structures - K Erler
- 29-11-1 Load Duration Effect on Structural Beams under Varying Climate Influence of Size and Shape - P Galimard and P Morlier
- 30-11-1 Probabilistic Design Models for the Durability of Timber Constructions - R H Leicester

LAMINATED MEMBERS

- 6-12-1 Directives for the Fabrication of Load-Bearing Structures of Glued Timber - A van der Velden and J Kuipers
- 8-12-1 Testing of Big Glulam Timber Beams - H Kolb and P Frech
- 8-12-2 Instruction for the Reinforcement of Apertures in Glulam Beams - H Kolb and P Frech
- 8-12-3 Glulam Standard Part 1: Glued Timber Structures; Requirements for Timber (Second Draft)
- 9-12-1 Experiments to Provide for Elevated Forces at the Supports of Wooden Beams with Particular Regard to Shearing Stresses and Long-Term Loadings - F Wassipaul and R Lackner
- 9-12-2 Two Laminated Timber Arch Railway Bridges Built in Perth in 1849 - L G Booth
- 9-6-4 Consideration of Combined Stresses for Lumber and Glued Laminated Timber - K Möhler
- 11-6-3 Consideration of Combined Stresses for Lumber and Glued Laminated Timber (addition to Paper CIB-W18/9-6-4) - K Möhler
- 12-12-1 Glulam Standard Part 2: Glued Timber Structures; Rating (3rd draft)
- 12-12-2 Glulam Standard Part 3: Glued Timber Structures; Performance (3rd draft)
- 13-12-1 Glulam Standard Part 3: Glued Timber Structures; Performance (4th draft)
- 14-12-1 Proposals for CEI-Bois/CIB-W18 Glulam Standards - H J Larsen
- 14-12-2 Guidelines for the Manufacturing of Glued Load-Bearing Timber Structures - Stevin Laboratory
- 14-12-3 Double Tapered Curved Glulam Beams - H Riberholt
- 14-12-4 Comment on CIB-W18/14-12-3 - E Gehri
- 18-12-1 Report on European Glulam Control and Production Standard - H Riberholt
- 18-10-2 Longitudinal Shear Design of Glued Laminated Beams - R O Foschi
- 19-12-1 Strength of Glued Laminated Timber - J Ehlbeck and F Colling
- 19-12-2 Strength Model for Glulam Columns - H J Blaß
- 19-12-3 Influence of Volume and Stress Distribution on the Shear Strength and Tensile Strength Perpendicular to Grain - F Colling
- 19-12-4 Time-Dependent Behaviour of Glued-Laminated Beams - F Zaupa

- 21-12-1 Modulus of Rupture of Glulam Beam Composed of Arbitrary Laminae - K Komatsu and N Kawamoto
- 21-12-2 An Appraisal of the Young's Modulus Values Specified for Glulam in Eurocode 5- L R J Whale, B O Hilson and P D Rodd
- 21-12-3 The Strength of Glued Laminated Timber (Glulam): Influence of Lamination Qualities and Strength of Finger Joints - J Ehlbeck and F Colling
- 21-12-4 Comparison of a Shear Strength Design Method in Eurocode 5 and a More Traditional One - H Riberholt
- 22-12-1 The Dependence of the Bending Strength on the Glued Laminated Timber Girder Depth - M Badstube, W Rug and W Schöne
- 22-12-2 Acid Deterioration of Glulam Beams in Buildings from the Early Half of the 1960s - Preliminary summary of the research project; Overhead pictures - B A Hedlund
- 22-12-3 Experimental Investigation of normal Stress Distribution in Glue Laminated Wooden Arches - Z Mielczarek and W Chanaj
- 22-12-4 Ultimate Strength of Wooden Beams with Tension Reinforcement as a Function of Random Material Properties - R Candowicz and T Dziuba
- 23-12-1 Bending Strength of Glulam Beams, a Design Proposal - J Ehlbeck and F Colling
- 23-12-2 Probability Based Design Method for Glued Laminated Timber - M F Stone
- 23-12-3 Glulam Beams, Bending Strength in Relation to the Bending Strength of the Finger Joints - H Riberholt
- 23-12-4 Glued Laminated Timber - Strength Classes and Determination of Characteristic Properties - H Riberholt, J Ehlbeck and A Fewell
- 24-12-1 Contribution to the Determination of the Bending Strength of Glulam Beams - F Colling, J Ehlbeck and R Görlacher
- 24-12-2 Influence of Perpendicular-to-Grain Stressed Volume on the Load-Carrying Capacity of Curved and Tapered Glulam Beams - J Ehlbeck and J Kürth
- 25-12-1 Determination of Characteristic Bending Values of Glued Laminated Timber. EN-Approach and Reality - E Gehri
- 26-12-1 Norwegian Bending Tests with Glued Laminated Beams-Comparative Calculations with the "Karlsruhe Calculation Model" - E Aasheim, K Solli, F Colling, R H Falk, J Ehlbeck and R Görlacher
- 26-12-2 Simulation Analysis of Norwegian Spruce Glued-Laminated Timber - R Hernandez and R H Falk
- 26-12-3 Investigation of Laminating Effects in Glued-Laminated Timber - F Colling and R H Falk
- 26-12-4 Comparing Design Results for Glulam Beams According to Eurocode 5 and to the French Working Stress Design Code (CB71) - F Rouger
- 27-12-1 State of the Art Report: Glulam Timber Bridge Design in the U.S. - M A Ritter and T G Williamson
- 27-12-2 Common Design Practice for Timber Bridges in the United Kingdom - C J Mettem, J P Marcroft and G Davis
- 27-12-3 Influence of Weak Zones on Stress Distribution in Glulam Beams - E Serrano and H J Larsen
- 28-12-1 Determination of Characteristic Bending Strength of Glued Laminated Timber - E Gehri

- 28-12-2 Size Factor of Norwegian Glued Laminated Beams - E Aasheim and K H Solli
- 28-12-3 Design of Glulam Beams with Holes - K Riipola
- 28-12-4 Compression Resistance of Glued Laminated Timber Short Columns- U Korin
- 29-12-1 Development of Efficient Glued Laminated Timber - G Schickhofer
- 30-12-1 Experimental Investigation and Analysis of Reinforced Glulam Beams - K Oiger

PARTICLE AND FIBRE BUILDING BOARDS

- 7-13-1 Fibre Building Boards for CIB Timber Code (First Draft)- O Brynildsen
- 9-13-1 Determination of the Bearing Strength and the Load-Deformation Characteristics of Particleboard - K Möhler, T Budiando and J Ehlbeck
- 9-13-2 The Structural Use of Tempered Hardboard - W W L Chan
- 11-13-1 Tests on Laminated Beams from Hardboard under Short- and Longterm Load - W Nozynski
- 11-13-2 Determination of Deformation of Special Densified Hardboard under Long-term Load and Varying Temperature and Humidity Conditions - W Halfar
- 11-13-3 Determination of Deformation of Hardboard under Long-term Load in Changing Climate - W Halfar
- 14-4-1 An Introduction to Performance Standards for Wood-Base Panel Products - D H Brown
- 14-4-2 Proposal for Presenting Data on the Properties of Structural Panels - T Schmidt
- 16-13-1 Effect of Test Piece Size on Panel Bending Properties - P W Post
- 20-4-1 Considerations of Reliability - Based Design for Structural Composite Products - M R O'Halloran, J A Johnson, E G Elias and T P Cunningham
- 20-13-1 Classification Systems for Structural Wood-Based Sheet Materials - V C Kearley and A R Abbott
- 21-13-1 Design Values for Nailed Chipboard - Timber Joints - A R Abbott
- 25-13-1 Bending Strength and Stiffness of Izopanel Plates - Z Mielczarek
- 28-13-1 Background Information for "Design Rated Oriented Strand Board (OSB)" in CSA Standards - Summary of Short-term Test Results - E Karacabeyli, P Lau, C R Henderson, F V Meakes and W Deacon
- 28-13-2 Torsional Stiffness of Wood-Hardboard Composed I-Beam - P Olejniczak

TRUSSED RAFTERS

- 4-9-1 Long-term Loading of Trussed Rafters with Different Connection Systems - T Feldborg and M Johansen
- 6-9-3 Deflection of Trussed Rafters under Alternating Loading During a Year - T Feldborg and M Johansen
- 7-2-1 Lateral Bracing of Timber Struts - J A Simon
- 9-14-1 Timber Trusses - Code Related Problems - T F Williams
- 9-7-1 Design of Truss Plate Joints - F J Keenan
- 10-14-1 Design of Roof Bracing - The State of the Art in South Africa - P A V Bryant and J A Simon
- 11-14-1 Design of Metal Plate Connected Wood Trusses - A R Egerup

- 12-14-1 A Simple Design Method for Standard Trusses - A R Egerup
- 13-14-1 Truss Design Method for CIB Timber Code - A R Egerup
- 13-14-2 Trussed Rafters, Static Models - H Riberholt
- 13-14-3 Comparison of 3 Truss Models Designed by Different Assumptions for Slip and E-Modulus - K Möhler
- 14-14-1 Wood Trussed Rafter Design - T Feldborg and M Johansen
- 14-14-2 Truss-Plate Modelling in the Analysis of Trusses - R O Foschi
- 14-14-3 Cantilevered Timber Trusses - A R Egerup
- 14-7-5 The Effect of Support Eccentricity on the Design of W- and WW-Trusses with Nail Plate Connectors - B Källsner
- 15-14-1 Guidelines for Static Models of Trussed Rafters - H Riberholt
- 15-14-2 The Influence of Various Factors on the Accuracy of the Structural Analysis of Timber Roof Trusses - F R P Pienaar
- 15-14-3 Bracing Calculations for Trussed Rafter Roofs - H J Burgess
- 15-14-4 The Design of Continuous Members in Timber Trussed Rafters with Punched Metal Connector Plates - P O Reece
- 15-14-5 A Rafter Design Method Matching U.K. Test Results for Trussed Rafters - H J Burgess
- 16-14-1 Full-Scale Tests on Timber Fink Trusses Made from Irish Grown Sitka Spruce - V Picardo
- 17-14-1 Data from Full Scale Tests on Prefabricated Trussed Rafters - V Picardo
- 17-14-2 Simplified Static Analysis and Dimensioning of Trussed Rafters - H Riberholt
- 17-14-3 Simplified Calculation Method for W-Trusses - B Källsner
- 18-14-1 Simplified Calculation Method for W-Trusses (Part 2) - B Källsner
- 18-14-2 Model for Trussed Rafter Design - T Poutanen
- 19-14-1 Annex on Simplified Design of W-Trusses - H J Larsen
- 19-14-2 Simplified Static Analysis and Dimensioning of Trussed Rafters - Part 2 - H Riberholt
- 19-14-3 Joint Eccentricity in Trussed Rafters - T Poutanen
- 20-14-1 Some Notes about Testing Nail Plates Subjected to Moment Load - T Poutanen
- 20-14-2 Moment Distribution in Trussed Rafters - T Poutanen
- 20-14-3 Practical Design Methods for Trussed Rafters - A R Egerup
- 22-14-1 Guidelines for Design of Timber Trussed Rafters - H Riberholt
- 23-14-1 Analyses of Timber Trussed Rafters of the W-Type - H Riberholt
- 23-14-2 Proposal for Eurocode 5 Text on Timber Trussed Rafters - H Riberholt
- 24-14-1 Capacity of Support Areas Reinforced with Nail Plates in Trussed Rafters - A Kevarinmäki
- 25-14-1 Moment Anchorage Capacity of Nail Plates in Shear Tests - A Kevarinmaki and J. Kangas
- 25-14-2 Design Values of Anchorage Strength of Nail Plate Joints by 2-curve Method and Interpolation - J Kangas and A Kevarinmaki
- 26-14-1 Test of Nail Plates Subjected to Moment - E Aasheim

- 26-14-2 Moment Anchorage Capacity of Nail Plates - A Kevarinmäki and J Kangas
- 26-14-3 Rotational Stiffness of Nail Plates in Moment Anchorage - A Kevarinmäki and J Kangas
- 26-14-4 Solution of Plastic Moment Anchorage Stress in Nail Plates - A Kevarinmäki
- 26-14-5 Testing of Metal-Plate-Connected Wood-Truss Joints - R Gupta
- 26-14-6 Simulated Accidental Events on a Trussed Rafter Roofed Building - C J Mettem and J P Marcroft
- 30-14-1 The Stability Behaviour of Timber Trussed Rafter Roofs - Studies Based on Eurocode 5 and Full Scale Testing - R J Bainbridge, C J Mettem, A Reffold and T Studer

STRUCTURAL STABILITY

- 8-15-1 Laterally Loaded Timber Columns: Tests and Theory - H J Larsen
- 13-15-1 Timber and Wood-Based Products Structures. Panels for Roof Coverings. Methods of Testing and Strength Assessment Criteria. Polish Standard BN-78/7159-03
- 16-15-1 Determination of Bracing Structures for Compression Members and Beams - H Brüninghoff
- 17-15-1 Proposal for Chapter 7.4 Bracing - H Brüninghoff
- 17-15-2 Seismic Design of Small Wood Framed Houses - K F Hansen
- 18-15-1 Full-Scale Structures in Glued Laminated Timber, Dynamic Tests: Theoretical and Experimental Studies - A Ceccotti and A Vignoli
- 18-15-2 Stabilizing Bracings - H Brüninghoff
- 19-15-1 Connections Deformability in Timber Structures: a Theoretical Evaluation of its Influence on Seismic Effects - A Ceccotti and A Vignoli
- 19-15-2 The Bracing of Trussed Beams - M H Kessel and J Natterer
- 19-15-3 Racking Resistance of Wooden Frame Walls with Various Openings - M Yasumura
- 19-15-4 Some Experiences of Restoration of Timber Structures for Country Buildings - G Cardinale and P Spinelli
- 19-15-5 Non-Destructive Vibration Tests on Existing Wooden Dwellings - Y Hirashima
- 20-15-1 Behaviour Factor of Timber Structures in Seismic Zones. - A Ceccotti and A Vignoli
- 21-15-1 Rectangular Section Deep Beam - Columns with Continuous Lateral Restraint - H J Burgess
- 21-15-2 Buckling Modes and Permissible Axial Loads for Continuously Braced Columns - H J Burgess
- 21-15-3 Simple Approaches for Column Bracing Calculations - H J Burgess
- 21-15-4 Calculations for Discrete Column Restraints - H J Burgess
- 21-15-5 Behaviour Factor of Timber Structures in Seismic Zones (Part Two) - A Ceccotti and A Vignoli
- 22-15-1 Suggested Changes in Code Bracing Recommendations for Beams and Columns - H J Burgess

- 22-15-2 Research and Development of Timber Frame Structures for Agriculture in Poland - S Kus and J Kerste
- 22-15-3 Ensuring of Three-Dimensional Stiffness of Buildings with Wood Structures - A K Shenghelia
- 22-15-5 Seismic Behavior of Arched Frames in Timber Construction - M Yasumura
- 22-15-6 The Robustness of Timber Structures - C J Mettem and J P Marcroft
- 22-15-7 Influence of Geometrical and Structural Imperfections on the Limit Load of Wood Columns - P Dutko
- 23-15-1 Calculation of a Wind Girder Loaded also by Discretely Spaced Braces for Roof Members - H J Burgess
- 23-15-2 Stability Design and Code Rules for Straight Timber Beams - T A C M van der Put
- 23-15-3 A Brief Description of Formula of Beam-Columns in China Code - S Y Huang
- 23-15-4 Seismic Behavior of Braced Frames in Timber Construction - M Yasumara
- 23-15-5 On a Better Evaluation of the Seismic Behavior Factor of Low-Dissipative Timber Structures - A Ceccotti and A Vignoli
- 23-15-6 Disproportionate Collapse of Timber Structures - C J Mettem and J P Marcroft
- 23-15-7 Performance of Timber Frame Structures During the Loma Prieta California Earthquake - M R O'Halloran and E G Elias
- 24-15-2 Discussion About the Description of Timber Beam-Column Formula - S Y Huang
- 24-15-3 Seismic Behavior of Wood-Framed Shear Walls - M Yasumura
- 25-15-1 Structural Assessment of Timber Framed Building Systems - U Korin
- 25-15-3 Mechanical Properties of Wood-framed Shear Walls Subjected to Reversed Cyclic Lateral Loading - M Yasumura
- 26-15-1 Bracing Requirements to Prevent Lateral Buckling in Trussed Rafters - C J Mettem and P J Moss
- 26-15-2 Eurocode 8 - Part 1.3 - Chapter 5 - Specific Rules for Timber Buildings in Seismic Regions - K Becker, A Ceccotti, H Charlier, E Katsaragakis, H J Larsen and H Zeitter
- 26-15-3 Hurricane Andrew - Structural Performance of Buildings in South Florida - M R O'Halloran, E L Keith, J D Rose and T P Cunningham
- 29-15-1 Lateral Resistance of Wood Based Shear Walls with Oversized Sheathing Panels - F Lam, H G L Prion and M He
- 29-15-2 Damage of Wooden Buildings Caused by the 1995 Hyogo-Ken Nanbu Earthquake - M Yasumura, N Kawai, N Yamaguchi and S Nakajima
- 29-15-3 The Racking Resistance of Timber Frame Walls: Design by Test and Calculation - D R Griffiths, C J Mettem, V Enjily, P J Steer
- 29-15-4 Current Developments in Medium-Rise Timber Frame Buildings in the UK - C J Mettem, G C Pitts, P J Steer, V Enjily
- 29-15-5 Natural Frequency Prediction for Timber Floors - R J Bainbridge, and C J Mettem
- 30-15-1 Cyclic Performance of Perforated Wood Shear Walls with Oversize Oriented Strand Board Panels - Ming He, H Magnusson, F Lam, and H G L Prion
- 30-15-2 A Numerical Analysis of Shear Walls Structural Performances - L Davenne, L Daudeville, N Kawai and M Yasumura

- 30-15-3 Seismic Force Modification Factors for the Design of Multi-Storey Wood-Frame Platform Construction - E Karacabeyli and A Ceccotti
- 30-15-4 Evaluation of Wood Framed Shear Walls Subjected to Lateral Load - M Yasumura and N Kawai

FIRE

- 12-16-1 British Standard BS 5268 the Structural Use of Timber: Part 4 Fire Resistance of Timber Structures
- 13-100-2 CIB Structural Timber Design Code. Chapter 9. Performance in Fire
- 19-16-1 Simulation of Fire in Tests of Axially Loaded Wood Wall Studs - J König
- 24-16-1 Modelling the Effective Cross Section of Timber Frame Members Exposed to Fire - J König
- 25-16-1 The Effect of Density on Charring and Loss of Bending Strength in Fire - J König
- 25-16-2 Tests on Glued-Laminated Beams in Bending Exposed to Natural Fires - F Bolonius Olesen and J König
- 26-16-1 Structural Fire Design According to Eurocode 5, Part 1.2 - J König

STATISTICS AND DATA ANALYSIS

- 13-17-1 On Testing Whether a Prescribed Exclusion Limit is Attained - W G Warren
- 16-17-1 Notes on Sampling and Strength Prediction of Stress Graded Structural Timber - P Glos
- 16-17-2 Sampling to Predict by Testing the Capacity of Joints, Components and Structures - B Nörén
- 16-17-3 Discussion of Sampling and Analysis Procedures - P W Post
- 17-17-1 Sampling of Wood for Joint Tests on the Basis of Density - I Smith, L R J Whale
- 17-17-2 Sampling Strategy for Physical and Mechanical Properties of Irish Grown Sitka Spruce - V Picardo
- 18-17-1 Sampling of Timber in Structural Sizes - P Glos
- 18-6-3 Notes on Sampling Factors for Characteristic Values - R H Leicester
- 19-17-1 Load Factors for Proof and Prototype Testing - R H Leicester
- 19-6-2 Confidence in Estimates of Characteristic Values - R H Leicester
- 21-6-1 Draft Australian Standard: Methods for Evaluation of Strength and Stiffness of Graded Timber - R H Leicester
- 21-6-2 The Determination of Characteristic Strength Values for Stress Grades of Structural Timber. Part 1 - A R Fewell and P Glos
- 22-17-1 Comment on the Strength Classes in Eurocode 5 by an Analysis of a Stochastic Model of Grading - A proposal for a supplement of the design concept - M Kiesel
- 24-17-1 Use of Small Samples for In-Service Strength Measurement - R H Leicester and F G Young
- 24-17-2 Equivalence of Characteristic Values - R H Leicester and F G Young
- 24-17-3 Effect of Sampling Size on Accuracy of Characteristic Values of Machine Grades - Y H Chui, R Turner and I Smith
- 24-17-4 Harmonisation of LSD Codes - R H Leicester

- 25-17-2 A Body for Confirming the Declaration of Characteristic Values - J Sunley
- 25-17-3 Moisture Content Adjustment Procedures for Engineering Standards - D W Green and J W Evans
- 27-17-1 Statistical Control of Timber Strength - R H Leicester and H O Breitingner
- 30-17-1 A New Statistical Method for the Establishment of Machine Settings - F Rouger

GLUED JOINTS

- 20-18-1 Wood Materials under Combined Mechanical and Hygral Loading - A Martensson and S Thelandersson
- 20-18-2 Analysis of Generalized Volkersen - Joints in Terms of Linear Fracture Mechanics - P J Gustafsson
- 20-18-3 The Complete Stress-Slip Curve of Wood-Adhesives in Pure Shear - H Wernersson and P J Gustafsson
- 22-18-1 Perspective Adhesives and Protective Coatings for Wood Structures - A S Freidin

FRACTURE MECHANICS

- 21-10-1 A Study of Strength of Notched Beams - P J Gustafsson
- 22-10-1 Design of Endnotched Beams - H J Larsen and P J Gustafsson
- 23-10-1 Tension Perpendicular to the Grain at Notches and Joints - T A C M van der Put
- 23-10-2 Dimensioning of Beams with Cracks, Notches and Holes. An Application of Fracture Mechanics - K Riipola
- 23-19-1 Determination of the Fracture Energie of Wood for Tension Perpendicular to the Grain - W Rug, M Badstube and W Schöne
- 23-19-2 The Fracture Energy of Wood in Tension Perpendicular to the Grain. Results from a Joint Testing Project - H J Larsen and P J Gustafsson
- 23-19-3 Application of Fracture Mechanics to Timber Structures - A Ranta-Maunus
- 24-19-1 The Fracture Energy of Wood in Tension Perpendicular to the Grain - H J Larsen and P J Gustafsson
- 28-19-1 Fracture of Wood in Tension Perpendicular to the Grain: Experiment and Numerical Simulation by Damage Mechanics - L Daudeville, M Yasumura and J D Lanvin
- 28-19-2 A New Method of Determining Fracture Energy in Forward Shear along the Grain - H D Mansfield-Williams
- 28-19-3 Fracture Design Analysis of Wooden Beams with Holes and Notches. Finite Element Analysis based on Energy Release Rate Approach - H Petersson
- 28-19-4 Design of Timber Beams with Holes by Means of Fracture Mechanics - S Aicher, J Schmidt and S Brunold
- 30-19-1 Failure Analysis of Single-Bolt Joints - L Daudeville, L Davenne and M Yasumura

SERVICEABILITY

- 27-20-1 Codification of Serviceability Criteria - R H Leicester

- 27-20-2 On the Experimental Determination of Factor k_{def} and Slip Modulus k_{ser} from Short- and Long-Term Tests on a Timber-Concrete Composite (TCC) Beam - S Capretti and A Ceccotti
- 27-20-3 Serviceability Limit States: A Proposal for Updating Eurocode 5 with Respect to Eurocode 1 - P Racher and F Rouger
- 27-20-4 Creep Behavior of Timber under External Conditions - C Le Govic, F Rouger, T Toratti and P Morlier
- 30-20-1 Design Principles for Timber in Compression Perpendicular to Grain - S Thelandersson and A Mårtensson
- 30-20-2 Serviceability Performance of Timber Floors - Eurocode 5 and Full Scale Testing - R J Bainbridge and C J Mettem

CIB TIMBER CODE

- 2-100-1 A Framework for the Production of an International Code of Practice for the Structural Use of Timber - W T Curry
- 5-100-1 Design of Solid Timber Columns (First Draft) - H J Larsen
- 5-100-2 A Draft Outline of a Code for Timber Structures - L G Booth
- 6-100-1 Comments on Document 5-100-1; Design of Solid Timber Columns - H J Larsen and E Theilgaard
- 6-100-2 CIB Timber Code: CIB Timber Standards - H J Larsen and E Theilgaard
- 7-100-1 CIB Timber Code Chapter 5.3 Mechanical Fasteners; CIB Timber Standard 06 and 07 - H J Larsen
- 8-100-1 CIB Timber Code - List of Contents (Second Draft) - H J Larsen
- 9-100-1 The CIB Timber Code (Second Draft)
- 11-100-1 CIB Structural Timber Design Code (Third Draft)
- 11-100-2 Comments Received on the CIB Code
- a U Saarelainen
 - b Y M Ivanov
 - c R H Leicester
 - d W Nozynski
 - e W R A Meyer
 - f P Beckmann; R Marsh
 - g W R A Meyer
 - h W R A Meyer
- 11-100-3 CIB Structural Timber Design Code; Chapter 3 - H J Larsen
- 12-100-1 Comment on the CIB Code - Sous-Commission Glulam
- 12-100-2 Comment on the CIB Code - R H Leicester
- 12-100-3 CIB Structural Timber Design Code (Fourth Draft)
- 13-100-1 Agreed Changes to CIB Structural Timber Design Code
- 13-100-2 CIB Structural Timber Design Code. Chapter 9: Performance in Fire
- 13-100-3a Comments on CIB Structural Timber Design Code
- 13-100-3b Comments on CIB Structural Timber Design Code - W R A Meyer
- 13-100-3c Comments on CIB Structural Timber Design Code - British Standards Institution
- 13-100-4 CIB Structural Timber Design Code. Proposal for Section 6.1.5 Nail Plates - N I Bovim

- 14-103-2 Comments on the CIB Structural Timber Design Code - R H Leicester
- 15-103-1 Resolutions of TC 165-meeting in Athens 1981-10-12/13
- 21-100-1 CIB Structural Timber Design Code. Proposed Changes of Sections on Lateral Instability, Columns and Nails - H J Larsen
- 22-100-1 Proposal for Including an Updated Design Method for Bearing Stresses in CIB W18 - Structural Timber Design Code - B Madsen
- 22-100-2 Proposal for Including Size Effects in CIB W18A Timber Design Code - B Madsen
- 22-100-3 CIB Structural Timber Design Code - Proposed Changes of Section on Thin-Flanged Beams - J König
- 22-100-4 Modification Factor for "Aggressive Media" - a Proposal for a Supplement to the CIB Model Code - K Erler and W Rug
- 22-100-5 Timber Design Code in Czechoslovakia and Comparison with CIB Model Code - P Dutko and B Kozelouh

LOADING CODES

- 4-101-1 Loading Regulations - Nordic Committee for Building Regulations
- 4-101-2 Comments on the Loading Regulations - Nordic Committee for Building Regulations

STRUCTURAL DESIGN CODES

- 1-102-1 Survey of Status of Building Codes, Specifications etc., in USA - E G Stern
- 1-102-2 Australian Codes for Use of Timber in Structures - R H Leicester
- 1-102-3 Contemporary Concepts for Structural Timber Codes - R H Leicester
- 1-102-4 Revision of CP 112 - First Draft, July 1972 - British Standards Institution
- 4-102-1 Comparison of Codes and Safety Requirements for Timber Structures in EEC Countries - Timber Research and Development Association
- 4-102-2 Nordic Proposals for Safety Code for Structures and Loading Code for Design of Structures - O A Brynildsen
- 4-102-3 Proposal for Safety Codes for Load-Carrying Structures - Nordic Committee for Building Regulations
- 4-102-4 Comments to Proposal for Safety Codes for Load-Carrying Structures - Nordic Committee for Building Regulations
- 4-102-5 Extract from Norwegian Standard NS 3470 "Timber Structures"
- 4-102-6 Draft for Revision of CP 112 "The Structural Use of Timber" - W T Curry
- 8-102-1 Polish Standard PN-73/B-03150: Timber Structures; Statistical Calculations and Designing
- 8-102-2 The Russian Timber Code: Summary of Contents
- 9-102-1 Svensk Byggnorm 1975 (2nd Edition); Chapter 27: Timber Construction
- 11-102-1 Eurocodes - H J Larsen
- 13-102-1 Program of Standardisation Work Involving Timber Structures and Wood-Based Products in Poland
- 17-102-1 Safety Principles - H J Larsen and H Riberholt

- 17-102-2 Partial Coefficients Limit States Design Codes for Structural Timberwork - I Smith
- 18-102-1 Antiseismic Rules for Timber Structures: an Italian Proposal - G Augusti and A Ceccotti
- 18-1-2 Eurocode 5, Timber Structures - H J Larsen
- 19-102-1 Eurocode 5 - Requirements to Timber - Drafting Panel Eurocode 5
- 19-102-2 Eurocode 5 and CIB Structural Timber Design Code - H J Larsen
- 19-102-3 Comments on the Format of Eurocode 5 - A R Fewell
- 19-102-4 New Developments of Limit States Design for the New GDR Timber Design Code - W Rug and M Badstube
- 19-7-3 Effectiveness of Multiple Fastener Joints According to National Codes and Eurocode 5 (Draft) - G Steck
- 19-7-6 The Derivation of Design Clauses for Nailed and Bolted Joints in Eurocode5 - L R J Whale and I Smith
- 19-14-1 Annex on Simplified Design of W-Trusses - H J Larsen
- 20-102-1 Development of a GDR Limit States Design Code for Timber Structures - W Rug and M Badstube
- 21-102-1 Research Activities Towards a New GDR Timber Design Code Based on Limit States Design - W Rug and M Badstube
- 22-102-1 New GDR Timber Design Code, State and Development - W Rug, M Badstube and W Kofent
- 22-102-2 Timber Strength Parameters for the New USSR Design Code and its Comparison with International Code - Y Y Slavik, N D Denesh and E B Ryumina
- 22-102-3 Norwegian Timber Design Code - Extract from a New Version - E Aasheim and K H Solli
- 23-7-1 Proposal for a Design Code for Nail Plates - E Aasheim and K H Solli
- 24-102-2 Timber Footbridges: A Comparison Between Static and Dynamic Design Criteria - A Ceccotti and N de Robertis
- 25-102-1 Latest Development of Eurocode 5 - H J Larsen
- 25-102-1A Annex to Paper CIB-W18/25-102-1. Eurocode 5 - Design of Notched Beams - H J Larsen, H Riberholt and P J Gustafsson
- 25-102-2 Control of Deflections in Timber Structures with Reference to Eurocode 5 - A Martensson and S Thelandersson
- 28-102-1 Eurocode 5 - Design of Timber Structures - Part 2: Bridges - D Bajolet, E Gehri, J König, H Kreuzinger, H J Larsen, R Mäkipuro and C Mettem
- 28-102-2 Racking Strength of Wall Diaphragms - Discussion of the Eurocode 5 Approach - B Källsner
- 29-102-1 Model Code for the Probabilistic Design of Timber Structures - H J Larsen, T Isaksson and S Thelandersson
- 30-102-1 Concepts for Drafting International Codes and Standards for Timber Constructions - R H Leicester

INTERNATIONAL STANDARDS ORGANISATION

- 3-103-1 Method for the Preparation of Standards Concerning the Safety of Structures (ISO/DIS 3250) - International Standards Organisation ISO/TC98

- 4-103-1 A Proposal for Undertaking the Preparation of an International Standard on Timber Structures - International Standards Organisation
- 5-103-1 Comments on the Report of the Consultation with Member Bodies Concerning ISO/TC/P129 - Timber Structures - Dansk Ingeniorforening
- 7-103-1 ISO Technical Committees and Membership of ISO/TC 165
- 8-103-1 Draft Resolutions of ISO/TC 165
- 12-103-1 ISO/TC 165 Ottawa, September 1979
- 13-103-1 Report from ISO/TC 165 - A Sorensen
- 14-103-1 Comments on ISO/TC 165 N52 "Timber Structures; Solid Timber in Structural Sizes; Determination of Some Physical and Mechanical Properties"
- 14-103-2 Comments on the CIB Structural Timber Design Code - R H Leicester
- 21-103-1 Concept of a Complete Set of Standards - R H Leicester

JOINT COMMITTEE ON STRUCTURAL SAFETY

- 3-104-1 International System on Unified Standard Codes of Practice for Structures - Comité Européen du Béton (CEB)
- 7-104-1 Volume 1: Common Unified Rules for Different Types of Construction and Material - CEB

CIB PROGRAMME, POLICY AND MEETINGS

- 1-105-1 A Note on International Organisations Active in the Field of Utilisation of Timber - P Sonnemans
- 5-105-1 The Work and Objectives of CIB-W18-Timber Structures - J G Sunley
- 10-105-1 The Work of CIB-W18 Timber Structures - J G Sunley
- 15-105-1 Terms of Reference for Timber - Framed Housing Sub-Group of CIB-W18
- 19-105-1 Tropical and Hardwood Timbers Structures - R H Leicester
- 21-105-1 First Conference of CIB-W18B, Tropical and Hardwood Timber Structures Singapore, 26 - 28 October 1987 - R H Leicester

INTERNATIONAL UNION OF FORESTRY RESEARCH ORGANISATIONS

- 7-106-1 Time and Moisture Effects - CIB W18/IUFRO 55.02-03 Working Party

**INTERNATIONAL COUNCIL FOR BUILDING RESEARCH STUDIES AND DOCUMENTATION
WORKING COMMISSION W18 - TIMBER STRUCTURES**

BEAM-COLUMN FORMULA FOR SPECIFIC TRUSS APPLICATIONS

by

W Lau

F Lam

J D Barrett

Department of Wood Science

University of British Columbia

Canada

MEETING THIRTY

VANCOUVER

CANADA

AUGUST 1997

Beam-Column Formula For Specific Truss Applications

Wilson Lau
Frank Lam
J.D. Barrett

Department of Wood Science
University of British Columbia
Canada

1 Introduction

In Canada, there are basically two typical residential roof structures — the traditional rafters and joists (usually cut and fabricated on site) and the metal plated wooden roof trusses (usually prefabricated). Whereas the former dominant the residential market before 1960s and are still used for roofs with unusual configurations, the latter has been playing a major role in the residential market since its introduction.

From structural theories, it is expected that lighter section can be used to fabricated roof trusses due to the load sharing effect. However, when prefabricated roof trusses were first studied in the 1960s, trusses designed according to the timber design codes resulted in member sizes larger than those obtained from the traditional rafters and joists method. A series of prefabricated roof trusses were then tested which showed satisfactory performance even though they did not meet the standard wood design procedures as set forth in CSA Standard O86.1 “Engineering Design in Wood”. Consequently, the roof framing requirements in the code were rewritten stating that residential roof trusses no longer required to satisfy the wood engineering design code as long as they passed the test as described in CSA Standard S307 “Load Test Procedure for Wood Roof Trusses for Houses and Small Buildings.” Since most roof trusses are different, it is impossible to test all possible truss configurations. As a result, the Truss Plate Institute of Canada (TPIC) developed a set of design procedures based on which trusses can be designed with confidence to pass the S307 procedures. According to the TPIC design procedures, an increase of 33 % of allowable stresses as specified in the working stress design version of CAN3-O86.1-M84 is allowed. This increase was explained as the load duration factor for structures supporting loads of 24 hours, which is the test duration of the S307 procedures. These ad hoc procedures were developed based on many years of experience and proven satisfactory in service performance.

In 1995, the Working Stress Design version of CAN3-O86-M84 was no longer referenced in the National Building Code of Canada (NBCC). The 1994 edition of the Limit States Design criteria in O86.1-94 did not provide for a 33 percent increase in design properties for the one day load duration. Along with changes in characteristic strengths, the removal of the 33 percent increase for one day load duration resulted in the combined stress indices of the top chords, designed using the TPIC procedures at the time, exceeding unity for trusses previously accepted in Part 9 of NBCC. Therefore, if the new Limit States Design criteria were used in designing residential trusses, member sizes would need to be increased significantly. These

issues brought forth a research program engaged by the truss industry, Canadian Wood Council, Forintek Canada Corporation and University of British Columbia to develop new design procedures which are consistent with the modern limit states design philosophy and reflect the proven in-service performance of residential trusses. However, testing of two types of Part 9 trusses by Forintek Canada Corp. showed that the top chords of these two truss designs are adequate with sufficient reliability (Lum *et al.* 1996).

Currently, the TPIC procedures and the O86.1-94 assume a linear relationship between the axial load and bending load. It has the form of

$$\frac{M_f}{M_r} + \frac{P_f}{P_r} \leq 1.0 \quad (1)$$

where P_f is the factored axial force, M_f is the factored bending moment, M_r is the factored bending moment resistance, and P_r is the factored compressive load resistance parallel to grain. Many studies have shown that this linear interaction equation is conservative when considering dimensioned lumber under combined loading (Buchanan 1984, Leicester 1989, Hart 1995).

The factored bending moment resistance, M_r , was derived based on the Canadian Wood Council Lumber Properties in-grade testing program conducted during the 1980's from which characteristic values were obtained from third-point bending test results. Modification factors such as size and treatment factors were then applied to these characteristic values to develop this factored bending moment resistance. It has been shown by many researchers that loading conditions have a significant effect on member strengths and the derived characteristic values are test method dependent (Buchanan 1984, Madsen 1990, Madsen and Buchanan 1986). Usually beams with higher stressed volume are expected to fail in lower loads compared to beams with less stressed volume. This dependence of member strength on the loading conditions is called stress distribution effect (or known as the load configuration effect). Madsen (1990) made a comparison of derived strengths based on different testing methods and reported a difference as much as 40%. Since the stress distribution factor was not included in the interaction equation of the current O86.1, there is a need to account for this factor to represent more realistic material behaviour under combined loading.

The objective of this paper is to provide the background and derivation to the new design procedures for wood trusses top chord members under axial compression and lateral loads which have been adopted by the O86 technical committee and will be included in the supplement No.1 to O86.1-94 (1997) timber design standard.

2.0 New Design Philosophy

The new interaction equation for specific truss applications, as given in Supplement No.1-97 to O86.1-94, is based on a new design philosophy that the equation is non-linear and a new bending capacity modification factor is included to account for the stress distribution effect.

2.1 Non-linear interaction equation

In the U.S., a non-linear quadratic interaction equation has already been adopted in the National Design Specification (NDS) for Wood Construction (1991) which has the format of

$$\left(\frac{f_c}{F'_c}\right)^2 + \frac{f_{b1}}{F'_{b1}\left(1 - \frac{f_c}{F_{cE1}}\right)} \leq 1 \quad (2)$$

where:

- F'_{b1} = allowable bending stress modified by lateral stability factor C_L
- F'_c = allowable compressive stress modified by stability factor C_p
- f_c = compression stress from axial force
- f_{b1} = stress due to bending about axis 1

and

$$f_c < F_{cE1} = \frac{K_{CE}E'}{\left(\frac{l_e}{d}\right)^2} \quad (3)$$

where:

- l_e = effective column length
- d = column depth
- E' = adjusted allowable value of modulus of elasticity
- K_{CE} = Euler buckling coefficient for columns

Equation (2) has also incorporated the moment amplification concept in which the moment caused by the axial load is magnified by the lateral displacement. As both the axial and bending terms should be positive and less than unity, squaring of the axial term will yield a smaller combined stress index which implies higher factored loads can be sustained by the same member in comparison with a linear interaction equation. However, the NDS equation does not address problems such as unequal end moments, moments with varying shapes, and maximum moment not occurring at the mid-span.

2.2 Stress distribution effect (Bending capacity modification factor)

Stress distribution effects are a manifestation of the natural variation of lumber properties that occurs along the length of the member. This within member variation in strength properties also leads to size effects. For instance, structural lumber members tested at different lengths have different strengths.

Recognising that bending members, especially the low quality material, fail in tension which is very similar to specimens under pure tensile loads, the ultimate bending strengths can be predicted by their ultimate tensile strengths using a weakest link failure concept. It is especially true for low quality lumber in bending because material strength under compressive stresses well exceeds material strength under tensile stresses. However, in high quality material under bending, the tension strength in general exceeds the compression strength resulting in significant yielding in the compression zone prior to final failure in the tensile mode.

Experimental studies on quantifying these size factors for different orientations were conducted by many researchers (Madsen and Nielsen 1976, Madsen and Nielsen 1978a, Johnson *et al.* 1989, Barrett and Fewell 1990, Madsen and Tomoi 1991). Using the 5th percentile values, weakest link theory based length effect factor of 0.17 and width effect factor of 0.23 were obtained for both tension and bending (Barrett *et al.*, 1992). These factors are consistent across a number of species and grades.

Although procedures for deriving stress distribution factors for bending, tension or compression members were proposed (Barrett *et al.* 1992, Leicester 1992a,b, Madsen 1990). Truss design procedures based on O86.1-94 ignored stress distribution effects in the calculation of design properties and the prediction of member capacity under combined loading. In the supplement to O86.1-94, a bending capacity modification factor (K_M) was introduced in the interaction equation to modify the factored bending moment resistance due to stress distribution effect. With the incorporation of this stress distribution factor (or bending capacity modification factor as referenced in the supplement), members for specific truss applications subject to combined bending and compression axial are required to satisfy the following interaction equation as specified in Clause 5.5.13.4 of Supplement No.1-97 to O86.1-94:

$$\left(\frac{P_f}{P_r}\right)^2 + \frac{M_f}{K_M M_r} \leq 1.0 \quad (4)$$

where P_f , P_r , M_f and M_r were previously defined and K_M is the bending capacity modification factor as defined in Table 5.5.13.5 in the supplement and Equation (8) in this paper.

Based on the Weibull weakest link failure criteria that members will fail in higher load if less volume is under stress, size factors have been applied to predict the ultimate loads of columns and beam-columns (Buchanan 1984). In order to predict the ultimate loads, several failure criteria including tensile failures, initiation of yielding, and buckling failures have to be checked. As yielding does not always lead to immediate failure a criterion for compression failure has to be specified. Koka (1987) assumed failure in compression when the column is unable to develop the compression stresses required to achieve equilibrium.

3.0 Derivation of Bending Capacity Adjustment Factors

The rationale and background for the derivation of the bending capacity modification factors K_M are presented in this section. In developing K_M , the following assumptions were made :

- (a) The axial compression load component of the combined bending and compression is ignored which yields more conservative bending capacity factors;
- (b) The stress distribution across a section is assumed to be linear in both tension and compression regions until failure;

- (c) Failure of the member is defined as the extreme fibre stress at the tension side reaches a ultimate value predicted by considering the stress distribution effect; and
- (d) Stress distribution effect is based on the weakest-link brittle failure model.

The factored bending moment resistance M , mentioned in the design proposal and referenced in the Code on Engineering Design of Wood is based on test results from the Canadian Wood Council Lumber Properties In-Grade Testing Program. The testing program followed ASTM standard D4761 (1990) where dimension lumber specimens were tested in third point bending under a span to depth ratio of 17:1. In application to top chord members of roof trusses under uniformly distributed loads, the dimension lumbars are of different lengths and subjected to bending moments with a form shown in Figure 1. Based on the weakest link failure concept, the ultimate capacity of a member depends on the stressed volume and thus the loading conditions. The derivation of the bending capacity adjustment factors is based on the comparisons of the theoretical cumulative probability distributions of bending strengths of the material tested in the Ingrade test program and the material subjected to bending moments of the form as shown in Figure 1.

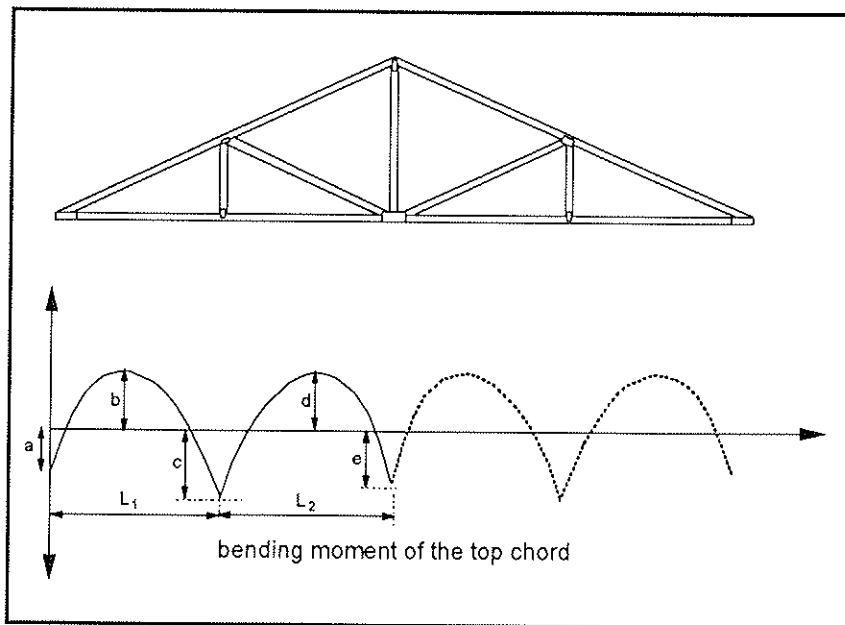


Figure 1 Typical Howe Truss and its Moment Distribution along top chord

Assuming that the strength of a member is governed by brittle tension failure mode, for an arbitrary member of volume V and subjected to a stress distribution $\sigma(x,y,z) = \sigma_{ref} f(x,y,z)$, the Weibull based cumulative probability of strength for the members can be represented by:

$$F = 1 - e^{-\int_{V_t} \left(\frac{\sigma(x,y,z)}{m} \right)^k dV} = 1 - e^{-\sigma_{ref}^k \int_{V_t} \left(\frac{f(x,y,z)}{m} \right)^k dV} \quad (5)$$

where V_t is the volume of material in the member under tensile stress, $f(x,y,z)$ is a dimensionless normalized stress function in the member with respect to a reference stress σ_{ref} , and m and k are the 2-parameter Weibull scale and shape parameters, respectively.

Consider now the bending strength of members under third point loading, the Weibull based cumulative probability distribution of strength for the members is represented by:

$$F = 1 - e^{-V \frac{1+k/3}{2(1+k)^2} \left(\frac{MOR}{m}\right)^k} \quad (6)$$

where V is the volume of the member and MOR is bending strength of the members obtained from the In-grade third point bending tests.

Consider a common level of failure probability in the arbitrary and third point loading cases, the two cumulative probability distributions in equations 5 and 6 can be equated to a bending capacity adjustment factor, K_M , relating the standard In-grade third point bending test results to the same material subjected to any arbitrary stress distribution (with brittle tension failure mode).

$$K_M = \frac{\sigma_{ref}}{MOR} = \left[\frac{V(1+k/3)}{2I(1+k)^2} \right]^{1/k} \quad (7)$$

where

$$I = \int_{V_i} f(x,y,z)^k dV$$

In our work the integral I was evaluated using the Gauss-Legendre numerical integration scheme for a given normalized stress function.

For the top chord of a typical Howe truss with schematic drawing and hypothetical moment distribution as shown in Figure 1, the moment distribution within each panel is assumed to have a parabolic shape. Assuming that the panel point moments at both ends are the same, we can characterize the moment distribution of each panel by the panel length-to-depth ratio, (L/d) , and the ratio of the mid-panel moment (M_1) to panel point moment (M_2) as shown in Figure 2.

By varying these two parameters, a set of K_M factors with different span to depth ratios for the working range of trusses are generated according to Eqn. (7) and are shown in Figure 3. Most of the residential trusses manufactured have a M_1/M_2 ratio in the range of -0.5 and -1.0 (TPIC personal communication).

For a simply-supported uniformly loaded member with no end-moment, M_1/M_2 will approach positive or negative infinity and will have a K_M of $1.67(L/d)^{-1/6}$. Observing the shape of the plot, regression equations were fitted to four regions of M_1/M_2 . This yields a cubic equation for M_1/M_2 between -1 and 1, a linear equation for M_1/M_2 between 1 and 3, and a constant equation for other M_1/M_2 ratios. The regression lines given in equation 8 are shown in Figure 3 as solid lines.

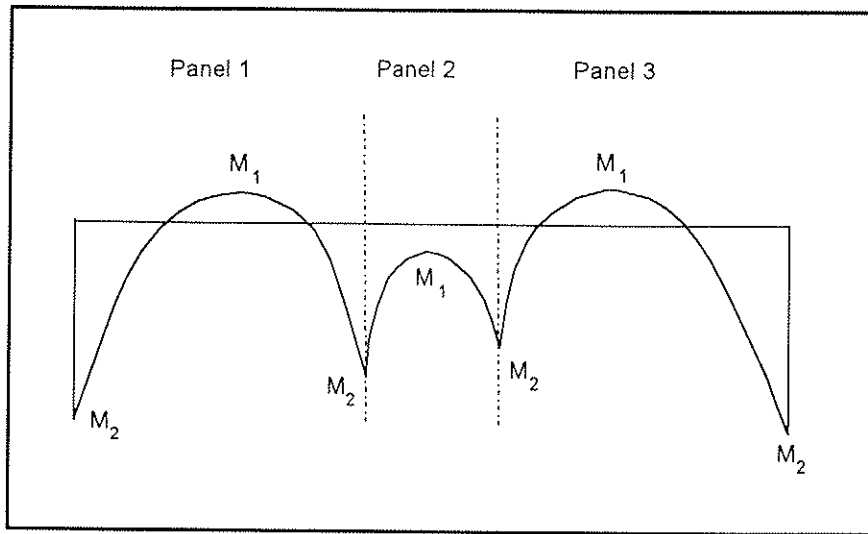


Figure 2 Moment Distribution along a Top Chord Truss Member for Unequal Spans

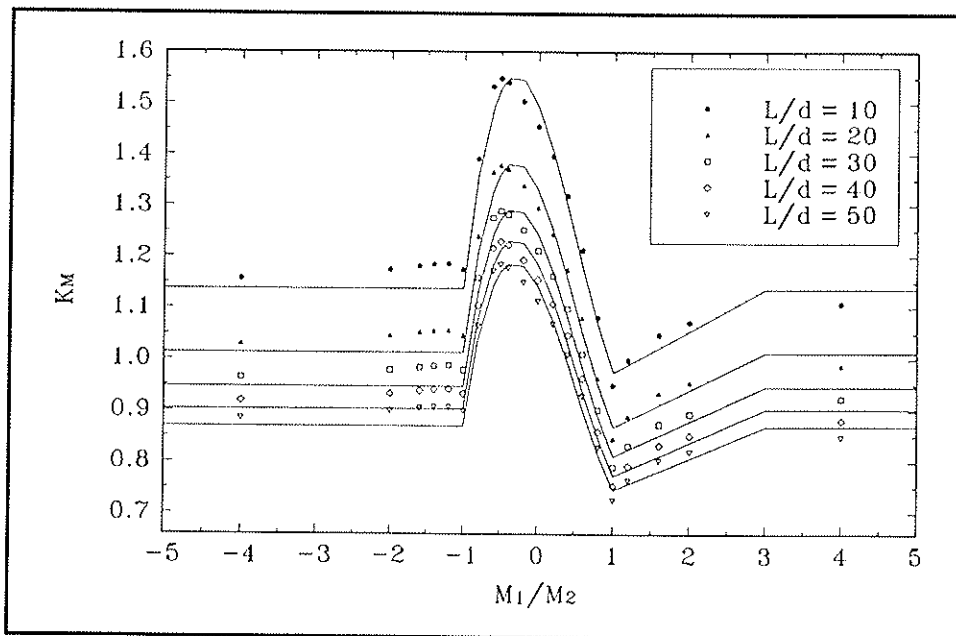


Figure 3 Bending Capacity Modification Factors for Combined Bending and Axial Compression

$$K_M = \left[2.20 - 0.53 \cdot \left(\frac{M_1}{M_2} \right) - 0.64 \cdot \left(\frac{M_1}{M_2} \right)^2 + 0.41 \cdot \left(\frac{M_1}{M_2} \right)^3 \right] \cdot \left(\frac{L}{d} \right)^{-\frac{1}{6}} \leq 1.30 \text{ for } -1.0 \leq \frac{M_1}{M_2} \leq 1.0$$

$$K_M = \left[1.31 + 0.12 \cdot \left(\frac{M_1}{M_2} \right) \right] \cdot \left(\frac{L}{d} \right)^{-\frac{1}{6}} \leq 1.30 \quad \text{for } 1.0 \leq \frac{M_1}{M_2} \leq 3.0 \quad (8)$$

$$K_M = 1.67 \cdot \left(\frac{L}{d} \right)^{-\frac{1}{6}} \leq 1.30 \quad \text{for any other cases}$$

In using these equations, M_1 and M_2 are obtained by appropriate structural analysis methods such as TPIC procedures and plane frame structural analysis program. The signs of both M_1 and M_2 have to be considered in the calculation. For example, in Figure 2, M_1/M_2 gives a negative value in panel 1 while it is positive when both M_1 and M_2 are having the same sign in panel 2. There is a maximum permitted value for K_M of 1.30 for all combination of L/d and M_1/M_2 .

Since the K_M factors are derived assuming that the panel point moments are the same at both ends. In cases where panel point moments within a panel differ, the greater (in absolute magnitude) of the two panel point moments should be used in the calculation of the K_M factor for each panel. Checking should progress along the truss.

Amplified moments (or P-delta effect) should be used for the factored bending moment in the interaction equation if possible. Although P-delta effect is significant for some structures especially at the mid-panel moments with large axial loads, some structures can be analysed accurately without the considerations of the moment amplification. It can be achieved by a proper analogue assumptions and structure configuration limitations.

Results from the truss testing at Forintek Canada Corp. reveal that trusses designed according to the TPIC procedures has satisfactory structural performances even though amplified moments were not considered. The TPIC procedures do not incorporate the P-delta effect; however, limitations were applied to the total span of the chord and the mid-panel deflection to ensure that the P-delta effect is still within the tolerance limit of the factored bending resistance. This deflection criteria may govern in some designs of the top chord span even the strength requirement is met. If the deflection criteria as given in the TPIC procedures is violated, then there is no assurance that bending capacity modification factors, K_M , would be appropriate in the interaction equation.

4.0 Verifications and Conclusions

Extensive testing of columns and beam-columns were performed by Buchanan (1984). Based on his experimental results, interaction equations were developed and were compared with the size and stress distribution effects based theoretical interaction curves. Good agreement between experimental data and stress distribution based strength model was observed (Figure 4). In addition, the linear interaction curve used in the previous engineering code has also been shown to be over conservative in most applications. Recent test results of columns under different eccentric axial compression also confirm the non-linear behaviour of the interaction curve (Figure 5, experiment in progress).

Considering some typical truss configurations manufactured as given by TPIC, a comparison of the combined stress indices computed using different criteria is shown in Table 1. In general, designs based on the proposed procedures have combined stress indices that are similar to the indices computed using the CSA-O86-M84/ TPIC-88 procedures. In almost all cases, the CSA-O86-M84/TPIC-88 procedures produce slightly smaller CSI than the proposed procedures.

The same trusses designed according to CSA-O86.1-M94 give combined stress indices which are up to 60% higher than the CSA-O86.1/TPIC-88 procedures. However, results of typical Part 9 trusses (designed using current TPIC procedures) by Forintek Canada Corp. show that they have adequate short-term capacities. Clearly the CSA-O86-M84/TPIC-88 procedures are too conservative and the new procedures are more reasonable.

The new interaction equation and the associated K_M factors, which based on the stress distribution effect and experimental results, appear to better reflect the behaviour of structural lumber under combined bending and axial compression loading and thus it is appropriate for the design of top chord members of wood trusses.

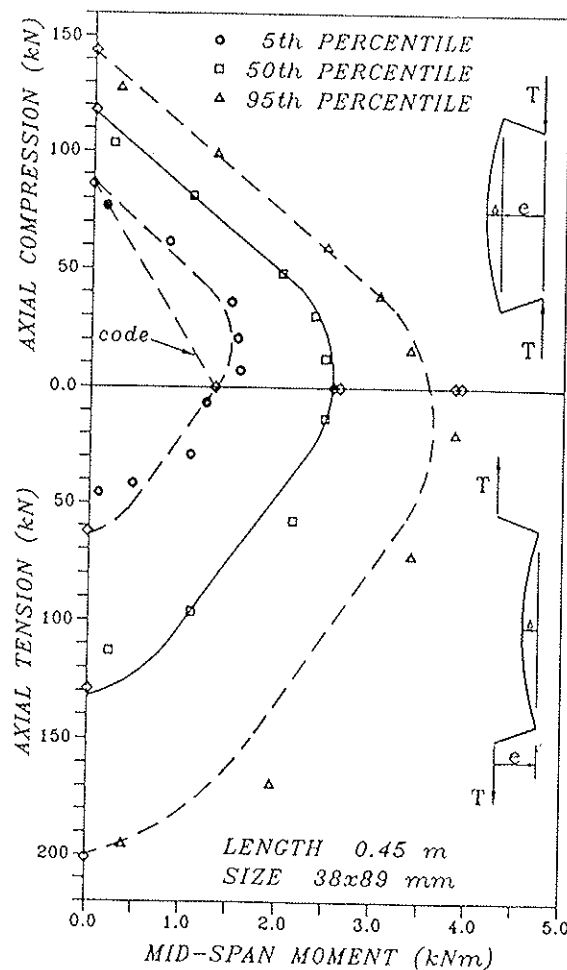


Figure 4 Strength Model and Test Results of Beam-Column (Buchanan 1984)

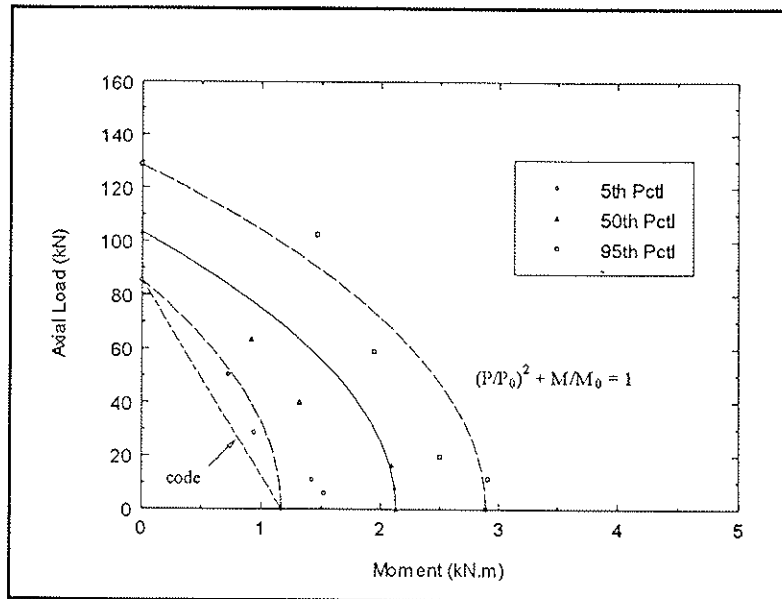


Figure 5 Test Results of Column under Eccentric Axial Compression (In progress)

Truss	CSA-O86.1-M94 + New Iteration Eqn.+TPIC-95	CSA-O86.1-M94	CSA-O86-M84 +TPIC-88
30 ft, 4 bay 2/12 Howe with 2×4 chords	0.92	1.14	0.79
30 ft, 4 bay 4/12 Howe (test truss) with 2×4 chords	1.03	1.45	0.99
30 ft, 4 bay 7/12 Howe (test truss) with 2×4 chords	0.99	1.47	0.99
30 ft, 4 bay fink truss with 2×4 chords	1.07	1.50	0.99
40 ft, 4 bay 4/12 Howe with 2×8 chords	0.86	1.24	0.99
40 ft, 6 bay 4/12 Howe with 2×4 chords	1.18	1.33	0.95
32 ft, 6 bay 4/12 Howe with 2×4 chords and variable panel lengths	1.00	1.24	0.90
30 ft, 5 bay flat truss with 2×4 chords	0.92	1.27	1.04

Table 1 Summary of Combined Stress Indices for different design criteria.

5.0 References

- Barrett, J.D. and Fewell, A.R., 1990. Size factors for the bending and tension strength of structural lumber. Proc. CIB Working Commission W18A - Timber Structures Meeting 23 Lisbon, Portugal.
- Barrett, J.D., Lam, F. and Lau, W., 1992. Size Effects in visually graded softwood structural lumber. CIB-W18/25, Ahus.
- Buchanan A.H. 1984. Strength model and design methods for bending and axial load interaction in timber members. Thesis presented to the University of British Columbia (Dept. Civ. Eng.), in partial fulfilment of the requirements of the degree of Doctor of Philosophy.
- CSA, 1984. Engineering design in wood (working stress design). CSA CAN/CSA-O86.1-M84. Rexdale (Toronto), Ont.: Canadian Standards Association. 206 p.
- CSA, 1994. Engineering design in wood (limit states design). O86.1-94. Rexdale (Toronto), Ont.: Canadian Standards Association. 191 p.
- CSA, 1980. Load test procedure for wood roof trusses for house and small buildings. CSA Standard S307-M1980. Rexdale (Toronto), Ont.: Canadian Standards Association. 18 p.
- Johns, K.C. and Buchanan, A.H., 1982. Strength of Timber Members in Combined Bending and Axial Loading. Proc. IUFRO Wood Engineering Group, S5.02, Boras, Sweden, 343-368.
- Johnson, L.A., Evans, J.W. and Green, D.W., 1989. Volume Effect Adjustments for the in-grade data. In Ingrade Testing of Structural Lumber. Forest Products Research Society, Madison, WI.
- Koka, N.E., 1987. Laterally Loaded Wood Compression Members: Finite Element and Reliability Analysis. M.A.Sc. Thesis, Department of Civil Engineering, Univ. Brit. Col., Vancouver, B.C.
- Madsen, B. and Nielsen, P., 1976. In-grade testing - size investigation on lumber subjected to bending. Struct. Res. Ser. Rept. No. 15., Dept. Civil Eng., Univ. Brit. Col., Vancouver, B.C., Canada.
- Madsen, B. and Nielsen, P., 1978a. In-grade testing: Bending tests in Canada. June 1977-May 1978. Struct. Res. Ser. Rept. No. 25. Dept. Civil Eng., Univ. Brit. Col., Vancouver, B.C., Canada.

- Madsen, B. and Buchanan, A.H., 1986. Size effects in timber explained by modified weakest link theory. *Canadian Journal of Civil Engineering*, Vol. 13, No. 2, pp. 218-232.
- Madsen, B. and Tomoi, M., 1991. Size effects occurring in defect-free spruce-pine-fir bending specimens. *Can. J. Civil Eng.*, 18(4), 637-643.
- National Forest Products Association. 1991. *National Design Specification for Wood Construction*. NFPA, Washington, D.C.
- Truss Plate Institute of Canada. 1988. *Truss design procedures and specifications for light metal plate connected wood trusses*. TPIC-1988. 42 p.
- Zahn, J.J., 1982. *Strength of Lumber under Combined Bending and Compression*. USDA, For. Serv. Res. Paper. FPL 391. For. Prod. Lab., Madsen, WI.
- Zahn, J.J., 1986. Design of Wood Members under Combined Load. *Journal of Struct. Eng.* ASCE 12, 9, Sept. 3109-3126.

6.0 Acknowledgements

The authors wish to express their appreciation to the following people and organizations. Conroy Lum of Forintek Canada Corp. is to be thanked for providing the results of the truss testings. Brian Hintz of Jager Industries Inc., for his assistance of providing the typical load cases for truss applications. In addition, the support of the Canadian wood truss fabricators and the Canadian Wood Council are also gratefully acknowledged.

This research was partially funded by the B.C. Science Council through the G.R.E.A.T scholarship awarded to the first author with Forintek Canada Corp. as the industry sponsor.

**INTERNATIONAL COUNCIL FOR BUILDING RESEARCH STUDIES AND DOCUMENTATION
WORKING COMMISSION W18 - TIMBER STRUCTURES**

**STRENGTH RELATIONSHIPS IN STRUCTURAL TIMBER
SUBJECTED TO BENDING AND TENSION**

by

N Burger
P Glos
Institute for Wood Research
University of Munich
Germany

MEETING THIRTY

VANCOUVER

CANADA

AUGUST 1997

Strength relationships in structural timber subjected to bending and tension

N. Burger and P. Glos

Institute for Wood Research, University of Munich, Germany

1 Introduction

As a rule small, clear specimens have greater tension strength than bending strength. In early standards for the design of timber structures bending and tension were usually assigned the same design values for timber members. However, tests conducted from the mid-60ies onwards using specimens in structural dimensions have shown, that in comparison to bending strength tension strength is more strongly affected by material defects such as knots and related local grain deviations than originally assumed. Tension strength is therefore lower than bending strength in specimens in structural sizes.

Based on these findings the design values for timber members loaded in tension were gradually reduced for almost all structural timber design standards. Tensile strength (f_t) to-day is about 60 % in relation to bending strength (f_m) for all commonly used strength class systems for structural timber (Green and Kretschmann, 1990). The characteristic strength values for European strength classes according to EN 338, too, are based on a factor of $f_t/f_m = 0.6$. The relative values for permissible tension stresses according to DIN 1052 amount to between 0.57 and 0.71, in relation to the grade.

Literature references indicate that the relationship of strength values depends on timber quality and dimensions (Galligan et al. 1979, Steiger 1996). The ratio of tension to bending strength tends to increase with rising timber quality and decreasing dimensions. Regarding the safety (for low timber quality) and the economy (for high timber quality) of timber structures it would be desirable to take these effects into consideration when determining characteristic strength values.

2 Derivation of the relationship by a modified brittle fracture theory

Assuming brittle material behaviour the model developed by Weibull (1939) to simulate brittle fracture was repeatedly used to describe strength in timber. According to this theory, the survival probability of a structural member is derived from eq. (1).

$$1 - S = e^{-\int_V \left(\frac{\sigma - \sigma_u}{\sigma_m} \right)^k dV} \quad (1)$$

- where
- S probability of failure of the structural element
 - V volume of the structural element
 - σ existing stress in volume element dV
 - σ_u location parameter of Weibull distribution for material strength (minimum material strength)
 - σ_m scale parameter of the Weibull distribution for material strength
 - k shape parameter of the Weibull distribution for material strength

For non-constant stress distribution stress σ within the volume element is expressed as a function of location in the structural element with $\sigma = \sigma(x,y,z)$. A non-constant stress distribution when loading in bending is taken into account by so-called fullness parameters λ (see Colling 1986). For load in tension stresses in the element are assumed to be constantly distributed over the length and the cross-section, so that fullness parameters in this case are 1. Survival probabilities are derived as a function of maximum stress σ and strengths f_t and f_m with a probability of failure S may be calculated from eq. (2a) and eq. (2b) using the 2-parameter-Weibull distribution ($\sigma_n = 0$).

$$\text{Bending: } 1-S = e^{-V \cdot \left(\frac{\sigma}{\sigma_m}\right)^k \cdot \lambda_l \cdot \lambda_h} = e^{-V \cdot \left(\frac{\sigma}{\sigma_m}\right)^k \cdot \left(\frac{1+\frac{1}{3} \cdot k}{(k+1)^2}\right)} \quad (2a)$$

$$\Rightarrow f_m = \sigma_m \cdot \left[-\frac{1}{V} \cdot \frac{(k+1)^2}{1+\frac{1}{3} \cdot k} \cdot \ln(1-S) \right]^{1/k}$$

$$\text{Tension: } 1-S = e^{-V \cdot \left(\frac{\sigma}{\sigma_m}\right)^k} \Rightarrow f_t = \sigma_m \cdot \left[-\frac{1}{V} \cdot \ln(1-S) \right]^{1/k} \quad (2b)$$

where λ_l, λ_h fullness parameters taking into account variable stress distributions over length and height respectively

Assuming equal survival probabilities the relationship between tension and bending strength of a structural element, using the brittle fracture theory, is calculated by

$$\frac{f_t}{f_m} = \left(\frac{1+\frac{1}{3}k}{(k+1)^2} \right)^{1/k} \quad (3)$$

According to EN 408 bending and tension tests shall be carried out using a span of $l_{St} \geq 18 \cdot h$ and a test length of $l_0 \geq 9 \cdot b$ respectively. The values of tension strength f_t thus refer to a different specimen volume than for bending strength f_m . Using minimum test lengths ($l_0 = 9 \cdot b$ resp. $l_{St} = 18 \cdot h$), equation (3) becomes

$$\frac{f_t}{f_m} = \left(2 \cdot \frac{1+\frac{1}{3}k}{(k+1)^2} \right)^{1/k} \quad (4)$$

where f_t, f_m tension and bending strength respectively
 k shape parameter of the Weibull distribution for material strength

Eq. (4) can be used provided bending strength is determined by loading points at thirds of specimen length, geometric conditions according to EN 408 are used and the distribution parameters for strength distributions are material constants, i.e. are the same for loading in tension and in bending. In this case the ratio f_t/f_m between tension and bending strength is a constant value.

However, material behaviour of timber in tension and in bending is different. Loaded in tension timber usually shows a brittle behaviour and tends to fail abruptly. In bending tests plastic deformations are increasingly encountered in the compression zone before failure of the tension zone, in particular with rising wood quality. While distribution of bending

strength may be approximated by a Weibull distribution, the distribution parameters are different from those for tensile strength.

Given equal geometric conditions for each sample the survival probability (see eq. 1) can be represented in simplified form by eq. (5).

$$1-S = e^{-\int_V \left(\frac{\sigma-\sigma_u}{\sigma_m}\right)^k dV} = e^{-\left(\frac{\sigma-\sigma_u}{\sigma_v}\right)^k} \Rightarrow f_m \text{ bzw. } f_t = \sigma_u + \sigma_v \cdot [-\ln(1-S)]^{1/k} \quad (5)$$

In eq. (5) the distribution parameters contain the dimensions and the stress distribution. By differentiating between the distribution parameters (using indices t for tension and m for bending) the relationship between strengths, given equal dimensions, can be deduced from eq. (5) as follows:

$$\frac{f_t}{f_m} = \frac{\sigma_{u,t} + \sigma_{v,t} \cdot [-\ln(1-S)]^{1/k_t}}{\sigma_{u,m} + \sigma_{v,m} \cdot [-\ln(1-S)]^{1/k_m}} \quad (6)$$

and, with $1-S = e^{-\left(\frac{f_m - \sigma_{u,m}}{\sigma_{v,m}}\right)^{k_m}}$ and $1-S = e^{-\left(\frac{f_m}{\sigma_{v,m}}\right)^{k_m}}$ for the 3-parameter and 2-parameter-distribution respectively

$$\text{3-parameter-expression: } \frac{f_t}{f_m} = \frac{\sigma_{u,t} + \frac{\sigma_{v,t}}{\sigma_{v,m}^{k_m/k_t}} \cdot (f_m - \sigma_{u,m})^{k_m/k_t}}{f_m} \quad (7a)$$

$$\text{2-parameter-expression: } \frac{f_t}{f_m} = \frac{\sigma_{v,t}}{\sigma_{v,m}^{k_m/k_t}} \cdot \frac{f_m^{k_m/k_t}}{f_m} = \frac{\sigma_{v,t}}{\sigma_{v,m}^{k_m/k_t}} \cdot f_m^{(k_m/k_t - 1)} \quad (7b)$$

Eq. (7a,b) are applicable to strength relationships for tests following the geometric dimensions stipulated in EN 408. Deviating specimen dimensions may be taken into account by the usual size factor according to eq. (8):

$$\frac{f_{t,r}}{f_{t,r}} \text{ resp. } \frac{f_{m,r}}{f_{m,r}} = \left(\frac{V_r}{V}\right)^{m_V} \cong \left(\frac{l_r}{l}\right)^{m_l} \cdot \left(\frac{b_r}{b}\right)^{m_b} \cdot \left(\frac{d_r}{d}\right)^{m_d} \quad (8)$$

where $f_{t,r}, f_{m,r}$ tension and bending strength for specimens in reference dimensions

V_r, l_r, b_r, d_r reference volume and dimensions of specimens

V, l, b, d volume and dimensions of tested specimens

m size effect parameter according to the Weibull theory ($m = 1/k$)

If size effects in tension and in bending are different the size effect for tension and bending has to be considered separately. Using standard geometry according to EN 408 with $l_{m,r} = 2 \cdot l_{t,r}$ and $b_{m,r} = b_{t,r}$ the strength relationship f_t/f_m according to eq. (9) is derived from eq. (7a,b) (for the sake of simplicity the larger cross-sectional width is generally denoted with b). The significance of specimen thickness is negligible (Burger and Glos, 1996) and has therefore not been included in the equation, but may, in analogy, be taken into account where necessary.

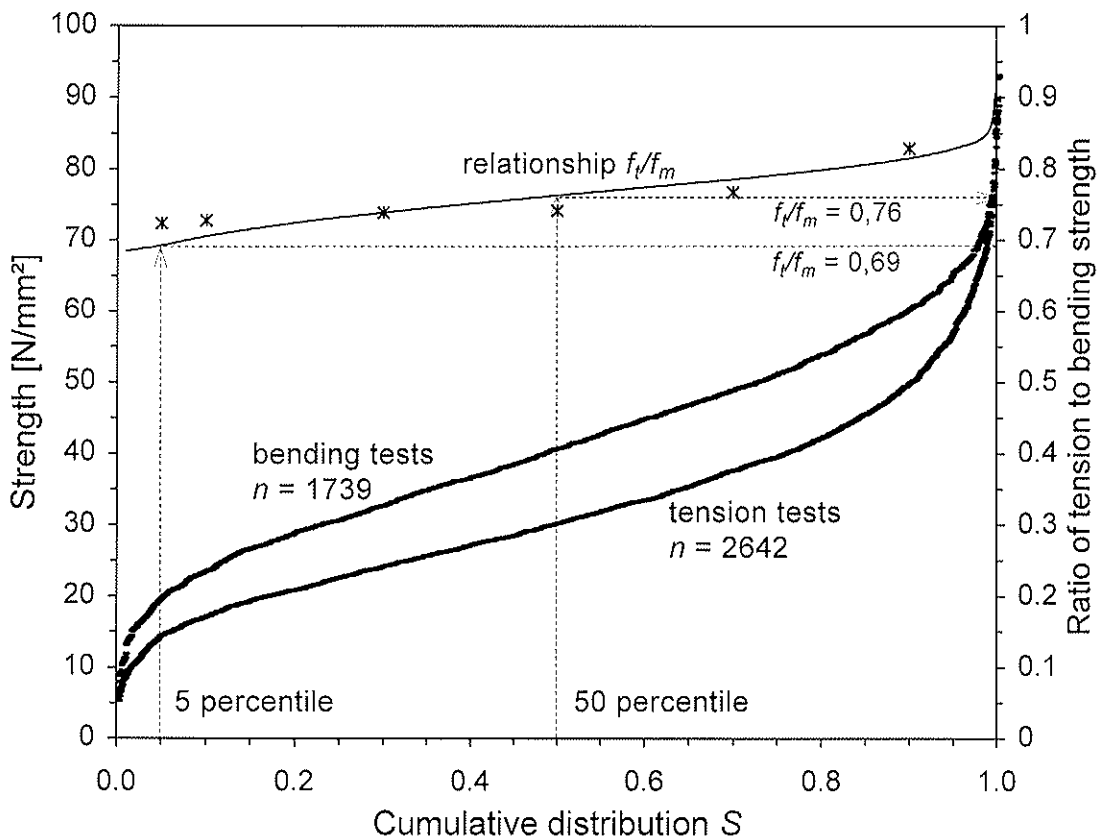
$$\frac{f_t}{f_m} = A \cdot \left(\frac{l_{t,r}}{l_t}\right)^{m_{l,t}} \cdot \left(\frac{l_{m,r}}{l_m}\right)^{-m_{l,m}} \cdot \left(\frac{b_{t,r}}{b_t}\right)^{m_{b,t}} \cdot \left(\frac{b_{m,r}}{b_m}\right)^{-m_{b,m}} = A \cdot \left(\frac{l_{m,r}}{l_m}\right)^{(m_{l,t}-m_{l,m})} \cdot \left(\frac{b_{m,r}}{b_m}\right)^{(m_{b,t}-m_{b,m})} \quad (9)$$

where A expression according to eq. (7a) or eq. (7b)

3 Parameter determination

In recent years a great number of bending and tension tests using specimens in structural sizes were conducted at the Institute for Wood Research, University of Munich, as part of various research programs. The results of these investigations are available as a data base and have been re-evaluated in this study. It involves only those test specimens which correspond to EN 408 specifications as regards test equipment, test conditions and specimen geometry. Data from a total of 2,642 tension tests using specimens with cross-sectional dimensions of 20 to 60 mm thickness and 75 to 260 mm width and of 1,739 bending tests with cross-sectional dimensions of 40 to 80 mm width and 50 to 250 mm height were available.

Fig. 1 shows the strength values of the tests plotted in terms of relative cumulative distribution. As expected the curve for tensile strength is below that for bending strength.



- * ratio f_t/f_m of ranked percentile values
- ratio f_t/f_m derived from the 3-Parameter-Weibulldistributions

Fig. 1: Plots showing relative cumulative distribution for 2,642 tension and 1,739 bending tests respectively from the data base of the Institute for Wood Research, University of Munich and curve for strength ratio f_t/f_m in relation to relative cumulative distribution.

The test specimens were broken down into separate samples according to dimensions, with adjusted 2- and 3-parameter Weibull distributions. Mean values, standard deviations and coefficients of variation of parameter estimates for 27 and 28 samples of bending and tension tests respectively are shown in Table 1. There was no evidence of an effect of specimen size on distribution parameters. For comparison the parameters are also given for all test data.

Fig. 1 plots the calculated ratio f_t/f_m from the 3-parameter Weibull distribution for all test data in relation to cumulative distribution. For comparison the curves are offset against the ratio from the ranked percentiles. The ratio of tension to bending strength rises with increasing cumulative frequency and thus with increasing strength or wood quality. For the 5 percentiles the value for f_t/f_m is 0.69 while that for the 50 percentiles is 0.76.

		Biegung					Zug				
		3-Parameter-Verteilung			2-Par.-Verteilung		3-Parameter-Verteilung			2-Par.-Verteilung	
		σ_u	σ_v	k	σ_v	k	σ_u	σ_v	k	σ_v	k
All data		5.3	40.7	2.82	46.1	3.42	4.6	31.2	2.37	36.0	2.95
Samples	Mean m	8.0	38.6	2.77	47.0	3.64	7.6	28.7	2.13	36.9	3.04
	Std.dev. s	7.2	10.3	0.75	6.4	0.59	5.2	9.1	0.52	7.2	0.49
	COV [%]	90	27	27	14	16	69	32	25	19	16

Tab. 1: Mean values, standard deviations and coefficients of variation of parameter estimates for the samples of the data base.

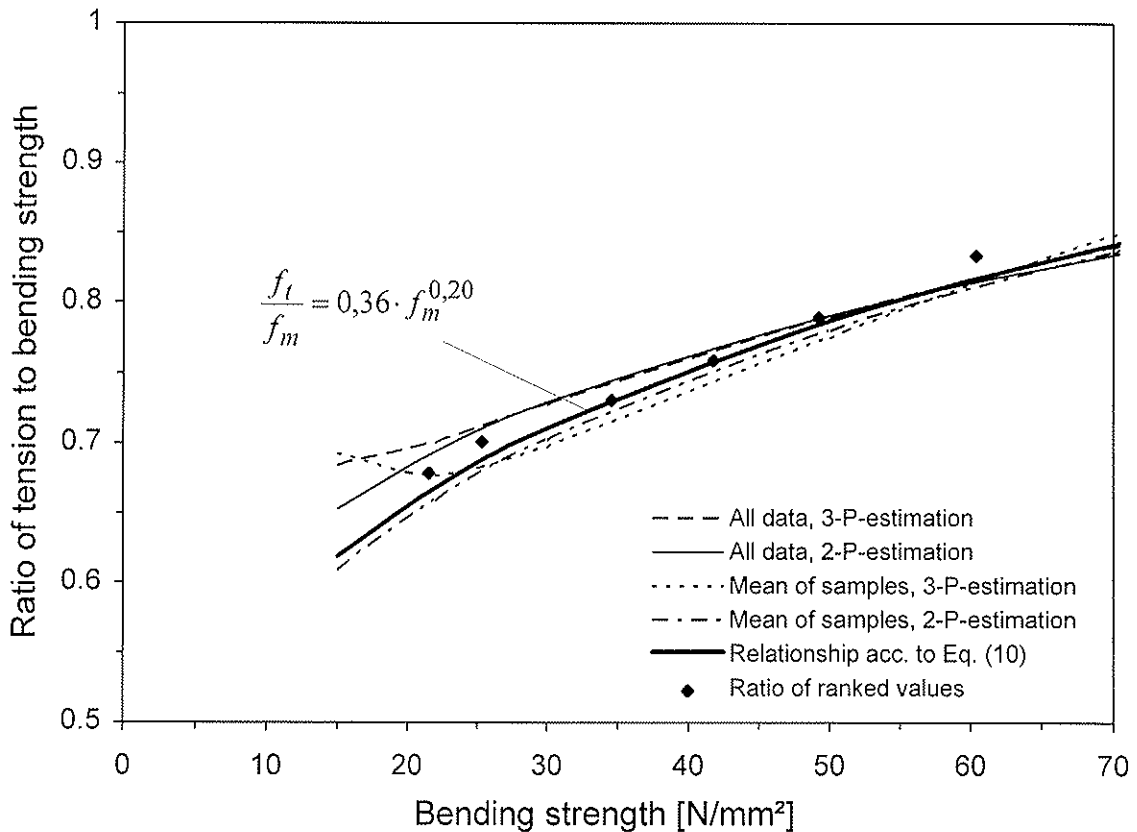


Fig. 2: Comparison of analytical curves for the ratio f_t/f_m .

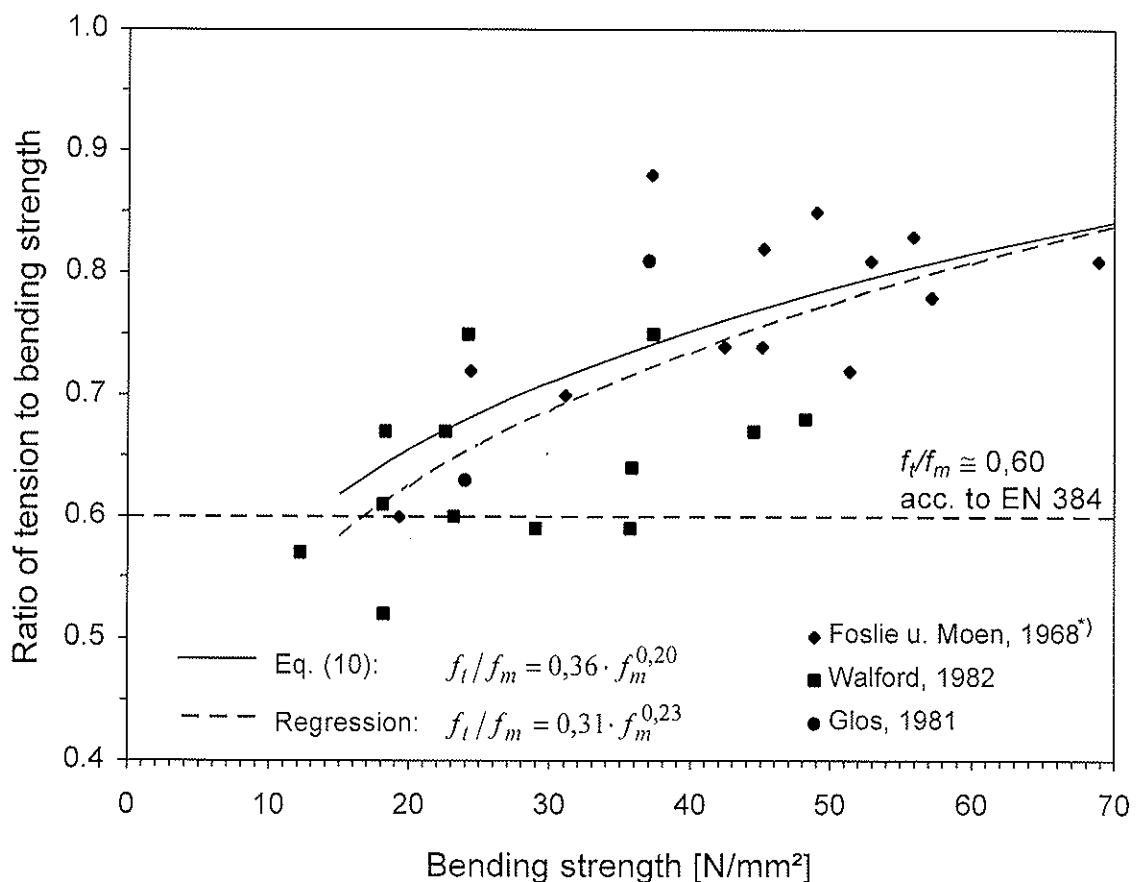
Four curves, shown in Figure 2, are derived from eq. (7a) and (7b) using the parameter estimates for the 2- and 3-parameter Weibull distributions for all test data and for the mean values from the samples respectively. For comparison the mean values of the ratio f_t/f_m from the ranked 5, 10, 30, 50, 70 and 90 percentiles are also shown.

For low wood quality the differences in the curves are attributed to the estimates for the location parameter $\sigma_u = 0$ which represents the minimum strength of the distribution. Since estimates for this parameter showed considerable variations (see Table 1) and the 2-parameter-expression moreover provides a conservative estimate for the ratio f_t/f_m on account of the minimum strength $\sigma_u = 0$, the relationship f_t/f_m of tension to bending strength is expressed by the 2-parameter-expression according to equation (7b) as follows

$$\frac{f_t}{f_m} = 0,36 \cdot f_m^{0,20} \quad (10)$$

4 Comparison with published values

Fig. 3 shows a compilation of ratios f_t/f_m from published test data. Here, too, the ratio f_t/f_m is seen to rise with increasing wood quality, however with considerable scatter. A regression analysis formally based on eq. (10) results in eq. (11).



^{*)}The results from the tension tests were converted to a test length of $l_0 = 9 \cdot b$ using a size factor of $(b_1/b_2)^{0,10}$.

Fig. 3: Ratio f_t/f_m of tension to bending strength in relation to bending strength from published test results and comparison with eq. (10).

$$\frac{f_t}{f_m} = 0,31 \cdot f_m^{0,23} \quad (11)$$

The difference between eq. (10) and eq. (11) amounts to about 5 percent for lower bending strengths.

Both own data and published values refer to bending tests with the weakest section positioned in the tension zone. In contrast according to EN 384 the weakest section has to be located randomly in the tension and compression zone. The position of weak sections has an effect on the ratio f_t/f_m , as the lower percentiles of bending strength are higher with random positioning of weak sections. The corresponding curve for these tests is thus shown to have lower values.

5 Relationships for strength graded material

From a practical point of view the ratio of tension to bending strength is important when determining characteristic strength values for the design of timber structures which have to be determined from the 5 percentiles of the strength distributions. The characteristic bending strength in tests where the weakest section is located within the tension zone are determined on the basis of the 7.5 percentiles of bending strength (vgl. Glos u. Burger, 1994).

The samples from the data base were visually graded according to DIN 4074 and the 5 percentiles of tension strength ($f_{t,05}$) as well as the 5 and 7.5 percentiles of bending strength ($f_{m,05}$ resp. $f_{m,075}$) were determined using 3-parameter Weibull distributions. Table 2 compiles the calculated ratios f_t/f_m . Compared with the ratio $f_{t,05}/f_{m,05}$ the ratio $f_{t,05}/f_{m,075}$ is about 7 % lower and on average about $f_{t,05}/f_{m,075} = 0.66$. There is no recognizable effect of wood quality.

To estimate the ratio f_t/f_m for machine grading about 300 and 350 tension and bending tests respectively from an ongoing research project were used, where specimens had been machine graded. Since the grading machine used is still being cleared for commercial use and no limiting values for the determination of strength classes had as yet been determined, the flatwise MOE in bending determined by the grading machine was used for the break-down into quality classes. For bending machines this parameter is the essential classification criterion, making it possible for the relationships for machine graded material to be assessed in this manner.

The ranges of MOE values were chosen so as to contain from 50 to 200 specimens in the individual quality classes:

MS I	9500 N/mm ²	≤	MOE _{flat}		
MS II	7000 N/mm ²	≤	MOE _{flat}	<	9500 N/mm ²
MS III	5000 N/mm ²	≤	MOE _{flat}	<	7000 N/mm ²

	S 13	S 10	S 7	MS I	MS II	MS III
$f_{t,05}/f_{m,05}$	0.74	0.67	0.72	0.81	0.66	0.60
$f_{t,05}/f_{m,075}$	0.68	0.62	0.68	0.73	0.61	0.56

Tab. 2: Ratio f_t/f_m of tension to bending strength for strength graded specimens. Visual grading according to DIN 4074 and estimation for machine grading. Comparison of calculations based on the 5 and 7.5 percentiles of bending strength.

As for visually graded material the ratios $f_{t,05}/f_{m,05}$ and $f_{t,05}/f_{m,075}$ were determined for the individual quality classes MS I to MS III (see Table 2). In contrast to visually graded material, however, the effect on wood quality in this case is quite distinct. Compared with ratio $f_{t,05}/f_{m,05}$ the ratio $f_{t,05}/f_{m,075}$ is about 8 % lower.

Fig. 4 represents the ratios $f_{t,k}/f_{m,k}$ for characteristic tension and bending strength for visually and machine graded timber. It shows data from our own investigations as well as values from literature for which characteristic strength values were available. In addition the ratios for ungraded material (mean of samples) and a matched sample containing tension and bending specimens cut from a single piece of sawn timber are plotted. From this data a regression analysis leads to

$$\frac{f_t}{f_m} = 0,38 \cdot f_m^{0,16} \quad (12)$$

When comparing the plotted data the relationship according to eq. (12) appears too high so that for safety reasons a ratio is proposed for the relationship between characteristic tension to bending strength which is derived by weighting the lower values and is closer to the lower ratios of f_t/f_m (see eq. 13).

$$\frac{f_{t,k}}{f_{m,k}} = 0,24 \cdot f_{m,k}^{0,28} \quad (13)$$

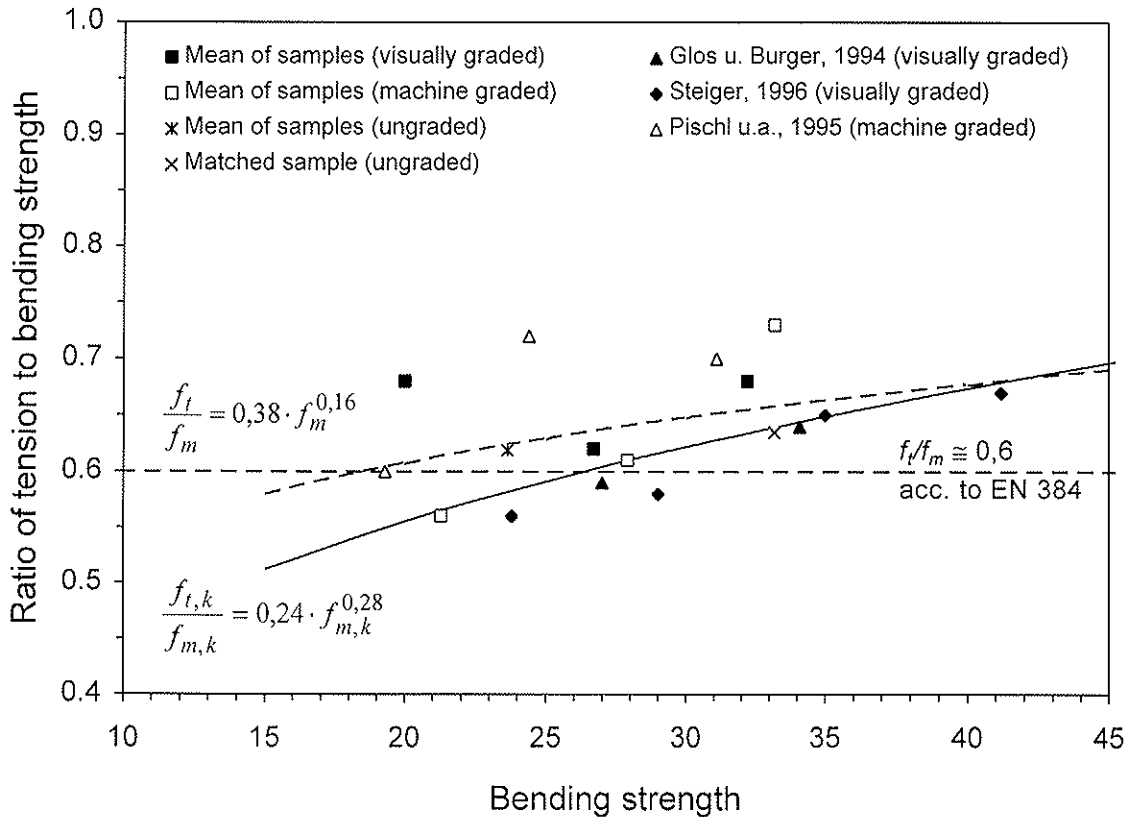


Fig. 4: Dependence of ratio $f_{t,k}/f_{m,k}$ of characteristic tension to characteristic bending strength for tests carried out according to EN 384 and EN 408 and related to the 7.5 percentiles of bending strength respectively.

6 Effect of specimen size

For load in tension and in bending a common size factor has to be taken into account when determining characteristic strength values according to EN 384 and designing structural timber elements according to EN 1995-1-1. The ratio f_t/f_m is hence independent of timber dimensions.

Recent results, however, have revealed differences in size effects (see Glos and Henrici 1993, Burger and Glos 1996), linked with an effect of timber dimensions on the relationship f_t/f_m .

All tests evaluated in this study were carried out with a constant ratio b/l , so that the effects of width and height respectively and length cannot be determined separately. The size effect for ungraded and visually graded material is therefore determined by the factor $\left(\frac{l_r \cdot b_r}{l \cdot b}\right)^{m_k}$. The calculated values for size effect parameters m_k are compiled in Table 3. For ungraded material the size effect parameter m_k shows hardly any and then only non-uniform differences in tension and in bending.

Compared with the ungraded material the size effect appears to be more pronounced for visual grading, in particular for load in tension. The difference in size effect parameters for load in tension and in bending comes to about $\Delta m_k = 0.06$ for the 50 percentiles and $\Delta m_k = 0.09$ for the 5 and 7.5 percentiles.

	50%-Fraktile		5%- bzw. 7,5%-Fraktile	
	Biegung	Zug	Biegung	Zug
unsortiert	0.06	0.03	0.03	0.05
S 13	0.05	0.07	0.01	0.08
S 10	0.04	0.17	0.09	0.16
S 7	0.04	0.08	-0.01	0.12
$m_{k,t} - m_{k,m}$	0.06		0.09	

Tab. 3: Size effect parameter m_k for the 50 percentiles and 5 percentiles of tension and bending tests respectively from the data base.

7 Discussion and conclusions

The present investigations involving structural timber from Central Europe (mainly spruce) confirm that the ratio between tensile and bending strength depends on timber quality. This relationship can be derived using brittle fracture theory and expressed in terms of dependence on bending strength.

According to the brittle fracture theory there is a constant relationship f_t/f_m which is independent of timber quality and dimensions. When taking into account the different material behaviour of timber loaded in tension and in bending by calculating different parameters for the strength distributions, the ratio of f_t/f_m increases with strength and can be said to be more realistic.

For 2,642 tension and 1,739 bending tests in 28 and 27 samples respectively using test specimens in structural dimensions (constant dimensions per sample) ungraded timber resulted in the relationship

$$\frac{f_t}{f_m} = 0,36 \cdot f_m^{0,20} \quad \text{bzw.} \quad f_t = 0,36 \cdot f_m^{1,20}$$

The bending tests were conducted with the weakest section located in the tension zone, so that a relationship in conformity with EN 384 based on bending tests involving random location of weak sections shows lower ratios.

With consideration of test conditions involving non-random positioning of weak sections the 5 percentiles of tension strength were related to the 7.5 percentiles of the bending strength. For strength graded timber there is a noticeable effect of both grading method and dimensions on the f_t/f_m ratio. There is no clear effect of timber quality on the ratio f_t/f_m in timber visually graded according to DIN 4074, while increase in ratio is remarkable for machine graded timber.

No size effect was found for ungraded timber. A more pronounced size effect in strength graded timber loaded in tension lead to a size effect, on average, of $\left(\frac{l_{m,r} \cdot b_{m,r}}{l_m \cdot b_m}\right)^{0,09}$ for visually graded specimens tested according to EN 408. Due to a constant ratio of b/l the effects of test length or span and specimen width or height could not be determined separately.

There is considerable scattering regarding the ratio f_t/f_m . For safety reasons the lower ratios were more strongly weighted when determining the relationship for characteristic strength values $f_{t,k}/f_{m,k}$. In conjunction with the test data on visually and machine graded timber from literature the following equation was derived:

$$\frac{f_{t,k}}{f_{m,k}} = 0,24 \cdot f_{m,k}^{0,28} \quad \text{bzw.} \quad f_{t,k} = 0,24 \cdot f_{m,k}^{1,28} \quad (14)$$

Table 4 compares characteristic tensile strength values for strength classes according to EN 338 derived from this equation with currently valid strength values. This reveals that tensile strength is being overrated as regards the lower strength classes while in the higher strength classes tension strength is being given too conservative. For economy and safety reasons proper consideration of the influence of timber quality would therefore be desirable, which would adequately highlight the particular advantages of machine graded timber.

[N/mm ²]	Festigkeitsklassen nach EN 338								
	C 14	C 16	C 18	C 22	C 24	C 27	C 30	C 35	C 40
$f_{m,k}$	14	16	18	22	24	27	30	35	40
$f_{t,k}$	8	10	11	13	14	16	18	21	24
$f_{t,Gl.(14)}$	7.0	8.3	9.7	12.5	14.0	16.3	18.7	22.7	27.0

Tab. 4: Comparison of characteristic strength values for strength classes according to EN 338 for load in bending and in tension with tension strength values calculated acc. to eq. (14).

Literature

- Burger, N.; Glos, P.; 1996: Effect of size on tensile strength of timber. Int. Council Build. Res. Stud. Doc., CIB-W18, Meeting 29, Bordeaux, 1996
- Colling, F.; 1986: Einfluß des Volumens und der Spannungsverteilung auf die Festigkeit eines Rechteckträgers. Holz als Roh- und Werkstoff 44, 1986, pp. 121-125 and pp. 179-183
- Foslie, A.M.; Moen, K.; 1968: Strength properties of Norwegian spruce - 1. Bending strength, modulus of elasticity and tensile strength tested on the structural sizes 3"x8" and 2"x4". Norwegian Institute of Wood Working and Wood Technology, Report No. 33, 1968
- Galligan, W.L.; Gerhards, C.C.; Ethington, R.L., 1979: Evolution of tensile design stresses for lumber. USDA, Forest Service, Forest Products Laboratory, Report FPL-28, 1979
- Glos, P.; 1981: Zur Modellierung des Festigkeitsverhaltens von Schnittholz bei Zug-, Druck- und Biegebeanspruchung. Institut für Holzforschung, Universität München, Berichte zur Zuverlässigkeit von Bauwerken, SFB, 1981
- Glos, P.; Burger, N.; 1994: Vergleichende Betrachtungen europäischer Bauprodukten-Normen mit nationalen Bestimmungen - Teilprojekt: Erstellung von Eigenschaftsprofilen von Bauholz für tragende Zwecke. Institut für Holzforschung, Universität München, Bericht 93507, 1994
- Glos, P.; Henrici, D.; 1993: Einfluß der Querschnittshöhe auf die Biegefestigkeit von Fichtenschnittholz mit kleinen Querschnitten Institut für Holzforschung, Universität München, Bericht Nr. 91508, 1993
- Green, D.W.; Kretschmann, D.E.; 1990: Stress class systems - An idea whose time has come ? USDA, Forest Service, Forest Products Laboratory, Research Paper FPL-RP-500, 1990
- Green, D.W.; Kretschmann, D.E.; 1991: Lumber property relationships for engineering design standards. Wood and Fiber Science 23 (3), 1991, pp. 436-456
- Madsen, B.; Buchanan, A.H.; 1986: Size effects explained by a modified weakest link theory. Canadian Journal of Structural Engineering 13(2), 1986, S. 218-232
- Pischl, R.; Schickhofer, G.; Seiner, Ch.; Steinberger, A.; Gehri, E.; Mauritz, R.; 1995: Entwicklung leistungsfähiger Holzleimbauteile. Zusammenfassender Bericht zum FFF-Forschungsprojekt 'Entwicklung leistungsfähiger Holzleimbauteile durch den Einsatz von maschinell festigkeitssortiertem Holz', Institut für Stahlbau, Holzbau und Flächentragwerke, Technische Universität Graz, 1995
- Steiger, R.; 1996: Mechanische Eigenschaften von Schweizer Fichten-Bauholz bei Biege-, Zug-, Druck- und kombinierter M/N-Beanspruchung. Institut für Baustatik und Konstruktion, Bericht Nr. 221, ETH Zürich, 1996
- Walford, G.B.; 1982: Comparison of the tensile and bending strengths of 100 x 50 mm radiata pine. Forest Research Institute, New Zealand Forest Service, FRI Bulletin No. 21, 1982
- Weibull, W.; 1939: A statistical theory of the strength of materials. Royal Swedish Institute for Engineering Research, Report No. 151, Royal Technical University, Stockholm, Sweden, 1939

**INTERNATIONAL COUNCIL FOR BUILDING RESEARCH STUDIES AND DOCUMENTATION
WORKING COMMISSION W18 - TIMBER STRUCTURES**

**CHARACTERISTIC DESIGN STRESSES IN TENSION FOR RADIATA PINE
GROWN IN CANTERBURY**

by

A Tsehaye
J C F Walker
School of Forestry
University of Canterbury
A H Buchanan
Department of Civil Engineering
University of Canterbury

MEETING THIRTY

VANCOUVER

CANADA

AUGUST 1997

CHARACTERISTIC DESIGN STRESSES IN TENSION FOR RADIATA PINE GROWN IN CANTERBURY

Addis Tsehaye*, A.H. Buchanan** and J.C.F. Walker*

*School of Forestry, University of Canterbury. **Department of Civil Engineering, University of Canterbury.

Abstract

This paper presents a study on mechanical properties of radiata pine timber from Canterbury Plains. Variations of axial stiffness and tensile strength within a tree and the effect of machine and visual grades on these properties of timber are examined. The results show that the mean values for the modulus of elasticity and the characteristic stress values for tensile strength vary significantly across the diameter of the tree while changing very little up the height of the tree. As expected, the modulus of elasticity and tensile strength increase on going from lower to higher grades. Comparison with previous studies on radiata pine timber from New Zealand, Australia and Chile reveals that timber from the Canterbury Plains has similar mechanical properties to similarly aged wood from Kaingaroa Forest selected as representative of future wood supply in New Zealand; modulus of elasticity for the Chilean timber is superior to that for New Zealand timber while there is little difference in mechanical properties between timber from New Zealand and Australia.

Introduction

New Zealand has 1.3 million ha of plantation forest of which 90% is radiata pine. The South Island contains 382000 ha of plantation forest, of which 72000 ha is located in the Canterbury region (New Zealand Forest Owners' Association, 1994). The Canterbury region contributes about 6% the country's total plantation forestry area or 19% of the South Island's planted production forests. In terms of wood quality, previous work (Walford, 1985; Hadi, 1992) has shown that some of the least stiff timber in New Zealand comes from the drier, stonier sites on the Canterbury Plains. This study examines the properties of timber from trees grown in such stands, investigating:

- a. variability of stiffness and strength with position in the tree;
- b. variability of stiffness and strength with grade; and
- c. comparison of test results with code values and previous studies.

Material and methods

Forty eight unpruned trees from a 25-year-old stand near Dunsandel in the Canterbury Plains in the South Island, New Zealand were felled and cross-cut to give three logs. These logs were milled to yield 915 90x35 mm dressed, dried (12% M.C.), machine stress graded boards, 3.6 m long. Each board was identified according to log type (butt, middle, top) and distance from the pith (positions 1 to 4), and visually graded. The detail regarding sample preparation is reported in Addis Tsehaye (1995) and Addis Tsehaye *et al.* (1995a, b).

The boards were machine graded by a stress grading machine in a sawmill, using normal commercial settings to mark each board with intermittent coloured paint marks. Each board was allocated the machine stress grade corresponding to the lowest grade mark in its length.

For each board the modulus of elasticity and tensile strength were measured by testing in tension to failure. The tensile strength of each board was determined using a horizontal tension test machine, having a span of 2.6 metres between the grips which were 450 mm long. This is a standard span according to the specifications in SAA (1992). The hydraulically operated grips applied a sufficient gripping force to prevent specimens slipping at the grips while low enough to avoid crushing of wood in the grips. The tensile force was applied by a 200 kN capacity hydraulic ram connected at one end of the test machine. At the other end a load cell measured the applied force which was continuously recorded. The failure load ranged between 25 kN to 150 kN.

The modulus of elasticity in axial tension was determined by measuring the elongation of the boards at low load levels (up to 35 kN) over a length of 2.46 m. In all except the weakest boards, the recording transducers were removed before failure to avoid the risk of damage. Almost identical values were obtained from flat-wise bending of each board (Addis Tsehaye, 1995; Addis Tsehaye *et al.*, 1995a).

5th percentile values

For structural use the issue is not how strong a piece of timber is, rather how weak it might be. That is a question of probability and reliability theory. The design stress in most modern codes is the "characteristic" stress, which is the lower 5th percentile value for the population determined with a specified confidence (Addis Tsehaye *et al.*, 1991). The 5th percentile values of tensile strength were calculated by the method described in SAA (1992), where the individual values are ranked in ascending order, and each is assigned a rank value, R_i as described by the following equation:

$$R_i = (i - 0.5)/(N) \quad [1]$$

Where: $i = 1, 2, 3, \dots$ etc. for the first, second, third etc. ranked values;

N = total sample size;

The 5th percentile corresponds to $R_i = 0.05$.

Characteristic Stress

According to the New Zealand standard (NZS, 1993) the characteristic stress or strength (R_k) for strength properties is defined as an estimate of the lower 5th percentile value determined with 75% confidence from tests on a representative sample of full-size test specimens. For stiffness the characteristic value (E_k) is the mean value.

The characteristic stresses (R_k) for tensile strength for this study were estimated from the lower 5th percentile values in accordance with SAA (1992). The lower 5th percentile is reduced by a factor (F) as follows:

$$F = (1 - 2.7V_R/\sqrt{n}) \quad [2]$$

where: V_R = coefficient of variation of the measured data and
 n = sample size.

This adjustment reflects the confidence with which the lower 5th percentile value of a population can be estimated when using a small sample. The normalised characteristic value, for use in the design code, is a normalised value given by:

$$R_{k, \text{norm}} = [1.35/\phi] \times [R_k/(1.3+0.7V_R)] \quad [3]$$

Where: ϕ = capacity factor specified in the limit state design code (0.8 for timber properties).

Results

a) Positions within the tree

A summary of characteristic stress ($R_{k, \text{norm}}$), mean, coefficient of variation (c.v.) and fifth percentile value for tensile strength and mean stiffness for the tested timber is presented in Tables 1 - 4.

Table 1 Characteristic stresses for tensile strength and mean modulus of elasticity based on log types.

Log	Tensile strength (MPa)					MOE (GPa)	
	N	Mean	c.v.	5%-ile	$R_{k, \text{norm}}$	Mean	c.v.
Top	221	15.2	0.35	7.2	7.4	6.6	0.26
Middle	295	17.9	0.32	10.0	10.5	7.0	0.24
Butt	399	20.9	0.40	10.2	10.3	6.8	0.31
All	915	18.6	0.39	9.0	9.3	6.8	0.28

Table 2 Characteristic stresses for tensile strength and mean modulus of elasticity based on position relative to the pith: position 1 is timber with boxed-pith while position 4 is adjacent to the cambium (see Addis Tsehaye et al., 1995a for more detail).

Position	Tensile strength (MPa)					MOE (GPa)	
	N	Mean	c.v.	5%-ile	$R_{k, norm}$	Mean	c.v.
1	206	13.5	0.28	7.8	8.3	5.0	0.22
2	440	17.8	0.33	8.9	9.4	6.7	0.21
3	269	23.2	0.35	11.4	11.7	8.5	0.18
4	19	29.1	0.33	n/a	n/a	9.5	0.16
All	915	18.6	0.39	9.0	9.3	6.8	0.28

n/a = not applicable because of the small sample size.

In Table 1 the mean values for the modulus of elasticity and the characteristic stress values for tensile strength change little in going from the butt log to the top log. The only exception is the mean value for tensile strength which decreases steadily from the butt to the top log.

In contrast to the lack of variation along the length of the tree the changes in the mean and characteristic stress values for stiffness and strength properties across the diameter of the tree (Table 2) are significant. In moving from position 1 to 2, 2 to 3 and 3 to 4, the percentage increase in stiffness is 36%, 27% and 11% respectively. The percentage increases in characteristic stress values for tensile strength in moving from position 1 to 2 and 2 to 3 are 13% and 25% respectively.

Figure 1 shows cumulative frequency distribution curves for tensile strength on the basis of position relative to the pith.

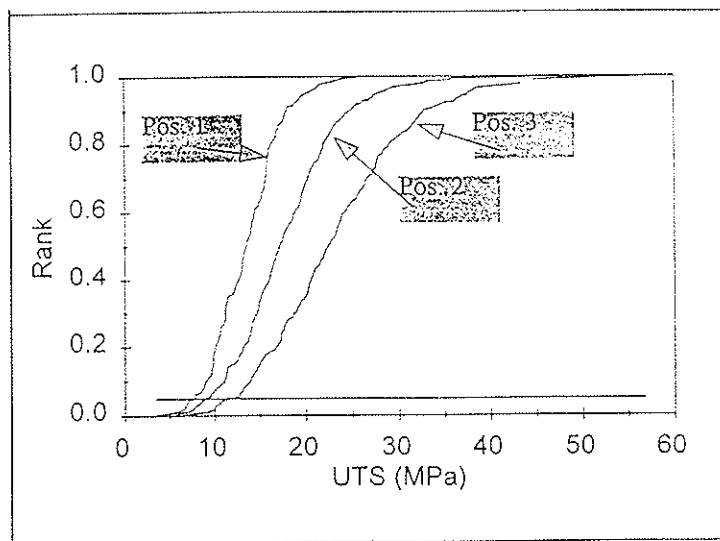


Figure 1 Cumulative frequency distribution curves for tensile strength on the basis of positions relative to the pith.

b. Grades

Summaries of characteristic stresses for tensile strength and mean modulus of elasticity of the tested timber on the basis of machine stress and visual grades, together with the specified code values for mechanically graded timber (AS1720, 1988) and visually graded timber (NZS, 1993) are presented in Tables 3 and 4.

Table 3 Characteristic stresses for tensile strength and mean modulus of elasticity based on machine stress grades, and code values (AS1720, 1988).

MSG	N	Tensile strength (MPa)					MOE (GPa)		
		Mean	c.v.	5%-ile	$R_{k, norm}$	Code values	Mean	c.v.	Code values
F4	132	13.1	0.33	6.8	6.9	6.5	4.8	0.27	6.1
F5	593	17.8	0.35	9.6	10.1	8.2	6.6	0.23	6.9
F8	179	24.2	0.31	14.0	14.6	13.0	8.7	0.14	9.1
F11	11	34.6	0.29	n/a	n/a	16.6	10.6	0.10	10.5
All	915	18.6	0.39	9.0	9.3	F5*	6.8	0.28	F4*

n/a = not applicable because of small sample; * = equivalent grade in the code.

Table 4 Characteristic stresses for tensile strength and mean modulus of elasticity based on visual grades, and code values (NZS, 1993).

Visual grade	N	Tensile strength (MPa)					MOE (GPa)		
		Mean	c.v.	5%-ile	$R_{k, norm}$	Code values	Mean	c.v.	Code values
Box	194	11.6	0.34	6.8	7.0	n.s	5.6	0.29	n.s
No.2F	208	15.3	0.22	11.2	12.5	n.s	6.3	0.27	n.s
No.1F	513	22.5	0.30	14.0	15.1	10.6	7.5	0.24	8.0
All	915	18.6	0.39	9.0	9.3		6.8	0.28	

n.s = not specified by code.

As expected in Tables 3 and 4 the modulus of elasticity and tensile strength show a very regular pattern of dependency on both machine and visual grades, in that they increase on going from lower to higher grade. The main difference between visual and machine stress grades is that visual grades provide much better differentiation than do machine grades of tensile strength, but the reverse is true for modulus of elasticity (as would be expected). An indication of the much better ability of visual grading to identify tensile strength is the observation that with visually graded timber more than half the boards (513) are No.1 Framing grade having a characteristic stress of 15.1 MPa, whereas for machine stress graded timber the "best" 179 boards have a characteristic stress of 14.6 MPa.

Comparing the machine stress grades with the respective code values (Table 3), it can be seen that all the machine stress grades exceed their respective code value in tensile strength. For stiffness, the modulus of elasticity for both F5 and F8 grades was about 96% of the code value for each grade. This proportion was lower for F4, and above the grade value for the few F11 boards. These figures suggest that the grading machine setting may have been slightly low, but the analysis in Table 3 and Table 8 is still considered an important indication of the properties of commercially machine graded timber in New Zealand. The bottom row of Table 3 shows that if all the pieces are lumped together as one population, the characteristic stress would put the population well into grade F5 for tensile strength and almost into F5 for stiffness.

Figure 2 shows cumulative frequency distribution curves for tensile strength on the basis of machine stress grades.

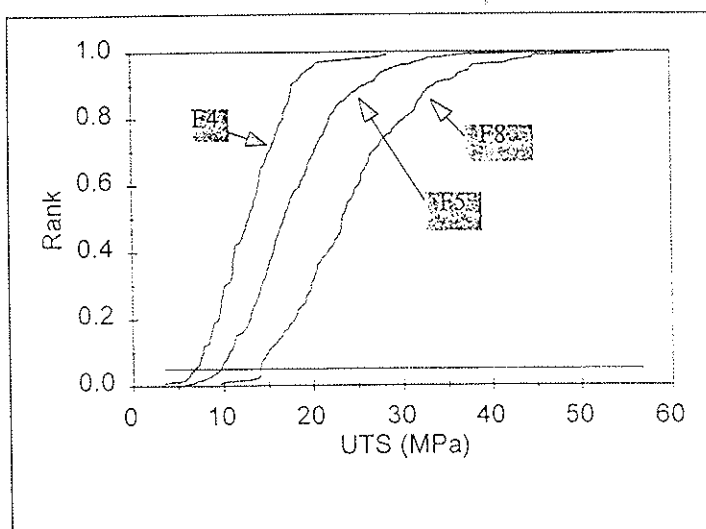


Figure 2 Cumulative frequency distribution curves of tensile strength for boards segregated into machine stress grades.

c. Comparison with previous studies

The results of the current study can be compared with those of previous work on full-sized members of radiata pine (Table 5). The studies selected are those Addis Tsehaye (1989), Hadi (1992), Walford (1994) and Smith *et al.* (1993).

Table 5 Mean and characteristic stress values of the current study compared with others (all grades).

Source, age, cross-section and clear span length	Tensile strength (MPa)				MOE (GPa)
	Mean	c.v.	5%-ile	$R_{k, norm}$	
<u>Boxed-pith timber</u>					
Addis Tsehaye (1989), mill run timber from Nelson Forests, 90x45x2000 mm	16.8	0.34	9.4	9.7*	6.4
Hadi (1992), 7-year-old stand from Canterbury Plains forests, 90x45x1200 mm	10.7	0.25	6.1	6.7*	2.9
Current study, 90x35x2600 mm	13.5	0.28	7.8	8.3	5.0
<u>Omitting butt log</u>					
Walford (1994), 25-year-old, thinned and pruned stand from Kaingaroa Forest					
90x45x650 mm	17.1	0.60	6.4	5.7*	6.2
90x45x1800 mm	12.1	0.58	3.8	3.4*	6.5
Current study, 90x35x2600 mm	16.7	0.34	9.8	9.0	6.8
<u>Corewood</u>					
Smith <i>et al.</i> (1993) mill run timber from Chile, 95x45x855** mm	20.4	0.57	8.5	7.7*	8.3
Current study***, 90x35x2600 mm	16.4	0.34	8.5	8.8	6.1
<u>Whole tree</u>					
Current study, 90x35x2600 mm	18.6	0.39	9.0	9.3	6.8

* Values for characteristic stress are calculated by ourselves; ** The 855 mm span length (i.e. 9 x specimen width) complies with the specification of ISO (1985); *** Data for corewood in the current study is calculated by merging data for positions 1 and 2 in Table 2.

From Table 5 it can be seen that various clear span lengths were used by these authors. According to the principle of the weakest link (Madsen and Buchanan, 1986) this span length variation will have a large effect on the results, with larger spans giving lower strength values. Hence, in order to make a fair comparison, the data in Table 5 need to be standardized to a 2.6 m and 0.86 m span lengths by applying a length effect parameter, k_1 , as recommended in the AS/NZS 4063 (SAA, 1992).

$$k_1 = (L_o/L_s)^{c.v.} \quad [4]$$

Where: L_o = non-standard span (m);
 L_s = standard span (m); and
c.v. = coefficient of variation.

The length effect in structural timber arises because of within-board variability, which is the variable strength of wood and defects along the length of each board. The term c.v. in equation 4 is the coefficient of variation for between-board variability, which is a measure of the variation of strength of the weakest points in each of a population of boards. Equation 4 is based on the assumption that these two sources of variability are the same. This assumption is not necessarily true, but may be reasonably used in most cases, given the difficulty of measuring within-board variability.

A summary of the adjusted characteristic stress values for tensile strength is presented in Table 6.

Table 6 Mean and characteristic stress values for tensile strength adjusted to 2.6 m and 0.65 m clear spans and the values for the length effect parameter, k_1 .

Source and clear span length in tension	Long span values Tensile strength (MPa) (adjusted to 2.6 m span length)					Short span values Tensile strength (MPa) (adjusted to 0.86 m span length)				
	Mean	c.v.	5%-ile	R_{k_1} norm	k_1	Mean	c.v.	5%-ile	R_{k_1} norm	k_1
<u>Boxed-pith</u>										
Addis Tsehay (1989, Nelson), 2.0 m	15.4	0.34	8.6	8.9	0.91	22.4	0.34	12.5	12.9	1.33
Hadi (1992, Canterbury), 1.2 m	8.8	0.25	5.0	5.5	0.82	11.6	0.25	6.6	7.3	1.09
Current study, 2.6 m	13.5	0.28	7.8	8.3	1.00	18.4	0.28	10.6	11.3	1.36
<u>Omitting butt log</u>										
Walford (1994, Kangarooa)										
Short specimen, 0.65 m	7.4	0.60	2.8	2.5	0.44	14.5	0.60	5.4	4.8	0.85
Long specimen, 1.8 m	9.8	0.58	3.1	2.8	0.81	18.6	0.58	5.8	5.2	1.53
Average	8.6	0.59	3.0	2.7	-	16.6	0.59	5.6	5.0	-
Current study, 2.6 m	16.7	0.34	9.8	9.0	1.00	24.3	0.34	14.3	13.1	1.46
<u>Corewood</u>										
Smith et al. (1993, Chile), 2.9 m	21.7	0.57	9.1	8.2	1.06	40.8	0.57	17.0	15.4	2.00
Current study, 2.6 m	16.4	0.34	8.5	8.8	1.00	23.9	0.34	12.4	12.8	1.46
<u>Whole tree</u>										
Current study, 2.6 m	18.6	0.39	9.0	9.3	1.00	28.6	0.39	13.9	14.0	1.54

The data of Smith *et al.* (1993) requires separate consideration as specimens were cut from 3 or 4 m lengths of timber in such a way that the grade determining feature (as detected by visual inspection) was included in the 855 mm test span. Thus in order to adjust to 2.6 m clear span the original data for the 855 mm test span must be deemed to apply to the original material (pers. com.) which we have taken to be 3.5 m, on average, minus 0.9 m to allow for end gripping, i.e. a clear span of 2.9 m.

Table 6 demonstrates the way in which the original data in Table 5 changes as the span length is increased or reduced. It also shows that the coefficient of variation has an extremely significant effect on the characteristic stress values. With the smallest coefficient of variation (c.v. = 0.25, Hadi 1992) the characteristic stress for the long span is 75% of the value for the short span whereas with the largest coefficient of variation (c.v. = 0.60 Walford 1994) the characteristic stress for the long span is only 52% of the short span value. This creates a possible problem because the between-board variation is dominating the calculation of the length effect, whereas the unmeasured within-board variation may be similar for all of the tested populations. More research on length effects is needed.

The extremely high dependence of characteristic tensile strength on test specimen length suggests three important points. First, it is important that in-grade tensile testing be carried out using a consistent specimen length representative of real world applications. Secondly, it would be desirable for the very large difference between test specimen lengths in different codes (such as AS/NZ and ISO) to be rationalised. Thirdly, and most importantly for designers, a length effect correction factor such as equation 4 should be introduced into NZS 3603 and other timber design code, following research to obtain the correct numbers.

The mean stiffness and tensile strength values for the boxed-pith timber in the current study (Tables 5 and 6) are comparable to but somewhat greater than the results of Hadi (1992). With Hadi the pith at both ends of 7-year-old logs was centred before milling so that his boxed-pith boards would contain wood from only the first 4 or so growth rings: in the current study the pith wandered between 2 or 3 boxed-pith boards so including some older wood in all the boxed-pith timber. The present finding again confirms that boxed-pith radiata pine from the Canterbury Plains is inferior in stiffness compared with that of boxed-pith material from the Nelson Region of New Zealand (Addis Tsehaye, 1989).

Our mean values of tensile strength (Table 6) and modulus of elasticity (Table 5) for timber from the tree, but omitting that from the butt logs, are superior to those recorded by Walford (1994). Walford's very low characteristic stress values for tensile strength are anomalous and should be treated with caution.

Comparing the data in Tables 5 and 6, the mean and characteristic stress values of the tensile strength for Canterbury timber are comparable, but a little inferior to that for Chile. The major difference is in stiffness. The Chilean timber is 22 - 34% stiffer compared with the values recorded both in this study and by Walford (1994). The large coefficient of variation for Chilean timber may reflect regional variations in growth, stocking and silviculture.

This wide difference in stiffness between the New Zealand and Chilean timber might be attributed to the difference in stocking between the two countries. In Chile, according to a report by the Instituto Forestal (1990) the traditional silvicultural practice for the production of pulpwood and sawlogs assumes an initial stocking of 1400 - 2000 stems/ha. The first thinning applies at an age of 12 - 13 years leaving 700 - 1000 stems/ha. A second thinning occurs at age 14 - 15 leaving a final-crop stock of 400 stems/ha. Whereas in New Zealand a typical stand grown for sawlogs starts with an initial stocking of 1500 stems/ha followed by two thinnings between the ages of 4 and 9 years, leaving a final-crop stock of 200 - 400 stems/ha (West *et al.* 1982). The higher stocking in Chilean stands reduces branch size and suppresses the diameter of the juvenile core so affecting wood quality.

A summary of characteristic stress values on the basis of grades is presented in Tables 7 and 8. Table 7 shows the characteristic stress values from the current study on the basis of visual grade which parallel the results of Walford (1994). Table 8 presents a summary of the characteristic stress values for machine stress grades F5 and F8 from the current study, Walford (1995), Bolden *et al.* (1994) and the draft AS 1720. Walford (1995) tested F5 and F8 grade radiata pine timber using samples 70 and 90 mm wide by 35 mm thick which were collected from all the New Zealand mills producing machine graded timber.

Bolden *et al.* (1994) tested 90x35 mm radiata pine timber (with length according to the specifications in SAA, 1992) taken from various mills throughout Australia. Note that the values in Tables 7 and 8 are not corrected for length.

Table 7 Summary of characteristic stress values compared with Walford (1994) on the basis of visual grades.

Source	Characteristic stress		
	Bending (MPa)	Tension (MPa)	MOE (GPa)
<u>Box</u>			
Walford (1994)	6.3	2.0*	5.0
Current Study	(12.8)	7.0	5.6
<u>No.2 Framing</u>			
Walford (1994)	12.2	3.5*	6.3
Current study	(23.8)	12.5	6.3
<u>No.1 Framing</u>			
Walford (1994)	17.2	4.1*	6.3
Current study	(29.2)	15.1	7.5
NZS (1993)	17.7	10.6	8.0

Values in parenthesis are derived values (2 x tensile stress); * Data for Walford (1994) has been recalculated (pers. com. Walford, 1996), and the average of his short and long specimens is used.

Table 8 Summary of characteristic stress values compared with others on the basis of machine stress grades.

	Bending (MPa)	Tension (MPa)	MOE (GPa)
<u>F5</u>			
Bolden (1994)	16.2	8.9	10.0
Walford (1995)	17.4	6.5	9.4
Current study	(20.2)	10.1	6.6
Draft AS1720	16.2	8.2	6.9
<u>F8</u>			
Bolden (1994)	28.0	15.0	12.7
Walford (1995)	29.0	10.7	13.7
Current study	(29.2)	14.6	8.7
Draft AS1720	25.4	13.0	9.1

n/a = not available; Values in parenthesis are derived values (2 x tensile stress).

Discussion

a. Comparison within New Zealand

The observations in Tables 5, 6 and 7 are surprising in that this timber from the Canterbury Plains has better mechanical properties to similarly aged wood from Kaingaroa Forest selected as representative of future wood supply (Walford, 1994). This is a significant finding because older trees from Kaingaroa Forest have been the traditional bench mark for New Zealand timber. The Nelson boxed-pith timber (Addis

Tsehaye, 1989) has comparable properties, and one might deduce that the outerwood quality for Nelson timber would be much superior to that studied here. A re-evaluation of regional variations of wood properties may be needed as the age of plantation forests readjusts to the end of clear felling of older stands (> 40 years) and the age of clear felling settles at between 25 and 30 years.

b. Comparison with the code values

The results of this study are compared with code values for visual grades in Tables 4 and 7. These show that the No.1 Framing grade material has higher tensile strength and slightly lower stiffness than the code values.

The comparison for machine stress grades (Tables 3 and 8) shows that for a given stiffness, the tensile strength of the tested material is higher than would be expected from the code values.

c. Comparison with the Australian timber

Walford (1996) compared radiata pine timber from New Zealand and Australia using the data from Walford (1995) and Bolden *et al.* (1994). He reported that timber from the two countries have the same values in bending, compression and modulus of elasticity. Walford (1996) suggests that the differences observed in tensile strength may be affected by different testing equipment (but does not elaborate any further). The higher tensile strength values observed in the current study (Table 7) are comparable with the Australian timber. Table 8 shows clearly that for any given values of mean modulus of elasticity, the New Zealand wood has higher tensile strength than the Australian wood.

Conclusions

1. The mean values for the modulus of elasticity change little in going from the butt log to the top log;
2. The characteristic stress values for tensile strength change significantly from the butt log to the top log;
3. The changes in the mean stiffness and characteristic stress values for tensile strength across the diameter of the tree are significant;
4. As expected, the modulus of elasticity and tensile strength show a regular pattern of dependency on both machine and visual grades, in that they increase on going from lower to higher grade;
5. The timber from the Canterbury Plains has similar mechanical properties to similarly aged wood from Kaingaroa Forest selected as representative of future wood supply;
6. Comparison of the characteristic stress values of the current study with those of the draft AS1720 shows that for a given stiffness, radiata pine timber from Canterbury generally has a higher characteristic tensile strength than would be predicted by the code;
7. Comparison of the characteristic stress values of the current study with a recent Australian study show that the New Zealand wood has a higher ratio of tensile strength to stiffness than the Australian wood;
8. The high dependence of characteristic tensile strength on test specimen length suggests that a length effect correction factor such as equation 4 should be introduced into NZS 3603 and other timber design codes. More research on this topic is needed.

Acknowledgments

The authors would like to acknowledge the New Zealand Foundation for Research, Science and Technology (Contract # UOC 502) for support towards this project.

References

- Addis Tsehaye (1995). Within- and between-tree variations in the wood quality of radiata pine. Ph.D thesis, University of Canterbury.
- Addis Tsehaye (1989). Proof testing of juvenile wood. M.For.Sc. thesis, University of Canterbury.
- Addis Tsehaye, Buchanan, A.H. & Walker, J.C.F. (1991). Juvenile Pinus radiata for structural purposes. *J.Ins.Wood Sci.* 12 (4) 211 - 16.
- Addis Tsehaye, Buchanan, A.H. & Walker, J.C.F. (1995a). Stiffness and tensile strength variation within

- and between radiata pine trees. *J.Ins.Wood Sci.* 13 (5) 513-18.
- Addis Tsehaye, Buchanan, A.H. & Walker, J.C.F.(1995b). A comparison of density and stiffness for predicting wood quality. *J.Ins.Wood Sci.* 13 (6) 539 - 43.
- AS1720 (1988). Timber Structure Code, Part 1 - Design methods. Standards Association of Australia, North Sydney.
- Bolden, S, Walsh, R., Grant, D., Leicester, R.H., Young, F. and Seath, C. (1994). In-grade evaluation of Australian pine. *Proc. of Pacific Timber Engineering Conf.*, Gold Coast, Australia. Vol. 2: 716-724.
- Hadi, P. (1992). Proof testing of radiata pine boxed-pith timber. M.For.Sc. thesis, University of Canterbury.
- Instituto Forestal (1990). Availability of radiata pine wood in Chile between 1990 and 2019. Institute of Forestry, Santiago, Chile. Technical Information No.125. (Spanish).
- ISO (1985). Solid timber in structural sizes - Determination of physical and mechanical properties. ISO 8375. International Organization for Standardization, ISO, Geneva, Switzerland.
- Madsen, B. and Buchanan, A.H. (1986). Size effects in timber explained by a modified weakest link theory. *Canadian Journal of Civil Engineering* 13(2) 218 - 32.
- New Zealand Forest Owners Association (1994). Forestry facts and Figures. New Zealand Forest Owners Association, New Zealand Min. of Forestry. Wellington.
- NZS (1993). New Zealand Timber Structures Standard, NZS 3603. Standards New Zealand, Wellington.
- Smith, I., Chui, Y.H., Vincente Perez and Alberto Campos (1993). Machine stress grading of Chilean radiata pine lumber. *J.Ins.Wood Sci.* 13 (2) 386 - 90.
- SAA (1992). Timber- Stress Graded - In-grade Strength and Stiffness Evaluation, AS/NZS 4063. Standards Association of Australia, North Sydney.
- Walford, G.B. (1985). The mechanical properties of New Zealand grown radiata pine for export to Australia. *New Zealand For. Serv., FRI Bulletin No.93*.
- Walford, G.B. (1994). Preliminary results of an in-grade evaluation of juvenile radiata pine. *Proc. of Pacific Timber Engineering Conf.*, Gold Coast, Australia. Vol. 2: 725-30.
- Walford, G.B. (1995). Machine-graded radiata pine evaluated to new standard. *New Zealand Timber Design Journal* 4(1): 10 - 12.
- Walford, G.B. (1996). An in-grade evaluation in compression of machine-graded timber. *Proceedings IPENZ Annual Conference 1996. Dunedin. Volume 1 - Part 1: 186 - 88.*
- West, G.G., Knowles, R.L. and Koeher, A.R. (1982). Model to predict the effects of pruning and early thinning on the growth of radiata pine. *New Zealand For. Serv., FRI Bulletin No.5*.

**INTERNATIONAL COUNCIL FOR BUILDING RESEARCH STUDIES AND DOCUMENTATION
WORKING COMMISSION W18 - TIMBER STRUCTURES**

**TIMBER AS A NATURAL COMPOSITE:
EXPLANATION OF SOME PECULIARITIES IN THE MECHANICAL BEHAVIOUR**

by

E Gehri
Chair of Wood Technology
ETH Zürich
Switzerland

**MEETING THIRTY
VANCOUVER
CANADA
AUGUST 1997**

Timber as a natural composite: explanation of some peculiarities in the mechanical behaviour

Case: Assessment of the modulus of elasticity of timber parallel to grain

E. Gehri, Chair of Wood Technology, ETH Zurich, Switzerland

1. Introduction

For the design of timber structures, the values of the modulus of elasticity parallel to the grain are needed. The characteristic values (mean or 5-percentiles) are normally given in the national design codes. In the frame of european standards they are fixed in EN 338 (solid timber) and EN 1194 (glulam).

It is the prevailing understanding that the modulus of elasticity for wood parallel to the grain should be independent of the type of forces applied: tension, compression or bending actions. Therefore the european standards for solid timber and for homogeneous glued laminated timber foresee a uniform modulus of elasticity parallel to the grain.

Following to Burger/Glos (1995) and based on their data-bank, noticeable differences between the modulus of elasticity (MOE) on bending and on tension were found. They stated the following (free translation):

„The european standards foresee for solid timber and for the three types of actions: tension, compression and bending a uniform value of modulus of elasticity parallel to the grain. It is of general understanding that this value corresponds to the MOE on bending, determined by a bending test according to EN 408. To clear up the correlation with the other modulus of elasticity, the following study has been made“.

Burger/Glos found, between others, for the ratio between the MOE's on bending and on tension – using the procedure given in EN 408 – a value of 1,09. That means that the MOE on bending is about 9 % higher than the corresponding MOE on tension.

No reasons for such an anomaly are given.

2. Actual situation

Most research was done on clear wood. Only reference is made here to Thunell (1941). Under the headline „different modulus of elasticity“ parallel to the grain he states the following:

„The stresses due to normal forces are tensile or compression stresses. A third case are the bending stresses, which may be led back to tensile and compression stresses. From the σ - ϵ -diagramm (see figure 1) it can be seen, that the MOE's on tension and compression, $E_{t,o}$ resp. $E_{c,o}$, are quite the same. Therefore the same value is used for both.“

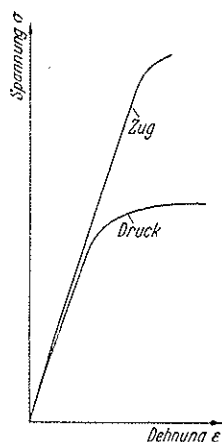


Figure 1: Stress-strain diagramm for clear wood from Thunell (1941)

The MOE on bending ($E_{m,o}$) should therefore correspond to the middle value of $E_{t,o}$ and $E_{c,o}$; therefore the difference between $E_{t,o}$ and $E_{m,o}$ should be even smaller. Furthermore – following to Thunell – the value of $E_{m,o}$ should be smaller than $E_{t,o}$.

Why this contradiction?

Different measuring techniques used for tension and bending may affect the results; higher precision on the measuring devices are required for tension. It seems that a systematic error can be excluded.

Burger/Glos made their measurements on the same portion of the timber element. They found the following relationship:

$$E_{m,o} = 88 + 1,077 \cdot E_{t,o} \quad [\text{in N/mm}^2]$$

with $E_{m,o}$ for edgewise bending.

The correlation found of $R = 0,94$ seems very good, but it has to be noted that for individual specimens extreme values of $E_{m,o} / E_{t,o} = 0,77$ to $1,48$ were found (see figure 2). For the whole collective, a ratio of $1,09$ was calculated.

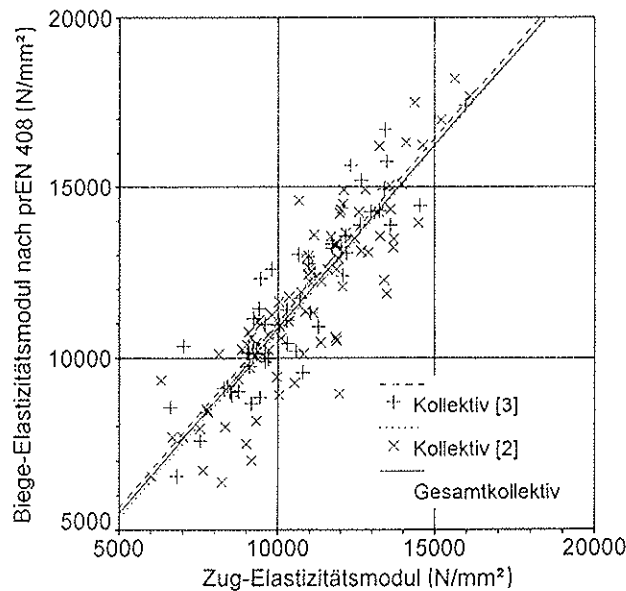


Figure 2: Relationship between MOE on tension and on bending (from Burger/Glos)

The above measured deviations are in contradiction with the results of Thunell. The MOE's on bending and on tension should be the same and are the same for a homogeneous material as clear wood used by Thunell. When using a non-homogeneous material as solid timber or lumber, only an apparent MOE can be determined.

3. Solid timber as composite material

Researchers have made their measurements on small, defect free, homogeneous specimens. Of course nowadays are made the measurements on larger specimens of solid timber, but considerations are made as when the material tested is still homogeneous like small wood specimens and not as the tested composite material „structural timber“.

Structural timber is produced from round wood through sawing. Therefore a few facts must be considered (see figure 3):

- The raw-material round wood is a composite material with a more or less rotary-symmetrical structure;
- The mechanical properties parallel to the grain increase from the center to the border of the round wood.

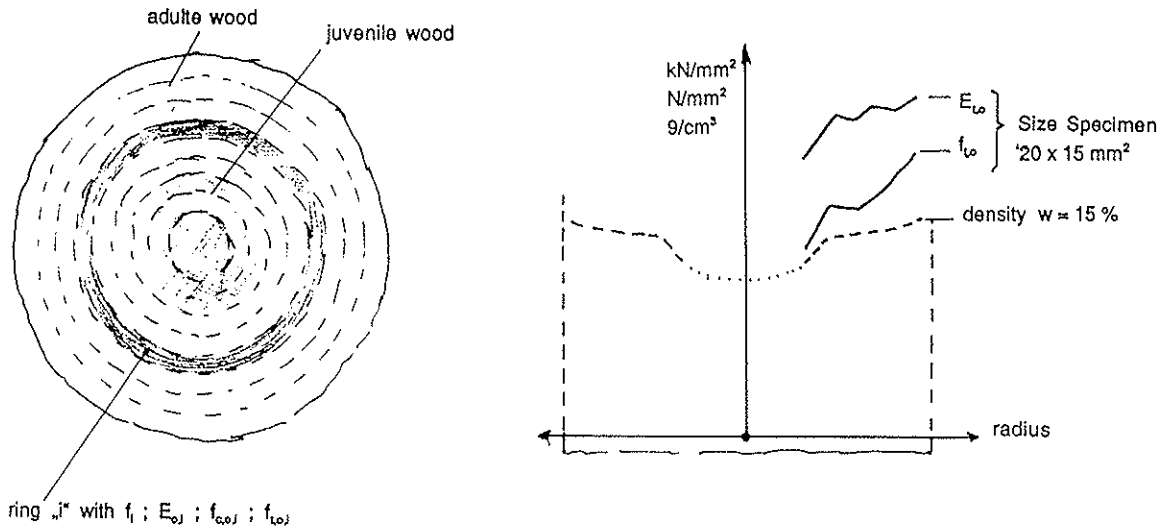


Figure 3: Round wood as a composite material

The above structure of the section has an excellent behaviour when considering the different age stages of the tree and the varying direction of the bending forces. This structure will now be differently disturbed depending on the cutting pattern. Following the position of the sawn timber, different behaviour and different apparent MOE will be obtained (see figure 4).

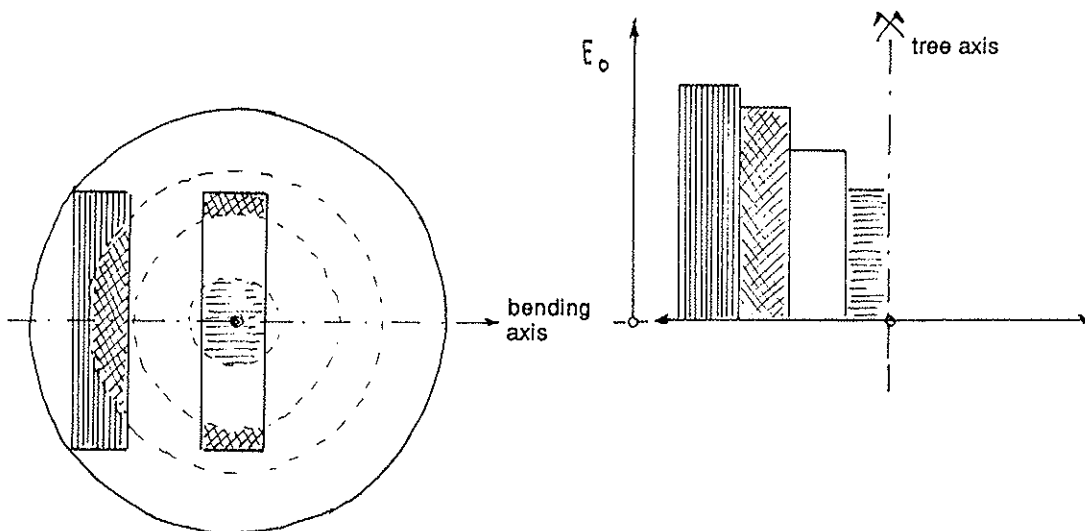


Figure 4: Differences between side board and pith board

The two typical boards: side and with pith are differently composed. Not only the side boards are stronger and stiffer than boards with pith but they show a different ratio between MOE on bending to MOE on tension.

It is interesting to note that glued laminated timber has been recognized as composite material. The same should be done for solid wood, at least to understand the measured differences in MOE's in bending and in tension.

4. Conclusions

The modulus of elasticity of wood (small clear specimens) parallel to the grain is independent of the type of actions involved (compression, tension or bending). When looking on round wood the material has to be considered as a composite material. The measured properties depend on the lay-up of the section.

The same is valid for sawn timber or structural timber cut-out from such a composite material with rotary-symmetrical lay-up; cutting pattern plays therefore an important role.

By cutting the boards according to figure 5.a it can be expected that the apparent MOE on edgewise bending is about 10 to 15 % higher than the apparent MOE in tension. A more detailed information about the influence of the position of the board on the apparent modulus of elasticity is given in Gehri et al (1997).

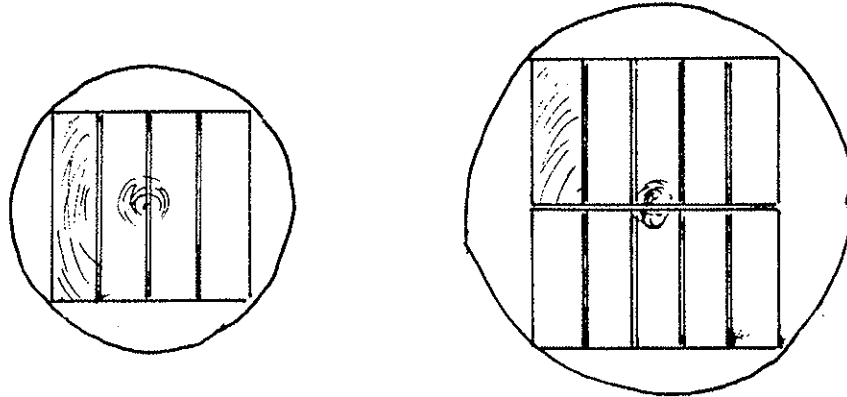


Figure 5: Influence of the cutting pattern on the apparent modulus of elasticity using the same composite raw-material

The higher apparent MOE on bending of the composite sections following the cutting pattern in figure 5a is a logical consequence of the position of the stiffer layers in the outside parts of the section, where they are more effective on bending.

5. References

- Burger, N./Glos, P.: Verhältnis zwischen Zug- und Biege-Elastizitätsmoduln von Vollholz. Holz als Roh- und Werkstoff, 1995, S. 73-74.
- Gehri, E./Fabris, A./ Scapozza, C.: Höhere Wertschöpfung beim Einschnitt von Rundholz (in Ausarbeitung).
- Thunell, B.: Über die Elastizität schwedischen Kiefernholzes. Holz als Roh- und Werkstoff, 1941, S. 15-18.

**INTERNATIONAL COUNCIL FOR BUILDING RESEARCH STUDIES AND DOCUMENTATION
WORKING COMMISSION W18 - TIMBER STRUCTURES**

**FLEXURAL BEHAVIOUR OF GLT BEAMS END-JOINTED BY
GLUED-IN HARDWOOD DOWELS**

by

K Komatsu
Wood Research Institute
Kyoto University
A Koizumi, T Sasaki, J L Jensen, Y Iijima
Institute of Wood Technology
Japan

MEETING THIRTY

VANCOUVER

CANADA

AUGUST 1997

Flexural Behavior of GLT Beams End-Jointed by Glued-in Hardwood Dowels

Kohei Komatsu^{*1}

^{*1}:Wood Research Institute, Kyoto University, Gokasyou, Uji, Kyoto,611 JAPAN

Akio Koizumi^{*2}, Takanobu Sasaki^{*2}, Jørgen L. Jensen^{*2,*3} and Yasuo Iijima^{*2}

^{*2}:Institute of Wood Technology, Akita Prefectural College of Agriculture,
11-1 Kaieizaka, Noshiro, Akita, 016 JAPAN

^{*3}:Visiting Research Scientist from Denmark

1 Introduction

Recent in Japan, hardwood dowel has been getting a new reputation as an alternative jointing device for engineered timber joints because it can be harmonized with timber structural members more gently than such jointing system as steel drift-pins or bolts with steel gusset plates. As the first step of utilizing this natural jointing device for engineered timber structures, a series of pull-out shear strength test has been done on single dowel joints glued with polyurethane adhesive (Koizumi et al. 1997).

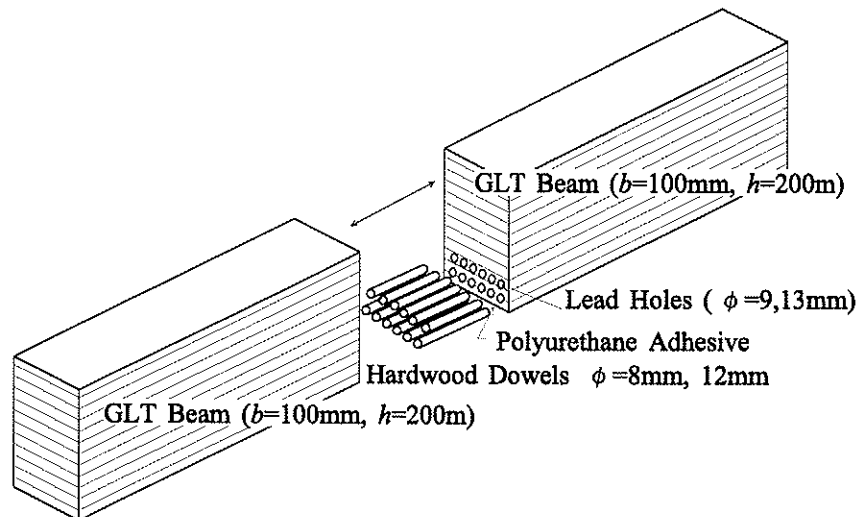


Fig.1 End-jointed GLT beams using adhesive and hardwood dowels.

This paper follows after the first step mentioned above, and gives preliminary results on the theoretical prediction of flexural behavior of GLT beams which were end-jointed using several hardwood dowels with polyurethane adhesive as shown in Fig.1.

2. Theory

2.1 Determination of Neutral Axis

Figure 2 shows the strain and stress distribution along the cross section of the end-jointed GLT beam. Strain at the i -th dowel line ϵ_{iT} is expressed as equation 1);

$$\epsilon_{iT} = \frac{g_i - \lambda}{\rho} \quad (i=1,2,3) \dots 1)$$

where,

g_i : distance from compression outer surface to the center of i -th dowel line ($i=1,2,3$)
 λ : distance from compression outer surface to the neutral axis ($N-N$).
 ρ : radius of curvature of GLT beam.

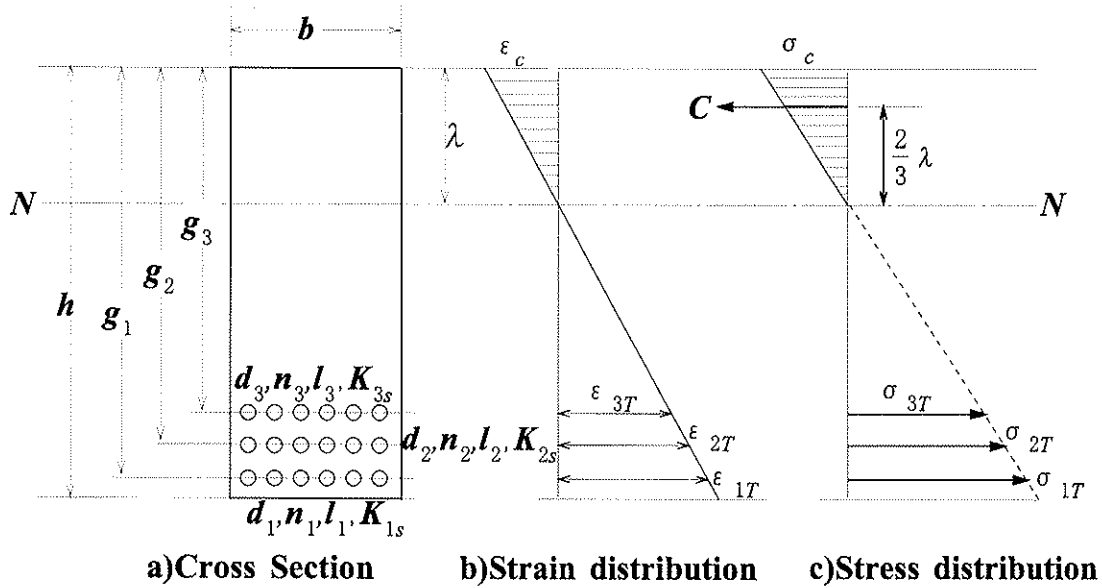


Fig.2 Strain and stress distribution.

Putting E_{iT} as an apparent modulus of elasticity along the i -th dowel line, the stress corresponding to the strain ϵ_{iT} is;

$$\sigma_{iT} = E_{iT} \cdot \epsilon_{iT} = E_{iT} \frac{(g_i - \lambda)}{\rho} \quad (i=1,2,3) \dots 2)$$

On the other hand, strain at the most outer surface of compression side ϵ_c is;

$$\epsilon_c = \frac{\lambda}{\rho} \dots 3)$$

Putting E_w as the modulus of elasticity of glulam member, the stress corresponding to the strain ϵ_c is;

$$\sigma_c = E_w \frac{\lambda}{\rho} \dots 4)$$

The resultant compression force C is;

$$C = b \int_0^\lambda \frac{y}{\lambda} \sigma_c dy = \frac{b E_w \lambda^2}{2 \rho} \dots 5)$$

While, the resultant tensile force T_i which is to be sustained by the i -th dowel line is;

$$T_i = \sigma_{iT} \cdot A_{id} \cdot n_i = \frac{E_{iT} A_{id} n_i (g_i - \lambda)}{\rho} \dots 6)$$

where,

A_{id} : cross sectional area of the hardwood dowel belonging to the i -th line.

n_i : number of dowels belonging to the i -th line.

In fact, however, the apparent modulus of elasticity E_{iT} at the i -th dowel line should be related to the displacement (slip S_i) of the hardwood dowel which is to be pulled out

from glulam member by the tensile force q_i as shown in Fig.3.

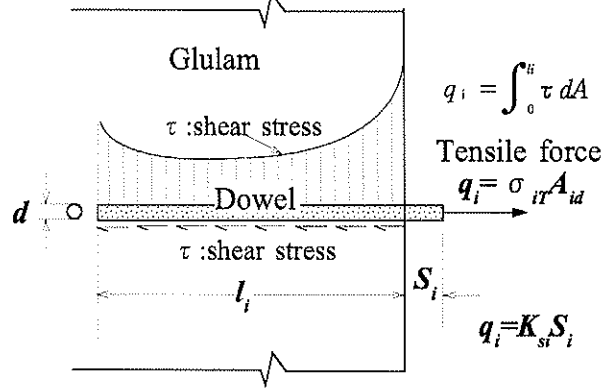


Fig.3 Dowel's displacement (slip) S_i due to tensile force q_i

It might be reasonable to assume a linear relationship between tensile force q_i and dowel's displacement (slip) S_i as equation 7)

$$q_i = \sigma_{iT} A_{id} = K_{si} \cdot S_i \dots 7)$$

where, K_{si} is the slip modulus of glued-in dowel which is to be evaluated by a series of pull-out tests on single glued-in dowel joints (Koizumi et al. 1997).

From equation 7);

$$\sigma_{iT} = \frac{K_{si}}{A_{id}} S_i \dots 7)'$$

The apparent mean tensile strain ϵ_{iT} at the i -th dowel line might be defined as;

$$\epsilon_{iT} = \frac{S_i}{l_i} \dots 8)$$

where,

l_i : embedding length of i -th dowel

From equations 7)' and 8);

$$\sigma_{iT} = \frac{K_{si}}{A_{id}} S_i = \frac{K_{si} l_i}{A_{id}} \epsilon_{iT} \dots 9)$$

By considering the apparent Hooke's law for σ_{iT} and ϵ_{iT} , we can express the apparent modulus of elasticity E_{iT} by slip modulus of the dowels as;

$$E_{iT} = \frac{K_{si} l_i}{A_{id}} \text{ or } E_{iT} A_{id} = K_{si} l_i \dots 10)$$

Thus, the resultant tensile force T_i can be expressed as;

$$T_i = \frac{E_{iT} A_{id} n_i (g_i - \lambda)}{\rho} = \frac{K_{si} l_i (g_i - \lambda) n_i}{\rho} \dots 11)$$

The equilibrium condition of the resultant forces is;

$$C = \sum_{i=1}^3 T_i \dots 12)$$

Substituting equations 5) and 11) into equation 12), we obtained the following equation

for determining the location of the neutral axis λ .

$$\lambda^2 + 2\beta\lambda + \mu = 0 \quad \dots 13)$$

Thus, the location of neutral axis was derived as follows;

$$\lambda = -\beta + \sqrt{\beta^2 + \mu} \quad \dots 14)$$

where,

$$\beta = \frac{\sum K_{s,i} l_i n_i}{bE_w} \quad \dots 15)$$

$$\mu = \frac{2\sum g_i K_{s,i} l_i n_i}{bE_w} \quad \dots 16)$$

2.2 Moment-Resisting Capacity

The equilibrium condition between external moment and internal moment is;

$$M = \frac{2}{3} \lambda C + \sum_{i=1}^3 (g_i - \lambda) T_i \quad \dots 17)$$

By considering equation 12), M can be expressed by the tensile force q_i acting on each hardwood dowels as;

$$M = \sum_{i=1}^3 (g_i - \frac{\lambda}{3}) q_i n_i \quad \dots 18)$$

where,

q_i : tensile force per dowel ($i=1,2,3$)

n_i : number of dowel at i -th dowel line

The maximum pull-out strength of dowels q_{i-max} depends on many parameters such as dowel diameter d_i , dowel embedment length l_i , and combination of mechanical properties of adhesive and timber used. Thus the following three possibilities for predicting maximum moment-resisting capacity of end-jointed GLT beams should be considered;

a) Case-1: in the case when dowel line 1 ($i=1$) reaches its maximum value

$$M_{max} = q_{1-max} \left\{ n_1 \left(g_1 - \frac{\lambda}{3} \right) + n_2 \left(g_2 - \frac{\lambda}{3} \right) \left(\frac{g_2 - \lambda}{g_1 - \lambda} \right) + n_3 \left(g_3 - \frac{\lambda}{3} \right) \left(\frac{g_3 - \lambda}{g_1 - \lambda} \right) \right\} \quad \dots 19)$$

b) Case-2: in the case when dowel line 2 ($i=2$) reaches its maximum value

$$M_{max} = q_{2-max} \left\{ n_1 \left(g_1 - \frac{\lambda}{3} \right) \left(\frac{g_1 - \lambda}{g_2 - \lambda} \right) + n_2 \left(g_2 - \frac{\lambda}{3} \right) + n_3 \left(g_3 - \frac{\lambda}{3} \right) \left(\frac{g_3 - \lambda}{g_2 - \lambda} \right) \right\} \quad \dots 20)$$

c) Case-3: in the case when dowel line 3 ($i=3$) reaches its maximum value

$$M_{max} = q_{3-max} \left\{ n_1 \left(g_1 - \frac{\lambda}{3} \right) \left(\frac{g_1 - \lambda}{g_3 - \lambda} \right) + n_2 \left(g_2 - \frac{\lambda}{3} \right) \left(\frac{g_2 - \lambda}{g_3 - \lambda} \right) + n_3 \left(g_3 - \frac{\lambda}{3} \right) \right\} \quad \dots 21)$$

In deriving equations 19), 20) and 21), the following relationship among tensile forces q_1 , q_2 , and q_3 was assumed as shown in Fig.4

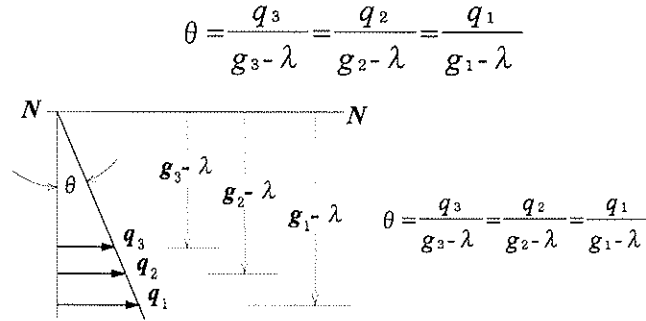


Fig.4 Relationship among tensile forces Q_i .

2.3 Rotational Rigidity of the End Joint

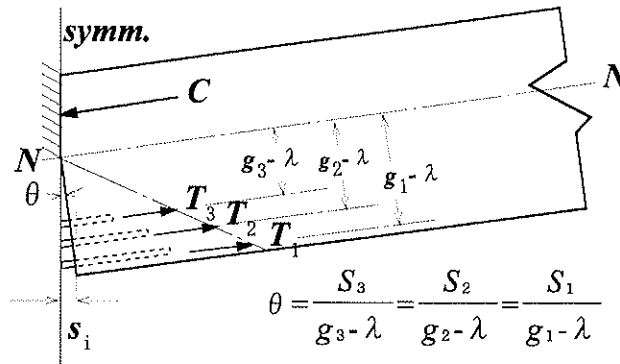


Fig.5 Rotation at the end-joint

By referring the schematic model for the rotation at the end-joint shown in Fig.5, the half rotation angle θ at the end-jointed part can be approximately defined as;

$$\theta = \frac{S_i}{g_i - \lambda} \dots 22)$$

Substituting equations 7), 22) into equation 18), following relationship between the external moment M and the half rotation angle θ is obtained;

$$M = \left\{ \sum \left(g_i - \frac{\lambda}{3} \right) (g_i - \lambda) n_i K_{s_i} \right\} \theta \dots 23)$$

Thus, the rotational rigidity R_J of half side of end-joint in GLT beam is defined as;

$$R_J = \sum_{i=1}^3 \left(g_i - \frac{\lambda}{3} \right) (g_i - \lambda) n_i K_{s_i} \dots 24)$$

2.4 Mid-Span Deflection of End-Jointed GLT Beam

According to the virtual work theory, mid-span deflection of beam having any joints whose rotational rigidity is R_{Ji} can be estimated as follows;

$$\delta = \int \frac{MM}{EI} dx + \int \kappa \frac{QQ}{GA} dx + \sum \frac{M_{Ji} \overline{M}_{Ji}}{R_{Ji}} \dots 25)$$

where,

M : moment in members due to external force

\overline{M} : moment in members due to unit load applied at where the deflection δ is assigned.

Q : shear force in members due to external force

\overline{Q} : shear force in members due to unit load (same as the case of \overline{M})

M_i : moment at i-th joint due to external force

\overline{M}_i : moment at i-th joint due to unit load (same as the case of \overline{M})

R_i : rotational rigidity of i-th joint

E : modulus of elasticity of members. G : modulus of rigidity of members

A : cross sectional area of members. I : moment of inertia of members

κ : shape coefficient for shear deformation (=1.2 for rectangular section)

In the case of four points bending tests used in this research shown in Fig.7, the mid-span deflection δ is derived as follows;

$$\delta = \frac{P(3l_s L^2 - 4l_s^3)}{48EI} + \frac{\kappa Pl_s}{2GA} + \frac{Pl_s L}{4R_j} \dots 26)$$

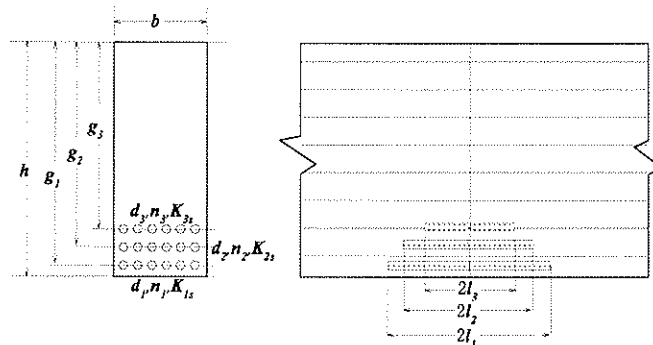
where,

l_s : shear span defined in Fig.7 In equation 26), notice should be paid that the number of end-joint was counted as "two".

3. Experiments

3.1 Test Specimens

Figure 6 shows number and location of dowels in test specimens.



Specimen	d (mm)	g_1 (mm)	n_1	l_1 (mm)	K_{s1} (kN/m m)	q_{1m11} (kN)	g_2 (mm)	n_2	l_2 (mm)	K_{s2} (kN/m m)	q_{2m11} (kN)	g_3 (mm)	n_3	l_3 (mm)	K_{s3} (kN/m m)	q_{3m11} (kN)
No.1 ~ No.3	8	184	6	80	11.8	9.61	168	6	48	9.16	7.46	—	0	—	—	—
No.4 ~ No.6	8	184	6	80	11.8	9.61	168	6	48	9.16	7.46	—	0	—	—	—
No.7 ~ No.9	8	184	6	80	11.8	9.61	—	0	—	—	—	—	0	—	—	—
No.10 ~ No.12	8	184	6	80	11.8	9.61	168	6	48	9.16	7.46	152	6	29	6.26	5.10
No.13 ~ No.15	12	182	4	120	22.93	18.68	158	4	72	18.97	15.45	—	0	—	—	—

Fig.6 Number, location and tensile strength of dowels in test specimens

Fifteen joint specimens were prepared using Japanese Cedar (*Cryptomeria japonica*) GLT beams which were originally produced in Institute of Wood Technology, Akita prefecture. Mean MOE value of GLT beams used was 8.2GPa. While, mean MOE value of hardwood dowels made of Japanese maple (*Acer mono*) was 15GPa.

3.2 Bending Test Method

Figure 7 shows a four points bending test set-up for joint specimens.

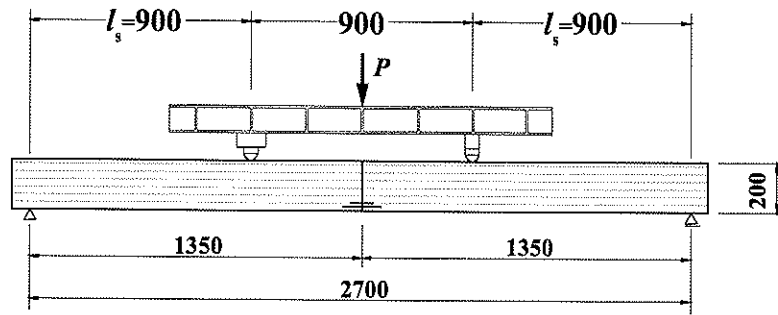


Fig.7 Four points bending test set-up.

One-sided static cyclic loads shown as follows were applied;

- 1st cycle : 0 \Leftrightarrow $\sigma_x = 5\text{MPa}$
- 2nd cycle : 0 \Leftrightarrow $\sigma_x = 10\text{MPa}$
- 3rd cycle : 0 \Leftrightarrow $\sigma_x = 15\text{MPa}$
- Last cycle : 0 \rightarrow P_{\max} (σ_x : most outer fiber stress)

4 . Results and Discussion

Figure 8 shows some comparisons between observed load(P)- deflection(δ) relationship and calculated ones.

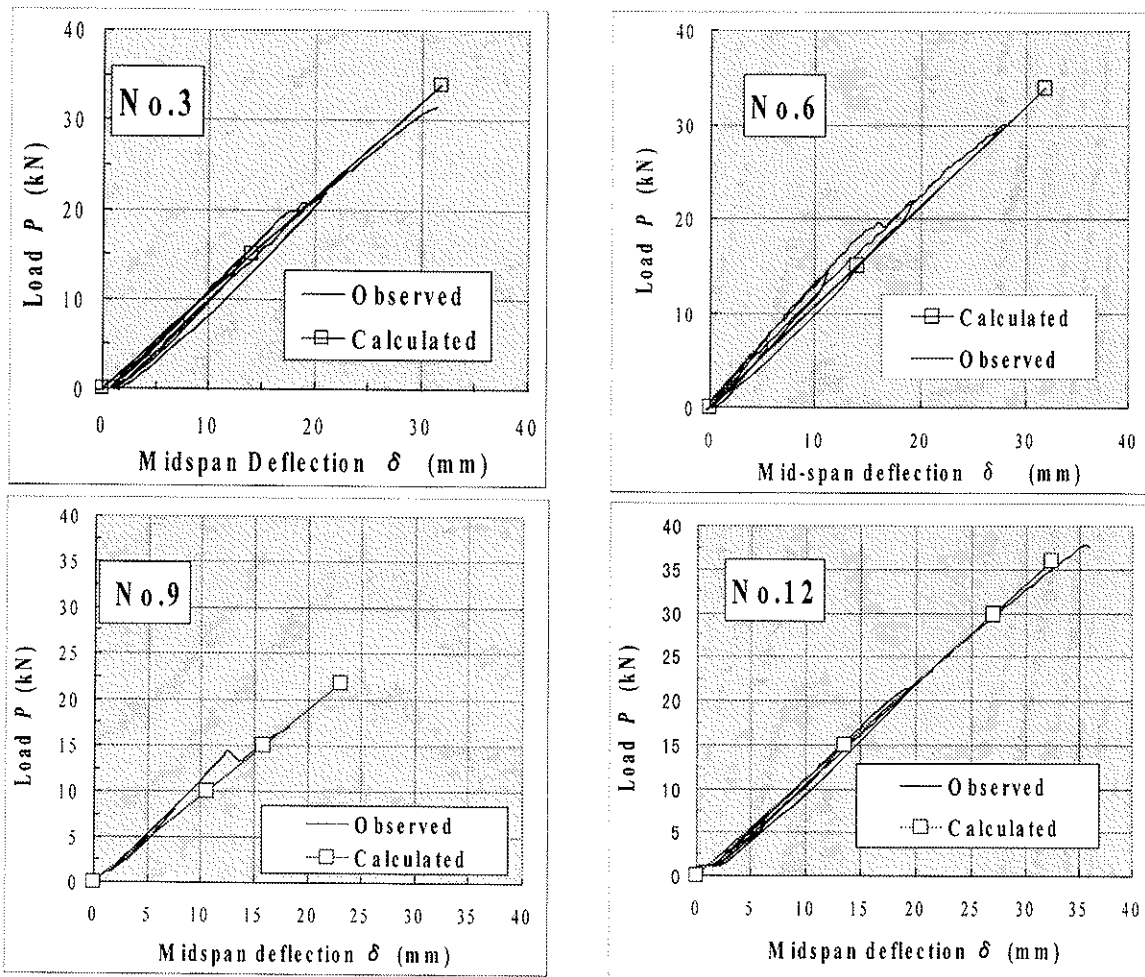


Fig. 8 Comparisons between observed load(P)- mid-span deflection(δ) relationship and predicted ones

Relatively good agreements were obtained for the specimens in which dowels of 8mm diameters were used (No.1-No.12). Contrary to this, however, exceptions were observed for the cases of specimens which were composed of dowels of 12mm diameter as shown in Fig.9. It is not clear why this big discrepancy happened.

Fig.9

Comparison between observed load(P)- midspan deflection(δ) relationship and predicted one for the case of specimen composed of 12mm dowels.

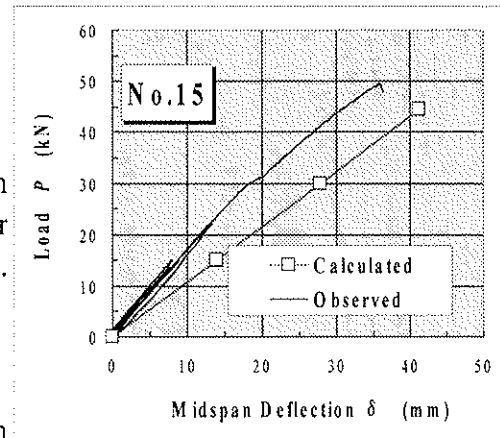


Table 1 shows total results for maximum moment-resisting capacity as well as for deflection. Agreements between observed maximum moment-resisting capacity and predicted ones were not so bad, while for deflection there were uncertain disagreements for the particular specimens.

Table 1 Total results

Specimen No.	d (mm)	λ (mm)	$P_{max-cal}$ (kN)	$P_{max-obs}$ (kN)	P_{obs}/P_{cal}	δ_{member} (mm) at $P=15kN$	R_j (kNm m/rad.)	δ_{joint} (mm) at $P=15kN$	$\delta_{total-cal}$ (mm) at $P=15kN$	δ_{obs} (mm) at $P=15kN$	$\delta_{obs}/\delta_{cal}$
No.1	8.0	50.9	33.93	28.19	0.831	10.47	2546407	3.58	14.05	13.84	0.985
No.2	8.0	50.9	33.93	28.95	0.853	10.47	2546407	3.58	14.05	14.37	1.023
No.3	8.0	50.9	33.93	31.51	0.929	10.47	2546407	3.58	14.05	14.55	1.035
No.4	8.0	50.9	33.93	28.77	0.848	10.47	2546407	3.58	14.05	13.44	0.956
No.5	8.0	50.9	33.93	28.22	0.832	10.47	2546407	3.58	14.05	14.28	1.016
No.6	8.0	50.9	33.93	30.48	0.898	10.47	2546407	3.58	14.05	12.78	0.909
No.7	8.0	44.0	21.71	15.31	0.705	10.47	1679034	5.43	15.90	13.97	0.879
No.8	8.0	44.0	21.71	16.42	0.756	10.47	1679034	5.43	15.90	15.50	0.975
No.9	8.0	44.0	21.71	16.92	0.780	10.47	1679034	5.43	15.90	15.62	0.982
No.10	8.0	53.0	35.99	36.21	1.006	10.47	2992304	3.05	13.52	14.65	1.084
No.11	8.0	53.0	35.99	36.34	1.010	10.47	2992304	3.05	13.52	13.25	0.980
No.12	8.0	53.0	35.99	37.78	1.050	10.47	2992304	3.05	13.52	14.00	1.036
No.13	12.0	65.9	44.49	38.71	0.870	10.47	2654702	3.43	13.91	9.05	0.651
No.14	12.0	65.9	44.49	49.05	1.103	10.47	2654702	3.43	13.91	9.54	0.686
No.15	12.0	65.9	44.49	49.55	1.114	10.47	2654702	3.43	13.91	7.90	0.568

5. Conclusions

In this report, equations, for predicting maximum moment-resisting capacity as well as deflection of GLT beams which are end-jointed using glued-in hardwood dowels with polyurethane adhesive, were derived based on the RC beam assumptions. Agreements between theoretical predictions and experimental observations were not so bad except one particular case for the specimens composed of 12mm dowels. This discrepancy should be investigated more deeply to obtain better theoretical model.

References

Koizumi, A. et al. : "On Shear Strength of Glue-in-Dowel Joints", to be published in the Journal of Japan Wood Research Society.

**INTERNATIONAL COUNCIL FOR BUILDING RESEARCH STUDIES AND DOCUMENTATION
WORKING COMMISSION W18 - TIMBER STRUCTURES**

**MODELLING OF THE BLOCK TEARING FAILURE
IN NAILED STEEL-TO-TIMBER JOINTS**

by

J Kangas
VTT Building Technology
K Aalto
A Kevarinmäki
Helsinki University of Technology(HUT)
Finland

MEETING THIRTY

VANCOUVER

CANADA

AUGUST 1997

Modelling of the Block Tearing Failure in Nailed Steel-to-Timber Joints

by

Jorma Kangas

VTT Building Technology,

Katariina Aalto and

Ari Kevarinmäki

Helsinki University of Technology (HUT)

Finland

Abstract

Block tearing failure mode has been found in the testing of nailed steel-to-timber joints with small nail spacings. The capacity of the nailed connection with given spacings depends on the nail capacity up to a certain joint length, after which the block tearing failure may occur, i.e., a block of timber will be cut out from the joint. The increase in the joint capacity due to additional nails will be less than the full capacity of nails.

The length of the connection is determined by this turning point, where the limiting factor of capacity changes from the capacity of nails to that of timber. A common way to model this kind of behaviour has been to multiply the capacity of a single nail by a reduction factor after this changing point.

This paper presents a method for modelling the block tearing failure and for designing the capacity of the connection. The model depends on the block tearing mode and on the dimensions of the timber torn off from the timber member. The capacity of the joint is limited by the sum of the nail capacities and by the sum of the tensile and shear capacities of the timber in the joint area.

Nail spacings and distances can be chosen to achieve the optimum capacity of the joint, without the unfavourable block tearing failure mode occurring. The maximum capacity of the nails can also be utilized without any reduction in the effective number of nails. A suitable reduction of the nails will increase the capacity of the connection.

1 Introduction

Multiple Nail Connectors (MNC) and Kerto-S-LVL have been used in the first phase to model the block tearing failure of steel-to-timber joints in tension. These test results (e.g., Väänänen et al. 1995, Ehlbeck 1992 & 1987, Kalliomäki et al. 1986) and a proposed model derived from them have already been presented by Kangas et al. (1996). To generalize and verify this design method, more joint tests were conducted using either sawn timber, Kerto-S-LVL or Kerto-Q-LVL as the timber member, and perforated steel plates with round profiled nails as fasteners. These tests were conducted at VTT in the spring of 1997 (Aalto et al. 1997). Other test results presented and analysed here are the following: "Multi-Krallen-Dübel (MKD) als Holzverbindungsmitel", tests carried out with MNC connectors and Kerto-S-LVL, Kerto-Q-LVL or glued laminated timber (Ehlbeck 1992); "Tests with

Multiple Nail Connectors used as fasteners for load-bearing timber members”, a test report from which results of glued laminated timber will be analysed (Ehlbeck 1987).

According to Eurocode 5, the capacity of bolted or dowelled joints with more than six fasteners in line with the load direction will have reduced capacity per fastener. The capacity of these extra fasteners is 2/3 of their full capacity (Eurocode 5 1993). No such reduction is suggested for nailed connections, yet certain reduction factors have been used for MNC connectors, e.g., in Germany. The new test results presented in this paper (Aalto et al. 1997) also suggest that a reduction in nailed connections is needed, and should be taken into account when modelling the block tearing failure capacity of the joint area.

2 Joint Members

2.1 Timber Members: LVL, Sawn Timber and Glulam

Laminated veneer lumber (LVL) is a product consisting of 3 mm thick spruce veneers bonded together with fenol-resin adhesive. The orientation of veneers can be parallel in the longitudinal direction of the LVL member (Kerto-S-LVL), or partly parallel and partly perpendicular (Kerto-Q-LVL). For example, in a 63 mm thick Kerto-Q-LVL, five out of the 21 veneers are cross veneers. On average, the percentage of cross veneers in Kerto-Q-LVL is approximately 20. Due to this, the strength properties of Kerto-Q-LVL are different from those of Kerto-S-LVL. The average density (ρ_w) and the average moisture content (ω) used for all the analysed Kerto-LVL, as well as the characteristic strength values are presented in Table 1.

Table 1 - Average density, average moisture content and characteristic strength values of timber members analysed.

Material	ρ_w (RH=65%) kg/m ³	ω %	f_{t0} Nmm ²	f_{v0} N/mm ²
Kerto-S-LVL	520	10	42	3.0 ¹⁾
Kerto-Q-LVL	520	10	30	1.5 ²⁾
Glulam	460	11.8	40	3.8
Heavy spruce	495	13.8	40	3.8
Light spruce	380	12.8	30	2.5

¹⁾ flatwise shear strength of parallel veneers (Ranta-Maunus 1995)

²⁾ rolling shear strength of cross veneers (Ranta-Maunus 1995)

In the tests carried out at VTT with nailed joints, sawn timber was used as joint members in comparison to Kerto-LVL. The joint area of test pieces made of spruce was selected so that no large knots were left in the middle of the nailed area. Both light and heavy spruce were used in these tests. The frequency and size of knots was considerably less in heavy spruce than in light spruce. Table 1 shows the average density and moisture content, as well as the characteristic strength values used for timber materials in the analysis.

Glued laminated timber was used in the tests conducted at Karlsruhe University in 1987 and 1992. The average density and the average moisture content at the time of the testing and the strength values used are presented in Table 1.

2.2 Connectors: Nailed Perforated Steel Plates and MNC Connectors

In the tests conducted at VTT, the steel plates used were made of plain structural steel (Fe 52 D) and of two thicknesses: 4 mm and 6 mm depending on the nails chosen. The nails used were BMF 4.0×40 mm and BMF 6.0×60 mm annular ringed shank nails with penetration lengths of 36 mm and 54 mm, respectively (see Figure 1). The diameter and depth of predrilled holes in timber were 3.5 mm and 30 mm for 4.0×40 nails, and 5.0 mm and 50 mm for 6.0×60 nails. The diameter of predrilled holes in steel plates was 4.3 mm and 6.5 mm, respectively.



Figure 1 - BMF annular ringed shank nails.

Multiple Nail Connectors (MNC) are connectors originally created for long-span trusses made of Kerto-LVL. The connector consists of a 10 mm thick steel plate with 50 mm long flat cone nails. The nails are rectangular in shape ($3.0 \times 4.0 \text{ mm}^2$) and welded perpendicularly on both sides of the plate. Each nail has a 4 mm long cone in the base to increase its effective length, and the longer sides of nails are profiled to increase the anchorage strength. Steel plates are of structural steel Fe 52 D.

3 Tests of Nailed Joints

3.1 Test Programme

Twenty-one test series were conducted altogether, 14 of which were done with 4 mm nails and seven with 6 mm nails. Kerto-S-LVL and Kerto-Q-LVL were both used in six series and sawn timber (spruce) in nine series. All test series consisted of three parallel test pieces, except for series with heavy spruce (2×2 test pieces). Test series were labelled as series A, B, C and D according to the joint type used (see Figure 2). Table 2 shows the nail arrangement and the effective width of the nailed area in each series.

Table 2 - Test programme: nail arrangements and effective widths of nailed area.

Series	Nails 4.0×40 mm		Nails 6.0×60 mm	
	Nail rows × nails in a row, $n_l \times n_b$	Effective width b_{ef} , mm	Nail rows × nails in a row, $n_l \times n_b$	Effective width b_{ef} , mm (see Page 7)
A	3 × 7	89	3 × 5	87
B	7 × 13	65	7 × 9	63
C	3 × 13	65	3 × 9	63
D	6 × 8	85	6 × 6	81

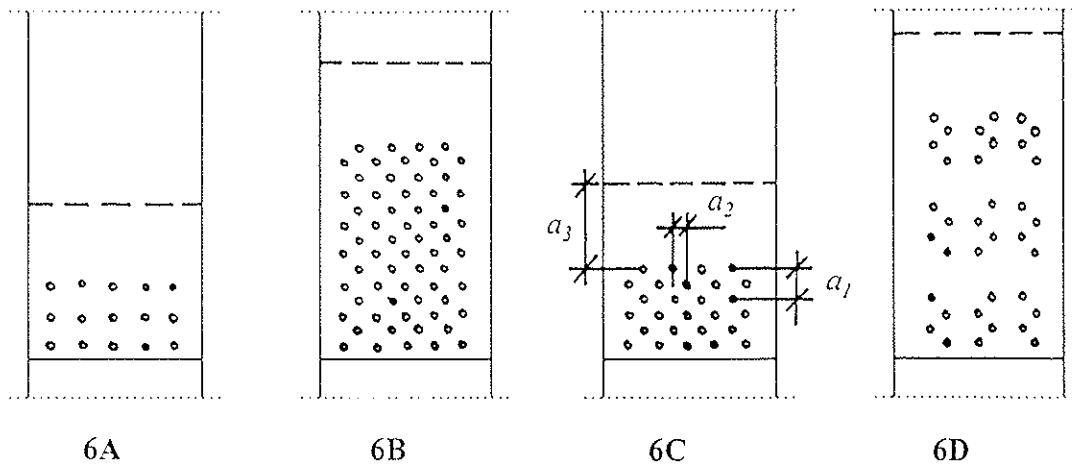


Figure 2 - Joint type of each test series, 6.0×60 mm nails.

3.2 Test Pieces and Test Arrangements

Test pieces consisted of one timber member and one steel plate nailed to it. All test pieces were made by hand using a drilling machine in the predrilling of holes prior to nailing, and were tested shortly after their construction. The total width of test pieces was 150 mm, whereas the thickness (either 45 mm or 63 mm) and the length of timber member varied according to the nail spacing used. The minimum length of a timber member was 1 m. In all the series with sawn timber, two out of three test pieces were nailed on the heartwood side and one on the sapwood side of the timber member.

Nail spacings were chosen according to Eurocode 5 (Table 6.3.1.2a), resulting in staggered nail rows. In series B and C, the minimum spacings and distances of predrilled holes were used, along with the reduction factor (0.7) due to the use of a steel member. In series D, the reduction factor was neglected. Since the steel plates were perforated according to one pattern only (the minimum nail density), this nail arrangement was achieved by leaving some of the nail rows and lines unnailed. The average nail spacings corresponded, however, to the nail density desired. In series A, nails were placed in straight rows with the nail spacing of a_2 being twice the minimum, in order to obtain pure yield of nails.

Table 3 shows examples of nail spacings and distances, as well as relative nail areas for Kerto-LVL members. The concept of relative nail area is used here to describe the density of nails used in each test series, in comparison to the minimum density by EC 5.

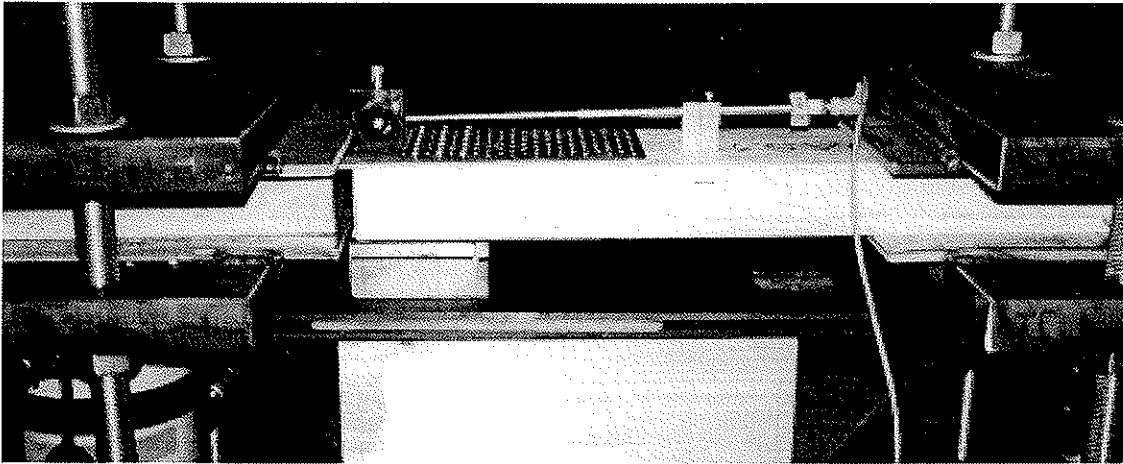
Tension tests were performed so that specimens were pulled with a hydraulic jack at a constant speed of 7...25 kN min directly to failure. The duration of tests was 5...10 min. Deformations of connections were measured with one inductive measuring gauge with a measuring range of ± 10 mm. Since the joint geometry was chosen to be asymmetrical (single shear), a simple support made of ball bearings was provided on the free side of the joint. The test arrangements are presented in Figure 3.

Table 3 - Nails spacings, distances and relative nail areas of Kerto-LVL members.

	Minimum values of EC5	Nail spacings used, mm			Relative nail area $(a_1 \times a_2)_{series} / (a_1 \times a_2)_{EC5}$		
		Series			Series		
		A	B&C	D	A	B&C	D
a_1	$4.9d$	$5d$	$5d$	$5d$ or $10d$	2.0	1.0	2.0
a_2	$2.1d$	$4.2d$	$2.1d$	$2.1d$ or $4.2d$			
a_3	$12d$	$12d$	$12d$	$12d$			
a_4	$3d$	$> 3.8d$	$> 3.8d$	$> 3.8d$			

Parameters in Table 3: a_1 = spacing parallel to the grain direction
 a_2 = spacing perpendicular to the grain
 a_3 = distance from the loaded end of timber member
 a_4 = distance from the loaded edge of timber member

(a)



(b)

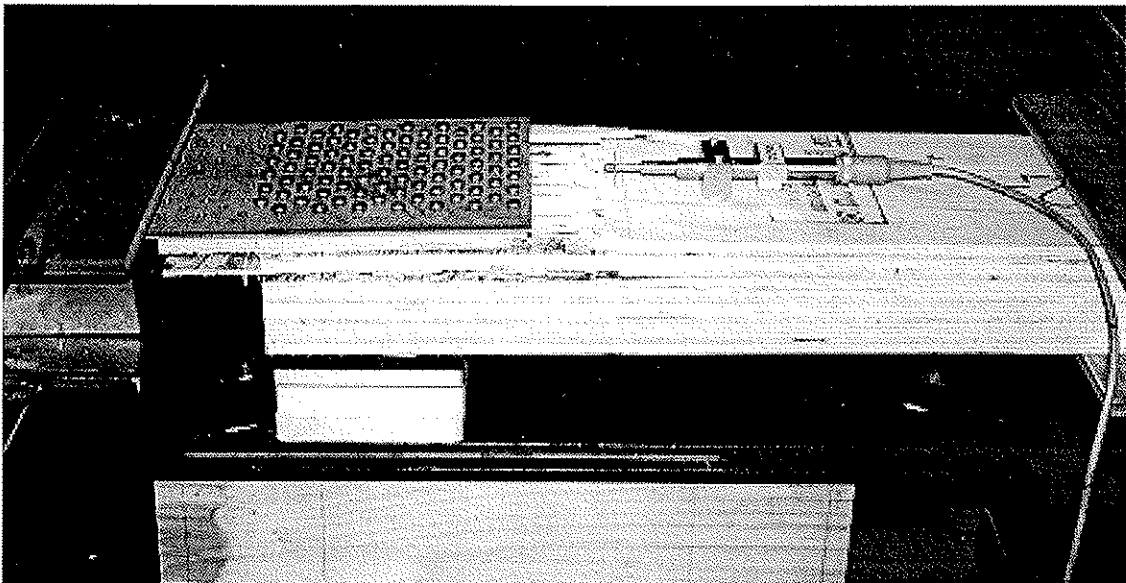


Figure 3 - Test arrangements: Test pieces (a) prior to and (b) after testing.

4 Load-Carrying Capacity of Nailed Steel-to-Timber Joints

4.1 Material Properties and Nail Capacities

The embedding strength ($f_{h,d}$) for all fasteners presented in this paper can be calculated according to Eurocode 5 (equations 6.3.1.2a and 6.3.1.2b) based on Johansen's theory. Parameters affecting this material property are the nail diameter (d) and timber density (ρ_k). The equations given in EC5 are for timber, but can also be used for Kerto-LVL.

The yield moment of annular ringed shank nails have been calculated according to the following formula, given by the manufacturer:

$$M_{y,k} \geq 6.7 \cdot (20-d) \cdot d^3 \text{ Nmm.} \quad (1)$$

A joint made of a thick steel plate and nails represents a rigid connection. A typical yield mechanism of such a joint is one with two plastic hinges - one at the interface of the plate and timber and the other at a distance t_{ef} from this interface. A free-body diagram of a nail in single shear is shown in Figure 5 (Hilson 1995).

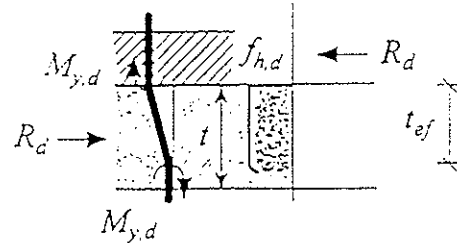


Figure 5 - A free-body diagram of a nail with two plastic hinges.

4.2 Modelling of the Peeling

In the peeling failure of a steel-to-timber joint, a block of timber is torn off from the timber member. The width of this block corresponds to the width of the nailed joint, and the depth to the distance of the second plastic hinge from the timber surface. The total capacity of the joint is limited by the sum of the nail capacities (R_N) and by the sum of the tensile and shear capacities of the timber member with the reduced dimensions, as presented in the following formula (Kangas et al. 1996):

$$R = \min \begin{cases} n_b \cdot n_l \cdot R_N \\ b_{ef} \cdot t_{ef} \cdot f_{t,0} + b_{ef} \cdot (l_N + a_3) \cdot f_{v,90} \end{cases} \quad (2)$$

where	n_b	is the number of nails perpendicular to the grain
	n_l	is the number of nails in the grain direction
	R_N	is the nail capacity
	b_{ef}	is the effective width of the nailed area
	t_{ef}	is the effective thickness of the nailed area
	l_N	is the length of the nailed area
	a_3	is the distance from the loaded end of the timber member
	$f_{t,0}$	is the tensile strength of timber in the grain direction
	$f_{v,90}$	is the flatwise shear strength of Kerto-S-LVL, or the rolling shear strength of Kerto-Q-LVL, or the shear strength of sawn timber.

The predrilling of holes cuts the grains of timber, so that the effective width of the nailed area (b_{ef}) is to be reduced by the sum of the width of the nails. For example, the effective width of a nail row consisting of $9 \times (6.0 \times 60 \text{ mm})$ nails is $9 \cdot (a_2 - 6 \text{ mm})$.

Formula (2) is valid only for such materials that are homogeneous in the grain direction, e.g. sawn timber and Kerto-S-LVL. For Kerto-Q-LVL, the effect of cross veneers can be taken into account by increasing the effective width (b_{ef}) by a factor of $2 \cdot b_{ad}$, where b_{ad} is the additional width of a timber block, due to the edgewise shear capacity of cross veneers. Thus, the increased width of a Kerto-Q-LVL member equals the following:

$$b_{ef}' = b_{ef} + 2 \cdot b_{ad}, \quad (3)$$

where $b_{ad} \leq a_4 - 0.5 \cdot a_2$ and

a_2 is the nail spacing perpendicular to the load
 a_4 is the distance from the edge of the timber member.

The cross-section of Kerto-Q-LVL in tension is assumed to be the same as for Kerto-S-LVL. Thus, the difference in the tensile capacity is due to the different strength values used. The shear capacity of veneers in the direction edgewise perpendicular to the grain is considerably greater (5.1 N/mm^2) than the shear capacity of cross veneers (1.5 N/mm^2) (Ranta-Maunus 1995). The failure mode of such veneers is also more ductile. This effect is taken into account by increasing the width of the timber block torn off from the timber member. The additional width (b_{ad}) is calculated by multiplying the shear strength ratio of Kerto-Q-LVL by the thickness (3 mm) and the number of cross veneers acting in the block. For example, for a joint with 63 mm thick Kerto-Q-LVL and $t_{ef} = 20 \text{ mm}$, the b_{ad} is calculated as $(5.1/1.5) \cdot (2 \cdot 3) \text{ mm} = 20 \text{ mm}$.

5 Analysis of Test Results

5.1 MNC Tests

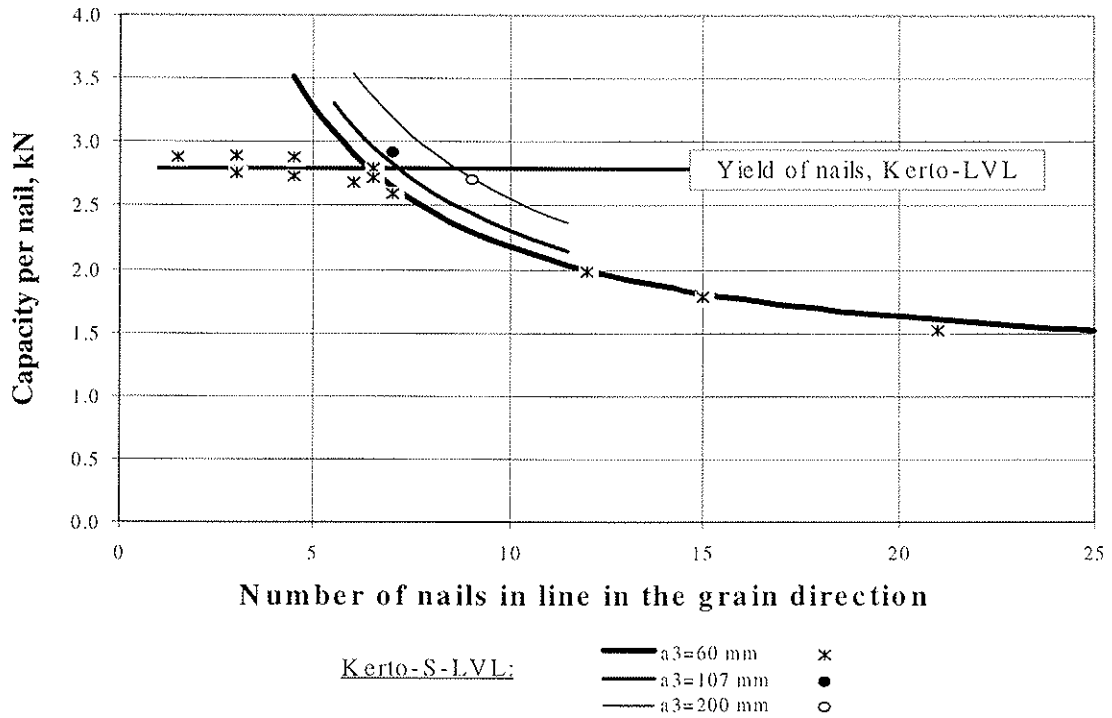
Numerous test series have been carried out with MNC connectors both in the University of Karlsruhe and at Helsinki University of Technology. The nail spacings used have been 40 mm in the load direction (a_1) and 12 mm perpendicular to it (a_2). The end distance used in most of the cases has been 60 mm (a_3). End distances of 107 mm and 200 mm have also been used in tests with Kerto-S-LVL. The number of nails in the grain direction (n_1) has varied between 1.5...21 and the number of nails perpendicular to the grain (n_b) in the range of 5...30.

A reduction method, similar to the method presented in EC5 for bolted joints, has been used to calculate the capacities of more than six MNC nails in line with the load direction. The load-carrying capacity of the additional nails has been reduced by 60 % resulting in the effective number (n_{ef}) of nails of $n_{ef} = 6 + 2 \cdot (n-6) / 5$ (Kevarinmäki 1995). This equation corresponds well to the test results obtained with Kerto-S-LVL. However, such a reduction can be used only for the above-mentioned nail spacings and the end distance of 60 mm.

Tests carried out with Kerto-S-LVL have been the basis for the model developed. This model has already been presented by Kangas (1996). The strength values used in the modelling for Kerto-LVL and glulam are presented in Table 1. The mean load-carrying nail capacity (R_m) obtained for Kerto-LVL in tests was 2.8 kN and 2.5 kN for glulam, and the calculated

location of the plastic hinge (t_{ef}) 28 mm and 29 mm, respectively. Figure 6 presents the mean values of test results with Kerto-S-LVL (five parallel test pieces) and all test results with Kerto-Q-LVL and glulam (three parallel test pieces).

(a)



(b)

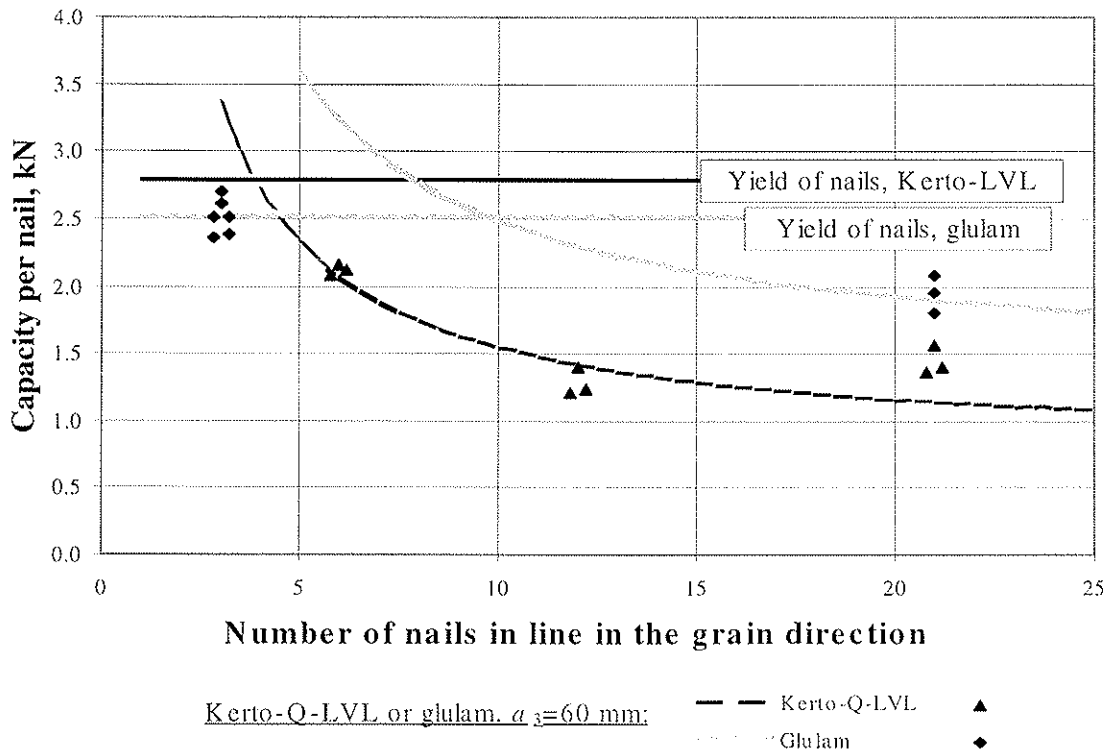


Figure 6 - Test results per nail and corresponding curves according to the model. (a) Kerto-S-LVL (mean values), (b) Kerto-Q-LVL and glulam (all test results).

5.2 Tests with Nailed Joints

5.2.1 Modes of Failure

The tests with series A resulted in clear yield of nails regardless of the material used as timber members. An exception to this was series 6AS, where small blocks of timber were torn off with the yield of nails, which was, however, the primary mode of failure. Test series B and C resulted in clear block tearing failure. In test series D, the dominant failure mode was block tearing. With the test pieces made of sawn timber, this was accompanied with yield of nails and therefore larger joint slips.

Figure 7 presents a few examples of the joint load per nail as a function of the joint slip. The curves show how brittle the block tearing failure was compared to the yield of nails. Figure 8 presents the block tearing failure of test pieces 4CS2, 4BQ1 and 6CT2.

The timber material used influenced the dimensions of the timber torn off from the timber member. Homogeneous materials in the grain direction, such as Kerto-S-LVL and sawn timber, were torn off similarly. The block tearing failure of Kerto-Q-LVL was different from these, since the width of the torn off piece was larger due to the greater shear strength of cross veneers. This was taken into account in the model by increasing the effective width (b_{ef}).

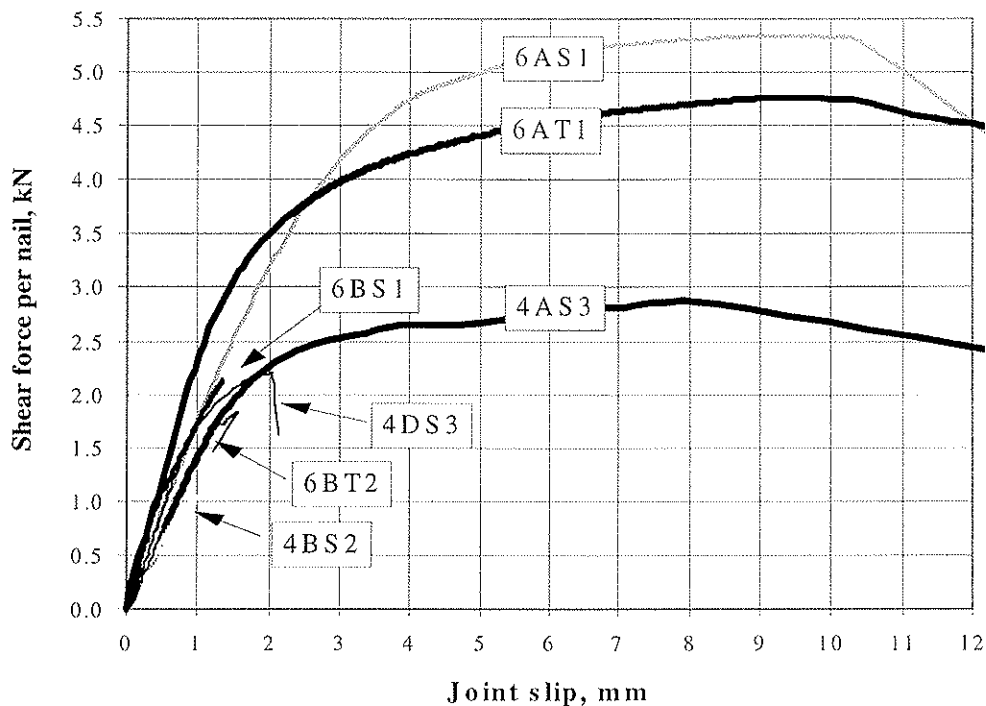


Figure 7 - Shear force-joint slip -curves of Kerto-S-LVL and sawn timber with connection types A, B and D.

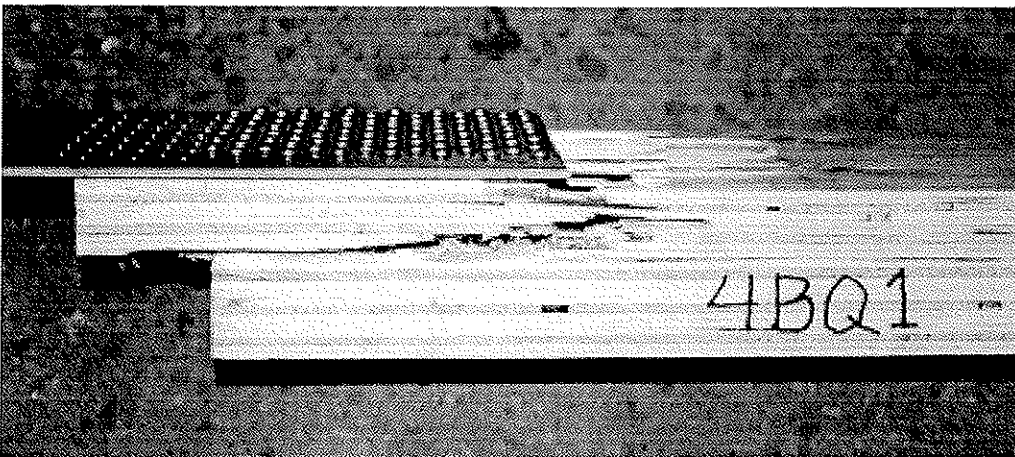
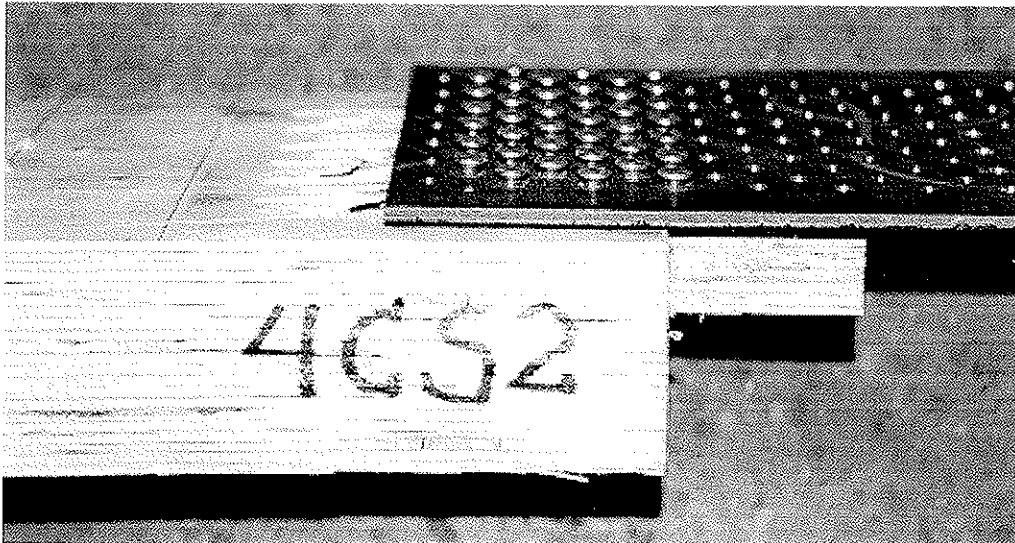


Figure 8 - Block tearing failure of test pieces made of Kerto-S-LVL (S), Kerto-Q-LVL (Q) or sawn timber (T).

5.2.2 Measured Mean Capacities of Test Pieces

Table 5 shows the measured mean capacities of joints with Kerto-S-LVL, Kerto-Q-LVL and sawn timber, and the shear capacities of each joint per nail. Table 5 also presents the calculated location of the plastic hinge (t_{ef}) (see Figure 5) and the capacity according to the formula (2). The strength values used in the modelling are presented in Table 1 (see Page 2). Figures 9, 10 and 11 present curves of this analysis model for different timber materials and the individual test results.

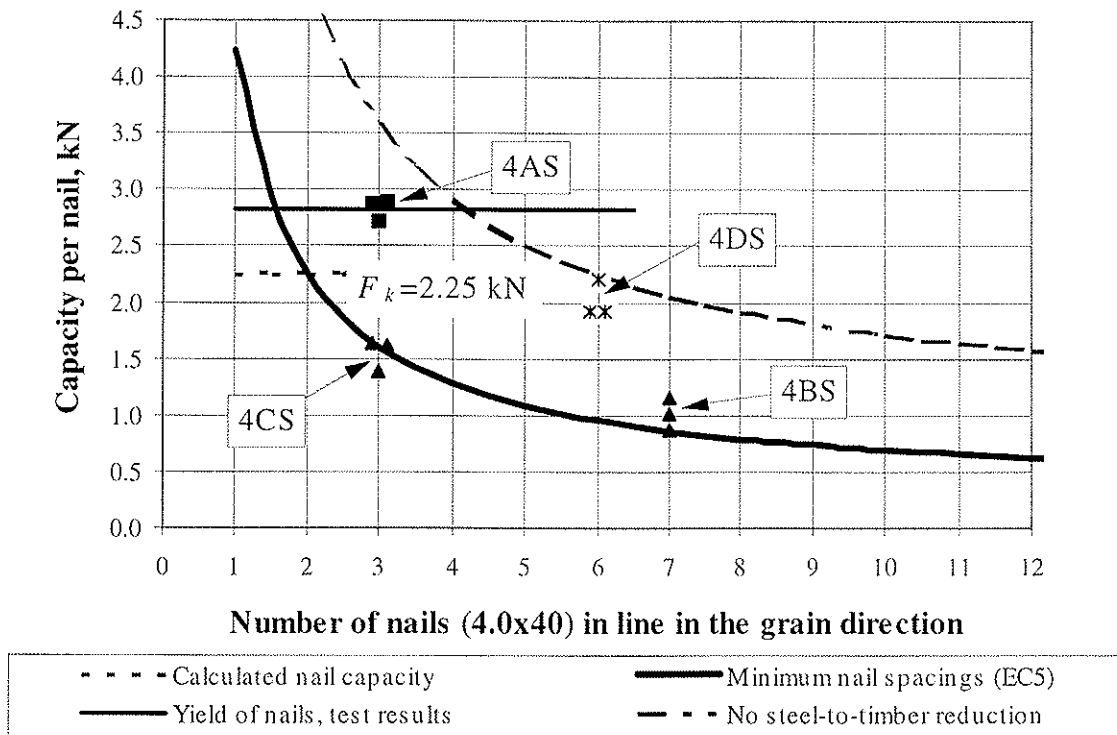
In the test series A and D, the nail spacings of a timber-to-timber joint were reduced by a factor of 0.7, corresponding to either predrilling of timber or steel-to-timber connection, and referred to here as a single reduction. In the test series B and C, a double reduction of 0.7×0.7 was used corresponding to both predrilling and a steel-to-timber connection. Such a double reduction is, however, not acceptable because of the significant decrease in the allowable number of nails in line in the grain direction, yet avoiding the block tearing failure. The single reduction, e.g. with light spruce, allows four nail rows to be used with full capacity, whereas with no reduction at all the number of nail rows is 14.

The nailing of the steel plate on the sapwood side of sawn timber resulted in about 10 % greater failure capacity than the nailing on the heartwood side.

Table 5 - Measured mean capacities and shear capacities per nail of test pieces with 4 or 6 mm nails. Calculated characteristic capacities of series A (EC5) are in parenthesis.

BMF 4.0×40	Test Series	R_{test} kN	R_{test} / n kN/nail	Mode of failure	t_{ef} mm	R_{model} / n kN/nail
Kerto-S-LVL	4AS	69.5	2.84	yield	17	(2.25)
	4BS	92.6	1.01	block tearing		0.86
	4CS	60.4	1.55	block tearing		1.61
	4DS	96.6	2.01	block tearing		2.24
Kerto-Q-LVL	4AQ	59.4	2.83	yield	17	(2.25)
	4BQ	76.3	0.84	block tearing		0.59
	4CQ	51.3	1.32	block tearing		1.12
	4DQ	72.7	1.51	block tearing		1.51
Light spruce	4AT	48.9	2.33	yield	20	(1.92)
	4BT	83.9	0.92	block tearing		0.63
	4CT	64.9	1.66	block tearing		1.15
	4DT	88.3	1.84	block tearing		1.66
Heavy spruce	4CT	93.8	2.41	block tearing	17	(1.70)
	4DT	114.0	2.37	tearing + yield		2.48
BMF 6.0×60						
Kerto-S-LVL	6AS	80.8	5.39	yield + tearing	24	(4.68)
	6BS	138.3	2.20	block tearing		1.75
Kerto-Q-LVL	6AQ	77.9	5.19	yield	24	(4.68)
	6BQ	82.5	1.31	block tearing		1.35
Light spruce	6AT	69.0	4.60	yield	28	(4.00)
	6BT	105.1	1.67	block tearing		2.06
	6CT	90.6	3.36	block tearing		3.75

(a)



(b)

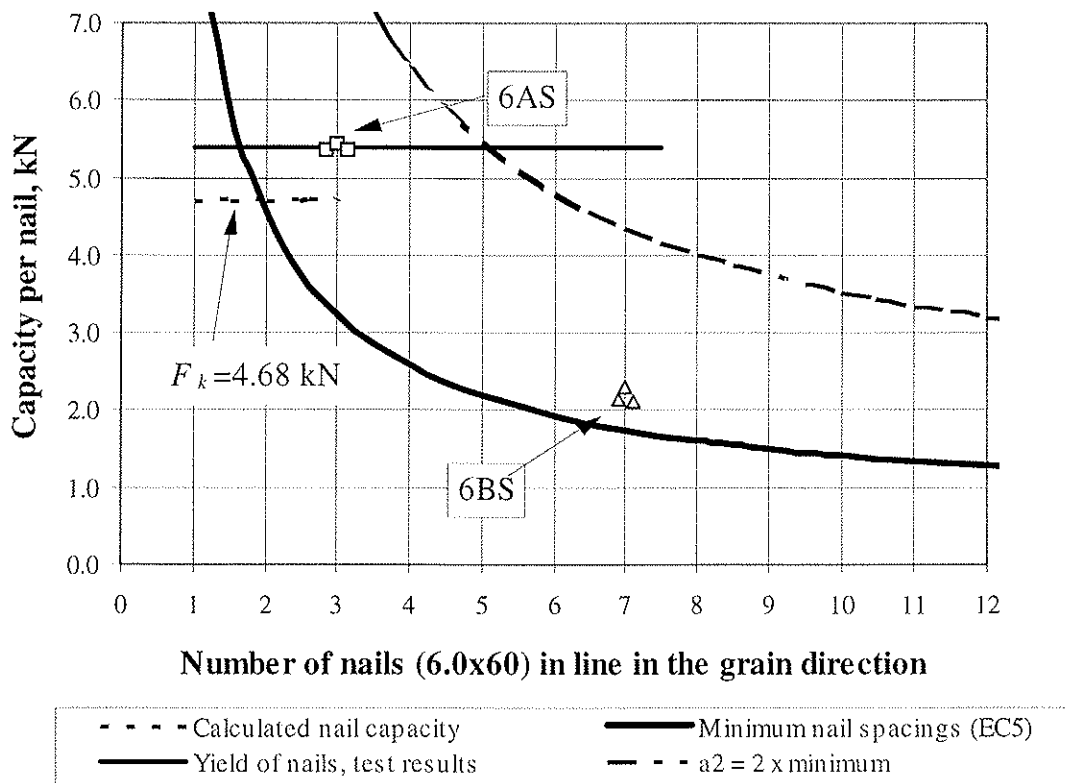
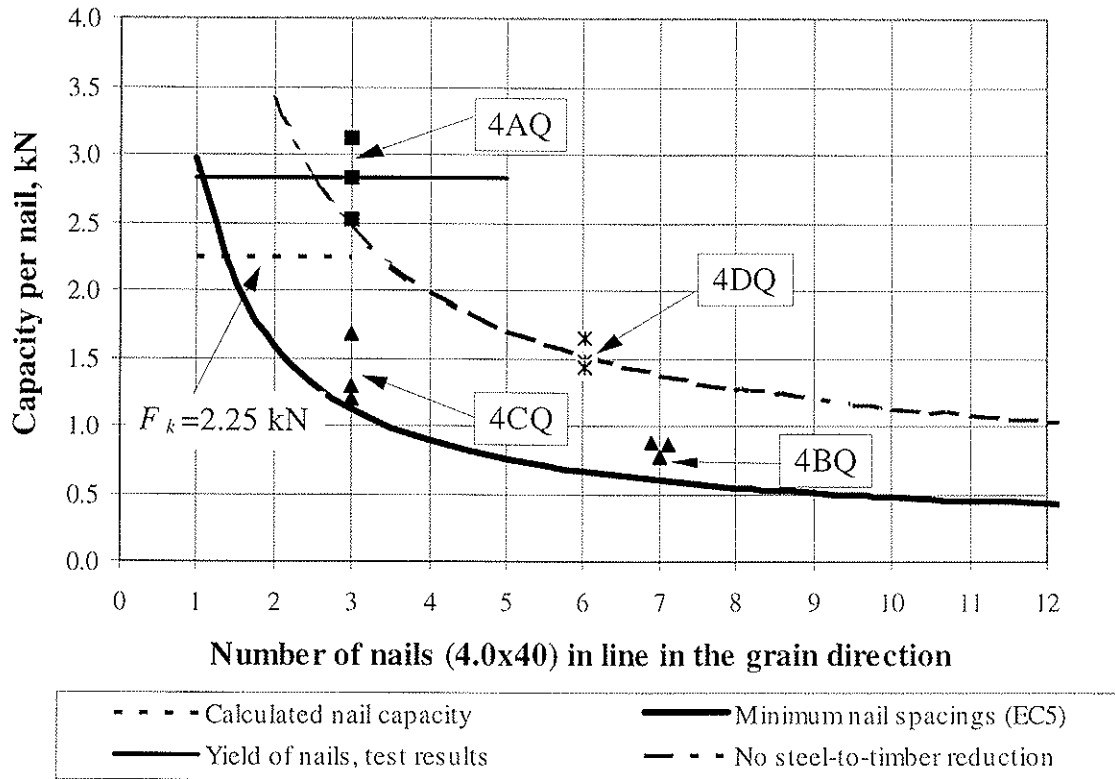


Figure 9 - Shear capacity per nail of Kerto-S-LVL test pieces and corresponding curves according to the model. (a) BMF 4.0x40 mm nails, (b) BMF 6.0x60 mm nails.

(a)



(b)

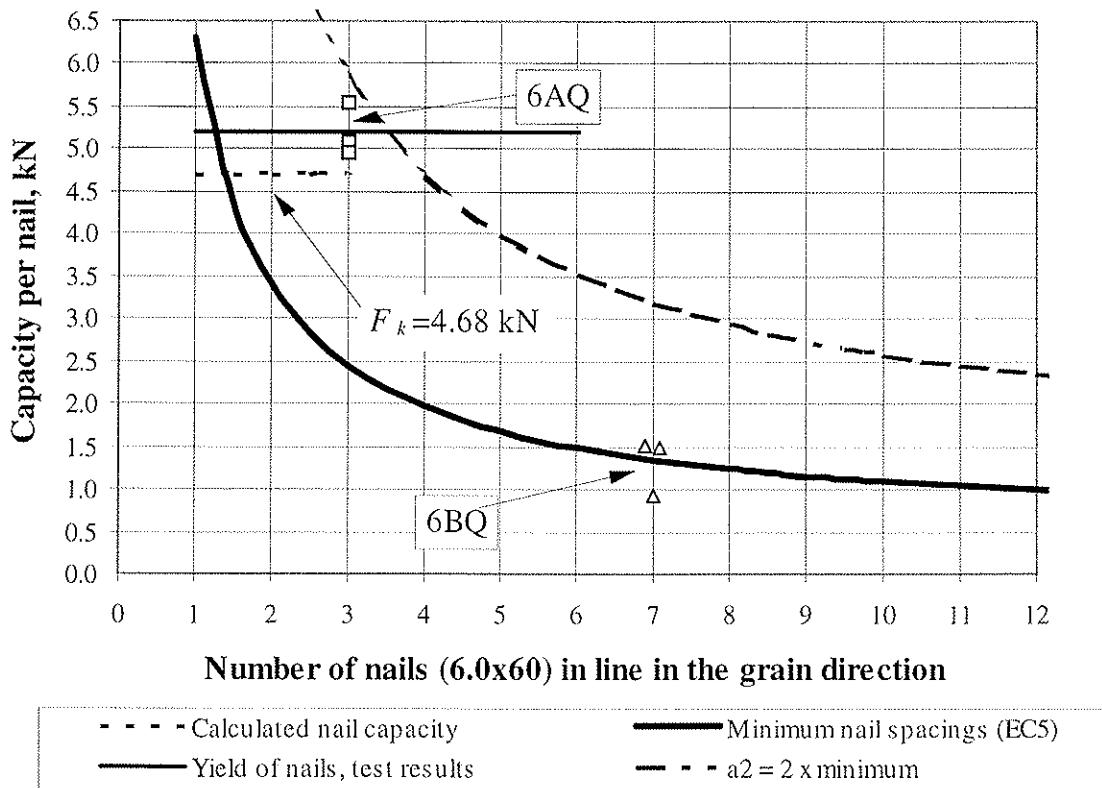


Figure 10 - Shear capacity per nail of Kerto-Q-LVL test pieces and curves according to the model. (a) BMF 4.0×40 mm nails, (b) BMF 6.0×60 mm nails.

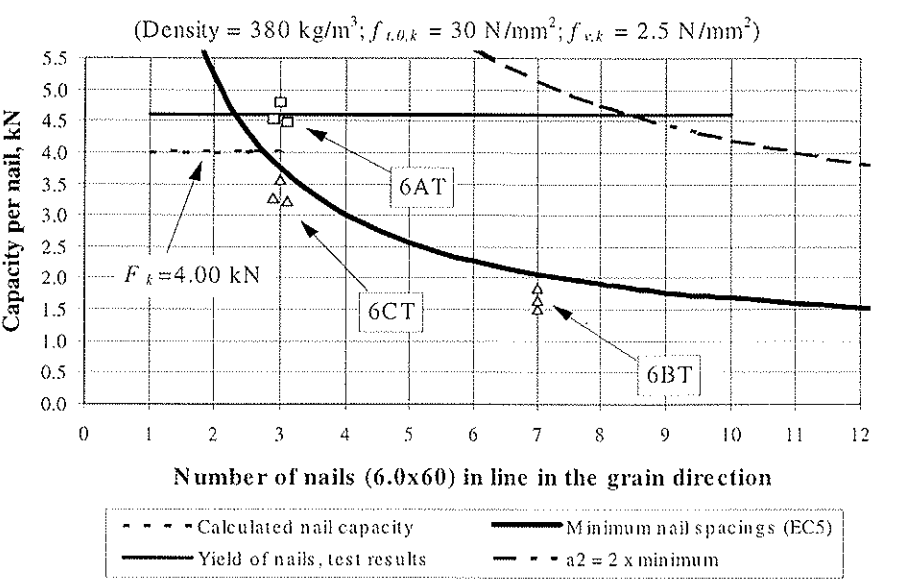
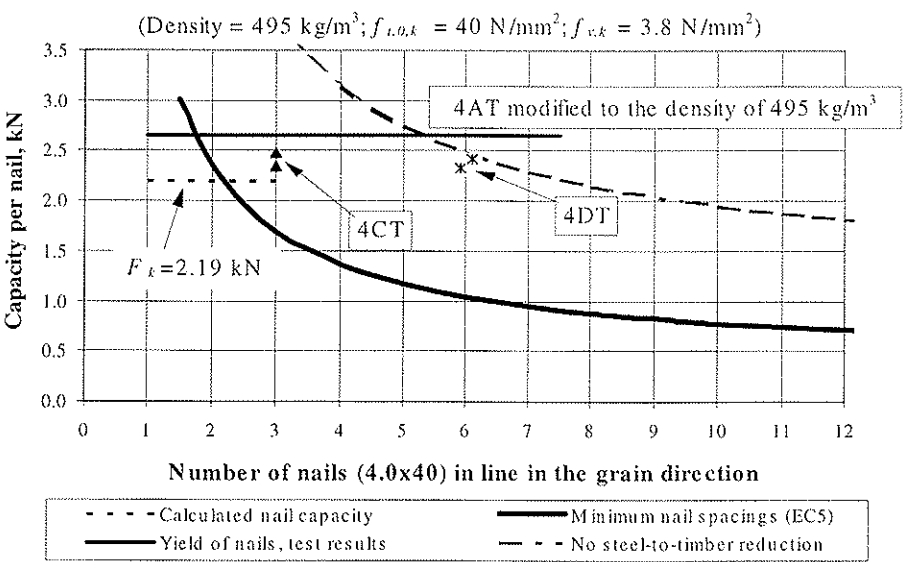
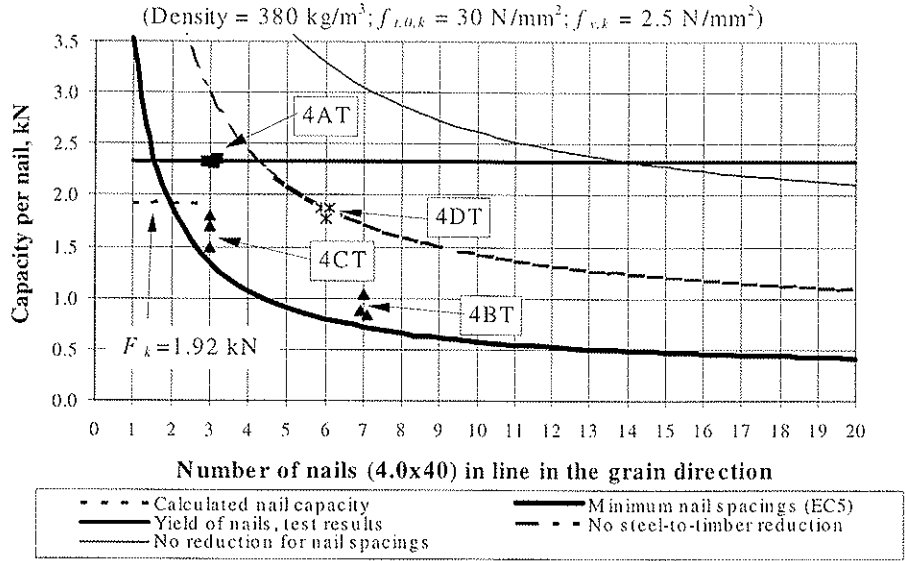


Figure 11 - Shear capacity per nail of sawn timber test pieces and curves according to the model (BMF 4.0x40 & light spruce / heavy spruce; BMF 6.0x60 & light spruce).

6 Concluding Remarks

In nailed timber connections, nail spacings are mainly given to avoid splitting during nailing. In the case of predrilled holes and steel-to-timber connections increased nail density is allowed by design codes. This leads to the exceeding of the tensile and shear capacity of the timber member in the joint area, and the unfavourable brittle mode of failure with reduced capacity of the joint.

The block tearing failure can be avoided by using the proposed method to model nailed steel-to-timber joints in tension. This method takes into account the dimensions of the torn off piece of timber member, and the tensile and shear capacity of timber in the joint area. Thus, the model can be used for optimizing nail spacings and distances of nailed joints made of different timber materials. The allowable nail spacings of EC5 are, therefore, found too small for nailed steel-to-timber connections, since the reduction in nail spacings due to both predrilling and steel connectors is not acceptable. In long timber joints, no reduction should be allowed at all. The reduction in the effective number of nails should also be replaced by increasing the joint area with maximum nail capacity or by determining the block tearing failure capacity of the joint area.

References

- Aalto, K., Kangas, J. & Kevarinmäki, A. 1997. Modelling of peeling failure in nailed steel-to-timber joints. Publication 65. Helsinki University of Technology. Laboratory of Structural Engineering and Building Physics. Espoo, Finland.
- Eurocode 5. 1993. Design of timber structures - Part 1-1: General rules and rules for buildings. ENV 1995-1-1:1993: European Committee for Standardization. Brussels, Belgium. 110 p.
- Ehlbeck, J. 1992. Ergänzende Versuche mit Multi-Krallen-Dübeln (MKD) als Holzverbindungsmittel. Prüfzeugnis Nr. H 9206. Versuchsanstalt für Stahl, Holz und Steine. Universität Karlsruhe. Karlsruhe, Germany.
- Ehlbeck, J. 1987. Tests with Multiple Nail Connectors used as fasteners for load-bearing timber members. Test Report No. H 8604. Versuchsanstalt für Stahl, Holz und Steine. Universität Karlsruhe. Karlsruhe, Germany.
- Hilson, B. O. 1995. Joints with dowel-type fasteners - Theory. In: Blass, H. J. & al. Timber Engineering STEP 1, lecture C3. Centrum Hout, The Netherlands.
- Kalliomäki, J., Hirsi, H. & Kanerva, P. 1986. Kerto-Laminated Veneer Lumber Truss. Report 14. Helsinki University of Technology. Laboratory of Structural Engineering and Building Physics. Espoo, Finland.
- Kangas, J. & Väänänen, H. 1996. The Capacity of Multiple-Nail-Connector / Kerto-LVL Joints. In: Proceedings of the International Wood Engineering Conference (IWEC), New Orleans, Louisiana, USA. October 28-31, 1996. Volume 3. p. 279-282.
- Kevarinmäki, A. 1995. Trusses made from laminated veneer lumber. In: Blass, H. J. & al. Timber Engineering STEP 2, lecture E6. Centrum Hout, The Netherlands.
- Ranta-Maunus, A. 1995. Laminated veneer lumber and other structural sections. In: Blass, H. J. & al. Timber Engineering STEP 1, lecture A9. Centrum Hout, The Netherlands.
- Väänänen, H. & Kangas, J. 1995. Tensile connection tests with Multi-Nail-Connector and Kerto-S laminated veneer lumber. Test Report. Technical Research Centre of Finland (VTT) and Helsinki University of Technology (HUT).

**INTERNATIONAL COUNCIL FOR BUILDING RESEARCH STUDIES AND DOCUMENTATION
WORKING COMMISSION W18 - TIMBER STRUCTURES**

CYCLIC TESTING OF JOINTS WITH DOWELS AND SLOTTED-IN STEEL PLATES

by

E Aasheim
Norwegian Institute of Wood Technology
Norway

MEETING THIRTY

VANCOUVER

CANADA

AUGUST 1997

Cyclic Testing of Joints with Dowels and Slotted-in Steel Plates

Erik Aasheim
Norwegian Institute of Wood Technology
Norway

1 Background and objective.

In this paper tests performed in the project "Joints for Timber Bridges" are described. This project is a part of the "Nordic Timber Bridge Program".

The objectives of the project were to evaluate and develop mechanical fasteners with regard to dynamic actions and moisture conditions. Different types of fasteners were considered, and it was soon clear that the project had to be limited to one main type of joints. The project team chose to concentrate the work to testing of joints with steel dowels and slotted-in steel plates exposed to dynamic loads. The main reasons for this were that these joints are heavily used for timber bridges and that this type of joints is typical for all kinds of dowel type fasteners.

Few test results concerning dynamic testing of joints are available. In the draft for Eurocode 5 - Design of timber structures - Part 2: Bridges. (Draft ENV 1995-2) k_{fat} for joints are introduced. k_{fat} is a factor to transform characteristic short term static strength to characteristic strength for dynamic loads, $f_{fat,k}$. The aim of the project was to obtain more detailed information about k_{fat} than those indicated in Eurocode 5. By studying draft Eurocodes and national design rules, the maximum number of load cycles during testing was set to 10^7 . The tests were performed to determine the load level where the dynamic loading resulted in rupture at this number of cycles.

2 Project plan.

The tests were mainly performed at Dansk Teknologisk Institutt (DTI) in Denmark. One series was tested dynamically at Høgskolen i Gjøvik (HIG) in Norway.

The testing of this type of joints with dynamic loads turned out to be rather complicated and many technical problems appeared (heating problems, clamping problems, noise problems in the laboratory and in the adjacent offices, etc.). The original test plan involved test pieces with different dowel diameters and test pieces with 90° angle between force and grain, but the number of test specimen had to be reduced. Five series are tested, and the test plan is showed in figure 1 and figure 2. The numbering from the original test plan is still used.

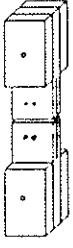
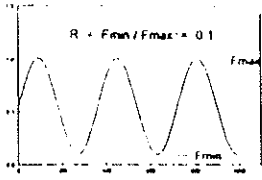
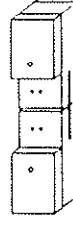
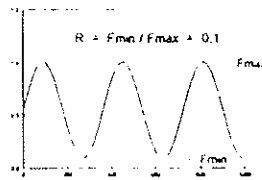
SERIES NO.		Static tests	Dynamic tests
1		5 test specimens	 <p>5 test specimens</p>
2		5 test specimens	 <p>14 test specimens</p>

Figure 1.

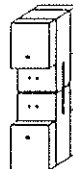
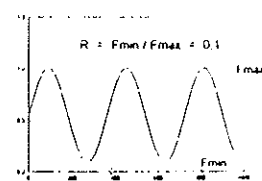
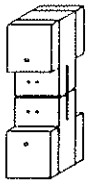
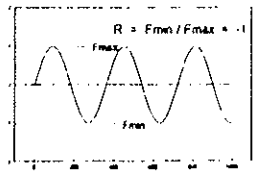
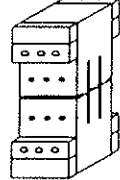
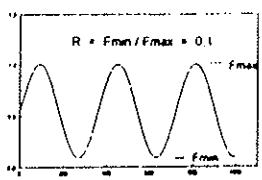
SERIES NO.		Static tests	Dynamic tests
2A	 <p>wet test specimens</p>	results from series 2	 <p>3 test specimens</p>
3		results from series 2	 <p>6 test specimens</p>
5		5 test specimens	 <p>5 test specimens</p>

Figure 2.

3 Test specimens.

In the design of the test specimens, the theoretical failure modes for joints with steel dowels and slotted-in steel plates were taken as the basis. For static loads three failure modes are possible. These failure modes are shown Eurocode 5 - Design of timber structures - Part 1-1: General rules, figure 6.2.2.e, 6.2.2.f and 6.2.2.g. For test series 1 the timber thickness was chosen to avoid yield moments by static testing (6.2.2.e). For the remaining test pieces in double shear the timber thickness was chosen to reach one yield moment (6.2.2.f). The results show that for none of the statically loaded test pieces visible yield moments were developed. One of the reasons for this is that the steel quality appeared to be higher than expected.

The test specimens were manufactured at Norsk Treteknisk Institutt (NTI), Norwegian Institute of Wood Technology.

3.1 Timber.

Density graded Norwegian Spruce was used with a density $\rho_{0,15}$ ranging from 360 to 410 kg/m³. The two timber pieces in each test specimen were cut from the same plank to balance the density. In test series 5 two pieces were glued together to obtain necessary thickness. The ends of the test pieces were reinforced with 15 mm birch plywood.

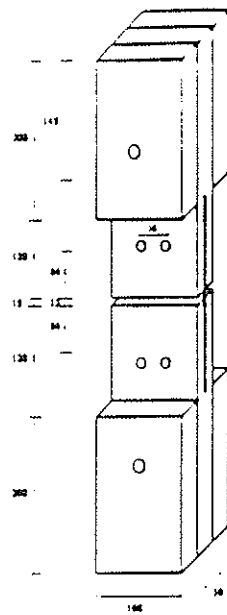
3.2 Steel dowels and steel plates.

The thickness of the slotted-in steel plates was 8 mm. The holes in the steel plates had a diameter of 12,5 mm.

The diameter of the steel dowels was 12 mm. All dowels were electrolytic galvanized. The steel quality was originally declared to be minimum ST 52 with a yield point of 355 N/mm². As the initial tests did not result in the expected failure modes, the Norwegian importer was contacted. He informed us that the dowels were produced from rolled steel and were cold drawn to obtain the correct diameter. Test from the importer showed that the actual yield point was 650 N/mm².

Spacing and distances for the dowels were chosen in accordance with Eurocode 5 - Design of timber structures - Part 1-1.

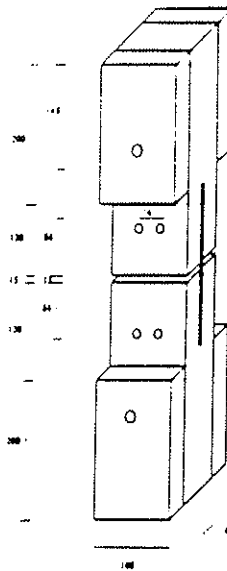
The geometry of the test specimens are shown in the figures 3, 4 and 5.



Slotted-in steelplate 8x100x250 mm

Dowels d=12 mm

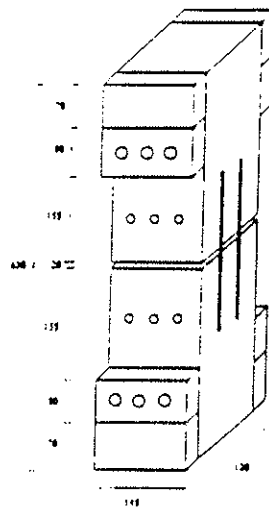
Figure 3. Test series 1.



Slotted-in steelplate 8x100x250 mm

Dowels d=12 mm

Figure 4. Test series 2 + 2A + 3.



2 slotted-in steelplates 8x120x250 mm

Dowels d=12 mm

Figure 5. Test series 5.

3.3 Conditioning of the test specimens.

The timber pieces were conditioned at 85% RH and 20°C prior to the manufacturing of test specimens. The test specimens were stored at 65% RH and 20°C until testing. The actual testing hall for the dynamic tests did not have constant climate. Due to the long testing periods the test specimens dried out during testing. To try to avoid this, the test specimens were wrapped up in plastic film. This is further discussed in section 7.3.

The test pieces in series 2A were vacuum/pressure treated with water. After manufacturing the test specimens were submerged in water in plastic tubs. The tubs were placed in an autoclave and exposed to a vacuum of 0,1 bar for 1 hour and a pressure of 7 bar for 1 day and night. The moisture content in the timber was approx. 100 % after this impregnation.

4 Static tests.

To establish a basis to settle the load level for the dynamic tests, parallel test series were manufactured and tested for the different series. The tests were performed as tension tests according to ISO 6891. Except test series 5, all static tests were done at DTI. Series 5 was tested at NTI.

5 Dynamic tests.

“Dynamic test” means alternating load intensity, either by changing from tension to compression (reversed cyclic loading) or by changing tension or compression loads (non-reversed cyclic loading). The loading cycles are shown in figures 6 and 7, and they are described by sine waves.

Due to the very high number of load cycles (10^7), each test was very time-consuming. For this reason the tests were performed with as high frequency as possible. The possible frequency is dependent on the amplitude, which again is dependent on the stiffness of the joints.

Test series 1,2,2A and one sample in series 3 were tested at 25 Hz. Test series 5 was tested at 12 Hz (Last specimen 20Hz). The above mentioned tests were performed at DTI.

Test series 3 was terminated after one specimen at DTI due to noise problems. The remaining specimen in series 3 were tested at HIG. In this series reversed loading was applied, which resulted in a larger amplitude. The frequency was chosen to be between 3 Hz and 6 Hz.

The load levels for dynamic testing were determined with the mean values from static testing as a basis.

The test machines were controlled by the loads, i.e. maximum and minimum loads are maintained and the test machines give the specimen the deformations that are necessary to obtain the relevant loads.

At the starting point of the project, it was assumed that the deformations in the joints would increase to an unacceptable level. Thus definitions of rupture were discussed. However, the tests showed that this problem was irrelevant, because other failure modes than expected were decisive.

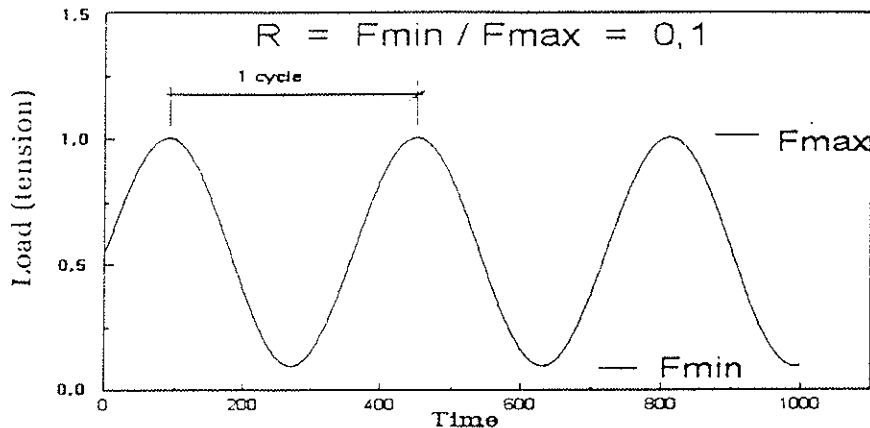


Figure 6. Loading for test series 1, 2, 2A and 5.

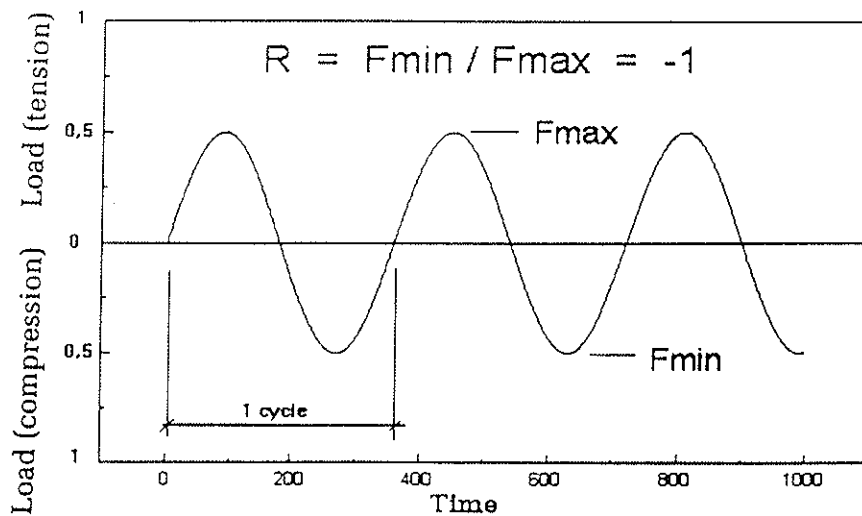


Figure 7. Loading for test series 3.

$$\Delta F = +0,5 - (-0,5) = 1,0$$

The difference in loads is the same for test series 3 and for the other test series, even if the maximum load is the half value.

6 Evaluation of the test results.

The figures 8 - 12 show graphs of the test results. The load levels are shown as a function of the number of load cycles to failure (logarithmic). The results are not adjusted with regard to moisture content and density. Results from test specimen with special problems (failure in the clamping system, motion of the dowels, etc.) are disregarded.

The mean values from the static tests are used as reference levels. It should be noticed that the static test results are somewhat lower than the values calculated according to Eurocode 5 Part 1.

It should also be noticed that for 3 of the test specimen in series 3, the failure modes were different in the static tests (timber failure) compared to the dynamic tests (steel failure in the dowels).

In the figures the values for k_{fat} from Eurocode 5 Part 2, Draft June 1996 are shown.

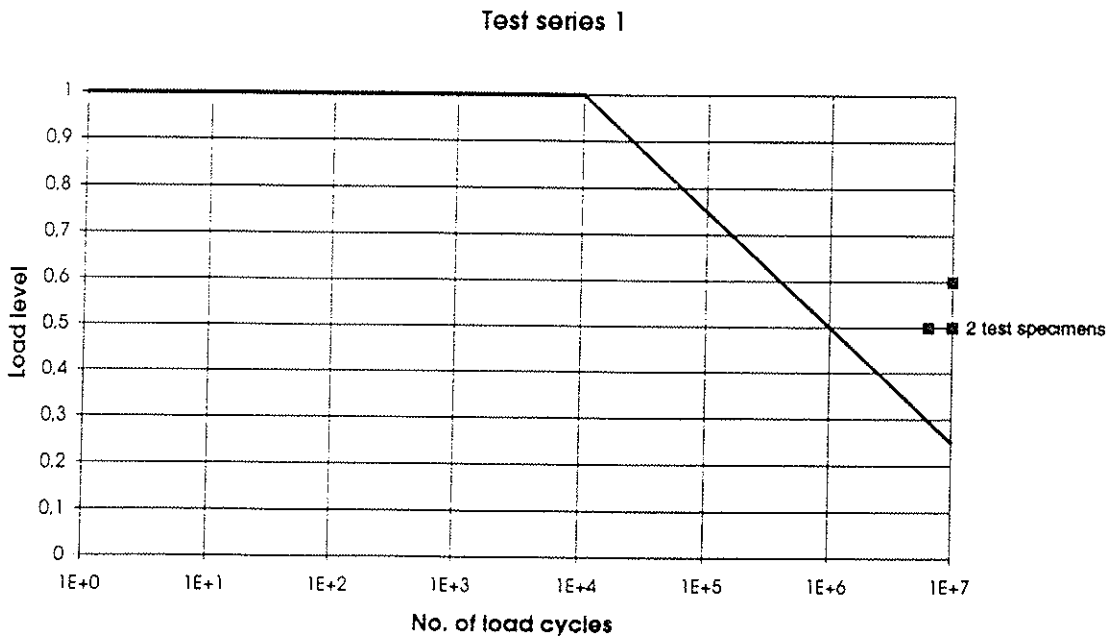


Figure 8.

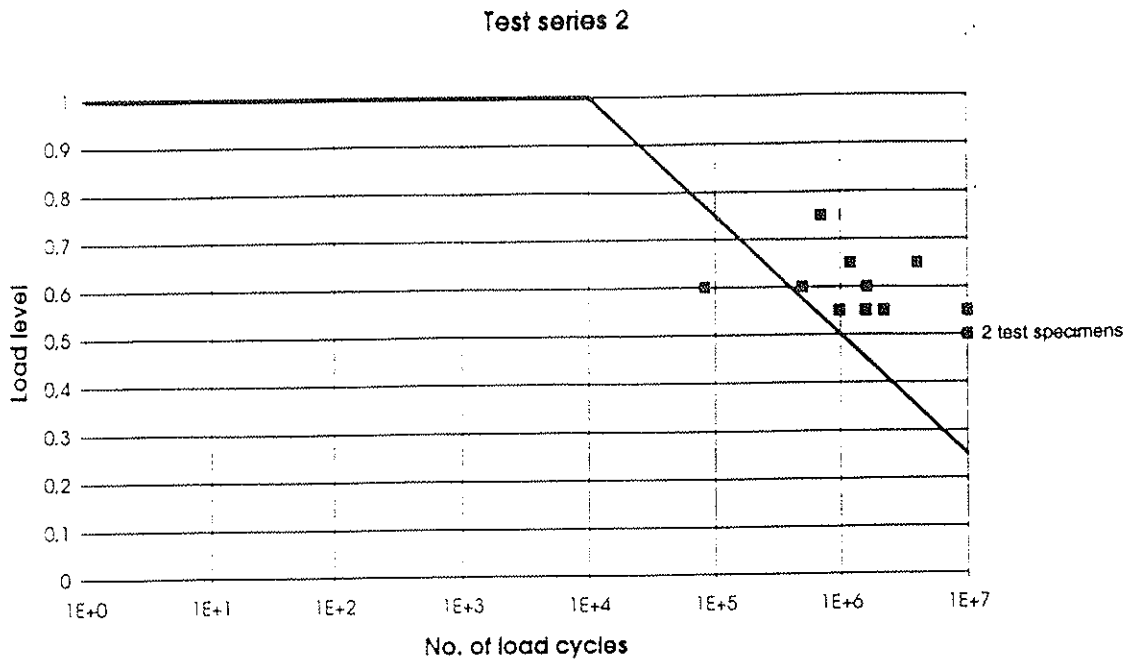


Figure 9.

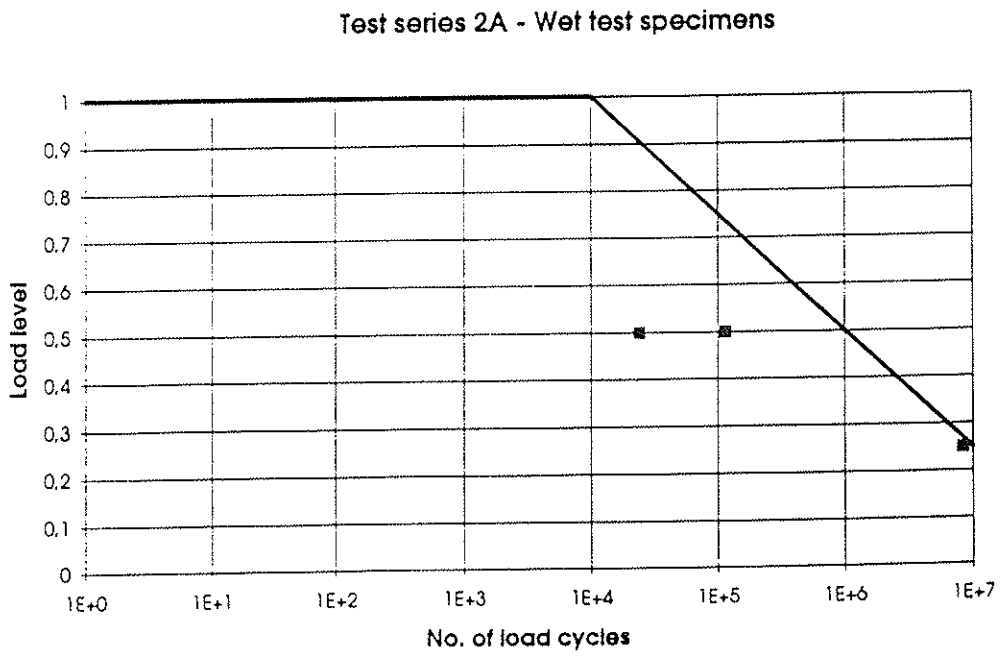


Figure 10.

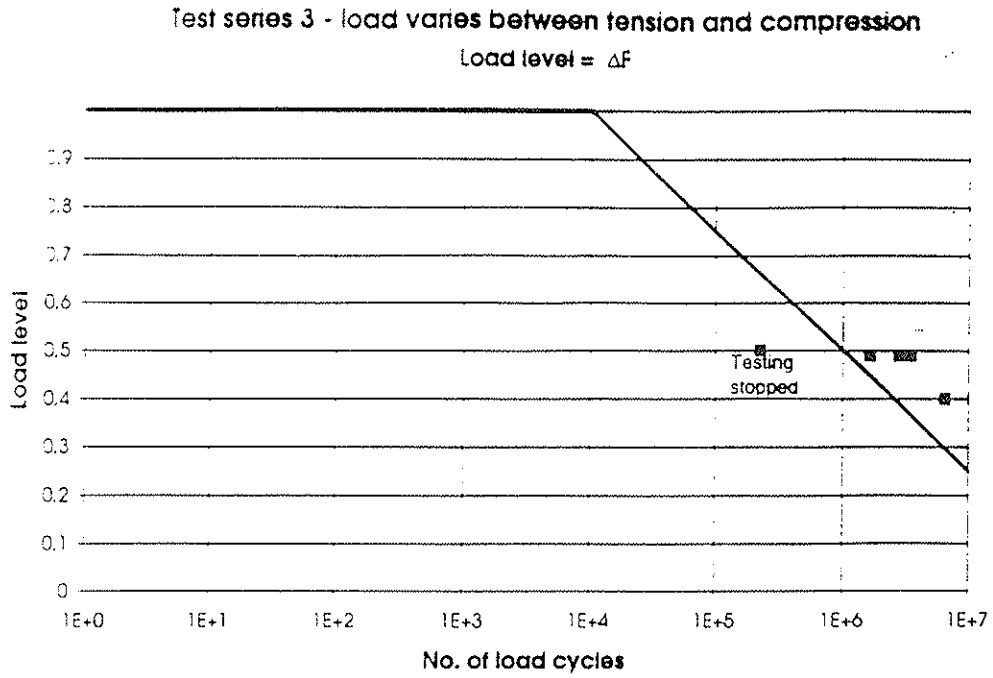


Figure 11.

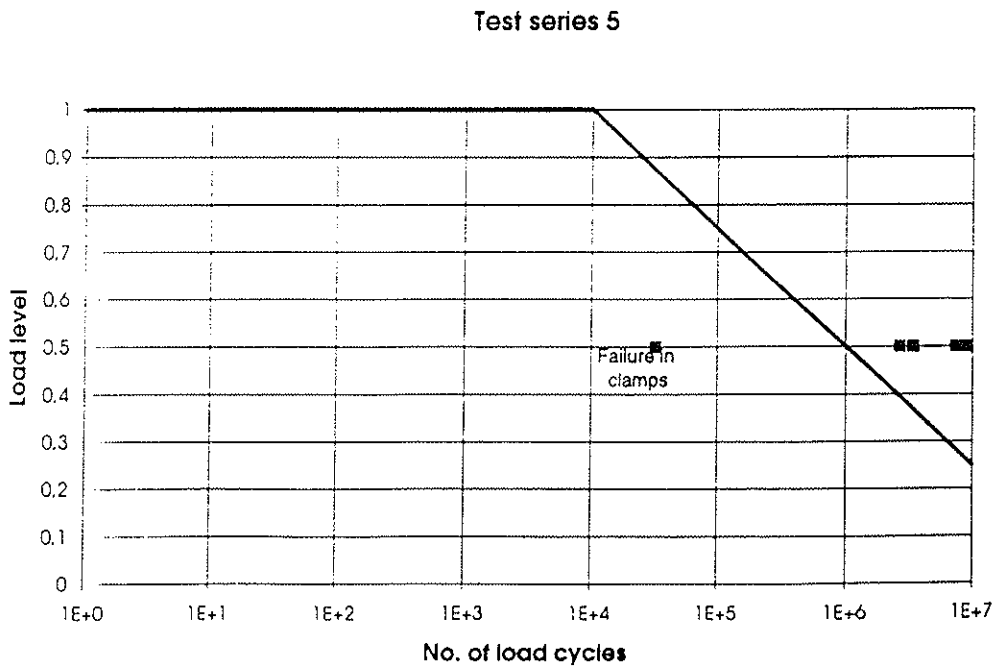


Figure 12.

7 Comments to the tests.

7.1 Failure mode.

All static tests resulted in crushing of the timber in the embedding area. The dowels had no visible yield moments.

For the dynamic tests of the series 1, 2 and 5 the failure modes were almost identical for all test specimen, namely failure in the timber at the dowels. The timber piece against the dowel was pressed out (shear failure in the timber). The failure modes were with that different at static and dynamic testing of identical test specimen.

For the dynamic tests of series 2A (high moisture content) the failure modes were compression failures in the timber against the dowels and cracks in the timber.

For the dynamic tests of series 3 (reversed cyclic loading) the failure modes were different from the other series. Fatigue failures in the dowels arose, and the dowels broke in two.

7.2 Motion of the dowels.

Pilot tests showed that some of the dowels moved out of their holes during the dynamic testing. This resulted in failure in the remaining dowels at early stages. This phenomenon was observed for both reversed and non-reversed cycling loading. For this reason the bolts were secured to prevent this moving-out motion. This was done in some cases by cotter pins at each end of the dowels and in other cases with a dash of glue at each of the dowel ends outside the timber.

7.3 Temperature and moisture content in the test samples.

In the course of the dynamic tests it was observed that the steel parts and the timber pieces were warmed up. The main reason for this is friction in the joints. The temperature increase is dependent on the fit between the parts in the joints, the frequency and the deformations (stiffness). The maximum observed temperatures in the dowels were about 65°C and in the steel plates about 75°C. These high temperatures resulted in drying of the timber parts, and a dry climate in the testing rooms increased this drying effect. The joints were wrapped in plastic films; but this could not totally stop the process.

The total time to failure varied. At DTI the time to failure was from 5 days up to 10 days. At HIG one test could last for up to 4 weeks. At both laboratories the result was a moisture content of about 6,5 % at failure.

The temperature increases during testing may have different effects. High temperatures may decrease the strength, and low moisture content may increase the strength.

8 Recommendations and conclusions.

No guidelines for fatigue testing of timber joints are found in Eurocode 5 or in other documents known to the project team. The tests described in this report may be regarded as a first proposal from the project team about how to test and evaluate joints with regard to fatigue actions. The experience gained during the testing shows that many factors should be discussed and that further research and tests are desirable. Some of the factors that are not investigated in this project are:

- Different failure modes.
- The difference between reversed and non-reversed cycling.
- The influence of the steel quality of the dowels.
- Other dowel diameters.
- Other angles between the load and the direction of the grain.
- The effect of several dowels in line with the load direction.
- The effect of the frequency of the load cycles.
- The effect of temperature and moisture content in the specimen.

The figures 8, 9, 11 and 12 show that the load levels in the range from 10^6 to 10^7 load cycles are slightly higher than $k_{fat}=0,25$ from Eurocode 5. In other words, Eurocode 5 seems to give values on the safe side.

The results from the specimen with high moisture content are shown in figure 10. The preliminary conclusion is that dowel joints exposed to fatigue loads are sensitive to the moisture content in the timber.

9 References.

Eurocode 5 - Design of timber structures - Part 2: Bridges (Draft June 1996).

Høgskolen i Gjøvik: Utmattingstest av dybelforbindelser i trekonstruksjoner, datert juni 1996.

Jens Ljørring, DTI: Broer i træ, forbindelsesmidler. Prøvningsrapport, datert 1996-05-07.

**INTERNATIONAL COUNCIL FOR BUILDING RESEARCH STUDIES AND DOCUMENTATION
WORKING COMMISSION W18 - TIMBER STRUCTURES**

**A STEEL-TO-TIMBER DOWELLED JOINT OF HIGH PERFORMANCE IN
COMBINATION WITH A HIGH STRENGTH WOOD COMPOSITE (PARALLAM)**

by

E Gehri
Chair of Wood Technology
ETH Zürich
Switzerland

**MEETING THIRTY
VANCOUVER
CANADA
AUGUST 1997**

A steel-to-timber dowelled joint of high performance in combination with a high strength wood composite (Parallam)

E. Gehri, Chair of Wood Technology, ETH Zurich, Switzerland

1. Introduction

A lot of research work has been done and is still going on for the development of high strength wood composites like Parallam. The main problem consists now in the transfer of larger forces in such materials, that means the development of adequate connections of high performance and reliability. The Blumer system (BSB), a steel-to-timber dowelled joint, developed and mainly used for connections in glued laminated timber of spruce, showed to be also adequate with Parallam.

2. Test material – Parallam

The test material was directly received from McMillan–Bloedel (Canada). The dimensions of the 20 test specimens were: section of 200 by 200 mm and length of 1 m. No quality control was made; only the density was measured, which varied between 628 and 670 kg/m³ (middle value: 645 kg/m³; coefficient of variation: 0,02).

3. BSB–connections

Two types of BSB–connections were used (see figure 1): with 3 and 4 steel plates. The number of dowels in a row varied between 3 and 5. Besides the normal BSB–dowel (diameter 6,25 mm and nominal tensile strength of 550 N/mm²) a serie was made with diameter 6,0 mm and ETG–steel (nominal tensile strength of 1000 N/mm²).

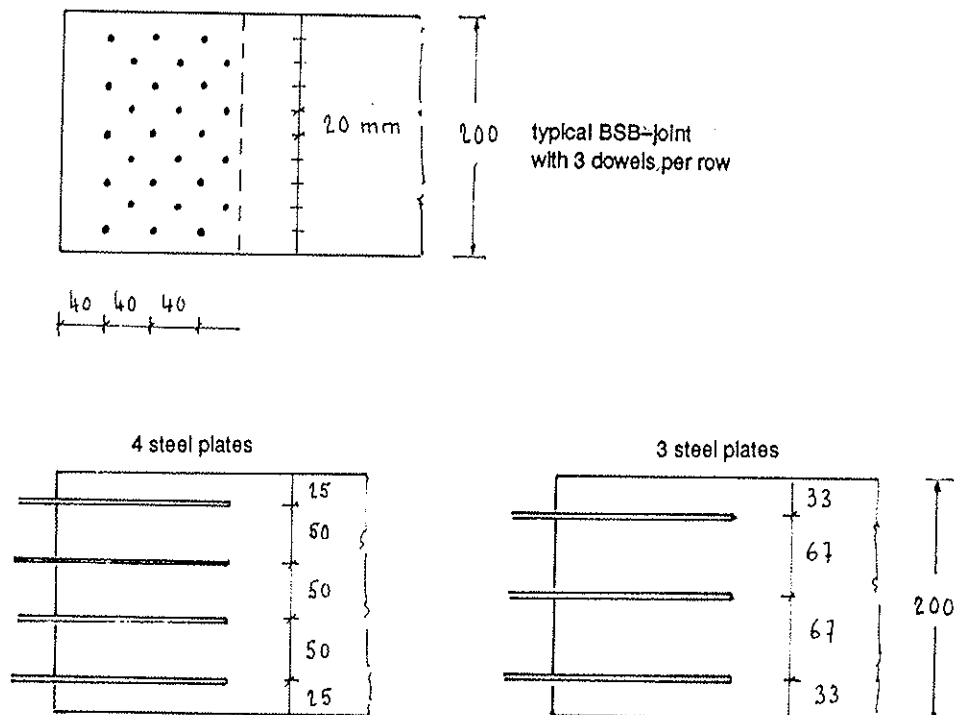


Figure 1: Type of BSB-connections used

4. Test arrangement and procedure

The test arrangement can be shown in figure 2. By using the indicated arrangement and symmetrical test specimens, a total of 38 connections were tested. Registered were 38 load-deformation curves and 19 load-carrying capacities (the lower of two values). The load was applied at a constant deformation increment rate of 1,40 mm per minute.

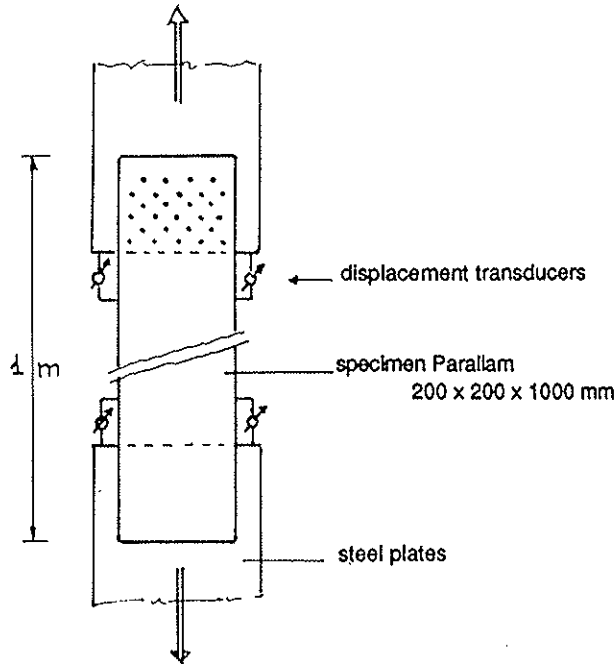


Figure 2: Test arrangement and position of displacement transducers

5. Test results

5.1 BSB-typ 67 and normal BSB-dowels

For this configuration the number of dowels in a row was varied between 3 and 5. The rest results are given in table 1.

3 steel plates in distances of 67 mm, 3 dowels per row

Specimen	Dowels [-]	Density [kg/m ³]	F _u [kN]	F _u per dowel and shear plane	σ_t gross [N/mm ²]	σ_t net [N/mm ²]
Mean value		644	801	4.95	20.03	30.72
P3R-67-1	27 BSB	650	801	4.94	20.03	30.71
P3R-67-2	27 BSB	640	795	4.91	19.88	30.48
P3R-67-3	27 BSB	642	815	5.03	20.38	31.25
P3R-67-4	27 BSB	645	794	4.90	19.85	30.44

3 steel plates in distances of 67 mm, 4 dowels per row

Specimen	Dowels [-]	Density [kg/m ³]	F _u [kN]	F _u per dowel and shear plane	σ_t gross [N/mm ²]	σ_t net [N/mm ²]
Mean value		652	1043	4.83	26.06	39.97
P4R-67-1	36 BSB	670	1050	4.86	26.25	40.26
P4R-67-2	36 BSB	647	1055	4.88	26.38	40.45
P4R-67-3	36 BSB	636	1012	4.69	25.30	38.80
P4R-67-4	36 BSB	654	1053	4.88	26.33	40.38

3 steel plates in distances of 67 mm, 5 dowels per row

Specimen	Dowels [-]	Density [kg/m ³]	F _u [kN]	F _u per dowel and shear plane	σ _t gross [N/mm ²]	σ _t net [N/mm ²]
Mean value		646	1198	4.44	29.94	45.92
P5R-67-1	45 BSB	656	1244	4.61	31.10	47.70
P5R-67-2	45 BSB	635	1149	4.26	28.73	44.06
P5R-67-3	45 BSB	648	1200	4.44	30.00	46.01

Table 1: Test results

The values per bolt and shear plane are calculated assuming 6 identical shear planes (the two outside parts have a smaller contribution).

The load-deformation curves are given in figure 3. From them the following can be seen:

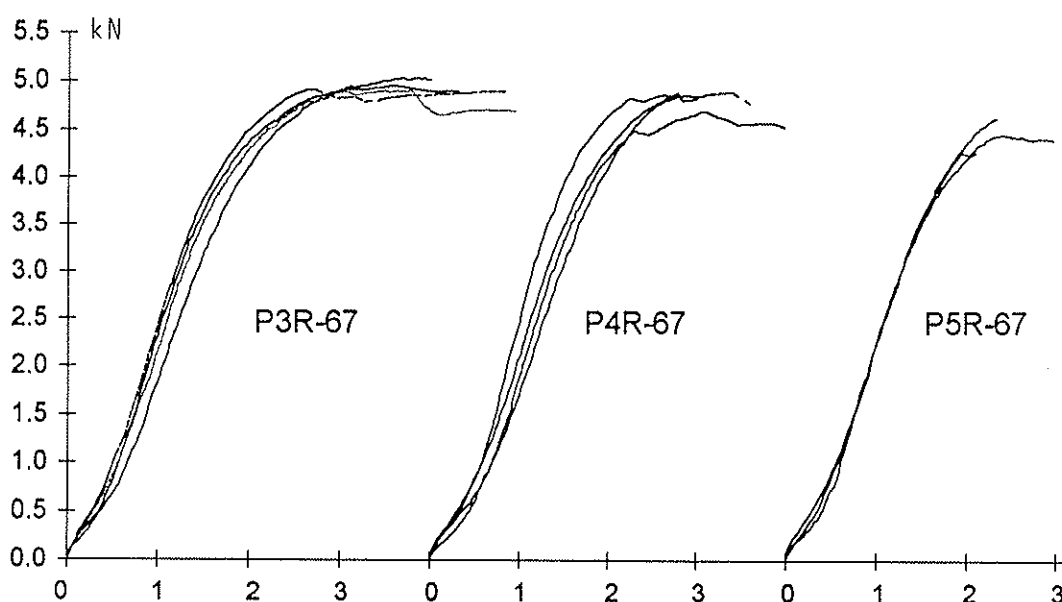


Figure 3: Load-deformation curves for 3, 4 and 5 dowels in a row; forces per dowel and shear plane in kN

- ◆ The strength per dowel and shear plane reduces slightly with increasing number of dowels in a row; with 5 dowels in a row the tensile stress in the net section has reached the ultimate capacity of the Parallam.
- ◆ Ductility of the joint decreased with increasing number of dowels; for 5 dowels in a row brittle failures occurred.

5.2 BSB-typ 67 and higher strength dowels

Through the use of dowels with steel strength $f_u \cong 1070 \text{ N/mm}^2$ instead of $f_u \cong 650 \text{ N/mm}^2$ (effective value of BSB-dowels used) and diameter of 6,0 mm instead of 6,25 mm, the load-carrying capacity was only increased by about 6 % (see table 2).

3 steel plates in distances of 67 mm, 4 dowels per row

Specimen	Dowels [-]	Density [kg/m ³]	Fu [kN]	Fu per dowel and shear plane	σt gross [N/mm ²]	σt net [N/mm ²]
Mean value		640	1105	5.12	27.63	42.38
P4R-67-A	36 ETG	665	1185	5.49	29.63	45.44
P4R-67-B	36 ETG	644	1050	4.86	26.25	40.26
P4R-67-C	36 ETG	623	1074	4.97	26.85	41.18
P4R-67-D	36 ETG	628	1112	5.15	27.80	42.64

Table 2: Test results with ETG-dowels

Following Johansen a little higher increase should be achieved (about 15 %). Due to earlier failure in the wood, the conditions for a mode 3 failure could not be fulfilled (see figure 4) in two of 4 cases.

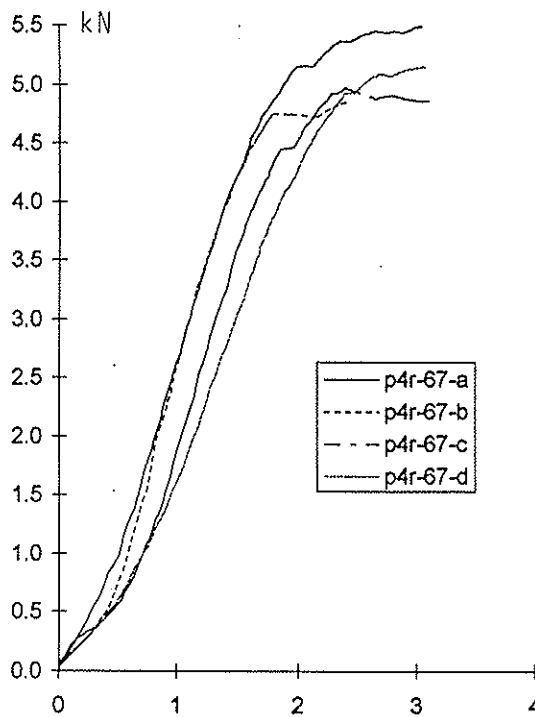


Figure 4: ETG-dowel

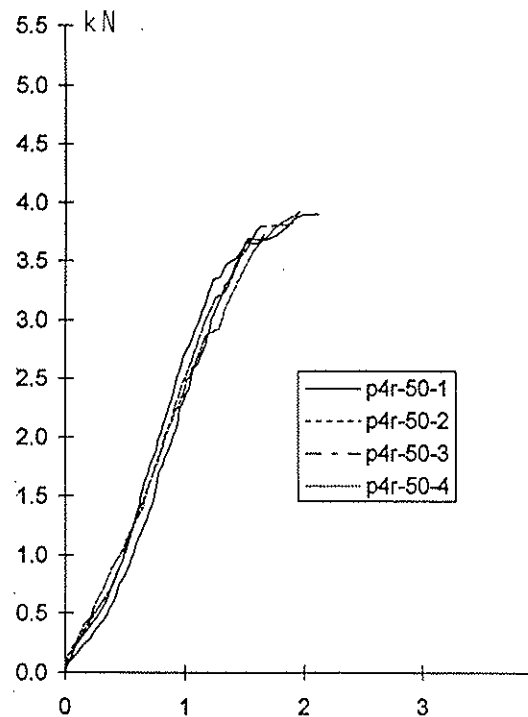


Figure 5: BSB-dowel and 4 steel plates

5.3 BSB-typ 50 and normal BSB-dowel

The use of a smaller spacing of the steel plates allows the use of 4 plates instead of 3 for the same dimension of the timber. The number of shear planes increases from 6 to 8 per dowel but the load-carrying capacity decreases per shear plane, as can be seen in table 3 and figure 5.

4 steel plates in distances of 50 mm, 4 dowels per row

Specimen	Dowels [-]	Density [kg/m ³]	Fu [kN]	Fu per dowel and shear plane	σt gross [N/mm ²]	σt net [N/mm ²]
Mean value		642	1107	3.84	27.68	43.86
P4R-50-1	36 BSB	630	1072	3.72	26.80	42.47
P4R-50-2	36 BSB	635	1105	3.84	27.63	43.78
P4R-50-3	36 BSB	653	1123	3.90	28.08	44.49
P4R-50-4	36 BSB	648	1128	3.92	28.20	44.69

Table 3: Test results for connections with 4 steel plates and BSB-dowels

A better comparison is given when comparing directly the load-carrying capacities (see figure 6).

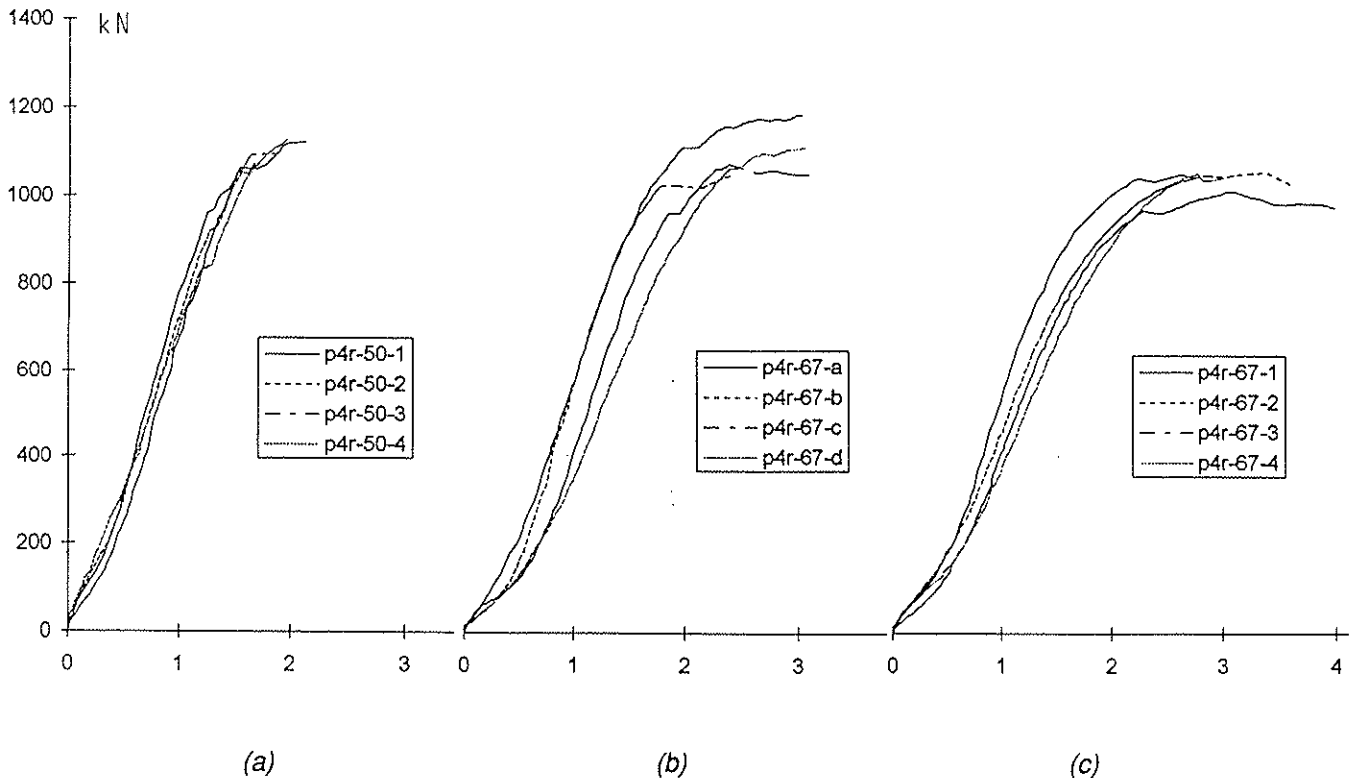


Figure 6: Load-carrying capacities of the 3 different joints using the same number of dowels (36 in 9 rows of 4 dowels) per connection:

- (a) with 4 steel plates and BSB-dowels $\varnothing 6,25$ mm
- (b) with 3 steel plates and ETG-dowels $\varnothing 6,0$ mm
- (c) with 3 steel plates and BSB-dowels $\varnothing 6,25$ mm

From figure 6 a it can be seen that the joint with 4 steel plates leads to a stiffer joint but with very brittle behaviour. A better behaviour could be found when using only 3 steel plates (and higher slenderness of the dowel) as seen in figure 6 b or 6 c.

6. Conclusions

The BSB connections are meanwhile (the tests with Parallam were made in 1991) made with a distance of the steel parts of 60 mm. Using normal BSB-dowels a similar behaviour as seen in figure 6 c will result and a slightly higher load-carrying capacity achieved.

The connection length is – independent of the section – when using 4 dowels in a row only about 220 mm, that is a very short connection.

The reliability is high; the variation of the connection load-carrying capacity is small, since the failure is connected to the formation of plastic hinges in the steel dowels.

The performance of the connected wood composite is high. Based on the net section (for 3 steel plates about 2/3 of the total section) the tensile strength of Parallam ($f_t \cong 45$ N/mm²) has been reached. Therefore the performance of the joint – based on the total section – reaches about 2/3.

The group effect is directly considered, since the test were made with full size joints and corresponding high number of dowels (about 36 dowels) or more than 200 shear planes per joint.

**INTERNATIONAL COUNCIL FOR BUILDING RESEARCH STUDIES AND DOCUMENTATION
WORKING COMMISSION W18 - TIMBER STRUCTURES**

**MULTIPLE FASTENER TIMBER CONNECTIONS WITH DOWEL TYPE
FASTENERS**

by

A Jorissen
Department of Civil Engineering
Delft, University of Technology
The Netherlands

MEETING THIRTY

VANCOUVER

CANADA

AUGUST 1997

Multiple Fastener Timber Connections with Dowel type Fasteners

André Jorissen, Section Steel & Timber Structures, Department of Civil Engineering, Delft University of Technology, the Netherlands

Abstract

The load carrying capacity of a connection with a number of fasteners, a so called multiple fastener connection, does generally not equal the load carrying capacity of a single fastener multiplied by this number. Often the connection fails at a lower load because the timber splits. The result can be a brittle failure. The geometrical parameters, material properties and the number of fasteners determine the load carrying capacity and the type of failure. To investigate the governing parameters a comprehensive research, both theoretical and experimental, started at the Delft University of Technology at the beginning of 1994. About 950 tests on single and multiple bolted connections have been carried out. The tests will be presented and discussed.

KEY Words: Timber, Multiple Fasteners, Bolts, Load Distribution, Fracture Mechanics.

Introduction

This paper deals with the load carrying capacity of multiple fastener timber connections, timber to timber, with dowel type fasteners in a row parallel to the grain. Symmetrical double shear connections are studied. The connection is in the grain direction.

The fact that the load carrying capacity of a multiple fastener connection, $F_{multiple}$, does not equal the load carrying capacity of a single fastener connection, F_{single} , multiplied by the number of fasteners n is taken into account in many national design codes. An effective number of fasteners n_{ef} ($n_{ef} < n$) has been introduced. $F_{multiple}$ is calculated according to equation (1).

$$F_{multiple} = n_{ef} F_{single} \quad (1)$$

In most countries F_{single} is calculated according to the so called European Yield Model, first described by Johansen (1941 and 1949), which allows n_{ef} , as defined in the national design codes, to be compared. As shown by Jorissen (1996), hardly any agreement on the design values for n_{ef} exists. Even if the background of the design rules are more or less the same there is no agreement. For instance, the design rules for Europe and Canada are both experimentally based. Nevertheless, n_{ef} for Europe is two to three times higher than n_{ef} for Canada.

The last fifty years research have been carried out to determine the load carrying capacity of multiple fastener connections. H. Fahlbusch (1949) was the first who presented a design equation for n_{ef} for bolts.

Lantos (1969), Cramer (1968) and v/d Put (1976) presented an analytical method for the calculation of the load distribution among the individual fasteners based on the assumption of identical linear elastic behaviour of all fasteners. Van der Put (1976) extended his model by a plastic analyses.

Wilkinson (1986) developed a numerical model where fabrication tolerances and variability of single fastener non-linear load-slip behaviour are taken into account. The result of this model is a randomly non uniform load distribution among the individual fasteners. Moss (1996) extended Wilkinson's research by simulation of a large number of joints. Moss used a piecewise linear approximation of the actual fastener load-slip curve measured by Wilkinson.

As discussed by Jorissen (1996) the equations according to the European Yield Model for rigid dowels can be replaced by an equation based on fracture mechanical considerations: equation (2). As a consequence, fracture mechanical considerations may be of importance for the analyses of multiple fastener timber connections.

$$F_{single} = t \sqrt{\frac{G_c E d (2 h - d)}{h}} \quad (2)$$

- With:
- F_{single} load carrying capacity of the single fastener connection [N]
 - G_c fracture mechanical energy [Nmm/mm²]. To determine this value a model presented by Gustafsson (1992) and Petersson (1995) can be used. This model results in $G_c \approx 0.43$ Nmm/mm².
 - E modulus of elasticity parallel to the grain [N/mm²]
 - d actual bolt diameter [mm]
 - h timber width [mm]
 - t summation of the timber thicknesses of the side members ($= 2 t_s$) or the middle member ($= t_m$) respectively

Behaviour of multiple fastener timber connections with rigid dowels

The embedding stresses in the timber introduced by the dowel type fastener are more or less uniform along the fastener axis, because the fastener does not bend. As shown by Jorissen (1995) by finite element calculations (two bolts in the row) the stresses perpendicular to the grain and shear are both at maximum near the bolt surface. An illustration of these stresses is shown in figure 1. First cracks develop near the bolt hole. Because the tension perpendicular to the grain

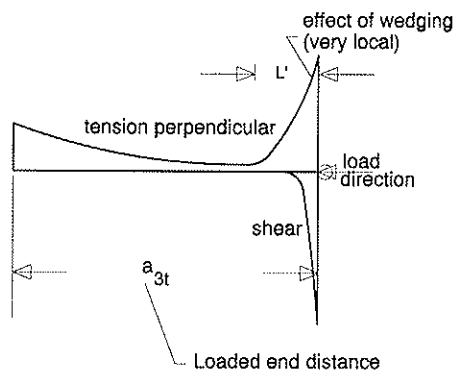


Figure 1: Stress distributions

and the shear parallel to the grain reach their maximum, it is a so called mixed mode fracture.

The stresses perpendicular to the grain are governed by the number of fasteners and the spacing. The shear stresses are determined by the force transferred by the fastener itself. There is no influence on the shear stresses of the other fasteners in the row. Therefore, fracture in a multiple fastener connection is predominantly governed by tension perpendicular to the grain. Cracks caused by tension perpendicular to the grain develop at a lower load than cracks caused by shear.

For this reason, a multiple fastener connection with rigid dowel type fasteners will fail at a load $F_{multiple} = n_{ef} F_{single}$, with $n_{ef} < n$. This is illustrated in figure 2.

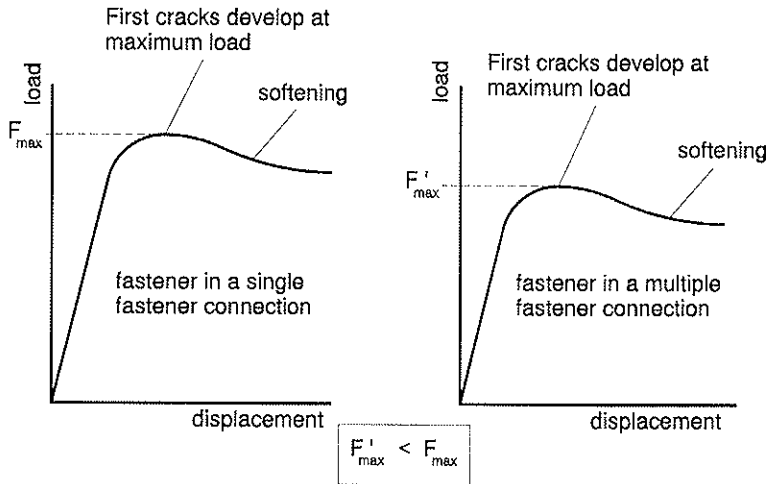


Figure 2: Load-displacement of a fastener in a single fastener connection and in a multiple fastener connection

Influence of the load distribution

Fabrication tolerances and the variability in load-slip behaviour of the single fastener result in a random load distribution among the individual fasteners. Consequently, the fasteners do not all reach maximum load, F_{max} or F'_{max} in figure 2, at the same moment.

However, the connection does not fail if one fastener reaches its ultimate load. As shown in figure 3, the load carried by the fastener slightly decreases if the displacement increases. This is called softening. This softening results in re-distribution of the load among the individual fasteners. For large end slip (displacement at failure load) the load will be uniformly distributed among the fasteners. This depends strongly on the spacing and the loaded end distance and the fastener slenderness.

Additionally, the load carried by the maximum loaded fastener must reduce because of the increased load carried by the other fasteners. As discussed before, the crack development in a multiple fastener connection is predominantly governed by tension perpendicular to the grain and not by shear. Therefore, the load carried by the maximum loaded fastener must decrease if the load carried by the other fasteners increases. This is illustrated by figure 3.

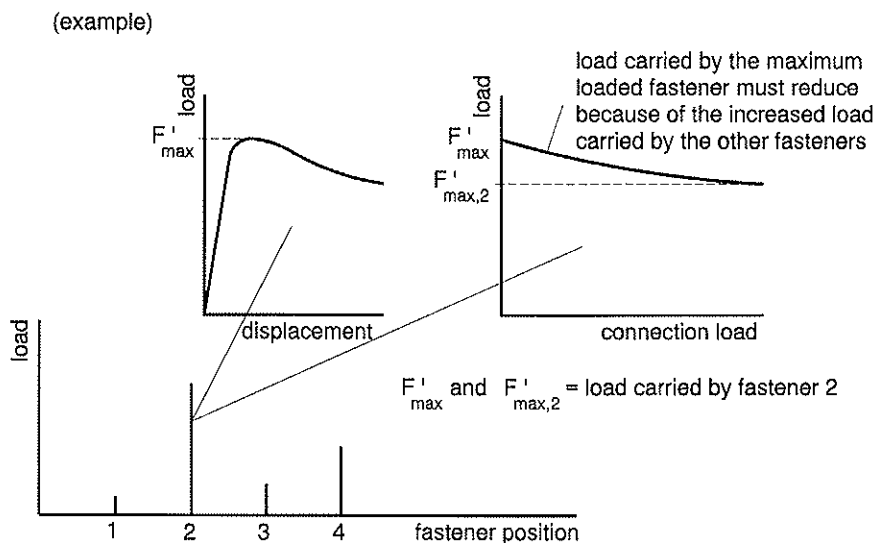


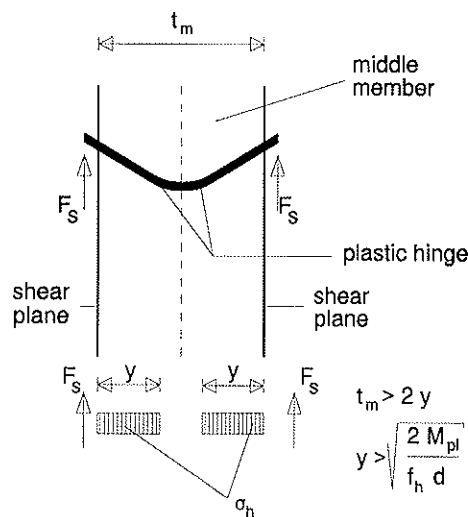
Figure 3: Reduction of the load carried by the maximum loaded fastener after some redistribution of the load

Experiments on multiple fastener timber connections with rigid dowel type fasteners often fail at rather small end slip. Consequently, complete redistribution of the load is prevented. The connection will fail at a low load.

Behaviour of multiple fastener timber connections with *slender* dowels

The embedding stresses in the timber, introduced by the dowel type fastener, are not uniform along the fastener axis, because the fastener bends. The connection often shows large deformations at failure load and behaves ductile. Therefore, the result will be a uniform load distribution. There will be hardly any load reduction per fastener: $n_{ef} \approx n$.

In some cases, however, the middle member splits prematurely. The uniformity of the tensile stresses perpendicular depends on the thickness of the middle member t_m : uniformity decreases when t_m increases. This is illustrated in figure 4.



The dimension of y must satisfy a minimum value, otherwise the dowel type fastener cannot be regarded as slender. The minimum value for y in figure 4 is given by Meyer (1957); it is assumed that the embedding strength f_h is identical for the side and middle members.

Figure 4: More or less uniform embedding stresses σ_h in the middle member depending on the timber thickness t_m

A multiple fastener connection with slender dowel type fasteners and t_m slightly higher than the minimum values given in figure 4 will fail at a load $F_{multiple} = n_{ef} F_{single}$, with $n_{ef} \leq n$. This is illustrated in figure 2. In this case the capability of load redistribution must be assured by softening.

Behaviour of multiple fastener timber connections with dowels in general

The slenderness of dowel type fasteners is, by definition, determined by the fastener diameter and the timber thickness. The slenderness, and the effect on the failure mode, is illustrated by the graphical presentation of the European Yield Model for connections in double shear in figure 5 (identical embedding strength for side- and middle members assumed).

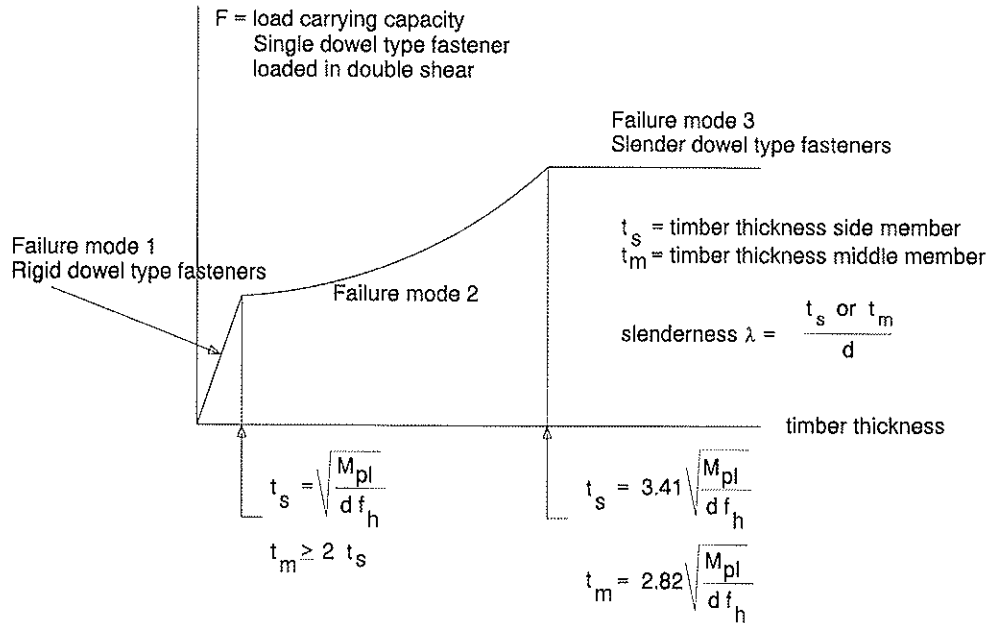


Figure 5: Graphical presentation of the European Yield Model for connections in double shear

Experimental research

About 950 experiments have been carried out and will briefly be reported in this paper.

Test specimen

The wood species was North European Spruce. The tests have been carried out under constant climate conditions: temperature = 20 °C and the relative air humidity = 65 %.

Most of the tests have been carried out using so called M 12 'black' bolts (nominal diameter = 12 mm; yield strength ≥ 240 N/mm²). The tests with these bolts will be discussed in this paper. The timber dimensions were taken so that all three failure modes (see figure 5) could be expected.

Thus, with $M_{pl} = 69120$ Nmm and $f_h = 27$ N/mm², it follows:

$$\text{Rigid fasteners: } t_s \leq \sqrt{\frac{M_{pl}}{d f_h}} = \sqrt{\frac{69120}{12 \cdot 27}} = 15 \text{ mm}$$

$$t_m \leq 2 t_s = 30 \text{ mm}$$

$$\text{Slender fasteners: } t_s \geq 3.41 \sqrt{\frac{M_{pl}}{d f_h}} = 3.41 \sqrt{\frac{69120}{12 \cdot 27}} = 50 \text{ mm}$$

$$t_m \geq 2.82 \sqrt{\frac{M_{pl}}{d f_h}} = 2.82 \sqrt{\frac{69120}{12 \cdot 27}} = 41 \text{ mm}$$

Based on these considerations the timber thicknesses for the side members (t_s) and middle members (t_m) are chosen according to table 1.

expected failure mode (see figure 5)	1	2	3
t_s [mm]	12	24	59
t_m [mm]	24	48	72

Table 1: Expected failure modes and the timber thicknesses

Furthermore the number of bolts (n), the spacing (a_1), the end distance (a_3), the number of rows (m) and the load direction (tension - compression) have been varied. An overview of the test specimen for tests on multiple fastener connections is given in figure 6 and table 2.

thickness [mm]		spacing a_1	end distance a_{3c} resp. a_{3t}	number of bolts per row n	number of rows m
t_s	t_m				
12	24		7d	1	1
		3d	7d	5	1, 2
		5d	7d	3, 5, 9	1
		7d	7d	3, 5, 9	1
		7d	7d	5	2
		11d	7d	3, 5	1
24	48		7d	1	1
		3d	7d	5	1, 2
		5d	5d	3, 5, 9	1
		5d	7d	3, 5, 9	1
		7d	5d	5	1
		7d	7d	3, 5, 9	1
		7d	7d	5	2
11d	7d	3, 5, 9	1		
59	72		7d	1	1
		3d	7d	5	1
		5d	5d	3, 5, 9	1
		5d	7d	3, 5, 9	1
		7d	5d	5, 9	1
		7d	7d	3, 5, 9	1
		11d	7d	3, 9	1
<p>Remarks: - specimens with two rows are tested in compression in combination. - the tests on specimens with three bolts in the row are not completed yet. Therefore the results can not be reported in this paper. On the other hand, the completed results on connections with 3 bolts are taken for the regression analysis, presented in this paper. - specimens with 3 and 9 bolts are tested in tension. - from the specimens with 5 bolts are 10 replicas tested in compression and 10 replicas tested in tension. - mostly, 20 replicas of each specimen have been tested. - d = nominal bolt diameter (= 12 mm)</p>					

Table 2: Overview of the test specimens.

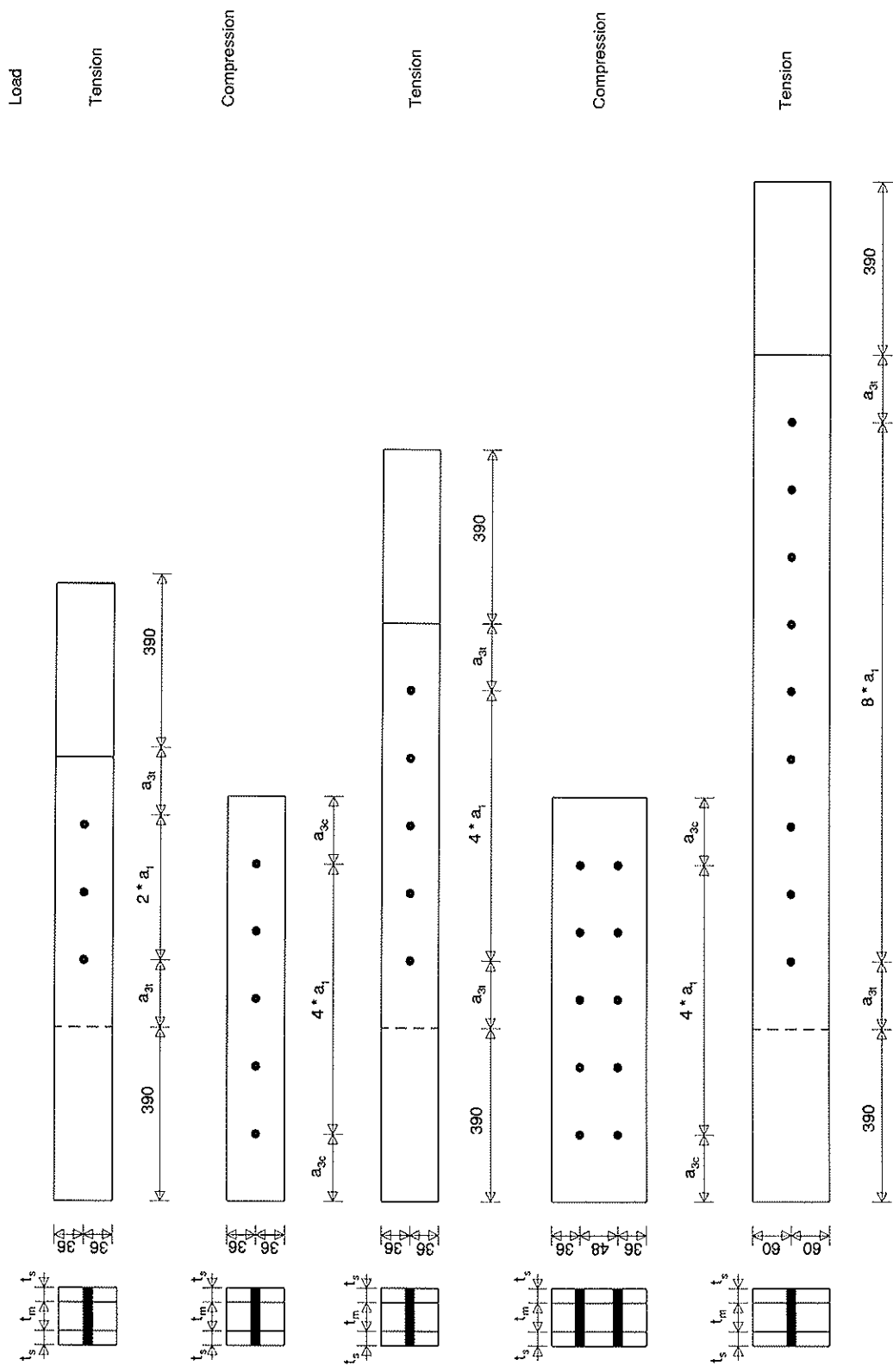


Figure 6: Specimen for the tests on multiple bolted connections

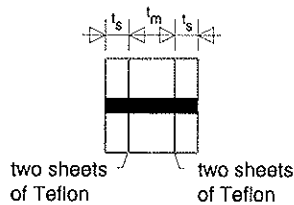


Figure 7

To reduce friction between the timber parts, two sheets of Teflon are placed in both shear planes. This is illustrated in figure 7. Furthermore, the nuts and washers have been left out and it has been taken care of that the bolt head did not touch the timber surface.

As shown in table 3 tests on single fastener connections have been carried out as well. The test specimens were cut from a multiple fastener connection with 5 bolts. This is illustrated in figure 8. These specimens were tested in compression.

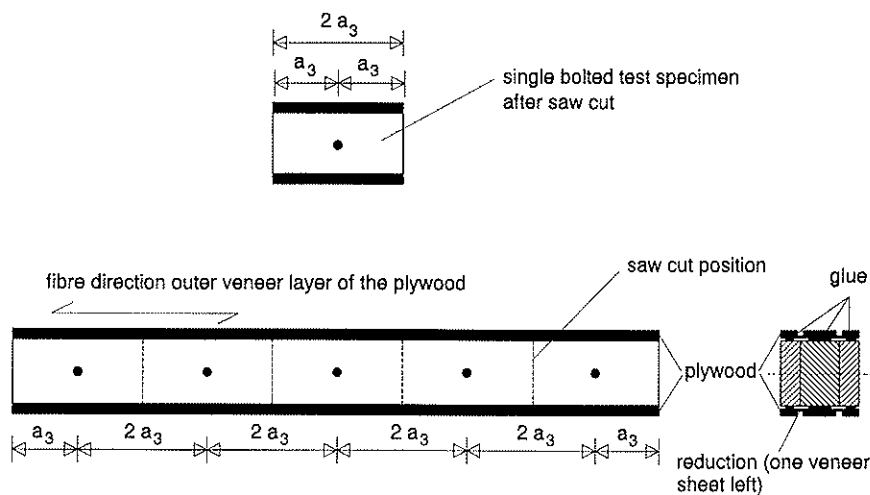


Figure 8: Test specimen for the single bolted connections

It is thought that the differences in hole clearances of the individual fasteners in a multiple fastener connection is important for the load carrying capacity. To verify this the individual hole clearances were fixed by the plywood as illustrated in figure 8. The thickness of the plywood was reduced to one veneer sheet (fibre direction in the load direction) to reduce its strength. Then the test specimens were sawn cut.

Thus, firstly the tests on single fastener connections were carried out to record the hole clearances. Secondly, these tests provide a reference for the load carried by the multiple fastener connections.

Measurements

The moisture content and density of all timber pieces, side and middle members, have been taken. The timber density is of importance for the fracture mechanical wood properties and for the estimation of the embedding strength.

Furthermore, the actual bolt diameter of all bolts used, have been recorded. The yield strength of all types of bolts (10 replicas each) have been tested according to EN 409, which standard is meant for the determination of the yield capacity of nails..

The tests on the connections have been carried out according to EN 26891. The slip is taken on both sides of the test specimen.

Results

The mean density of the timber was, at a moisture content of 12 %, 460 kg/m³, with a coefficient of variation of 9 %.

The yield strength of the bolts varied from about 300 to 600 N/mm². This variation is of no concern to the test on connections with rigid dowel type fasteners. On the other hand this variation does affect the results of the tests connections with slender dowel type fasteners.

The bolt diameter varies as well. Although a nominal bolt diameter of d = 12 mm was ordered, the actual bolt diameters delivered were between 10.65 mm and 11.75 mm. In every joint bolts of equal diameter and yield strength were chosen.

Table 3 shows the test results together with the results according to the European Yield Model (EYM) and equation (2).

thickness [mm]		actual bolt diameter [mm]	load carrying capacity						number of tests
t _s	t _m		Test result		EYM		Equation (2)		
			Mean [N]	c.o.v. [%]	Mean [N]	c.o.v. [%]	Mean [N]	c.o.v. [%]	
12	24	11.81	7465	8	9640	2	8790	7	25
24	48	10.65	11905	5	13674	1			25
59	72	11.81	18795	10	16070	3			20

Table 3: Results of the tests on *single* fastener connections

Load carrying capacity of multiple fastener connections

The test results will be presented in relation to the test results of the single fastener connections. An effective number of fasteners is calculated according to equation (3).

$$n_{ef} = \frac{\text{characteristic value of the test result multiple fastener}}{\text{characteristic value of the test result single fastener}} \quad (3)$$

The characteristic values (lower 5%) are calculated according to: charact. = (1 - 1.64 * c.o.v.) * Mean. See table 4^a, 4^b and 4^c.

timber thickness t _s = 12 mm actual bolt diameter = 11.75 mm t _m = 24 mm									
n	a ₁	a ₃	Test result Multiple fastener connection			n _{ef}	end slip		number of tests
			Mean [N]	c.o.v. [%]	Charact. [N]		Mean [mm]	c.o.v. [%]	
5	3 d	7d	18313	17	13128	2.0	3.9	17	20
	5 d	7d	26671	11	21708	3.4	3.2	21	20
	7 d	7d	31716	8	27381	4.2	6.1	9	20
	11 d	7d	35112	9	30184	4.7	8.8	19	20

Table 4^a: Results of tests on multiple fastener connections with rigid bolts

The end slip (= displacement at failure) is very important for the analyses. As discussed before, the end slip indicates whether the load is uniformly distributed among the fasteners or not. Therefore the end slip is reported in the tables 4^a, 4^b and 4^c as well.

timber thickness $t_s = 12$ mm actual bolt diameter = 11.75 mm $t_m = 24$ mm									
n	a_1	a_3	Test result Multiple fastener connection			n_{ef}	end slip		number of tests
			Mean [N]	c.o.v. [%]	Charact. [N]		Mean [mm]	c.o.v. [%]	
9	5 d	7 d	54162	19	37372	5.8	2.9	33	20
	7 d	7 d	52513	21	34470	5.3	3.1	40	20

Table 4^a: Results of tests on multiple fastener connections with rigid bolts (continuation)

timber thickness $t_s = 24$ mm actual bolt diameter = 10.65 and 11.75 mm $t_m = 48$ mm									
n	a_1	a_3	Test result Multiple fastener connection			n_{ef}	end slip		number of tests
			Mean [N]	c.o.v. [%]	Charact. [N]		Mean [mm]	c.o.v. [%]	
5	3 d	7d	35863	12	28882	2.6	3.9	12	20
	5 d	5d	52870	11	43602	4.0	4.9	37	20
	5 d	7d	50885	8	43946	4.0	4.5	23	20
	7 d	5d	56575	7	50229	4.6	8.6	34	20
	7 d	7 d	55876	5	51742	4.7	13.1	20	20
	11 d	7 d	56491	4	52505	4.8	18.4	17	20
9	5 d	5 d	78977	17	57466	5.3	4.6	42	20
	5 d	7 d	95162	6	85066	7.8	4.9	33	20
	7 d	5 d	96450	8	83337	7.6	7.0	43	20
	7 d	7 d	100830	4	94213	8.6	8.8	26	20
	11 d	7d	100324	5	91739	8.4	5.0	38	10

Table 4^b: Results of tests on multiple fastener connections

timber thickness $t_s = 59$ mm actual bolt diameter = 11.75 mm $t_m = 72$ mm									
n	a_1	a_3	Test result Multiple fastener connection			n_{ef}	end slip		
			Mean [N]	c.o.v. [%]	Charact. [N]		Mean [mm]	c.o.v. [%]	number of tests
5	3 d	7 d	45393	15	33893	2.2	3.8	30	20
	5 d	5 d	70841	8	61675	3.9	9.3	19	20
	5 d	7 d	61897	4	57383	3.7	8.7	24	20
	7 d	5 d	78272	6	70582	4.5	13.8	25	20
	7 d	7 d	76562	8	66292	4.2	9.2	45	20
9	5 d	5 d	115557	10	96823	6.2	6.5	15	20
	5 d	7 d	117467	7	103308	6.6	6.5	32	20
	7 d	5 d	130524	7	115824	7.4	10.5	21	20
	7 d	7 d	128443	12	104003	6.6	10.0	28	20
	11 d	7 d	164456	7	145253	9.2	12.5	24	10

Table 4^e: Results of tests on multiple fastener connections with slender bolts

Regression Analysis

Some preliminary regression calculations have been carried out. All the test results have been taken into account. Three of the possible regression equations will be presented here, equations (4), (5) and (6).

$$F_{multiple} = 0.31 * n^{0.96} * m^{0.97} * \left(\frac{a_1}{d_n}\right)^{0.44} * \left(\frac{t_m}{d_n}\right)^{0.22} * F_{single-ECS} \quad (4)$$

$$F_{multiple} = 1575 * n * m^{0.88} * \left(\frac{a_1}{d_n}\right)^{0.43} * \left(\frac{t_m}{d_n}\right)^{0.82} \quad (5)$$

$$F_{multiple} = 1440 * n * m * \left(\frac{a_1}{d_n}\right)^{0.45} * \left(\frac{t_m}{d_n}\right)^{0.83} \quad (6)$$

With: $F_{multiple} \leq n * m * F_{single}$
 $F_{single-ECS}$ = load carrying capacity of the single fastener connection. This means that the density is not varied. The density $\rho = 380$ kg/m³ in all cases.

The correlation coefficient is for all three equations about 0.925. The coefficient of determination is therefore about 0.85. The coefficient of determination is just slightly different if the real density, determined for each individual piece of wood, is taken into account. Therefore the density is not varied.

The end distance is not in either three regression equations. The end distance seems to be

of no significant influence on the load carrying capacity. Note that only two different end distances have been regarded in this research (see table 2).

Furthermore, the coefficient of determination does hardly change if $F_{\text{single-EC5}}$ is not in the regression equation. This means that $F_{\text{single-EC5}}$ is almost completely explained by the thickness of the middle member. The stress distribution will be more or less uniform along the bolt axis as shown in figure 4.

The timber thickness of the side members is not in the regression equation either. The connections were designed in such a way that the correlation between the thicknesses of the side- and middle members is very high (more than 0.90). Furthermore, the thickness of the middle member affects the coefficient of determination much more than the thickness of the side members. Therefore the thickness of the timber side members has been left out.

Concluding remarks

For most configurations no significant difference has been found in the load carrying capacity between tests carried out in compression or in tension.

The differences in individual hole clearances can be of some importance if the end slip is rather low (smaller than 2 to 3 mm). In most cases the end slip is higher. As a consequence, in most cases the individual hole clearances does not affect the load carrying capacity.

The reduction factor R in load carrying capacity is calculated according to equation (7).

$$R = \frac{n_{ef}}{n} \quad (7)$$

Table 5 shows the reduction factor R for the presented test results in table 4 (characteristic values). The values for $(1 - R)/n$ are added for the indication of the reduction per fastener. These indicate that the reduction per fastener reduces if the number of fasteners increases.

timber sizes [mm]		spacing a_1	end distance a_3	n	R	$\frac{1-R}{n}$
t_s	t_m					
12	24	5d	7d	5	0.68	0.064
				9	0.64	0.040
		7d	7d	5	0.84	0.032
				9	0.59	0.034
24	48	5d	5d	5	0.80	0.040
				9	0.60	0.044
		5d	7d	5	0.80	0.040
				9	0.87	0.014
		7d	7d	5	0.94	0.012
				9	0.95	0.006
59	72	5d	5d	5	0.78	0.044
				9	0.69	0.023
		5d	7d	5	0.74	0.052
				9	0.73	0.030
		7d	7d	5	0.84	0.032
				9	0.73	0.030

Table 5: Reduction factors R

The effective number of fasteners n_{ef} is calculated according to equation (3). This means that the results from tests on the single fastener connections are compared to the results from tests on the multiple fastener connections. The results from tests on single fastener connections are, however, for the connections with rigid bolts significantly below the calculated values according to the European Yield Model. Consequently, the reduction factors for connections with rigid bolts decrease if the strength values for the single fastener connections according to the European Yield Model are compared to the results from tests on multiple fastener connections. This results in a more significant influence of the timber thickness (a slenderness influence). This comparison has not been made, because this is not a comparison between equal quantities. Consequently, it must be investigated why the results from tests on single fastener connections differ so significantly from the theoretical values.

It is quite remarkable that the load carrying capacity, presented by the regression equations (4), (5) and (6), is almost linear to the number of bolts (the coefficients turn out to be almost one). If this is true, the fact that the effective number of bolts n_{ef} does not equal the actual number of bolts n is explained by the spacing and the timber thickness of the middle member.

More remarks are shown in table 6.

	rigid failure mode 1	failure mode 2	slender failure mode 3	
			$t_m > 2.82 \sqrt{\frac{M_{pl}}{d f_h}}$	$t_m \approx 2.82 \sqrt{\frac{M_{pl}}{d f_h}}$
Ductility provided by	limited softening (low ductility)	softening (low ductility)	plastic deformations in wood and fastener	full softening
spacing	very important	very important	important	very important
loaded end distance	not important	not important	not important	not important
Hole clearances	important in combination with small spacing and/or end distance	important in combination with small spacing and/or end distance	not important	not important

Table 6

Table of symbols

a_1	spacing parallel to the grain
a_3	end distance
n	number of fasteners in the row
n_{ef}	effective number of fasteners in the row
F_{single}	load carrying capacity of a single fastener connection
$F_{singleEC5}$	load carrying capacity of a single fastener connection according to Eurocode 5. This means that the density $\rho = 380 \text{ kg/m}^3$ in all cases (the density is not varied).
$F_{multiple}$	load carrying capacity of a multiple fastener connection
t	timber thickness
t_s	timber thickness of the side member
t_m	timber thickness of the middle member
d	diameter of the dowel type fastener
M_{pl}	plastic bending capacity of the dowel type fastener
f_h	embedding strength
σ_h	embedding stress

Acknowledgements

This research is supported by the Dutch Technology Foundation (STW).

References

- Johansen, K.W. 1941. Forsøg med træforbindelser. (In Danish. Tests with timber connections). Bygningsstatistiske Meddelelser, årgang XII.
- Johansen, K.W. 1949. Theory of timber connections. International Association for Bridge and Structural Engineering. 9: 249 - 262.
- Jorissen, A.J.M. 1995. Wood research at the Lund Institute of Technology, Division of Structural Mechanics. Report 25.4.95.02/MFJ-1, Delft University of Technology, Delft, The Netherlands.
- Jorissen, André. 1996. Multiple Fastener Timber Connections with Dowel Type Fasteners. In: Proceedings of the International Wood Engineering Conference (IWEC), New Orleans, Louisiana, USA: 4-189 - 4-196.
- Fahlbusch, H. 1949. Ein Beitrag zur Frage der Tragfähigkeit von Bolzen in Holz bei statischer Belastung. Dissertation T.H. Braunschweig.
- Lantos, G. 1969. Load Distribution in a Row of Fasteners subjected to Lateral Load. Wood Science. 1(3): 129 - 136.
- Cramer, Calvin O. 1968. Load Distribution in Multiple-bolt Tension Joints. Journal of the Structural Division, Proceedings of the American Society of Civil Engineers: 1101 - 1117.
- Van der Put, T.A.C.M. 1976. Proeven op stiftverbindingen hout op hout en staal op hout in horizontaal gelamineerd hout en in constructiehout. Resultaten van het studentenpracticum 1975-1976. (In Dutch. Tests on timber connections with dowel type fasteners in glulam and sawn structural timber. Results of tests carried out by students in 1975-1976). Rapport 4-76-2, Stevin Laboratorium, Technische Hogeschool Delft.
- Wilkinson, Thomas Lee. 1986. Load Distribution among bolts parallel to Load. Journal of Structural Engineering: 112(4): 835-851.
- Moss, Peter J. 1996. Research Into Row Modification Factors for Multiple-bolted Timber Joints. In: Proceedings of the International Wood Engineering Conference (IWEC), New Orleans, Louisiana, USA: 4-197 - 4-204.
- Meyer, Adolf. 1957. Die Tragfähigkeit von Nagelverbindungen bei Statischer Belastung. In: Holz als Roh- und Werkstoff, 15 (2): 96-109.
- Gustafsson, P.J. 1992. Some test methods for fracture mechanics properties of wood and wood adhesive joints, RILEM TC133-TF workshop, Bordeaux, France.
- Petersson, Hans. 1995. Fracture design analyses of wooden beams with holes and notches. Paper 28-19-3, Proceedings CIB-W18 meeting, Copenhagen, Denmark.

**INTERNATIONAL COUNCIL FOR BUILDING RESEARCH STUDIES AND DOCUMENTATION
WORKING COMMISSION W18 - TIMBER STRUCTURES**

**INFLUENCE OF DUCTILITY ON LOAD-CARRYING CAPACITY OF JOINTS
WITH DOWEL-TYPE FASTENERS**

by

A Mischler
Chair of Wood Technology
ETH Zürich
Switzerland

**MEETING THIRTY
VANCOUVER
CANADA
AUGUST 1997**

Influence of Ductility on the Load-carrying Capacity of Joints with Dowel-type Fasteners

Adrian Mischler, Wood Technology, ETH Zurich, Switzerland

1. Introduction

The load-carrying capacity of joints with laterally loaded dowel-type fasteners is, in Eurocode 5–1–1, based on a plastic design method, which was developed by Johansen (1949). In this model, it is assumed that both the dowel and the timber behave like rigid-plastic materials. Brittle failure modes such as splitting or plug shear are not taken into account by this design method.

Plastic analysis methods are only valid to describe the load-carrying capacity on condition that no premature brittle failure will occur.

The deformations in the joint before failure have to be large enough, so that the dowel can reach the yield moment. In all other cases the failure-load will be less than the calculated load-carrying capacity. In Eurocode 5–1–1 no indication is given about ductility conditions. It is assumed that minimum requirements for spacing, end- and edge distances prevent brittle failure modes. However, tests on multiple fastener joints show sometimes brittle failure in timber splitting even if minimum requirements are satisfied.

In this paper, the importance of ductile failure is shown. It is also discussed how the joint has to be designed to achieve these ductile failure modes.

2. Importance of ductility

In timber construction, joints constitute the weak points of the construction. Therefore, joints should always be designed of such a kind that their failure occurs only after great deformations (i.e. ductile).

The ductility of a joint exercises a decisive influence

– *on the general behaviour of the structure*

Especially when loaded in tension, wood behaves extremely brittle. In the joint range, the cross-sectional area is reduced by holes for the dowels and by slits for steel plates, according to the respective design. These notches create stress concentrations which cannot be reduced by plastic deformations because of the brittle failure of wood in tension. Therefore, ductile behaviour of a timber structure is only obtainable if the joints develop large plastic deformations before failure. Even if the load-carrying capacity of a single joint is reduced by such a ductile design, the collapse load of the whole structure increases, because a plastic redistribution of the internal forces becomes possible.

– *on the bearing behaviour of the joint*

When the dowels are stressed up to their plastic moment, the maximum load-carrying capacity of the dowel joint is reached. For this, large elastic and plastic bending deformations of the dowels are necessary. Thus, the whole joint has to allow enough big deformations before failure. If the joint fails before achieving these deformations, the plastic load-carrying capacity cannot be reached. As an example, this would be the case when splitting failure in the wood occurs.

– *on the load-carrying capacity of a group of fasteners*

A mechanical joint in timber construction normally consists of more than one fastener. The load-carrying capacity of the hole joint depends on how far the sum of the individual fasteners capacities have to be reduced. There is an unequal distribution of load among the fasteners if the fasteners are placed in a line parallel to the direction of loading. A certain balancing of these unequal forces is possible in case of large plastic deformations before failure of the joint. As for wood, the failure in embedment is not ductile enough to allow the necessary deformations, the balancing of the forces has therefore to occur by plastic deformations of the dowels. Even if the design of the joint is ductile

(slender dowels) the load-carrying capacity of the joint is smaller than the sum of the individual fastener capacities. For further informations see Gehri [1992], [1997] and Jorissen [1996].

The demand for a high ductility of the joint is not contradictory to the demand for high stiffness: The slip modulus for the serviceability limit state is determined between 10 and 40 % of the load-carrying capacity, i.e., in the linear range of deformation. Given a certain ultimate strength deformation w_u , the ductility of the joint becomes bigger with smaller elastic deformations w_y (see figure 1).

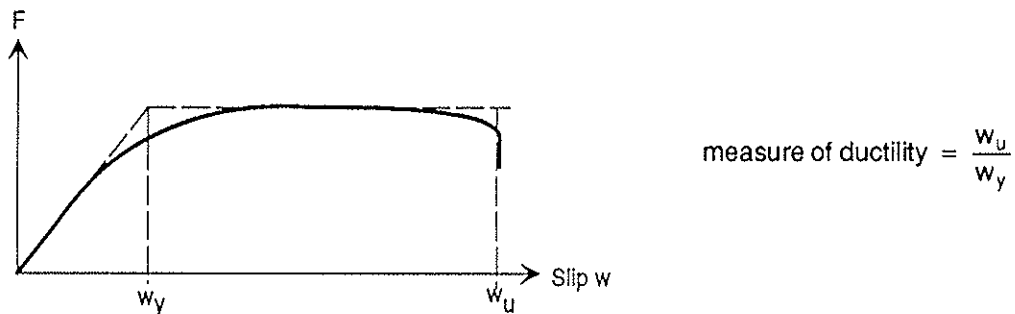


Figure 1: Ductility of a joint

3. Failure modes of joints with dowel-type fasteners

3.1 Failure of the timber in the joint

In the joint range, the cross-sectional area of the timber is reduced by boreholes for the dowels. This is together with stress concentration along the dowels the cause of a local weak point in the timber. If the joint itself has a higher resistance than the timber in the joint range, a tensile failure without deformation occurs in the reduced section of the timber.

According to Gehri and Fontana [1983] an optimal adjustment of the number of fasteners on the tensile resistance of the timber section allows to eliminate this brittle failure.

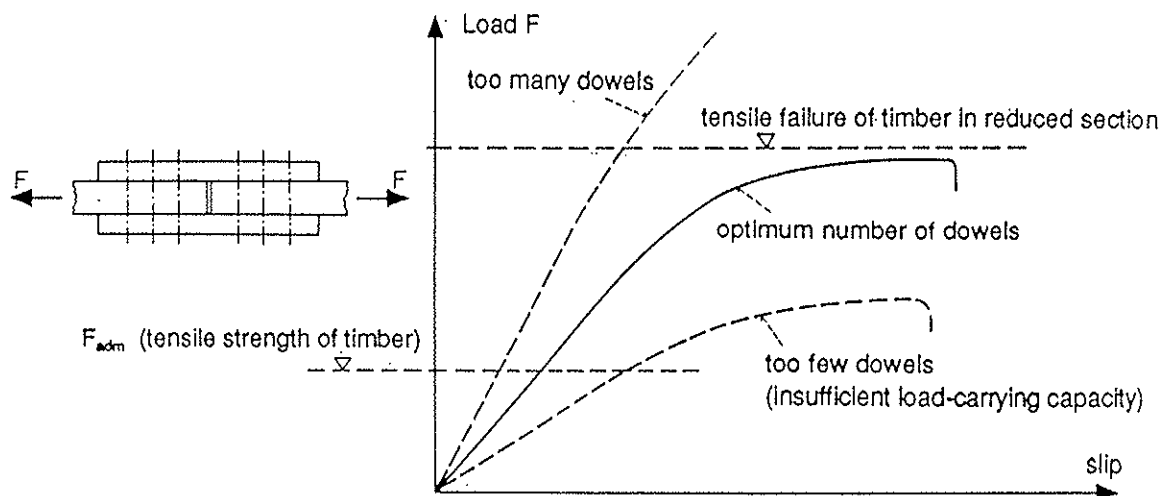


Figure 2: Influence of the number of dowels on the deformation behaviour of a joint, according to Gehri and Fontana [1983] ($F_{adm} = F_{allowable}$)

Splitting of the wood parallel to grain in a line of dowels is the other possible failure mode of timber in joints (see figure 3).

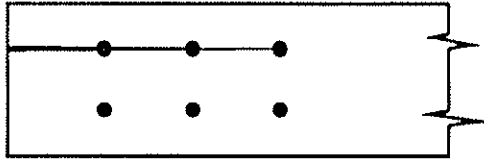


Figure 3: Failure mode: Splitting parallel to grain

The cause of splitting is the bursting effect of the dowels. If the dowels are impressed in the timber as it happens in dowelled joints, the wood in front of the dowel is not only compressed but also laterally pushed away.

If several dowels are arranged in a row parallel to grain, a plane of failure with tension perpendicular to grain is built up (figure 4).

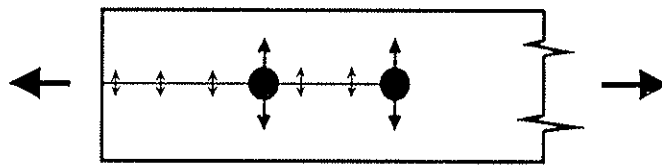


Figure 4: Failure plane with tension perpendicular to grain

On the weakest point of this plane failure starts and continues across the hole plane.

3.2 Failure modes of the joint

If preliminary timber failure is avoided by an adequate design of the joint, the failure will occur in the joint.

Depending on the dowel slenderness, three different failure modes are observed in joints with one single dowel.

3.2.1 Mode I: Small dowel slenderness: failure of embedment

The stocky dowel remains straight in the joint. Therefore the embedding stress is constant over the whole dowel length. The failure occurs when the embedding strength of the timber is reached. If there is only one dowel in line, this failure occurs after plastic wood deformations (Figure 5). But if there are several dowels in line parallel to the load direction, this ductile kind of failure can hardly happen because the wood splits in a very brittle way, as described before.

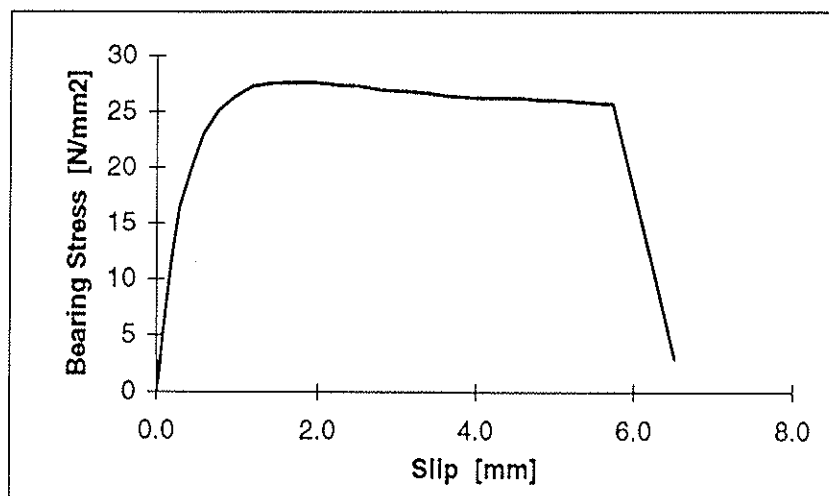


Figure 5: Bearing stress–embedment curve of one individual stocky dowel

3.2.2 Mode II: Medium dowel slenderness: combined failure

If the dowel has a medium slenderness, it is deformed in the joint without reaching its full plastic load-carrying capacity. The embedding pressure is no more constant, so wood failure occurs at a lower average stress level. In multiple fastener joints the wood splits before reaching this failure mode II. According to Jorissen [1996] the equation of this failure mode is therefore not valid for multiple fastener joints.

3.2.3 Mode III: Big slenderness of the dowel: plastic failure of the dowel

If the dowel slenderness is raised further, the plastic bending moment of the dowel becomes determinative. This case occurs only after large plastic deformations and after the formation of yield hinges in the dowel. Hence this is a ductile failure mode. This failure mode is valid for single and multiple fastener joints.

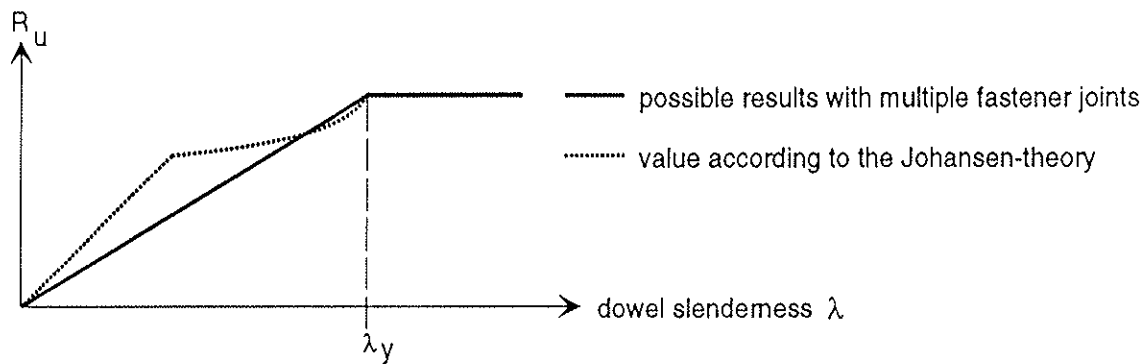


Figure 6: Load carrying capacity in function of the dowel slenderness λ for a single dowel and for a multiple fastener joint according to Jorissen [1996]

Consequently, a ductile behaviour of the joint is not possible unless plastic failure of the dowels occurs (failure mode III) and the other failure modes (mode I and II) may be avoided.

4. Premature failure of a joint as a consequence of lacking ductility

If the ductility of a joint with several fasteners one behind another is too small, the failure takes place before the load-carrying capacity according to the Johansen-theory is reached. This becomes obvious when the tests with joints with five dowels in line of Gehri [1996] are observed (figure 7).

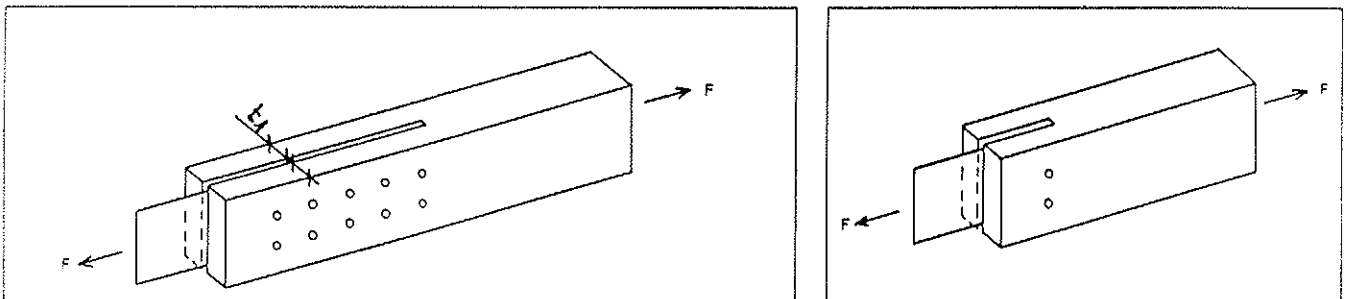


Figure 7: Test setup according to Gehri [1996]

The thickness t_1 of the wooden parts is 100 mm. A GL 28 with $\rho_k = 410 \text{ kg/m}^3$ was used. The dowels (diameter 24 mm) had a characteristic tensile strength $f_{u,k}$ of 510 N/mm^2 .

Identical tests have also been carried out with only one dowel in line. Load-deformation-curves (figure 8) show a completely different behaviour of the two joints, one with one dowel in line, the other one with five dowels in line.

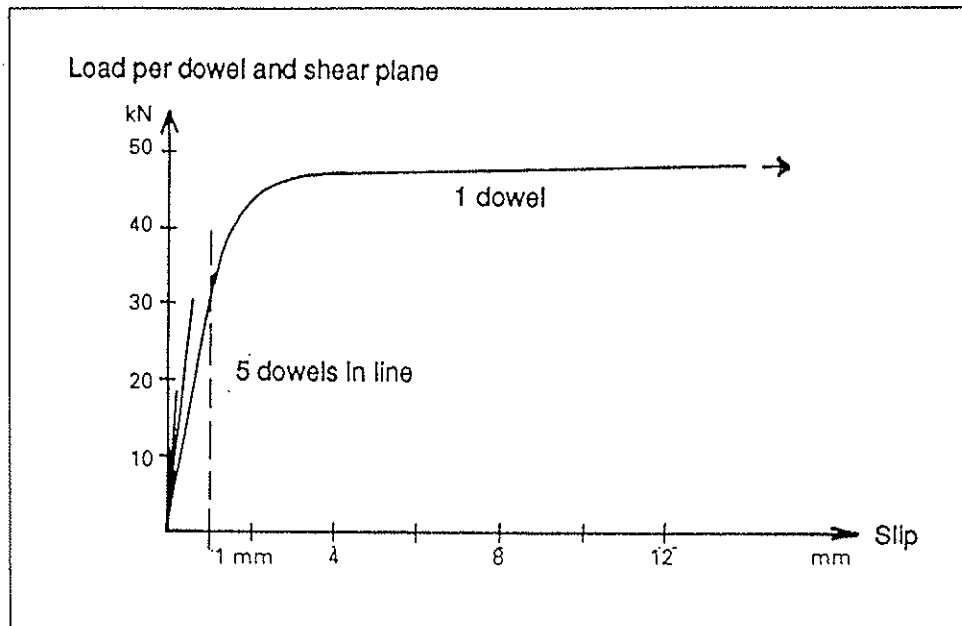


Figure 8: Load-deformation-plot of the joints

The observed load-carrying behaviour of the joints with one dowel in line is in accordance with the theory of Johansen: the dowels are deformed plastically, the consequence is a ductile failure.

On the other hand, in the joint with five dowels in line, the failure already happens after smallest displacements of only 0,4 to 0,7 mm, by splitting of the wood. The dowels are not deformed. Consequently, the plastic load-carrying cannot be reached.

Those tests prove that the ductility of the whole joint with several fasteners in line has to be ensured. The proof of ductility of a joint with one single fastener is not sufficient.

5. How to influence the ductility of doweled joints

5.1 The BSB-joint

The BSB-joint is a very efficient multiple-shear steel-to-timber joint with 6,25 mm diameter dowels. By means of this joint type, the influence of the constructive design on the load-carrying behaviour is demonstrated. All tests with the BSB-joint were carried out with specimens of 200 x 200 mm cross-sectional area. The mean tensile strength of the regular BSB-dowel is 650 N/mm².

5.2 Effect of the distance between the steel plates

The effective dowel slenderness has a major impact on the load-carrying behaviour of the joint. The diameter of the dowels is constant with BSB-joints. Hence, the dowel slenderness is controlled by the distance between the steel plates. The different joints shown in figure 9 have been investigated. Each configuration was tested with 3 specimens, each specimen with one joint on both ends.

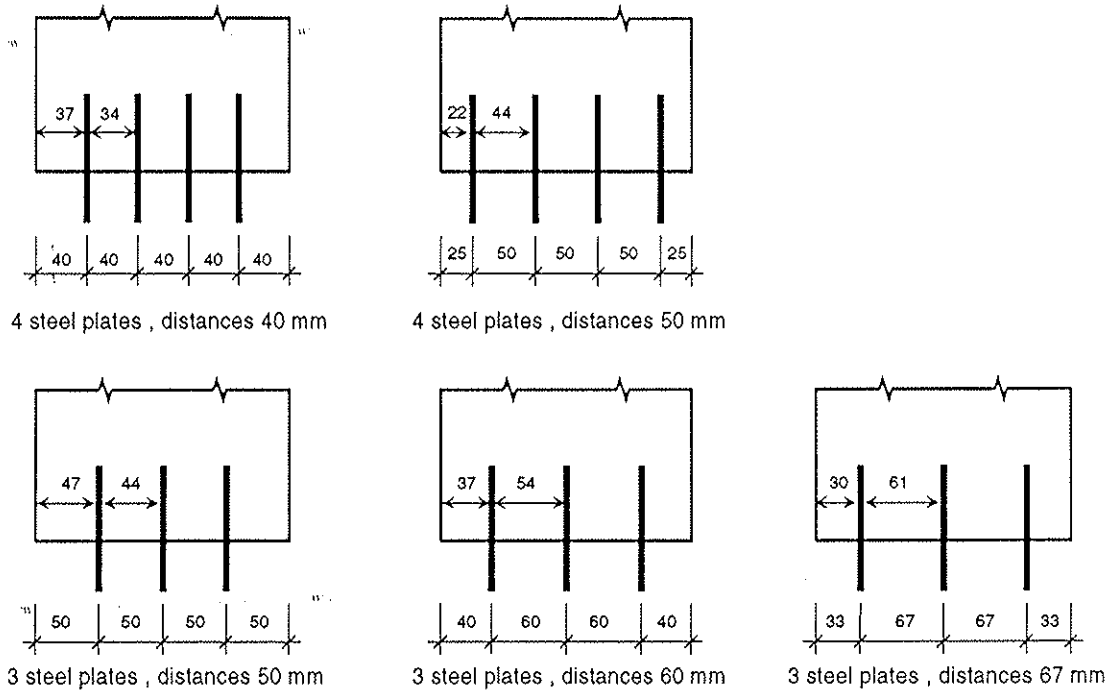


Figure 9: BSB-Joints with different distances between the steel plates

Figure 10 and 11 show the load-deformation curves each of one test.

For distances between the plates from 40 to 50 mm, the failure happens very brittle. From a distance between the plates of 60 mm upwards, the ductility of the joint is big enough, so that plastic hinges are formed. Afterwards, the failure takes place by splitting of the wood. A further increase of the distance between the plates to 67 mm results in no further delay of the splitting. The load-carrying capacity decreases a little bit because the side members become too small.

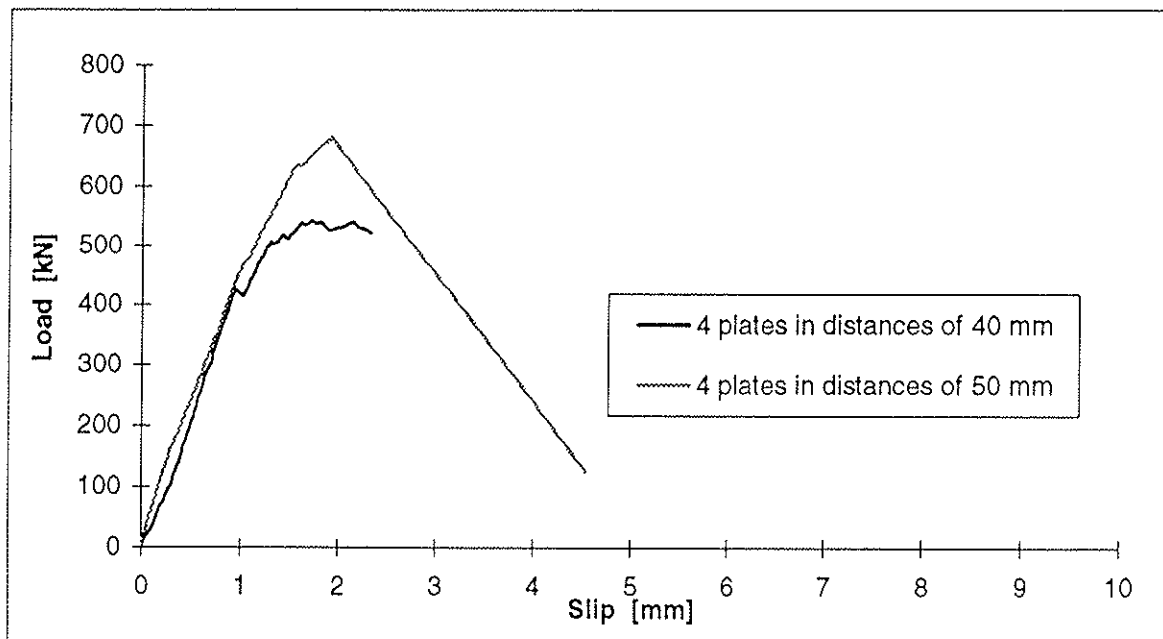


Figure 10: Load-deformation plot of the specimens with 4 steel plates

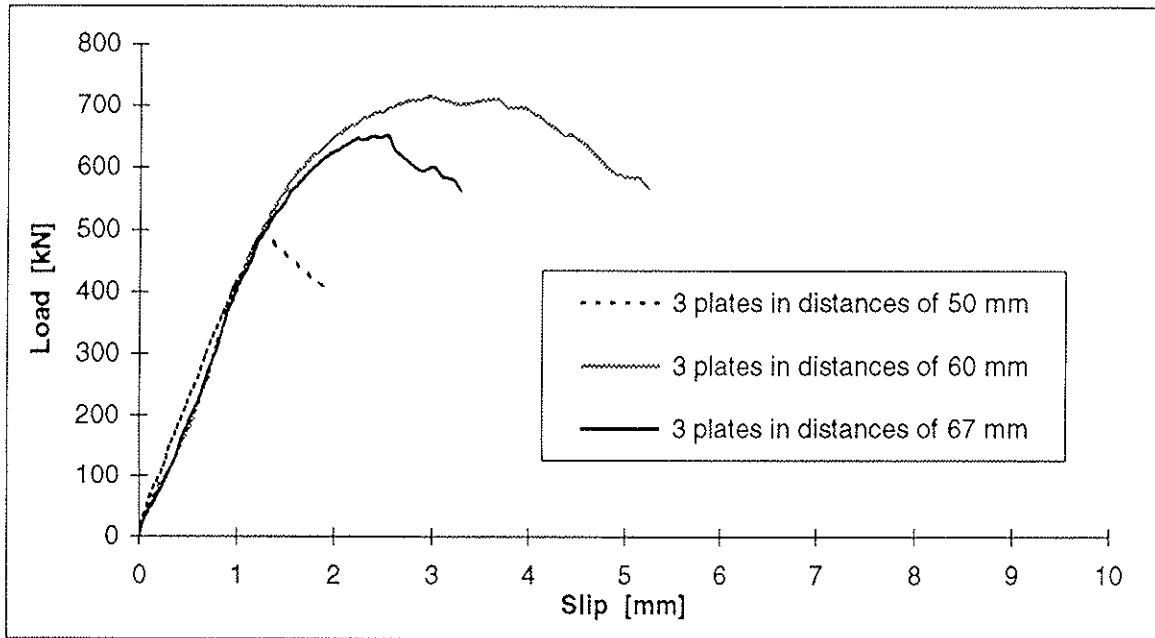


Figure 11: Load-deformation plot of the specimens with 3 steel plates

5.3 Effect of the tensile strength of the dowels

In failure mode III, according to the Johansen-theory the load-carrying capacity is proportional to the square root of the yield moment of the dowel. The results of tests carried out with single dowel joints correspond excellently with the theory of Johansen [Gehri 1997].

The dowels with higher tensile strengths cause higher stress in the wood in the joint range. If in a joint with more than one dowel the tensile strength of the dowels is increased without simultaneously increasing the distances between the fasteners, higher loads are induced in the same surface of wood. The resulting higher stresses increase the danger of splitting in the wood. This was proved by tests carried out with two different tensile strengths of the dowel steel.

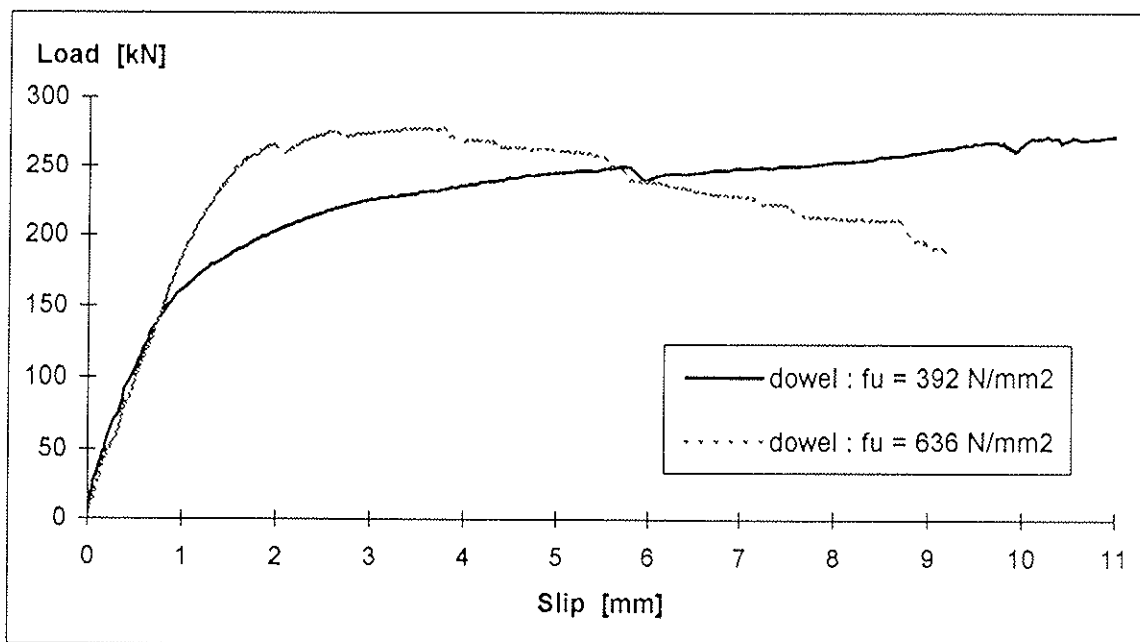


Figure 12: Testing in tension parallel to the grain of BSB-joints with dowels of different tension strength

Consequently, the end distance and the spacings among the dowels have to be adjusted to the tensile strength of the dowels. Unless this is taken into consideration, the higher load-carrying capacity of the dowel with higher strength cannot be exploited, because of the wood failure.

5.4 Effect of the number of dowels in line

The risk of splitting in a joint with several fasteners in line is much higher than in a joint with one single fastener. That's why the load-carrying capacity of a joint that fails in splitting is smaller than the sum of the single fastener's capacity.

To show the effect of the number of dowels in line on the BSB-system, two test series with especially density-sorted glued-laminated wood were performed. The cross-section measured 200 by 200 mm² and the distance among the steel plates was 60 mm, which is the regular distance in the BSB-joint.

The series with a mean density ρ_{mean} of 480 kg/m³ had 9 rows of dowels each. The specimens were executed with either one, two or three dowels per row (see figure 13). No setup with more than three dowels in line and 9 rows was tested, because otherwise the wood would have failed in tension.

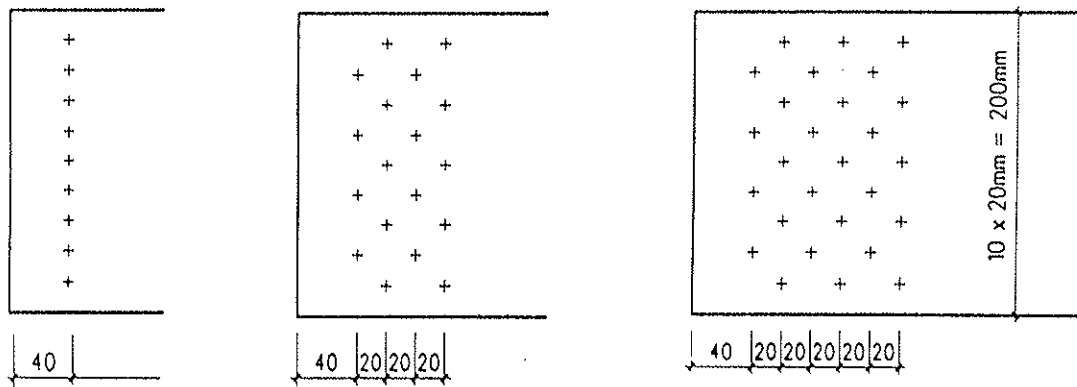


Figure 13: Arrangement of the dowels in specimens with $\rho_{\text{mean}} = 480 \text{ kg/m}^3$

5 specimens with two joints each have been tested for each arrangement (one, two or three dowels per row).

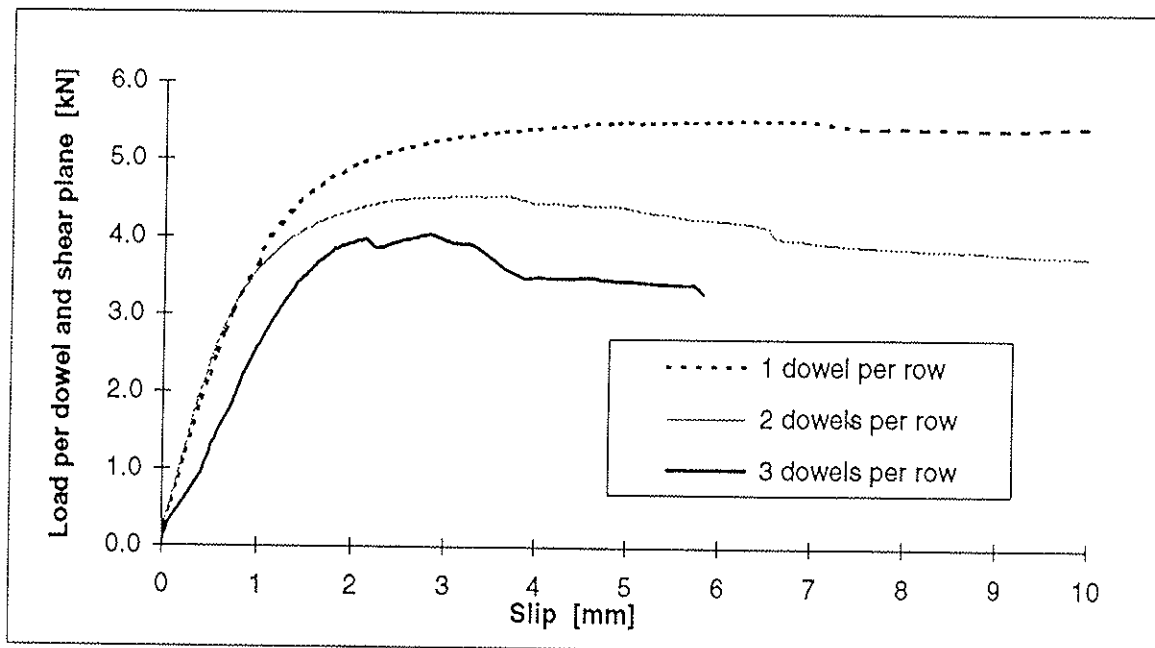


Figure 14: Load-slip-curves of joints with 1, 2 and 3 dowel per row

The joints with one dowel per row behave very ductile with great plastic deformations in the dowels. Because of strain hardening of the steel dowel the load-carrying capacity still increases even after reaching the yield point.

The joints with two dowels per row still show a very ductile failure mode. Splitting in the wood occurs after about 3,5 mm slip between timber and steel plates. This leads to a decrease of resistance of the joint.

The joints with three dowels per row show larger elastic deformations than the other two joints. This is caused by an unequal distribution of load among the dowels. The dowels are deformed plastically but the splitting in the wood takes place already after 2 mm of slip between timber and steel plates.

The load-carrying capacity of the joints with different numbers of dowels in line is compared with the formula proposed by Gehri [1992 and 1996]:

$$n_{ef} = 2 \left(\frac{n}{2} \right)^{k \cdot \lambda_r}$$

for $\lambda_r \leq 1$

with $\lambda_r = \frac{\lambda_{ef}}{\lambda_y}$

λ_{ef} : effective slenderness of fastener

λ_y : limit slenderness as defined in figure 15

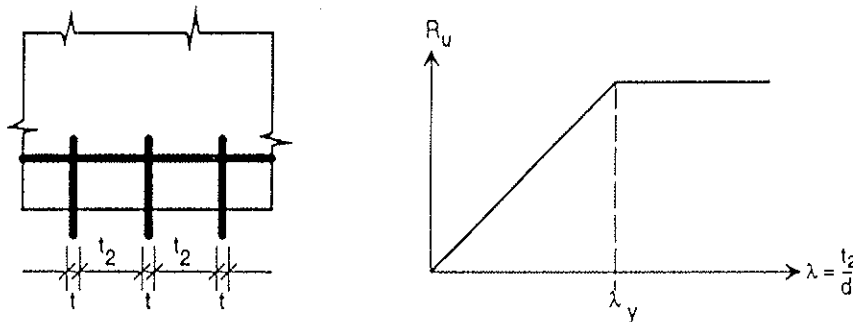


Figure 15: Definition of the limit slenderness λ_y for multiple-shear joints

As for the BSB-joint with distances among the plates of 60 mm, the slenderness λ_{ef} is bigger than λ_y , so that $\lambda_r = 1$.

The best correspondence with the test values was found for $k = 0,7$ (see figure 16).

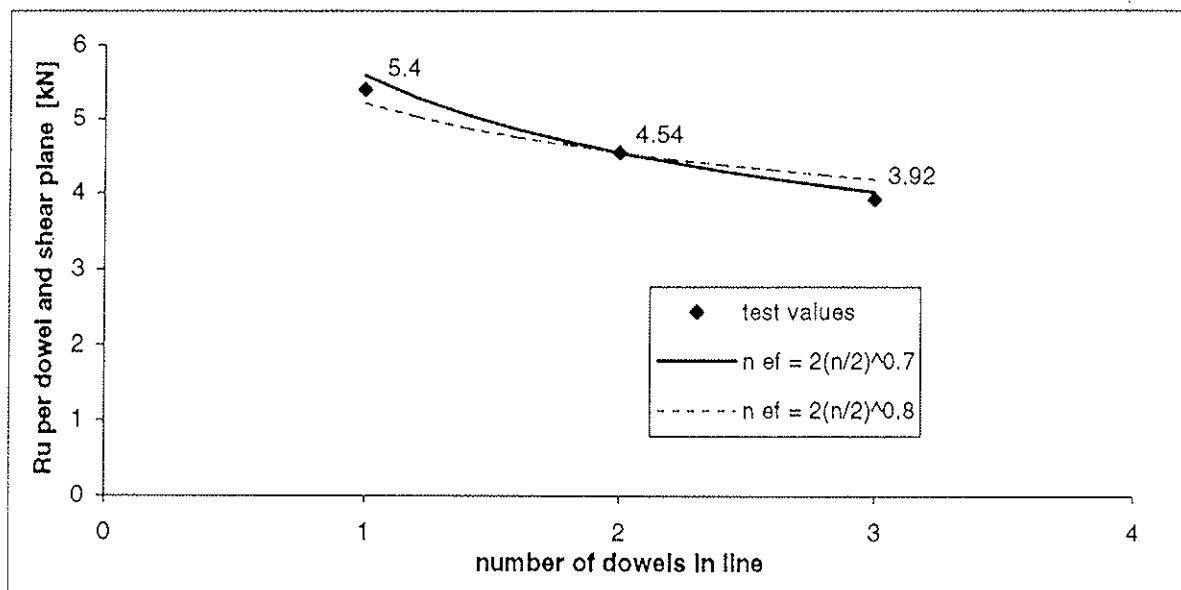


Figure 16: Group effect on load-carrying capacity per dowel and shear-plane (series with $\rho_{mean} = 480 \text{ kg/m}^3$, each point represents the mean value of 5 tests with 2 joints each)

As for the series with an average density ρ_{mean} of 410 kg/m^3 , the tensile strength of the wood parallel to the grain was too low to test a joint with 27 dowels. Therefore, the tests were carried out in such a way that the five types of joints were tested with a number of dowels between 8 and 12 (see table 1).

Number of dowels in line:	1	2	3	4	6
Number of rows:	9	4	4	2	2
Number of dowels totally:	9	8	12	8	12

Table 1: Number of dowels in the specimens with $\rho_{\text{mean}} = 410 \text{ kg/m}^3$

The only goal of these tests was to prove that even if the stress level of the entire joint is almost constant, the number of dowels in line has a certain impact. They are of no practical importance for the BSB-system, because a joints with 12 dowels would never be carried out with 6 dowels in line.

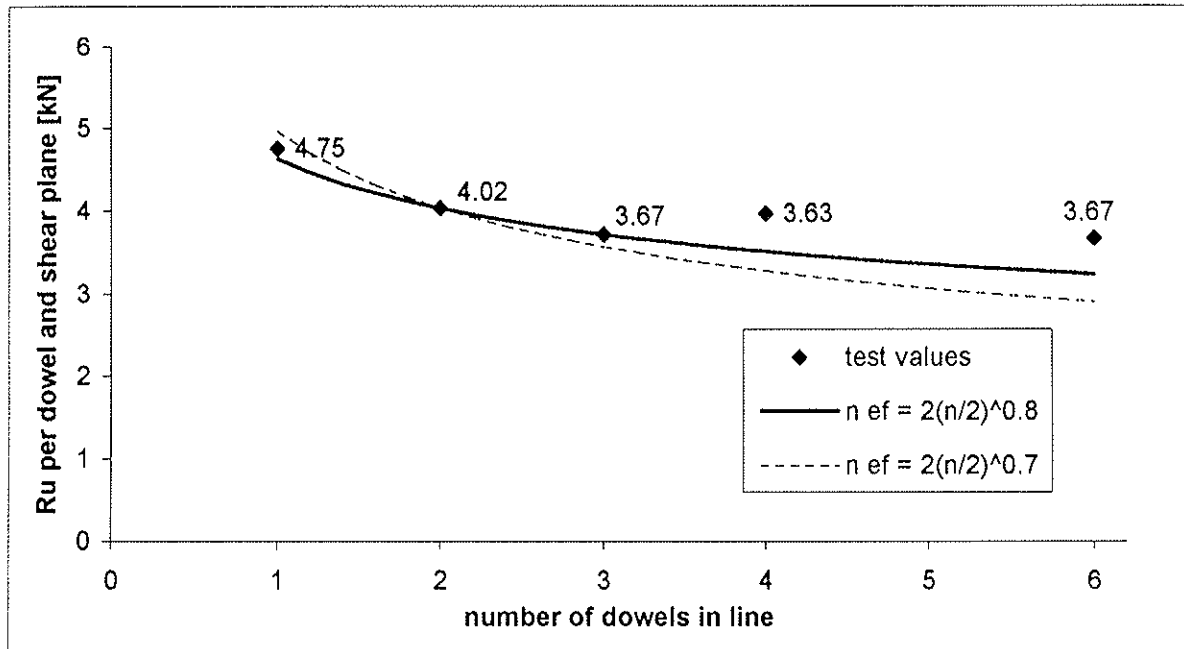


Figure 17: Group effect on load-carrying capacity per dowel and shear-plane (series with $\rho_{\text{mean}} = 410 \text{ kg/m}^3$, each point represents the mean value of 5 tests with 2 joints each)

With this test setup, a group effect was observed only from one to three dowels in line. From 3 up to 6 dowels in line the load-carrying capacity per dowel remains constant. The best correspondence for 1 to 3 dowels was found for

$$n_{\text{ef}} = 2 \left(\frac{n}{2} \right)^{0.8 \cdot \lambda_r}$$

The formula above for the effective number of fasteners in line is only valid for the BSB-joints.

This small reduction factor for several dowels in line parallel to the load direction is caused by:

- The use of very thin (size effect) and slender dowels
- The ductile failure of the joint
- The small fabrication tolerances of the BSB-system

5.5 Effect of end distance and spacing among dowels

In timber constructions, compact joints with small steel plates are preferred to longer joints with heavy steel plates. But if the spacing among the dowels is too small, the timber fails in splitting.

Spacing and end distance of a joint have to be adapted to the following variables:

- diameter of the dowel
- tensile strength of the dowel
- shear strength and tensile strength perpendicular to grain
- angle between the force and the grain direction

5.5.1 Effect of spacing parallel to grain

End distance and spacing parallel to grain in the BSB-joint normally measure $6,4 d = 40$ mm. Tests with this configuration were carried out with glulam GL 36 and 3 dowels in line. In these test the wood splitted after only 2 until 3 mm of slip between wood and steel plates (Figure 18).

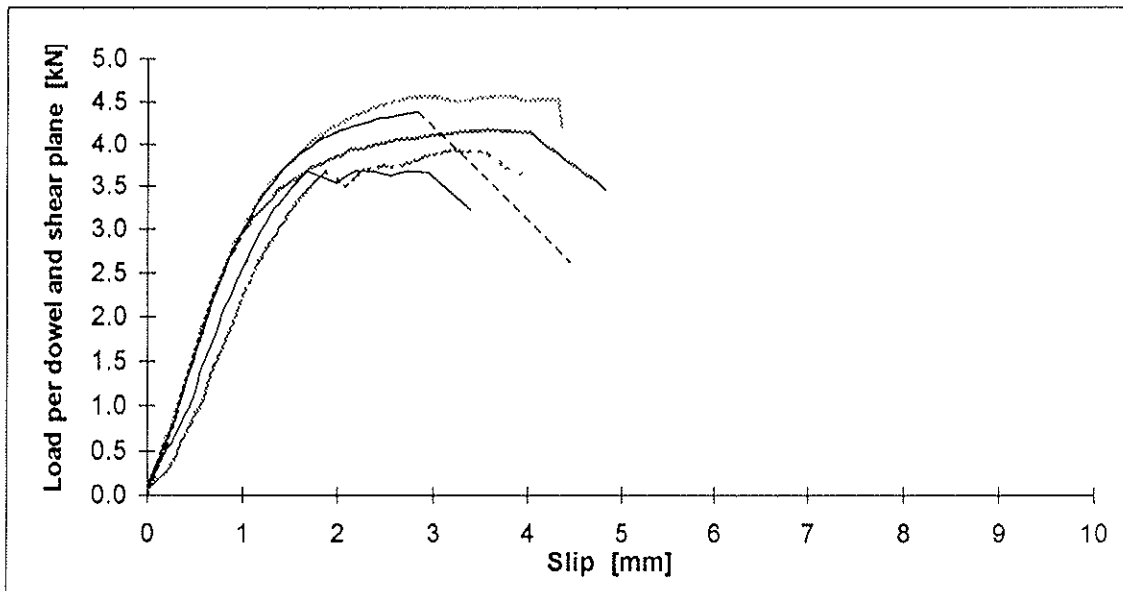


Figure 18: Load-slip curves for BSB-joints with spacing and end distance of 40 mm

Because of the small ductility of these tests, another series of specimens was produced with end distances and spacings of 50 mm. The ductility was bigger than with the smaller spacings but 2 of 7 specimens splitted after a slip of only 2 to 2,5 mm (Figure 19).

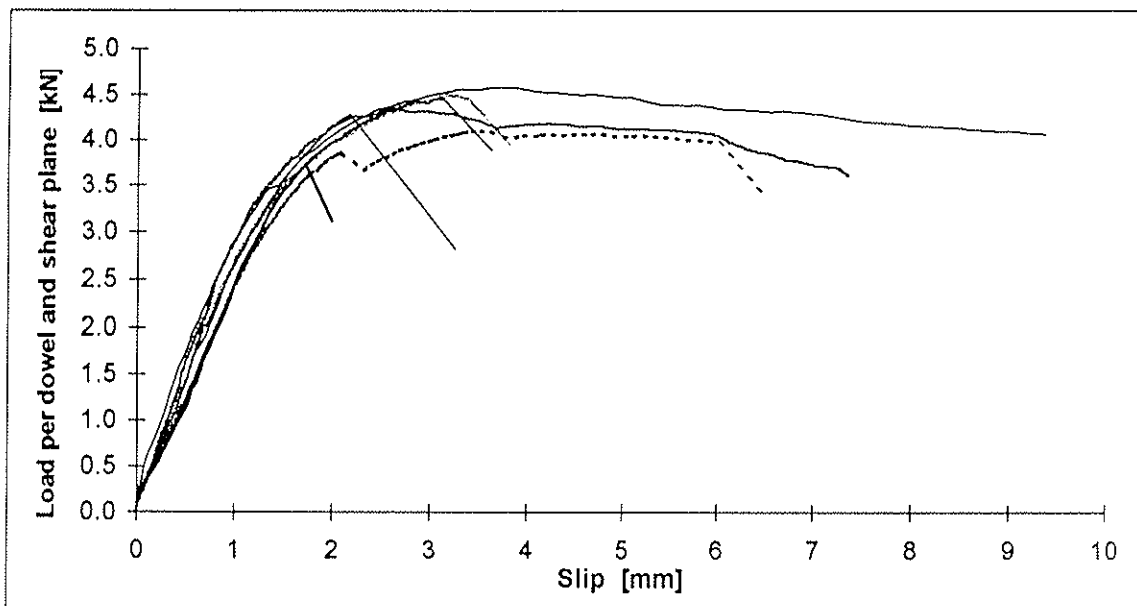


Figure 19: Load-slip curves of the BSB-joints with end distance and spacing of 50 mm

5.5.2 Effect of end distance

To optimize the end distance of the BSB-joint test series were carried out in 1991 with a constant spacing parallel to grain of 40 mm and a variable end distance of 20 up to 120 mm.

The distance among the steel plates measured with 67 mm, 7 mm more than the regular distance of 60 mm. The intention was that also the specimens of low density would achieve the failure mode III.

One of these series was made of spruce, the other one of douglas-fir.

For both species there was no significant effect of the end distance neither on the load-carrying capacity, nor on the ductility of the joints. Therefore the regular end distance in the BSB-joint was laid down to 40 mm.

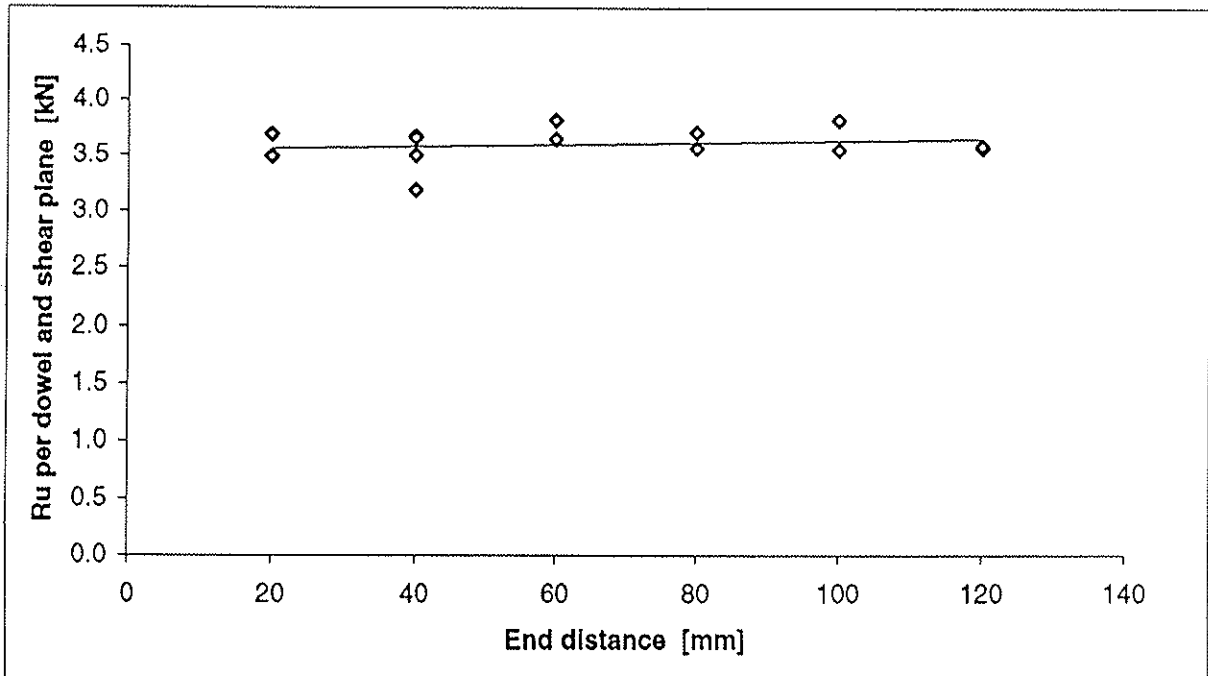


Figure 20: Effect of end distance for joints with spruce

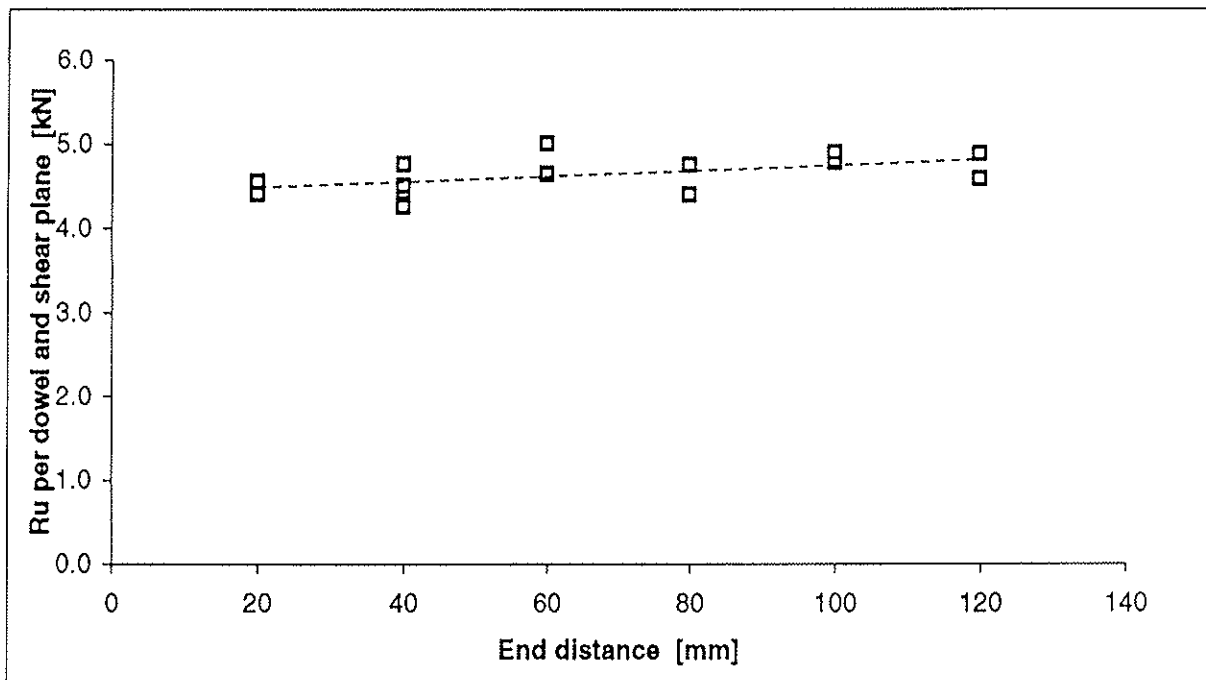


Figure 21: Effect of end distance for joints with douglas-fir

In Eurocode 5-1-1 the minimum end distance for dowel joints is prescribed to 80 mm. For this reason, test series were made with spacing parallel to grain of 40 mm and end distance of 80 mm. The specimens were made of the same GL 36 as the specimens for the joint with only 40 mm of end distance (Figure 18). The ductility of the joint with end distance 80 mm (Figure 22) is higher than the ductility of joints with end distance 40 mm (Figure 18) and 50 mm (Figure 19).

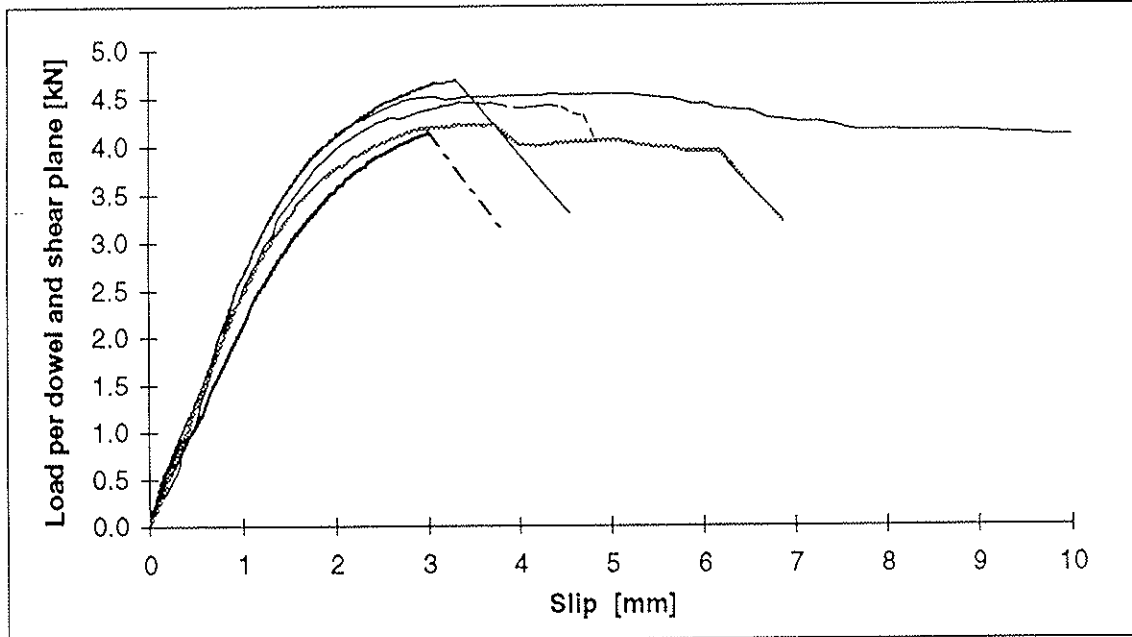


Figure 22: Load-slip curves of the BSB-joint with 80 mm of end distance

Series	spacing	end distance	ρ_{mean}	$F_{u,\text{mean}}$
A: Douglas-fir	40 mm	20 to 120 mm	523 kg/m ³	751 kN
B: spruce	40 mm	20 to 120 mm	408 kg/m ³	584 kN
C: spruce	40 mm	40 mm	471 kg/m ³	675 kN
	40 mm	80 mm	479 kg/m ³	715 kN
	50 mm	50 mm	484 kg/m ³	696 kN

Table 2: Results of tests with different end distances

In the series A and B (Table 2), no positive effect of an end distance longer than 40 mm was found, neither on ductility nor on failure load.

However, the series C (Table 2) showed an improvement of ductility and failure load by enlarging the end distance from 40 mm up to 80 mm.

As the forces per dowel in series C are higher than in series B, the splitting effect of the dowels have increased too. The splitting resistance of the spruce in series C has not raised up enough. That's why the longer end distance has a positive effect in series C but not in series B.

The load-carrying capacity of the joints in douglas-fir are still higher than these in spruce GL 36. The splitting resistance of the douglas-fir in Serie A was high enough so that an end distance of 40 mm is sufficient to reach a ductile failure.

6. Conclusions

The Johansen-theory was developed and validated for single fastener connections. The equations given in Eurocode 5-1-1 are based on this theory but they are used without any reduction for multiple-fastener joints up to 6 dowels in line.

It is shown that the model of Johansen is only valid for ductile failure modes. The investigations made by Jorissen [1996] prove that a multiple fastener joint shows a ductile failure only under condition that mode III according to Johansen is reached. Therefore doweled joints have to be designed in such a way that they develop large plastic deformations before failure. This is only possible if the dowel slenderness λ is higher than λ_y as defined in Figure 6 and 16.

Even if the multiple fastener joint fails in a ductile way, the load-carrying capacity is smaller than the sum of the individual fastener capacities. The formula for the effective number of fasteners in load direction n_{ef} proposed by Gehri [1992] is validated by tests with the BSB-joint.

7. References

- Gehri, E. , Fontana M. [1983]: Betrachtungen zum Tragverhalten von Passbolzen in Holz-Holz-Verbindungen, Baustatik und Stahlbau, Publ. Nr. 83-1, ETH Zürich, 1983.
- Gehri, E. [1992]: Eurocode 5, Part 1-1. Swiss proposals for new formulations and comments. 3rd november 1992.
- Gehri E.: Joints with dowel-type fasteners. A system factor or a systematic error? Paper prepared for the CIB-meeting in Sidney, 1994.
- Gehri, E. [1996] Design of joints and frame comers using dowel-type fasteners. CIB-W18/29-7-6, Bordeaux, 1996.
- Gehri, E. [1997]: Einfluss der Lagerungsbedingungen auf das Tragverhalten einer Stahl-Holz-Bolzenverbindung, Professur für Holztechnologie, ETH Zürich, 1997.
- Gehri, E.: Timber connections with dowel type fasteners. Group effect or reduction factor on single fastener load carrying capacity, chair of wood technology, ETH Zürich, 1997 (Background paper, doc CEN/TC 250/SC5
- Indermühle, D.: Zur optimalen Auslegung der BSB-Verbindung. In „Brettschichtholz“ Schweiz. Arbeitsgemeinschaft für Holzforschung, Weinfelden, 1996.
- Johansen, K.W.: Theory of timber connections. IABSE, 98, 249-262, Zurich, 1949.
- Jorissen, A. [1996]: Multiple fastener timber connections with dowel type fasteners. Int. Wood Eng. Conf. 1996.
- Mischler, A.: Passbolzenverbindungen. In „Brettschichtholz“ Schweiz. Arbeitsgemeinschaft für Holzforschung, Weinfelden 1996.
- Mischler, A.: Einfluss der Duktilität auf das Tragverhalten von Stahl-Holz-Passbolzenverbindungen, Professur für Holztechnologie, ETH Zürich (erscheint 1997)
- Werner, H.: Tragfähigkeit von Holz-Verbindungen mit stiftförmigen Verbindungsmitteln unter Berücksichtigung streuender Einflussgrössen, 1993. Berichte der Versuchsanstalt für Stahl, Holz und Steine der Uni Karlsruhe, 4. Folge – Heft 28.
- Wilkinson, T.L.: Load distribution among bolts parallel to load. Journal of Structural Engineering, Vol. 112, No. 4, April 1986.

**INTERNATIONAL COUNCIL FOR BUILDING RESEARCH STUDIES AND DOCUMENTATION
WORKING COMMISSION W18 - TIMBER STRUCTURES**

**DOL EFFECT IN TENSION PERPENDICULAR TO THE GRAIN OF GLULAM
DEPENDING ON SERVICE CLASSES AND VOLUME**

by

S Aicher
G Dill-Langer
FMPA-Otto-Graf-Institute
Germany

MEETING THIRTY

VANCOUVER

CANADA

AUGUST 1997

DOL effect in tension perpendicular to the grain of glulam depending on service classes and volume

Aicher, S., Dill-Langer, G.

FMPA – Otto-Graf-Institute
Department of wood and timber construction
Stuttgart, Germany

Abstract

This paper reveals the concept and today's results of an extensive experimental and theoretical research work on the DOL effect of glulam in tension perpendicular to the grain with special respect to different climates and volumes. In the different test series with about 180 large scale specimens the primarily examined parameters were the influence of climate conditions – service class 1 and two different service class 2 environments – and the influence of volume (0,01 resp. 0,03 m³) comprising two cross-sectional widths of 90 resp. 140 mm. The investigated glulam volumes, built-up from machine graded laminations, conformed acc. to characteristic densities to high grade European glulam strength classes (GL 32 resp. 36). Due to time ranges of applied stepwise loading regime the empiric results apply primarily for short and medium-term duration of load classes. It is shown by means of damage model considerations that the stepwise loading regime has almost no influence on the DOL median in constant climate. The empiric results reveal that today's modification factors for short and medium term duration of load classes, specified in Eurocode 5 for service class 2 conditions, are highly non-conservative in case of tension strength perpendicular to the grain.

1 Introduction

The DOL effect, i. e. the combined influence of stress level, accumulated loading time and climate conditions is one of the most important characteristics of the material wood and respective derivatives, whereby a size dependency can be incorporated, too. The material degradation is usually expressed in codes by scalar modification factors on ramp load reference values obtained from standard test volumes resp. sizes at 12 % equilibrium moisture contents.

Primarily due to lacking empiric data for European lumber species, Eurocode 5 gives an equal DOL effect for solid wood and glulam, then being equal for all strength properties and further without any differences concerning indoor (service class 1) and sheltered outdoor (service class 2) conditions. The stepping of the modification factors for DOL, i. e.

the k_{mod} values given in EC 5 for different classes of accumulated duration of load, conforms roughly to the slope of stress level (SL) vs. logarithm of time to failure (t_f) according to the linear Madison curve

$$\text{SL}(t_f) \approx a - 6,3 \lg t_f . \quad (1)$$

The applicability of the linear Madison curve, derived from small clear specimens, to structural size European spruce lumber in tension and compression and thus for bending parallel to grain was proved by Glos et al. (1987) for the case of constant climate (20 °C/65 % RH) and hence may also be assumed roughly for service class 1.

The indisputable impact of increased and especially varying moisture content on failure stress level resp. k_{mod} -factors (i. a. Schniewind, 1967; Mohager, 1987; Hoffmeyer, 1990, Barrett, 1996) is recognised in EC 5 only for service conditions delivering an average moisture content above 20 % (service class 3). For strength properties *parallel* to fiber this non differentiating strategy in the moisture range between 12 and 20 % nevertheless might be acceptable. However, it is obvious from literature (i. a. Mindess et al. , 1979; McDowall, 1982) that the quoted lumping is too crude in the case of tension *perpendicular* to the grain where significant eigenstresses normal to grain induced by varying climate are superimposed to external load stresses. An evaluation of DOL tests in tension perpendicular to the grain on structural size glulam (stressed volume 0,002 m³) from Canadian Douglas Fir with constant load levels in nominally constant climate conditions, however showing non neglectible variations (Mindess et al., 1979) reveals a drastically well 2times increased slope of SL vs. logarithm of time to failure compared to the Madison slope

$$\text{SL}(t_f) \approx a - 15 \lg t_f . \quad (2)$$

In order to verify the latter results and to separate the influences of time, climate and size a research project was started including a total of 6 DOL test programs with two different glulam volumes (0,01 m³ and 0,03 m³) at three different climate conditions, being constant climate (20 °C/65 % RH), sheltered outdoor climate and cyclic variable climate (RH between 55 % RH and 90 % RH). In all cases a stepwise loading regime was applied with a step length of 28 days. In each DOL test series 15 specimens were tested; the related ramp load test series comprised 44 specimens for each volume.

The choice of the 0,01 m³ volume is bound to EC 5 were this volume magnitude serves as the reference volume with respect to size effect; consequently this size serves in EN 1193 for the derivation of characteristic values.

2 Wood material, specimen sizes and built-ups

All wood came from a selected spruce stand in the south east part of Sweden. The sawing was performed as so-called 3x-log sawing, forwarding i. a. a center board with pith, which was excluded nearly throughout. The boards, all with a thickness of 39 mm and two widths of 120 and 160 mm, were graded to yield strength classes C 35 and better. After grading, the lamellas were processed by a Finnish company to glulam by means of phenolic resorcinol adhesive. Two dimensions of beams were manufactured: a small size with a finished nominal cross-section of 90 x 462 mm (14 lamellas) and a beam length of 5000 mm resp. a large size with nominal dimensions of 140 x 595 (18 lamellas) x 5000 mm. In total, 11 and 13 beams of the smaller and larger cross-sectional size, respectively, formed the material population for ramp and especially DOL tests. The cutting pattern of the test volumes from the beams was laid-out with two aims: To receive a highest possible number of matched samples in different climates and second to obtain an even distribution of the different specimen types within the beams. In total 142 small ($V = 0,01 \text{ m}^3$) and 138 large ($V = 0,03 \text{ m}^3$) test volumes with dimensions of 90 x 400 x 275 mm and 140 x 528 x 405 mm, respectively, were cut from the beams. The densities of the material determined from all specimens were for small and large volumes, respectively, $530 \pm 24 \text{ kg/m}^3$ (C.O.V. = 4,6 %) and $493 \pm 10 \text{ kg/m}^3$ (C.O.V. = 2,0 %). According to densities, the investigated glulam material conformed in case of the small and large volumes (widths), respectively, to high quality glulam grades GL 32 and GL 36 acc. to European glulam strength class standard prEN 1194.

The built-ups and nominal dimensions of the small and large specimens, related to small and large test volumes, are shown in Fig. 1. The test volumes were glued between two intermediate blocks of glulam with grain direction parallel to the load axis as recommended in the informative annex B of EN 1193. The onglings were then adhered to two steel plates, used to transfer the loads from the test machine. The lengths of the intermediate blocks and the thickness of the adhered steel plates have a pronounced influence on the stress distribution in the specimen's cross-section. Based on a compromise between the results of a 3D finite element study of the stress issue vs. manufacture and handling aspects of the specimens, the lengths of the intermediate wooden blocks were set to 300 mm equally for both specimen sizes, thus two times longer as a minimum length recommended by Ehlbeck and Kürth (1994); the thickness of the steel plates was set to 40 mm acc. to recommendations of the same authors.

The glue lines between the test volume and the both sided intermediate wooden blocks were performed with a 2component epoxy „Wevo EP 20/VP1“, without facing any problems with these parallel to the grain vs. end grain face connections. However, the reliability of the glue lines between steel plates and wooden end grain faces imposed more difficulties than expected. The mentioned 2component epoxy delivered insufficient results in preliminary tests in varying climate conditions. Thus, the suitability of adhesives for such applications was evaluated in a test series, where a 2component polyurethane „Plastic-Mastic“ performed best. As only a few glue line failures could severely endanger the interpretation of the long-term test results (15 specimen for each test series), additionally two threaded steel bolts of 150 mm length were glued parallel to grain into each intermediate block and fixed to the steel plates.

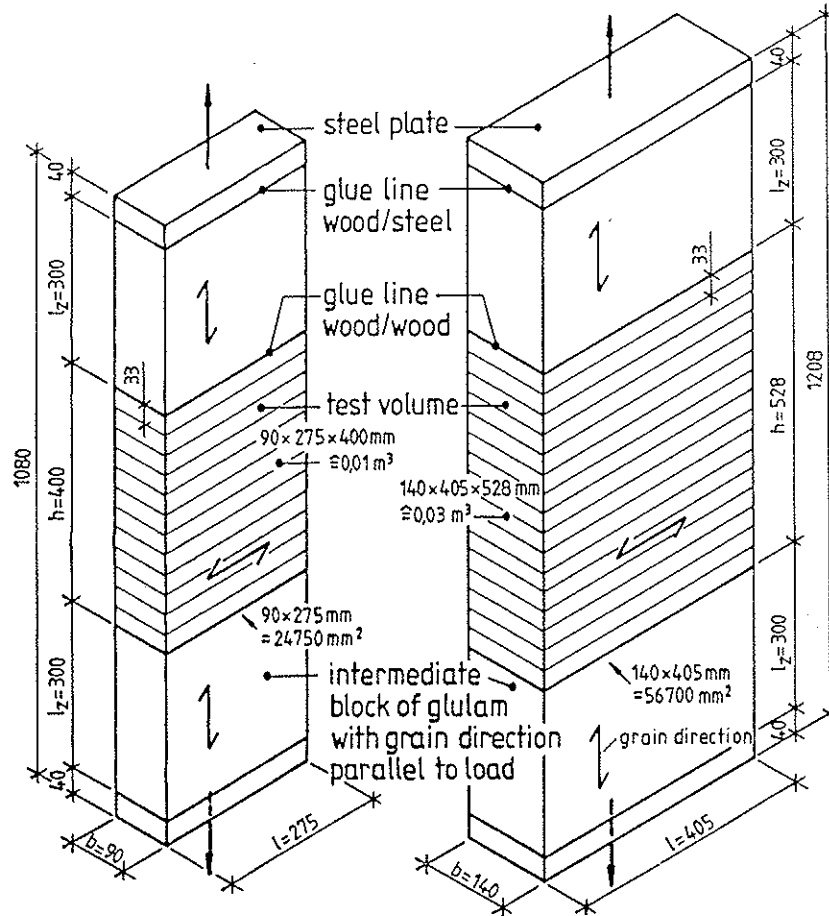


Figure 1 Built-up and dimensions of small and large glulam specimens for ramp-load and DOL tests with test volumes of 0,01 resp. 0,03 m³

3 Ramp load tests

Preliminary tests on the influence of specimen fixings (Aicher and Dill-Langer, 1995) confirmed widely the results by Feldborg (1991). No statistical significant difference with respect to strength values was obtained for hinged fixation as opposed to two different realisations of rigid fixation, in order to enforce an even translation displacement. However, strain eccentricity, defined as the ratio of maximum strain at one of the 4 edges vs. mean strain, is larger for hinged fixation. All ramp load and also the DOL tests were performed with hinged fixation.

The ramp load tests with the small volumes were performed in stroke control with a constant cross-head speed of 0,4 mm/min. Stroke control, the loading procedure also prescribed by EN 1193 enables sudden pre-peak load drops, due to micro-cracking, followed by load recovery eventually exceeding the load level before the load drop. That behaviour is possible due to redistribution of stresses in an inhomogeneous continuum. The rather frequent occurrence of pre-peak load drops followed by load recovery (65 % of all 0,01 m³ ramp load specimens) led to the question what impact this phenomenon which should in principle not occur in load controlled tests really has. This has to be seen in view of the

DOL tests where specimens are not loaded by constant deformation but by constant (gravity) loads. It was thus decided to conduct the majority of the ramp load tests (30 out of 44 tests) with the larger volumes in load control at a rate of 0,125 kN/sec; the others were tested in stroke control with a constant cross-head speed of 0,47 mm/min.

The difference between the mean strength values of stroke controlled vs. load controlled tests (large specimens) was minor; the specimens tested in stroke control yielded a slightly higher strength.

A compilation of the test results concerning tension strengths resp. MOE perpendicular to the grain and densities is given in Table 1. The obtained strength values were fitted by Gauß, lognormal and 3parameter Weibull distributions delivering rather equal results. For 3parameter Weibull distribution the parameters $m = 3,99$, $\sigma_{\min} = 0,555 \text{ N/mm}^2$ resp. $\sigma_0 = 0,364 \text{ N/mm}^2$ for small specimens and $m = 5,50$, $\sigma_{\min} = 0,302 \text{ N/mm}^2$ and $\sigma_0 = 0,399 \text{ N/mm}^2$ for large specimens were obtained.

volume (number of specimens)	strength $f_{t,90}$			MOE $E_{t,90}$			density ρ_{12}		
	mean	C.O.V.	x_{05}	mean	C.O.V.	x_{05}	mean	C.O.V.	x_{05}
m^3	N/mm^2	%	N/mm^2	N/mm^2	%	N/mm^2	kg/m^3	%	kg/m^3
0,01 (44)	0,885	10,5	0,740	446	6,8	398	530	4,6	490
0,03 (44)	0,670	11,5	0,548	419	6,5	375	493	2,0	447

Table 1 Compilation of ramp-load test results for tension strengths and MOE's perpendicular to the grain and of specimen densities; given are mean values, C.O.V.'s and 5 % fractiles (due to fitted lognormal distributions).

The size effect obtained was $k_{\text{mean}} = (f_{t,90} (V = 0,03 \text{ m}^3)) / (f_{t,90} (V = 0,01 \text{ m}^3)) = 0,76$ for mean values and $k_k = 0,74$ for characteristic values, yielding shape factors $m_{\text{mean}} = \lg (V = 0,01 \text{ m}^3 / V = 0,03 \text{ m}^3) / \lg k_{\text{mean}} = 4,0$ resp. $m_k = 3,7$ due to Weibull theory. Thus, the obtained empiric size effect is at first hand more severe than stated in EC 5 as $m = 5$ based on results by Barrett (1974). However, when normalizing size effect by mean densities of both volumes one obtains $k'_{\text{mean}} = (530 \text{ kg/m}^3) / (493 \text{ kg/m}^3) \cdot k_{\text{mean}} = 0,81$ resp. $k'_k = 0,80$ and hence $m'_{\text{mean}} = 5,2$ resp. $m'_k = 5,0$ for mean and characteristic values, respectively.

4 DOL test set-ups

Figures 2a, b show the realised test configuration resp. test rigs in sheltered outdoor and controlled cyclic climate. The end-grain faces of the glulam volumes were sealed with a diffusion tight foil to simulate the hygromechanical situation in the apex area of curved or tapered beams. Eight specimens per test series were equipped with two electronic gauges each for continuous deformation measurement. Besides the DOL specimens also unloaded control specimens were installed in the individual climates. These were used to monitor transient moisture distribution by means of both oven-drying and electrical resistance method and to record deformations due to pure temperature resp. relative humidity influence.

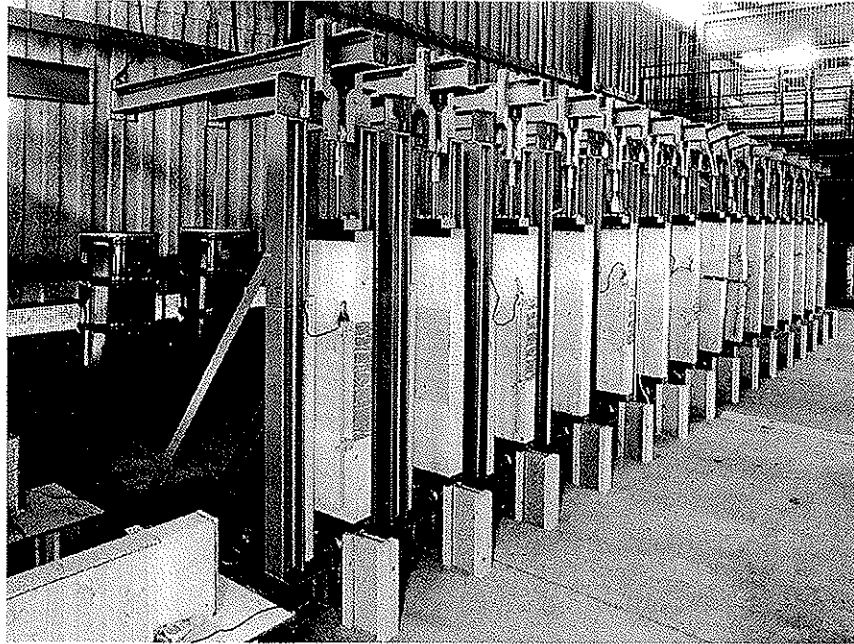
5 Imposed climate environments, loading regime

The DOL tests were conducted at three climate conditions, being

- constant climate of 20 °C/65 % RH representing service class 1 conditions,
- sheltered outdoor climate with temperature variations between –8 °C and 29 °C and relative humidity variations between 25 % and 99 % ,
- controlled cyclic climate in a climate chamber (constant temperature of 20 °C) with relative humidity of 55 % (11 days), 75 % (3 days), 90 % (11 days), 75 % (3 days) yielding a cycle length of 28 days.

The variable climates represent different kinds of service class 2 conditions.

The loading regime was stepwise with step lengths of 28 days, starting in the first load step at 45 % of mean ramp load strength $f_{t,90,mean}$ in constant and outdoor climate resp. at 0,40 $f_{t,90,mean}$ in cyclic climate, whereby load increments in all cases were 0,05 $f_{t,90,mean}$. The stepped load history is one of the most important project characteristics, imposing of course several questions with respect to interpretation of results (see discussion of damage accumulation in chap. 6.2). Figures 3a–c illustrate the loading regime, the relative humidity histories and the times to failure for the three climate conditions and two different test volumes.



a)

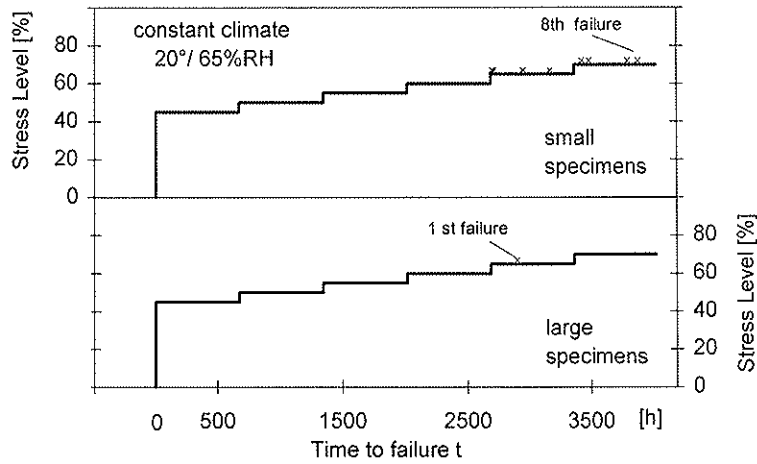


b)

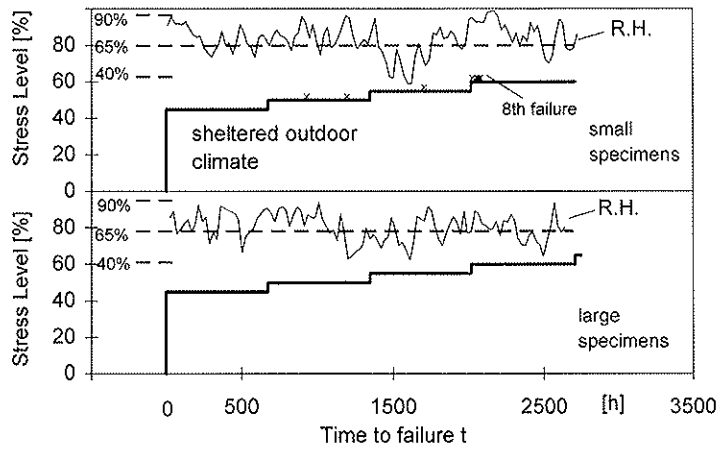
Figures 2a, b View of DOL test set-ups with mounted specimens ($V = 0,01 \text{ m}^3$) for tension perpendicular to grain tests

a) loading rigs installed in sheltered outdoor climate

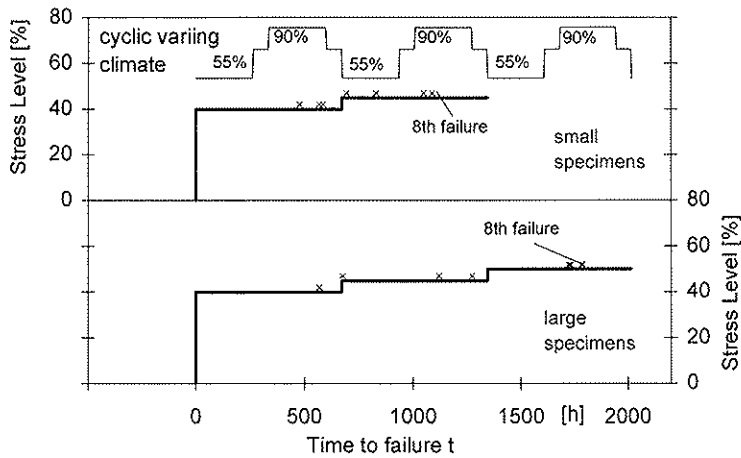
b) loading rigs installed in a climate chamber (cyclic climate)



a)



b)



c)

Figures 3a–c Illustration of the stepwise loading regime for small and large specimens in the three different climates investigated; also given are times to failure (obtained so far) at respective nominal stress levels

- a) constant climate tests (20 °C/65 % RH)
- b) sheltered outdoor climate tests (–8 °C – 29 °C, 25 % RH – 99 % RH)
- c) cyclic variable climate tests (20 °C/55 % RH – 20 °C/90 % RH)

6 DOL results for standard volumes acc. to EN 1193

6.1 Empiric results

So far a comprehensive evaluation of the DOL effect in different climates can be performed for the small specimens ($V = 0,01 \text{ m}^3$). In case of the large specimens ($V = 0,03 \text{ m}^3$) the DOL tests at sheltered outdoor climate (no failure so far) and at constant climate (two failures) are still in progress; the finished cyclic climate tests of the $0,03 \text{ m}^3$ volumes are compared to the results from small volumes in chap. 7.

Figure 4 shows the results of the DOL tests ($V = 0,01 \text{ m}^3$) in the three investigated climates altogether with the ramp load reference tests as cumulative distributions of the strength values perpendicular to the grain. The pronounced influence of a varying climate resp. relative humidity compared to the constant climate DOL effect is apparent. The most important data to be compared are mean and characteristic values, whereby the mean is subject to the least interpretation problems resulting from the chosen stepwise loading regime. In the following judgement of the data it is assumed that no resp. negligible damage has occurred at previous load steps; this argument will lateron be highlighted in more detail (see chap. 6.2).

A qualitative and quantitative discussion of the DOL data is preferably performed on the basis of normalised strength values, i. e. stress levels. The failure stress level of the individual specimens may be determined by two methods, being a deterministic one by matched specimens and a probabilistic one by ranking. The latter, pursued here, determines the unknown short term strength of the individual DOL specimen by relating the cumulative long term failure frequency to short term strength with same probability level. This implies of course the assumption that comparable failure mechanisms occur in short and long term loading. In detail, the ranking was not performed on the basis of empiric ramp load results but on the basis of the fitted 3parameter Weibull distributions given in chap. 3. It may be noted that the individual stress levels of the specimens can divert considerably from the nominal values assigned to the stepwise loading regime. All failures before the mean have a higher stress level compared to the nominal and solely for the mean DOL failure nominal and individual stress level coincide¹.

Figure 5 gives the individual stress levels, SL, vs. logarithms of times to failure, t_f , of the individual specimens for the three different climates. The times to failure refer solely to the time within the failure load step, i. e. loading times at lower load steps are disregarded. The mean failure stress level in each climate is denoted by a filled square, rhomb resp. triangle.

¹ In detail, slight differences may occur with respect to the latter due to limited number of DOL specimens. In case of the constant climate tests one specimen out of the 15 had to be excluded due to a pure glue line failure, delivering for the 7th and 8th failure cumulative probabilities of 0,464 resp. 0,536.

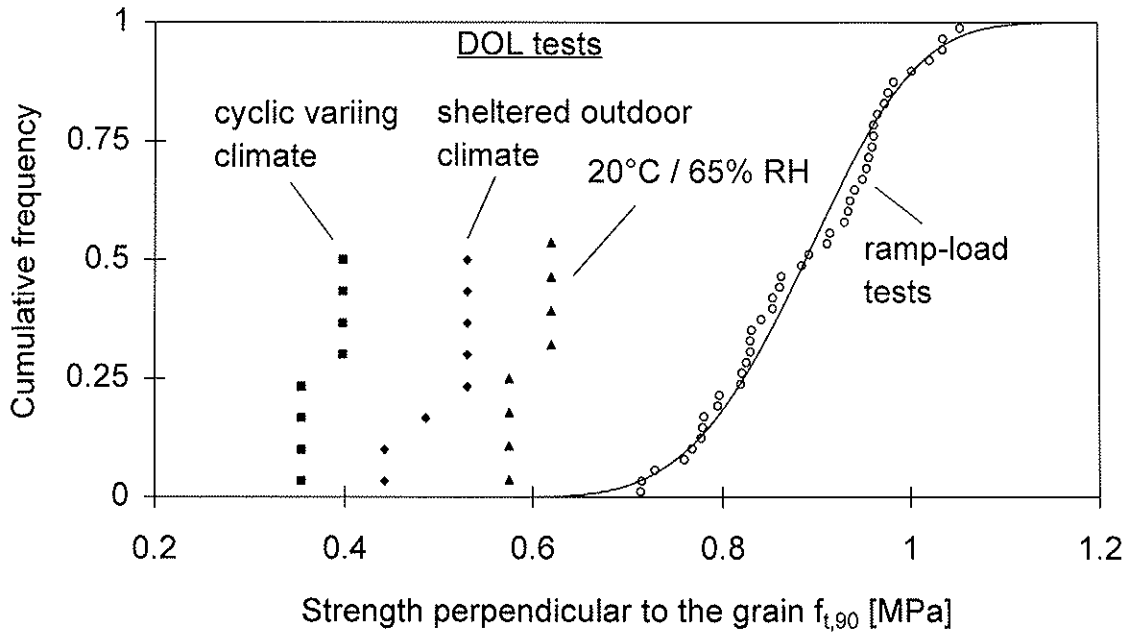


Figure 4 Cumulative frequencies of strength results from DOL tests in three different climates and ramp load reference values

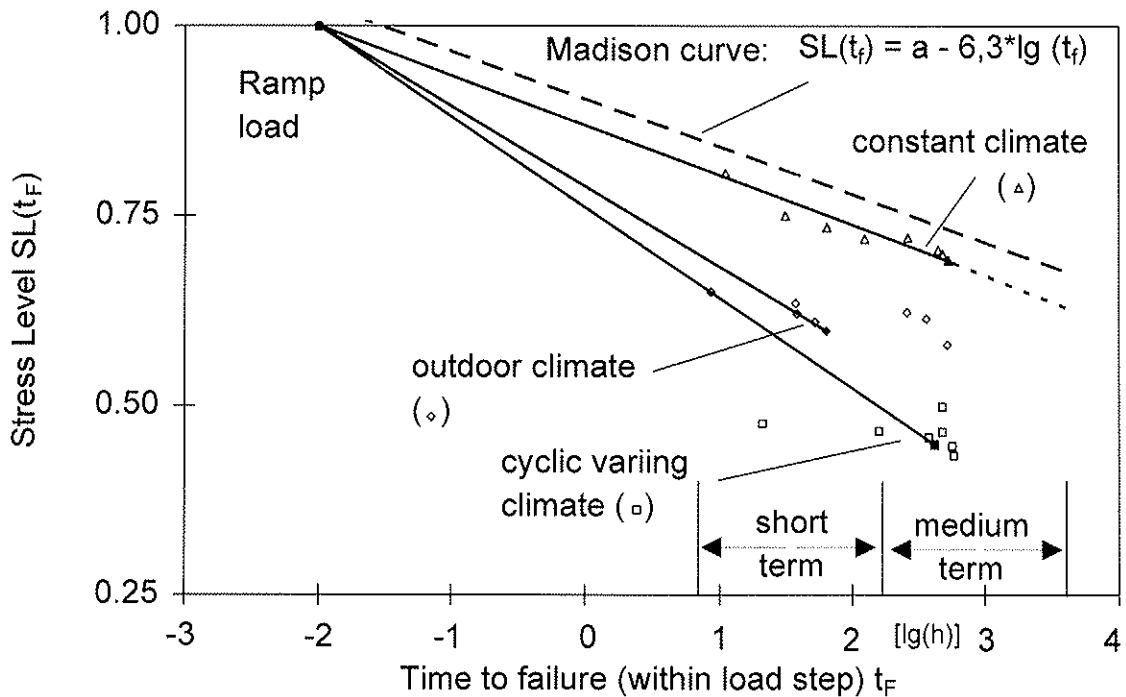


Figure 5 Stress levels vs. logarithm of times to failure (within failure load step) of DOL tests in three different climates. Given are individual specimen results and straight lines through DOL mean value and ramp load mean, the latter with damage model adjusted t_F -value

6.1.1 Constant climate (service class 1 conditions)

For constant climate conditions a constant slope of SL vs. $\lg(t_F)$ would be anticipated from the linear type Madison curve - derived from constant load tests - and actually was obtained rather well. A linear regression ($SL(t_F) = a - m \lg(t_F)$) through the empiric constant climate data delivers for the slope 5,63, being slightly less steep compared to the slope of the Madison curve ($m = 6,3$). The coefficient of correlation for the linear regression is 0,95, i. e. rather high. Instead of the regression line through the empiric DOL data points, Fig. 5 shows - equally for all three climates - a straight line through the DOL mean and a semi-empiric point, denoted by ramp load stress level $SL = 1$ and a time to failure of $10^{-2} \text{ h} = 36$ seconds. The given time value represents the equivalent dead load time of the ramp load stress level. Its derivation based on damage modelling and engineering judgement is discussed later (see chap. 6.2).

With respect to absolute values of the DOL effect in constant climate, the following numbers of $SL(t_F) = k_{\text{mod}}$ can be given for short and medium term load duration times, i. e. for accumulated loading times of less than one week resp. between one week and six months. Not regarding what type of fit to the empiric data is applied, sensible k_{mod} -values for short and medium term duration of load classes are in the range of 0,8 and 0,7 (see Fig. 5), so, rather close to today's EC 5 specifications for service class 1 conditions.

6.1.2 Sheltered outdoor and cyclic climate (service class 2 conditions)

In case of sheltered outdoor and cyclic varying climate the SL vs. $\lg(t_F)$ data points due to the high dependency on the transient eigenstress levels may not be assumed to lay on a rather straight line. The DOL medians of both climates differ of course, however revealing the anticipated trend that the imposed cyclic climate forms the conservative lower bound of realistic outdoor climate conditions. The k_{mod} -values for both climates, obviously being extremely low, may be assumed as 0,6 and 0,5 for short and medium term DOL class, respectively. These values differ extremely from those specified in EC 5 (there 0,9 resp. 0,8).

The obtained extreme DOL effect can be explained by the occurrence of transient moisture gradients along the cross-sectional width of the glulam specimens: Uneven moisture distributions interacting with stresses due to external load lead to restrained shrinkage/swelling and to mechano-sorptive creep. This results in a complex stress state with pronounced tensile eigenstresses at the centreline of the cross-section during wetting periods (Dill-Langer and Aicher, 1997a). FEM calculations for the cyclic climate yielded for the end of the first climate cycle an increase of about 90 % for the damage relevant Weibull stresses, σ_{wei} , compared to σ_{wei} -stresses from pure external loads. Thus, the impact of moisture variations on stresses was of an equal order of magnitude compared to applied loads.

6.2 Assessment of damage at previous load steps

Figure 6 illustrates schematically the major open question of the applied stepwise loading regime, i. e. whether and to what extent the previous load steps lead to a damage accumulation in the specimens. A damage accumulation at earlier load steps inevitably shifts the

sample mean to smaller times to failure compared to the median curve, ideally determined by testing comparable populations at different constant nominal stress levels. In a more precise manner, it should be said that not only the accumulated damage but primarily – in case of not too excessive primary damage – the damage gradient in the respective stress level is relevant for time to failure.

The answers to the forwarded uncertainties on pre-damage are bound to a suitable damage modelling pursued in this project on the basis of the Canadian damage model (Foschi et al., 1989). The differential equation describing the time and stress level dependant damage evolution $\alpha(t)$ is

$$\frac{d\alpha}{dt} = a [\text{SL}(t) - k_0]^b + c [\text{SL}(t) - k_0]^d \alpha(t) \quad (3)$$

where $\text{SL}(t) = \sigma(t) / f_0$, $\sigma(t)$, f_0 and k_0 are, respectively, time dependant stress level, current stress, ramp load strength and threshold stress ratio below which no damage accumulates. The fitting of the independent parameters a , b , c , d and k_0 , assumed to be constant for a single specimen, depends whether the behaviour of a population or of discrete specimens shall be simulated.

In the following it is solely focused on the constant climate tests (small specimens). For details and the extension of the Canadian model to variable climate conditions see Dill-Langer and Aicher, 1997b. The fitting of eq. (3) to the individual stress level histories of the first and eighth failed specimen delivered, respectively, the following parameter values (exponential damage accumulation assumed),

$$\begin{array}{ccccc} a = 1,045 \cdot 10^9, & b = 17,428, & c = 0,104, & d = 1,676, & k_0 = 0,566, \\ a = 3,294 \cdot 10^7, & b = 16,435, & c = 0,105, & d = 1,544, & k_0 = 0,497 \end{array}$$

whereby quantity a was determined from the other model parameters b , c , d , k_0 in order to ensure model consistency between long term and ramp load calibration data (Foschi and Yao, 1986).

Assuming that no damage has occurred in the previous load steps, the times to failure for both specimens were computed for the individual stress levels at failure step from

$$t_F = \frac{1}{c [\text{SL}(t) - k_0]^d} \ln \left\{ \frac{c}{a} [\text{SL}(t) - k_0]^{d-b} + 1 \right\} \quad (4)$$

and compared to the actual empiric times to failure².

² The time to failure acc. to eq. (4) results from integration of eq. (3). Consideration of additional damage terms due to ramp loading up to the respective stress level (Foschi and Yao, 1986) turned out to have negligible influence on the t_F results.

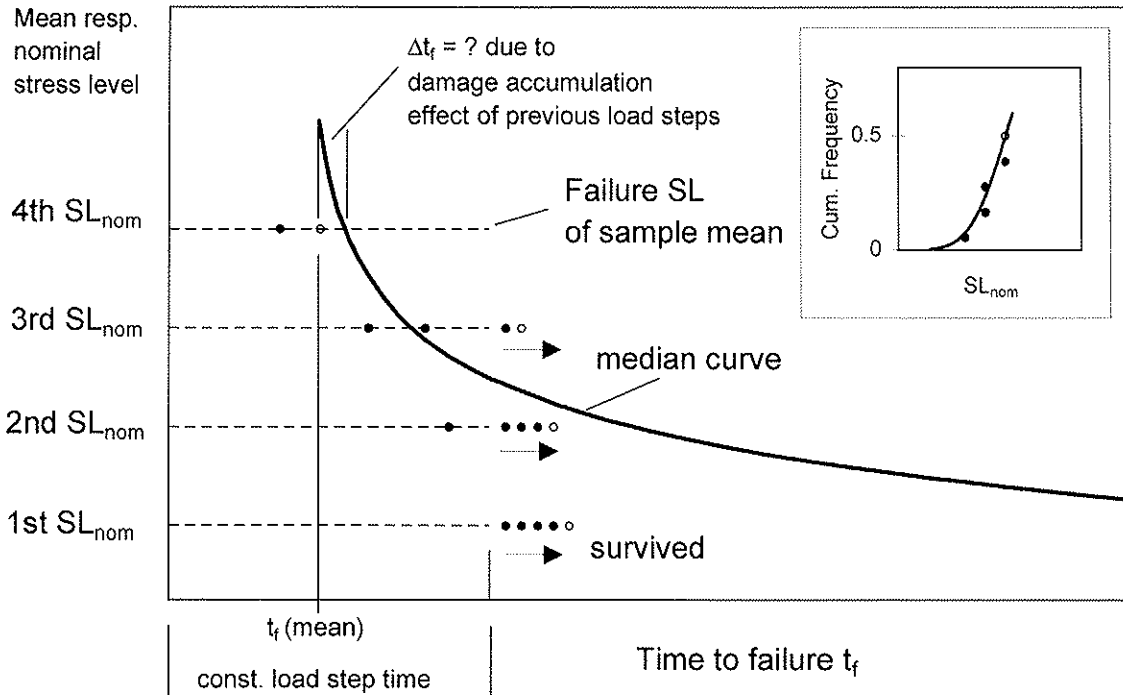


Figure 6 Schematic illustration of inherent problem of stepwise loading regime, being the question of damage accumulation at previous load steps potentially shifting the DOL mean to lower t_f -values compared to constant load tests

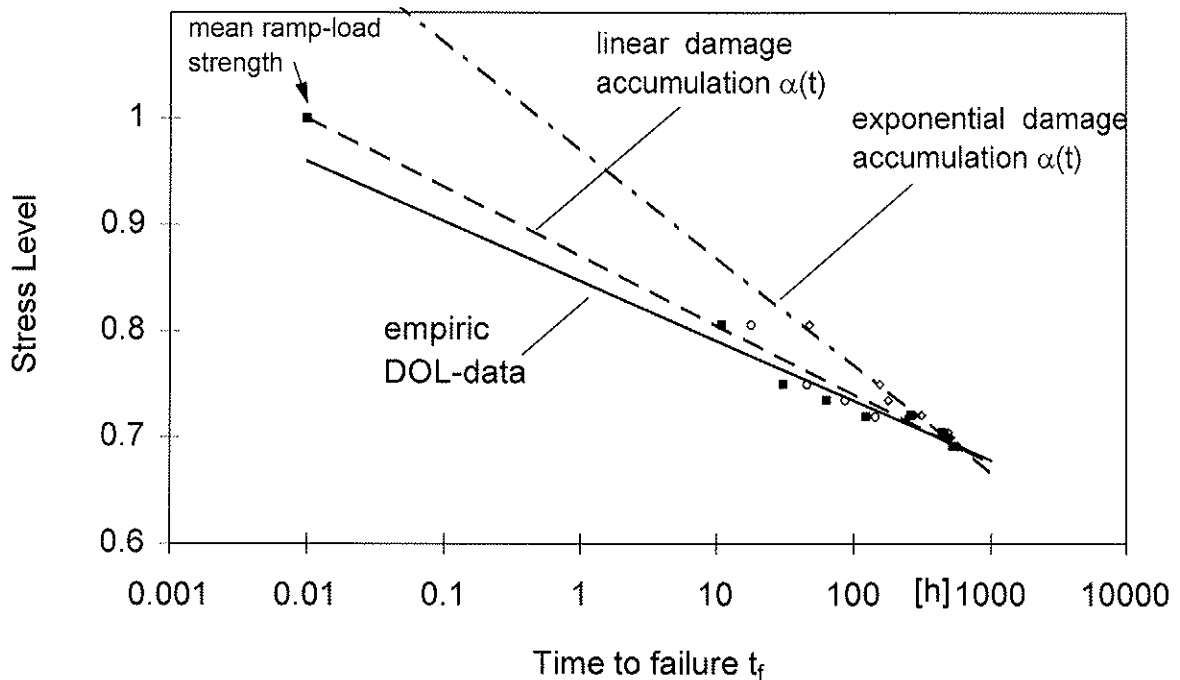


Figure 7 Stress levels vs. times to failure in failure load step in constant climate acc. to empiric results and acc. to Canadian damage model with assumed zero damage accumulation at previous load steps; the theoretical values are given for two different damage evolution types (linear resp. exponential damage accumulation)

Employing the failure stress levels of 0,806 and 0,691 for the 1st and 8th failed specimen altogether with above given parameter sets delivers times to failure of 47 resp. 572 hours . These times have to be compared to the empiric times to failure, being 11 and 525 hours. Apparently the times to failure obtained by the assumption that damage accumulation starts in the failure load step should be longer than the empiric ones and can minimally be equal.

The comparison of the empiric and theoretical t_F values shows that in case of the 1st failed specimen, representing roughly the 5 % fractile of the population, considerable damage ($\alpha = 0,69$) has accumulated at lower load steps, resulting in a rather short empiric survival time at the failure load level compared to the theoretical t_F value with no previous damage (t_F (empiric)/ t_F (theoretical) = 23 %). A completely different situation occurs for the 8th failed specimen, i. e. the DOL median (exactly: 0,536) were empiric and theoretical t_F values coincide very good, i. e. previous damage ($\alpha = 0,004$) has only small impact on survival time at failure stress level (t_F (empiric)/ t_F (theoretical) = 92 %). This means that the stepwise loading regime delivers for the population mean, respectively for its coinciding nominal and individual failure stress level, a time to failure which is shifted negligible to a shorter t_F -value compared to the true median value to be received when the whole population is tested at the respective nominal failure stress level. The reason that damage accumulation is not negligible for earlier failures, i. e. that determination of the lower 5th percentile boundary of the DOL curve is questionable with stepwise loading, results from the very high individual stress levels of the weakest part of the population.

Figure 7 illustrates the above graphically. For the individual failure stress levels of all constant climate specimens the graph gives the empiric times to failure (solely survival time in the failure stress level) and then the theoretical t_F -values with no damage accumulation at previous load steps, i. e. what has been given explicitly for specimen failures No. 1 and 8, above. In detail, the theoretical times to failure are given for two qualitatively different sets of material parameters a, b, c, d, k_0 incorporating a linear resp. exponential type of damage evolution. The data points of the empiric and theoretical DOL failures are then fitted with linear regression lines coinciding for the population mean.

The derivation of the equivalent dead load time for the ramp loading is of decisive importance with respect to the slope of SL vs. $\lg(t_F)$ representations of DOL data. Direct empiric investigation of very short dead load times are difficult. The use of ramp load results with a time to failure of 300 seconds has to be based on damage model calculations. The times to failure for SL = 1 were calculated via eq. (4), whereby the model parameters calibrated from DOL and ramp-load data were used. The resulting dead load times being damage equivalent to the empiric ramp-load test times turned out to be in the range of 7 to 11 seconds. As, due to the small sample size, these t_F values might lead to a non-conservative DOL slope, a reasonably increased value of $t_F = 0,01$ h was used.

7 Size effect in cyclically changing climate

Figure 8 illustrates the cumulative distributions of DOL strength values at cyclic varying climate for small ($0,01 \text{ m}^3$) and large ($0,03 \text{ m}^3$) volumes altogether with the related ramp-load results. The size effect denoted by the ratio of large vs. small specimens' strength values was 0,84 when regarding the 8th failed specimens (i. e. the mean values) resp. 0,76 in the case of the 1st failed specimens (roughly representing the characteristic level). Thus, in case of the mean values, the size effect in DOL tests under cyclic varying climate was slightly less severe compared to ramp-load tests ($k_{\text{mean}} = 0,76$, see chap. 3). An interpretation of the results on the characteristic level, due to the small sample size is dubious. The first results of ongoing DOL tests with large specimens at constant and sheltered outdoor climate seem to confirm the trend obtained at cyclic climate.

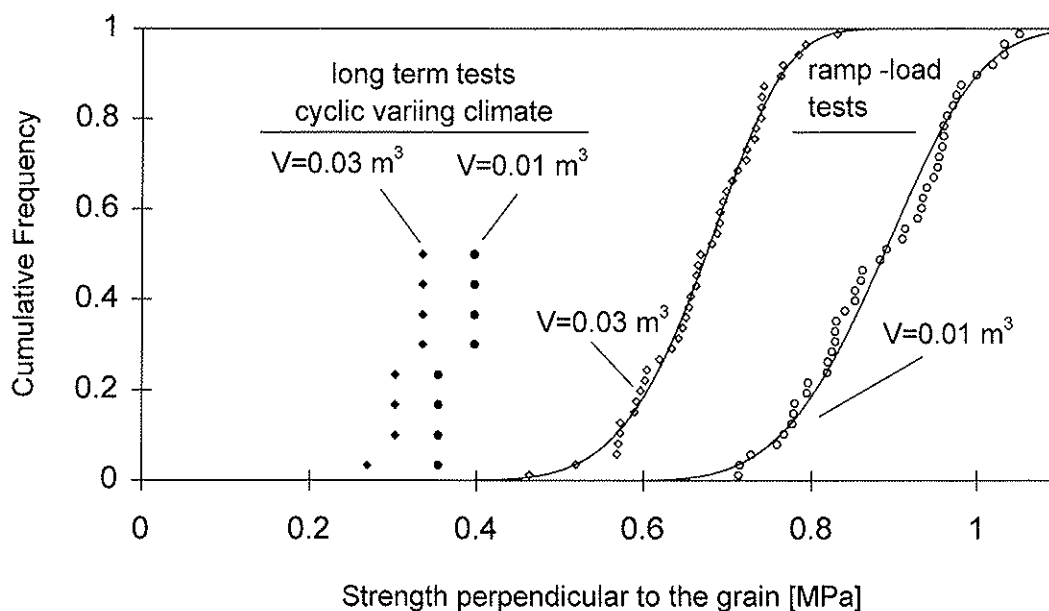


Figure 8 Cumulative frequencies of DOL and ramp load strength values of small and large specimens in cyclic varying climate

8 Proposal on empiric based k_{mod} -values

Based on the DOL results at three different climates and the related ramp-load tests, a set of k_{mod} values is proposed which in contrast to EC 5 accounts for the strength reduction due to climate influence at service class 2 conditions.

Whereas the k_{mod} values for service class 1 as given in EC 5 and derived here coincide roughly, the values for service class 2 in EC 5 should be reduced significantly by about 40 %. It shall be mentioned that the proposed service class 2 values are slightly higher

compared to empiric values for the $0,01 \text{ m}^3$ volumes, thus accounting for the slightly reduced size effect in DOL tests.

load duration class	service class			
	1		2	
	EC 5	proposed	EC 5	proposed
short term (< 1 week)	0,9	0,8	0,9	0,6
medium term (1 week – 6 months)	0,8	0,7	0,8	0,5

Table 2 Compilation of k_{mod} values acc. to EC 5 and proposals based on the empiric results of the reported DOL tests

9 Conclusions

The results of the presented research work prove a significant and extreme difference of the DOL effect in service class 1 and 2 in case of tension perpendicular to the grain of glulam. Consequently the empiric k_{mod} values for primarily design relevant short and medium term duration of load classes are well below those assumed today in Eurocode 5 for service class 2 conditions.

Finished and still ongoing DOL tests with the larger volumes ($V = 0,03 \text{ m}^3$) indicate that the volume effect, conforming to a Weibull shape factor of about 5 in ramp load tests, might be slightly less severe in long term loading.

The investigations were conducted with glulam of high strength classes; it should be checked whether the results apply in equal rigidity to lower quality material.

10 Acknowledgements

The funding of the presented research work through European Community via grant of research project AIR PL 94 1057 and the considerable financial support of Stuttgart University is gratefully acknowledged. Many thanks are indebted to Prof. Reinhardt, chair of building materials at Stuttgart University and director of FMPA, as well as to Mr. Radovic, head of department of wood and timber construction, for their expressed interest and financial support of the work.

11 References

Aicher, S., Dill-Langer, G. (1997): Duration of load effect in tension perpendicular to the grain of solid wood and glulam, FMPA Report (to be published), Stuttgart

- Aicher, S., Dill-Langer, G. (1995): Tension strength perpendicular to the grain of supreme quality glulam conforming to CEN strength classes GL 32 and GL 36. *Otto-Graf-Journal*, Vol. 6, pp. 246–274, FMPA – Otto-Graf-Institute, Stuttgart
- Aicher, S., Dill-Langer, G. (1996): Influence of cylindrical anisotropy of wood and loading conditions on off-axis stiffness and stresses of a board in tension perpendicular to the grain. *Otto-Graf-Journal*, Vol. 7, pp. 216–242, FMPA – Otto-Graf-Institute, Stuttgart
- Barrett, J. D. (1974): Effect of size on tension perpendicular-to-grain strength of Douglas-Fir. *Wood and Fiber*, Vol. 6 (2), pp. 126–143
- Barrett, J. D. (1996): Duration of load – the past, present and future. *Proceedings 1996 International Conference on Wood Mechanics*, pp. 119–137, Stuttgart
- Dill-Langer, G., Aicher, S. (1997a): Influence of cyclic climate on DOL and creep of glulam in tension perpendicular to the grain. *Proceedings COST Action E8 Conference*, (in press), Copenhagen
- Dill-Langer, G., Aicher, S. (1997b): Damage modelling of glulam in tension perpendicular to grain in variable climate. *Proceedings CIB–W18 Meeting 30*, paper CIB–W18/30-9-2, Vancouver
- Ehlbeck, J., Kürth, J. (1994): Ermittlung der Querkzugfestigkeit von Voll- und Brettschichtholz; Entwicklung eines Prüfverfahrens. *Versuchsanstalt für Stahl, Holz und Steine, Abteilung Ingenieurholzbau, Universität Karlsruhe*
- Feldborg, T. (1991): Determination of some mechanical properties of timber in structural sizes. *Proceedings 1991 International Timber Engineering Conference*, Vol. 2, pp. 2.189–2.199, London
- Foschi, R. O., Yao, Z. C. (1986): Another look at three duration of load models. *Proceedings CIB W18 Meeting 19*, paper CIB-W18/19-9-1, Florence
- Glos, P., Heimeshoff, B., Kellertshofer, W. (1987): Einfluß der Belastungsdauer auf die Zug- und Druckfestigkeit von Fichten-Brettlamellen. *Holz als Roh- und Werkstoff* 45, pp. 243–249
- Hoffmeyer, P. (1990): Failure of wood as influenced by moisture and duration of load. Ph. D. thesis, State University of New York, Syracuse
- Madsen, B. (1972): Duration of load tests for wood in tension perpendicular to grain. *Structural Research Series, Report No. 7*, Department of Civil Engineering, University of British Columbia, Vancouver
- McDowall, B. J. (1982): The duration of load effect in tension perpendicular to the grain for Douglas-Fir. Ph. D. thesis, University of British Columbia, Vancouver
- Mindess, S., Madsen, B., Barrett, J. D. (1979): Rate of loading and duration of load tests on Douglas-Fir in tension perpendicular to the grain. *Proceedings of the 1st Conference on Wood Fracture*, pp. 143–157, Banff
- Mohager, S. (1987): Studies of creep of wood (in Swedish). Ph. D. thesis, Royal Technical University, Stockholm
- Schniewind, A. P. (1967): Creep-rupture life of Douglas-Fir under cyclic environmental conditions. *Wood Science and Technology* 1, pp. 278–288

**INTERNATIONAL COUNCIL FOR BUILDING RESEARCH STUDIES AND DOCUMENTATION
WORKING COMMISSION W18 - TIMBER STRUCTURES**

**DAMAGE MODELLING OF GLULAM IN TENSION PERPENDICULAR TO GRAIN
IN VARIABLE CLIMATE**

by

G Dill-Langer
S Aicher
FMPA-Otto-Graf-Institute
Germany

**MEETING THIRTY
VANCOUVER
CANADA
AUGUST 1997**

Damage modelling of glulam in tension perpendicular to the grain in variable climate

Dill-Langer, G., Aicher, S.
FMPA – Otto-Graf-Institute
Department of Wood and Timber Engineering,
Germany

1 Introduction

So far, the so-called Canadian damage model has been applied primarily to model the damage evolutions of North American lumber subjected to long term bending loading (Foschi and Yao, 1986; Foschi et. al, 1989). Hereby load history results solely from gravity loads and climate is perceived as a parameter implicitly included in the damage state variable. A few attempts are known for an explicit recognition of the effect of transient moisture history in a damage model, either based on the US-model (Fridley et al., 1991) or on the Canadian model (Toratti, 1992); in all cases bending was regarded.

The application of a damage model to DOL in tension perpendicular to the grain is not stated in the literature. On the other hand DOL effects in this loading mode, especially in variable climate situations are still a largely unresolved matter with high importance for curved and tapered glulam beams.

In case of tension perpendicular to the grain of glulam in variable climate conditions the damage relevant load history has to incorporate the moisture gradient dependant eigenstress component as it is in the same order of magnitude of stresses from imposed service loads. The resulting combined stress state accounting for interacting transient stresses due to actions and moisture, strongly influenced by the cylindrical material orthotropy (Hanhijärvi and Ranta-Maunus, 1996; Aicher and Dill-Langer, 1996) can be suitably described by a damage relevant integral Weibull stress (Ranta-Maunus, 1996). The latter scalar then represents the load history.

The applicability of the sketched approach is demonstrated on the basis of empiric data sets obtained in an extensive research project on DOL of glulam and solid wood from North European spruce (Aicher, S. and Dill-Langer, G., 1997). In said investigations the loading regime of applied tension loads was stepwise and different test series were performed in presence of either constant resp. variable climate. Here exclusively the small volumes ($V = 0,01 \text{ m}^3$) are considered.

The paper first reveals the calibration of the Canadian damage model parameters, from constant climate DOL and ramp load tests. Then the model is applied for damage and time to failure simulation in variable climate. It is shown that the modelling approach with an

integral transient Weibull stress level is suited to predict times to failure in pronounced varying climate.

2 Calibration of damage model parameters

2.1 Description of the empiric data set at constant climate

The empiric DOL data set consisted of 15 specimens loaded to failure in stepwise loading at constant climate 20 °C/65 % RH conditions. One specimen had to be excluded due to an early glue line failure; the specimen was located at the end grain face of the original beam. In each step of 28 days the load was kept constant. The initial nominal load level was 45 % of the mean ramp load strength $f_{t, 90, \text{mean}}$ (ramp-load) = $f_{\text{mean, ramp}} = 0,885 \text{ N/mm}^2$; the load increment for each following load step was 5 % of $f_{\text{mean, ramp}}$. Figure 1 shows the stepwise loading regime and gives the times to failure of the individual specimens. The test was ended after the 8th specimen, roughly representing the median, had failed in the sixth load step at a nominal stress level of $SL_{\text{nom}} = 0,7$ resp. at an absolute stress value of $0,62 \text{ N/mm}^2$.

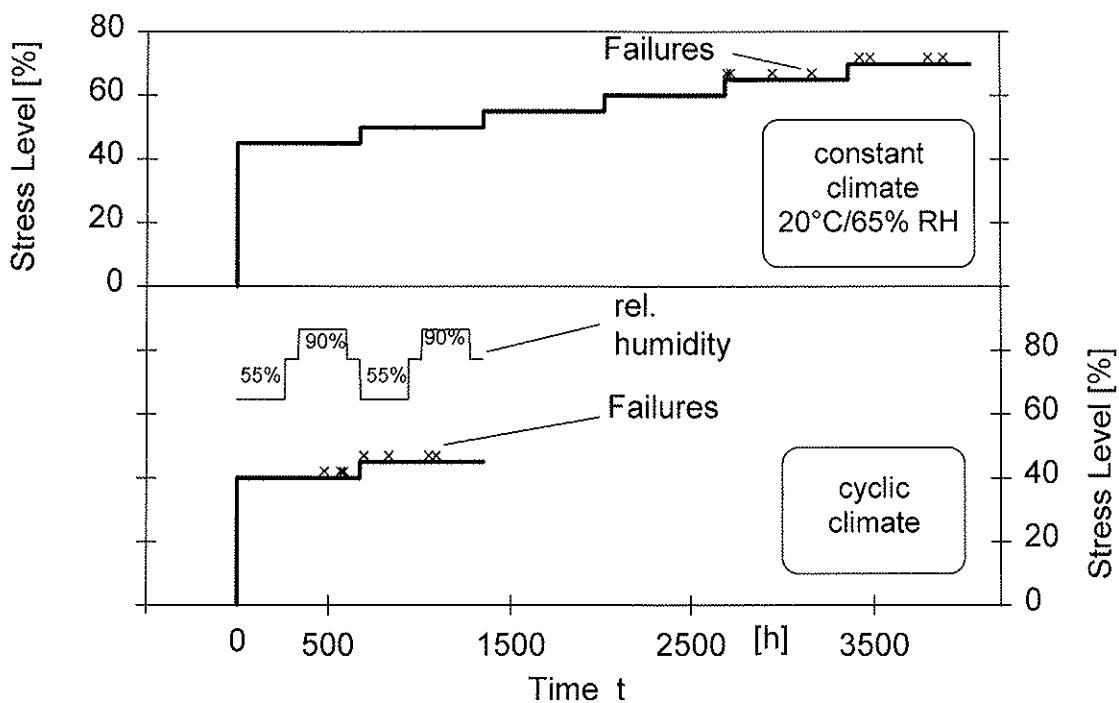


Figure 1 Loading history and times to failure of DOL tests in constant and cyclic climate conditions

The individual stress levels of the specimens were then determined by ranking method, i. e. determining the unknown strength of the individual specimen by relating the cumulative long term failure probability to a short term strength with same probability level. Hereby the short term strength distribution was described by a fitted 3parameter Weibull distribution

$$F_{(ft,90)} = 1 - \exp \left\{ - \left[(\sigma - \sigma_{\min}) / \sigma_0 \right]^m \right\} \quad (1)$$

where $m = 3,99$, $\sigma_0 = 0,364 \text{ N/mm}^2$, $\sigma_{\min} = 0,555 \text{ N/mm}^2$.

Table 1 contains a compilation of the experimental data and of the actual failure stress levels according to ranking method.

No. of specimen	Empiric cumulative failure probability in DOL test at 20 °C/65 % RH	Applied tension stress (resp. nominal stress level)		No. of failure load step	Estimated ramp load strength based on 3parameter Weibull distribution	Actual failure stress level	Times to failure	
		at load step 1 N/mm ²	at failure load step N/mm ²				total h	in failure load step h
1	0,036	0,398 (0,45)	0,575 (0,65)	5	0,714	0,806	2699	11
2	0,107				0,767		2719	31
3	0,179				0,798		2948	260
4	0,250				0,822		3165	477
5	0,321	0,620 (0,70)	0,620 (0,70)	6	0,843	0,735	3424	64
6	0,393				0,861		3483	123
7	0,464				0,879		3800	440
8	0,536				0,896		3885	525

Table 1 Compilation of empiric DOL test data in constant climate experiment and individual stress levels

2.2 Calibration procedure and results

The so-called Canadian damage model (Foschi et al., 1989) can be stated as

$$\dot{\alpha}(t) = a [\text{SL}(t) - k_0]^b + c [\text{SL}(t) - k_0]^d \alpha(t) \quad (2)$$

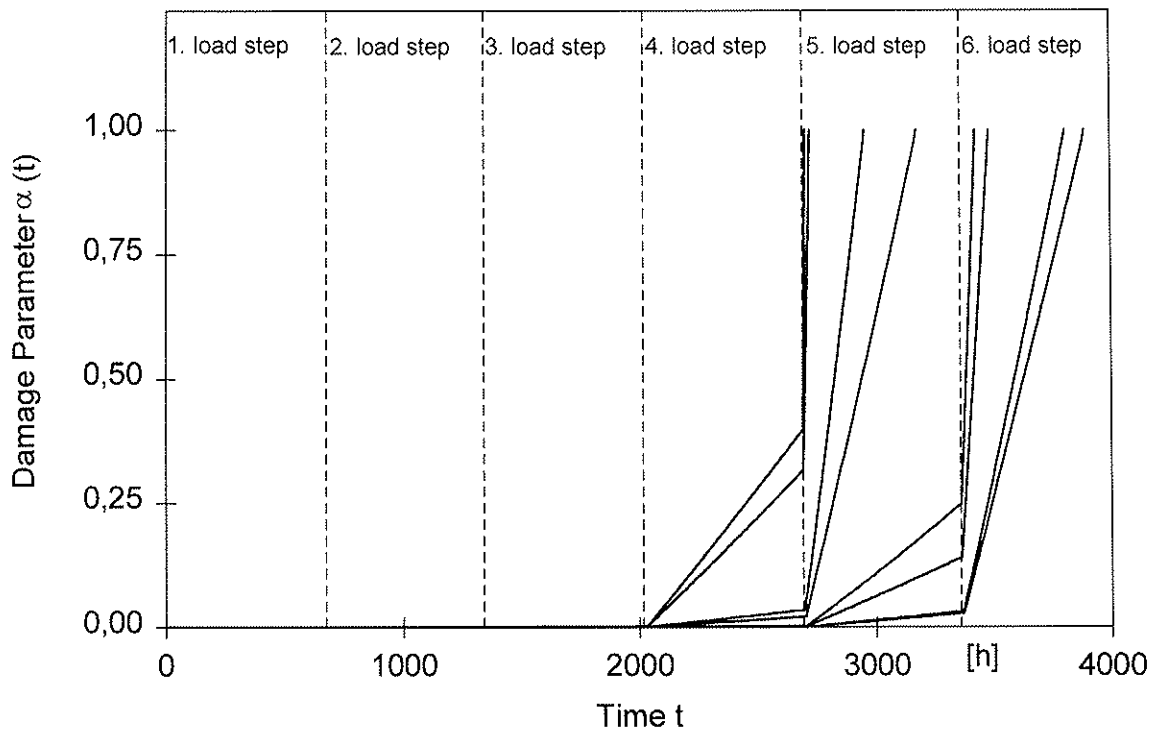
where $\text{SL}(t) = \sigma(t)/f_0$, $\sigma(t)$, f_0 and k_0 are, respectively, time dependant stress level, current stress, ramp load strength and threshold stress ratio where no damage accumulates for $\text{SL}(t) < k_0$. Quantities a , k_0 , b , c , d are independent parameters which are constant for a single member of the population but may vary considerably throughout the population depending i. a. on species and grade. Calibration of parameters k_0 , a , b , c , d has to be performed by non-linear minimization whereby quantity a can be derived in an approximation from the other model parameters in order to provide model consistency between long term and ramp load calibration data (Foschi and Yao, 1989)

$$a = \frac{f_0}{t_{F,0}} (b+1) / [1 - k_0]^{(b+1)} \quad (3)$$

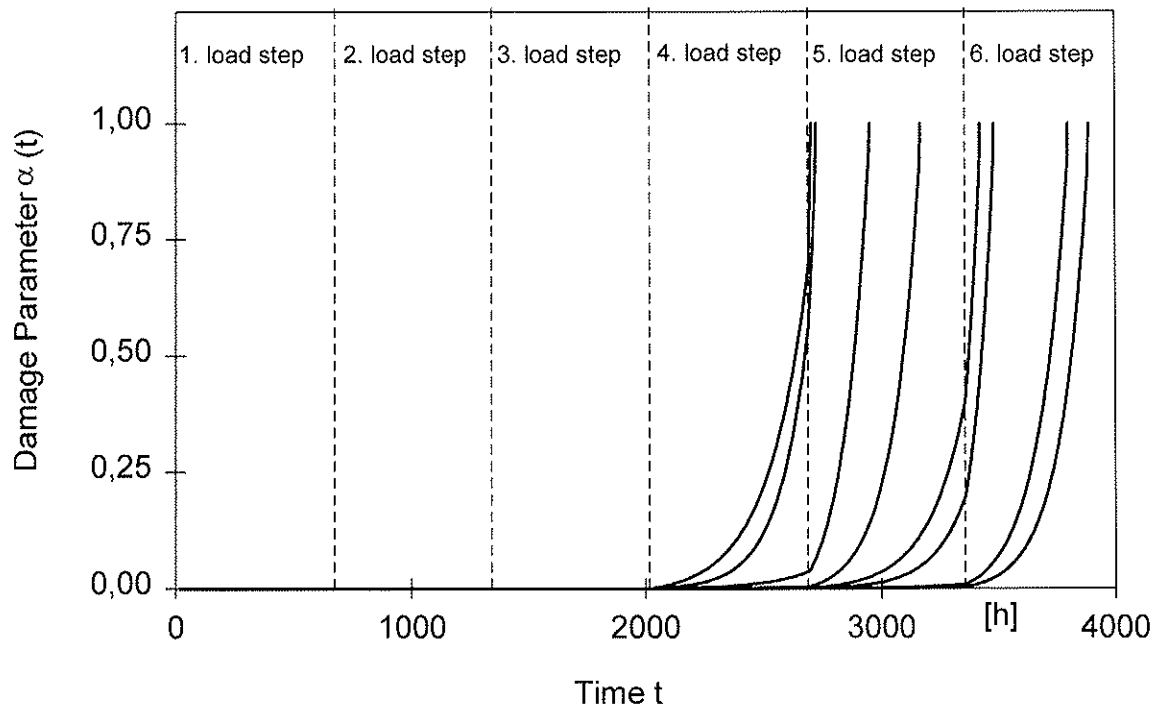
where $f_0/t_{F,0}$ is the ramp loading rate.

Integration of eq. (2) was performed by an iterative solution procedure (Foschi et al., 1989) being applicable for stepped load functions. However, the calibration of the model parameters due to the small sample size was performed different compared to the procedure stated in Foschi et al. The parameters were determined by fitting eqs. (2) and (3) to the explicit stress level history of eight failed specimens through iterative non-linear minimization of the squared difference between estimated and empiric times to failure. Thus a set of parameters for each individual specimen was obtained with a certain variation compared to the iteration start values, given equal for all specimens.

A matter of decisive importance for the parameter determination consists in the appropriate choice of the iteration start values, actually defining the type of damage evolution. From a variety of start value sets two sets delivered rather equal approximation results for times to failure with a rather different damage evolution. Set 1, see Table 2, delivers a quasi linear damage accumulation in each load step, whereas set 2 produces a more pronounced exponential damage evolution. Figures 2a, b illustrate the different damage evolutions for both types of start sets. Table 2 contains the parameter values for all eight specimens and further the means and C.O.V.'s of the parameters for set 1 and 2. The differences of the damage model parameters between the specimens are rather small. The C.O.V.'s for the parameter means resulting from set 1 and 2 start values were in the range of 2 to 5 %.



a)



b)

Figures 2a, b Individual damage evolution $\alpha(t)$ of eight specimens at constant climate conditions until damage $\alpha(t_f) = 1$ at empiric times to failure t_f for two different start sets of parameters for the Canadian damage model.
 a) start value set 1 resulting in quasi linear damage curves
 b) start value set 2 resulting in exponential damage curves

Iteration parameter start set	No. of specimens	Fitted damage model parameters and start set parameters				Total time to failure	
		b	c	d	k ₀	empiric h	damage model h
set 1	–	12,5	1	5	0,5	–	–
	1	14,565	1,081	5,569	0,576	2699	2699
	2	12,865	1,008	5,060	0,528	2719	2719
	3	13,300	1,00	5,008	0,518	2948	2948
	4	13,134	1,005	5,218	0,501	3165	3165
	5	13,711	1,000	5,016	0,500	3424	3425
	6	13,104	1,000	5,258	0,501	3483	3483
	7	13,546	1,005	5,081	0,500	3800	3801
	8	12,617	1,000	5,453	0,500	3885	3885
	mean	13,355	1,012	5,208	0,516		
	C.O.V.	4,2	2,6	3,8	4,8		
set 2	–	16	0,1	1,5	0,5	–	–
	1	17,428	0,104	1,676	0,569	2699	2699
	2	17,391	0,101	1,514	0,504	2719	2720
	3	16,450	0,100	1,608	0,500	2948	2949
	4	16,325	0,102	1,552	0,501	3165	3166
	5	16,091	0,101	1,626	0,500	3424	3425
	6	16,202	0,106	1,526	0,496	3483	3483
	7	16,403	0,100	1,610	0,500	3800	3801
	8	16,435	0,105	1,544	0,497	3885	3886
	mean	16,591	0,102	1,582	0,508		
	C.O.V.	2,9	2,9	2,1	4,5		

Table 2 Compilation of fitted damage model parameters for two different parameter start sets

3 Application of the model to DOL in transient moisture conditions

A first attempt of extending the Canadian damage model (2) to consider the superimposed effect of transient moisture conditions was performed by Toratti (1992) by introducing an additive term in eq. (2) to account for mechano-sorptive damage impact:

$$\dot{\alpha}(t) = a [SL(t) - k_0]^b + c [SL(t) - k_0]^d + e SL(t)^f |\dot{u}| . \quad (4)$$

An obvious problem of the latter approach is, that the additive mechano-sorptive damage term incorporates no stress threshold ratio for coupled stress-moisture induced damage

accumulation and further that the introduction of two further free parameters increases the calibration problem significantly. It was found that the mechano-sorptive term, as might be anticipated, is dominant and that the other terms did not contribute significantly to the damage rate for the studied stress levels and cyclic environments. The model therefore was reduced solely to the mechano-sorptive term. Another approach to introduce transient environmental effects on damage was made by Fridley et al. (1991) by extending the original US damage model (Gerhards and Link, 1987) by mechano-sorptive as well as constant moisture and temperature terms. For discussion of the inherent basic approach, see Foschi and Yao, 1986.

In this paper a new strategy for consideration of transient environmental conditions is employed. The basic idea is to keep the original Canadian model (2) and to incorporate the transient moisture conditions resp. the resulting complex transient (eigen)stress history by a suitably integrated scalar stress level history. The reduction of the complex 2dimensional transient cross-sectional stress field to a damage representative stress scalar was performed by computation of Weibull stresses. Hereby the integration, as presented following, is not performed for total stressed cross-section but for the highest stressed line parallel to width in the cross-section. The Weibull stress level was obtained as the ratio of actual Weibull stress $\sigma_{wei}(t)$ divided by the Weibull short term strength $f_{wei, ramp}$

$$SL_{wei}(t) = \frac{\sigma_{wei}(t)}{f_{wei, ramp}}, \quad \sigma_{wei}(t) = \left[\frac{1}{b} \int_0^b \sigma_{max}(x, y = const., t)^m \right]^{1/m}. \quad (4a, b)$$

According to EC 5 the shape parameter m was chosen as $m = 5$, thus, somewhat less severe than obtained in this investigation (chap. 2.1). Some details with respect to computation of $\sigma_{wei}(t)$ and its basis, being the transient stress field $\sigma_{max}(x, y, t)$, are given following.

3.1 Details of derivation of transient Weibull stress level

The 2D-structural modelling of the glulam cross-section built-up is performed on the basis of individual polar orthotropic material coordinate systems origins for the individual boards in the staggered built-up. The origin of the polar coordinate system is described by quantities d and e , being, respectively, distance of pith from right (= closer to pith oriented) board edge and eccentricity from mid-width. The assumed cutting pattern of the boards is based on an empiric evaluation of 30 glulam cross-sections of specimens employed in the tension perpendicular to the grain tests. The evaluation yielded for the means and C.O.V.'s of d and e , respectively, 30 mm (C.O.V. = 25 %) and 5 mm (C.O.V. = 25 %).

Figure 3 shows the cross-sectional built-up used for the hereinafter described calculations whereby in an approximation, for distance d throughout the mean value was assumed. For eccentricities e a simple periodic series of ± 5 mm was prescribed. Further, Fig. 3 reveals the vertical distribution of principal stress at mid-width exhibiting concentrations near the glue-lines; the horizontal distribution given for the lower edge of one board in the middle,

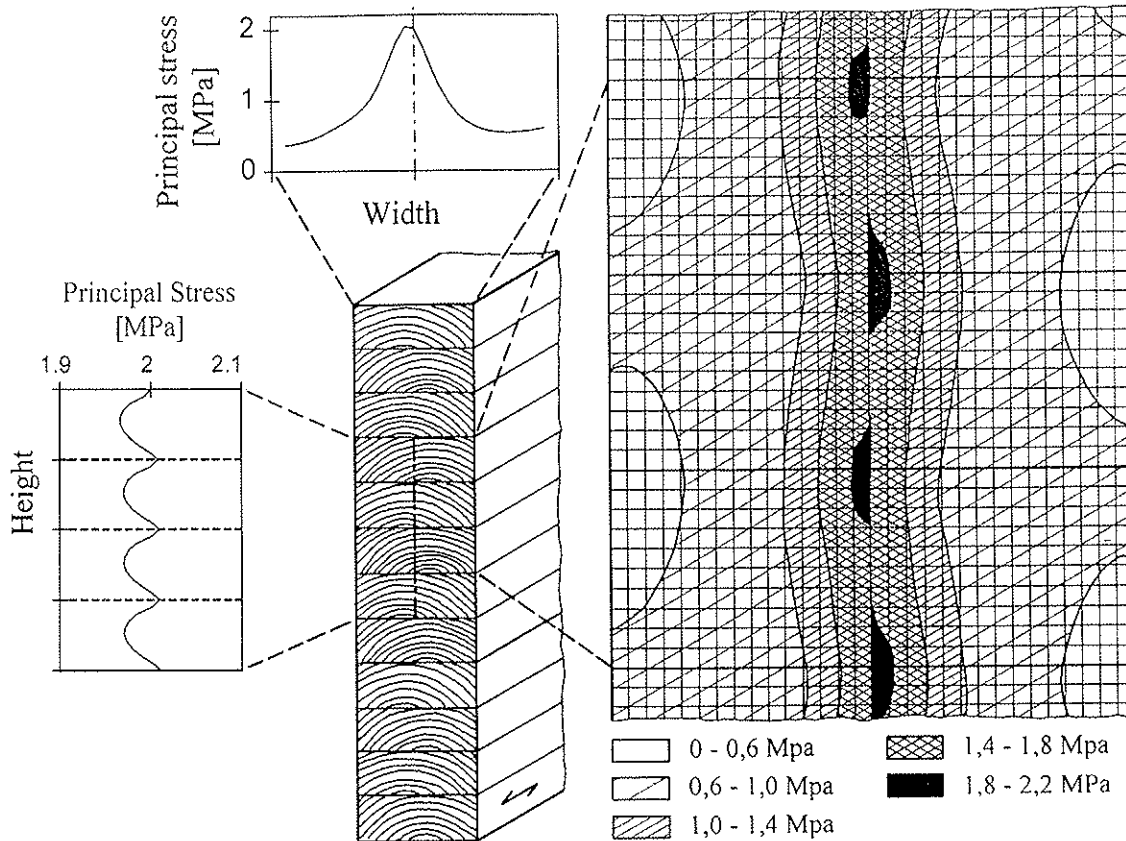


Figure 3
 Built-up of glulam cross-section altogether with principal stress distributions along height and width due to uniformly distributed tensile loading perpendicular to the grain in vertical direction (applied stress: $f_{\text{mean, ramp}} = 0.885 \text{ N/mm}^2$)

Figure 4
 Two-dimensional principal stress distribution of three boards out of a glulam cross-section with a built-up as given in Fig. 3

shows a pronounced stress peak near mid-width due to shear coupling effects (Hanhijärvi and Ranta-Maunus, 1996). In Fig. 4 the two-dimensional stress distribution is graphed as a contour plot. According to the empiric fact that most failures occur near the glue lines in both, ramp load and DOL tests, decision was made to base the calculation of Weibull stresses on the 1D horizontal stress distribution parallel to width at the lower edge of the board.

The constitutive equation used for computation of the mechanical behaviour expressed in a rate formulation for total strain rate $\dot{\epsilon}$ is

$$\dot{\epsilon} = \dot{\epsilon}_{\text{el}} + \dot{\epsilon}_{\text{ss}} + \dot{\epsilon}_{\text{visc}} + \dot{\epsilon}_{\text{ms}} \quad (5)$$

where

$$\dot{\epsilon}_{\text{el}} = \frac{\dot{\sigma}}{E}$$

is the elastic term,

$\dot{\varepsilon}_{ss} = \alpha \cdot \dot{u}$ is the linear shrinkage/swelling term,

$\dot{\varepsilon}_{visc} = \frac{\sigma}{E} \cdot \dot{J}$ is the viscoelastic creep term and

$\dot{\varepsilon}_{ms} = -\beta \cdot \sigma \cdot \dot{u} + m \cdot \sigma \cdot |\dot{u}|$ is the mechano-sorptive term.

The parameters E , α , β and m are, respectively, modulus of elasticity, shrinkage/swelling coefficient and two mechano-sorptive coefficients; \dot{J} denotes the rate of visco-elastic creep compliance. Transient moisture content $u(t)$ is derived by diffusion analysis based on Ficks law and boundary conditions of the convective type. For details of the adopted model, the FEM calculations and the calibration of the material parameter set see Dill-Langer and Aicher (1997).

3.2 The empiric data set

The DOL tests at cyclic varying climate were conducted similarly to those at constant climate conditions: 15 specimens were loaded stepwise starting at a level of 40 % of mean ramp load strength (i. e. one step below the level of the constant climate tests) with an increment of 5 % of $f_{mean, ramp}$. Figure 1 shows the stepwise loading regime, the cyclic climate variation between 55 % RH and 90 % RH with a cycle length of 28 days = 672 hours and the individual times to failure of 8 specimens.

The short term Weibull strength of the mean value was calculated as outlined in chap. 3.1. Based on this result the individual ramp load Weibull strengths were determined by ranking method (see chap. 2.1). A transient diffusion and mechanical analysis was then performed to calculate Weibull stresses $\sigma_{wei}(t)$. The verification of the mechanical model and the used material parameter set was performed via deformation results: Calculated and empiric deformations showed good agreement for two different cross-sectional widths and for both loaded and unloaded specimens (for details see Dill-Langer and Aicher, 1997).

4 Results of damage modelling in transient moisture conditions

Figure 5 shows the transient principal stresses at mid-width and at the edges of the cross-sectional built-up altogether with the resulting Weibull stress of the entire horizontal stress distribution. At the edges there are compressive stresses during wet and tensile stresses during dry periods as shrinkage/swelling is constrained by the inner part of the cross-section which exhibits smaller amplitudes of moisture changes. Vice versa the varying moisture gradient leads to high tensile stresses near mid-width during wet periods. The Weibull stress $\sigma_{wei}(t)$ follows qualitatively the course of the mid-width stresses: an increasing course during wetting periods then decreasing during drying periods. At the beginning of the second load step the stress curve shows a small peak due to external load increment.

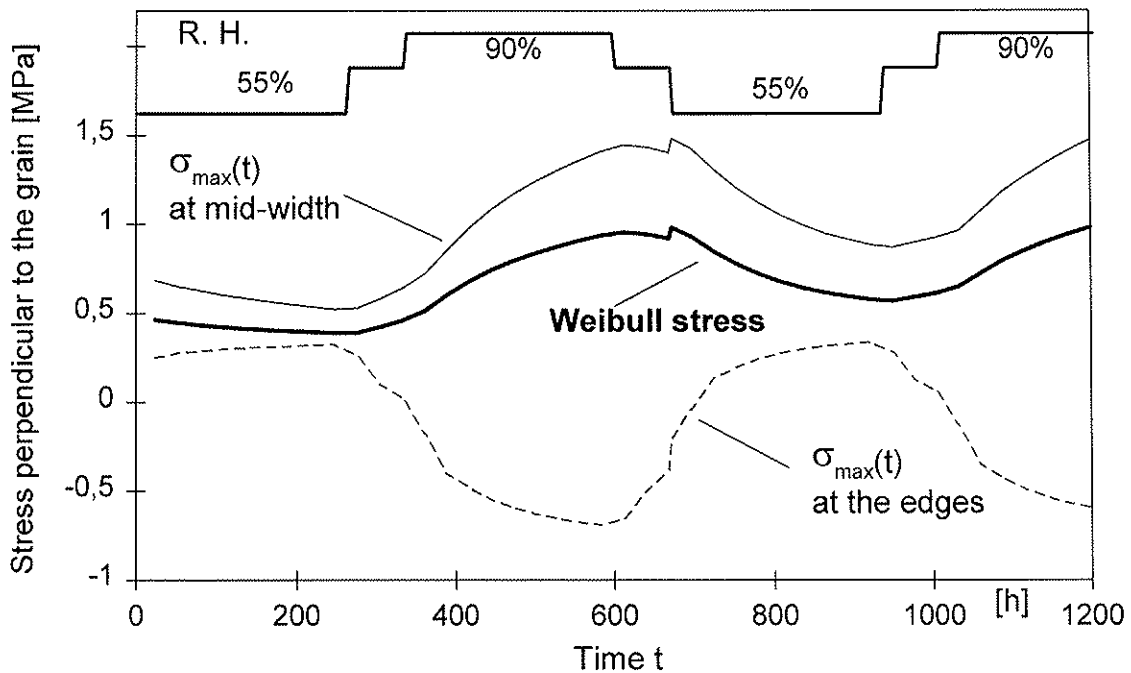


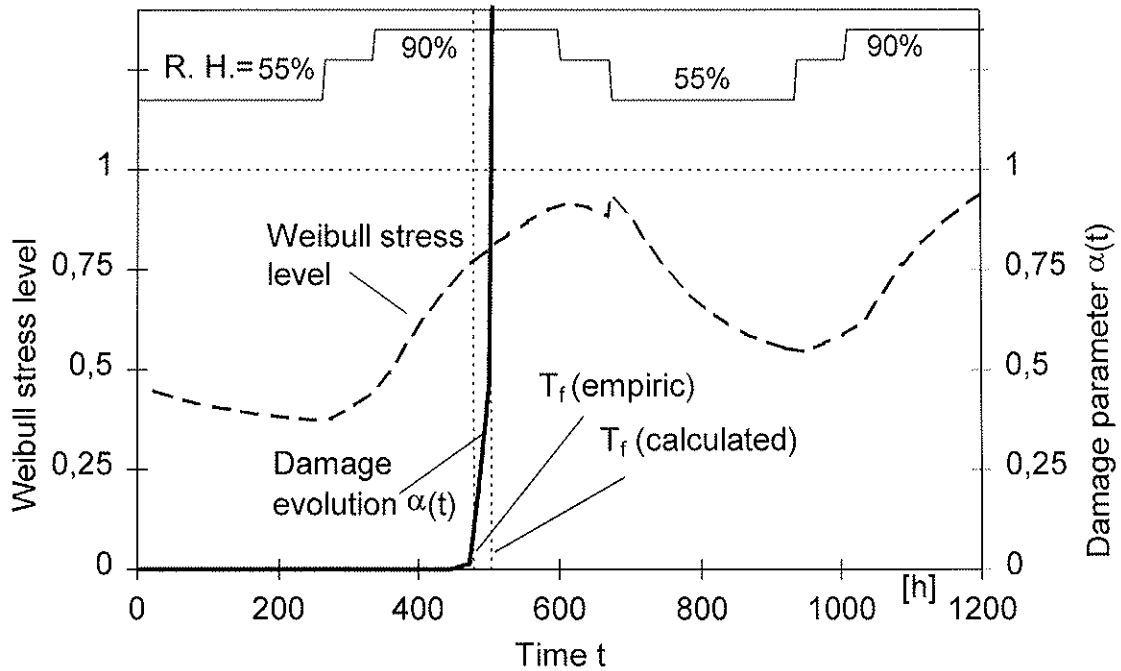
Figure 5 FEM-calculated evolutions of principal stresses vs. time at mid-width and at the edges of a glulam cross-section and the related evolution of the integral Weibull stress (simulation of DOL tests at cyclic varying climate)

The transient Weibull stress divided by the respective ramp load Weibull strength gives the individual transient Weibull stress level for each specimen. As direct integration of eq. (2) is difficult for random load histories the course of $SL_{wei}(t)$ was divided into intervals of 1 h length. The resulting step function was used as load history input data for the damage calculations. As model parameters a, b, c, d, k_0 the respective values of the calibration results (Table 2, parameter set 2) were used.

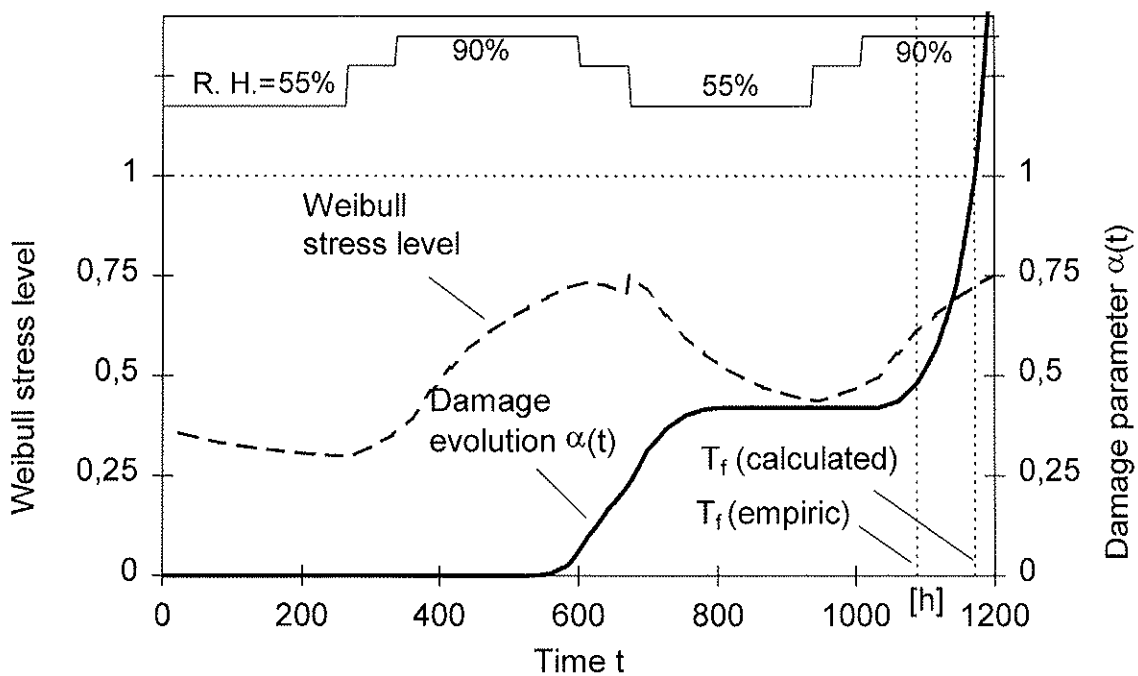
The stress level history $SL_{wei}(t)$ and the resulting evolution of the damage parameter $\alpha(t)$ is presented in Figs. 6a, b for the first and the 8th (mean value) failure of the cyclic climate DOL tests. Due to model assumptions both specimens were exposed to the same climate depending stress history $\sigma_{wei}(t)$ but to quantitatively different stress level histories $SL_{wei}(t)$.

In the case of the first failure the threshold value of damage accumulation is exceeded 400 hours after beginning of the first wetting period and damage evolution accelerates until the critical value is reached at $T_f = 504$ h (empiric: 479 h).

The damage evolution of the 8th specimen shows a different behaviour. Significantly increased damage values are reached at the end of the first wetting period. Although Weibull stress level $SL_{wei}(t)$ decreases due to lower relative humidity the cumulative damage grows until about 750 h. Between 800 h and 1000 h a plateau is reached as the stress level decreases beyond the threshold value. Damage acceleration occurs during the second wetting period and the damage parameter reaches the critical value at $T_f = 1172$ h (empiric: 1088 h).



a)



b)

Figures 6a, b FEM-calculated evolutions of Weibull stress level (dashed line) and resulting damage evolution vs. time for two specimens with distinct different failure times; the empiric and calculated times to failure are given as dotted lines.

a) SL_{wei} and α for 1st specimen representing roughly the characteristic value

b) SL_{wei} and α for 8th specimen being the mean value of the DOL tests

Table 3 contains a compilation of the individual short term Weibull stresses and the empiric altogether with the calculated times to failure for all eight failed specimens. It may be seen that damage calculations based on transient Weibull stress level yield in general a good qualitative prediction of times to failure. The quantitative agreement is satisfactory for most specimens, except specimens No. 5 and 6. In these cases the damage evolution curve exhibits a plateau which leads to major deviations in failure time due to minimal variations of damage parameters or load history.

No. of specimen	Short term Weibull strength $f_{wei, ramp}$ [MPa]	Time to failure t_F	
		empiric [h]	calculated [h]
–			
1	1,041	479	504
2	1,122	479	531
3	1,172	568	559
4	1,198	595	579
5	1,226	693	595
6	1,252	830	655
7	1,275	1049	1059
8	1,301	1088	1172

Table 3 Compilation of estimated individual short term Weibull strength due to ranking method and empiric resp. damage model calculated times to failure; all failed specimens in DOL tests at cyclic climate conditions

5 Conclusions

The Canadian damage model was applied to DOL tests of glulam loaded in tension perpendicular to the grain at constant and changing climate conditions.

The calibration of the model parameters was performed on the basis of empiric data obtained from constant climate tests with stepwise increased loading and from related results of ramp load tests. Hereby, two different sets of parameter start values, representing two qualitatively different shapes of damage accumulation functions, turned out to yield equally good fits of times to failure.

The idea of the presented damage modelling approach in case of varying climate conditions with resulting high eigenstress terms was to keep the basic Canadian model. In an extension the stress level should be expressed by an adequately derived damage relevant Weibull stress level. The stress history of DOL tests at cyclic varying humidity was derived through transient diffusion and mechanical FEM-calculations including mechano-sorptive creep and the structural effect of polar orthotropy due to annual ring curvature. The resulting

transient stress field was integrated to a damage relevant Weibull stress which was related to short term Weibull strength by ranking method. The derived Weibull stress levels were used as load history input for the Canadian damage model. The results of the damage calculations yielded a qualitatively good prediction of times to failure.

The presented new approach to incorporate changing climate influences into damage calculations through an apt stress scalar (Weibull stress level) seems to be promising for all cases where moisture gradient dependant eigenstresses are important.

6 Acknowledgements

The funding of the presented research work through European Community via grant of research project AIR PL 94 1057 is gratefully acknowledged. Many thanks are indebted to Prof. Reinhardt, chair of building materials at Stuttgart University and director of FMFA, as well as to Mr. Radovic, head of department of wood and timber construction, for their expressed interest and financial support of the work.

7 References

- Aicher, S., Dill-Langer, G. (1997): DOL effect in tension perpendicular to the grain of glulam depending on service classes and volume. Proceedings CIB W18 A Meeting 30, paper 30-9-1, Vancouver
- Aicher, S., Dill-Langer, G. (1996): Influence of cylindrical anisotropy of wood and loading conditions on off-axis stiffness and stresses of a board in tension perpendicular to the grain. *Otto-Graf-Journal*, Vol. 7, pp. 216–242, FMFA – Otto-Graf-Institute, Stuttgart
- Dill-Langer, G., Aicher, S. (1997): Influence of cyclic climate on DOL and creep of glulam in tension perpendicular to the grain. Proceedings COST Action E8 Conference, (in press), Copenhagen
- Foschi, R. O., Folz, B. R., Yao, F. Z. (1989): Reliability based design of wood structures. Structural Research Series, Report No. 34, Department of Civil Engineering, University of British Columbia, Vancouver
- Foschi, R. O., Yao, Z. C. (1986): Another look at three duration of load models. Proceedings CIB W18 A Meeting 19, paper CIB-W18/19-9-1, Florence
- Fridley, K. J., Tang, R. C., Soltis, L. A. (1991): Environmental effects of the load duration behaviour of structural lumber. Proceedings 1991 International Timber Engineering Conference, Vol. 4, pp. 4.180–4.187, London
- Gerhards, C. C., Link, C. L. (1987): A cumulative damage model to predict load duration characteristics of lumber. *Wood and Fiber Science*, 19 (2), pp. 147–164
- Hanhijärvi, A., Ranta-Maunus, A. (1996): Computational analysis of the effect of transverse anisotropy and annual ring pattern in cross-sections of curved glulam beams on the size effect of strength. Proceedings European Workshop on Application of Statistics and Probabilities in Wood Mechanics (in press), Bordeaux

- Larsen, H. J., Thelandersson, S., Isaksson, T. (1996): Model code for the probabilistic design of timber structures. Proceedings CIB W18 A, meeting 29, paper CIB-W18/29-102-1, Bordeaux
- Ranta-Maunus, A. (1996): The influence of changing state of stress caused by mechano-sorptive creep on the duration of load effect. Proceedings 1996 International Conference on Wood Mechanics, pp. 187–201, Stuttgart
- Toratti, T. (1992): Creep of timber beams in a variable environment. Report 31, Laboratory of Structural Engineering and Building Physics, Helsinki University of Technology

**INTERNATIONAL COUNCIL FOR BUILDING RESEARCH STUDIES AND DOCUMENTATION
WORKING COMMISSION W18 - TIMBER STRUCTURES**

**NONDESTRUCTIVE EVALUATION OF WOOD-BASED MEMBERS
AND STRUCTURES WITH THE HELP OF MODAL ANALYSIS**

by

P Kuklik
Czech Technical University in Prague
Czech Republic

MEETING THIRTY

VANCOUVER

CANADA

AUGUST 1997

Nondestructive Evaluation of Wood-based Members and Structures with the help of Modal Analysis

Petr Kuklik

Czech Technical University in Prague, Czech Republic

1 Introduction

Non-destructive testing of members and structures is a process during which we investigate the properties of the respective members and structures without their serious damage. There is a whole range of non-destructive methods and their accuracy is different.

The paper describes in detail the method of modal analysis which was most frequently used and evolved during its application to thin-flanged beams. For the verification of the modal analysis method thin-flanged beams were paralelly tested by means of statical tests without and up to the attainment of load carrying capacity (Fig.1.1,1.2).

Test samples of thin-flanged beams were made of spruce wood and water resistant spruce plywood. The ribs and the reinforcement of thin-flanged beams were connected by nails. The test samples were placed on the supports of the breaking path and they were loaded through distributing steel component of an overall mass of 2.94 kN (Fig. 1.1) by means of a hydraulic press of capacity of 100 kN. The loading force was measured with 1.5 percentage precision.

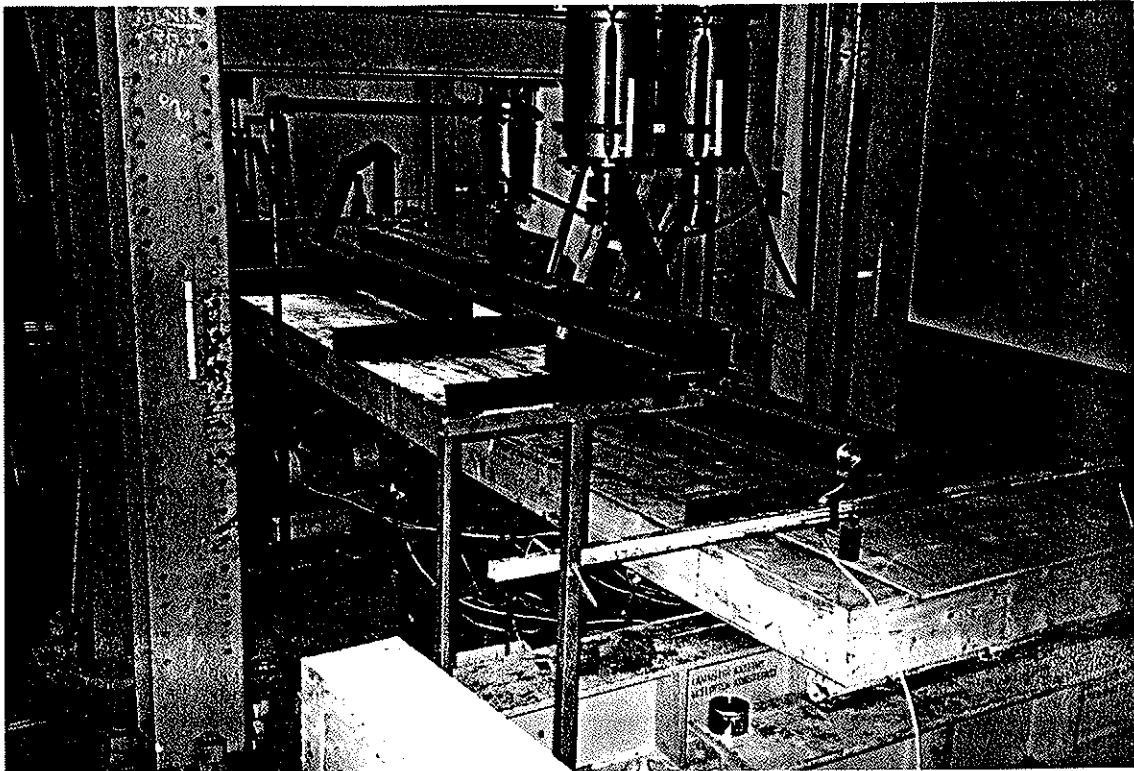


Fig.1.1 Arrangement of a loading test of thin-flanged beams

The thin-flanged beams were first loaded by the so-called test loading Q_t during a period of 72 hours. After unloading they were further loaded up to ultimate load (fracture)- Fig.1.2. The test load was determined according to the relationship :

$$Q_t = \frac{1+\gamma_{Q,i}}{2} \sum Q_{k,i} \quad (1.1)$$

where $Q_{k,i}$ are the characteristic values of variable actions,
 $\gamma_{Q,i}$ is the partial safety factor of variable actions $Q_{k,i}$.

The test without reaching the ultimate load capacity concerning thin-flanged beams was evaluated on the basis of the principle of a comparison of the values of permanent deflections (ascertained ideally 72 hours after the removal of the test loading) and the values of total deflections (after 72 hours of application of the test load).

On the basis of long-term experience it is possible during tests without reaching the ultimate load capacity to consider the component as possessing sufficient bearing capacity under the assumption that the deformation ratio (permanent deflection / total deflection) does not exceed the value 0.3. As regards this criterion experience has proved that it can be applied even in other cases. For example, in this way we have tested also frames with screwed corners of hall structures.

During the loading of thin-flanged beams up to fracture the loading mass increased as shown in Fig.1.2.

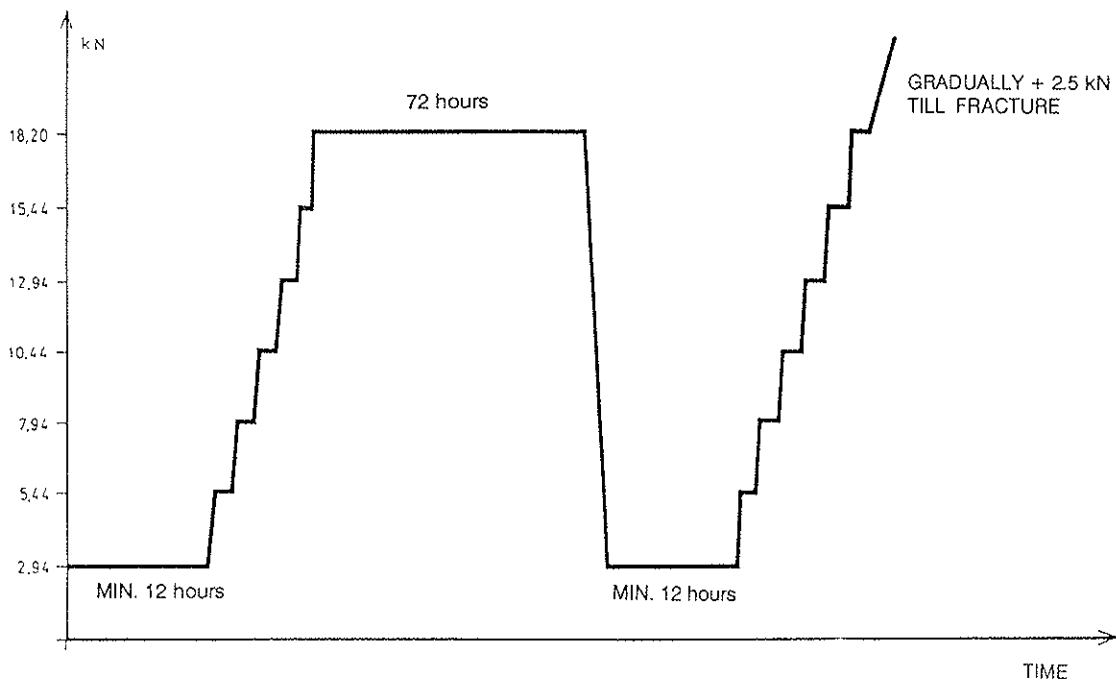


Fig.1.2 Time curve of a loading test of thin-flanged beams

2 Modal analysis

Modal analysis involves the determination of modal parameters for members and structures. Modal parameters are essentially dynamic characteristics of an element determined by the mechanical interaction of structural geometry and material. An element will freely vibrate at one or more of its natural frequencies when subjected to some form of external triggering force. At each natural frequency the element forms a certain shape called a "mode shape". The mode shape formed may be predicted by computer models but still requires measurement to determine accurately the modal frequency and amplitudes. Vibration can be caused by any number of external sources. Should the fundamental frequency of the external source coincide with any of the natural frequencies (particularly those with the most significant amplitudes) large amplitudes of vibration can occur. This phenomenon, known as resonance, results in large amplitudes that can have destructive effects on components and structures. In some cases this causes the deterioration of members, in general this contributes to increased fatigue of the specimen. Study in this area falls into the category of structural dynamics.

This examination is directed towards the modal analysis of thin-flanged beams. This work can be generally divided into two sections.

- 1) Experimental analysis: A large part of this work involves taking field measurements of thin flanged beams and an analysis of the obtained results.
- 2) Finite element analysis: The derivation of modal parameters and hence mode shapes using analytical models utilising a special finite element package capable of performing dynamic analysis on a model. In addition to this static load cases can be examined on models already validated with dynamic correlation between experimental and analytical results.

2.1 Fast Fourier Transforms

As part of the initial data processing of measurements the spectrum analyser must perform an algorithm known as the Fast Fourier Transform (FFT). Data read in the time domain are converted to the frequency domain using the FFT algorithm. It is necessary, as the majority of modal analysis packages require the data to be in this form. All of the data recorded in this study have been processed using the FFT, which is an inherent part of the spectrum analyser.

The following equation is representative of the Fourier series:

$$F(t) = \frac{F_{co}}{2} + \sum_{n=1}^{\infty} (F_{cn} \cos \omega_n t + F_{sn} \sin \omega_n t) = F_{st} + \sum_{n=1}^{\infty} F_n \sin(\omega_n t + \varphi_{Fn}). \quad (2.1)$$

In the transforming of the exiting force $F(t)$ into the Fourier series we consider in practical computations only a finite number of members of the series.

2.2 The transfer function

The transfer function is a mathematical model defining the input-output relationship of a physical system.

The system transfer function can be thought of as the intermediate section of the following block diagram (Fig. 2.1).

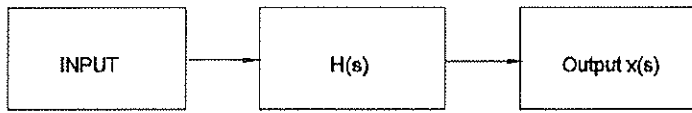


Fig.2.1 The block diagram outlines the three key segments in experimental analysis

The transfer functions of the linear system $H(p)$ is defined as the Laplace image of its weight function $h(t)$. The weight function $h(t)$ is defined as a response of a linear system as regards a unit impulse $\delta(t)$.

With the help of the weight function we can analyse the linear system by means of the so-called Duhamel integral:

$$v(t) = \int_{-\infty}^t h(t-\tau)F(\tau)d\tau = \int_0^{\infty} h(\tau)F(t-\tau)d\tau, \quad (2.2)$$

where $F(\tau)$ is an input value and $v(t)$ is an output value.

2.3 A system with a finite number of degrees of freedom

The solution in the normal system of coordinates.

We introduce a transformation of coordinates:

$$\{v\} = [v^0] \{n\}, \quad \{n\} = [v^0]^{-1} \{v\}, \quad (2.3)$$

where the new coordinates of the system $\{n\}$ are the so-called normal coordinates and the matrix $[v^0]$ is the so-called modal matrix composed of vectors describing the natural shapes of vibration,

$$[v^0] = [\{v^0_{(1)}\}, \{v^0_{(2)}\}, \dots, \{v^0_{(k)}\}, \dots, \{v^0_{(m)}\}]. \quad (2.4)$$

The transformation (2.3) enables us to obtain a system of statically and dynamically independent equations from the system of dependent equations.

For a system with a finite number of degrees of freedom with viscous damping it holds valid:

$$[M]^D \{v\} + [B]\{v\} + [C]\{v\} = \{F(x_s, t)\}, \quad (2.5)$$

where $[M]^D$ is the diagonal mass matrix,
 $[B]$ is the matrix of damping,
 $[C]$ is the stiffness matrix,
 $\{F(x_s, t)\}$ is the column matrix of the exciting forces.

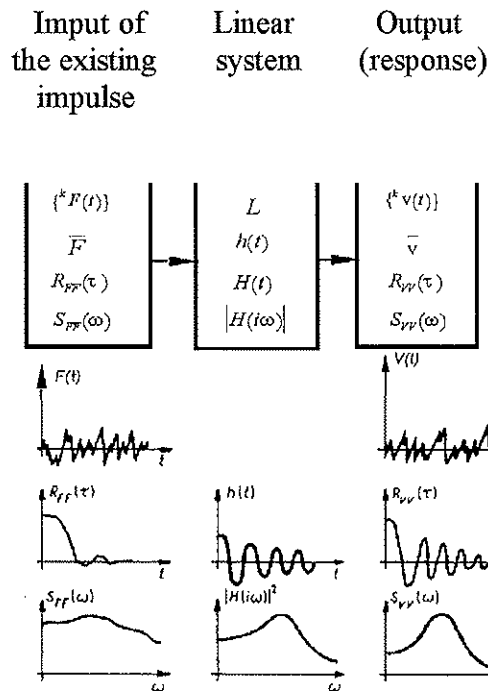


Fig.2.2 Response of a linear system to a stationary random exciting impulse

3 Linking finite element method with experimental modal analysis

M. Hermanki and H. Ostholt presented a paper in July 1987 examining a method for linking the finite element technique with experimental modal analysis. The method uses Lagrange polynomials and cubic spline functions to "... approximate the Rotational Degrees of Freedom (RDOF) at the linking points in the modal data base". In order to link correctly both the finite element data base and the experimental modal data base the RDOF of each base must be compared. Information of this sort is readily available from FEM analysis but requires some processing to achieve the same for experimental modal data.

4 Configuration

The selection of equipment for measuring the dynamic properties of any structure requires an evaluation of the type of measurements the analyst is to perform. The type of equipment is dependent on the measurement environment, i.e. depends on the ambient conditions around it, and the measurement required. The diagram below illustrates a typical instrument configuration used in the experimental investigation section of this work.

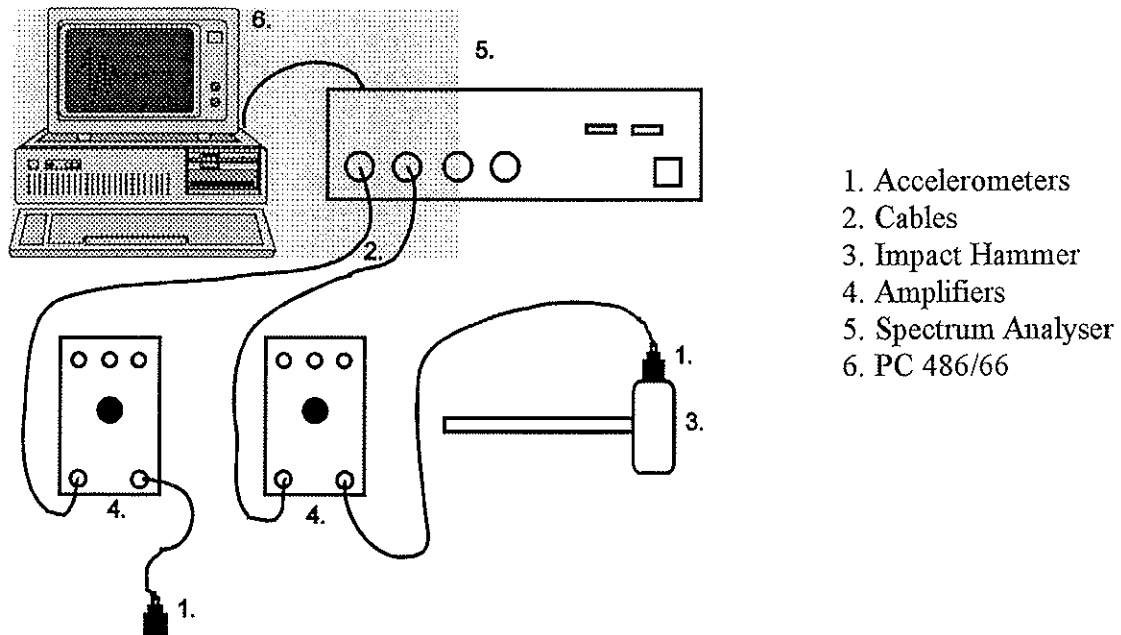


Fig.4.1 Typical configuration of the testing equipment used for dynamic measurements

4.1 Spectrum analyser

The spectrum analyser used for measurements was a four channel Tektronix. Four channels enable the dynamicist to have one accelerometer measuring the force input and three measuring the structural response, which is a common technique for checking the recorded data simply using measurement comparisons. Measurement checking should be practiced where possible to help to eliminate the possible recording and processing of extraneous data. The spectrum analyser performs Fast Fourier Transforms (FFT) on the measured data creating a continuous curve by joining the discrete measured points with the use of a mathematical series.

4.2 Impact hammer

The type of analysis undertaken here involves the use of an impact load to the element, classified as an impulsive impact type of loading.

The impact hammer used for all these investigations has been specially developed during the recent few years. Essentially the impact hammer has the character of a hammer of a mass about 3 kg. The drop height of the hammer is about 15 - 20 cm.

5 Testing of thin-flanged beams

5.1 Practical use of modal analysis

Test elements of thin-flanged beams (Fig. 5.1) were made of spruce wood and water resistant spruce plywood. The ribs and the reinforcement of thin-flanged beams were connected by nails.

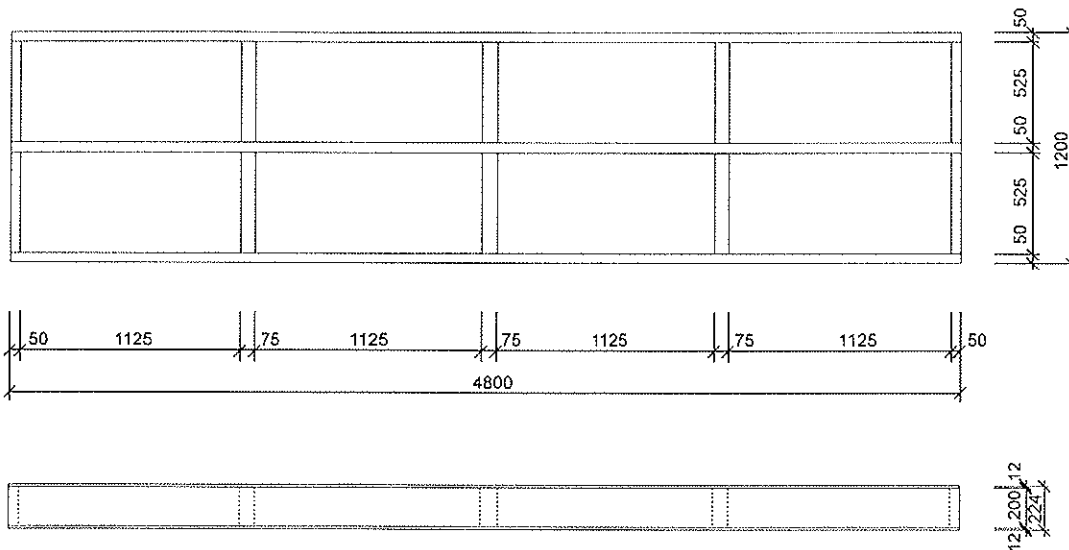


Fig.5.1 Dimensions of Test Elements

The test elements were placed on the supports (Fig. 5.2) and they were loaded by the impact hammer.

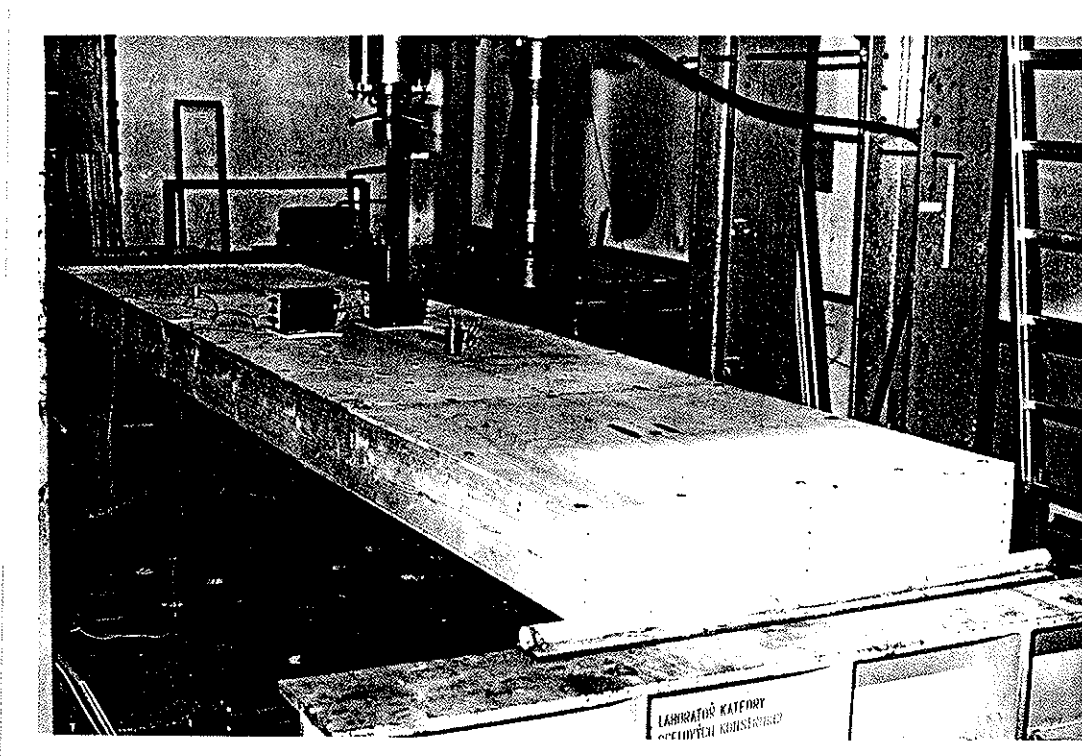


Fig.5.2 Arrangement of a Test

During the test steel targets were glued to the thin-flanged beams, as is shown in Fig. 5.3. One of the targets served as a reference target. The first accelerometer was connected with this target. At the remaining targets impulses were gradually excited by means of the impact hammer which was connected with the second accelerometer (Fig. 4.1).

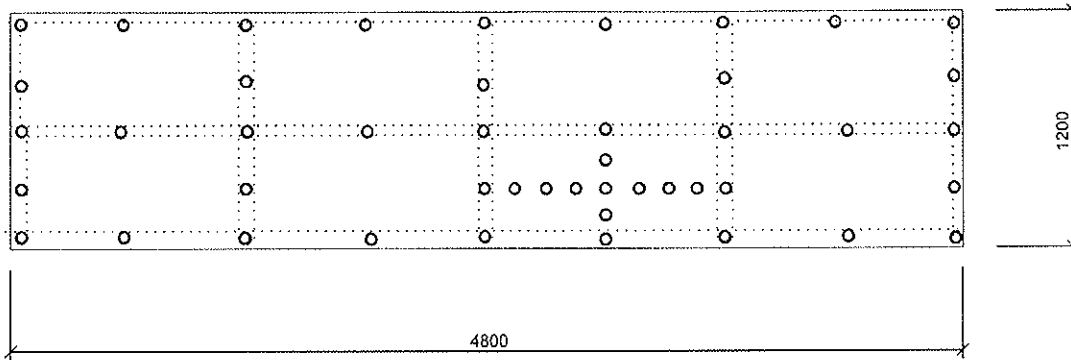


Fig.5.3 Spacing of the steel targets on thin-flanged beams

The impulses were repeatedly conveyed to each target (10 times) and the response to these impulses was evaluated with the help of a weighted arithmetic mean.

Beside the response test of thin-flanged beams also their plywood sheathing was tested separately for buckling in the section between the longitudinal and the transverse ribs (See Fig. 5.4). In this case the process of imparting the impulses was reversed. The power impulse was conveyed to the reference point and the response was measured at different places within the chosen target mesh.

```

Project      : plast
Trace A     : Mode#4 80.07 Hz
Mode #      : 4
Frequency   : 80.07 Hz
Damping     : 431.92m %
  
```

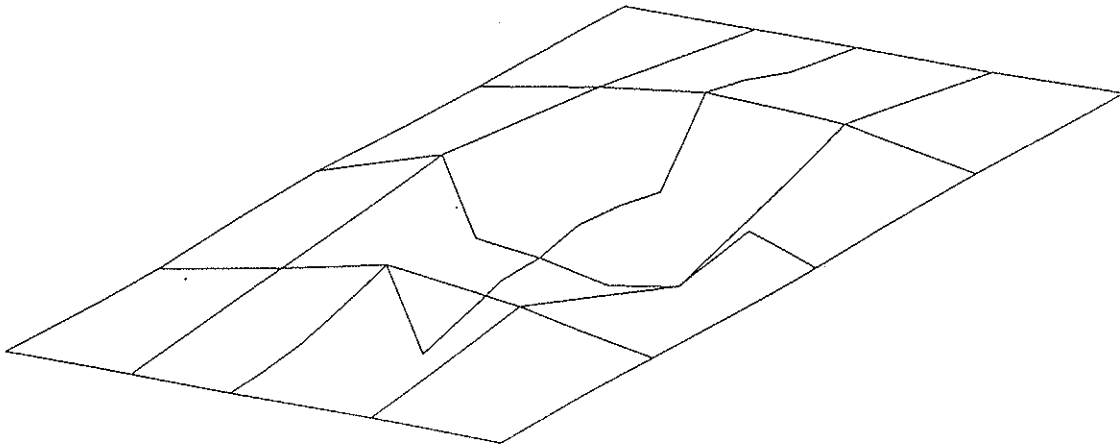
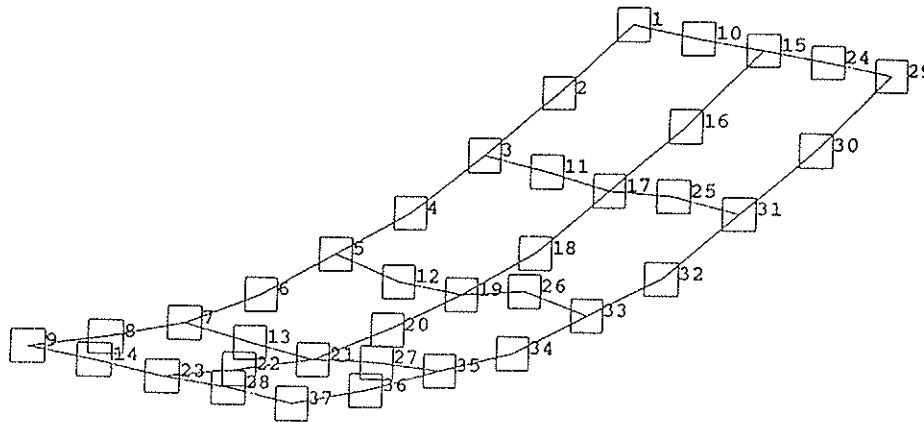


Fig.5.4 Buckling of thin-flanged beam sheathing

During the measuring the responses were simultaneously recorded with the help of a computer which at the same time decided if the magnitude of the imparted impulses was kept within tolerable limits. The panels were tested on both sides.

The individual measuring results were gradually evaluated with the help of the Star Program. The results of the evaluation were represented by the natural shapes and natural frequencies yielded by the program in the form of animation but also of graphic output. Examples are shown in Fig. 5.5.

Project : panel-1
 Trace A : Mode#1 17.38 Hz
 Mode # : 1
 Frequency : 17.38 Hz
 Damping : 91.65m %



Project : deskar
 Trace A : Mode#4 38.99 Hz
 Mode # : 4
 Frequency : 38.99 Hz
 Damping : 739.63m %

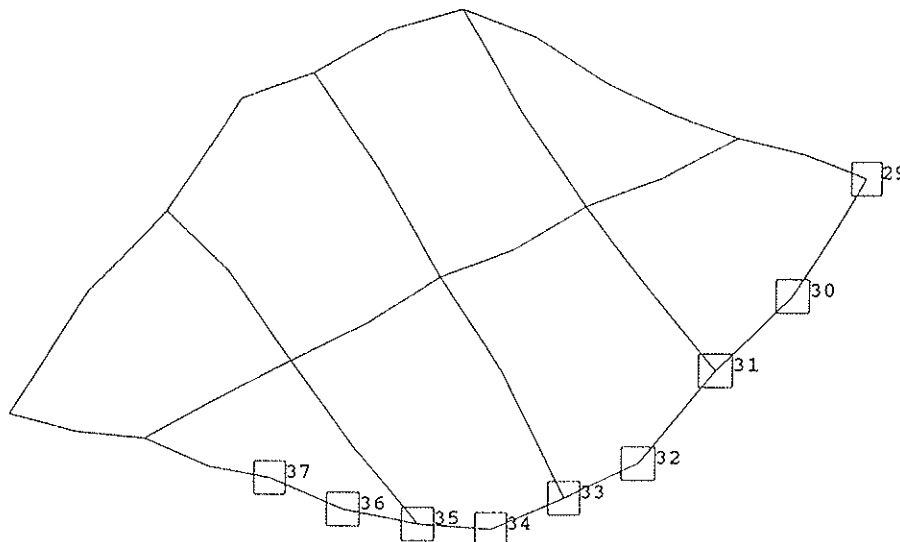


Fig.5.5 Natural shapes and natural frequencies of thin-flanged beams determined experimentally with the help of modal analysis

The first natural frequency and the first natural shape of the vibration of the tested element are of primary importance for practical use, because they are represented most frequent in the resulting vibration shape as regarded from the point of energy.

5.2 Investigation of natural shape and natural frequency by means of the Finite Element Method

In connection with the testing of thin-flanged beams by means of modal analysis a model was simultaneously elaborated with the help of the Finite Element Method. Natural shapes and natural frequencies were investigated at this model similarly to the experiments shown in Fig. 5.5.

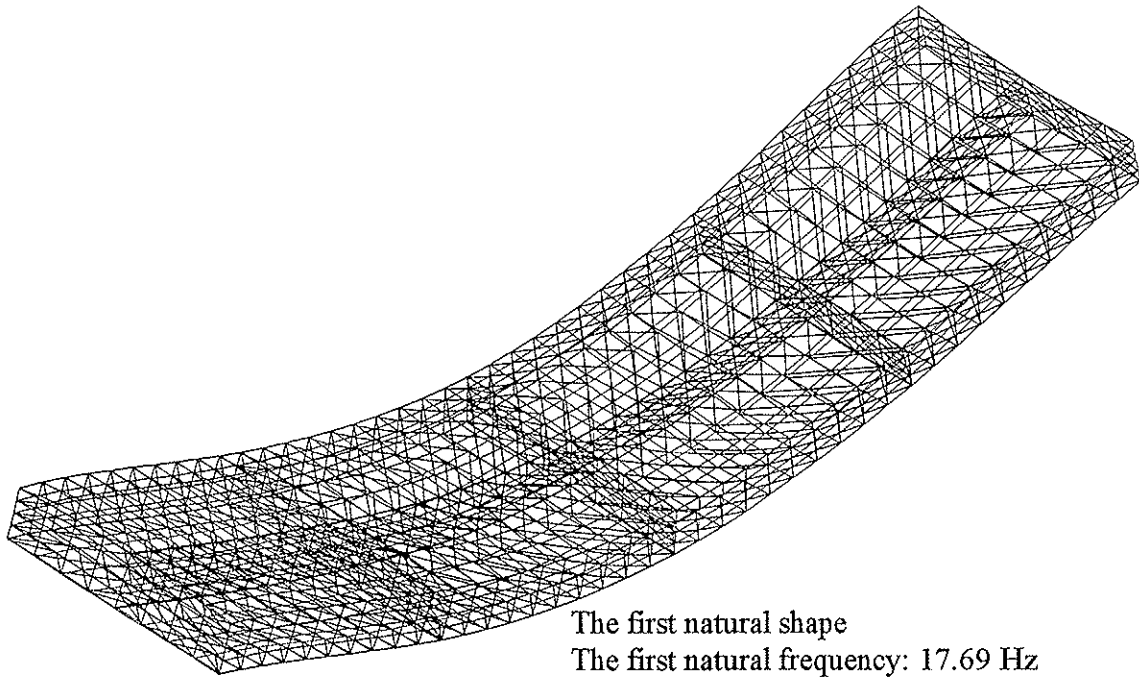


Fig.5.6 The first natural shape and the first natural frequency

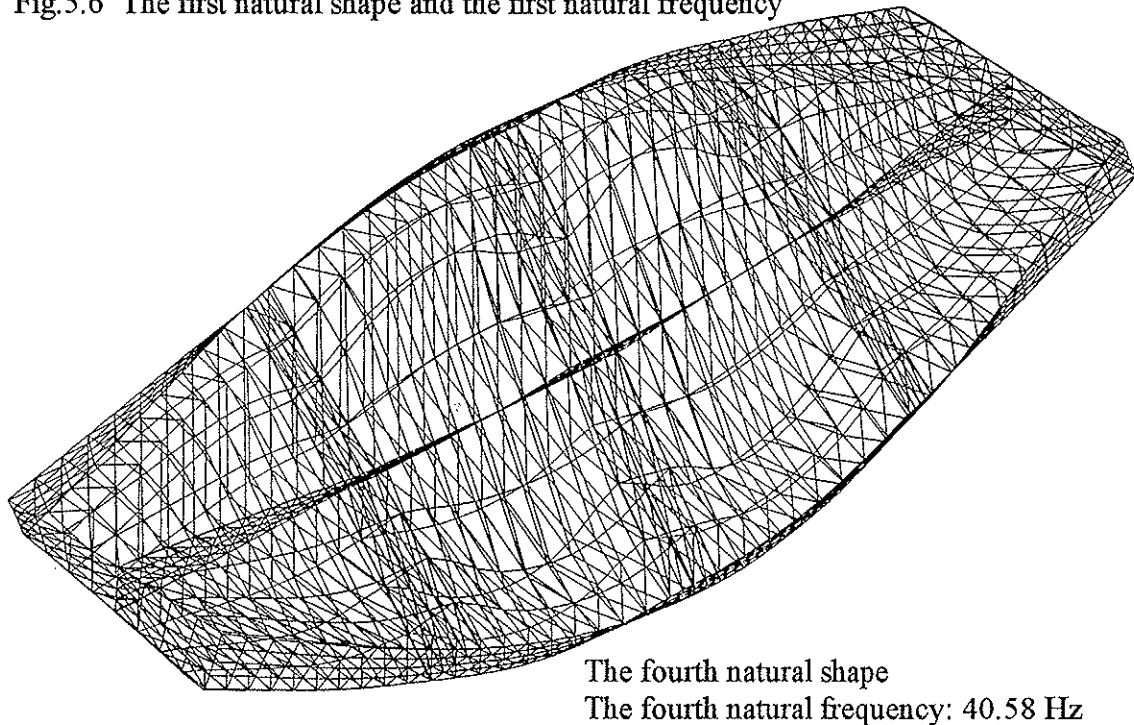


Fig.5.7 The fourth natural shape and the fourth natural frequency

6 Conclusion

It is obvious from the results of experimental testing of thin-flanged beams and their subsequent modelling by means of the Finite Element Method (See section 5) that modal analysis is a convenient method for the verification of computation models.

Modal Analysis has recently proved useful in the determination of characteristic values of the mechanical properties of structural timber and its grading. Up to the present day we have carried out three series of experiments with structural timber taken from three different regions of the Czech Republic. The tests were carried out with samples with the dimensions

of 100 mm x 120 mm x 2 800 mm and of 100 mm x 150 mm x 2 950 mm. Structural timber first underwent visual grading according to the standard DIN 4074. Further tests were carried out by means of the modal analysis method and the ultrasonic method. Eventually destructive tests were carried out according to the standards EN 408 and EN 384. The purpose of the destructive test was the verification of non-destructive test results. The test results of one series of 43 samples of structural timber, which corresponded to the strength class C 22 according to the standard EN 338, are shown in Figure 6.1.

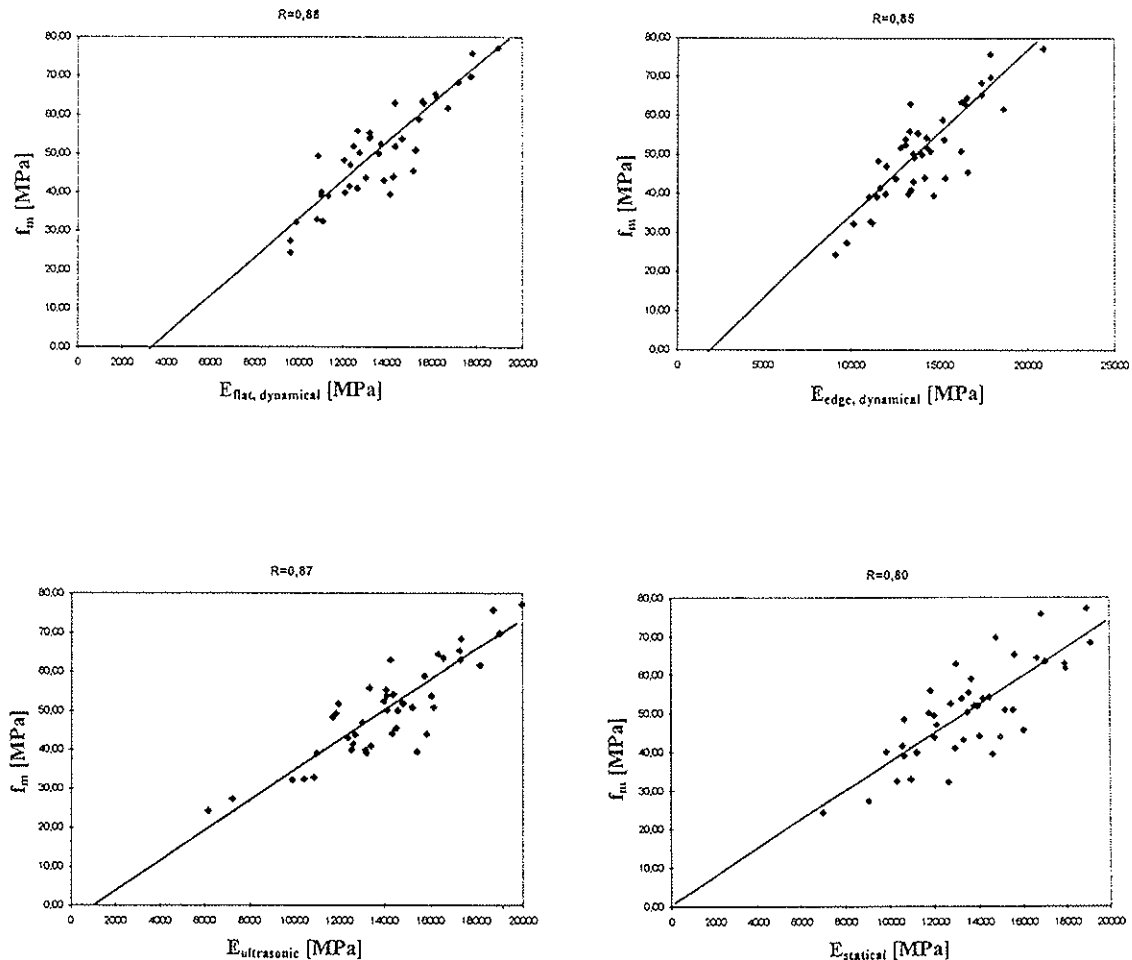


Fig.6.1 Results of experimental testing of structural timber

Another non-destructive method which we have recently applied in the analysis of a frame comes detail in the frame construction of a Prague sports hall, with a span of 50 m, was the photoelastic measuring method.

The structure of the frame consists of reinforced concrete columns to which laminated timber beams are connected with the help of anchors (Fig.6.2).

The modelling of the connection of the beam and the column of the respective frame has up to now been carried out with the application of the Finite Element Method (Fig.6.3) and and photoelastic measuring method (Fig.6.4).

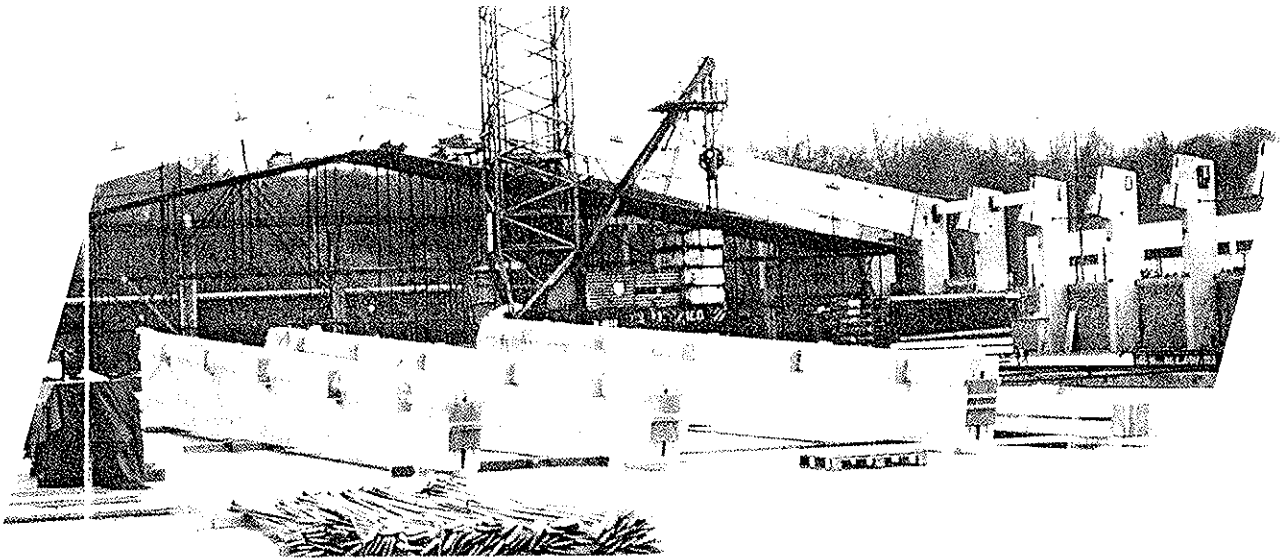


Fig.6.2 Frame structure of a Sports Hall

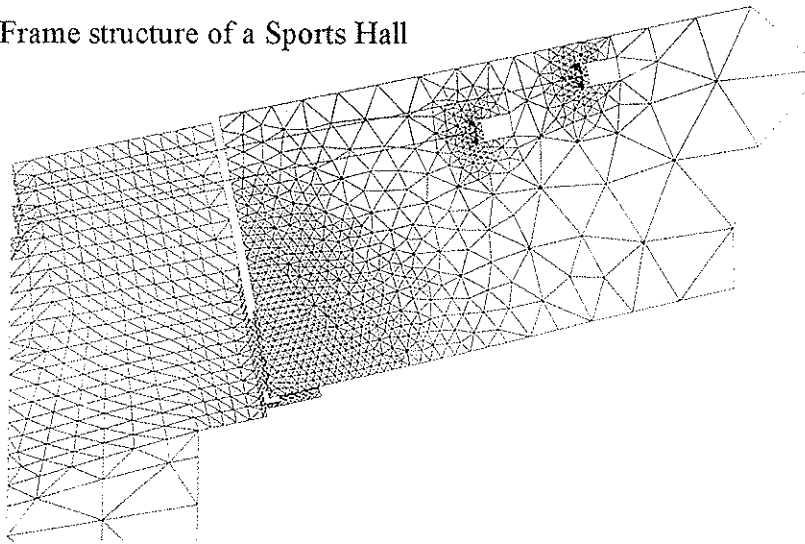


Fig.6.3 Detail of a frame investigated by means of the Finite Element Method



Fig.6.4 Detail of frame investigated by means of the photoelastic measuring method

7 References

Kuklík,P.,Mikeš,K.: Damage quantification of Wood based Thin-flanged Beams with the help of Modal Analysis, COST 508 Publication, pp. 237 - 255, ISBN 92-827-7187-3, Brussels 1996

INTERNATIONAL COUNCIL FOR BUILDING RESEARCH STUDIES AND DOCUMENTATION
WORKING COMMISSION W18 - TIMBER STRUCTURES

MEASUREMENT OF MODULUS OF ELASTICITY IN BENDING

by

L Boström
SP, Borås
Sweden

MEETING THIRTY

VANCOUVER

CANADA

AUGUST 1997

Measurement of modulus of elasticity in bending

Lars Boström
SP, Borås, Sweden

1 Introduction

When allocating timber to a strength class the characteristic values of bending strength, density and mean modulus of elasticity (MOE) parallel to the grain must be greater than or equal to the corresponding values in the European standard EN 338. The governing grade determining parameter varies depending on the grade combination to be graded. For Nordic spruce timber the bending strength is normally the property that controls the highest grade in a grade combination, while the MOE controls the intermediate and low grades, Chrestin and Boström (1997).

It is of great importance that the test methods used to determine these grade determining properties are consistent and give correct results. The test methods used today are given in European standard EN 408. Recent findings show that EN 408 does not give consistent results when used for determination of MOE in edgewise bending, see for example Boström et al. (1996) and Solli (1996). The guidelines, regarding the experimental set-up for measurement of edgewise MOE, given in EN 408 are not clear enough. Differences of 10% between two laboratories testing the same timber according to EN 408 have been reported.

One obvious problem is the very small deformations measured, leading to a high sensitivity of the experimental set-up. It has, for example, been shown by Boström et al. (1996) that the position of the measuring yoke has a great influence. Whether or not measurements are carried out on both sides can also have major effects, Solli (1996). The description of the experimental set-up and the test procedure in EN 408 is not accurate enough to give acceptable consistency in the experimental results.

In the present paper the EN 408 method is compared with a method in which the determination of MOE is based on the total deflection between the supports, and therefore includes a contribution from the shear deformations. The method is similar to the Australian standard AS/NZS 4063, but with one major difference, the worst strength reducing defect is centred within the middle third in the test, instead of being placed randomly. The method might have the advantage of being less sensitive to the experimental set-up and may therefore give more consistent results than EN408.

2 Test methods

The MOE was determined using two different methods, the method given in EN 408 and a method where the total deflection was measured. Figure 1 shows the experimental set-up. On the same beam the deformation was measured in two different ways: as given in EN 408 with yokes on both sides, placed in the neutral axis, and the mid-point deflection measured on the compression edge relative to the supports. The MOE determined according to EN 408 is denoted E_L (L as in local) and the MOE determined from the mid-point deflection is denoted E_G (G as in global).

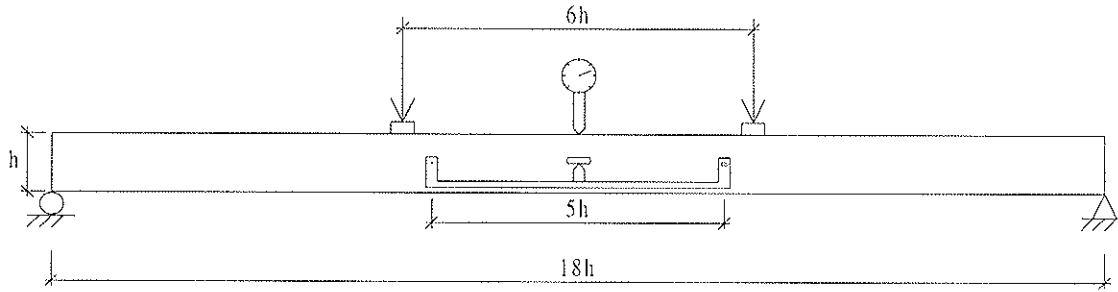


Figure 1. Experimental set-up.

3 Material

Two species, pine (*Pinus sylvestris*) and spruce (*Picea abies*), were included in the test program. Seven different sizes of spruce timber were tested, 34x70, 34x170, 45x70, 45x145, 45x190, 60x195, and 70x220 mm². Only one dimension of pine timber was studied, 45x140 mm². A total of 1672 pieces of timber were tested. Before testing the timber was kiln-dried and conditioned to a moisture content around $\omega=12\%$. The timber was planed on all four sides.

Table 1. Timber samples.

Sample	Species	Dimensions (mm ²)	Origin	Number of specimens
A	Spruce	34x70	Central Sweden	156
B	Spruce	34x170	Central Sweden	177
C	Spruce	45x70	Central Sweden	169
D	Spruce	45x145	Southern Sweden	201
E	Spruce	45x190	Central Sweden	177
F	Spruce	60x195	Southern Sweden	215
G	Spruce	70x220	Southern Sweden	222
H	Spruce	45x145	Southern Finland	152
I	Pine	45x140	Central Sweden	203

4 Experimental results

The mean MOE determined by the two methods for the different samples, and for all specimens, is presented in table 2. This level of the MOE is normal for Nordic grown spruce and pine.

A non-linear regression analysis was performed on each sample, and on the total population, and the results are presented in table 2. The results show that both the ratio between local and global MOE (E_L/E_G) and the coefficient of determination (R^2) increase with increasing size of the timber. The following may explain some of the differences between local and global MOE:

- The yoke length, over which the local MOE is measured, is based on the depth of the timber. For a short yoke length, i.e. small depth of the timber, influence of local defects, such as knots, is greater on the local MOE.
- The length used for measurement of global deflection is 3,6 times larger than for the local measurements. Thus local defects have a smaller influence on the results.

- When determining the global MOE, the measured deformation also includes shear deformations, leading to a lower value.
- The effects of the accuracy of the measurements.

Table 2. Mean MOE of the samples.

Sample	Dimension	Mean E_L	Mean E_G	\bar{E}_L/\bar{E}_G	$E_L = a \cdot E_G^b$		
					a	b	R^2
A	34x70	11990	12120	0,99	0,047	1,323	0,82
B	34x170	12530	11880	1,05	0,321	1,127	0,95
C	45x70	11840	11600	1,02	0,055	1,311	0,88
D	45x145	11500	11254	1,02	0,261	1,146	0,93
E	45x190	11900	11210	1,06	0,471	1,087	0,92
F	60x195	12510	11680	1,07	0,502	1,081	0,96
G	70x220	11380	10500	1,08	0,681	1,050	0,93
H	45x145	12040	11970	1,01	0,839	1,019	0,85
I	45x140	13280	12730	1,04	0,201	1,174	0,91
All	-	12240	11780	1,04	0,351	1,116	0,89

A non-linear regression analysis of all samples gave the following relation between local and global MOE and normalised timber dimensions;

$$E_L = 0,285 \cdot (h/150)^{0,047} \cdot (w/50)^{0,049} \cdot E_G^{1,139} \quad \text{Eq. (1)}$$

where h is the depth in mm and w is the width in mm. The coefficient of determination was $R^2=0,91$. The surface diagram presented in figure 2 show the level when the local and global MOE are equal. The diagram is based on eq. (1). Below the surface the local MOE is lower than the global MOE, and above the surface the local MOE is higher than the global MOE. The figure shows that for Nordic timber the local MOE is usually higher than the global MOE. Only for small sizes, and/or timber with low MOE, does the global MOE render higher values than the local MOE.

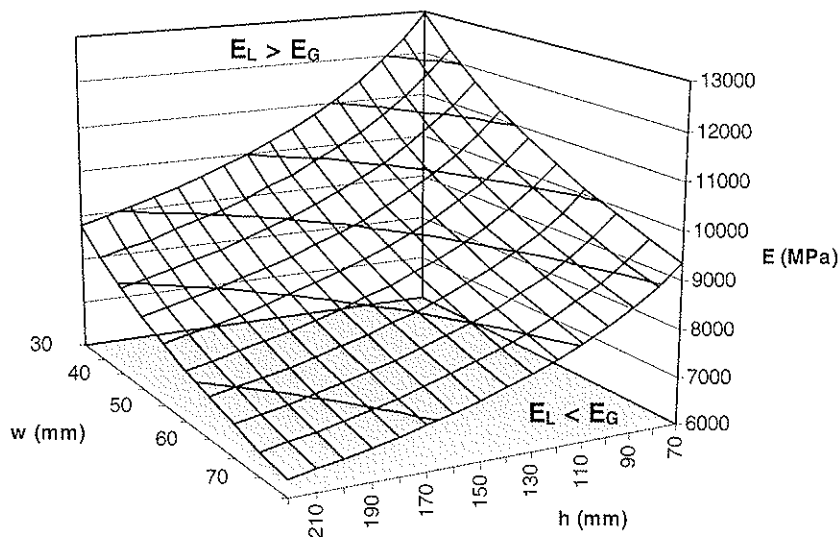


Figure 2. Diagram, based on eq. (1), showing when local and global MOE is equal for different timber sizes.

The surface plot given in figure 3, based on eq. (1), show how the ratio between the local and global MOE depends on the level of the global modulus of elasticity (timber quality) and the timber depth (the thickness was constant $w = 50$ mm). The ratio between local and global MOE increases with the timber quality and the timber depth. For high values of the MOE the local MOE is 15% higher than the global MOE, and for low values of the MOE the local MOE is 10% lower than the global MOE.

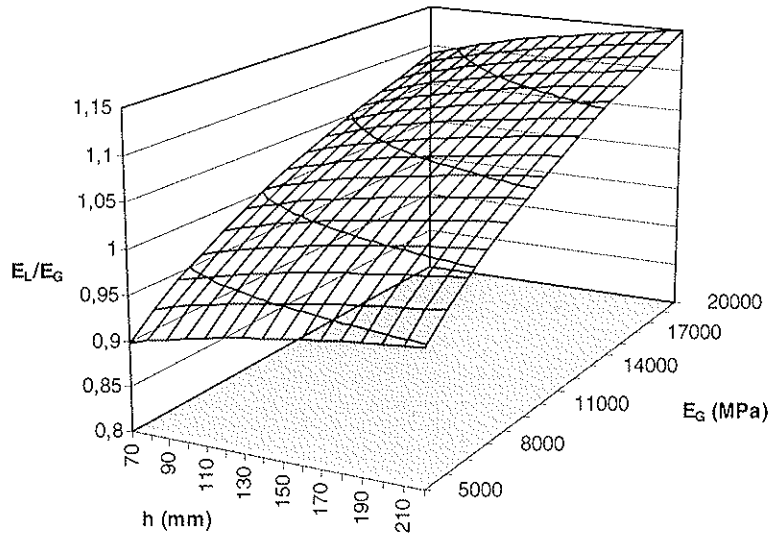


Figure 3. Diagram, based on eq. (1), showing the ratio between local and global MOE for different beam depths (constant thickness $w = 50$ mm).

The two methods for determination of MOE can be compared as regards correlation to bending strength. In table 3 the coefficient of determination, R^2 , of a linear regression relation between bending strength and MOE is shown. When measuring the local MOE the correlation to bending strength is better for small size timber, while for large size timber the global MOE give a better correlation.

Table 3. Coefficient of determination of the relation between bending strength and MOE for different timber sizes.

	34x70 Serie A	34x170 Serie B	45x70 Serie C	45x145 Serie D	45x190 Serie E	60x195 Serie F	70x220 Serie G	45x145 Serie H	45x140 Serie I
f_m-E_L	0,77	0,66	0,72	0,64	0,56	0,71	0,59	0,66	0,72
f_m-E_G	0,72	0,66	0,65	0,63	0,59	0,73	0,63	0,66	0,71

5 Discussion

The results obtained in the present study can be compared with the results obtained by Leicester and Young (1991) and Leicester et al. (1996) where small size timber, 35x90 mm, was examined. In the Leicester studies the global MOE, determined according to AS/NZS 4063, was higher than the local MOE determined according to EN 408. This could be explained by the small size timber where the effects of local defects are more pronounced when measuring the local MOE, and by the random location of the weakest point in the Australian standard when measuring the global MOE. Thus, the present results coincide well with the Leicester studies for small size timber. There is a size effect when

comparing local and global measurement of MOE. It is logical that the ratio between local and global MOE is low for small size timber because the effects of the defects are more pronounced on the measurement of local MOE.

The results show that the ratio between local and global MOE is low for timber with low MOE, i.e. timber with more defects. This effect was also found in the study by Leicester et al. (1996).

How well the MOE correlates to bending strength depends both on the method used for determining the MOE and the timber dimensions. For small size timber, the local MOE yields a better correlation, while for large size timber the correlation is better for the global MOE.

A method based on the measurement of the mid-point deflection instead of the existing method defined in EN 408 is preferable. There are, however, some drawbacks to this method. Owing to shear deformations, the MOE is underestimated. However, shear deformations are seldom taken into account in the design calculations. So including them in the MOE would be staying on the safe side.

When comparing the local and global measurements of MOE, there is a size effect. This size effect can be explained, at least to some extent, by the influence of local defects, which becomes more pronounced with smaller timber size.

Further testing would be needed in order to show whether the measurement of global deformations give a more consistent result than local measurements. A round-robin test in which different methods are tested at different laboratories would be preferable.

References

Boström L., Ormarsson S., Dahlblom O. (1996): On determination of modulus of elasticity in bending. CIB W18 meeting in Bordeaux, paper 29-10-3

Leicester R.H, Young F.G. (1991): Equivalence of characteristic values. CIB W18 meeting in Oxford, paper 24-17-2

Leicester R.H., Breitingner H.O., Fordham H.F. (1996): Equivalence of in-grade testing standards. CIB W18 meeting in Bordeaux, paper 29-6-2

Solli K. (1996): Determination of modulus of elasticity in bending according to EN408. CIB W18 meeting in Bordeaux, paper 29-10-2

INTERNATIONAL COUNCIL FOR BUILDING RESEARCH STUDIES AND DOCUMENTATION
WORKING COMMISSION W18 - TIMBER STRUCTURES

A WEAK ZONE MODEL FOR TIMBER IN BENDING

by

B Källsner

K Salmela

Swedish Institute for Wood Technology Research

Sweden

O Ditlevsen

Technical University of Denmark

Denmark

MEETING THIRTY

VANCOUVER

CANADA

AUGUST 1997

A weak zone model for timber in bending

B. Källsner¹, O. Ditlevsen², K. Salmela¹

¹Swedish Institute for Wood Technology Research

²Department of Structural Engineering and Materials
Technical University of Denmark

Summary

In order to verify a stochastic model for the variation of the bending strength within and between structural timber members, tests with long members subjected to constant bending moment have been performed. The span with constant moment contained between five and nine weak zones, i.e. zones with a cluster of knots. In a previous investigation test specimens, each containing one weak zone, have been tested in bending separately. Based on these tests a hierarchical model with two levels was formulated.

The test results show that the bending strength of the long timber members on the average is 5 to 15% lower than is predicted by the proposed hierarchical model. Energy considerations show that the reduction in strength of long beams may not be solely a statistical effect caused by an increased number of possible failure modes in the long beams as compared to the short test specimens. The large elastic energy released in a long highly bent beam at the onset of failure may mean that a later higher external load level cannot be realised as in a controlled slowly progressing failure.

It should be reflected in the codes that the elastic energy plays a role with respect to the size effect. Therefore, if the hierarchical model is codified, information should be given both on the largest load-carrying capacity of a weak zone, and on the capacity at the first occurring weakening of the zone.

1 Background

Compared to other structural materials, timber is characterised by a rather large variation of the strength properties. The grading of structural timber in Europe is usually based on the so called "grade determining defect" i.e. the defect which is believed to give the lowest strength. In traditional design of structural timber in bending, it is assumed that the load-carrying capacity is equal to the strength of this weakest part all over the length. A more accurate design based on a probabilistic method makes it possible to take advantage of the timber having higher strength in other parts. In order to do so, it is necessary to know the strength variation both within and between the timber members.

It is reasonable to assume that the variation of the bending strength within structural timber members to a large extent is connected to the occurrence of knots along the members. Structural timber in Sweden is produced from spruce (*Picea Abies*) and pine (*Pinus Silvestris*). In both species the branches grow in a rather regular pattern characterised by the branches forming whorls along the stem. Between these groups of branches, singular smaller branches exist, but these knots do not affect strength significantly.

It is complicated to determine the bending strength of all weak zones within a timber member experimentally since bending failure is often accompanied by fissures propagating along the member. Consequently it is difficult to obtain separate bending failures of sections close to each other without any mutual influence on the load-carrying capacity by the adjacent weak zones. There seem to be very few investigations where direct measurements have been carried out of the bending strength of weak zones along timber members.

Källsner and Ditlevsen (1994) presented a test method where the finger joint technique was used. In order to model the variation of the bending strength, a hierarchical model with two levels was used, see chapter 4. The experimental data were reasonably well represented by the formulated model. In order to further examine the validity of the model, the strength of long timber members subjected to a constant bending moment is investigated in a second phase of that project (Källsner, Ditlevsen and Salmela, 1997). The evaluation of these test results has not yet been finalised. A more detailed report will be published as a master thesis by Salmela (1997).

2 Objective

The purpose of this paper is to give a brief overview of the project and to present the most important results so far obtained and to compare the results with results obtained from other investigations.

3 Experimental investigation

3.1 Selection of timber

In order to obtain a test material with not too high a variation of the mechanical properties which could arise from different growth conditions, the timber was selected from a limited area of about 10 000 m². The intention is, in later phases of the project, to sample timber from other regions in order to see if the proposed model needs some modification with respect to different growth conditions. Only spruce was cut, and the trees were randomly taken from the area. One selection criterion, however, was that at least two logs, 4800 mm long, could be cut from each tree, and that at least two timber members could be sawn from each log. Another criterion was that logs with rot were excluded. All logs were sawn through the pith. After drying in a chamber kiln, the timber members were planed to their final dimension 45 mm x 120 mm. The total number of members was more than 500. Prior to testing all timber members were conditioned in a climate of 20 °C and 65 % relative humidity.

During the first two phases of the project only the two central twin members sawn from the second log (number 2 from the ground level) and closest to the pith were selected. In order to study the influence of the knot cluster frequency on the bending strength, all planks were grouped with respect to the number of weak zones. The number of weak zones was determined with all timber members belonging to the same log placed next to each other. This meant that a weak zone in one of the timber members always had a corresponding weak zone in the twin member. Consequently it often happened that, in a specific weak zone, there was only small knots or grain deviations while the corresponding weak zone of the twin member contained big knots. It must be pointed out that it was sometimes difficult to judge whether there was a weak zone or not, especially in the case of slow-grown timber with short distances between the knot whirls.

3.2 Method and scope

The main idea during the first phase of the project was to determine the bending strength of the timber at each weak zone (cluster of knots) separately. For that reason the timber members were cut into pieces, each of them containing one knot cluster. Each of these pieces were then finger jointed together with pieces of timber without defects, thus forming a specimen containing only one weak zone in the centre, see Figure 1. By this procedure the test specimens could be tested in the normal way. As has already been mentioned the timber members were grouped with reference to the number of weak zones within each member. The intention was to achieve about the same number of strength values in each group. Thus more timber members were taken from the groups with a few number of weak zones. The members were selected randomly from each group. The total number of timber members selected for the tests was 26.

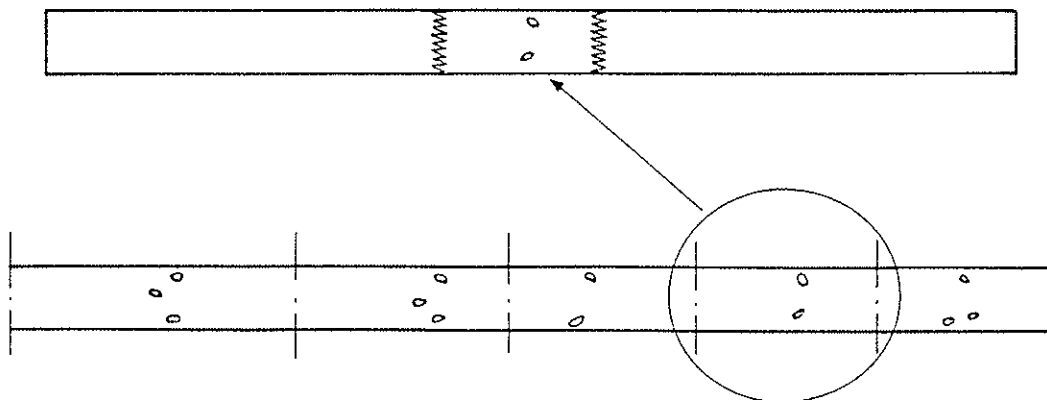


Figure 1 Example of how a timber member was cut into pieces and finger jointed with pieces of timber of high strength at the ends.

The purpose of the second phase of the project was to investigate if the hierarchical model of the bending strength variation, developed during the first phase, could be used to determine the strength of long timber members subjected to a constant bending moment. For that reason tests with long timber members containing many weak zones were performed. The bending tests with long timber members consisted of two series of specimens:

Test series 1 comprised the twin members of the 26 ones which were tested during phase 1 when the bending strength of each weak zone was determined separately.

Test series 2 comprised 14 pairs of twin members, each pair being sawn from each side of the pith.

3.3 Material parameters

A number of material parameters were measured. The most important ones were: The moduli of elasticity in edgewise and flatwise bending, knots, position of pith, annual ring width, density and moisture content.

3.4 Test equipment and test procedure

During phase 1 of the project, when each weak zone was tested separately (Figure 2), the test procedure given in the standard ISO 8375 was followed. Denoting the depth of the timber member by h , the distance subjected to constant bending moment was $6h$ and the total span was equal to $18h$. All the test specimens cut from the same timber member were tested with the same edge in tension. The tension side was chosen at random.

During phase 2 the test arrangements had to be modified according to Figure 3. The total span was increased from 18 h to 36 h, and the span with constant moment was increased from 6 h to 30 h. To prevent lateral buckling, the test specimens were braced at the third points. Due to the long span of the test specimens, the influence of large displacements had to be taken into account by correcting the measured bending moments. Each timber member belonging to test series 1 was tested with the same edge in tension as the corresponding twin member of phase 1. For the timber members belonging to test series 2, each pair was tested with the same edge in tension. The tension side for each pair was chosen randomly.

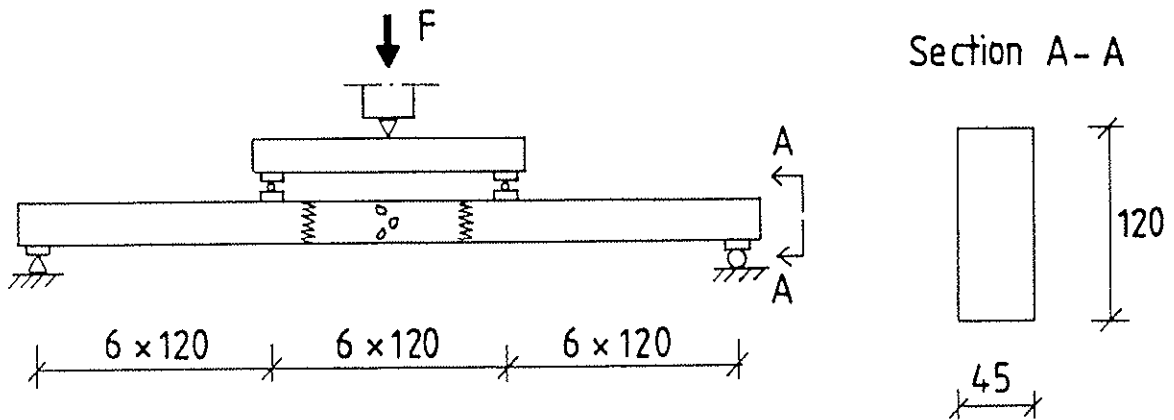


Figure 2 Principal test arrangement when one weak zone was tested at a time. All sizes in mm.

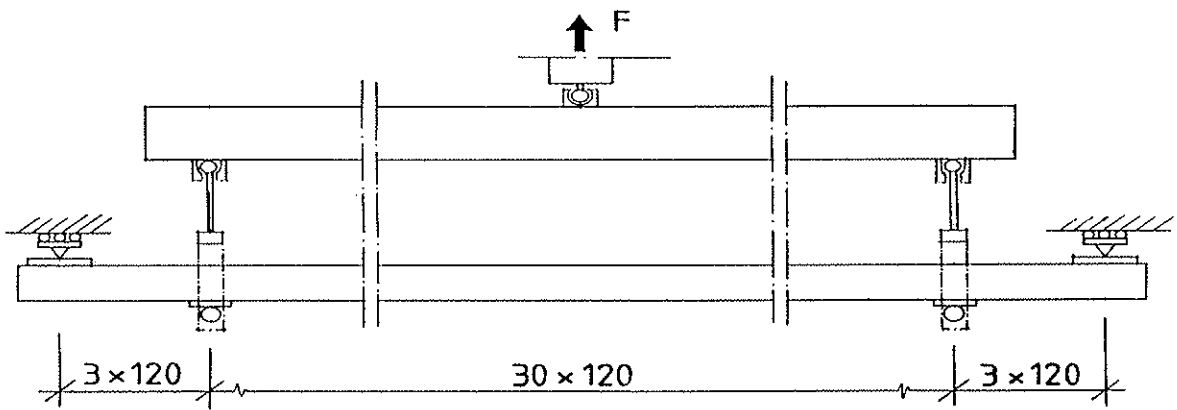


Figure 3 Principal test arrangement when timber members containing many weak zones were tested. All sizes in mm.

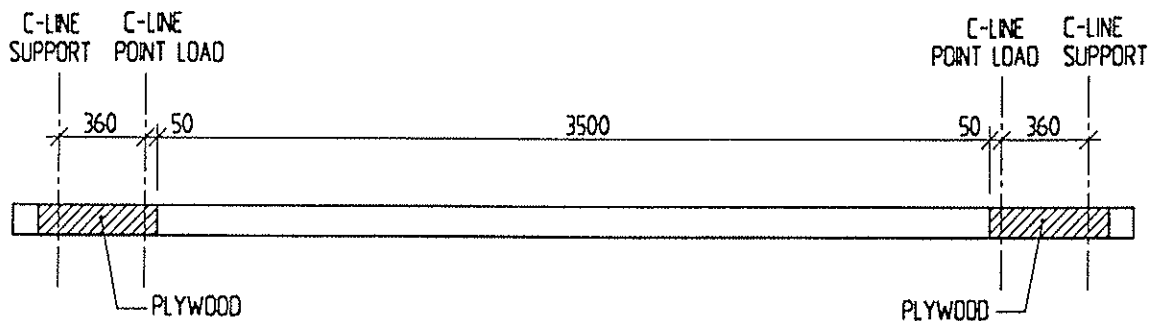


Figure 4 Test specimen reinforced with plywood. All sizes in mm.

To prevent failure in the zone between the supports and the point loads, all test specimens of phase 2 were reinforced with plywood at the ends according to Figure 4. The plywood was placed such that the distance between the edge of the plywood and the first weak zone in the centre span should be the same at both ends.

In both phase 1 and phase 2, the load was applied at a constant rate of displacement.

4 Probabilistic modelling

This chapter gives a brief description of the model used by Källsner and Ditlevsen (1994).

This is the simplest type of probabilistic model for describing equicorrelation between the bending strength values of the weak zones within the same timber member.

4.1 Hierarchical probabilistic model of weak cross-section strengths

In connection with the description of the models, a weak zone is idealised to be concentrated as a point. Thus the terminology "weak zone" is replaced by "weak cross-section".

Reported results show indications of equicorrelation (i.e., a constant correlation independent of separation) between the bending strengths of the weak cross-sections within the same beam, Riberholt and Madsen (1979), Williamson (1994), Isaksson (1996). The simplest type of probabilistic model with this property is the so-called hierarchical model with two levels. This model is as follows.

For a given beam with k identified weak cross-sections, it is assumed that the bending strengths of the k cross-sections are

$$X + Y_1, \dots, X + Y_k \quad (1)$$

where Y_1, \dots, Y_k are mutually independent random variables of zero mean and standard deviation σ_Y . The variable X is a random variable over the population of beams. If the variables Y_1, \dots, Y_k are assumed to be independent of X , the variance of the bending strength of a weak cross-section is

$$\text{Var}[X + Y_i] = \text{Var}[X] + \text{Var}[Y_i] = \sigma_X^2 + \sigma_Y^2 \quad (2)$$

The covariance between the strengths of two weak cross-sections in the same beam is

$$\text{Cov}[X + Y_i, X + Y_j] = \text{Var}[X] = \sigma_X^2 \quad (3)$$

such that the correlation coefficient becomes

$$\rho[X + Y_i, X + Y_j] = \frac{\sigma_X^2}{\sigma_X^2 + \sigma_Y^2} \quad (4)$$

Thus the correlation coefficient is independent of i and j for $i \neq j \leq k$, that is, the correlation is independent of the distance between the two weak cross-sections. Moreover, if it is assumed that the distributions of X and Y are independent of $k \geq 1$, it follows that the model is an equicorrelation model.

4.2 Probabilistic model for beam subjected to constant moment

The physical model for the beam strength is based on the assumption that failure can occur only at a finite number of weak cross-sections along the beam. The bending strength S of a beam subjected to a constant bending moment along the entire length and containing $k > 0$ weak cross-sections can be described by the random variable

$$S = X + \min\{Y_1, \dots, Y_k\} \quad (5)$$

where X and Y are defined as in the previous section. Assuming that X, Y_1, \dots, Y_k all have normal distributions (not a crucial assumption) it follows that the distribution function of the bending strength S is

$$F_S(z|k) = P(X + \min\{Y_1, \dots, Y_k\} \leq z) = \frac{1}{\sigma_X} \int_{-\infty}^{\infty} \left[1 - \Phi\left(-\frac{z-x}{\sigma_Y}\right)^k \right] \varphi\left(\frac{x-\mu_X}{\sigma_X}\right) dx \quad (6)$$

where $\varphi(\cdot)$ is the standardised normal density function, $\Phi(\cdot)$ is the standardised normal distribution function and μ_X is the mean of X . Since $F_S(z|0) = 0$ this formula is also valid for $k = 0$. Assuming that K is a random variable with $k \in \{0, 1, 2, \dots\}$ as outcome with probability p_k , the distribution function of S becomes

$$F_S(z) = \sum_{k=0}^{\infty} F_S(z|k) p_k = 1 - \frac{1}{\sigma_X} \int_{-\infty}^{\infty} E\left[\Phi\left(\frac{x-z}{\sigma_Y}\right)^K\right] \varphi\left(\frac{x-\mu_X}{\sigma_X}\right) dx \quad (7)$$

in which the expectation

$$E\left[\Phi\left(\frac{x-z}{\sigma_Y}\right)^K\right] = \sum_{k=0}^{\infty} \Phi\left(\frac{x-z}{\sigma_Y}\right)^k p_k \quad (8)$$

can be expressed by the so-called probability generating function $\psi(x) = E[x^K]$ of the integer random variable K .

5 Results and analysis

Three main types of failure modes were identified during the tests in phase I, namely:

- B Bending failure in the centre part between the finger joints
- F Failure in one of the finger joints
- S Failure in one of the end parts outside the finger joints

A combined type of failure mode BF could also be observed which normally started as a fissure in the vicinity of a knot and propagated to one of the finger joints where it caused a failure in the finger joint.

The test results obtained in phase I indicate that there exists an equicorrelation between the bending strength values of the weak zones within the same piece of structural timber. The simplest type of probabilistic model with this property is the hierarchical model

with two levels. Due to failure in the finger joints in a great number of the tests the hierarchical model had to be extended in the evaluation of the results (Källsner and Ditlevsen, 1994). The experimental data were reasonably well described by this extended model. By assuming that the failure modes B and BF were true bending failures, the following estimates of the parameters were obtained:

$$\begin{aligned}\mu_x &= 49.77 \text{ N/mm}^2 \\ \sigma_x &= 7.03 \text{ N/mm}^2 \\ \sigma_y &= 6.33 \text{ N/mm}^2 \\ \rho &= 0.55\end{aligned}$$

Two main types of failure modes, tensile and compression failure, were observed during the testing of the long-span timber members in phase 2. Only in a few cases were permanent deformations caused by excessive compressive stresses observed before the test specimens collapsed. The final failures developed very fast. They often started with a fissure propagating from one weak zone (e.g. a knot on the tensile side of the specimen) to an adjacent weak zone where the timber member was broken. This first failure was often followed by secondary failures in the weak zones closest to the point loads. Consequently the test specimens were often broken into three or even four pieces.

For a beam subjected to constant moment along the entire length and containing $k > 0$ weak zones, the distribution function of the bending strength $F_s^*(z | k)$ is given by equation (6). By using the bending strength values from phase 1 of the project, the curves in Figure 5 are obtained. It is obvious that the bending strength decreases with an increased number of weak sections.

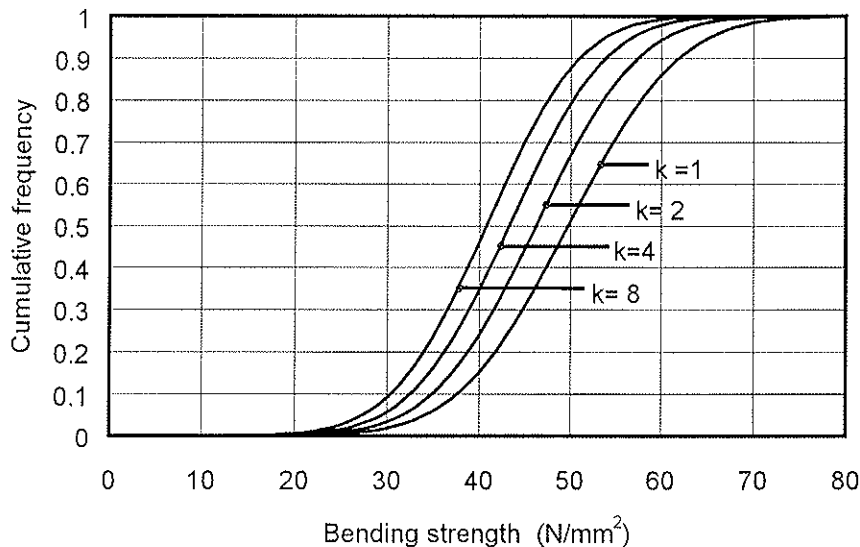


Figure 5 Distribution function for bending of timber members under constant bending moment and k weak zones.

Since test series 1 and 2 consist of timber members with different number of weak zones within the test span, it is better to compare the test results with a weighted distribution function $F_s^*(z)$ according to equation (7). In Figure 6 and Figure 7 the bending strength values obtained from test series 1 and 2 are plotted together with the weighted distribution functions (the curves to the left). The weighted distribution functions for test series 1 and 2 are almost identical, and they are also very close to the distribution function

$F_s(z | k)$ corresponding to 6 weak cross-sections. The curves to the right in the figures show the distribution function $F_s(z | k)$ according to equation (6) with $k = 1$, i.e. with one weak zone in the span subjected to constant moment.

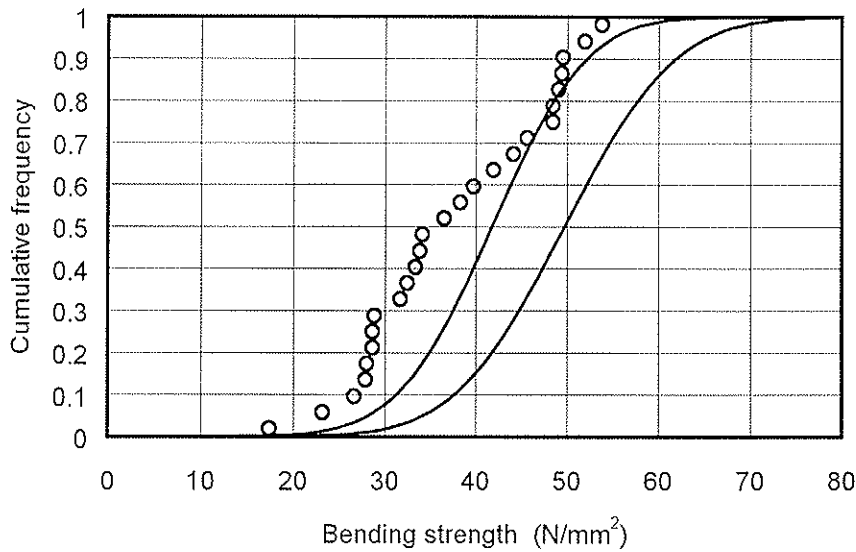


Figure 6 Empirical distribution function for the bending strength data of test series 1 plotted together with the estimated distribution function (7) obtained from the hierarchical model (left curve). The curve to the right shows the estimated distribution function (6) for one weak zone.

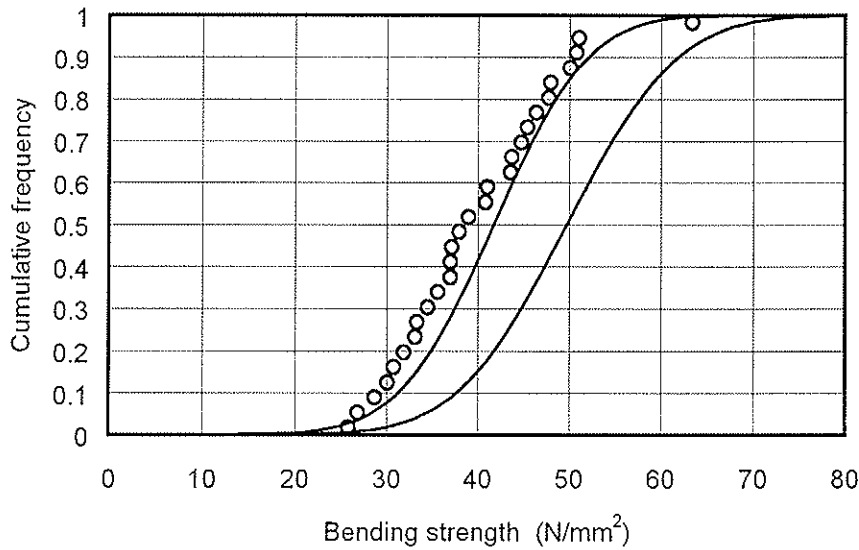


Figure 7 Empirical distribution function for the bending strength data of test series 2 plotted together with the estimated distribution function (7) obtained from the hierarchical model (left curve). The curve to the right shows the estimated distribution function (6) for one weak zone.

The plots show that the empirical distribution functions are shifted further to the left of the predicted distribution function than can be explained solely by referring to the statistical uncertainty related to the small sample size. It is also seen that the deviation to the left is largest for test series 1, where the test specimens are twins of the ones tested during phase 1. However, the difference between the positions of the two empirical distribution

functions cannot be excluded to be a result of statistical uncertainty combined with the fact that the predicted distribution functions also are affected by statistical uncertainty.

In part the general shift to the left relative to the predicted distribution functions can be explained as follows. During phase 1, where only one weak zone was tested at a time, two main types of failures were observed. These were bending failure in the weak zone and failure in the finger joint. The bending failures always took place or started at the weak zone in the test specimen. One type of failure that could be observed was when a fissure propagated from a knot on the tension side of the weak zone. Sometimes this fissure led to an immediate collapse at the weak zone and sometimes the fissure stopped propagating and the load could be further increased. Since there were no adjacent weak zones in the test specimens, there was no influence from fissures that started from other weak zones propagating to the weak zone tested. It is obvious that this kind of fissures would have led to lower strength values and that such failure types may be possible in long beams.

The reason for the shift to the left may also partly be that the long timber members tested during phase 2 of the project contained more elastic energy than the standard beams tested during phase 1. As argued in (Källsner, Ditlevsen and Salmela, 1997), it can be assumed that the large elastic energy stored in a long highly bent beam before the onset of failure causes the failure to progress to total failure directly at the first decrease of the load. At least partly, the shift to the left is then explainable by the external force variation measured during the deformation controlled bending test. During the slowly progressing failure the external force is observed to vary upwards and downwards with its largest global value not necessarily coinciding with the first occurring local maximal value. The appearance of a shift to the left is then a consequence of the applied definition of the load-carrying capacity as being the globally largest value of the measured load during the test.

It is seen that there is a tendency to a better fit between measured and theoretical values in the upper strength range than in the lower and medium ranges. This indicates that during the process of controlled slowly progressing failure, as observed in the experiments of phase 1, there are larger differences between the first observed local maximum of the external load and the global maximum of all the following local maxima for the low strength timber than for the high strength timber. For the high strength timber this confirms the expectation that the first local maximum of the load is also the global maximum. Such timber has only small knots on the tension side. The failure may start as a compression failure but the final failure is usually a tension failure. This type of failure develops as a total collapse of the timber and the external load cannot be increased further. Thus it makes no difference whether it is a short or a long beam. Moreover, the empirical distribution function in Figure 6 shows a decrease of the slope (that is, the probability density) in the medium range. This indicates that the carrying capacity distribution may be bimodal. Such bimodality can be caused by some separation of the carrying capacity distribution of the compression failure mode from the lower placed carrying capacity distribution corresponding to the tension failure mode. The same bimodality tendency is not seen in the data of series 2 plotted in Figure 7.

6 Comparison with other investigations

6.1 Size effect

From tests of structural timber in bending it is well-known that the strength of members decreases with increasing span and that the strength depends on the load configuration. This behaviour of the structural timber is often described as a "size effect". See for example

Madsen (1992) and Barrett and Fewell (1990). A major contribution to the basic theory for analysing of this phenomenon was developed by Weibull (1939a,b). The two basic assumptions of this "weakest link theory" are that the material is perfectly brittle and that the strength variation is locally homogeneous with appearance like white noise, that is, with statistical independence of the strengths of any set of non-coinciding cross-sections. Thus the Weibull theory does not take account of the existence of at most a finite random number of weak cross-sections and the possible observation of their positions along the beam. Nor does it take the strength correlation (equi-correlation, according to the two-level hierarchical model) along the beam into account.

The size factor found in different investigations varies considerably. Rouger and Fewell (1994) demonstrate that the "size effect" could be significantly influenced by the sawing pattern and by the grading method. For a beam in bending tested at constant depth but with different lengths L , the size effect is often expressed by an exponent S_L which is calculated from the relation

$$\frac{f_m}{f_{m,ref}} = \left(\frac{L_{ref}}{L} \right)^{S_L} \quad (9)$$

where f_m is the bending strength and where the subscript "ref" refers to a reference length of the beam. Madsen (1992) reports that the exponent S_L at the 50th percentile is in average equal to 0.18.

To be able to compare this value of S_L with the results presented in this paper, it seems reasonable to modify equation (9) so that the length L is replaced by the number of weak zones k , i.e.:

$$\frac{f_m}{f_{m,ref}} = \left(\frac{k_{ref}}{k} \right)^{S_L} \quad (10)$$

By considering the bending strength of one weak zone as the reference level, it is obvious that $k_{ref} = 1$ and $f_{m,ref} = 49.77 \text{ N/mm}^2$. If the 50th percentile of the empirical distribution function for the bending strength data of test series 1 and 2 are put into equation (10) assuming 6 weak zones (which is very close to the mean value), the exponent S_L obtains the values given in Table 1. These values are close to the value 0.18 reported by Madsen (1992). It is of special interest to compare these values with values obtained by the hierarchical model. Assuming 6 weak zones gives $S_L = 0.097$. This value will come out

Test series	$f_m \text{ N/mm}^2$	S_L
1	35.27	0.192
2	38.44	0.144

Table 1 Exponent S_L for test series 1 and 2.

larger when taking into account that the release of elastic energy may trigger the total failure during the period of damage development before reaching the maximal static carrying capacity of the weakest of the single weak zones of the beam. According to this the

strength reduction by length may possibly still be solely a statistical effect. Further analysis of the data including the measured force-deflection curves will reveal whether this conjecture can be confirmed.

6.2 The Lund investigation

Isaksson (1996) has presented results of an investigation similar to the one reported in this paper. Specially designed equipment for clamping of the structural timber when being tested in bending was used. The timber was sampled at a sawmill. The nominal dimension of the timber was 45 mm x 145 mm. For a timber length of 5.1 m it was possible to test 4-7 weak zones depending on how the distances between the zones were distributed.

The mean bending strength of the weak zones was estimated to 57.4 N/mm² i.e. considerably higher than in the investigation reported in this paper (49.8 N/mm²). The standard deviation of the bending strength was estimated to 13.4 N/mm² compared to 9.5 N/mm² reported here. The higher standard deviation found by Isaksson is probably an effect of a higher σ_x i.e. variation between the timber members. The reason for this may be a consequence of the sampling. The timber was probably taken from a larger area than the timber reported here.

In a simulation based on the test data from the separate timber members, Isaksson obtains $S_x = 0.106$ at the 50th percentile. This value is very close to the value 0.097 found by the hierarchical model and may indicate that the strength variation within the members is of the same magnitude as reported in this paper.

7 Conclusions

Tests with long timber members subjected to constant bending moment indicate that the bending strength is 5 to 15% lower than was predicted by the proposed hierarchical model.

It should be noted that there is a fundamental difference between the Weibull modelling and the discrete weak zone modelling. According to the Weibull model the number of weak zones is infinite, which for small timber members and members with peak moments means that the timber in the design is not fully utilised.

There are indications that in order to use the statistical information from single weak zone bending strength testing to predict the bending strength distribution for long beams, the release of stored elastic energy should be taken into consideration. It should therefore be reflected in the codes that the elastic energy plays a role with respect to the size effect. Therefore, if the hierarchical model is codified, information should be given both on the largest load-carrying capacity of a weak zone, and on the capacity at the first occurring weakening of the zone.

The test results are still subject to analysis, and the conclusions of this paper are therefore preliminary.

Acknowledgements

The project has been funded by the Swedish saw milling industry and the Swedish National Board for Industrial and Technical Development.

References

- Barrett J.D.; Fewell A.R. (1990): Size factors for the bending and tension strength of structural timber. Proc of the CIB-W18 Meeting, Lisbon, Portugal, Paper 23-10-3.
- Isaksson, T. (1996): Variability of bending strength within timber elements. Licentiate thesis at Department of Structural Engineering, Lund Institute of Technology, Sweden.
- Källsner, B.; Ditlevsen, O. (1994): Lengthwise bending strength variation of structural timber. Paper presented at the IUFRO/ S5.02 Meeting, Sydney, Australia.
- Källsner, B.; Ditlevsen, O.; Salmela, K. (1997): Experimental verification of a weak zone model for timber in bending. Paper presented at the IUFRO/ S5.02 Meeting, Copenhagen, Denmark.
- Madsen B. (1992): Structural behaviour of timber. Timber Engineering Ltd., North Vancouver BC, Canada.
- Riberholt, H.; Madsen, P. H. (1979): Strength distribution of timber structures, measured variation of the cross sectional strength of structural timber. Structural Research Laboratory, Technical University of Denmark, Report No. R 114.
- Rouger F.; Fewell T. (1994): Size effects in timber. Novelty never ends. Proc. of the CIB-W18 Meeting, Sydney, Australia, Paper 27-06-2.
- Salmela, K. (1997): Bending strength of timber in long-span testing (in Swedish). Master thesis at Building Materials, Department of Buildings and Building Services, Royal Institute of Technology, Stockholm, Sweden (under preparation).
- Weibull W. (1939a): A statistical theory of the strength of materials. Royal Swedish Institute for Engineering Research, Proceedings, No. 141, p. 45.
- Weibull W. (1939b): The phenomenon of rupture in solids. Royal Swedish Institute for Engineering Research, Proceedings, No. 153, p. 55.
- Williamson J.A. (1994): Statistical dependence of timber strength. Paper presented at the IUFRO/ S5.02 Meeting, Sydney, Australia.

INTERNATIONAL COUNCIL FOR BUILDING RESEARCH STUDIES AND DOCUMENTATION

WORKING COMMISSION W18 - TIMBER STRUCTURES

**LOAD CARRYING CAPACITY OF TIMBER BEAMS
WITH NARROW MOMENT PEAKS**

by

T Isaksson

Department of Structural Engineering

Lund University

Sweden

J Freysoldt

Department of Wood Science and Technology

University of Hamburg

Germany

MEETING THIRTY

VANCOUVER

CANADA

AUGUST 1997

Load Carrying Capacity of Timber Beams with Narrow Moment Peaks

Tord Isaksson

*M.Sc., Department of Structural Engineering,
Lund University, Box 118, S - 221 00 Lund, Sweden.*

Julia Freysoldt

*Student, Department of Wood Science and Technology
University of Hamburg, D - 21027 Hamburg, Germany*

1 Abstract

Timber exhibits quite a strong variability of properties within elements. The current design guidelines for timber structures only to a limited extent account for this variability. In a previous CIB-W18 paper (28-6-4) results from testing of several weak sections within an element were presented. This paper adds information about the strength between the weak section, i.e. strength of "defect" free wood. A sample of 150 boards of Norway spruce were subjected to a point load over a relatively short span with the intention of trying to reproduce the conditions at an inner support of a continuous beam. Both the weakest section, according to the Cook-Bolinder machine grader, and a strong section were tested in the same board. The results show that the difference between a "defect" free sections and weak sections is smaller than may be expected. The mean difference between these sections is 6.44 MPa. In 39 out of 149 successfully tested boards what was believed to be the weak section actually proved to be stronger than the selected "defect" free section.

2 Introduction

A special characteristic for timber, compared to other structural materials, is the strong variability of properties within elements, resulting in for example a length and load dependent load carrying capacity. This is to a limited extent accounted for by correction factors in the codes. As an example, the bending strength at moment peaks in a trussed rafter may be increased by a factor k_m . In order to be able to take these effects into account in a rational way, more information about the within member variability of material properties is needed.

In a previous CIB-W18 paper (28-6-4) the results from testing of several weak sections within an element were presented. Those results were fairly sufficient and adequate when studying single span beams without too narrow moment peaks. The assumption was that the boards could only fail in one of the tested sections within each board.

This is of course a too rudimentary model of the bending strength distribution within a board if the intention is to study beams with narrow moment peaks. Such moment peaks exist for example in the upper cord in a trussed rafter. In order to improve the model and enable studies of continuous beams and beams with narrow moment peaks complementary tests of the bending strength capacity under a point load over a relatively short span has been performed.

Within the same board both the weakest section, according to the Cook-Bolinder machine stress grader, and the section with as defect free wood as possible were tested. The

reason for testing both is to make the results comparable to the previous tests of weak sections where the strength of the weakest section according to the Cook-Bolinder also is represented. The thought is to use the Cook-Bolinder reading as the parameter to link together the different tests.

The set-up for testing a board under a narrow moment peak will be a single point load at mid span of a simply supported board. A compromise between having too large crushing of the wood under the point load and not increase the span too much and thus reducing the moment peak was found by testing a couple of different combinations.

In a CIB paper (CIB-W18A/22-14-1) Riberholt introduces a correction factor k_m aimed to increase the characteristic bending strength at moment peaks in the upper cord in a trussed rafter. The correction factor $k_{m,p}$ depends on the Coefficient of Variation, C.V, and is for a continuous beam given as:

$$k_{m,p} = \begin{cases} 1 + 0.4 \frac{C.V}{30\%} & \text{for } C.V \leq 30\% \\ 1.4 & \text{for } C.V > 30\% \end{cases}$$

3 Material and Methods

The test material consists of 154 boards with a cross section of 45 by 145 mm². The boards, with a length of 4.2 m, are kiln dried and planed. This length was chosen so that it would be possible to test two sections within each board. The material is taken from the same sawmill as in the previous investigation (Isaksson 1996) and the raw material is Norway spruce (*picea abies*) grown in southern Sweden. It was important to have as similar properties in the material as possible, making the two investigations comparable. The exact location of the stands is not known.

After sawing and drying, the boards are graded according to appearance. Pieces with excessive wane, twist, crook and bow are not included in the test sample. The material contains timber with quality o/s, V:th and the better part of VI:th according to the Swedish grading rules for sawn timber, Anon (1982). The test sample is believed to be fairly representative for structural timber produced in southern Sweden.

Before testing, the boards are graded using the Cook-Bolinder machine stress grader at the Swedish National Testing and Research Institute (SP) in Borås. The same settings and speed of the machine were used as in the previous investigation. In addition, the location and size of knots were recorded within a length of 1 m at the selected test section, using the same principles as in Isaksson (1996).

Prior to testing, the boards are stored in a climate of 16-20°C and a relative humidity of 60 to 65 % (MC≈ 12 %).

How well this new sample corresponds to the previous in material properties can be viewed in *figure 1* and *table 1*. In *figure 1* the distribution of the lowest Cook-Bolinder reading within the boards for the three samples are compared. The last sample (D) seems to have a somewhat higher strength level, at least according to the Cook-Bolinder. The density and ring width on the other hand indicates a somewhat weaker material in this study, *table 1*. Note that the bending strength presented in *table 1* is determined using two different test set-ups. Following the weakest link theory the same board would have a higher strength if loaded with a single point load instead of two point loads at the third points, that is the mean strength in this study is even lower if it was to be corrected. On the other hand the short span and the single point load may cause damage to the board and thus reduce the strength.

The outcome of the grading is that 128 boards ends up in the grade T30, 19 in T24, 2 in T18 and finally one is T12. In other words, this ungraded sample has a characteristic strength of 27.5 MPa, according to the testing of the Cook-Bolinder section.

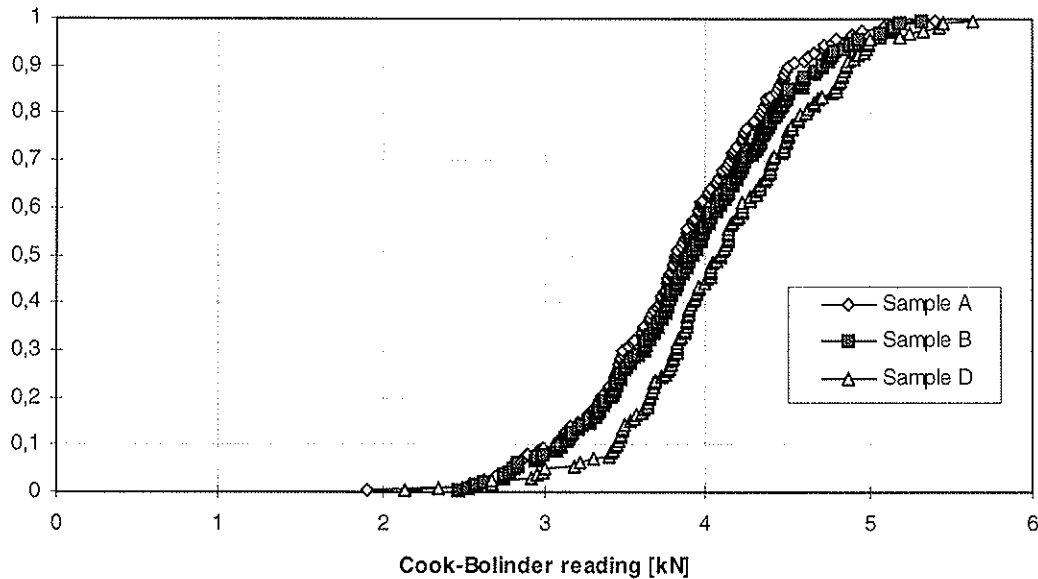


Figure 1. Distribution of lowest Cook-Bolinder reading within each board for the three samples, D being the one presented in this paper.

Table 1. A comparison between this study and the investigation in Isaksson (1996)

	$\rho_{12,12}$ (kg/m ³)		Ring width (mm)		Bending strength (MPa)	
	Mean	Std	Mean	Std	Mean	Std
This study	438	40	2.86	0.89	52.0*	12.2*
Isaksson (1996)	470	50	2.5	0.90	54.7	13.7

*) This is the results from a one point bending test, and not the ISO8375.

3.1 Selecting test section

The procedure for selecting the test sections is as follows. First, the section with the lowest Cook-Bolinder reading is selected. If this section is impossible to test with respect to the restrictions of the set-up (section being too close to the end of the board), the section with the next lowest reading is chosen. Thereafter a section with as defect free wood as possible is selected.

3.2 Test set-up

The idea with this investigation was to achieve a loading condition that is as similar as possible to what would be the case at an inner support of a continuous beam. But also to get an indication of what the in-between weak section strength is. Limited full scale bending tests on fairly defect free wood and relating the strong section strength to the density showed that this was not a practicable way to go. The predicted strong section strength was in most cases lower than the strength of actually tested weak sections. A relation between the strength of the weakest section according to the Cook-Bolinder and

the strength of a section with as defect free wood as possible could be a more accurate way to go. Practically such a section is located between two knot clusters. For Norway spruce grown in Sweden the distance between knot clusters is around 400 to 600 mm.

Four boards were used to find out a an appropriate span for the tests. A too short span (around 1 m) would lead to shear failures and severe crushing perpendicular to grain under the point load. A too long span (around 1.5 m) on the other hand would mean that the moment distribution would be less peaked and thus the board could fail in weaker sections. It was found that a span of nine times the depth of the board (1305 mm) would be a good compromise, *figure 2*.

At the supports and at the applied load steel plates with a length of 120 mm was used to limit the crushing of the board perpendicular to grain. In addition, a piece of tire rubber was placed between the plate and the board at the load. This smoothed the deformation perpendicular to grain so that the fibres were not cut off. However, as the tests are meant to reflect a realistic situation, deformation and crushing at a support are quite natural. It also adds to the redistribution of moment by becoming more or less a plastic hinge. This effect is not evaluated in this paper.

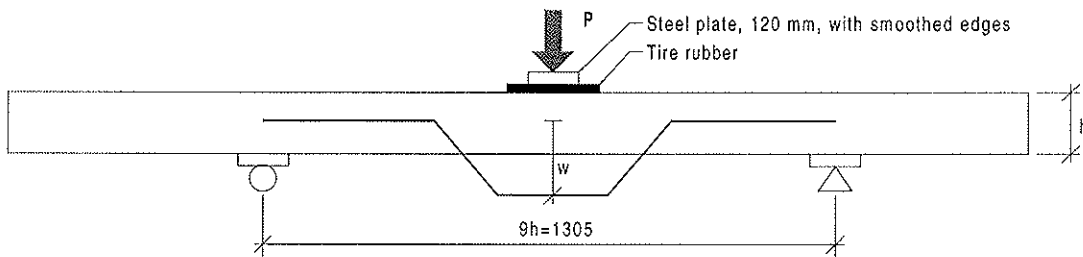


Figure 2. Test arrangement for determining the bending strength at a narrow moment peak.

3.3 Additional measurements

The edgewise MOE was measured on both sides of the board over the entire span, as shown in *figure 2*. The average of the two measurements is used as the MOE on the edge.

In addition the density, moisture content and mean annual ring width was measured.

Within a distance of 1 m in the centre of the span all knots were recorded using the same principles as described in Isaksson (1996).

4 Results

The tests show that the difference in bending strength between a weak section and a strong one is around 60 % at the 5:th percentile and the corresponding value at the mean value is 13 %, see *figure 3*. If the boards are ranked in an ascending order according to the weak section strength and the difference is taken between the strong and weak section, we get the result shown in *figure 4*. As can be seen, in quite a few cases what is believed to be the weak section is actually stronger than what is selected as a strong section.

It seems to be easier to find the weaker section in the generally weaker boards. This is shown by the downward trend of the difference of section strength. This is also the way it should be. In weaker boards of lower quality the knot clusters are often more pronounced as is the large ring width. In 39 out of 149 boards we failed in predicting which section was the weakest, or more correctly, the Cook-Bolinder again showed that locating a weak

section is not what it does best. The mean difference between the strong and weak section is 6.44 MPa with a standard deviation of 8.87 MPa.

The Coefficient of Variation, C.V., is 16 % and 23.5 % for the strong and weak sections respectively.

As can be seen in *figure 3* the distribution of weak section strength coincides well with the previous investigation (Isaksson 1996).

The relation between density and the strength of strong, defect free, sections is presented in *figure 5*. The R^2 is 0.372, which can be compared with the R^2 for the relation between weak section strength and density, 0.312.

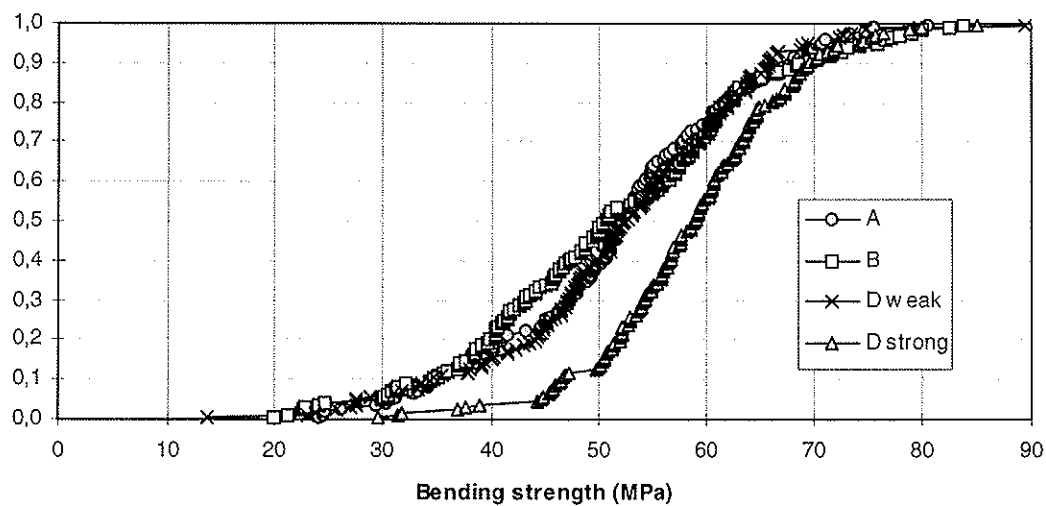


Figure 3. Distribution of bending strength for sample A, B (both in Isaksson 1996) and the present, D.

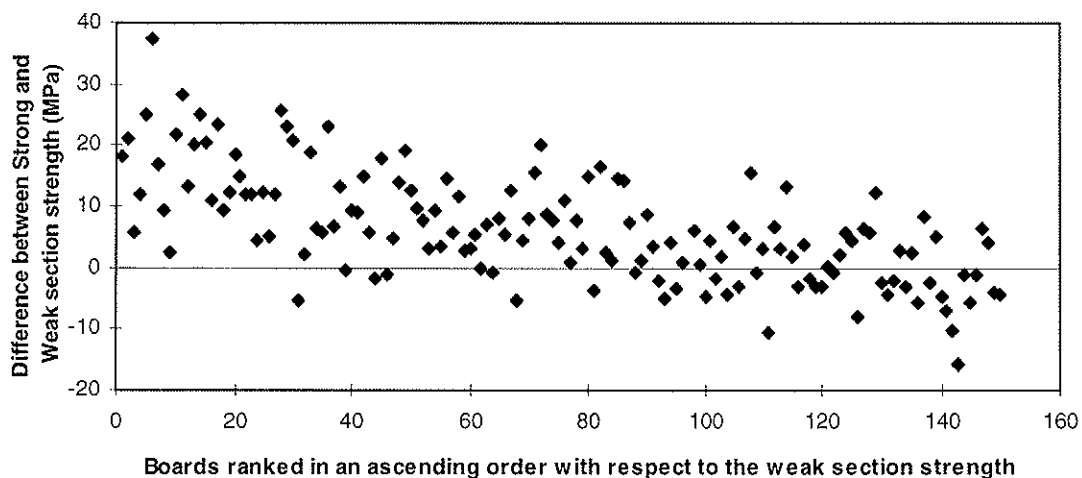


Figure 4. Difference between the bending strength in the selected strong (defect free) section and the weakest section according to the Cook-Bolinder. The boards are ranked in an ascending order with respect to the strength of the weak section.

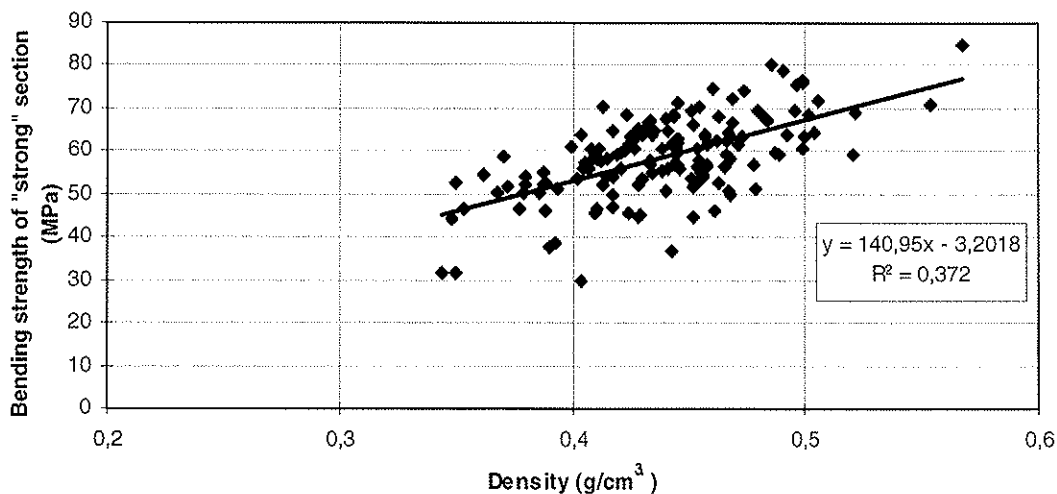


Figure 5. Relation between density and bending strength of "strong" sections.

5 Discussion and Conclusions

A sample of 150 boards were tested in a weak section, located using the readings from a Cook-Bolinder, and in a strong section based on visual inspection. The bending strength under a single point load at mid span was measured. Together with the results reported in Isaksson (1996) this study can provide necessary data about the variation of bending strength within timber elements. The present study gives information about the strength at moment peaks and the strength in stronger sections of fairly defect free wood.

Again, this study showed that the Cook-Bolinder often fails in predicting the location of the weak section as 39 out of 149 had higher strength in what was selected as weak sections compared to the selected strong ones.

A span of 9 times the depth of the board (1305 mm) was found to be a good compromise between having too much of crushing under the point load (a short span) and on the other hand having a less peaked moment distribution with the increasing risk of getting failures in weak sections outside the strong section.

Using the measured Coefficient of Variation for the weak sections, 23.5 %, the correction factor for bending strength can be determined according to Riberholt (1989). In this case the factor $k_{m,p}$ is 1.31, i.e. the bending strength may be increased with 31 % at the moment peak. From this study it can only be concluded that the factor is somewhere between 1.0 and 1.6. However, together with the previous test results (Isaksson 1996), a statistical model can be developed, providing a continuous bending strength variation profile within a board. With such a model it is possible to evaluate the correction factor $k_{m,p}$.

Based on the Coefficients of Variation for the weak and strong sections respectively, 16% and 23.5%, it can be assumed that the variation for a randomly selected section will be somewhere in-between these values.

The presented bending strengths are based on the assumption of single point load. However, a 120 mm long steel plate was used to distribute the load. This means, if assuming a uniformly distributed load over a length of 120 mm, the bending strengths will be 4.6 % lower.

Further, it can be concluded that there is no significant difference in the distribution of bending strength in tests with a single point load and a standardised testing according to ISO 8375, if the test section is selected using the same principles.

The relation between the density and bending strength of strong, defect free wood, is quite poor, at least for being used to predict the strength between weak sections ($R^2=0.372$).

6 References

Anon., 1982. Sortering av sågat virke av furu och gran. "Gröna boken". (Instructions for grading of sawn timber products of pine and spruce. In Swedish. AB Svensk Trävarutidning. Stockholm, Sweden.

Isaksson, T., 1995. Effect of test standard, length and load configuration on bending strength of structural timber. CIB-W18 Timber structures. Paper 28-6-4. Copenhagen, Denmark.

Isaksson, T., 1996. Variability of Bending Strength within Timber Elements. Lund Institute of Technology, Dept. of Structural Engineering, Sweden. Report TVBK-1011.

Riberholt, H., 1989. Guidelines for design of timber trussed rafters. CIB-W18A Timber structures. Paper 22-14-1. Berlin, Germany.

**INTERNATIONAL COUNCIL FOR BUILDING RESEARCH STUDIES AND DOCUMENTATION
WORKING COMMISSION W18 - TIMBER STRUCTURES**

**PROBABILISTIC DESIGN MODELS FOR THE DURABILITY OF
TIMBER CONSTRUCTIONS**

by

R H Leicester
CSIRO Building
Australia

**MEETING THIRTY
VANCOUVER
CANADA
AUGUST 1997**

PROBABILISTIC DESIGN MODELS FOR THE DURABILITY OF TIMBER CONSTRUCTION

by

R.H. Leicester

CSIRO Building, Construction and Engineering, Australia.

1. INTRODUCTION

The theory of structural engineering for timber construction is now sufficiently well defined that computational design procedures can be developed and even codified. By contrast, design for durability is still very much of an art, with design solutions varying from person to person. More usually, design for durability is omitted and the control of performance is undertaken by complying with 'good building practice'.

The key to developing a design procedure is first to have predictive models for durability. Because of the uncertainties associated with these models, they will of necessity have to be probabilistic models. Once such models are available computational design procedures can be developed and codified; optimised strategies for asset management involving design, maintenance and replacement can be derived; optimised procedures may be used to develop 'good building practice'. Perhaps most importantly, the availability of predictive models will enable innovative designs to be undertaken with confidence, and without the necessity of relying on past experience.

The purpose of this paper is to introduce a major investigation on timber durability being undertaken in Australia. It is a three year project, involving 5 research organisations at a cost of about one million dollars per year. An ambitious and key aspect of this project is to develop a probabilistic model for predicting the durability of any type of timber construction located anywhere in Australia.

The following describes the general concept of a probabilistic model, together with some of the practical aspects involved in developing such a model.

2. PROBABILISTIC MODEL

Figure 1 is a schematic illustration of the key elements of the prediction model. A set of input parameters are used to define the design situation, a particular hazard type is selected, and finally an attack model is used to predict the performance of the element or building system.

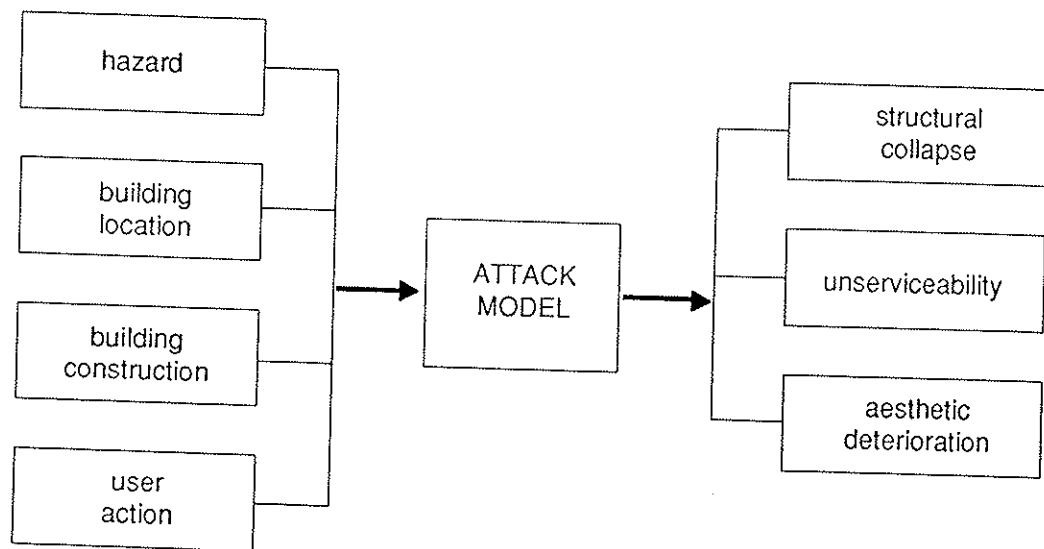


Figure 1. Schematic illustration of the prediction model.

Typical input parameters are those that relate to the hazard, building location, building construction, building element and maintenance programs. Performance criteria will be classified as either structural collapse, unserviceability (such as excessive deflections, water entry or loss of material) or aesthetic deterioration. Within the proposed scope of the project, the hazards investigated will include attack by the following:

- fungi
- bacteria
- termites
- marine borers
- corrosion agents
- mechanical degradation

In the above, the term mechanical degradation is taken to refer to the effects of rain, sun, wind and ultra violet rays on exposed timber. These parameters may lead to surface degrade, aesthetic deterioration, nail popping and extreme distortion of timber elements.

Each attack model is assumed to comprise a sequence of events as shown in Figure 2. The duration of each event is a random variable. This leads to a prediction in statistical terms of the time to failure as shown in Figure 3.

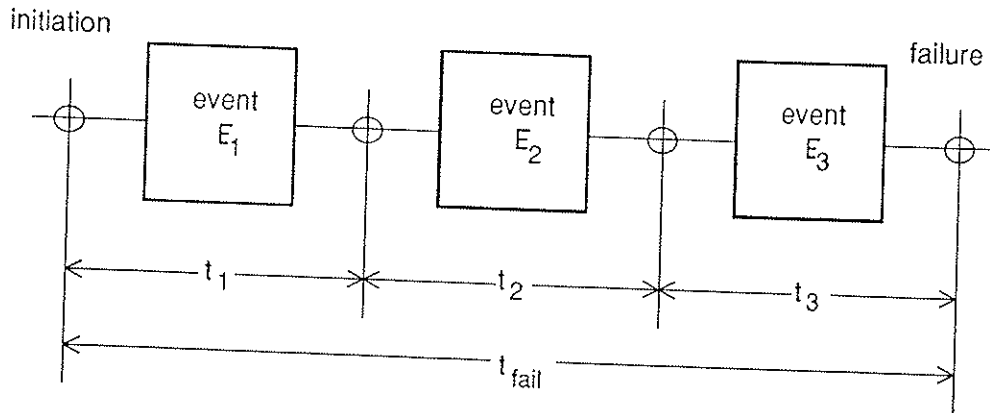


Figure 2. Statistical model of event times.

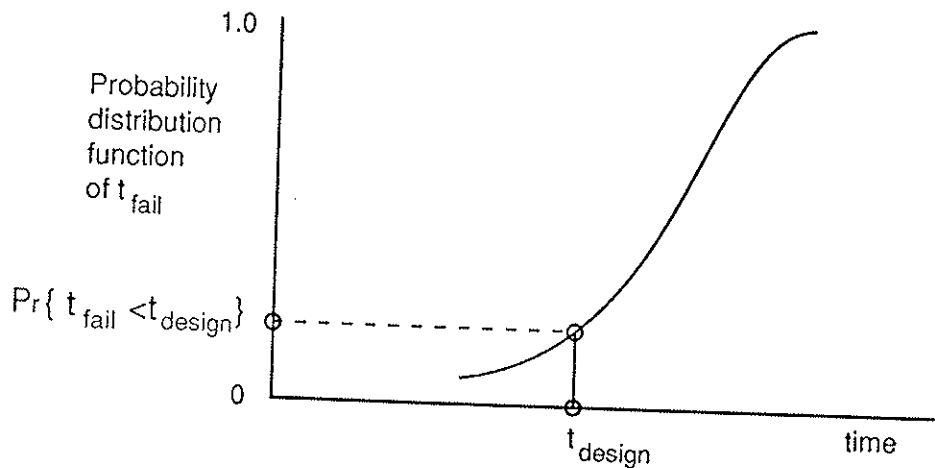


Figure 3. Statistical representation of time to failure.

The variability of the event times should take into consideration not only the natural in-service variability of these events, but also the additional variability that reflects the uncertainties arising from our inadequate knowledge or from the use of simplified models. Of particular interest is the risk parameter $\Pr\{t_{\text{fail}} < t_{\text{design}}\}$, the probability that the time to failure t_{fail} is less than the specified design life of the structural element, t_{design} . Typical acceptable values of the risk parameter are 0.05, 0.2, and 0.5 for structural collapse, unserviceability and aesthetic deterioration respectively.

3. METHODOLOGY

The most important aspect in the development of a design model is the choice of an attack scenario. Once this is done, all past experience and research data may be used to quantify the event times for such a scenario.

Index properties, usually measured through the application of standardised protocols, are useful input parameters for a prediction model. Some of these index properties apply only to specific materials or specific locations and hence their applicability is similarly limited. An example of this would be index properties derived for specific species in a standard grave yard test. More useful for modelling purposes are index properties that can be computed for any situation from readily available data, such as for example, the Scheffer climate index.

Accelerated tests, such as those involving accelerated field simulators may be regarded as providing index properties. However, care must be taken to ensure that the correct aspects are being accelerated, i.e. that the attack mechanism in the simulator is the same as that in real construction.

Statistical surveys may be applied to hazard, climate and soil parameters. If the surveys are comprehensive, i.e. they cover all of Australia, then the survey data may be used directly as input parameters for the prediction model. If the surveys are not comprehensive, then the data should be used to calibrate a sub-model that in turn acts as a comprehensive input for the prediction model.

Field studies involving full size real buildings or other timber construction will always be limited in scope. Hence the data from these studies should be used only to calibrate generic sub-models as discussed above.

4. ATTACK BY DECAY

4.1 Attack Mechanism

The simplest decay equation, illustrated schematically in Figure 4 is given by

$$dW/dt = f(s, m, T, \phi, p, b) \quad (1)$$

where W denotes the distance to the decay front, s denotes an index parameter related to timber species, m denotes a moisture potential, T denotes the temperature of the timber, ϕ denotes the osmotic potential of the water if solutes are present, p denotes an index parameter related to the preservative present (if any), and b denotes an index parameter related to the biological agents present. If the timber is not in ground contact, then the terms ϕ and b may be omitted. Hence, it can be seen that an important aspect of predicting decay is to be able to predict the moisture content and temperature history of a building element.

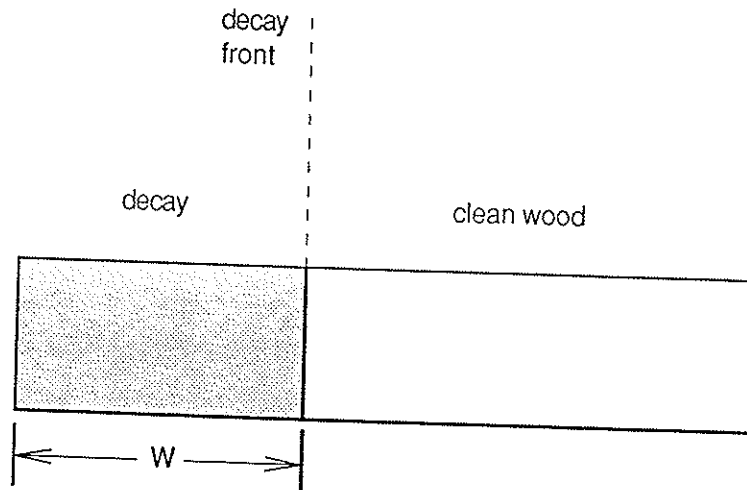


Figure 4. Notation for base model of decay.

For *timber protected and above ground*, such as timber in buildings, Figure 5, it is necessary to predict moisture condensation, moisture content and temperature of the critical elements due to both external and internal environmental effects.

For *timber above ground, but exposed to the weather*, Figure 6, moisture ingress is largely a function of 'time-of-wetness' arising directly from rain. For a given climate, both the moisture condition within the wood and the temperature of the timber must be predicted.

If the timber element has a protective skin arising either from a surface coating or a finite penetration of a preservative treatment, then it is convenient to treat the penetration of decay as two sequential events; the first is the penetration of the skin and the second is the attack on the inner core. Field observations indicate that cracking of the timber has a major effect on decay rate. This is partly due to the fact that cracks allow fungal and bacterial spores to bypass the protective skin, and partly because it allows the rain to accumulate and penetrate into the interior of the timber. Hence the penetration of surface cracks is an important part of this model.

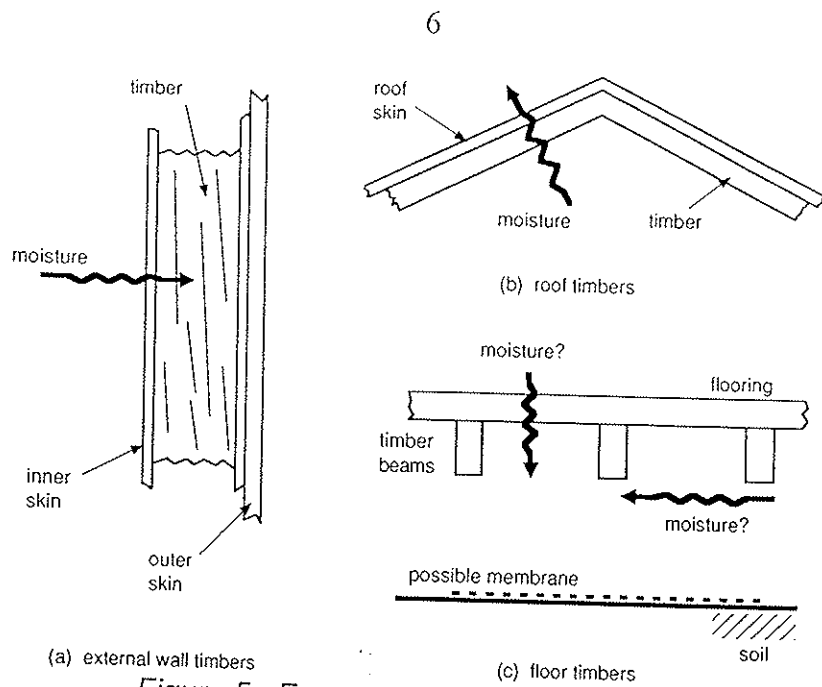


Figure 5. Examples of protected timber.

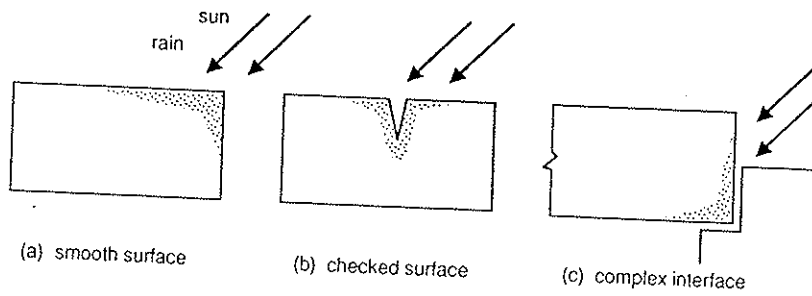


Figure 6. Examples of exposed timber, above ground.

For *timber in ground contact*, Figure 7, the model is similar to that of the exposed structure, with the additional concern of the ingress of moisture from the soil.

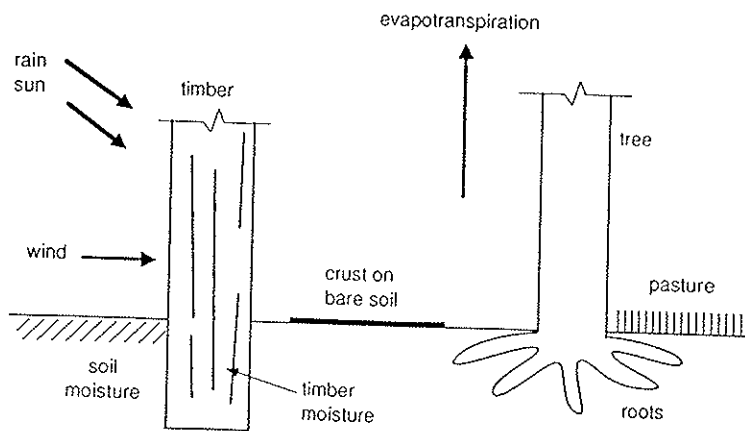


Figure 7. Example of exposed timber, in ground contact.

4.2. Sub Models

4.2.1 Climate models

Since Australia extends from latitude 10°S to 40°S, and includes both rainforest and desert regions, climate effects play a significant role in biodeterioration. For about 60 sites in mainland Australia (Figure 8), there is detailed climate data for a 10-year period; this data is given on an hourly basis and includes rainfall, wind, temperature, relative humidity, evaporation, cloud cover and the various components of solar radiation.

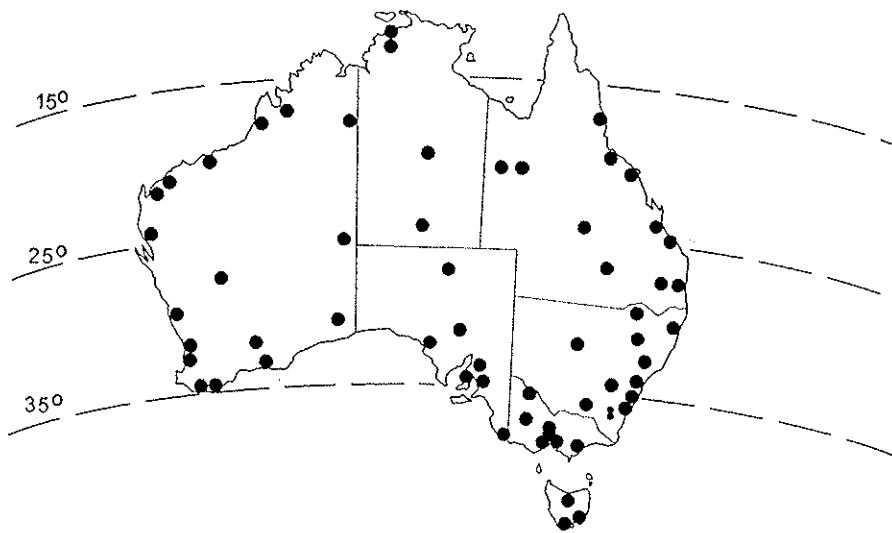


Figure 8. Site locations for detailed climate data.

To extend the value of this information, use can be made of a service by the Department of Primary Industry, Queensland, which provides a more limited set of data for a twenty year period that can be estimated for any location within Australia.

4.2.2 Model for solar heating

A simple model for solar heating such as that used by Gibbs (1990) will be used. Where total solar data is not available, estimation methods such as that proposed by Spencer (1982) will be applied.

4.2.3 Soil moisture model

Most of the water movement in soils is due to capillary action, although the vapour phase will also be examined. For capillary action, the relationships between soil moisture, pressure head and permeability will be expressed in terms of the model proposed by Genuchten (1980). Short duration water movements will be accurately calculated by numerical solution of the Richards equation (Ross 1990); long duration water movements will be computed using approximate but simpler equations such as the Green-Ampt equations (James and Larsen 1976). Refinements will include the effects of evapotranspiration by the local vegetation (Doorenbos and Pruitt 1977) and surface crust effects (Hillel and Gardner).

4.2.4 Model for heat and moisture movement in wood

Suitable models for heat and moisture movements in wood have been described by Siau (1995). For the vapour phase, the vapour pressure is a convenient driving force. However, for the purpose of working across a soil/timber or timber/masonry interface, the use of water potential as the driving force tends to be more convenient.

For capillary effects it is convenient to use models similar to those being used for soils. The most significant aspect of capillary action in timber is the high variability involved. As may be expected, permeability varies considerably between species. However, even within a single species permeability can vary considerably with location and direction; ratios of 100:1 are typical for sapwood to heartwood permeabilities and ratios of 10^5 :1 are typical for longitudinal to transverse permeabilities (Siau 1995).

In addition to the above, surface effects need to be considered. In particular, the effect of surface coating on moisture ingress due to wetting is important (Derbyshire *et al.* 1996)

4.2.5 Model for timber cracking

Models for cracking will be based on computing the transverse stresses arising from differential shrinkage effects near the surface of the wood.

4.2.6 Model for decay

The basic attack model for decay will be similar to that proposed by Griffin (1977). However, because of the lack of fundamental information, the validity of the model will depend very much on calibration to reported field studies. For Australia, these include the following:

- (a) Grave yard stake tests for 77 species at 5 sites shown in Figure 9; the test specimens have been monitored for 25 years (Thornton *et al.* 1996);
- (b) Ten types of painted panels exposed above ground at 20 sites, Figure 10; the test panels have been monitored for 9 years (Creffield *et al.* 1992).
- (c) L-joints exposed above ground at 11 sites, Figure 11; 27 species were placed at one site and 9 species at all others; the test specimens have been monitored for 9 years (Cause 1993).

In addition to the above, there have been several studies using accelerated field simulations that may provide useful information (Thornton *et al.* 1995). Finally, for modelling treated timber, the effective depth of preservatives must be estimated (Carey 1992).

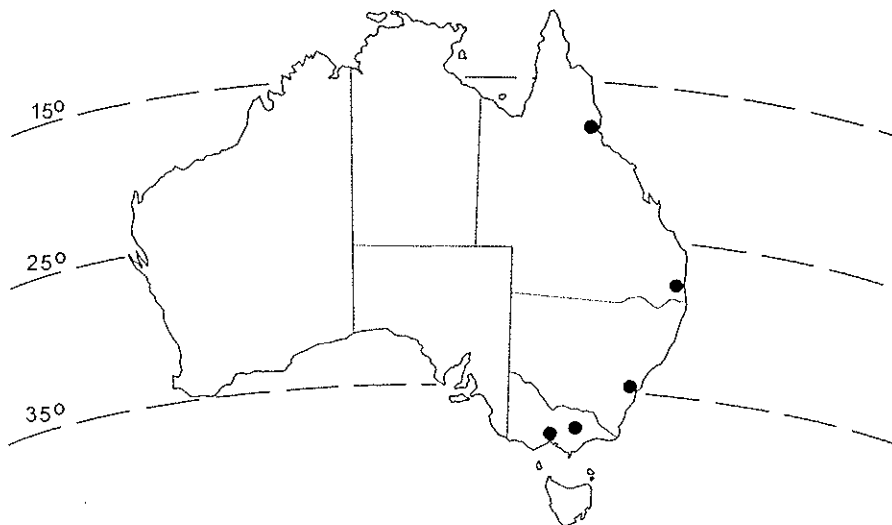


Figure 9. Site locations for grave yard tests.

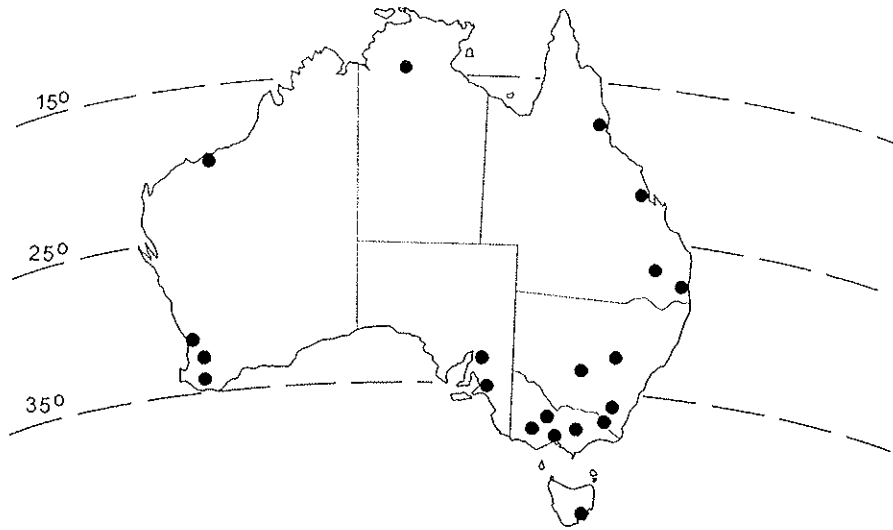


Figure 10. Site locations for exposure panels.

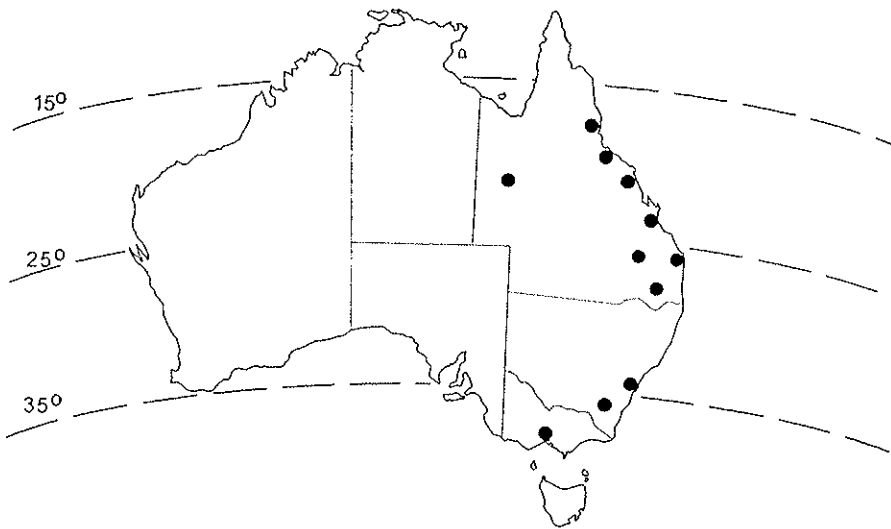


Figure 11. Site locations for L-joint tests.

4.2.7 Model for moisture movement in buildings

Modelling will be applied to sections of buildings as shown in Figure 5. Simple methods such as those outlined in the ASHRAE Handbook on Fundamentals (1993) and Tenwolde (1983) will be used. Calibration of these models will be by data from field monitoring of houses at the locations shown in Figure 12 (Cole *et al.* 1996).

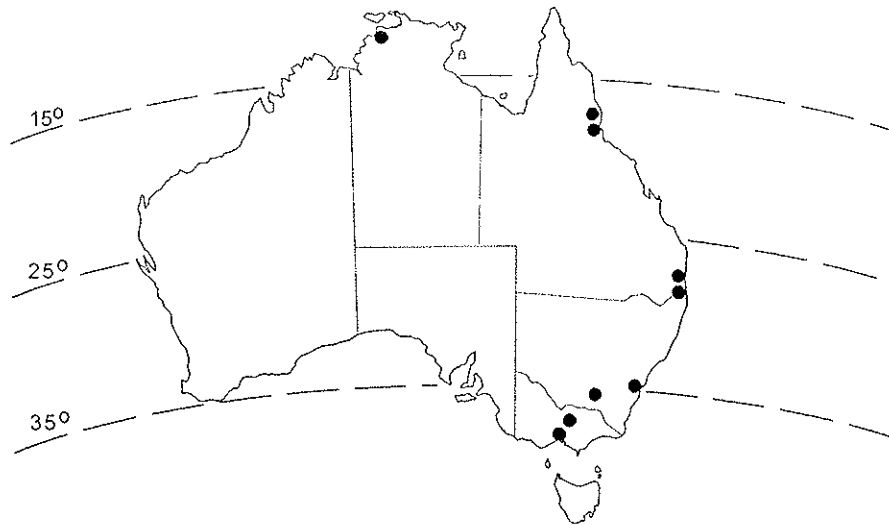


Figure 12. Site locations for monitored indoor climate.

5. ATTACK BY TERMITES

The model for attack by termites comprises the following components:

- (i) establishment of nests within 150 m of the building;
- (ii) movement from the nest to the building;
- (iii) movement from the ground upwards or into the building;
- (iv) movement within a structure;
- (v) destruction process.

There appears to be only limited data on the movement of termites (Ettershank *et al.* 1980; Lopez *et al.* 1994; Robson *et al.* 1995).

Consequently field experiments are being undertaken to assist in this matter; these will include the use of radioactive tracers to track termite movement (Easy and Holt 1988). The termite model will be calibrated against data obtained from a national survey on termite attack being undertaken by J.R. French and A. Bernhard (private communication). Major locations for this survey are shown in Figure 13.

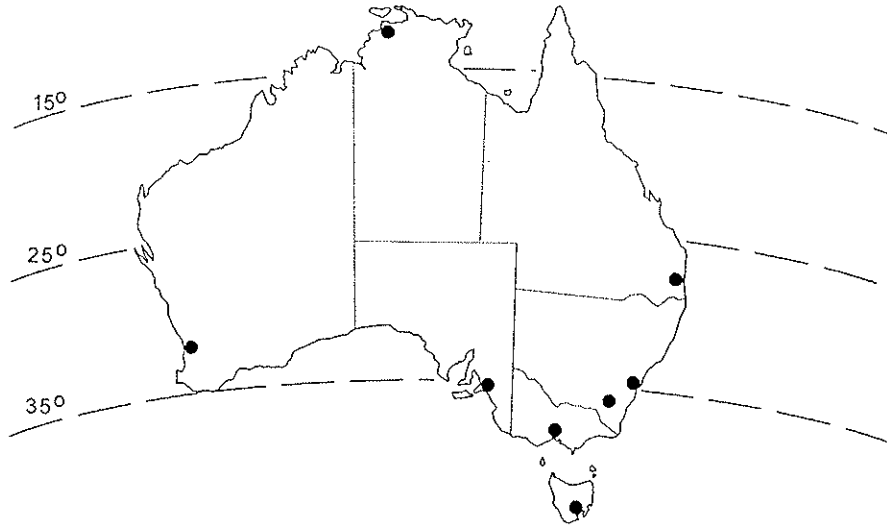


Figure 13. Site locations for termite surveys.

6. ATTACK BY CORROSION

Attack on metal connectors is by a combination of atmospheric corrosion on exposed steel elements and cathodic corrosion on embedded steel elements as illustrated in Figure 14. Relevant corrosion models are under development (Davis 1994; Cole *et al.* 1997) and field monitoring of atmospheric corrosion parameters is being undertaken at the sites shown in Figure 15.

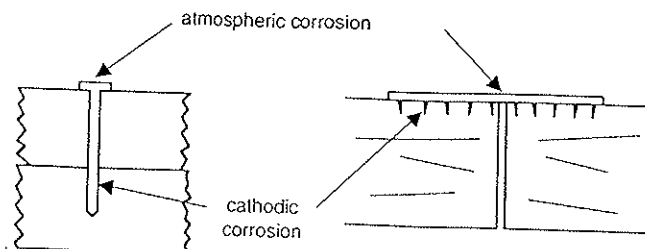


Figure 14. Types of corrosion of metal fasteners.

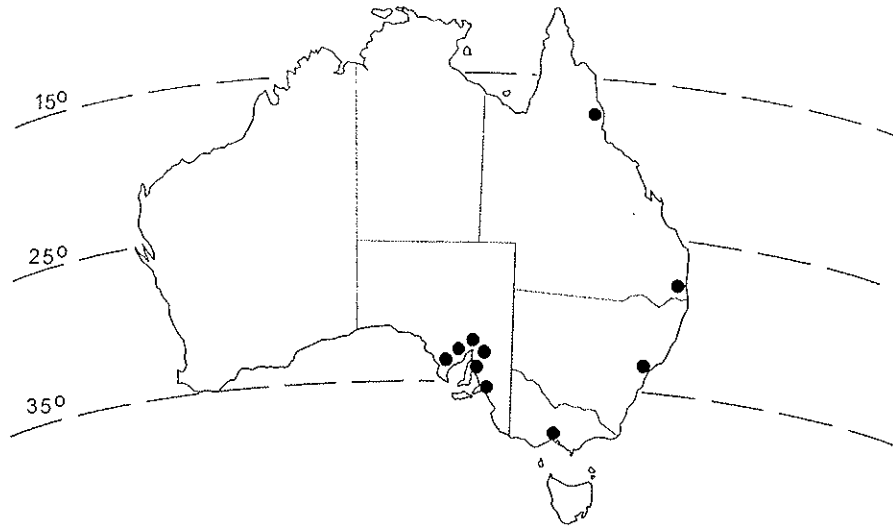
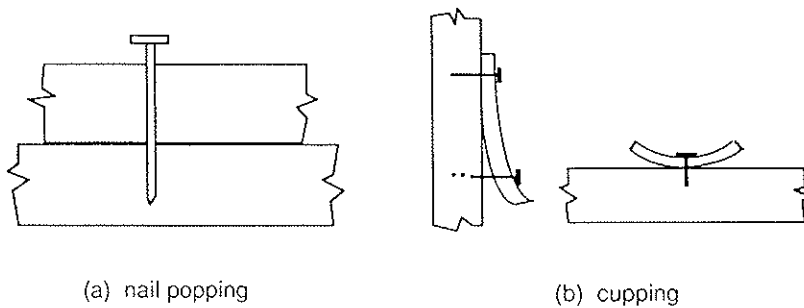


Figure 15. Site locations of corrosion surveys.

7. ATTACK BY MECHANICAL DEGRADATION

Examples of mechanical degradation that are planned to be modelled are shown in Figure 16.



(a) nail popping

(b) cupping

Figure 16. Examples of mechanical degradation.

8. CONCLUDING COMMENT

The project to develop prediction models has had a slow start, largely because of unanticipated difficulties in formulating suitable attack mechanisms. However, once this has been accomplished, the next phase will be to develop design procedures and/or software that are user friendly. The complex effects of climate may need to be reduced to simple index parameters, or failing this, to regional parameters; similarly it may be effective to reduce the complex features of building construction to index parameters or at least to idealised building types. However, in general it will be desirable as far as possible, for all aspects of the prediction model to be globally applicable.

Furthermore, it would be expected that the predictions on durability would be associated with a high degree of variability. As a result, the use of refined models and accurate parameter estimates are not warranted. For this reason alone, within the Australian project the use of sophisticated methods will be avoided and emphasis will be placed on the use of simple methods both for analysis and for estimating the required model parameters.

9. ACKNOWLEDGMENTS

This project involves many research scientists, and the author is indebted to all of them for providing data and assistance in the development of the models described herein. The major funding for this project is from the Forestry and Wood Products Research and Development Corporation; the overall project manager is Colin Mackenzie of the Timber research and Development Advisory Council of Queensland.

10. REFERENCES

1. ASHRAE. (1993). ASHRAE Handbook – Fundamentals, American Society of Heating, Refrigerating and Air-Conditioning Engineers Inc., Atlanta, GA.
2. Carey, J.K. (1992). The Preventative Effectiveness of Preservative Treatments Against Wood-rotting Fungi-preliminary Results. *Proc. 23 Annual Meeting of International Res. Group on Wood Preservation*, Harrogate, 10-15 May, BRI Paper PD143/92, March.

3. Cause, M. and Stringer, G. (1993). Performance of Timber Decking at a Brisbane Site After 5¹/₂ Years Weather Exposure. *Proceedings of 24th Forest Products Conference—Vol. 1*, CSIRO Division of Forest Products, Clayton, Victoria, Australia, November.
4. Cause, M. (1993). Establishment and Preliminary (5 Yr) Results of a Major Above-Ground Timber Durability Trial in Eastern Australia. *Proceedings of 24th Forest Products Conference—Vol. 1*, CSIRO Division of Forest Products, Clayton, Victoria, Australia, November.
5. Cole, I.S., Ganther, W. and Norberg, P. (1996). Estimation of the Moisture Condition of Timber Framewrok in Australian Houses. *Proc 25th Forest Products Research Conference*, Paper No. 3/7, 18–21 November, Melbourne, Australia, Vol. 1, 10 pages.
6. Cole, I.S., Neufield, A. and Ganther, W. (1997). A New Model of Corrosion in Tropical Conditions. *Proc 10th Asean Pacific Corrosion Control Conference*, Bali, October.
7. Creffield, J.W., Johnson, G.C., Thornton, J.D., Nguyen, N.K. and Chew, N. (1992). An Australian Test for Decay in Painted Timbers Exposed to the Weather for a Total of 9 Years. *Forest Products Journal*, **42** No. 1.
8. Davis, R. (1994). Timber and Metal – The Connection. *Proceedings of Pacific Timber Engineering Conference, Gold Coast, Australia*, July.
9. Derbyshire, H. and Miller, E.R. (1996). Moisture Conditions in Coated Exterior Wood. *J. Institute of Wood Science*, **14**(1), Issue 79: 40–47.
10. Doorenbos, J. and Pruitt, W.O. (1977). Guidelines for Predicting Crop Water Requirements. *FAO Irrigation and Drainage Paper*, No. 24, 145 pages.

11. Easey, J.F. and Holt, J.A. The Use of Gold-198 and Iodine-131 as Tracer Materials for the Study of Termite Behaviour. *Material und Organismen*, **10**, February, 1988, 133–145.
12. Ettershank, G., Ettershank, J.A. and Whitford, W.G. (1980). Location of Food Sources by Subterranean Termites. *Environ. Entomol.*, **9**, 645–648.
13. Gibbs, P. (1990). Calculating Building Element Surface Temperatures from Environmental Data. *Architectural Science Review*, **33**.
14. Genuchten, M.Th. van (1980). A Closed-form Equation for Predicting the Hydraulic Conductivity of Unsaturated Soils. *Soil Sci. Soc. Am. J.*, **44**, 892-898.
15. Griffin, D.M. (1977). Water Potential and Wood-Decay Fungi. *Ann. Rev. Phytopathol*, **15**, 319–329.
16. Hillel, D. and Gardner, W.R. (1969). Steady Infiltration into Crust-topped Profiles. *Soil Sci.*, **108**(2), 137–142.
17. James, L.G. and Larson, C.L. (1976). Modeling Infiltration and Redistribution of Soil Water During Intermittent Application. *Soil and Water Division of ASAE*, Paper No. 74–2571, February, 482–488.
18. Lopez, F., Acosta, F.J. and Serrano, J.M. (1994). Guerilla vs. Phalanx Strategies of Resource Capture: Growth and Structural Plasticity in the Trunk Trail System of the Harvester Ant *Messor barbarus*. *Journal of Animal Ecology*, **63**, 127–138.
19. Robson, S.K., Lesniak, M.G., Kothandapani, R.V. and Traniello, J.F.A. (1995). Nonrandom Search Geometry in Subterranean Termites. *Naturwissenschaften*, **82**, Springer Verlag, 526–528.

20. Ross, P.J. (1990). Efficient Numerical Methods for Infiltration Using Richards' Equation. *Water Resources Research*, Vol. **26**(2), February, 279–290.
21. Siau, J.F. (1995). *Wood: Influence of Moisture on Physical Properties*. Dept of Wood Science and Forest Products, Virginia Polytechnic Institute and State University, 227 pages.
22. Spencer, J.W. (1972). A Comparison of Methods for Estimating Hourly Diffuse Solar Radiation from Global Solar Radiation. *Solar Energy*, **29**(1), 19–32.
23. Tenwolde, A. (1983). The Kieper and MOISTWALL Moisture Analysis Methods for Walls. *Proc. ASHRAE/DOE Conference, ASHRAE SP 38*, Atlanta, GA, 1033–1051.
24. Thornton, J.D., Johnson, G.C. and Creffield, J.W. (1996). Hazard-based Natural Durability Ratings and Mean Rates of Biodeterioration Proposed for Use in the Reliability-based Durability Design Method. *Proc. 25th Forest Products Research Conference*, Melbourne, 18–21 November, Paper 1/19.
25. Thornton, J.D., Johnson, G.C. and Nguyen, N.K. (1995). Specimen Life Statistics of Untreated Heartwood of 35 Timber Species After Five Years' Exposure in the Accelerated Field Simulator. CSIRO Division of Forest Products, Melbourne, Victoria, Australia.

INTERNATIONAL COUNCIL FOR BUILDING RESEARCH STUDIES AND DOCUMENTATION
WORKING COMMISSION W18 - TIMBER STRUCTURES

EXPERIMENTAL INVESTIGATION AND ANALYSIS OF
REINFORCED GLULAM BEAMS

by

K Oiger
Tec. Univ. Tallinn
Estonia

MEETING THIRTY
VANCOUVER
CANADA
AUGUST 1997

Experimental Investigation and Analysis of Reinforced Glulam Beams

K. Oiger
Prof. Dr.Tech., Tec. Univ.Tallinn, Estonia

This paper discusses the the results of an experimental investigation and an analysis of reinforced and prestressed glulam beams. During many years experimental investigations have been carried out on models in the laboratory of Tallinn Technical University. The studies involved beams both, reinforced with deformed bars and prestressed with steel cables. The results show that prestressed glulam beams are applicable in some cases (in particular, by post-tensioning), though a relatively large portion of initial prestress disappears with time.

1 Introduction

It is well known, the strength of a small undefected test piece is much greater than that of a ordinary sawn timber with actual dimensions and natural defects. Thus to improve timber properties, various methods have been used. Composite structures are combined from different materials and elements where every material serves the purpose in the most suitable way.

One possibility is, for example, to reinforce glulam beams with steel bars. In this case steel bars inside the timber beam are protected against direct fire and increase the fire resistance of the structure. In addition to that, often the timber cover layer is chemically more durable then ordinary steel.

Various methods for reinfocing glulam beams with steel bars include ordinary staight reinforcing steel bars without the prestressing force, prestressed straight bars or cables and curved steel cables.

Variable experience has been gained in testing, designing and using reinforced glulam structures. On the basis of literature, the following advantages can be highlighted: reinforcing saves 30-40 % timber and glue, decreases 15-20 % of the weight of structures, 12-20 % of cost and 30-36 % of all expenses compared to ordinary unreinforced glulam beams. Reinforced glulam beams have usually 20-30 % smaller depth than ordinary beams, but in most cases, their width is 120-140 mm /1/.

No special devices are needed for manufacturing of reinforced glulam beams if the equipment for glulam structures is appropriate. Gluing of reinforcing bars is labour-consuming. Consequently manufacturing of reinforced glulam beams needs 10-15 %

more work.

Glues based on epoxyresin or phenol-resorcinol glues or polyurethane resins are generally recommended. According to Riberholt the bond of two- component polyurethane and other ductile glues appears to be slightly better (axial strength for bolts). Polyurethane resins remain more elastic than epoxy, making the stress distribution in ultimate limit state more uniform.

It is believed that neither epoxy nor polyurethane give complete corrosion resistance. However, epoxies are regarded as more impervious than polyurethane resins. So an epoxy primer treatment of steel surface should be applied when polyurethane resins are used.

Reinforced structures have a longer life-time and higher reliability than usual glulam, as the influence of natural wood defects is smaller. Because of wood creep over a long time, the redistribution of forces takes place so that normal stresses in steel bars increase about 25-40 %, and tension stresses in wood decrease.

In the 1980s in the former Soviet Union, glulam beams, prestressed with steel bars were developed and designed for spans of 9, 12 and 18 m (depth of beams 600, 700 and 1080 mm) and loading 32 kN/m. Straight reinforcing bars were used both in the tension and compression zone.

Prestressing (tensile) stresses in reinforcing steel exceeded 500 MPa and stresses in timber near the lower edge of the beam after hardening of glue and transfer of pretensioning forces from supports to the beam appeared to be between 5- 7.4 MPa, but before testing stresses decreased about 3-15 %. These prestressed beams had direct bond between bars and wood.

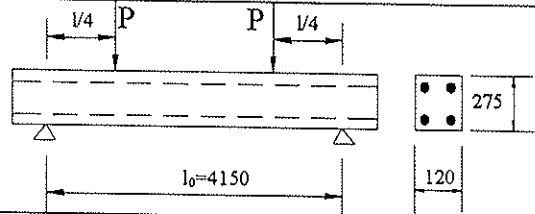
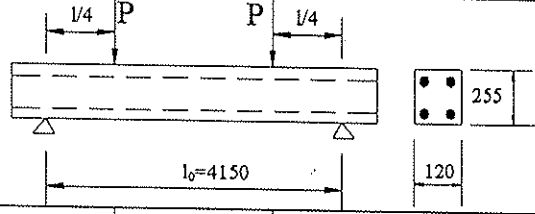
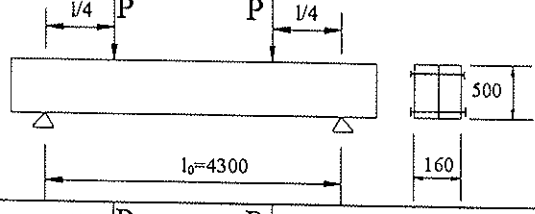
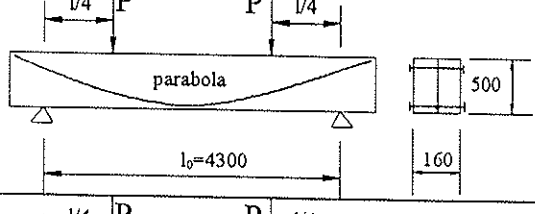
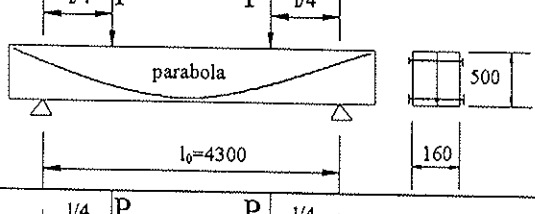
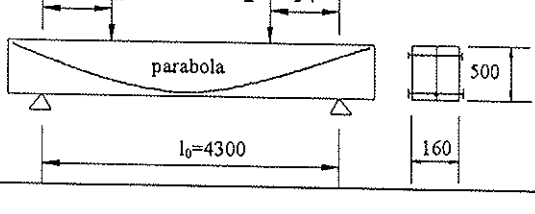
As a result, deflections of prestressed beams were 1.1-1.2 times smaller than ordinary gluelam beams. Failure of some beams occurred so that steel bars yielded and in compression edge of beam folds occurred. However, that happened by the load that exceeded the designed load more than twice.

2. Experimental investigations of reinforced and prestressed glulam beams

For over twenty years, research has been carried out at Tallinn Technical University on problems of reinforced glulam beams, the behaviour of ordinary reinforced glulam beams and beams prestressed with curved steel cables (tendons). Table 1 shows general parameters of some examined beam models. Mainly static short-term tests were carried out. As we can see, relatively little reinforcement was used.

For gluing steel bars glues based on epoxyresin or phenol-resorcinol glues were used.

Table 1

No of model	Scheme of model	Reinforcing bars	Prestressing force
1.		$\varnothing 12\text{mm}$ $f_y = 390\text{ MPa}$	—
2.		$\varnothing 12\text{mm}$ $f_y = 390\text{ MPa}$	lower bars were prestressed with $N_0 = 2 \times 35\text{ kN}$
3.		—	—
4.		$\varnothing 16\text{mm}$ $f_y = 235\text{ MPa}$	—
5.		$\varnothing 16\text{mm}$ $f_y = 235\text{ MPa}$	$N_0 = 30\text{ kN}$
6.		Cable $\varnothing 13\text{mm}$, $A_{ef} = 10,16\text{ mm}^2$ $f_y = 1875\text{ MPa}$	$N_0 = 40, 80, 100\text{ kN}$

2.1 Glulam beams reinforced with straight steel bars

This section discusses briefly the results of an experimental study of glulam beams reinforced with deformed reinforcing steel (yield point 390 MPa) only in the tension zone or both in the tension and compression zone, glued in square grooves with two-component epoxy glue (see model 1 and 2 in Table 1).

These models were built over twenty years ago and then tested with a design load. 10-20 days after manufacturing, the beams were tested with concentrated forces as shown on the scheme in Table 1. More than twenty years one of the beams was kept

in various conditions of humidity and temperature and now it has been again tested. Its carrying capacity and stiffness has not changed remarkably, though factors depending on time have taken place. Strength class of the glulam was GL 24, the thickness of the lamination layer 16 mm and wood moisture content 11 %.

Models were loaded until tension steel bars began to yield. No failure symptoms of compression edge timber or bond failure of steel bars in the support cross-section were observed. If the beams with parameters shown in Table 1 (model 1) are reinforced only in their lower edge (tension zone), then their load carrying capacity is about 1.2 times greater. The carrying capacity of the beams reinforced both in the upper and in lower edge have 1.5 times greater load carrying capacity than ordinary unreinforced glulam beam with similar parameters. The steel began to yield by the load $P = 40$ kN and deflection was 22.5 mm. In the last case design load was determined by the stiffness requirements. At the same time, shear capacity was within allowed limits.

Obviously, load carrying capacity and stiffness depend on the intensity of reinforcement, but shear capacity of the beam, which sometimes tends to be unsatisfactory, should be observed carefully in design process.

2.2 Glulam beams prestressed with straight reinforcing bars

This model (model 2 in Table 1) was made as described above in 2.1. The same material for reinforce steel as for the beams of model 1 was used. Unfortunately, because of small initial prestress force and loss of tension bar force in transfer process from supports to the beam (after hardening of glue) we couldn't have noticeable effects of prestressing.

3. Beams reinforced and prestressed with curved bars

The aim of using curved bars was to increase simultaneously bending strength, stiffness of the beam, and shear strength at the beam ends.

Model 4 was reinforced with round section bars fixed with nuts at the ends of the beam. Model 5 was reinforced with the same bars, which were posttensioned to the ends of the beam (both ends were active). Beam was built from two halves located side by side. This way making of grooves was simplified for curved bars (see photo Fig. 1). After planting bars into the groove of one side, both sides of the beam were connected with bolts (photo Fig. 2).

The model beam parameters were: the total length of the beam 4.5 m (span 4.3 m), cross-section $b \times h = 160 \times 500$ mm, the thickness of the lamination layer 29.4 mm, the strength class GL 24, wood moisture content 11-12 %.

Unprestressed reinforcement increased carrying capacity about 10 % and decreased deflections about 9 %.



Figure 1. Halves of the tested beam with grooves for steel bars.

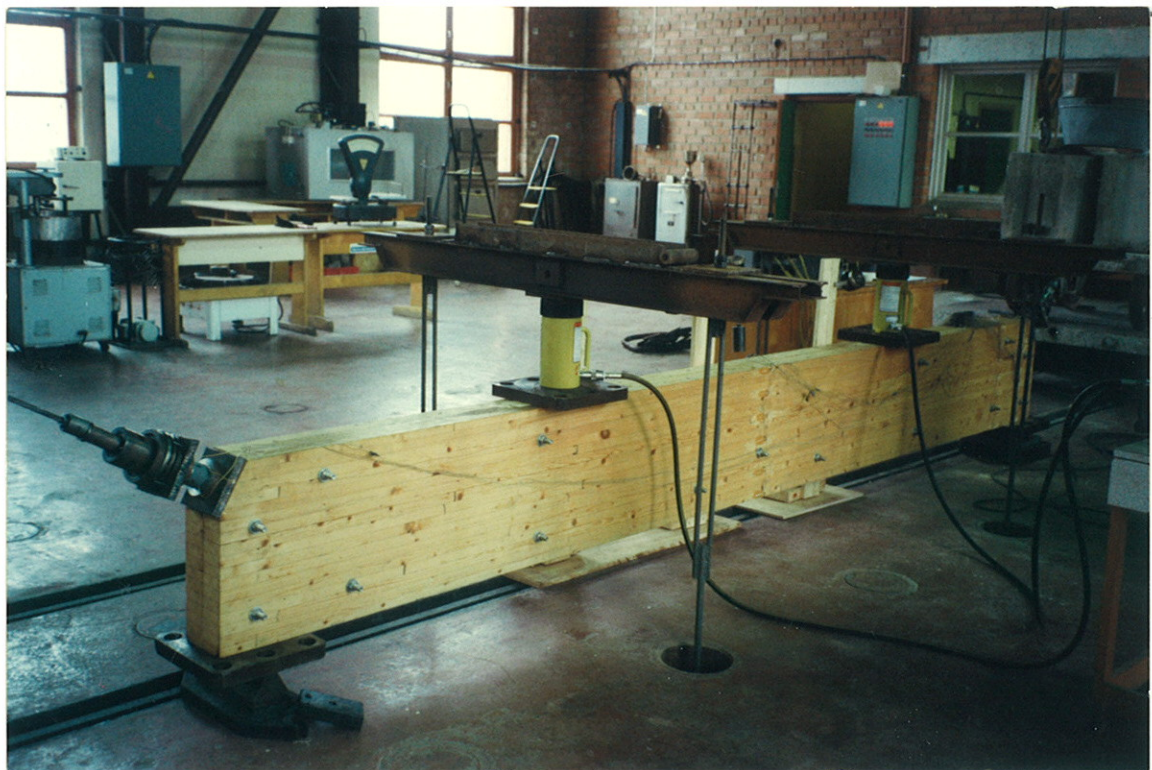


Figure 2. Loading of the prestressed glulam beam - model 6.

Post-tensioning bars of relatively low strength ($f_y = 235 \text{ MPa}$) and loss of prestress due to friction in grooves which caused essential decrease in prestress force in the center section of the beam about 3 times, increased carrying capacity only 4 % compared to the previous model.

4. Beam prestressed with curved high-tension cable

Model 6 (see Table 1 and Fig. 2) was a more successful structure, because we could apply sufficiently high prestressing forces, and loss of prestress due to elastic deformation of the member and due to relatively small friction. The beam parameters were the same as for the beams of model 5. The 7-wire cable (tendon) had cross-section area $A_{ef} = 10.16 \text{ mm}^2$ and $f_y = 1875 \text{ MPa}$. The tendons were locked by using conical-shape grips on the steel plate anchor. The beam was tested with prestressing forces of 40, 80 and 100 kN and loaded with concentrated loads up to $P = 180 \text{ kN}$ (summary load 360 kN).

Strains were measured by strain gauges (see Fig. 3). The deflection (camber) caused by tendon force was measured at the mid-span.

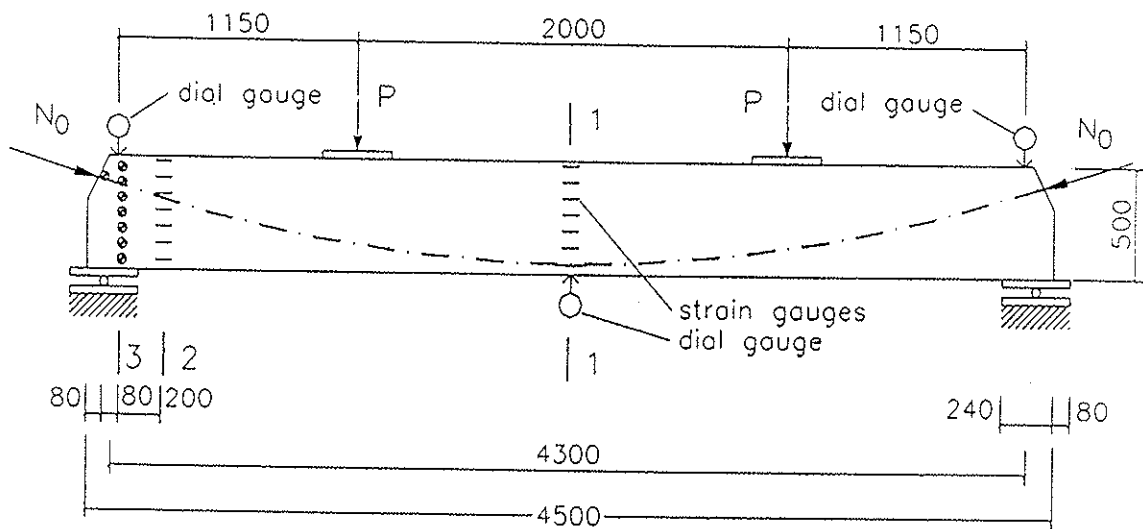


Figure 3. Scheme of the beam structure, loading, strain and dial gauge positions.

Typical distribution of stresses and their values is illustrated on graphs in Fig. 4.

As we can see the normal stresses in central section of the beam, caused by short-time loading at prestressing force $N_0 = 100 \text{ kN}$ and by load $P = 180 \text{ kN}$ do not significantly exceed designed values of stresses except for the bearing stresses $\sigma_{c,90}$ (σ_y) at the supports. The latter high stresses caused the breakage of support area. Nevertheless, the designed value of load P at $N_0 = 100 \text{ kN}$ cannot exceed 110 kN ($2 \times 110 \text{ kN}$).

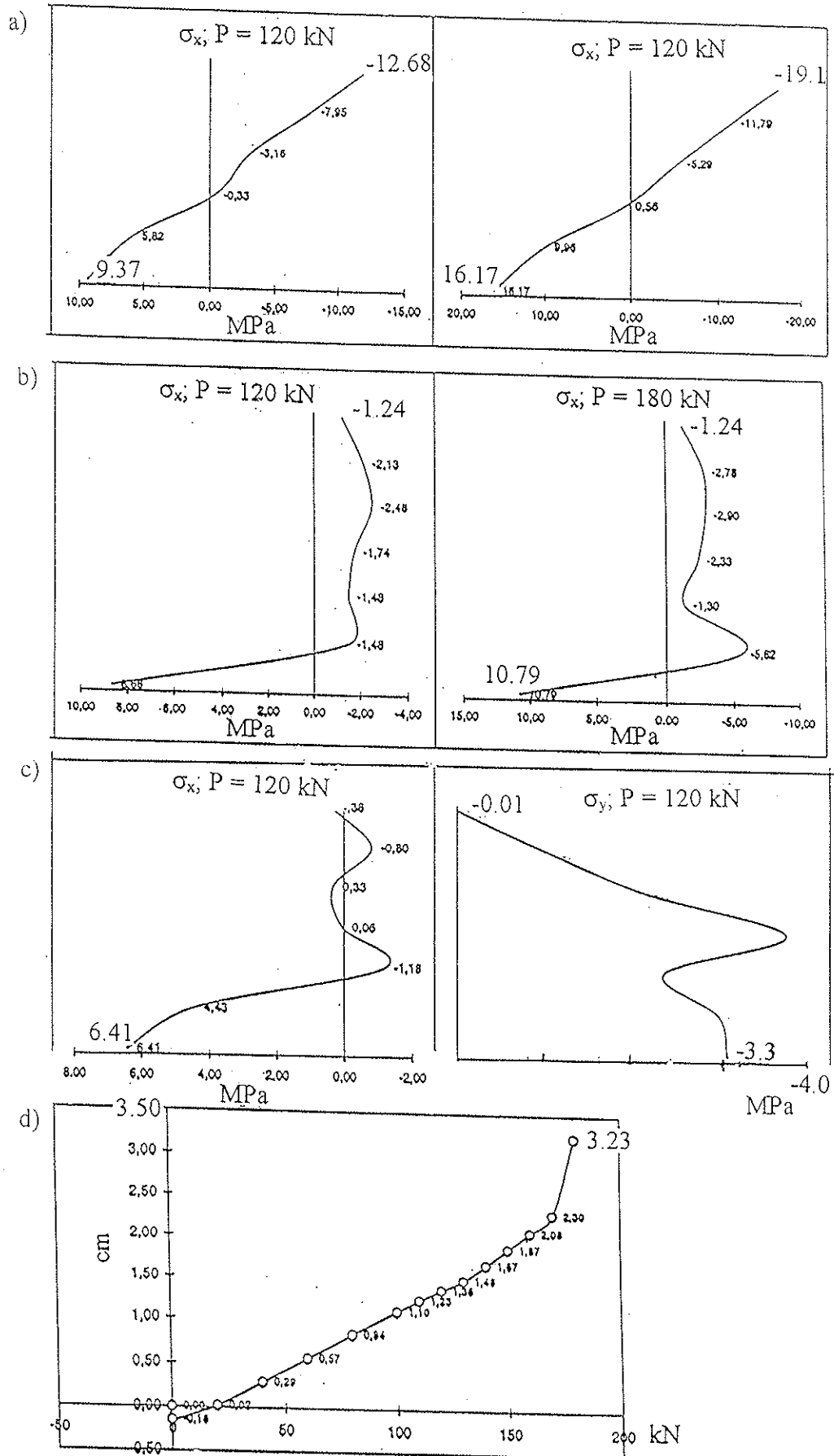


Figure 4. Distribution of stresses by $N_0 = 100$ kN: a) in section 1-1, b) in section 2-2 and c) in section 3-3; d) deflection f versus load P by $N_0 = 100$ kN.

The tested beam has relatively low shear strength. It is also necessary to take account that the loss of prestress can exceed 50 % of initial value if we cannot compensate it by posttensioning. In any case prestressed beam with tendon ($N_0 = 100$ kN) has about 1.4 times greater carrying capacity than unprestressed ordinary glulam beam with the same parameters. Such beams are reasonable to use if it is possible to realize posttensioning of tendon afterwards.

6. Analysis of reinforced beams

It can be concluded that relatively simple methods for calculating reinforced concrete beams could be used to analyse reinforced glulam beams, especially for unprestressed beams.

Using reduced (equivalent) section parameters it is possible simply and with sufficient accuracy to calculate strains and stresses of reinforced beams. For example, for beams (see model 1 in Table 1) differences between measured and calculated values for $P = 40$ kN in central cross-section of the beam are: $\sigma_{x,max}$ for timber beam edge 8.9 %, for steel bars in measured section 3 %, and for deflection 16.7 %. Calculated values for wood stresses were greater, and deflection was smaller than the measured values.

Obviously, more complicated analysis models based on nonlinear FEM, for example, can give more exact and comprehensive results. Influence of creep deformation should not be neglected.

6. Summary

Reinforced and prestressed glulam beams could be effectively used when slender heavy loaded beams are needed. Nevertheless the long-term behaviour of prestressed glulam beams needs further research. At present more reliable and simpler solution is given by reinforced glulam beams with glued-in deformed bars.

References

1. Štšurko, S. A., Štšuko, V.J., Kozulin, A. J., Osobennosti izgotovljenija kleenih armirovannyh konstruktsii. Proizvodstvo i povysenie katsestva derevjannyh kleenih konstruktsii. Moskva 1978.
2. Mäkipuro, R., Tommola, J., Salokangas, L., Jutila, A. Wood-Concrete Composite Bridges. Nordic Timber Bridge Project. 1996.

**INTERNATIONAL COUNCIL FOR BUILDING RESEARCH STUDIES AND DOCUMENTATION
WORKING COMMISSION W18 - TIMBER STRUCTURES**

**THE STABILITY BEHAVIOUR OF TIMBER TRUSSED RAFTER ROOFS
-STUDIES BASED ON EUROCODE 5 AND FULL SCALE TESTING**

by

R J Bainbridge
C J Mettem
TRADA Technology Ltd.
A Reffold
Gang-nail Systems Ltd.
T Studer
Truswal - Twinaplate Ltd.
United Kingdom

**MEETING THIRTY
VANCOUVER
CANADA
AUGUST 1997**

The Stability Behaviour of Timber Trussed Rafter Roofs - Studies Based on Eurocode 5 and Full Scale Testing

By: **R J Bainbridge**, TRADA Technology Ltd., UK
C J Mettem, TRADA Technology Ltd., UK
A Reffold, Gang-nail Systems Ltd., UK
T Studer, Truswal-Twinaplate Ltd., UK

Abstract

This paper describes recent research into the stability behaviour of timber trussed rafter roofs of non-domestic scale, in the light of Eurocode 5 [1] and the latest edition of BS5268 [2]. Testing of a full scale non-domestic timber trussed rafter test roof of 11m span is also detailed, employing diagonal bracing at rafter level to provide stability.

The comparative effects of different bracing angles are presented in terms of their influence upon the overall stiffness of the structure. Investigation is also made into the effects of variations in the fixity of the bracing members at wall plate locations.

The findings are also compared with theoretical behaviour based on a simplified three dimensional structural model and hand calculation.

1. Background

Permanent roof bracing for standard trusses in the UK performs two clear functions:

- stability bracing*, to hold the trusses firmly in place and keep them straight so that they can resist all the loads on the roof (with the exception of wind);
- wind bracing*, often required in addition to the stability bracing to withstand wind forces on the roof and walls of a building.

Stability bracing consists of tiling battens, longitudinal binders, diagonal rafter bracing, web chevron bracing and lateral web bracing (if required). There are deemed-to-satisfy rules for conventional, site applied bracing for domestic roofs, but it is not known whether these methods are excessive when extrapolated to non-domestic roofs.

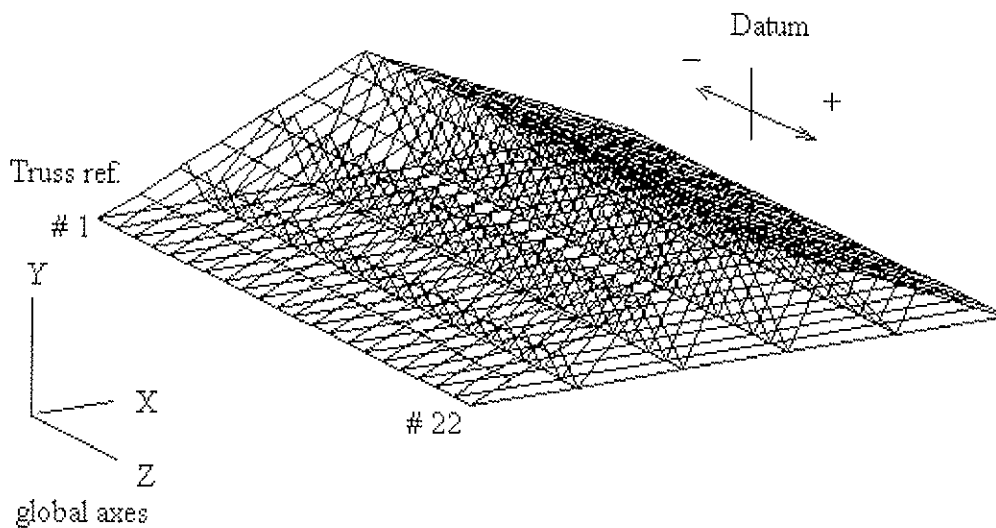
The work detailed in this paper is part of a three-year research project, the objective of which is to develop the information necessary to produce authoritative design guidance on bracing in non-domestic timber trussed roofs, for use by the truss rafter industry, structural engineers, architects and other roof designers, control and approving authorities.

A recent review of recurring faults in timber trussed rafter roofs [3] highlighted the importance of effective design and installation of roof bracing. Inadequate provision of roof bracing was linked to substantial lateral movement of roof and walls, often necessitating extensive remedial work and, occasionally, rebuilding of complete structures.

2. Test Method

2.1 Test Roof Specification

Experimental focus in this research programme has been placed upon a test roof consisting of 22 trusses of 11m span at a pitch of 22.5°, as detailed in Figure 1.



Span	11000 mm	Top Chord	35x120 mm
Top Chord Pitch	22.50°	Bottom Chord	35x97 mm
No. of Trusses	22	Web Members	35x72 mm
Truss Centres	600 mm	Overhang	410 mm
Top and Bottom Chord Grade	M75	Overhang Cut	Plumb
Web Grade	M50	Timber Treatment	Protim
Heel Joints	Standard	Nominal Bearing	100 mm

Figure 1 Test Roof Specification

Extra care was taken to construct the roof to the closest tolerance possible in an attempt to minimise the effects of deviations from plumb and straightness that are inevitably developed through the process of fabrication, transportation and erection of a structure of this type [4].

The roof is supported on a steel framework (see Figure 2) which was designed to cater for substantially greater loads than would be generated through testing of the roof.

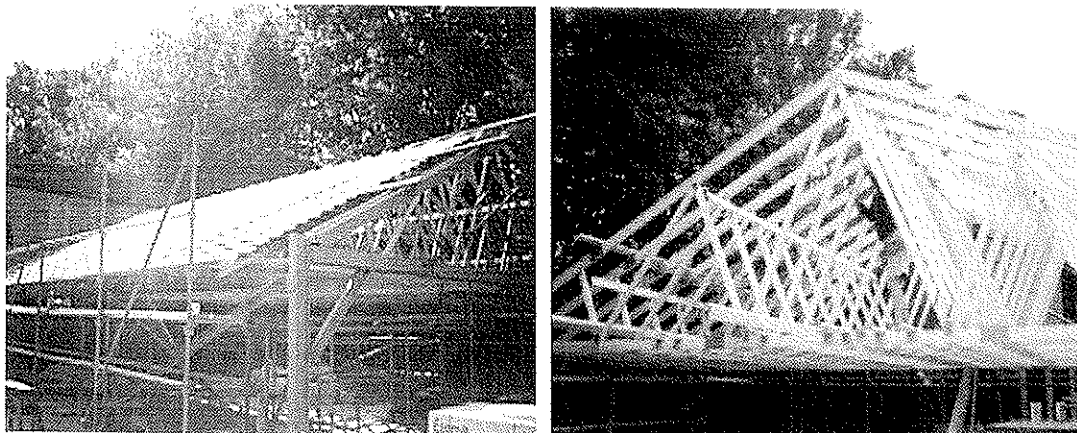


Figure 2 *Test Roof During Construction*

2.2 Test Series

The standard bracing details presented in Annex A of BS 5268 suggest that diagonal rafter braces should ideally be inclined at $45^\circ \pm 10^\circ$ in the plane of the rafter [2]. However, in some instances, especially in large roofs, designers may wish to consider steeper or shallower bracing angles. Tests were therefore carried out on a wider range of angles as described in Table 1.

The roof construction was varied between tests with respect to the bracing configuration employed. An initial test (i) was performed on the roof with only longitudinal bracing, tile battens and roof felt in place. Then a single line of diagonal bracing was introduced at rafter level, the angle being varied from 30° to 60° in subsequent tests.

Test	Diagonal Bracing Angle	Fixed at wall plate
i	no brace	n/a
ii	30°	✗
iii	30°	✓
iv	45°	✗
v	45°	✓
vi	60°	✗
vii	60°	✓

Table 1 *Outline Of Test Programme*

The standard details given in Annex A of BS5268 [2] also indicate that rafter braces should be nailed to the wall plate. This was found to be impractical in the case of the test roof due to the conflicting geometry of the various timber members that form the roof structure. This observation instigated an investigation of the implications of the fixity of the bracing at wall plate level on the whole roof performance. Tests were performed with no positive connection at the wall plate level and also with a simple detail for connection at this location, as shown in Figure 3. This detail was located as close to the wall plate as possible without conflicting with nail-plate locations (c. 250mm from wall plate), and was chosen on the basis that it is both simple to construct and not overly robust when compared to the rest of the structure.

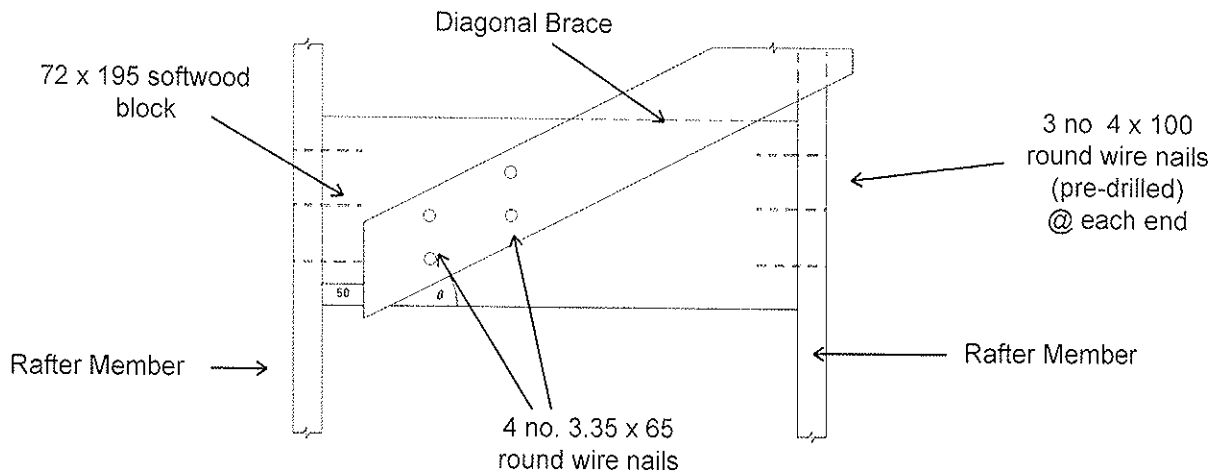


Figure 3 *Wall Plate/Bracing Connection Detail*

2.3 Load Application

In these tests, load was applied to the roof in the lateral direction only (global Z as identified in Figure 1).

Through consideration of previous tests on full scale roofs [5] it was decided that testing should comprise of repeated load cycles within a safe deflection limit range.

Load was applied at rafter level through a series of hydraulic jacks. The load application points were also locally stiffened with noggings (as shown in Figure 4) in an attempt to minimise any localised deformations induced in the members of the directly loaded rafter.

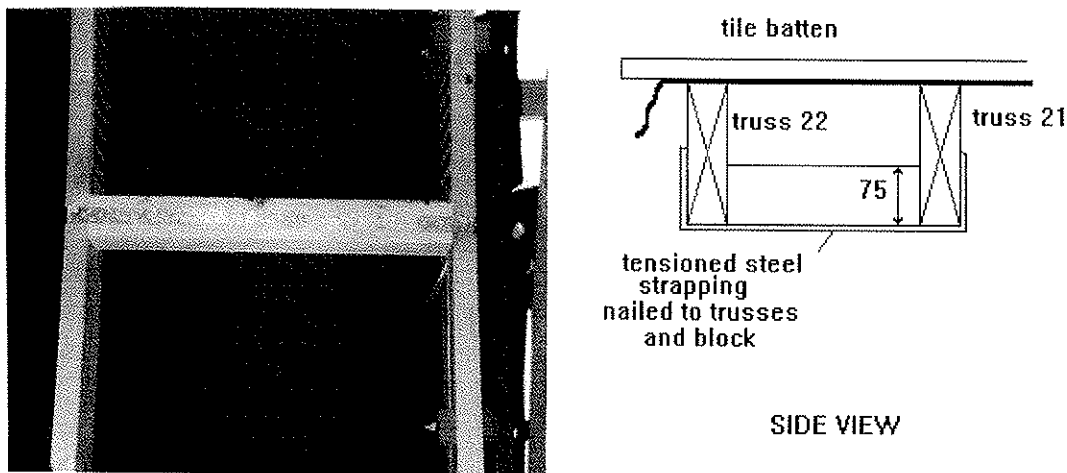


Figure 4 *Nogging Detail at Load Application Locations*

2.4 Deflection Measurement

Deflections were recorded using an arrangement of electronic transducers and visual gauges (see Figure 5) supported on a scaffold framework securely fixed to the steel test base.

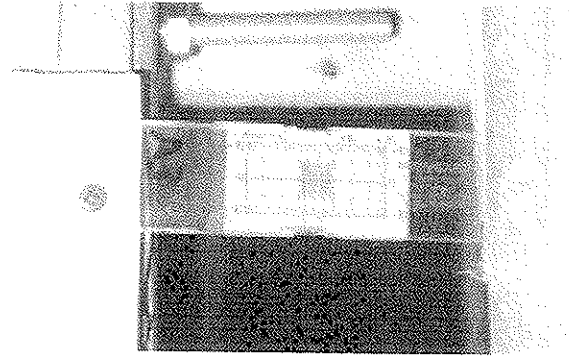


Figure 5 Visual Measurement Gauges

2.5 Test Procedure

Initial readings were taken from all gauges at zero load. The load was then applied in predetermined increments, recording deflections at transducer locations at each increment. At maximum load, instantaneous readings were taken, and the load was maintained whilst the visual gauges were read. During this time, periodic recordings were made of transducer deflections. Load was then released and instantaneous readings taken. The structure was then allowed to recover for approximately 5 minutes under no load. The visual gauges were then read, with periodic recordings being taken during this period. This procedure for loading and recording was repeated over four cycles for loads applied in both directions, (positive and negative senses of the Z-axis shown in Figure 1).

3. Results

3.1 Initial Tests on Unbraced Roof

The initial test on the roof system, carried out with only longitudinal binders, roof felt and tile battens in place, showed that the roof had a very low resistance to load in this unbraced state. This is as would be expected and is in agreement with previous work in this area [5,6].

This preliminary test also indicated that there was negligible bias between the two hands of the roof in terms of the stiffness, but that there was a slight directional bias in the stiffness of the unbraced roof subjected to lateral load in the global Z-axis described previously.

3.2 General Roof Behaviour

An example of a portion of the deflection curves recorded on successive loading cycles, in this case at the ridge position of the loaded rafter, is illustrated in Figure 6 which shows the progression of deflection (u/mm) with moment applied to the end rafter (M/kNm).

It can be seen that on successive loading cycles, the recorded deflections relative to the initial position increase, but that the difference between deflections on successive loading reduces. Comparing deflections on the third and fourth cycle of load, the difference is very low and the net deflection is almost identical.

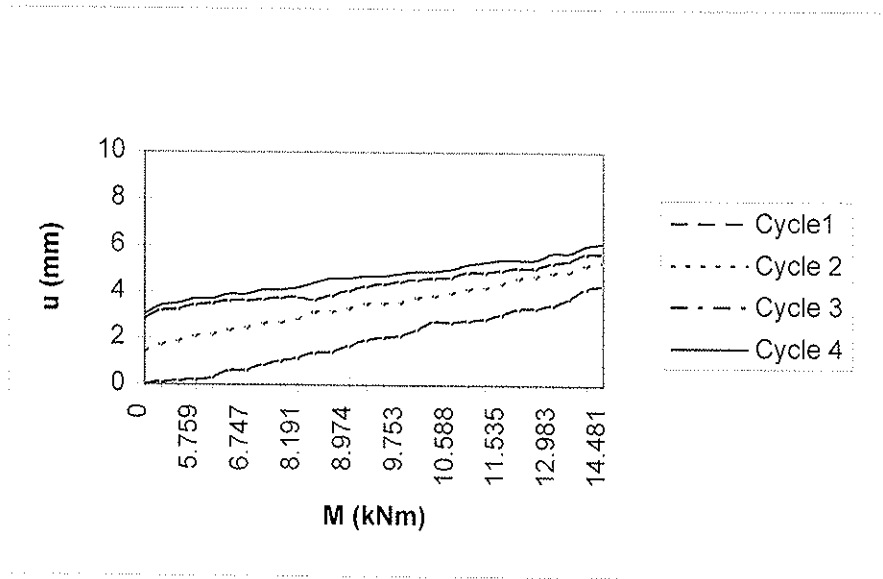


Figure 6 Extract From Cyclic Curve Set

3.3 Variations in Bracing Angle

The effect of the different bracing angles (in the case where the bracing ends are not fixed at wall plate locations) are compared to the unbraced roof results in Figure 7, for tests with lateral load applied in both directions (i.e. push and pull).

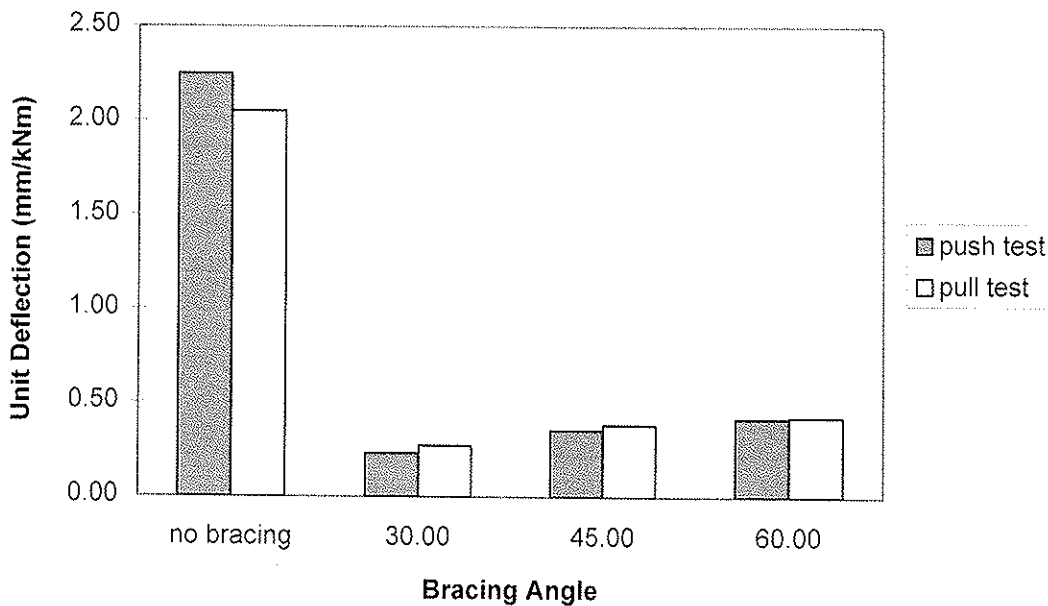


Figure 7 Relative Effectiveness Of Bracing Over A Range Of Angles As Compared To The Roof Structure With Only Longitudinal Binders.

From these results it is clear that the bracing has a substantial effect in stiffening the roof. The directional bias in the roof is also reduced in magnitude and a change in the direction of the bias is observed, also indicating that the effect of the bracing is dominant over the effect of the remainder of the roof. The reduction in deflection is expressed in percentage terms in Table 2.

Bracing Angle (°)	'Push' Test U Reduction (%)	'Pull' Test U Reduction (%)
30	90	87
45	84	81
60	82	80

Table 2 Percentage Deflection Reductions Related To Bracing Angle

3.4 Variations in Wall Plate / Bracing Connectivity

The effect of fixing the ends of bracing at wall plate level, using the simple detail illustrated previously, upon the deflection flexibility of the roof is illustrated in Figure 8.

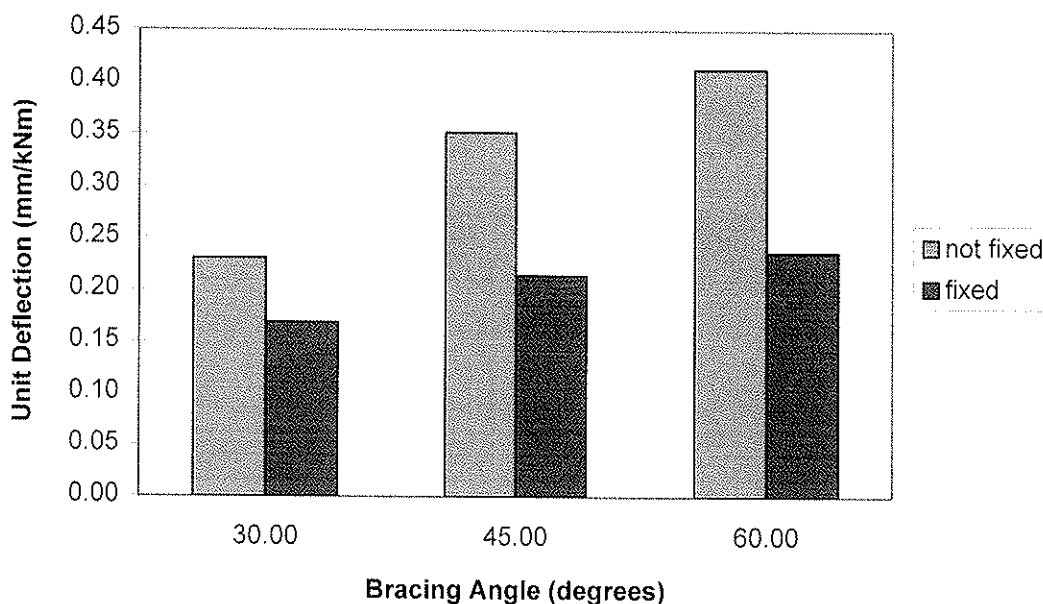


Figure 8 Relative Effectiveness Of Bracing With Free And Fixed Ends At Wall Plate Locations, Over A Range Of Bracing Angles.

From these results it is clear that enhancement of the fixity of the ends of bracing members, through the introduction of even a simple detail requiring minimal effort and material, can have a substantial effect upon the stiffness of the roof. The percentage reductions in ridge deflection in this instance are reported in Table 3. It is

interesting to note that the effect of this enhancement is greatest where the bracing is least effectual, i.e. at the steepest bracing angle.

Bracing Angle (°)	Ridge Deflection Reduction (%)
30	27
45	39
60	43

Table 3 Reduction in Ridge Deflections Where Bracing Fixity Enhanced At Wall Plate Level.

4. Comparison With Simplified Model

A simplified model of the roof for hand calculation purposes is shown in Figure 9.

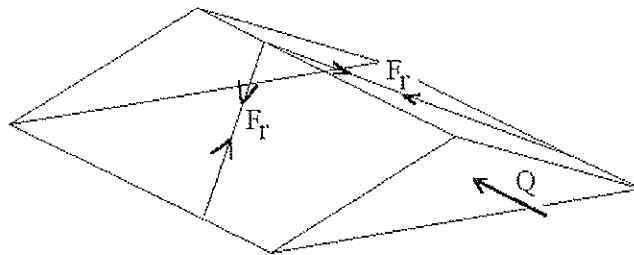


Figure 9 Basis of Simplified Roof Model For Hand Calculation

Considering an applied load 'Q' acting on the end of the roof, it is clear that there are two possible components that can develop resistance to the load:

- the inherent stiffness of the unbraced roof structure comprising trusses, binders and tile battens, as recorded in test i);
- the development of tension in the diagonal rafter braces.

$$R = 2 F_r \cos \theta + R_i \quad (1)$$

Where

- R= Resistance of roof against applied load
- F_r = Force developed in the diagonal brace on each side of the roof
- θ = Bracing slope angle
- R_i = Inherent resistance of the unbraced roof against applied load

The theoretical relative effectiveness of the bracing in the range of angles considered in the tests, based on equation (1), is shown in Table 4.

θ	R (kN/mm)
30°	1.73 $F_r + R_i$
45°	1.41 $F_r + R_i$
60°	1.00 $F_r + R_i$

Table 4 Load Resistance Over a Range of Bracing Angles

Assuming that the variation of force that can be developed in the diagonal bracing in each case is minimal, and subtracting the recorded stiffness of the unbraced roof from the results of the tests with braces fixed at wall plate locations, the relative effectiveness of bracing compared to the 'standard' 45° specification can be derived. Table 5 shows how this compares to the relative effectiveness from the simple calculation based on equation (1).

Angle	Simple Calculation	Tests iii), v) & vii)
30°	1.23	1.12
45°	1.00	1.00
60°	0.71	0.76

Table 5. Relative Effectiveness, Compared To 45° 'Standard' Bracing

It is clear that even from these simple approximations of bracing effectiveness, that the relative performance of bracing can be related to its angle of inclination to gain an approximate measure of its likely performance.

The simple relationship between approximation of the effectiveness of bracing and angle of inclination can also be observed in the data produced for previous tests carried out on smaller scale roofs [5,6].

5. Comparison With EC5 Bracing Requirements.

The bracing of truss systems is detailed in section 5.4.5.3 of EC5:Part1.1 [1]. The guidance relates to the definition of a load, q_d , which the brace should be able to resist in addition to the normal horizontal loads considered in the design:

$$q_d = k_1 \frac{nN_d}{30l} \quad (2)$$

where

$$k_1 = \min. \left\{ \begin{array}{l} 1 \\ \sqrt{15/l} \end{array} \right. \quad (3)$$

and

- n = number of members
- N_d = mean design axial compression force in member
- l = length of member

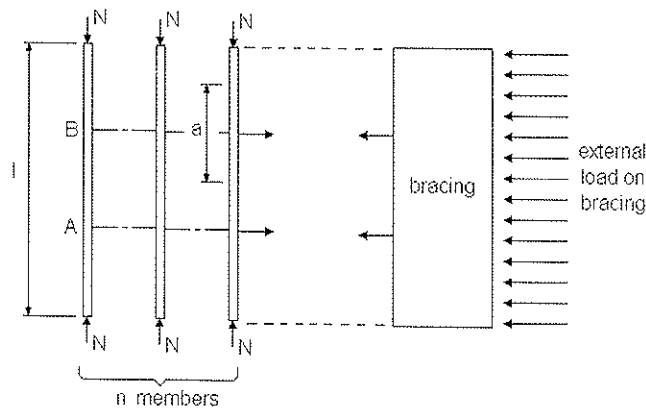


Figure 10. Truss System Requiring Lateral Supports [1]

The horizontal deflection permitted in EC5 under this load is set at a limit of $l/700$ (Cl. 5.4.5.3.(2)), which in the case of this test roof is approximately 8.6mm. Relating this limit to the moment induced by the buckling load results in a series of limiting unit deflections, as reported in Table 6 along with the values of q_d calculated for this roof.

Load Condition	q (kN/m)	u_{max}/M (mm/kNm)
Top Chord: Dead Load + snow Bottom Chord: Dead Load + Imposed Load	2.21	0.22
Top Chord: Dead Load + snow Bottom Chord: Dead Load + Imposed Load (No Uplift)	1.85	0.26
Top Chord: Dead Load Bottom Chord: Dead Load + Imposed Load (Snow & Uplift Cancel)	1.32	0.36

Table 6. Calculated Buckling Loads.

Comparing these values to those obtained in the tests (see Figure 8), it is apparent that the required effectiveness of the bracing given in Table 6 (0.22 mm/kNm for the braced roof) is satisfied by the ‘standard’ 45° brace when fixed at wall plate locations, but not where the ends are free. It should be noted that no other bracing elements (such as web chevrons) have been included in the tests, but would be incorporated following the BS5268 [2] standard details.

6. Discussion

It has been found that all of the aspects investigated in these tests have an appreciable effect upon the stiffness of the roof, which in its unbraced state is minimal.

Although a slight bias was observed in the directional performance of the roof with regard to resistance to lateral load, the introduction of bracing reduced such effects to a negligible level. This shows that the overall system is being dictated by the bracing and is in agreement with previous research which concluded that there is no

significant difference between the performance of such bracing acting in tension and compression [5].

The effectiveness of diagonal rafter bracing is related to the slope angle at which the bracing is installed. Based on the limited number of full scale tests possible, it has been found that consideration of the simple geometric relationship between forces to be resisted for equilibrium under applied load, produces a reasonable approximation of the effectiveness of the braces in these tests. It should however be remembered that these studies are based on a single geometric configuration, believed to be representative of a large proportion of UK non-domestic type timber trussed rafter roofs, and extrapolation of these results remains un-investigated to date.

Enhancing the fixity of the diagonal rafter braces at the wall plate locations has been found to increase the effectiveness of the bracing and hence enhance the overall stiffness of the roof. Although, within the serviceability limits of the structure this may be seen as beneficial, there are concerns associated with the promotion of localised stiffening. The roof structure has a number of systems for resisting load such as ceiling diaphragm action, chevron bracing, longitudinal binders, etc. In order to mobilise the contributions of each component, there must be interaction and hence distribution of load. Introduction of high localised stiffness may restrict the distribution of load, thus leading to a situation whereby the majority of the load within the structural system is concentrated in comparatively few elements. This is not a problem if the structure remains within its service limits, but in the case of a failure within one of these elements (through accidental loading for example), the resultant sudden release of load may be catastrophic upon the roof structure. Considerations such as this are recognised in reinforced concrete design [8], whereby ‘under-reinforcement’ is often preferred, in order to promote a gradual failure in preference to a sudden failure at higher load.

It is important to note that in constructing the roof, the bracing angle was found to have an influence upon the ease with which it could be incorporated. The 30° bracing, although found to be very efficient, was more problematic to install due to the geometric interference with truss rafter web members. Common faults encountered in roof bracing include incomplete diagonal bracing, inadequate lapping of bracing and incorrect fixing [3]. Since the ease of installation can have an effect upon the likely levels of obtainable workmanship, this might be an important consideration.

Adoption of shallower bracing angles also has implications regarding the erection sequence of a roof. It is common to install the diagonal rafter brace to permanently stabilise a number of trusses before proceeding to erection of further trusses. It is therefore desirable, from a safety point of view, to minimise the number of trusses reliant upon temporary bracing at any one instant. A decrease in the bracing angle will lead to an increase in the number of temporary braced trusses prior to fixing of a complete run of effective permanent diagonal bracing.

Additional practical considerations such as these, that may influence roof designers, may lead to adoption of target angles closer or equal to the conventional 45° [2,7] commonly used in the UK at present.

7. Conclusions

The results of these tests have shown that the roof structure with only longitudinal binders and tile battens in place offered only minimal resistance to applied lateral loads. The introduction of even a single diagonal bracing member in a roof of this type has a large influence on the stability and lateral stiffness.

The effectiveness of the bracing is affected by the angle of slope in the brace and the robustness of connection between brace end and wall plate connections. It has been found that the relative effectiveness of the bracing can be approximated to a reasonable degree by the cosine of the angle of inclination of the bracing. Improvements in the robustness of connection details at the wall plate end of bracing provide significant enhancement to the overall roof stiffness, reducing measured roof deflections by approximately 30 – 40 %, dependent on angle of inclination of bracing.

It is believed that although shallow angled bracing has been shown to be structurally more efficient than steep angled bracing, 45° is still a preferable target angle. Designers should consider aspects such as the ease of installation and effects on the erection process before varying from this 'standard' detail.

8. Further Work

Testing is continuing on the roof , investigating aspects such as contribution of plasterboard ceilings and relative effectiveness of different configurations of bracing elements; e.g. chevron bracing systems.

The results are also to be used for comparison with a computer model of the roof . If this model proves successful, then further aspects of performance not incorporated in the test programme can be investigated.

The overall aim of this project is to produce authoritative design guidance, which will draw on the findings of these studies.

References

- [1] BSI, (1994). DD ENV 1995-1-1:1994. Eurocode 5: Design of Timber Structures. Part1.1 General Rules and Rules For Buildings. BSI, UK.
- [2] BSI, (1997). BS5268:Part3:1995. Structural Use of Timber, Part3. Code of Practice For Trussed Rafter Roofs. Final Draft for Unofficial Comment, BSI Doc 97/102776, BSI, UK.
- [3] GORDON, J.A. (1993). Recurring Faults in Trussed Rafter Roofs. Building Control, November 1993 issue, UK.
- [4] BAINBRIDGE R.J., STUDER T. and REFFOLD A.(1997). Survey Of A Non-Domestic Timber Trussed Test Roof And Supplementary Nail Joint Tests. International Conference of IUFRO S5.02 Timber Engineering, Copenhagen, Denmark.
- [5] HARROD, P.S.K. (1978). Lateral Loading Tests On A Full Size Trussed Rafter Roof. Building Research Establishment Note N26/78, BRE, UK.
- [6] MAYO, A.P. (1982). Trussed Rafter Roofs - Load Distribution And Lateral Stability. Building Research Establishment Information Paper IP 14/82, BRE, UK.
- [7] I.T.P.A.(1995). I.T.P.A. Technical Handbook. SfB G12, Rev:0395, International Truss Plate Association, UK.
- [8] KONG, F.K. and EVANS, R.H. (1980). Reinforced and Prestressed Concrete, 2nd Edition. Van Nostrand Reinhold (UK) Co. Ltd., Wokingham, UK.

**INTERNATIONAL COUNCIL FOR BUILDING RESEARCH STUDIES AND DOCUMENTATION
WORKING COMMISSION W18 - TIMBER STRUCTURES**

**CYCLIC PERFORMANCE OF PERFORATED WOOD SHEAR WALLS
WITH OVERSIZE ORIENTED STRAND BOARD PANELS**

by

Ming He
H Magnusson
F Lam
H G L Prion
Department of Wood Science
University of British Columbia
Canada

MEETING THIRTY

VANCOUVER

CANADA

AUGUST 1997

Cyclic Performance of Perforated Wood Shear Walls with Oversize Oriented Strand Board Panels

Ming He
Henrik Magnusson
Frank Lam
Helmut G.L. Prion

Department of Wood Science
University of British Columbia
Canada

1 Abstract

This paper reports the test results obtained from a study to investigate the influence of openings on the lateral resistance of wood based shear walls built with both standard and oversize oriented strand board panels under monotonic and cyclic loading conditions. Eight walls were tested, using either standard 1.2×2.4 m panels or one full size 2.4×7.3 m oriented strand board panel. Commonly used wood frame construction details were employed, using 38×89 mm No. 2 and better Spruce Pine Fir framing components. Test results showed that the application of nonstandard oversize panels significantly improved the performance of the perforated shear walls compared with standard 1.2×2.4 m panels. Door and window openings caused a significant decrease in the strength and stiffness of the walls and precipitated a change in failure mode, especially for walls with full size panels. While nail failure modes were commonly observed in walls without openings, a combination of nail and panel failures were observed in shear walls with openings. Final failures typically affected the wall performance once the plastic deformation region was reached, which was displayed in the tests in the form of either panel buckling or panel tearing at the corners of door and window openings. A newly proposed cyclic test protocol was used which consisted of fewer but more severe displacement excursions, compared to many other test protocols. This was believed to better reflect typical earthquake excitation and avoid low cycle nail fatigue failures, which were observed previously with long cyclic test protocols.

2 Introduction

Wood based shear wall and diaphragm systems provide buildings with three major load carrying components to resist (i) vertical loads, (ii) transverse wind loads and (iii) in-plane lateral forces imposed by wind and seismic loading. These systems typically are composed of lumber framing members sheathed with 1.2×2.4 m plywood or oriented strand board panels and connected by nails. Wood frame construction has a history of excellent performance against lateral loading especially in residential applications. For example, in the 1995 Kobe earthquake in Japan, it was evident that residences built with North American wood based shear wall techniques (2x4 platform construction) survived major seismic forces with relatively little damage even in sites of serious liquefaction of the supporting ground.

Even though this type of construction has proven to be cost-effective and structurally sound for residential low-rise buildings, its structural integrity under the action of natural hazards such as earthquakes and wind is not necessarily guaranteed, especially in multi-storey buildings and when large openings exist. In the past few decades much experimental work was done on the structural behavior of wood based shear wall systems without or with openings. Based on the previous studies on full size shear walls or even full scale buildings under static lateral loads, perforated shear wall systems were studied under static and dynamic loading conditions (Patton-Mallory *et al.* 1985, Falk and Itani 1987, Sugiyama 1994, White and Dolan 1996, Line and Douglas 1996). Long shear walls (2.4×12 m) with openings (Johnson and Dolan 1996) and perforated shear walls with large panels (4.8×4.8 m) (Enjily and Griffiths 1996) have also been investigated. It was observed that under monotonic loading conditions the reduction in racking strength and stiffness of perforated shear wall were related to the area of the openings. Empirical equations were developed by Patton-Mallory *et al.* (1985) (specifying the ratio of effective wall length) and by Sugiyama (1994) (using the sheathing area ratio) to calculate the strength loss due to openings. Experimental results show that Patton-Mallory's equation tends to overestimate the initial stiffness and ultimate load capacity of shear walls with openings (Patton-Mallory *et al.* 1985), while Sugiyama's equation provides a conservative estimate of the shear load ratio at ultimate capacity (Johnson and Dolan 1996). The results also indicated that along with the increase of the area of openings, the governing design criterion may more reasonably be serviceability (stiffness) rather than ultimate load (strength) (Patton-Mallory *et al.* 1985, Enjily and Griffiths 1996). Under dynamic loading, shear walls with openings generally exhibited lower damping ratios than similar walls without openings (Falk and Itani 1987).

The study described in this paper was part of a comprehensive study on the lateral resistance of wood based shear walls built with regular and oversize oriented strand board panels. The previous phase of the study focused on the performance of walls without openings and produced encouraging results, showing significant improvements when full sized panels were used. The objective of this study was to experimentally investigate the structural performance of perforated wood based shear wall systems built with either standard 1.2×2.4 m or nonstandard large dimension 2.4×7.3 m oriented strand board panels under monotonic and cyclic lateral loading conditions.

3 Experimental Studies

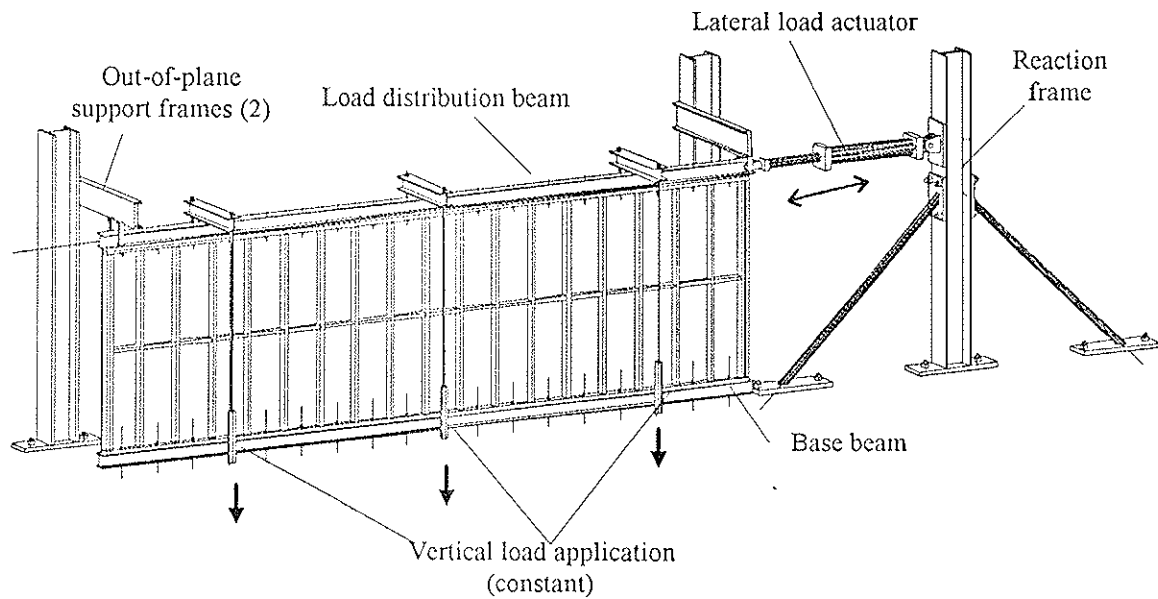
3.1 Test Facilities

Fig. 1 shows the schematics of a typical shear wall test specimen with staggered regular size sheathing panels. The test specimen was mounted in the load assembly with variable in-plane lateral load applied by a 222 kN servo-controlled hydraulic actuator along the top of the wall through a steel load distribution beam that was bolted to the wall. The actuator with an inline load cell was mounted onto the reaction frame through a pin connection 2.5 m from the ground. A MTS Micro-controller (458.10) and Material Testing Function Generator (Exact-340) were used to drive the actuator in a displacement control mode to develop the required lateral loading pattern.

The wall specimen was attached to the W150 × 22 steel load distribution and base beams using 12.7 mm diameter class 5 steel bolts at a spacing of 0.4 m. The assembly was then erected with the base beam attached to the test floor and the load distribution beam connected to the hydraulic actuator at one end. Out-of-plane supports were provided at the two ends of the load distribution beam.

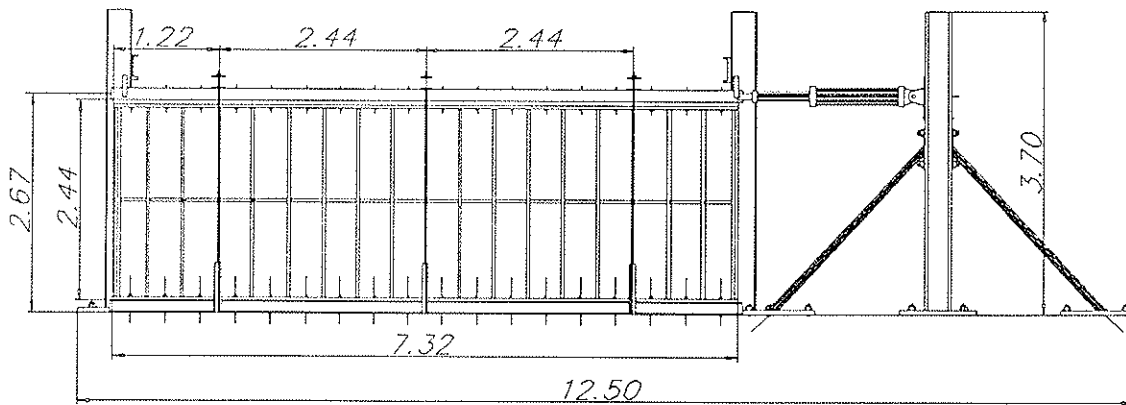
Six hydraulic jacks, each with a pressure capacity of 17.24 MPa, were mounted to the test floor and attached through 2.1 m long threaded steel rods (diameter 12.7 mm) to the top of the load distribution beam. The jacks were positioned symmetrically about the center of the wall with a spacing of 2.4 m, and provided a static distributed vertical load of 66.7 kN on the wall through the load distribution beam. The vertical load represented an equivalent occupancy load of 5.0 kPa from two stories over an area of 7.3 × 7.3 m, supported by 4 walls.

A 386/25 personal computer data acquisition system with 16 channels and LabTech Notebook® data acquisition software were used to collect the experimental data at regular time intervals. The data collected included the lateral load, vertical load, actuator displacements, lateral displacements at the top of the shear wall, uplift at the base of the shear wall, and relative movements between panel and frame at various locations. The sampling frequency was 10 Hz for cyclic load conditions.



(a)

Dimensions in meter



(b)

Fig. 1. The Scheme of Shear Wall Test Setup Assembly

3.2 Test Wall Configurations

The test shear walls, 2.44×7.32 m in dimension, were constructed in the laboratory, employing standard wood frame construction details and using No. 2 and better Spruce Pine Fir 38×89 mm lumber as framing members. A Bostitch-N80CB air driven nail gun with coil fed 76 mm common nails was used to connect the members. The stud members (2.4 m in length) were spaced 400 mm apart. The top plate and the end studs consisted of double members while the bottom plate and the interior studs consisted of single members. Performance Rated W24 oriented strand boards (CSA-0325.0-M88), 9.5 mm thick, were used

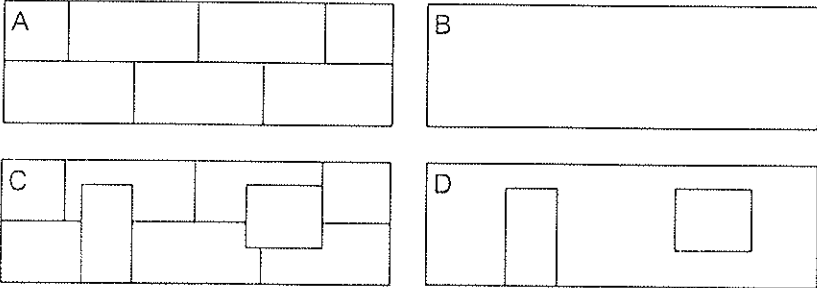
as sheathing panels. The sheathing panels were connected to the framing members with 50 mm air gun driven spiral nails.

Eight shear walls were tested with one replicate per test type (Table 1). In tests 1, 3, 5 and 7, regular 1.2 × 2.4 m panels were used with continuous blocking installed at mid-height of the walls. The regular size panels were staggered and oriented with their long axes parallel to the length of the wall, as shown in layout A, Table 1. In all the other tests, 2.4 × 7.3 m oversize panels were used (layout B, Table 1). Door and window openings were introduced to walls 3, 4, 7 and 8 as shown in layouts C and D in Table 1. The locations and dimensions of the door and window, as shown in Fig. 2, were selected in accordance with the “Canadian Wood-Frame House Construction” guide (Canada Mortgage and Housing Corporation 1985). At the vertical edges of openings, studs were doubled with the inner studs cut to reach the lintels which were end-nailed through the outer studs. The interior nail spacing in all the tests was 305 mm. In shear walls with regular 1.2 × 2.4 m panels, a standard nail spacing of 152 mm around the perimeter of the panels was used. In shear walls sheathed with oversize 2.4 × 7.3 m panels, two nail spacing patterns along the perimeter of shear wall were used: a 76 mm nail spacing in tests 2 and 6, and a 102 mm nail spacing in tests 4 and 8. These nail spacing patterns were used such that the total number of nails in the various walls was kept similar.

Table 1. Shear Wall Test Program

Wall No.	Panel size (m)	Openings	Panel layout ^a	Lateral load types	Nail spacing (mm)	No. of nails
1	1.2 × 2.4	N/A	A	Monotonic	152	424
2	2.4 × 7.3	N/A	B	Monotonic	76	409
3	1.2 × 2.4	YES	C	Monotonic	152	395
4	2.4 × 7.3	YES	D	Monotonic	102	391
5	1.2 × 2.4	N/A	A	Cyclic (FCC)	152	424
6	2.4 × 7.3	N/A	B	Cyclic (New)	76	409
7	1.2 × 2.4	YES	C	Cyclic (New)	152	395
8	2.4 × 7.3	YES	D	Cyclic (New)	102	391

^a Panel layout:



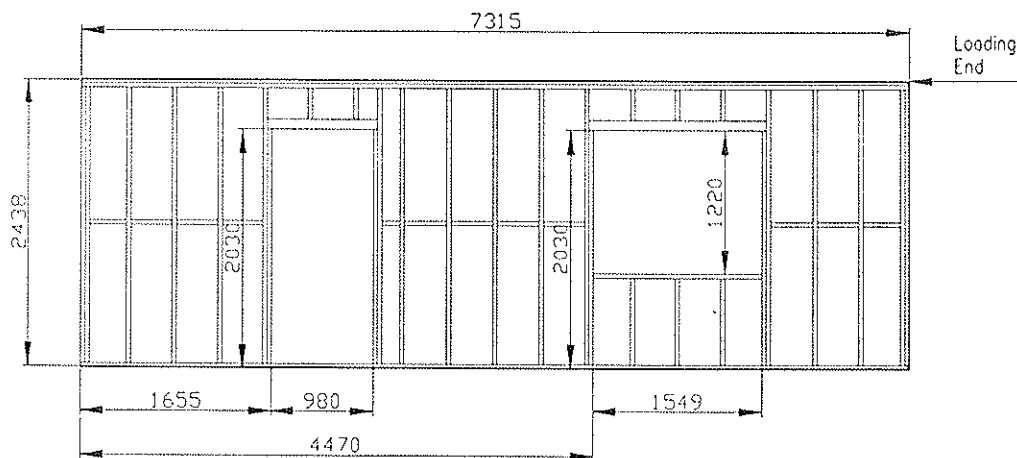


Fig. 2. Shear Wall Layout Showing Locations and Dimensions of Door and Window

3.3 Loading Schemes

Two types of loading schemes were used: monotonic loading for walls 1 to 4 and cyclic loading for walls 5 to 8. The loading rate for the monotonic tests was approximately 7.8 mm/min based on recommendations in the ASTM Standard E564-73.

In cyclic tests two protocols were used: Forintek Canada Corp. (FCC) cyclic test protocol in tests 5 and a newly proposed protocol in tests 6, 7 and 8 (He 1997).

Forintek Canada Corp. (FCC) Protocol (Karacabeyli 1995). The FCC protocol consists of a sequence of sinusoidal cycle groups, each of which contains three identical cycles (Fig. 3). The amplitude of each cycle group is taken as a percentage of the nominal yield slip (Δ_{yield}), and is increased stepwise, with inter-spaced decreasing cycles, until specimen failure (Fig. 3 and Table 3). The nominal yield slip is defined as the displacement at half of the maximum load obtained during a monotonic test. The maximum load (P_{max}) and yield point (Δ_{yield}) from the monotonic tests in wall 1, and cycle frequencies for shear wall 5 are listed in Table 2. The amplitudes of cycle groups as a percentage of the yield point for wall 5 are listed in Table 3. Both the amplitude schedules and the cycle frequencies were adjusted beyond cycle group 18 because of limited data storage capacity. At this cycle group, the maximum load had been well exceeded.

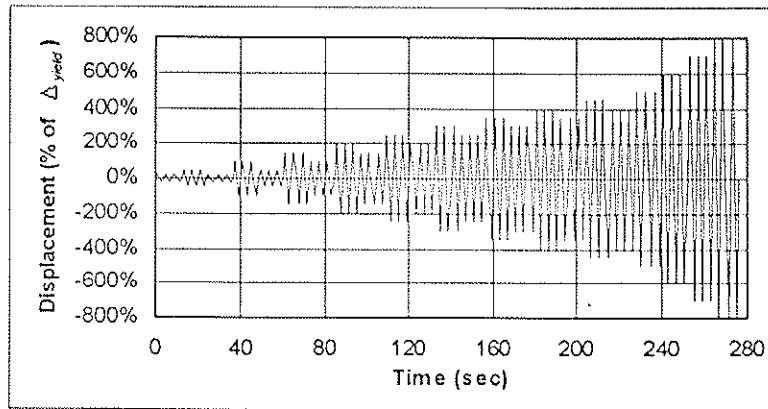


Fig. 3. FCC-Forintek Protocol

Table 2. Parameters in Cyclic Tests Using FCC Protocol

Wall	P_{max}^a (kN)	Δ_{yield}^a (mm)	Loading rate			
			Cycle group	Cycle frequency (Hz)	Cycle group	Cycle frequency (Hz)
5	62.8	10.0	1 to 19	0.25	20 to 22	0.083

^a The values were cited from the monotonic tests.

Table 3. Displacement Amplitude Schedule as a Percentage of Δ_{yield}

Cycle Group (1)	Wall No. 5 (2)	Cycle Group (1)	Wall No. 5 (2)	Cycle Group (1)	Wall No. 5 (2)	Cycle Group (1)	Wall No. 5 (2)	Cycle Group (1)	Wall No. 5 (2)	Cycle Group (1)	Wall No. 5 (2)
1	25%	5	50%	9	150%	13	250%	17	350%	21	700%
2	50%	6	150%	10	250%	14	350%	18	450%	22	800%
3	25%	7	100%	11	200%	15	300%	19	500%		
4	100%	8	200%	12	300%	16	400%	20	600%		

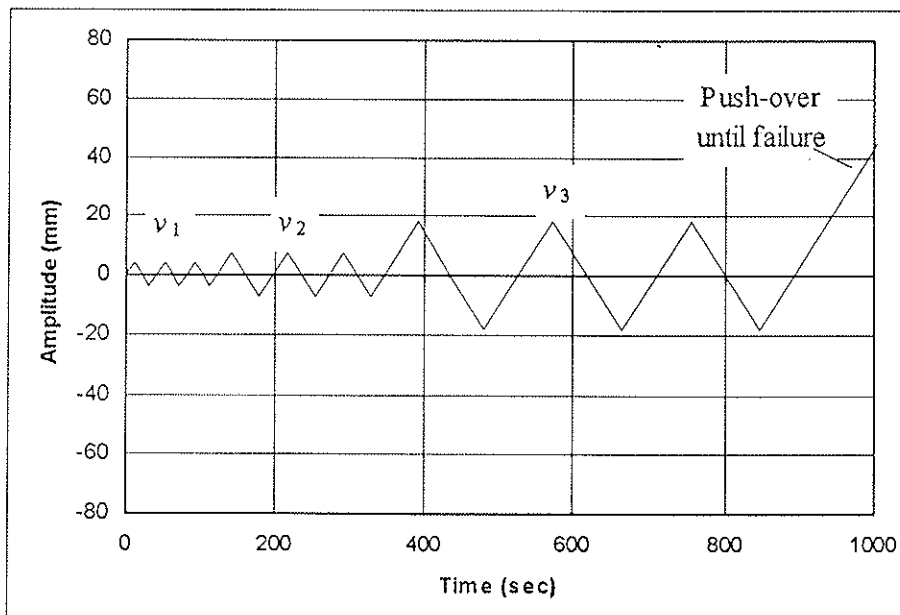
New cyclic loading protocol. The FCC test protocol is a particularly long test sequence, designed to capture the full stabilized load-deformation curve, which is typically obtained from the maximum load point of the third cycle in each group. Because of the extensive yielding induced in nails during the pre-ultimate part of the test, it was commonly observed that the nails failed due to low cycle fatigue and the wall would not be able to reach its maximum load carrying capacity. Such failures were rarely observed under real or simulated seismic conditions, however, and a new cyclic loading protocol was proposed to assure a more realistic failure mode. This proposed loading scheme, as used in shear wall tests 6, 7 and 8, consisted of two or three groups of cycles, three identical cycles in each

group, and one final unidirectional loading (push-over) until the wall failed. The amplitudes of these cycle groups, v_1 , v_2 and v_3 corresponded to the displacement at a certain percentage of the maximum load, obtained from the monotonic shear wall tests. All the parameters and the cyclic amplitude schedule are listed in Table 5 and illustrated in Fig. 4.

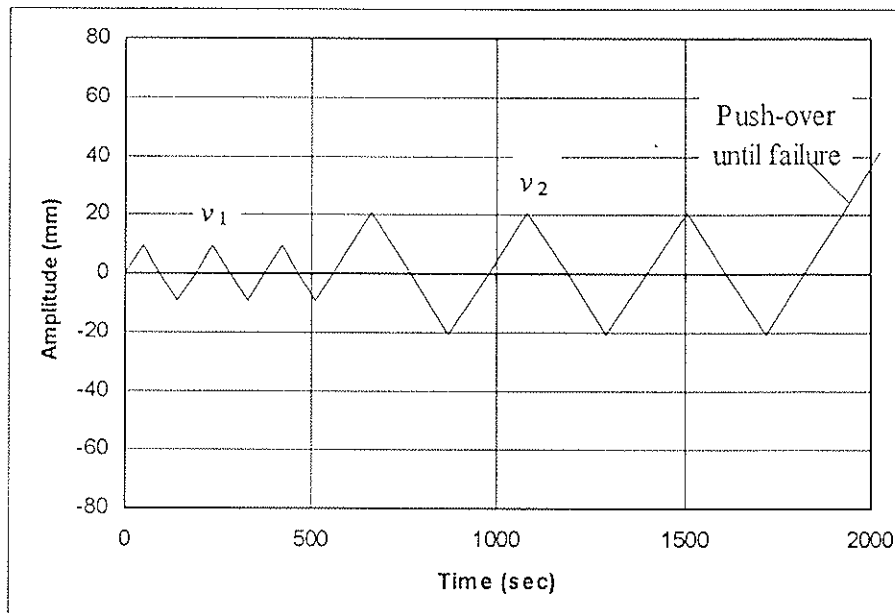
The number of cycle groups in tests 7 and 8 was reduced to two from three in test 6. In the first cycle group of the test 6 the displacement and degradation in strength and stiffness of shear wall were insignificant as this was well within the linear range of the wall (He 1997). As no data of importance was obtained during this cycle group, it was decided to eliminate this part of the test sequence in subsequent wall tests.

Table 5. The Parameters in Cyclic Tests Using New Protocol

Wall No.	P_{max} (kN)	v_1 (mm)		v_2 (mm)		v_3 (mm)		Loading rate (mm/sec)
		Value	Definition	Value	Definition	Value	Definition	
6	125.2	4.1	$\Delta_{0.35P_{max}}$	7.5	$\Delta_{0.5P_{max}}$	18.2	$\Delta_{0.8P_{max}}$	0.4
7	45.1	9.3	$\Delta_{0.5P_{max}}$	21.0	$\Delta_{0.8P_{max}}$	-	-	0.2
8	63.5	6.9	$\Delta_{0.5P_{max}}$	13.1	$\Delta_{0.8P_{max}}$	-	-	0.2



(a) Test protocol for wall 6



(b) Test protocol for walls 7 and 8

Fig. 4. New Cyclic Test Protocol

4 Test Results and Discussion

The following values, summarized in Table 6, were obtained from shear wall tests:

P_{max} : maximum load carrying capacity of shear wall (in cyclic tests for both positive and negative cycles), kN.

Δ_u : displacement of shear wall at maximum load, mm.

Δ_{yield} : yield slip defined as the top displacement of shear wall at half of maximum load, mm.

S_u : ultimate shear strength of shear wall, kN/m.

$$S_u = \frac{P_{max}}{L}, \text{ where: } L = 7.315\text{m, length of shear wall measured parallel to the loading direction.}$$

G' : shear stiffness of shear wall, MN/m.

$$G' = \frac{P_{max}H}{2\Delta_{yield}L}, \text{ where: } H = 2.438\text{m, height of shear wall.}$$

D : ductility factor.

$$D = \frac{\Delta_u}{\Delta_{yield}}$$

N : number of nail connectors between panels and frame.

Table 6. Shear Wall Summary Test Results

Wall	P_{max} (kN)	Δ_u (mm)	Δ_{yield} (mm)	S_u (kN/m)	G' (MN/m)	D	N
1	62.77	54.04	9.82	8.58	1.07	5.5	424
2	125.21	38.07	7.40	17.12	2.81	5.1	409
3	45.07	42.93	8.25	6.16	0.91	5.2	395
4	63.53	24.89	5.18	8.69	2.04	4.8	391
5	+59.29, -51.69 ^a	31.93	12.62	-	-	-	424
6	+115.33, -110.01	31.95	6.16	-	-	-	409
7	+46.15, -33.01	49.76	10.35	-	-	-	395
8	+68.74, -48.65	21.24	4.77	-	-	-	391

^a + \Rightarrow extension of the hydraulic cylinder, - \Rightarrow contraction of the hydraulic cylinder.

Note that in test 8 an error in the controlling system caused an instant push-forward of the hydraulic cylinder and an unexpected cycle was thus added to the wall before the stipulated loading scheme was applied. Degradations of both stiffness and strength in wall 8 can be observed in the cyclic test when the wall was subjected to a loading in the push-forward direction (upper right part in Fig. 9). It seemed that this impact load did not reduce the load capacity and stiffness of the wall in the pull-back loading condition (lower left part in Fig. 9).

4.1 Influence of Openings on Performance of Shear Walls

The monotonic test results (Table 6 and Fig. 5) show that openings significantly decreased the strength (S_u) and stiffness (G') of shear walls. With a 152 mm conventional nail spacing and built with regular sized panels, wall 3 (with openings) had a 28% drop in strength and a 15% reduction in stiffness compared to wall 1 (without opening). The static test results also show differences in the performance of shear walls built with oversize and regular panels. Comparisons between wall 2 (large panel, no opening) and wall 4 (large panel, with openings) indicate a 50% drop in strength and a 27% reduction in stiffness. By comparing the static test results between wall 4 (oversize panel with openings) and wall 3 (regular panel with openings) an increase of stiffness and strength of 124% and 41%, respectively, was observed. More significantly, compared to wall 1 (regular panels without opening), wall 4 had a much higher stiffness (91%) and reached a slightly higher peak load level with fewer nails.

It was also noticed that in wall 4, after the peak load level of 63 kN was reached, the oversize panel started to fail in the form of buckling and tearing at the corners of the door and window openings, resulting in an abrupt reduction of load carrying capacity. Upon continued loading, the sheathing panel was torn into three separate smaller panels. At approximately 45 mm wall displacement, the wall consisted essentially of three individual shear walls, similar to the wall

with regular panels, which was also demonstrated by the similar load-deformation curves of walls 4 and 3 after 45 mm of top wall displacement (Fig. 5).

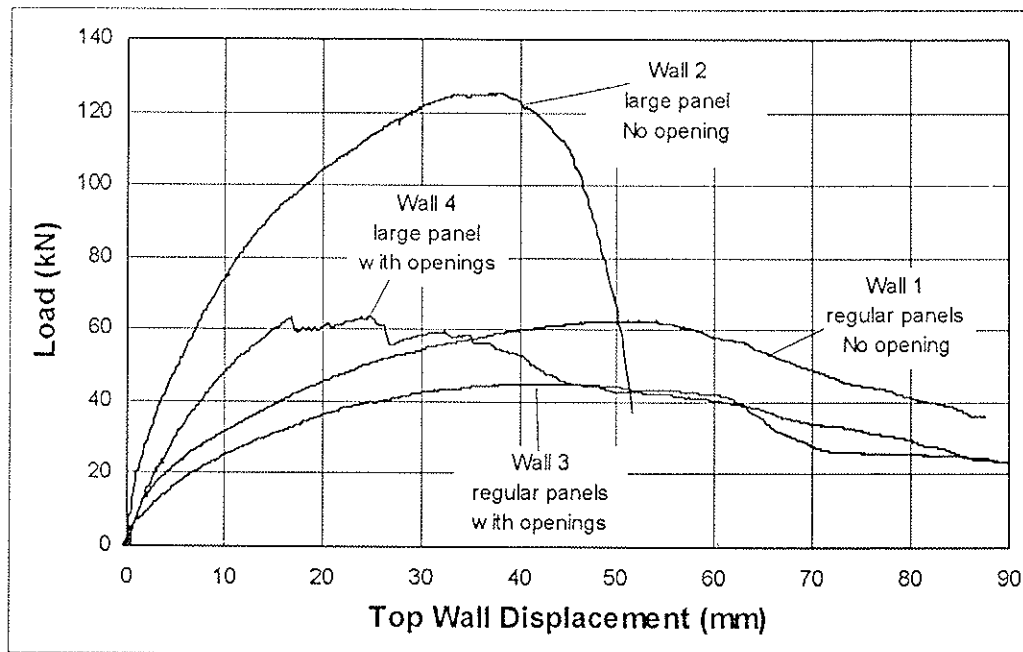


Fig. 5. Load Displacement Curves for Shear walls 1 to 4

Figs. 6 to 9 show the hysteresis curves from the cyclic tests together with the corresponding static envelope curves for walls 5 to 8, respectively. In each case, a mirror image of the monotonic curve was drawn in the lower left quadrant to compare with the cyclic curves during the negative displacement phases. The peak load values for the shear walls under cyclic loading conditions were very similar to those in the monotonic tests, with a variance ranging from 92% to 108%. Wall 5 (Fig. 6) was an exception in that it reached a maximum load of 59 kN at a much smaller displacement followed by a substantial drop in the load carrying capacity. This was caused by low cycle fatigue failure of the nails as a result of repeated reversed bending. To avoid nail fatigue failure, a new cyclic test protocol with fewer load cycles was proposed and used in tests 6, 7 and 8 (Fig. 4). All three walls reached their ultimate load in the push-over phase and exhibited very similar envelope curves for the monotonic and cyclic tests with slight variances in maximum load capacity and ductility. During these tests no nail fatigue failure was observed.

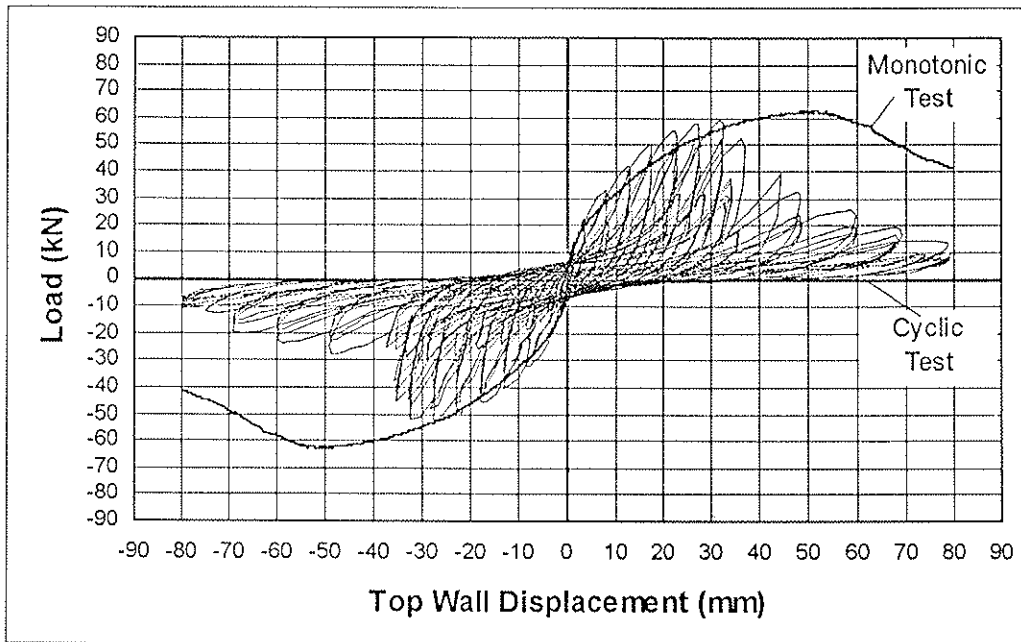


Fig. 6. Cyclic Load-Displacement Curve and Monotonic Envelope for Wall 5

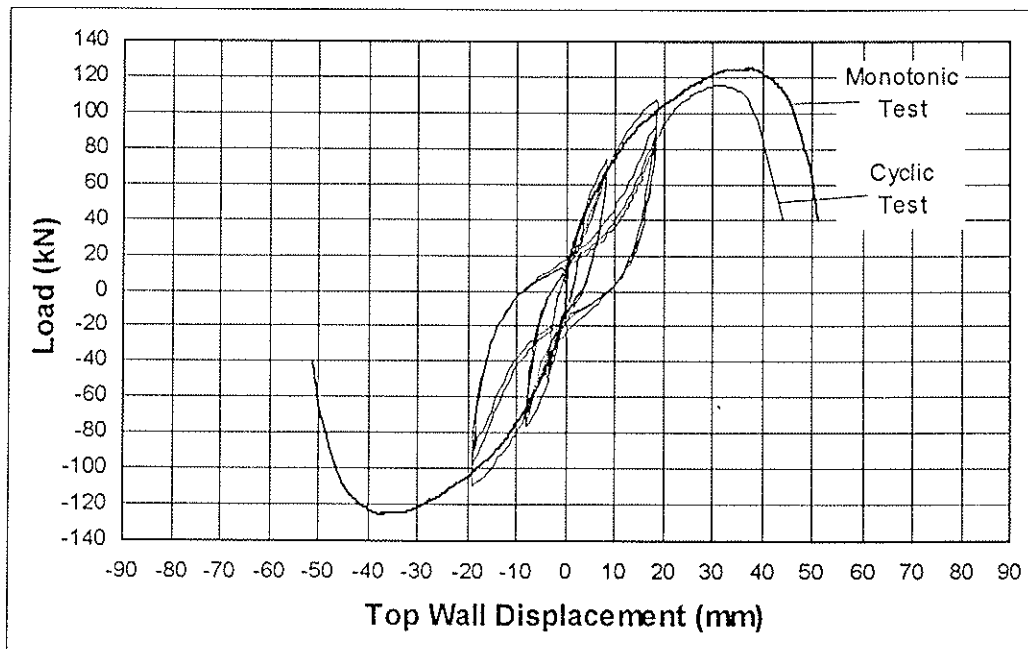


Fig. 7. Cyclic Load-Displacement Curve and Monotonic Envelope for Wall 6

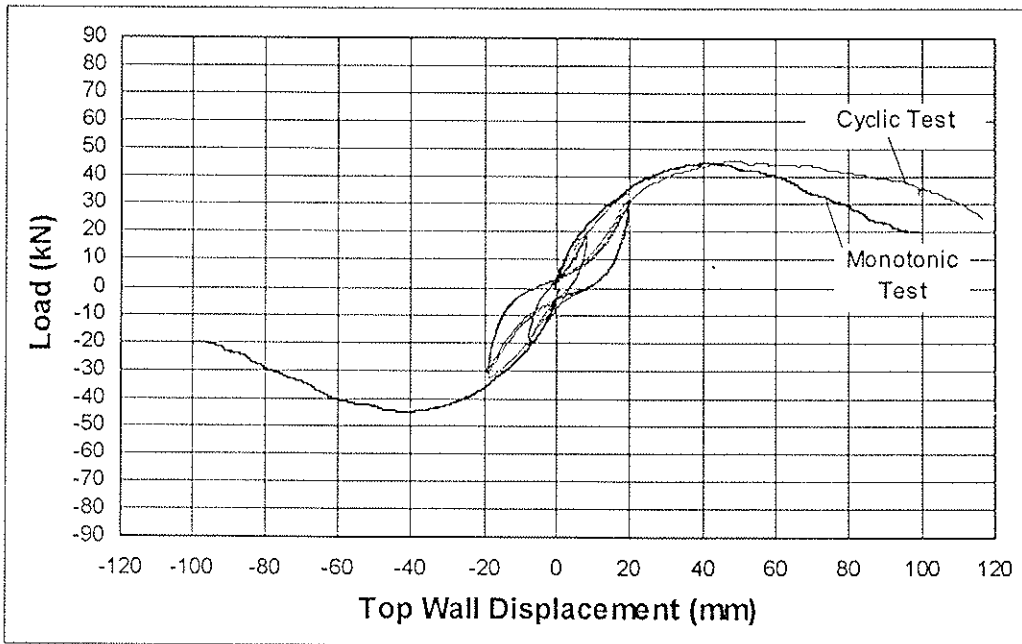


Fig. 8. Cyclic Load-Displacement Curve and Monotonic Envelope for Wall 7

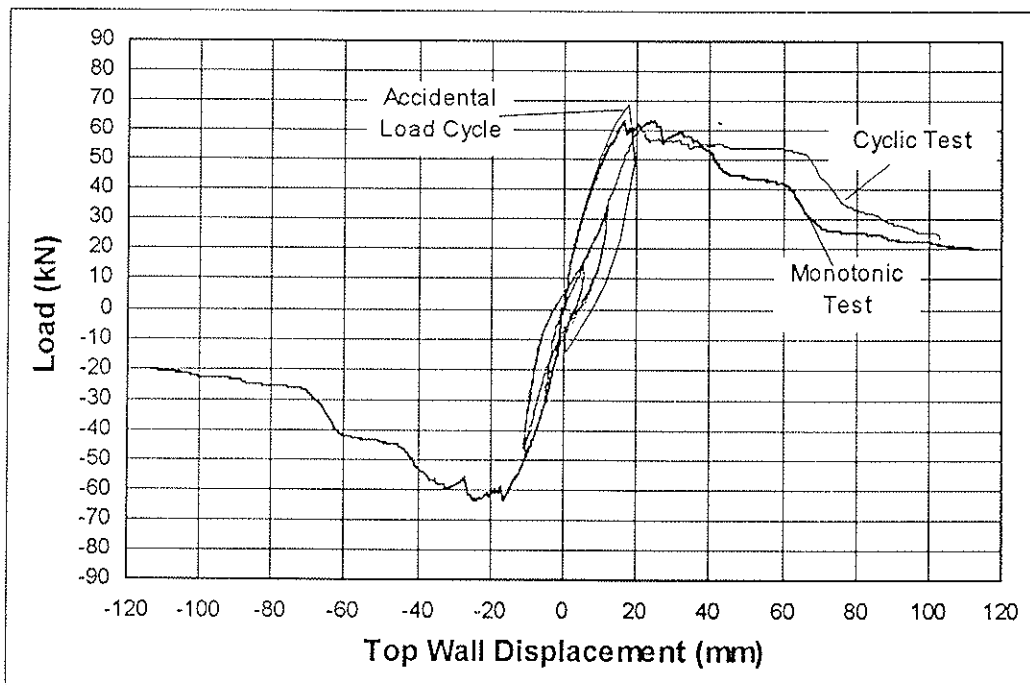
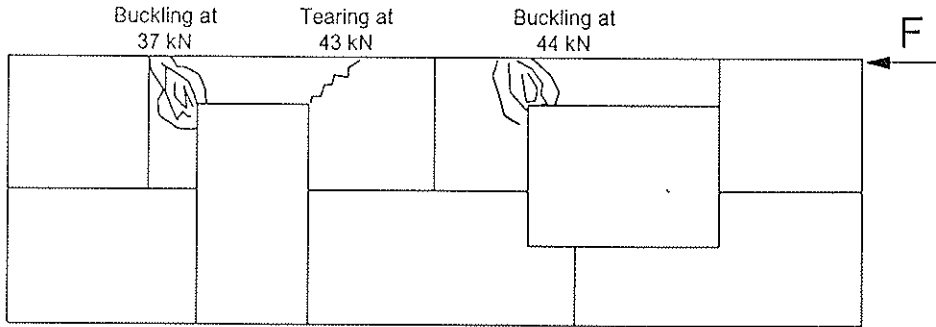


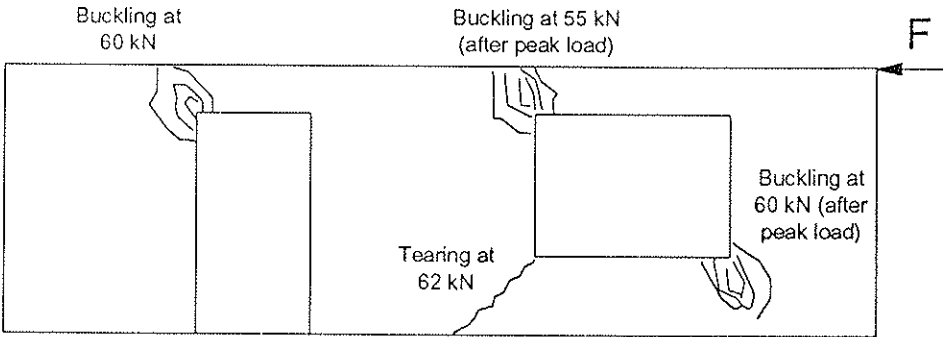
Fig. 9. Cyclic Load-Displacement Curve and Monotonic Envelope for Wall 8

4.2 Failure modes

The failure modes in walls with openings differed significantly from those without openings. In the latter, almost all the deformations occurred in the nails along the panel edges, while panel failures were observed in the walls with openings. The openings in the walls resulted in stress concentrations near the corners of openings, which precipitated failures in the panel material itself. These panel failures were particularly significant for the walls with one large panel and resulted in a relatively steep load decrease after ultimate. In the monotonic test on wall 4, the panel failure, which was first observed in the form of panel buckling at the top corner of the door opening at a load level of 60 kN (Fig. 10 (b)), occurred before significant nail deformations were observed. In the walls with regular panels, this type of panel failure occurred simultaneously with nail failures at a load level of 37 kN (Fig. 10 (a)). The occurrence of panel buckling and tearing at the top corners of both door and window openings eventually separated the regular panels into smaller pieces and the oversize panel into three pieces. The remaining shear strength appeared to result solely from these smaller solid pieces of panels with severe reduction in performance (Fig. 5). Nail withdrawal, the most common nail failure mode, occurred mainly along the edges of the panels at the mid-height of the wall sheathed with regular panel and along the bottom edge of the panel in the shear walls with oversize panel, which was the same as in the shear wall tests without opening.



(a) shear wall with regular panels



(b) shear wall with oversize panel

Fig. 10. Locations of panel failures with failure load levels

As concluded in the previous experimental study of shear walls without opening (Lam, Prion and He 1996), the performance of shear walls is governed by the performance of the fasteners between panel and frame. These test results from perforated shear walls indicate that their ultimate capacities were governed by panel failures. From this point of view, nail reinforcements will not significantly improve the performance of these perforated shear walls.

As discussed before, nail low cycle fatigue failures limited the load carrying capacity of wall 5. Since this type of failure, which is caused by excessive cyclic yielding, was rarely found in buildings subjected to earthquake loads, a more realistic test protocol was introduced. Under the new cyclic test procedures, as used in walls 6, 7 and 8, no nail fatigue failures occurred and more realistic degradation characteristics were observed. Both monotonic and cyclic test protocols produced similar load-deflection envelope curves and failure modes.

5 Conclusions

Openings in wood based shear walls caused a significant decrease in shear strength and stiffness of shear walls, due to the reduction in the effective sheathing area. To strengthen the racking resistance of shear walls with openings, large nonstandard panels were used. When shear walls with openings were built with these oversize panels, they presented a significant improvement in shear wall performance, obtaining shear strength and stiffness values even higher than for walls without openings built with regular panels. These results imply that the impact of openings on shear walls with oversize panel is more significant in contrast with the corresponding values in shear walls with regular panel. In addition, the ductility ratios of the walls with openings were slightly lower than those without openings.

The failure modes of shear walls with openings differed from those without openings. The performance of the walls was not only governed by the behaviour of the nail connectors between panel and frame, but a combination of nail and panel failure. Panel failure modes occurred in the form of panel buckling and panel tearing around the corners of openings. Nail withdrawal was the dominant nail failure mode in the tests (except for wall 5, in which nail low cycle fatigue occurred), which occurred mainly along the edges of the panels at the mid-height of the wall with regular panels and along the bottom edge of the panel in the wall with one oversize panel. Both panel and nail failure modes and locations were the same under monotonic and cyclic loading conditions. Considering the fact that panel failure locations were mainly concentrated in the corner areas of openings, localized reinforcement methods should be further investigated.

6 Acknowledgments

The authors gratefully acknowledge funding support received from the Structural Board Association and the National Research Council-Industry Research Assistant Program. Ainsworth Lumber Co. is also thanked for providing the testing material. The technical contribution from P. Symons in the research program is acknowledged with thanks.

7 References

- Canada Mortgage and Housing Corporation. (1985). *Canadian Wood-Frame House Construction*, Canada.
- Enjily, V. and Griffiths, R.D. (1996). "The racking resistance of large wall panels." *Proc. Int. Wood Engrg. Conf.*, 2:321-328, New Orleans, USA.
- Falk, R.H. and Itani, R.Y. (1987). "Dynamic characteristics of wood and gypsum diaphragms." *J. of Struct. Engrg.*, ASCE, 113(6), 1357-1370.
- He, M. (1997). "A study of wood based shear walls sheathed with oversize oriented strand board panels." M.A.Sc. Thesis, The University of British Columbia, Vancouver, Canada.
- Johnson, A.C. and Dolan, J.D. (1996). "Performance of long shear walls with openings." *Proc. Int. Wood Engrg. Conf.*, 2:337-344, New Orleans, USA.
- Lam, F., Prion, H.G.L. and He, M. (1996). "Lateral resistance of wood based shear walls with oversize sheathing panels." *Proc. Int. Council for Building Research Studies and Documentation*, Working Commission W18 - Timber Structures, Meeting Twenty-Nine, paper 29-15-1, Bordeaux, France.
- Line, Philip and Douglas, B.K. (1996). "Perforated shearwall design method." *Proc. Int. Wood Engrg. Conf.*, 2:345-349, New Orleans, USA.
- Patton-Mallory, M., Wolfe, R. W., Soltis, L. A. and Gutkowski, R. M. (1985). "Light-frame shear wall length and opening effects." *J. of Struct. Engrg.*, ASCE, 111(10), 2227-2239.
- Sugiyama, H. (1994). "Empirical equations for the estimation of racking strength of a plywood-sheathed shear wall with openings." Summaries of Technical Papers of Annual Meeting, Trans. of A.I.J.
- White, M.W. and Dolan, J. D. (1995). "Nonlinear shear-wall analysis." *J. of Struct. Engrg.*, ASCE, 121(11), 1629-1635.

**INTERNATIONAL COUNCIL FOR BUILDING RESEARCH STUDIES AND DOCUMENTATION
WORKING COMMISSION W18 - TIMBER STRUCTURES**

A NUMERICAL ANALYSIS OF SHEAR WALLS STRUCTURAL PERFORMANCES

by

L Davenne

L Daudeville

Laboratoire de Mécanique et Technologie

Cachan

France

N Kawai

Building Research Institute

Tsukuba, Ibaraki

M Yasumura

Shizuoka University

Japan

MEETING THIRTY

VANCOUVER

CANADA

AUGUST 1997

A Numerical Analysis of Shear Walls Structural Performances

Luc DAVENNE, Laurent DAUDEVILLE

Laboratoire de Mécanique et Technologie, ENS Cachan / CNRS / Univ. Paris 6

61 avenue du Président Wilson, 94235 Cachan, France

E-mail: davenne@lmt.ens-cachan.fr

Naohito. KAWAI

Building Research Institute, 1 Tatehara, Tsukuba, Ibaraki 305, Japan

Motoi YASUMURA

Department of Forest Resources Science, Faculty of Agriculture, Shizuoka University 836

Ohya, Shizuoka 422, Japan

Abstract

This paper deals with the numerical analysis of wood based shear walls made of lumber framing members and with sheathing plywood panels connected with nails. A model is presented for the simulation of the non linear response of the nailed connection under static monotonic or reversed cyclic loading. It has been implemented in the finite element code CASTEM 2000. Three kind of walls with different openings are simulated. The responses are close from the experimental results made at the Building Research Institute in Tsukuba, Japan.

1. Introduction

The wood based shear walls with plywood sheathing panels seems to have an excellent performance against lateral loading, especially in residential applications, and are often used in North America and in Japan. Many experimental programs have been conducted over full scale walls either under static, cyclic or dynamic loading (Lam *et al* 1996, Dolan 1989, kamiya 1988). But there are still some questions about the adopted cyclic load schedule in relation to the dynamic response of the shear wall and the failure modes in it (Karacabeyli and Ceccotti, 1996). To avoid costly experimental programs, simulation seems to be a good alternative. Some author have worked on the modeling of such shear walls under static loading (Dolan and Foschi 1991, Schmidt and Moody 1989, Falk and Itani 1989, Gupta and Kuo 1985) or under cyclic or dynamic loading (Tarabia and Itani 1997, Tarabia and Kamiya 1996, Kazal *et al* 1994). Some important phenomena, especially in the cyclic models,

where not taken into account in the literature. For example, for several cycles at the same imposed displacement, the strength degradation between the first cycle (loading cycle) and the other cycle (stabilized cycles) were not modeled. An other experimentally observed phenomenon is the difference between the monotonic curve and the peaks envelope of the loading cycles under cyclic loading. There is here also a strength degradation that may have an great influence over the shear wall response. In both cases, the dissipated energy is affected and the behavior of the wall under seismic loading may be very different. A model that takes these phenomena into account is presented in this paper.

2. Experimental observations

Two kinds of experiments were conducted at the Building Research Institute. The first one concerns tests of simple nailed joints under monotonic and cyclic loading (four nails, figure 1). It allows to obtain the response of one single nail. It is assumed to be one quarter of the whole response of the specimen. The second one is the real test of shear walls with several kinds of openings (doors, windows, ...), clamped in the ground and laterally loaded at the top (monotonic and cyclic) (figure 2).

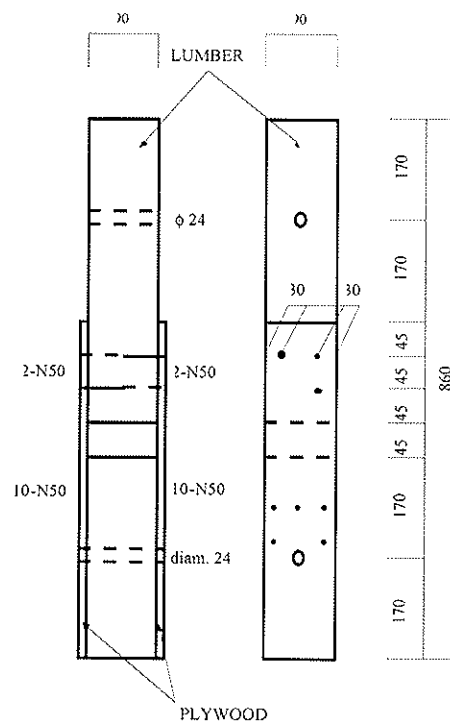


Figure 1 - Test set-up for single nailed joint response

The loading was made under displacement control. The cyclic displacement loading versus time is based on the CEN Standard (static cyclic test) and is given on figure 3. The typical response of a nail is shown on figure 4. This is the average response from six monotonic tests in each direction and from six cyclic tests. We can observe two main phenomena :

- The monotonic loading curve is higher than the (supposed) peaks envelope under cyclic loading : if the loading cycles (first cycle for a given displacement) were continued, it is evident that these curves wouldn't reach the monotonic loading curve.
- There is a pinching of the curve when cycling, and the peaks after cycling at the same displacement (stabilized cycles) are lower than those of the first cycles (loading cycles). Most of the strength degradation occurs between the first and the second cycles, the other cycles can be considered as stabilized. The same phenomena were observed by Karacabeyli and Ceccotti, 1996.

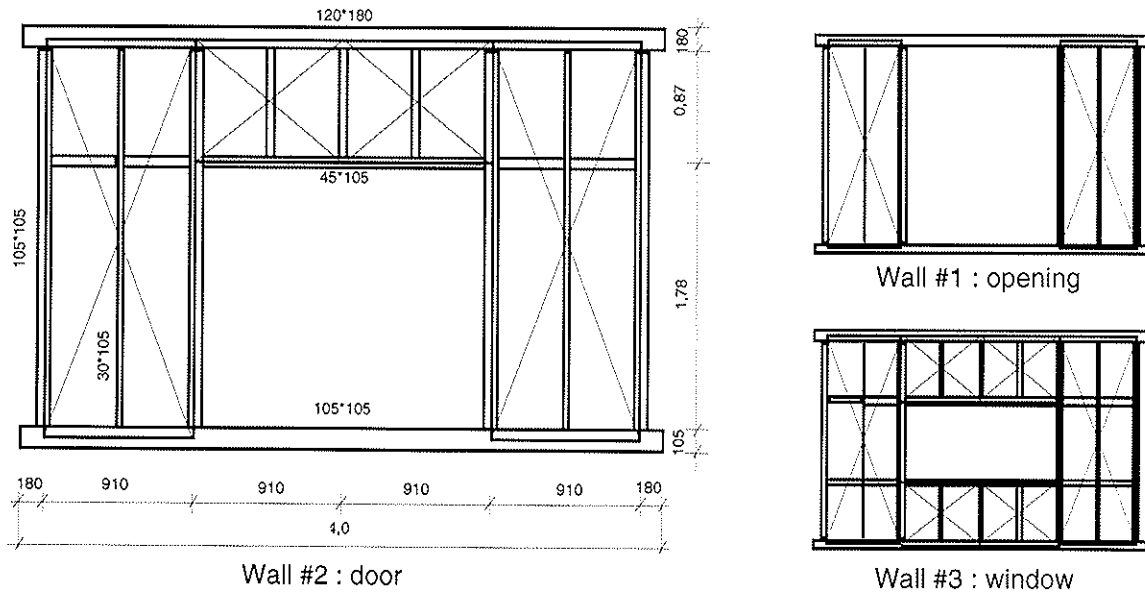


Figure 2 - Tested shear walls

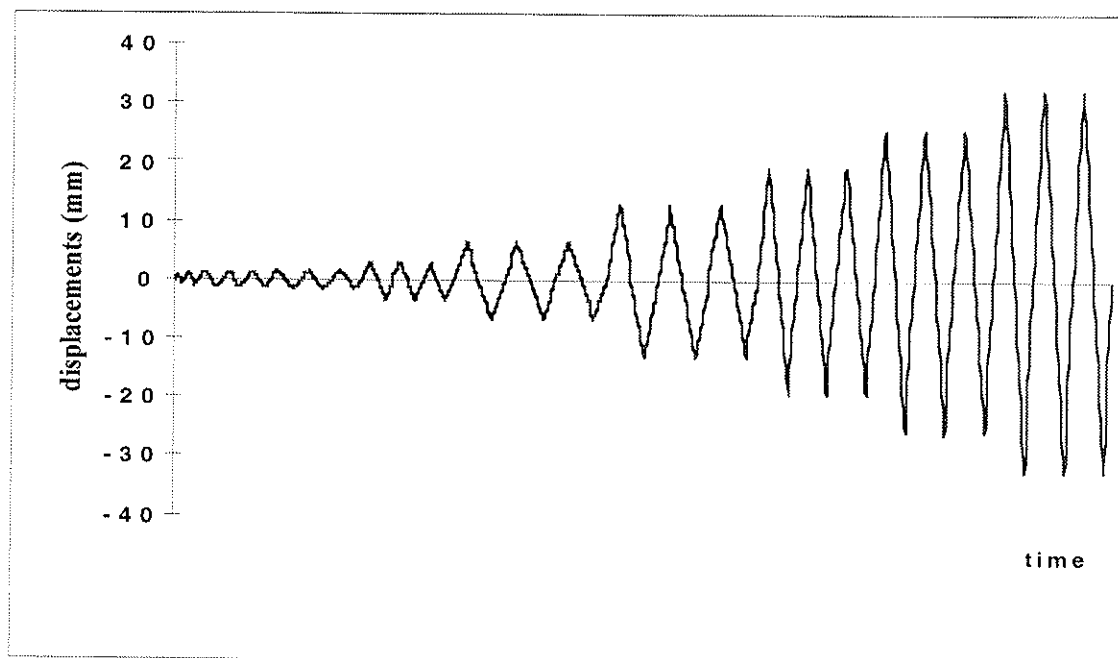


Figure 3 - Cyclic displacement control curve on the nailed test specimen

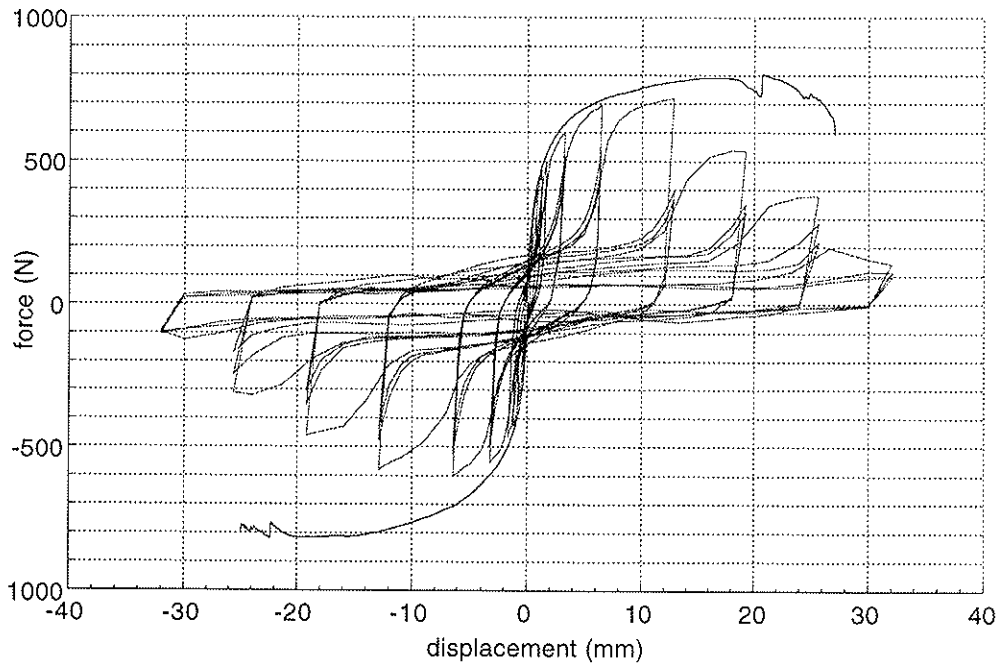


Figure 4 - Responses of a nailed joint

The same remarks can be made on the response of the walls. It is discussed in the section 4.

3. Modeling

3.1 General overview

In the simulation of the shear wall, the nailed joints are supposed to be the only place where non linearity occur. The computation is made in plane stress in the plane of the wall. The lumber frames are modeled with 2D beam elements (elastic, isotropic). The connection between two beams is modeled with a rotational spring whose stiffness is given between zero (free relative rotation) and infinity (clamped). The plywood sheathing plates are modeled with 2D plane stress elements (elastic, orthotropic). The fasteners between the beams and the plates are modeled with a two perpendicular spring system (figure 5). The beam node and the plate node have the same coordinates. The stiffness matrix of the nailed joint element which relates the nodal forces to nodal displacements is given in the program.

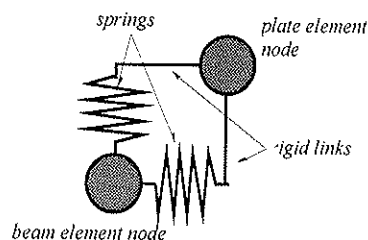


Figure 5 - Modeling of the fasteners

The non linear constitutive relation of the fastener relates the shear force to the relative displacement and is presented in section 3.2 and 3.3. It is to note that these constitutive relations are given in one dimension in the direction of the relative displacement between the beam and the plate nodes (slip). It is assumed that this direction (local, at the joint level) doesn't change a lot during the loading of the wall (global, at the wall level). Even with a radial loading path, this assumption may be violated if there are force redistributions. However, in the walls tested here, this assumption has been checked and can be kept. In the future, the constitutive relations will be written in two dimension with coupling between the directions.

The global equilibrium is solved with a simple initial stress algorithm. No dynamic effect are implemented until now.

3.2 Monotonic loading model of the nailed joint

Two models have been tested. One simple three-linear curve (model #1) and the model proposed by Foschi (Foschi 1977, Dolan and Foschi 1991) (model #2), modified with a cutting off in the descending branch . The first model is fully described with three points (that is three slips and three forces).

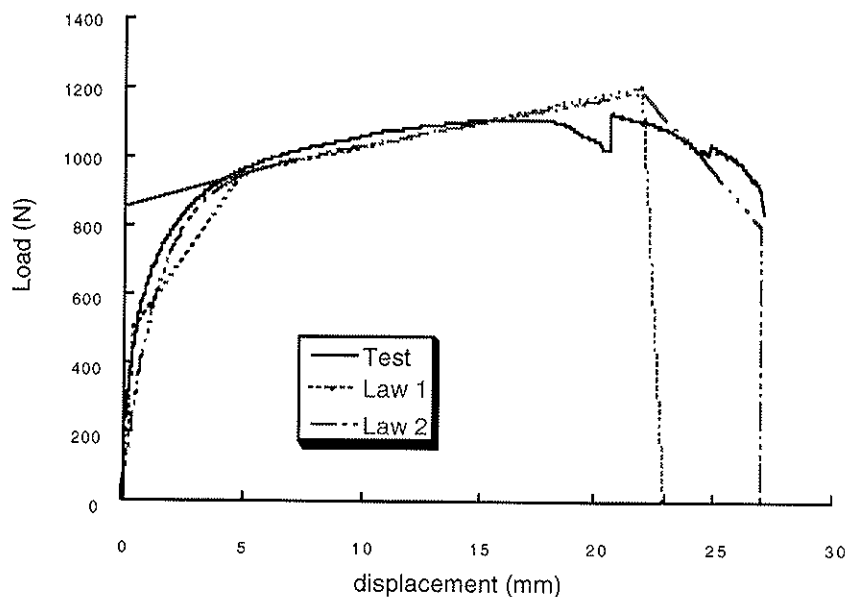


Figure 6 - The two models for monotonic loading

The equations of the second model are:

$$\left\{ \begin{array}{ll} F = (P_0 + K_2\Delta)(1 - e^{\frac{-K_1\Delta}{P_0}}) & \text{for } \Delta < \Delta_p \\ F = (P_0 + K_2\Delta_p)(1 - e^{\frac{-K_1\Delta_p}{P_0}}) - K_3(\Delta - \Delta_p) & \text{for } \Delta_p < \Delta < \Delta_{\max} \\ F = 0 & \text{for } \Delta > \Delta_{\max} \end{array} \right. \quad (1)$$

where Δ is the slip and F the load. Three stiffness K_1 , K_2 and K_3 , one load P_0 , and two slips Δ_1 and Δ_2 , are needed to describe the model.

The six parameters of each model are fitted with the experimental results of the nailed joint. The curves (for one nail) are presented on figure 6.

3.3 Cyclic model of the nailed joint

The proposed cyclic model is presented on the figure 7. The rules are the following :

- the first loading curve OA_1 (to the right) follows the monotonic loading curve, that is the monotonic model #2. This corresponds to the crushing of the wood and the flexional yielding of the nail,
- the unloading A_1B_1 is elastic with the initial stiffness K_1 ,
- if there is a new loading from B_1 , it is linear until A_1 and then it follows the monotonic loading curve,
- if the unloading continues from B_1 , it follows a strait line toward the fixed point J on the zero slip axis, it correspond to the flexional yielding in the reverse direction, and an allowance begins to occur,
- then the first loading in the other way (to the left) follows the monotonic loading curve OA'_1 , it is the wood crushing on the other side and the yielding of the nail, the allowance growth,
- during the path $B_1-J-A'_1$, it is assumed that it is the reached level of load (under the axis) that degrades the strength and enlarges the allowance, thus that define the point D_1 where the next loading curve will pass in the future loading in right direction, the point D is defined as follows:

$$\left\{ \begin{array}{l} \Delta_D = \Delta_A \\ F_D = F_A - \alpha(F_A - kF_{Dl}) \end{array} \right. \quad (2)$$

with

$$\alpha = \frac{\langle F \rangle_-}{F_{\max}} \quad (3)$$

where F_{\max} is the peak load and $\langle F \rangle_-$ the maximum load reached under the zero load axis during the reverse loading, F_{Dl} is the limit of F_D when it decreases, this is the point of slip Δ_{A_1} located on the line parallel to B_1-J which passes through I .

- the unloading from the point A'_1 is elastic until the point B'_1 ,

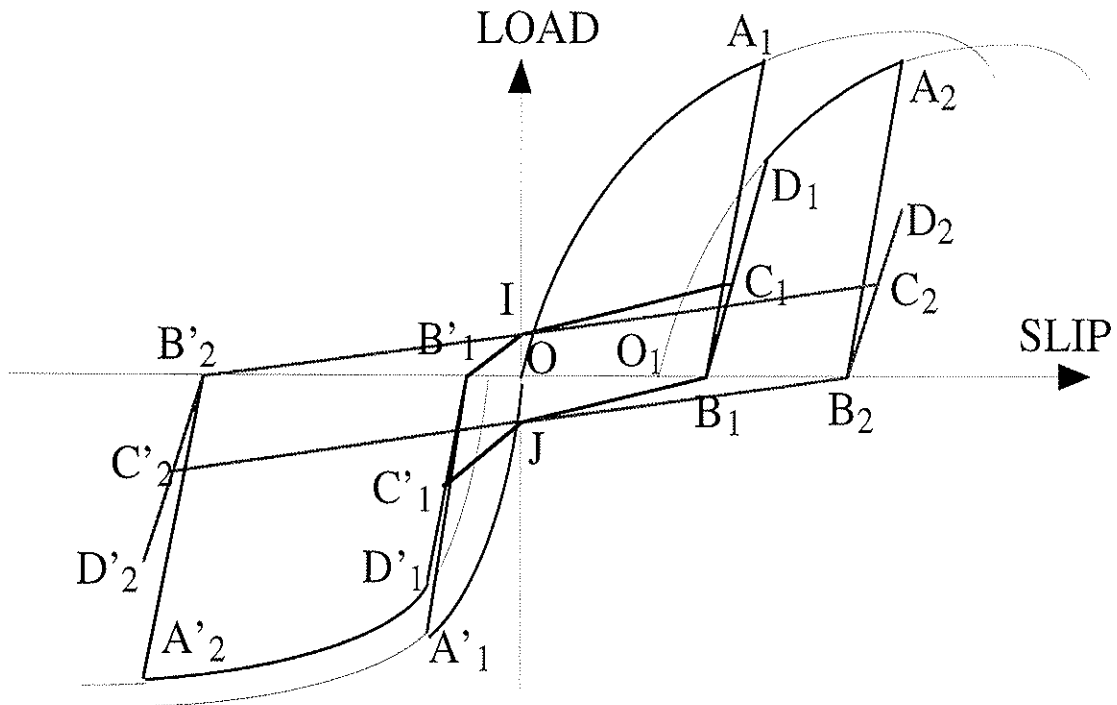


Figure 7 - proposed cyclic model for the nailed joint

- then the unloading to zero slip is a straight line toward the fixed point I, the physical sense is the same as the line B_1 -J,

- from I, the second cycle begins. Since there has been already a loading at the first cycle, the wood is already crushed and there is an allowance. Thus the following path is the line I - C_1 parallel to the line B_1 -J. The point C_1 is the intersection between the line I - C_1 and the line B_1 - D_1 .

- if the loading continues from point C_1 , it follows the line D_1 - B_1 (D_1 is assumed to have the same slip than A_1)

- during the path B'_1 - I - C_1 - D_1 , it is assumed that it is the reached level of load (over the axis) that degrades the strength and enlarges the allowance, thus that defines the point D'_1 where the next loading curve will pass in the future loading in left direction,

- from D_1 , there can be a stabilized cycle D_1 - B_1 - J - C'_1 - B'_1 - I - C_1 - D_1 ,

- or there can be a new loading D_1 - A_2 , in this case the new loading curve is the monotonic loading curve that is shifted of O - O_1 , and whose strength is affected by a parameter which depend on the maximum reached slip in the reverse direction $\Delta_{A'_1}$. The shift corresponds to the allowance and the strength degradation correspond to the nail withdrawal witch occurs after a slip threshold Δ_0 . The strength degradation is simulated by multiplying the monotonic loading curve by a parameter β :

$$\beta = \gamma \frac{|\Delta_{A'}| - \Delta_0}{\Delta_{\max} - \Delta_0} \quad (4)$$

Since the equation (1) cannot be inverted, the shift is computed with a local Newton iterative procedure.

The model has ten parameters which must be identified from the tests: The six parameters of the monotonic loading curve (eq. 1), one for defining the loads at zero slip $F_l = \phi$ and $F_r = -\phi$, the slip threshold of strength degradation Δ_0 , the maximum percentage of strength degradation γ and the parameter k in equation (2).

The non symmetry between the right and the left directions can be captured because there are variables α' and β' for the left direction which can have different values from and β defined in equations (3) and (4).

4. Results

4.1 Shear walls under monotonic loading

The three walls of the figure 2 have been tested under monotonic loading. For example, the response of the wall #2 is presented on figure 8.

The two models give a good prediction of the experimental results. The maximum load and the corresponding displacement are obtained in a range of 10%.

The simulation gives a too rigid response in the beginning of the loading, this is doubtless due to the modeling of the connections of the wall to the floor. There were possible allowances in the real test that are not taken into account in the simulation.

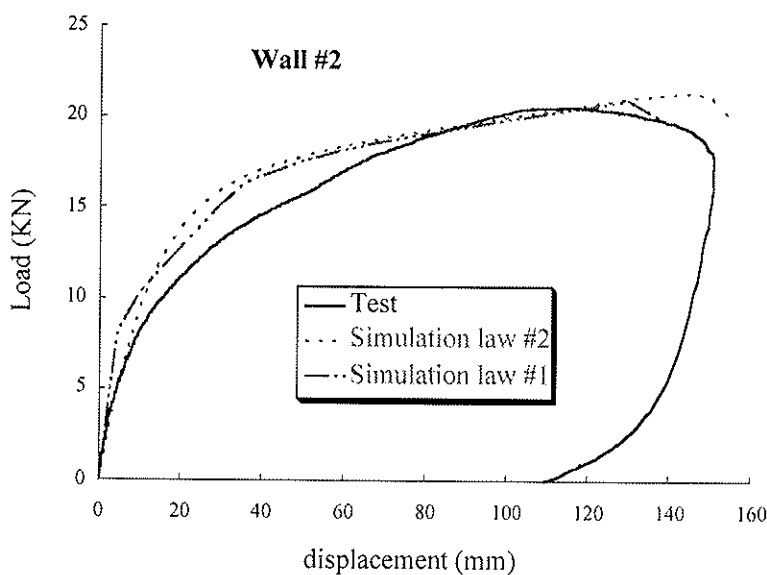


Figure 8 - Response of the wall #2 under monotonic shear loading

4.2 Nailed joint under cyclic loading

The proposed model presented in section 3.3 include several assumptions that must be checked on simple tests before running a wall simulation. The response of a nailed joint submitted to the same displacement loading as the nailed joints tests (given on figure 3) is presented on figure 9.

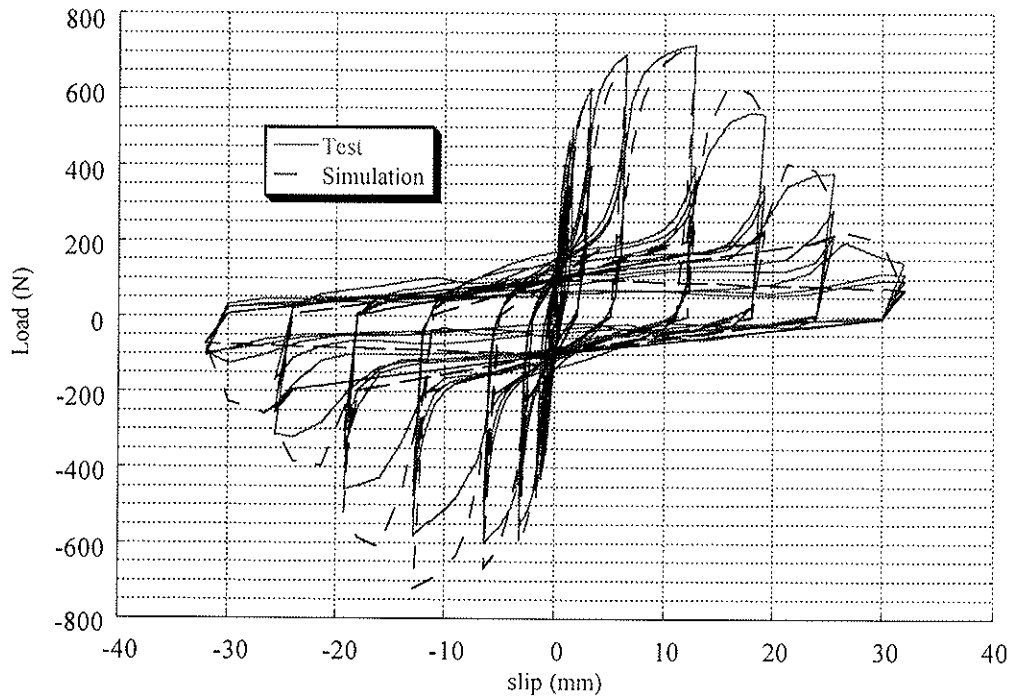


Figure 9 - Response of a nailed joint under cyclic loading

As a whole, the proposed rules seem to be in good agreement with the test. The only phenomenon that is not correctly taken into account is the strength degradation on the left. This effect, that brings non symmetry to the whole response, is due to the given loading. As seen on figure 3, each time there is a new loading cycle, it begins toward the right and brings a degradation that affects the left strength. Some modifications are in progress to better model this phenomenon, the evolution of the parameters β and β' (eq. 4) must be modified. The proposed model was developed from the given test observations (reverse displacement cycling loading). It has now to be tested under different loading histories to check if the proposed rules still work : for example cyclic imposed forces, non-symmetric cyclic loading.

4.2 Shear walls under cyclic loading

The simulation of shear walls under cyclic loading is in progress.

5. Conclusion

The authors presented a finite element code to compute the response of wood frames with nailed plywood sheathing panels. A model to simulate the non linear response of the nailed joints under cyclic loading is proposed. It gives a good response in the case of static reversed cyclic imposed displacements (CEN standard). The different strength degradations, pinching and allowance apparitions are modeled. The response of the walls under static monotonic loading is close from the tests. The cyclic loading of walls is in progress.

The one dimensional model must now be checked in other loading cases and with other type of nail (for example, nail fatigue may appear with other kind of nails, the behaviour may be different than the Japanese nails tested here).

In a future work, a three dimension model with degradation couplings must be developed to better simulate the reality.

Acknowledgments

The authors would like to thank Y. Cazal and J. Laflotte in master's course for their help.

They thank the STA (Science and Technology Agency), Japan, for financial support and Dr. K. Watanabe, Manager of this collaborative research for giving advice.

References

- Dolan J.D. 1989: The dynamic response of timber shear walls. Ph. D. Dissertation, Dept. of Civil Engineering, UBC, Vancouver, Canada.
- Dolan J.D. ; Foschi R.O. 1991: Structural analysis for static loads on timber shear walls, *Journal of Structural Engineering*, 117 (3), 851-861.
- Falk R.H. ; Itani R.Y. 1989: Finite element modeling of wood diaphragms, *Journal of Structural Engineering*, 115(3), 543-559.
- Foschi, R. 1977: Analysis of wood diaphragms and trusses, Part I: diaphragms, *Canadian Journal of Civil Engineering*, 17, 345-352.
- Gupta A.K. ; Kuo G.P. 1985: Behavior of wood-framed shear walls, *Journal of Structural Engineering*, 111(8), 1722-1733.
- Kamiya F. 1988: Nonlinear earthquake response analysis of sheated wood walls by a computer actuator on-line system, *Proc. Int. Timber Engineering Conference, Seattle, USA*, 1, 838-847.
- Karacabeyli E. ; Ceccotti A. 1996: Quasi-static reversed-cyclic testing of nailed joints, *Proceedings of the 29th CIB-W18 Meeting, Bordeaux, France*, paper 29-7-7.
- Kazal B. ; Leichti R.J. and Itani R.Y. 1994: Nonlinear finite-element model of complete light-frame wood structures, *Journal of Structural Engineering*, 120(1), 100-119.
- Lam F. ; Prion H.G.L. and He M. 1996: Lateral resistance of wood based shear walls panels with oversized sheathing panels, *Proceedings of the 29th CIB-W18 Meeting, Bordeaux, France*, paper 29-15-1.
- Schmidt R.J. ; Moody R.C. 1989: Modeling laterally loaded light-frame buildings, *Journal of Structural Engineering*, 115 (1), 201-217.
- Tarabia A.M. ; Itani R.Y. 1997: Static and dynamic modeling of light-frame wood buildings, *Computers and structures*, 63(2), 319-334.
- Tarabia A.M. ; Kamiya F. 1996: Analytical seismic response of wood shear walls using hysteresis models of nailed joints, *Mokuzai Gakkaishi*, 42(11), 1064-1071.

**INTERNATIONAL COUNCIL FOR BUILDING RESEARCH STUDIES AND DOCUMENTATION
WORKING COMMISSION W18 - TIMBER STRUCTURES**

**SEISMIC FORCE MODIFICATION FACTORS FOR THE DESIGN OF
MULTI-STOREY WOOD-FRAME PLATFORM CONSTRUCTION**

by

E Karacabeyli
Forintek Canada Corp.
Canada
A Ceccotti
University of Florence
Italy

**MEETING THIRTY
VANCOUVER
CANADA
AUGUST 1997**

Seismic force modification factors for the design of multi-storey wood-frame platform construction

Erol Karacabeyli, P.Eng.
Wood Engineering Scientist
Forintek Canada Corp.
Canada

and

Ario Ceccotti, Professor
Civil Engineering Dept.
University of Florence
Italy

Abstract

Time-history non-linear dynamic analyses using twenty-eight earthquake accelerograms were performed on a four-storey wood-frame platform structure. The results confirm the current Canadian seismic force modification factor ($R=3$) for lateral load resisting systems comprising of plywood nailed shear walls. An alternate seismic modification factor ($R=2$) which accounts for the contribution of the gypsum wall board (GWB) walls in design is also found to be appropriate.

1 Introduction

Most design codes contain force modification factors which account for the energy dissipating characteristics of the structural system under earthquake loads. In Part 4 of the National Building Code of Canada, NBCC (CCBFC 1995) force modification factors or "R" factors are provided for various types of steel, concrete and timber lateral load resisting systems. For timber structures, the R factors were first implemented in the 1990 edition of the NBCC which stipulates that large residential and non-residential timber structures (exceeding 600 m² in building area and three storeys) shall be designed and detailed according to the Canadian Code for Engineering Design in Wood, CSA O86.1 (Canadian Standards Association 1994). These factors were selected to result in designs of timber lateral load resisting systems that were consistent with the observed performance history. However, retention of these factors for subsequent editions of the code was contingent on the availability of technical data supporting such factors.

In order to assess the appropriateness of the R factors, time-history dynamic analyses using twenty-eight earthquake accelerograms and a hysteresis model for the shear wall

components were performed on a four-storey platform frame wood structure. This structure was used as an example by the members of the Wood Frame Committee of the Structural Engineering Consultants of B.C. (SECBC, Continuing Education for Engineering & Architecture, UBC 1995). Based on these analyses, recommendations about R factors have been made. A comparison between the Canadian force modification factor and European seismic behaviour factor for lateral load resisting systems with nailed shear walls is also made.

2 Approach

The floor plan of the selected building which was designed in accordance to the NBCC provisions for the city of Vancouver is given in Figure 1. In this paper, a two dimensional dynamic analysis of one of the shear walls parallel to the short dimension of the building was performed. The floors were assumed to be rigid because of the concrete topping. In the short direction, the building was symmetrical, and consequently torsional effects are not considered.

The study consisted of the following steps:

- a) shear wall specimens were tested (Figure 2) under monotonic and cyclic displacement schedules;
- b) a hysteresis model was fitted to the above cyclic test data (Figure 3). For systems containing shear walls sheathed with a combination of plywood and gypsum wall board (GWB), individual skeleton curves were superimposed. This method of superimposition has been shown (Karacabeyli and Ceccotti 1996) to be valid for displacements up to approximately 40 mm.;
- c) the hysteresis model was employed in a time-step dynamic analysis for twenty-eight different earthquake accelerograms. The peak ground acceleration for each accelerogram was scaled upwards until the ultimate displacement is achieved. This acceleration is then called " A_u ". The ultimate displacement, used as the collapse criteria, is defined as the displacement at 80 percent of the maximum load on the descending portion of the skeleton curve;
- d) a shake table test was conducted to verify the theoretical predictions.

The overall approach is shown in Figure 4.

3 Testing

A comprehensive database was established by testing wood-frame shear walls under monotonic and cyclic displacement schedules. The test program included wood frame shear walls sheathed with plywood, oriented strand board (OSB) and/or GWB. The detailed description and results of the test program are given in (Karacabeyli and Ceccotti 1996).

4 Time-history Dynamic Analysis

Time-history non-linear dynamic analysis were performed using a structural analysis program in which the in-elastic behaviour is modelled by a hysteresis model developed at the University of Florence (Ceccotti *et al.* 1994). In the analysis, the skeleton curve for the hysteresis model is selected based on the 5th percentile (determined by assuming a 10 percent coefficient of variation and a normal distribution) of the first envelope curves obtained in the cyclic tests. No further adjustments for safety were used. The analyses were performed using twenty-eight earthquake accelerograms of which six were accelerograms from real earthquakes; the remaining twenty-two were modified accelerograms to fit the Vancouver area design spectrum (Anderson 1996).

Three design cases (Figure 5) were considered:

- Case 1: $R=3$; Designed and analyzed only considering plywood shear walls. The effect of the GWB walls were neglected in the dynamic analysis.
- Case 2: $R=3$; Designed only considering plywood shear walls. In the dynamic analysis, considered plywood shear walls and accounted for the effect of the GWB walls.
- Case 3: $R=2$; Designed and analysed considering plywood and GWB shear walls. This case is proposed by the Wood Frame Committee of the SECBC (SECBC, Continuing Education for Engineering & Architecture, UBC 1995).

For Cases 2 and 3, the ratio of GWB to plywood walls was kept at 2.5, 2.5 and 5.0 for the first three storeys, respectively. No restriction was applied for the fourth floor. A 1 kN/m factored shear resistance for GWB walls is used in the design.

For Case 1, the European (Eurocode 8, 1993) seismic behaviour factors (q) for lateral resisting systems with nailed shear walls were also determined for the twenty-eight accelerograms. The factor " q " is calculated as the ratio of A_u and the acceleration which caused the yielding of the structure, A_y (as defined in CEN 1994).

The fundamental period of vibration of the structure (T_0) is calculated by using the NBCC, and also by dynamic analysis. The value of $T_0^{NBCC}=0.2$ sec was found to be much less than those (Figure 5) found for the three cases by dynamic analysis. In determining the design shear force, we used $T_0^{NBCC}=0.2$ sec.

5 Results

The results of non-linear dynamic analysis are shown in Figures 6, 7 and 8 where the peak ground accelerations (A_u) that "caused" the inter-storey drift to reach the shear wall's ultimate displacement are shown against the twenty-eight accelerograms, and also against the Peak Ground Acceleration (PGA_{CODE}) given in the NBCC. These results lead to the following conclusions:

- a) For Case 1, all values of A_u were found to be greater than PGA_{CODE} which confirms that the current force modification factor, $R=3$, is appropriate for plywood nailed shear walls. The median value of A_u is found to be three times the PGA_{CODE} .
- b) For Case 2, most values of A_u were found to be greater than those found for Case 1 suggesting that the existence of GWB walls did not impair the lateral resistance of the structure. Instead, GWB contributed positively to the response of the structure compared to plywood shear walls only.
- c) For Case 3, all values of A_u were also found to be greater than the PGA_{CODE} which shows that the alternate force modification factor, $R=2$ is adequate. Although the median value of A_u was found to be smaller than that found for Case 1, the lower quartile values of A_u for Case 1 and Case 3 were similar. This is due to the smaller variability obtained in the results of Case 3.
- d) Most values of q (Figure 9) were found to be greater than 3 which confirms that the seismic behaviour factor in Eurocode 8, $q=3$, for plywood or OSB nailed shear walls is appropriate. The median q was found to be between 5.0 and 6.0.
- e) Results from a shake table tests are currently being analysed to confirm or refute the above observations.

6 Conclusions

The results confirm the current Canadian seismic force modification factor ($R=3$) and the European behaviour factor ($q=3$) for lateral load resisting systems comprising of plywood nailed shear walls.

The results also show that the presence of walls sheathed with GWB has a positive influence on the response of the structure which was designed considering only plywood shear walls. An alternate seismic modification factor ($R=2$, recommended by the SECBC) which accounts for the contribution of the GWB walls in design is found to be appropriate.

Shake table test results will be used to confirm or refute these findings.

7 References

- Anderson, D.L. 1996. Personal communications.
- Canadian Commission on Building and Fire Codes. 1995. National Building Code of Canada. National Research Council Canada.
- Canadian Standards Association. 1994. O86.1-94. Engineering Design in Wood (limit States Design). CSA, Etobicoke, Ont., Canada.
- Ceccotti, A., Vignoli, A., and Giordano, S. 1994. Seismic Tests on Full-Scale Timber Structures. Proceedings. Pacific Timber Engineering Conference; Goald Coast, Australia:1:232-240.
- CEN TC124.117. 1994. Timber Structures - Test methods - Cyclic testing of joints made with mechanical fasteners. CEN, Bruxelles, Belgium.
- EUROCODE 8. 1993. Design of Structures in Seismic Regions (draft). Draft ENV 1998-1-1 CEN, Bruxelles, Belgium.
- Karacabeyli, E., and Ceccotti, A. 1996. Test Results on the Lateral Resistance of Nailed Shear Walls. Proceedings. International Wood Engineering Conference, New Orleans, USA. pp:V2,179-186.
- SECBC, 1995. Conventional Wood Frame Multi-Unit Residential Buildings. Continuing Education for Engineering and Architecture, UBC, 1995. Proceedings of a Workshop on Seismic Design of Buildings. University of BC

8 Acknowledgements

This work was undertaken under a Canadian Forest Service contract to Forintek Canada Corp. Authors thank their colleague Mr. Conroy Lum for his contributions.

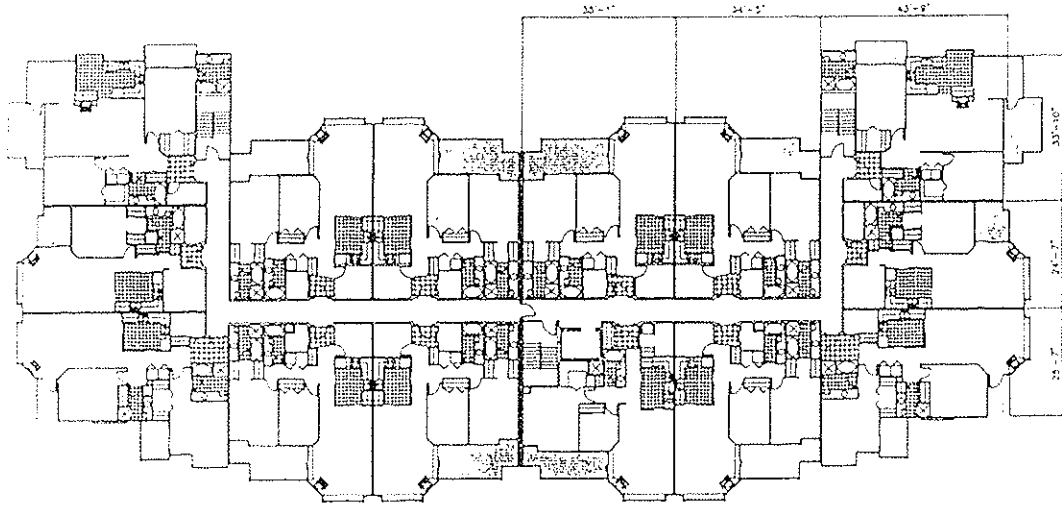


Figure 1 Floor Plan of the Sample Structure
(Courtesy of Wood Frame Committee of the SECBC)

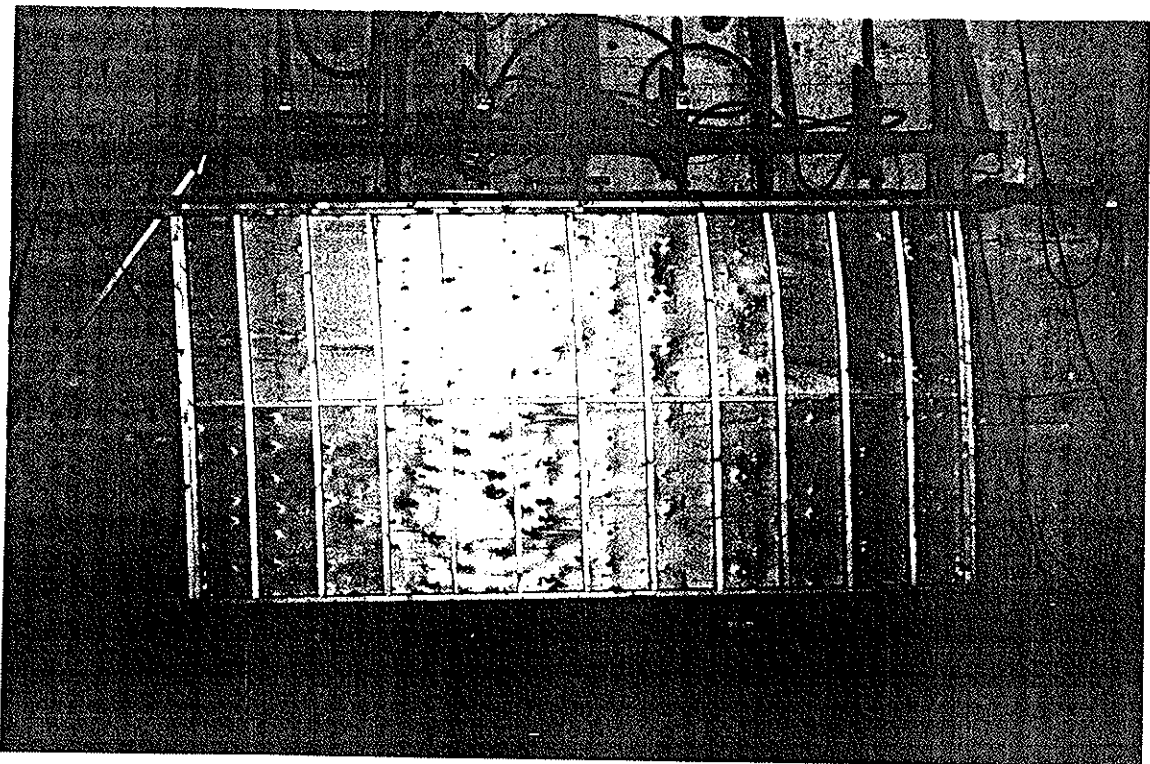


Figure 2 The Shear Wall Test Set Up

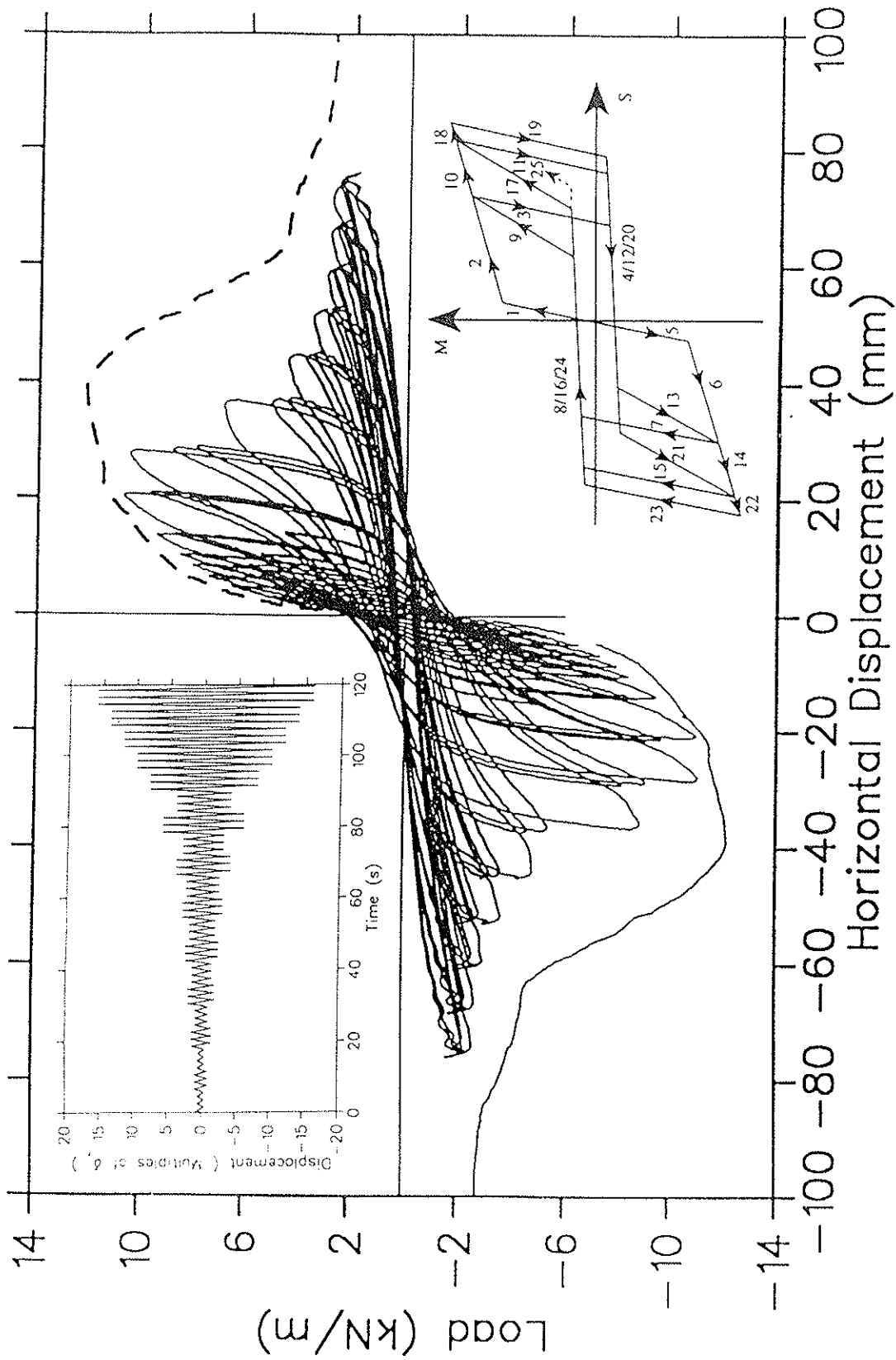


Figure 3 Typical Monotonic and Cyclic Test Data, the Hysteresis Model

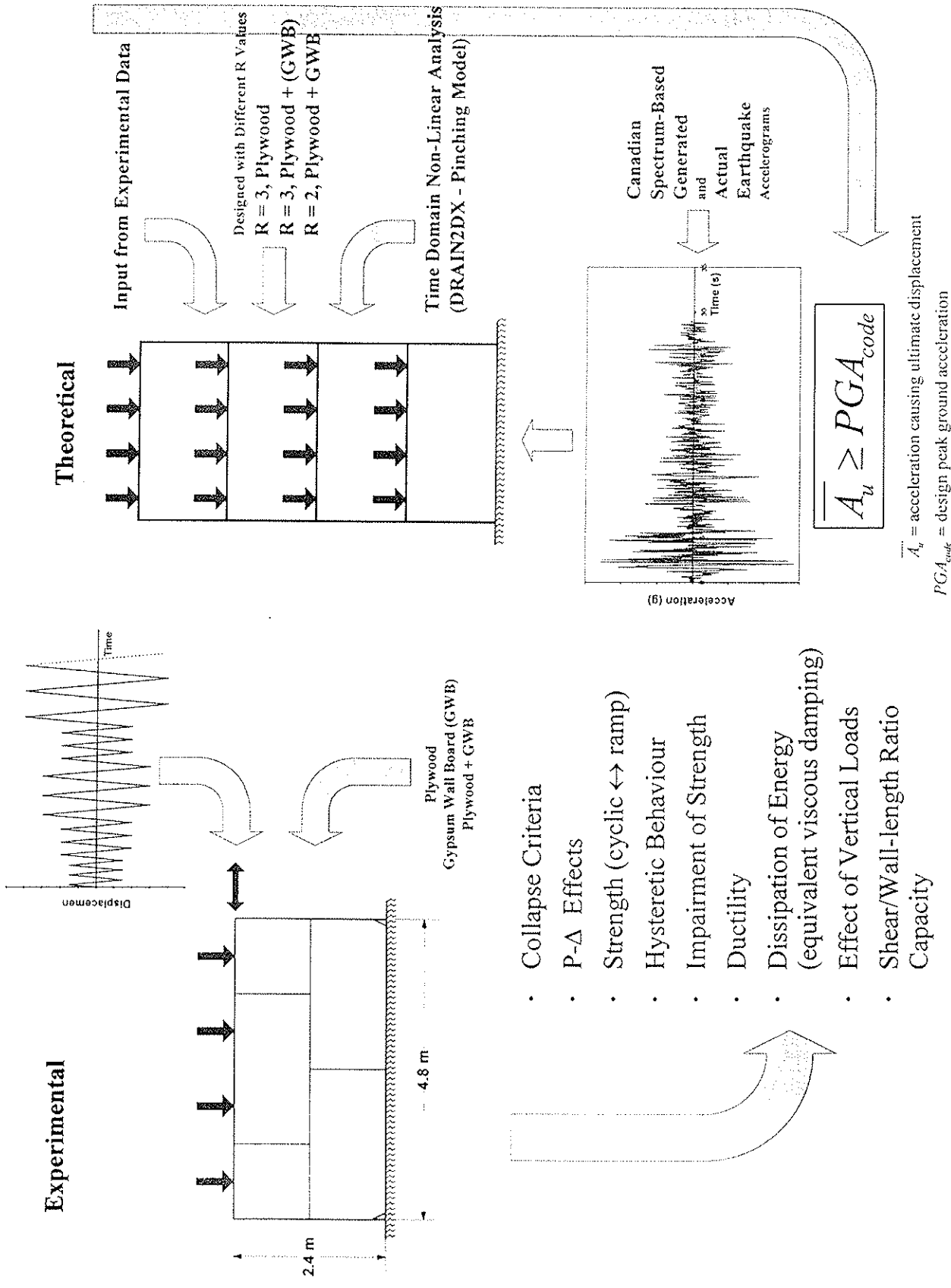
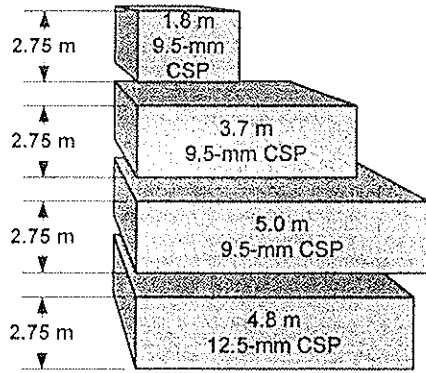
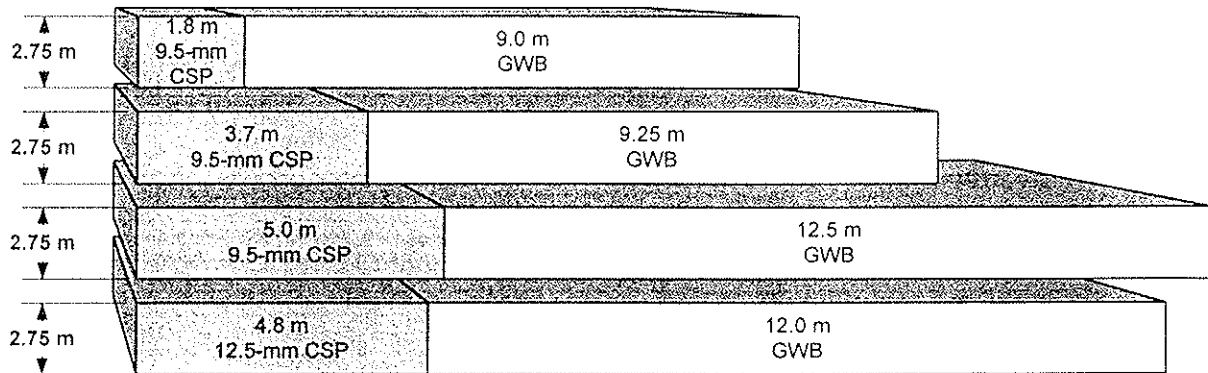


Figure 4 The Overall Approach

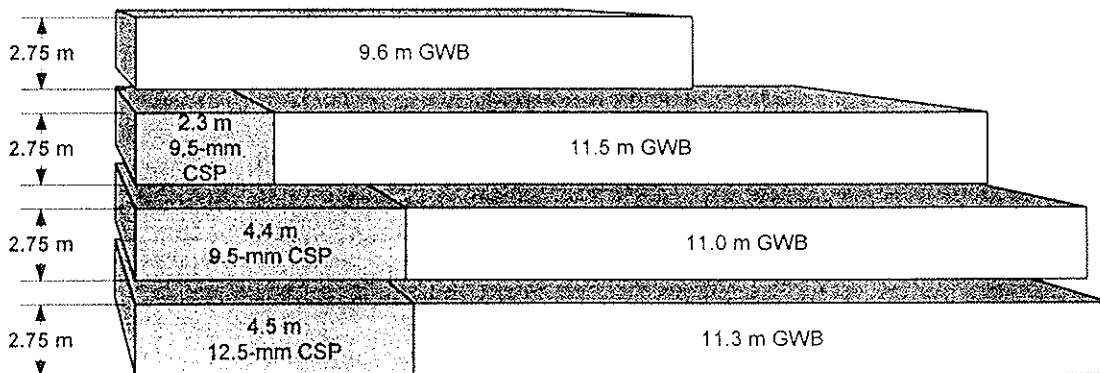
Figure 5 Three Cases Considered in the Design and Analysis



CASE 1 R=3; Designed only considering plywood shear walls. In analysis, neglected the effect of GWB walls.
 $T_o = 0.65$ sec. $v = 5\%$



CASE 2 R=3; Designed only considering plywood shear walls. In analysis, accounted for the effect of GWB walls.
 $T_o = 0.47$ sec. $v = 2\%$



CASE 3 R=2; Designed and analysed considering plywood and GWB shear walls.
 $T_o = 0.48$ sec. $v = 2\%$

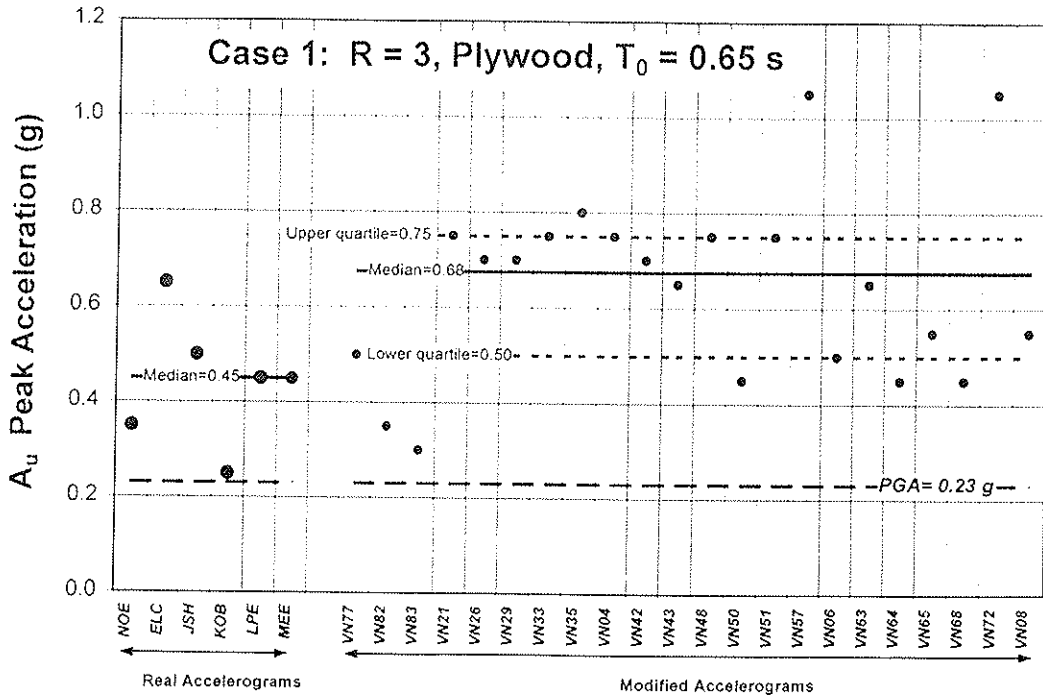


Figure 6 Results for Case 1

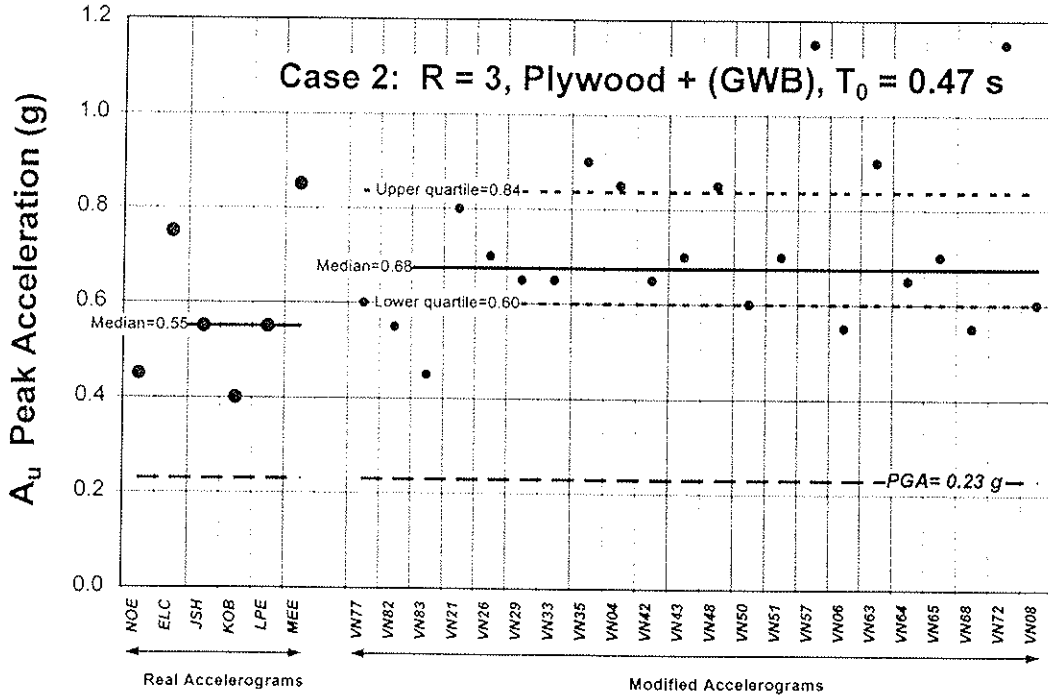


Figure 7 Results for Case 2

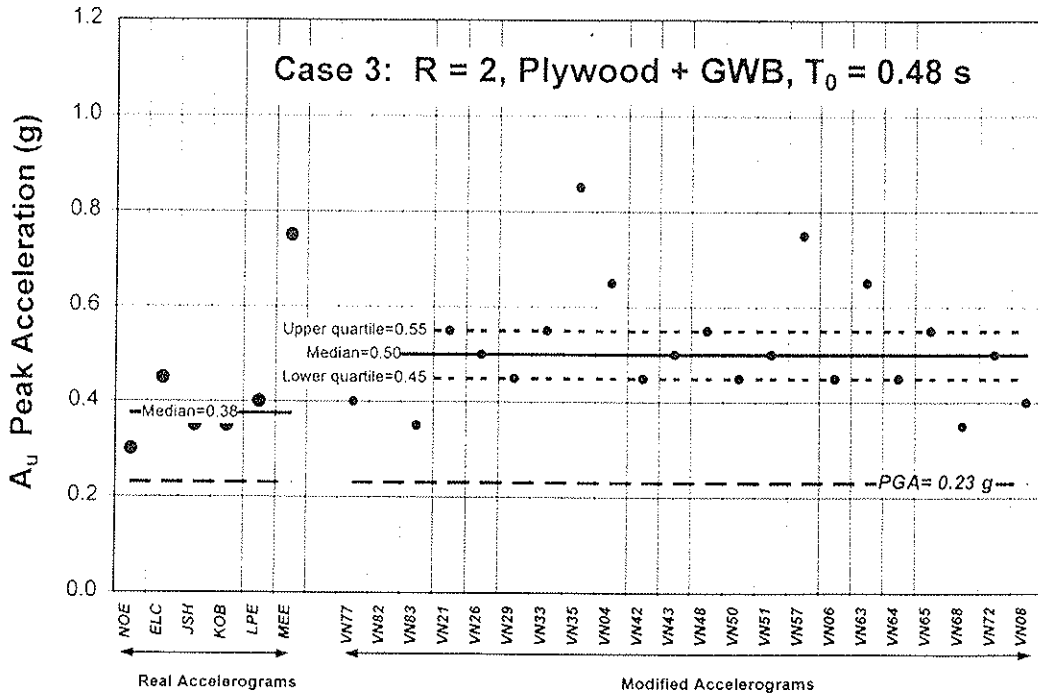


Figure 8 Results for Case 3

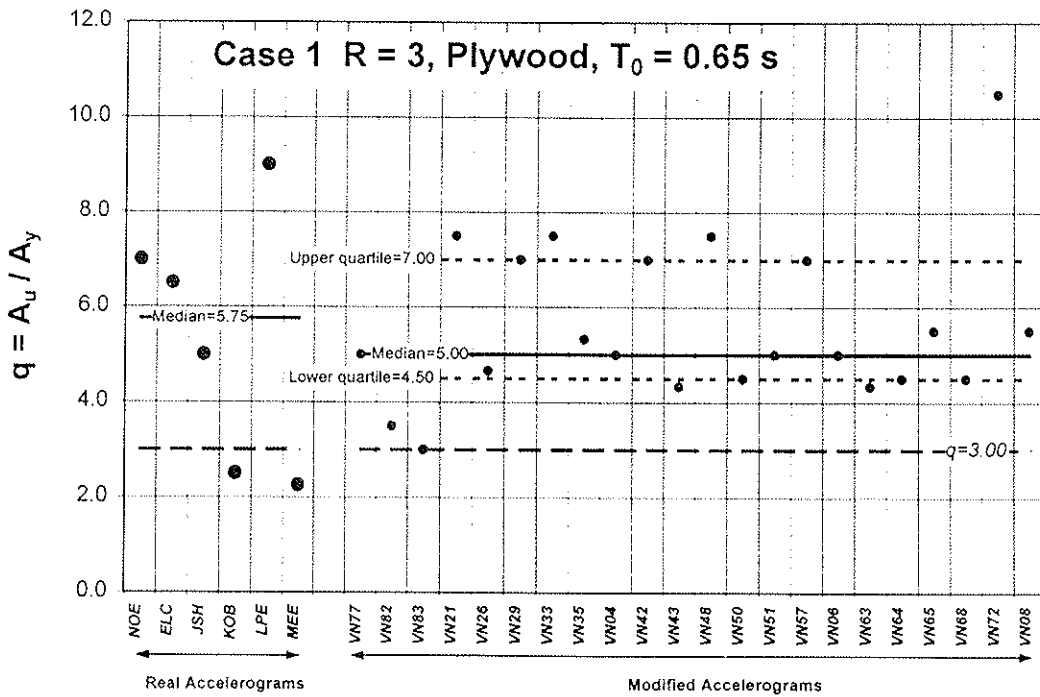


Figure 9 European Behaviour Factor for Case 1

INTERNATIONAL COUNCIL FOR BUILDING RESEARCH STUDIES AND DOCUMENTATION
WORKING COMMISSION W18 - TIMBER STRUCTURES

EVALUATION OF WOOD FRAMED SHEAR WALLS
SUBJECTED TO LATERAL LOAD

by

M Yasumura
Shizuoka University
N Kawai
Building Research Institute
Japan

MEETING THIRTY

VANCOUVER

CANADA

AUGUST 1997

Evaluation of Wood Framed Shear Walls subjected to Lateral Load

Motoi YASUMURA

Department of Forest Resources Science, Shizuoka University, Japan

Naohito KAWAI

Codes and Evaluation Research Center, Building Research Institute, Japan

Abstract

The purpose of this study is to establish the test method for evaluating the seismic performance of wood-framed shear walls. The quasi-static monotonic loading and the reversed cyclic loading were applied to the nailed joints and the wood-framed shear walls sheathed with the plywood, OSB and gypsum board. The yield load, ultimate load and the maximum displacement were determined by the several procedures, and the energy dissipation of the nailed joints and the shear walls is discussed.

1. Introduction

The revision of the Japanese standard for wood-framed building¹⁾ in March 1997 requires to ensure the ultimate safety of the structure against the severe earthquake motion in certain conditions such as, for example, in case the materials used for the structure and the structural design are not in conformity with the specification provided in this standard. This new design concept requires to estimate the load carrying capacity and the seismic performance of wood-framed structures by either testing or calculation. The seismic performance of wood-framed structures can be estimated on the basis of the load carrying capacity and the energy dissipation of the shear walls. The test methods for determining the seismic performance of joints made with mechanical fasteners has been provided in CEN Standard²⁾ and also discussed in ISO-TC165/WG7. In this study, the quasi-static monotonic loading and the reversed cyclic loading tests were carried out on the nailed joints and shear walls, and the test method and the evaluation of the seismic performance of wood-framed shear walls are discussed.

In the current Japanese design of wood-framed structures, the allowable shear strength of shear walls is determined by either the racking test of shear walls or the calculation based on the yield strength of a nailed joint connecting the sheathing material to the wooden frames³⁻⁴⁾. The racking test of the wood-framed shear walls to determine the permissible strength is in general based on ASTM E72 with tie rods. The test is in principle based on the monotonic

loading except for one subjected to the simple reversed cyclic loading. Following two definitions of the shear deformation is lead by the horizontal displacements of the top and bottom plates (δ_1 and δ_2) and the vertical displacements of the end studs (δ_3 and δ_4).

$$\text{Apparent shear deformation} = \frac{\delta_1 - \delta_2}{h}$$

$$\text{True shear deformation} = \frac{\delta_1 - \delta_2}{h} - \frac{\delta_3 + \delta_4}{a}$$

In general, the true shear deformation is applied to the evaluation of wood-framed shear walls, while the braced frames of Japanese

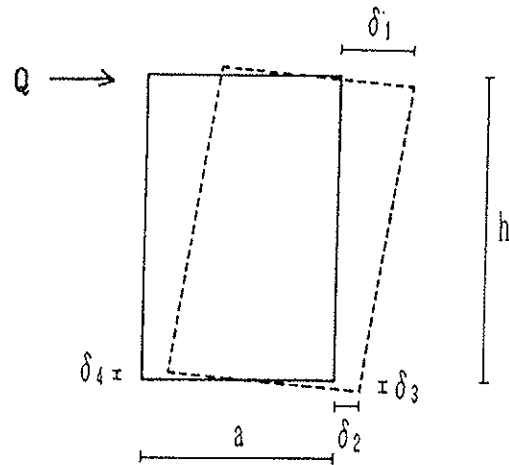


Fig.1 True shear deformation

conventional post-and-beam structures are evaluated with the apparent shear deformation as the tie rods to prevent the up-lift of the panel are not frequently used for the testing. The allowable shear strength is determined with the minimum value of the following three criteria.

$$Pa = \min \left\{ \begin{array}{l} P_{1/300} \\ \frac{2}{3} P_{\max} \\ P_{1/2\gamma_{\max}} \end{array} \right.$$

Where, $P_{1/300}$ is the load corresponding to the true shear deformation of 1/300 rad., P_{\max} is the maximum load, and $P_{1/2\gamma_{\max}}$ is the load corresponding to the half of the maximum deformation. The true shear deformation of 1/300 rad. is replaced by 1/120 rad. when the apparent shear deformation is applied. Although this method is simple and practical, it does not include of the evaluation of the ultimate load and the energy dissipation of the shear walls under the reversed cyclic loading.

The loading protocol and the determination of the yield load are provided in CEN standard on the joints made with the mechanical fasteners²⁾. The loading protocol as shown in Fig.2 is based on the yield displacement (D_y) corresponding to the yield load (P_y) which is defined by the intersection of two lines: the first line is determined by the drawn through the point on the load-slip curve corresponding to 0.1 P_{\max} and the point on the load-slip curve corresponding to 0.4 P_{\max} , the other drawn as the tangent having an inclination of 1/6 of the first line as shown in Fig.5. Different from CEN standard, D_y is defined as the point on the load-slip curve corresponding to P_y in this study.

The Yield load defined by this method has the trend to depend on the inclination of the

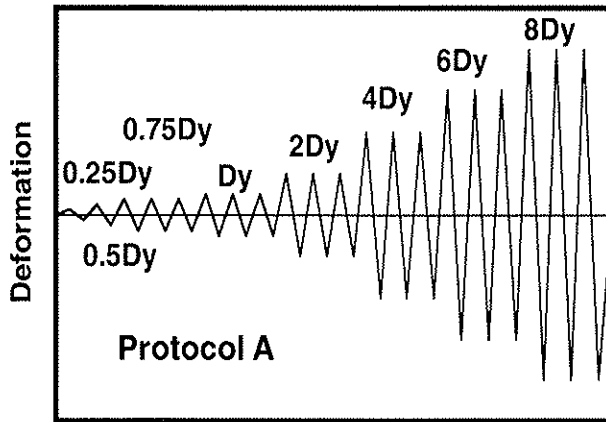


Fig.2 Loading protocol for the reversed cyclic loading test of joints and shear walls based on CEN 124.117. D_y represents the yield displacement.

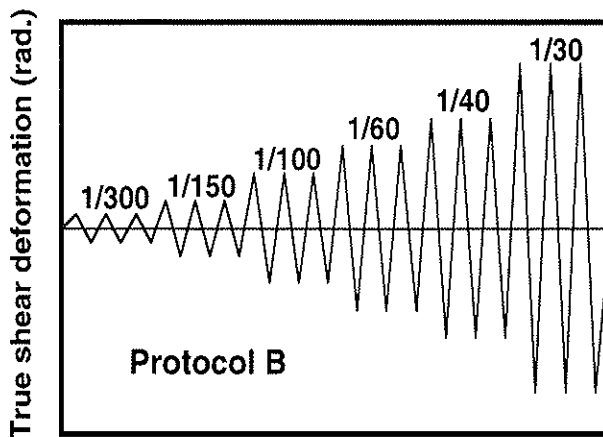


Fig.3 Loading protocol for the reversed cyclic loading test of shear walls based on 1/300 true shear deformation.

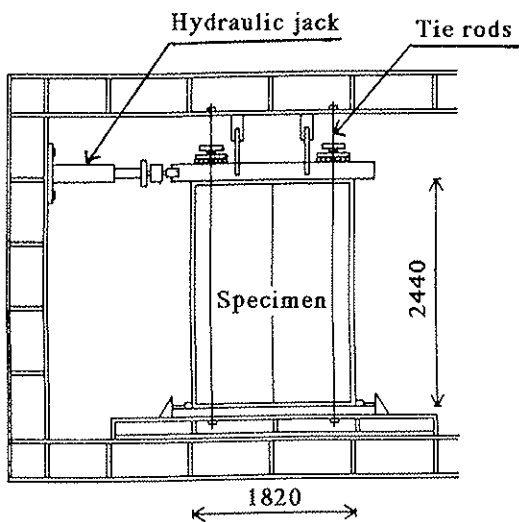


Fig.4 Racking test apparatus

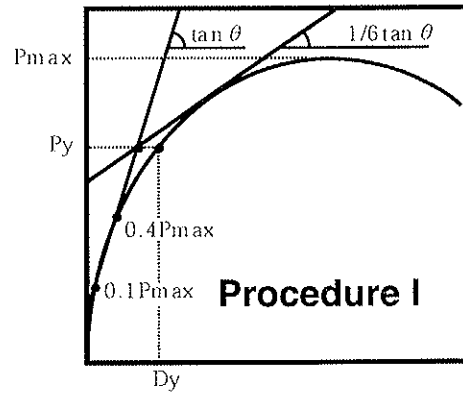


Fig.5 Definition of P_y by EN TC124.117

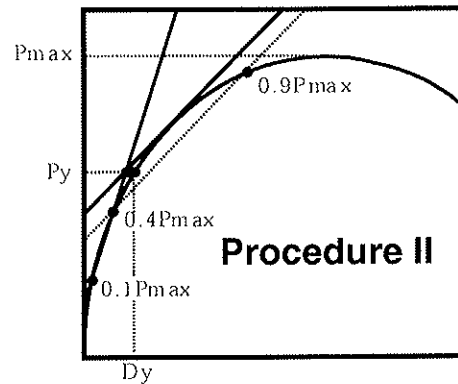


Fig.6 Proposed definition of P_y

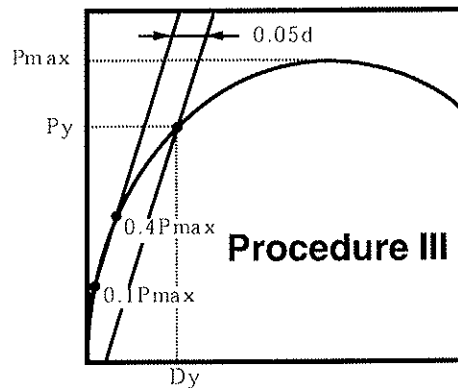


Fig.7 Definition of P_y by 5% off-set

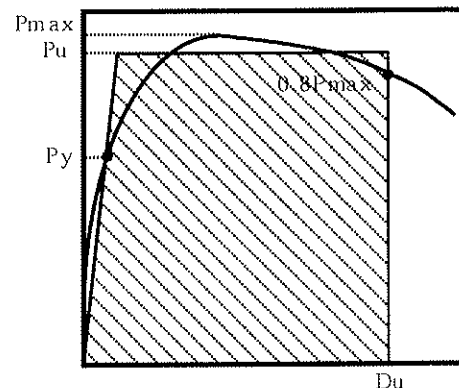


Fig.8 Definition of P_u and D_u

first line. It tends to give the higher yield load when the inclination of the first line is lower, and lower yield load when the inclination of the first line is higher. Therefore, new definition of the yield load is proposed in this study which is determined by the intersection of two lines: the first line is determined by the drawn through the point on the load-slip curve corresponding to 0.1 P_{max} and the point on the load-slip curve corresponding to 0.4 P_{max} , the other drawn as a parallel line having the inclination through the point on the load-slip curve corresponding to 0.4 P_{max} and the point on the load-slip curve corresponding to 0.9 P_{max} as shown in Fig.6.

2. Specimens and test methods

2.1 Single shear nailed joints

Specimens had two sheets of 9.5 millimeters thick spruce plywood , 9.5 millimeters thick Oriented Strand Board, 12 millimeters thick gypsum board connected to the nominal two-by-four lumbers of S-P-F with four common wire nails of 2.87 millimeters diameter (CN50) for plywood and OSB and gypsum nails of 2.34 millimeters diameter (GN40) for gypsum board. Six specimens of each type were subjected to the quasi-static monotonic lateral loading and six others to the reversed cyclic loading as shown in Fig.2. D_y for the reversed cyclic loading was determined by the Procedure II.

2.2 Shear walls

Specimens had the wooden framing of 1.82 meters length and 2.44 meters height and the sheathings of 9.5 millimeters thick plywood, 9.5 millimeters thick Oriented Strand Board and 12 millimeters thick gypsum board. Sheathing materials were connected to the frames of nominal two-by-four lumbers of S-P-F with CN50 and GN40. Nail spacing was 100 millimeters in the perimeters of a sheet material and 200 millimeters on the central support. Three specimens of each type were subjected to the monotonic loading, three others subjected to the reversed cyclic loading as shown in Figs.2 and two as shown in Figs. 3. The racking test of shear walls was conducted according to ASTM E72 as shown in Fig.4. Two tie rods were placed at the both ends of the specimen in the reversed cyclic loading test, and double studs were applied at the end of the frame to prevent the embedding of the end studs to the bottom plate. The horizontal displacements of the top and bottom plates and the vertical displacements of the end studs were measured by the electric transducers.

3. Results and discussions

3.1 Load-deformation relationship

Figs.9 and 10 show the load-deformation relationships of the nailed joints and shear walls, respectively. The degradation of the strength by the reversed cyclic loading was observed both in the nailed joints and the shear walls. The influence of the reversed cyclic loading on the strength characteristics was more remarkable in the nailed joints than the shear walls.

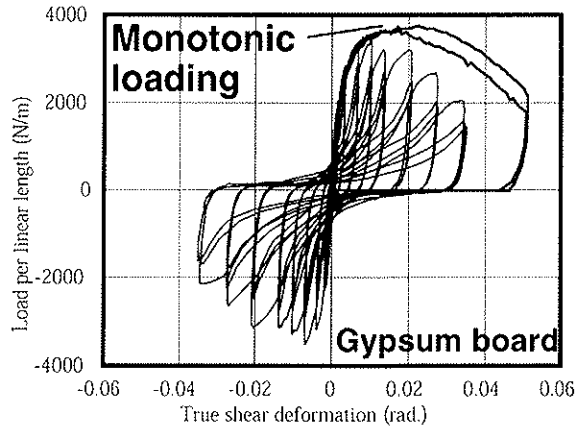
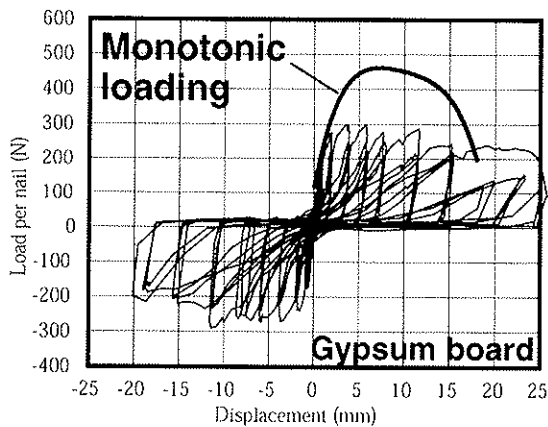
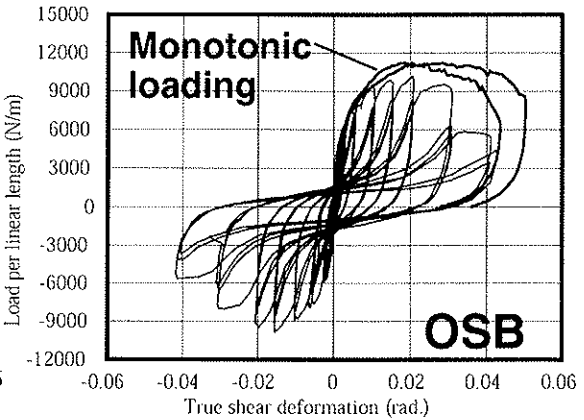
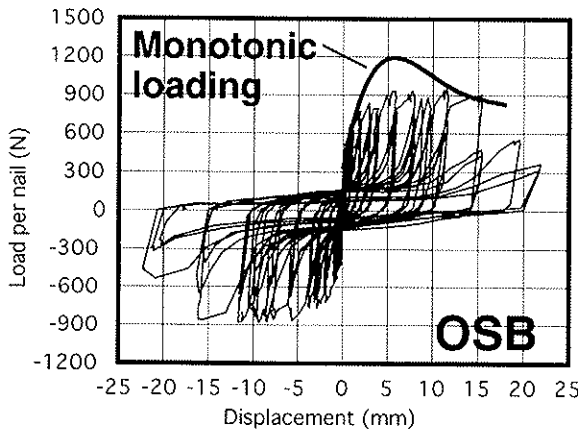
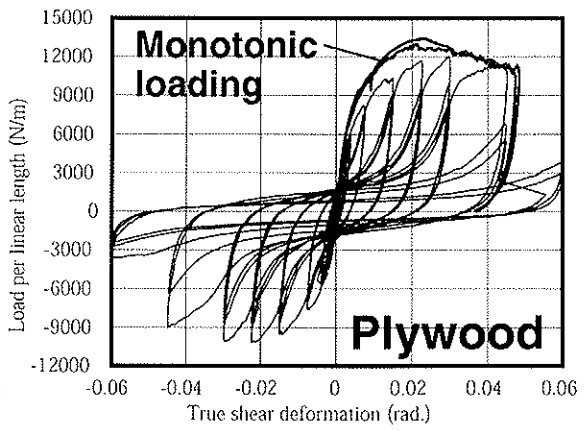
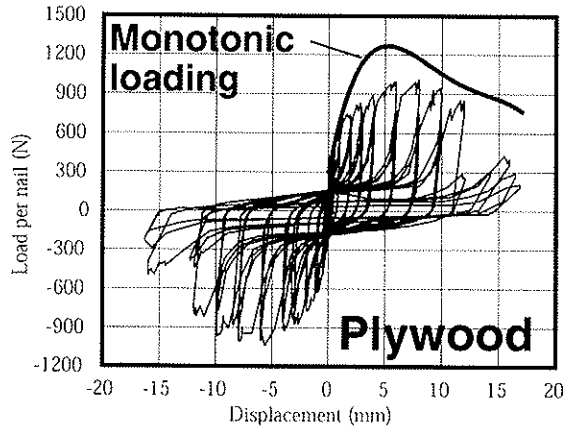


Fig.9 Load-displacement relationship of nailed joint

Fig.10 Load-displacement relationship of shear walls

3.2 Yield load

Table 1 compares the yield load of the nailed joints of the monotonic and reversed cyclic loading tests determined by the different evaluation procedures (I) to (III). The procedure (I) is based on CEN standard as shown in Fig.5, the procedure (II) is that proposed in this paper as shown in Fig.6 and the procedure (III) is based on 5% off-set of the diameter of the fastener. The yield load of the reversed cyclic loading test was 15 to 25% smaller in plywood and OSB sheathed specimens and 25 to 40% smaller in the gypsum board sheathed specimens than that of the monotonic loading test. The yield load determined by the procedure (II)

was in general the highest, followed by those by the procedures (III) and (II) except for some exceptions.

Table 2 shows the yield load of the shear walls of the monotonic loading test determined by the procedures (I) and (II). It is remarkable that the yield load determined by the procedure (II) with the apparent shear deformation was very close to that determined with the true shear deformation, while the yield load determined by the procedure (I) with the apparent shear deformation was 20 to 40% higher than that determined with the true shear deformation. The yield load determined by the procedures (I) and (II) was compared with the calculated values by the following formula:

$$P_y = q \cdot s$$

$$s = \min.\left(\frac{m-1}{a}, \frac{n-1}{h}\right)$$

Where, a and h are the width and the height of the wall having an unit of sheet material, m and n are the number of nails in an horizontal and vertical perimeter of the sheet material and q is the yield strength of the nailed joint. The q value can be obtained from either the single shear test of the nailed joint or the yield theory⁵⁾.

The yield strength of shear walls calculated from the experimental results of nailed joints (1) and the yield theory (2) agreed well with that obtained from the procedure (II). It also agreed with the load corresponding to the true shear deformation of 1/300. These results indicate that it is appropriate to apply the proposed procedure (II) to estimate the yield strength of wood-framed shear walls.

3.3 Ultimate load

Table 3 compares the ultimate load of the nailed joints in the monotonic and reversed cyclic loading tests. The ultimate load was determined by the bi-linear approximation of the

Table 1 Comparison of the yield load for nail joint determined by the procedures (I), (II) and (III).

Sheathing material	Evaluation method	Monotonic loading				Reversed cyclic loading			
		Py (N)		Dy (mm)		Py(N)		Dy (mm)	
		Av.	SD	Av.	SD	Av.	SD	Av.	SD
Plywood	I	569	36.0	0.245	0.100	485	70.5	0.528	0.227
	II	698	62.8	0.497	0.086	563	48.5	0.851	0.237
	III	639	62.5	0.357	0.062	481	59.7	0.517	0.133
OSB	I	528	60.4	0.191	0.114	440	72.5	0.264	0.127
	II	683	75.2	0.478	0.161	566	56.9	0.683	0.258
	III	627	73.8	0.322	0.087	471	76.9	0.351	0.089
Gypsum board	I	258	36.9	0.705	0.398	192	43.8	0.873	0.315
	II	288	30.0	0.948	0.333	167	31.7	0.654	0.254
	III	243	27.7	0.577	0.188	163	36.0	0.579	0.183

load-displacement relationship as shown in Fig.8. First the yield point and the maximum displacement were obtained from the load-deformation curves of the monotonic loading test and the envelop curves of the reversed cyclic loading test. The yield point was obtained from the procedure (II), and the maximum displacement corresponding to 80% of the maximum load after the peak load was determined. Then the ultimate load was obtained so that it has the equivalent energy dissipation as the original curves up to the maximum displacement. The ultimate load and the maximum displacement of the reversed cyclic loading test was respectively 10 to 15% and 10 to 30% smaller than those of the monotonic loading test. The

Table 2 Comparison of the yield load of the shear walls in the monotonic loading test

Sheathing material	Evaluation method	Py (kN/m)				Dy (x10 ⁻³ rad.)		P _{1/300} (kN/m)	2/3P _{max} (kN/m)
		Experiment		Calculation		True	Apparent		
		True	Apparent	(1)	(2)				
Plywood	I	8.22	10.0	5.69	6.83	4.68	13.51	6.95	8.81
	II	7.37	7.61	6.98		3.71	8.05		
OSB	I	6.08	8.44	5.28	5.81	2.47	11.9	6.79	7.47
	II	6.15	6.43	6.83		2.54	6.92		
Gypsum board	I	2.43	2.96	2.58	2.27	3.00	7.46	2.42	2.73
	II	2.11	2.24	2.88		2.29	4.53		

Calculation (1): calculated from the yield load determined by the testing of nailed joints.

Calculation (2): calculated by the Yield theory.

Table 3 Ultimate load and the maximum displacement of the nailed joints.

Sheathing material	Monotonic loading				Reversed cyclic loading			
	Pu (N)		Du (mm)		Pu(N)		Du (mm)	
	Av.	SD	Av.	SD	Av.	SD	Av.	SD
Plywood	1150	122	13.2	4.28	907	108	15.0	2.46
OSB	1100	122	14.7	3.76	872	77.5	16.2	3.55
Gypsum	435	20.8	13.9	1.28	282	33.0	14.3	4.57

Table 4 Ultimate load and the maximum displacement of the shear walls.

Sheathing material	Monotonic loading		Reversed cyclic loading				
	Pu (kN/m)	Du (x10 ⁻³ rad)	Pu(kN/m)		Du (x10 ⁻³ rad)		Pu Calculated (kN/m)
			Protocol A	Protocol B	Protocol A	Protocol B	
Plywood	12.0	47.7	9.51	10.0	42.5	35.6	9.07
OSB	10.3	43.8	8.69	8.97	33.9	32.4	8.72
Gypsum	3.43	37.8	2.84	3.05	26.9	28.2	2.82

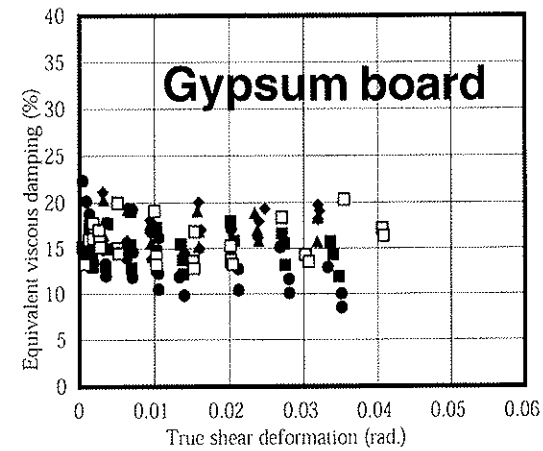
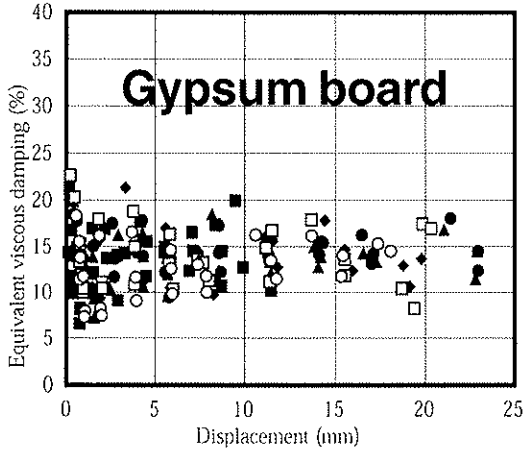
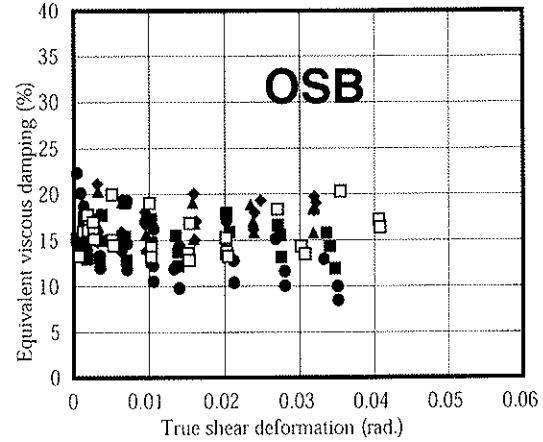
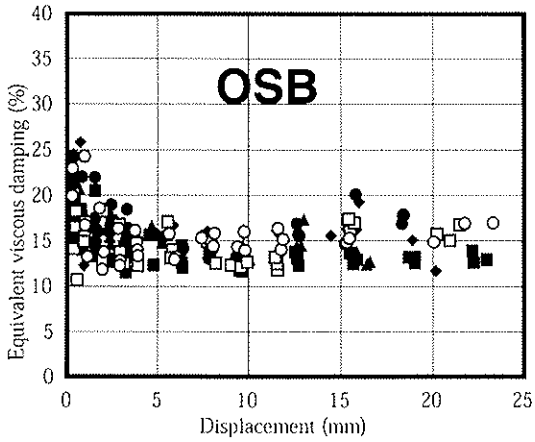
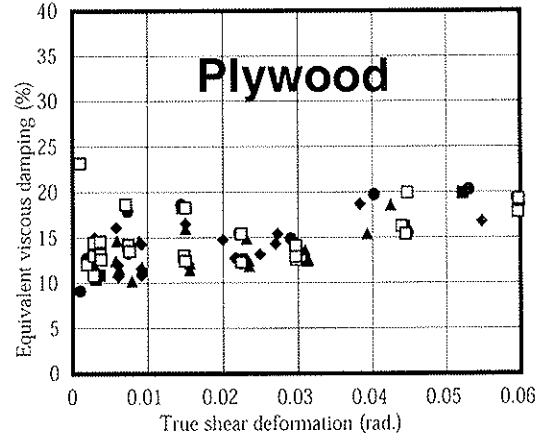
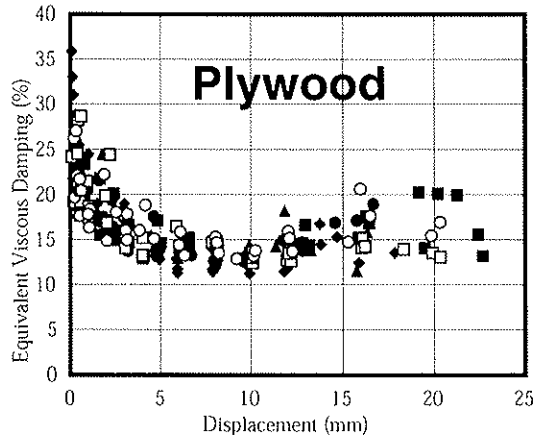


Fig.11 Equivalent viscous damping ratio of nail joints

Fig.12 Equivalent viscous damping ratio of shear walls

ultimate load was calculated from the following formula and compared with the experimental results.

$$Pu = q_u \cdot s$$

$$s = \min.\left(\frac{m-1}{a}, \frac{n-1}{h}\right)$$

Where, q_u is the ultimate load of the nailed joint. The calculated ultimate load agreed well with the experimental results. This indicates it possible to estimate the ultimate load of the

shear walls from the ultimate load of the nailed joints.

3.3 Energy dissipation

Figs.11 and 12 show the equivalent viscous damping ratio of the nailed joints and the shear walls, respectively. The equivalent viscous damping is obtained from the ratio of the dissipated energy in a cycle (E_d) to the potential energy (E_p) as follows:

$$h_{eq} = \frac{E_d}{2\pi \cdot E_p}$$

The equivalent viscous damping of the nailed joints varied from 15 to 25% when the displacement was smaller than 1mm and decreased to 15% in average when the displacement was larger than 5 mm in the plywood and OSB sheathed walls. This trend was not clear in the gypsum sheathed nailed joints. The equivalent viscous damping ratio of the shear walls was almost constant regardless of the displacement within the range of 10 to 20%.

Table 5 shows the total energy dissipation of the nailed joints and the shear walls during the monotonic loading test and the reversed cyclic loading test until the failure. The total energy dissipation of a nailed joint in the reversed cyclic loading test was 15 to 20 times as large as the monotonic loading, and that of the shear wall was about 10 times as large as this. There were few difference of the dissipated energy between the protocols (A) and (B) except for the plywood-sheathed shear walls, however this magnitude of the difference did not make an important effects on the test results. In the monotonic loading test, the sum of the energy dissipation of the nailed joints ($N \cdot E_n$) agreed well with the total energy dissipation of a shear wall (E_w) for the plywood and OSB sheathed shear walls. That of the gypsum board sheathed shear walls was 38% larger than E_w . This result indicates that the most of the energy of the monotonic loading test is dissipated by the nails placed in the perimeter of a sheet material. In the reversed cyclic loading test, the sum of the energy dissipation of the nailed joints ($N \cdot E_n$) was 30 to 90% larger than the total energy dissipation of a shear wall

Table 5 Total energy dissipation of the nailed joints and the shear walls.

Specimen	Monotonic			Reversed cyclic			
	En Nail (Nm)	Ew Wall (Nm)	N*En (Nm)	En Nail (Nm)	Ew Wall (Nm)		N*En (Nm)
					ProtocolA	ProtocolB	
Plywood	14.7	1187	970	299	14592	10292	19734
OSB	15.9	1060	1049	290	11588	11262	19140
Gypsum	5.72	274	378	87.1	3119	3556	5749

* N: total number of nails in the perimeter of a sheet material

** En: total energy dissipation of a nail, Ew: total energy dissipation of a unit sheathing (0.91m) of the shear wall.

(Ew). This indicates that the reversed cyclic loading by the protocol A is severer test for the nailed joints than the shear walls especially for the wall sheathed with the material having comparatively low rigidity such as plywood.

4. Conclusion

The yield load of the shear walls determined by the proposed procedure in this paper gives appropriate values both for the true and apparent shear deformations, while the yield load determined by CEN standard procedure gives 20 to 40% higher value for the apparent shear deformation than that for the true shear deformation. The yield load determined by this method agreed well with the yield strength calculated from the experimental results of the nailed joints and that with the yield theory. It also agreed well with the load corresponding to the true shear deformation of $1/300$.

The ultimate load and the maximum displacement under the reversed cyclic loading test was respectively 10 to 15% and 10 to 30% smaller than those of the monotonic loading test. The calculated ultimate load from that of the nailed joint under the reversed cyclic loading test agreed well with the experimental results.

The equivalent viscous damping of the nailed joints varied from 15 to 25% when the displacement was smaller than 1mm and decreased to 15% in average when the displacement was larger than 5 mm in the plywood and OSB sheathed walls. This trend was not clear in the gypsum sheathed nailed joints. The equivalent viscous damping ratio of the shear walls was almost constant regardless of the displacement within the range of 10 to 20%.

Sum of the total energy dissipated in the nailed joints agreed well with the total energy dissipation of a shear wall under the monotonic loading. Sum of the total energy dissipated in the nailed joints was 30 to 90% larger than the total energy dissipation of a shear wall under the reversed cyclic loading.

References

1. Ministry of Construction : Notification No.56, January 1982, revised March 1997
2. CEN: EN TC 124.117, May 1994
3. YASUMURA,M. : Japan overview:design of timber joints in seismic zones, Proceedings of International Workshop On Wood Connectores, 42-51, FPS, 1993
4. YASUMURA,M. : Japan overview:design concept and prospect of bolted joints and nailed joints, Proceedings of International Workshop On Wood Connectores, 114-121, FPS, 1993
5. YASUMURA,M. and T. Murota : Design Procedures for Wood-framed Shear Walls, Proceedings of The IUFRO S5.02, August 1992
6. Dolan, J.D. : Proposed Test Method for Dynamic Properties of Connections Assembled with Mechanical Fasteners, Proceedings of 26th CIB-W18, 26-7-1, August 1993
7. Karacabeyli, E.,A. Ceccottii : Quasi-static Reversed-cyclic testing of Nailed Joints, Proceedings of 29th CIB-W18, 29-7-7, August 1993

**INTERNATIONAL COUNCIL FOR BUILDING RESEARCH STUDIES AND DOCUMENTATION
WORKING COMMISSION W18 - TIMBER STRUCTURES**

**A NEW STATISTICAL METHOD FOR THE ESTABLISHMENT OF
MACHINE SETTINGS**

by

F. Rouger
CTBA
France

**MEETING THIRTY
VANCOUVER
CANADA
AUGUST 1997**

A new statistical method for the establishment of machine settings.

F. Rouger¹

CTBA, FRANCE

1. Abstract.

When verifying settings, a major concern is to quantify the effects of down- or up-grading, and give limits on these errors. Because we never know what is for a piece the correct strength class, which is only defined by fractiles, the first step is to assign a strength class regardless of the grading method. Once this target strength class is given for each piece, the result of the grading process is compared to the target value. For each error which occurs in this process, an elementary cost is assigned. This cost is based on safety concerns for up-grading and on economic losses for down-grading. It depends on the set of strength classes to be produced.

Another part of this paper is dedicated to verification of settings. Rather than making a separate sampling for verification, a crossed-validation procedure is proposed. This procedure aims at reducing the sampling, so that the sample can be used simultaneously for the establishment and verification of settings. Since this procedure is repeated several times on different parts of the sample, one can ensure that a piece is never used for both.

By using the cost assignment method and the crossed-validation procedure, a global cost matrix is formulated. It can subsequently be used for comparison to limiting values, the result being an agreement for a specific grading machine producing specific strength classes. Some examples illustrate the method.

2. Introduction.

When calculating machine settings in the field of machine strength grading, one must verify the accuracy and the reproductibility of these settings. The accuracy aims at measuring the capability of the machine to predict the correct grade for a given piece. Rather than measuring the accuracy of the sensing devices, it should be preferred to measure the accuracy of the grade prediction : a machine that has a poor sensing device could perform well if the target grades are limited. Since a grade is defined by statistical fractiles, it is impossible to know if the grade assignment is correct for an individual piece. Therefore, the method presented in this paper considers a whole sample. Once the accuracy is established, one must verify the reproductibility of the machine : if a sample is passed several times through the machine, the response of the machine should be as uniform as possible. Once again, it is preferable to check the reproductibility on the grade assignment rather than on the sensing devices.

¹ Head of Research Division, Timber Construction Group

3. Determination of the optimum grading.

This step aims at checking that the grade prediction is correct. If a grade would be defined by minimum values, i.e. minimum Modulus of Elasticity, minimum Modulus of Rupture and minimum density, it would be very easy to check that the actual values of an individual piece are larger than the minima, given for the grade corresponding to the machine prediction. But grade limits are defined by statistical fractiles, calculated on a sample :

- Mean Modulus of Elasticity $E_{0,\text{mean}}$
- Characteristic strength $f_{m,k}$ (*in the case of bending*)
- Characteristic density ρ_k

The characteristic values usually correspond to the lower 5th percentiles of the sample. The optimum grading of a sample should be such that, if this sample is graded into several grades, the characteristic values of each graded subsample are larger than target values. Of course, one can find different ways of achieving this requirement, but let us assume that the correct assignment is the one that maximises the yields in the top grades. An iterative procedure has been already described in [1]. It can be summarized in Annex 1.

After performing optimal ranking, some pieces are not ranked in the prescribed strength classes. For these pieces, one can determine the mean MOE and the 5% MOR.

4. Establishment of the elementary cost matrix.

Once the optimal grading is performed, a model is built to predict the strength from the measurements of the grading machine. This model could be a multi-regression, a neural networks or something else. The main aspect is that it produces a strength class for each piece that passes through the machine. The accuracy of the machine is thus a combination of the sensing devices accuracy and the goodness of fit of the model. To establish it, we compare the assigned grade of a piece to its optimum grade, on a sample which will be defined later. When the assigned grade is higher than the optimum grade, we can define it as an *upgrading*. In this case, there is a safety issue. When the assigned grade is lower than the optimum grade, we can define it as a *downgrading*. In this case, there is a material loss issue. The elementary cost matrix corresponds to a cost assignment for each down- or upgrading, as a function of the optimum grade and the assigned grade.

4.1. Upgrading.

Example : If a piece which should belong to C24 (called Optimum grade) is graded into C40 (called Assigned grade), it is upgraded. The consequence will be an increased probability of failure of the piece, which has a cost.

Procedure for determining the cost :

(1) From the characteristic value of the Optimum grade ($f_{m,k,\text{Optimum}}$), we calculate the mean value, $\mu(f_{m,\text{Optimum}})$, by assuming a LogNormal distribution and a coefficient of variation $cv = 30\%$, according to :

$$\mu(f_{m,\text{Optimum}}) = e^{\left[\ln(f_{m,k,\text{Optimum}}) + \left(\frac{1}{2}cv^2 + 1.65cv \right) \right]} \quad (4.1)$$

(2) By assuming a target safety $\beta_{target} = 3.0$, we can calculate the applicable stress to the piece of timber according to:

$$S_{Assigned} = \mu(f_{m,Assigned}) - \beta_{target} \mu(f_{m,Assigned}) cv \quad (4.2)$$

(3) If this stress is now applied to the real strength of the piece, the safety index will be :

$$\beta_{real} = \frac{\mu(f_{m,Optimum}) - S_{Assigned}}{\mu(f_{m,Optimum}) cv} \quad (4.3)$$

where $\mu(f_{m,Optimum})$ is calculated according to a similar expression than equation (4.1)

(4) The cost is the difference between β_{target} and β_{real} .

$$Cost (Upgrading) = \beta_{target} - \beta_{Real} \quad (4.4)$$

Numerical example :

Optimum grade : C24

Assigned Grade : C40

$\mu(f_{m,Assigned}) = 68.6$ Mpa

$\mu(f_{m,Optimum}) = 41.18$ MPa

$S_{Assigned} = 6.86$ MPa

$\beta_{real} = 2.778$

Cost = 0.222

4.2. Downgrading.

Example : If a piece which should belong to C40 (called Optimum Grade) is graded into C24 (called Assigned Grade), it is downgraded. The consequence will be an increased quantity of material as compared with what should be necessary for a given design. Because most of the timber is dimensionned according to the deformations, the loose of material is given by :

$$Cost (Downgrading) = \sqrt[3]{\frac{E_{Optimum}}{E_{Assigned}}} - 1 \quad (4.5)$$

where $E_{Optimum}$ and $E_{Assigned}$ are the MOE for the Optimum and Assigned Grades.

This equation is explained by the expression of the deformation, which has the form :

$$\delta = \frac{\alpha P L^\beta}{E b h^3} \quad (4.6)$$

where P is the applied load,
 L is the span,
 b, h are the cross-section dimensions,
 E is the modulus of elasticity,
 α, β are constants depending on the load configuration.

which, after transformation, gives :

$$h = \sqrt[3]{\frac{\alpha P L^\beta}{E b \delta}} = K \sqrt[3]{\frac{I}{E}} \quad (4.7)$$

4.3. Elementary Cost Matrix.

By using the equations (4.4) and (4.5), the elementary cost matrix for the strength classes of EN 338 [2] can be built. In the following matrix, the reject has been quantified as :

$$f_{m,k,Reject} = 12 \text{ Mpa} \quad E_{Reject} = 6 \text{ GPa}$$

Table 1 : Elementary Cost Matrix for EN 338 strength classes

Optimum Grade	Assigned Grade									
	C40	C35	C30	C27	C24	C22	C18	C16	C14	Reject
C40	0	0,025	0,053	0,068	0,084	0,119	0,159	0,205	0,26	0,326
C35	0,048	0	0,027	0,042	0,057	0,091	0,13	0,176	0,229	0,294
C30	0,111	0,056	0	0,014	0,029	0,063	0,101	0,145	0,197	0,26
C27	0,16	0,099	0,037	0	0,015	0,048	0,085	0,129	0,18	0,242
C24	0,222	0,153	0,083	0,042	0	0,032	0,069	0,112	0,163	0,224
C22	0,273	0,197	0,121	0,076	0,03	0	0,036	0,077	0,126	0,186
C18	0,407	0,315	0,222	0,167	0,111	0,074	0	0,04	0,087	0,145
C16	0,5	0,396	0,292	0,229	0,167	0,125	0,042	0	0,046	0,101
C14	0,619	0,5	0,381	0,31	0,238	0,19	0,095	0,048	0	0,053
Reject	0,778	0,639	0,5	0,417	0,333	0,278	0,167	0,111	0,056	0

5. Procedure for crossed-validation tests.

5.1. Principles of the method.

The idea of the crossed-validation tests is to use the same sample for establishing the settings of a grading machine and for testing them. To ensure the stability of this procedure, one has to divide the sample into n sub-samples (named SS_i , for $i=1$ to n), which are equally distributed. Let us assume that $n=10$. The number of sub-samples determines the number of required calculations. For each calculation i , a learning sample (named LS_i) and a check sample (named CS_i) are constituted according to the following equation :

$$LS_i = \sum_{\substack{j=1 \\ j \neq i}}^n SS_j \quad CS_i = SS_i \quad (5.1)$$

For each calculation i , a set of settings is determined by using the learning sample. These settings are applied to the check sample, in order to assign a grade (the assigned grade) to each specimen of the check sample.

By this way, each piece of the original sample is used (n-1) times for establishing settings (which might be different for each calculation) and 1 time for checking settings (which have been established without the specimen to be considered). Therefore, the original sample is used for the whole process.

Then, a size matrix (A) is constructed. This size matrix is a squared matrix, in which the rows correspond to the optimum grades and the columns to the assigned grades. Each piece, which is defined by its optimum grade and by its assigned grade, is assigned to the corresponding cell of the size matrix.

The global cost matrix (C) is then constructed according to the following equation, which applies on each cell of the matrix :

$$C_{ij} = \alpha - \frac{100A_{ij}B_{ij}}{\sum_i A_{ij}} \quad (5.2)$$

where C is the global cost matrix,

A is the size matrix,

B is a sub-matrix of the elementary cost matrix (see Table 1), defined by the choice of the grades;

$\alpha = 1.0$ (α is a value that will need further adjustments).

5.2. Requirements for checking the settings.

Once the procedure is applied, two requirements must be fulfilled :

- the characteristic values of the assigned grades (given for the check samples) should meet the requirements of EN 338 (at minimum for $f_{m,k}$ and ρ_k , within 5% for E_{mean})
- the global cost matrix should be such that no negative terms should exist in the lower triangle of the matrix (which corresponds to wrongly upgraded pieces).

If these requirements are fulfilled, the machine settings can be determined on the original sample.

5.3. Examples.

Example 1 : Machine A, strength classes = (C30, C18, Reject)

$$A = \begin{pmatrix} 207 & 43 & 1 \\ 37 & 174 & 13 \\ 3 & 46 & 68 \end{pmatrix} \quad B = \begin{pmatrix} 0.0 & 0.101 & 0.26 \\ 0.222 & 0.0 & 0.145 \\ 0.5 & 0.167 & 0.0 \end{pmatrix} \quad C = \begin{pmatrix} 1.0 & -0.65 & 0.68 \\ -2.33 & 1.0 & -1.30 \\ 0.39 & -1.92 & 1.0 \end{pmatrix}$$

$$\sum_i A_{ij} = (247 \quad 263 \quad 82)$$

The characteristic values for the assigned grades are the following :

Table 2 : Characteristic values for Example 1

Strength Class	MOR (N/mm ²)	MOE (kN/mm ²)
C30	34,1	11,8
C18	21,9	8,9

Although the characteristic values of the assigned grades are satisfied (see Table 2), these grading settings should be rejected because of C_{21} and C_{32} .

Example 2 : Machine A, strength classes = (C40, C30, C24, C18, Reject)

$$A = \begin{pmatrix} 110 & 193 & 39 & 9 & 1 \\ 7 & 67 & 54 & 20 & 2 \\ 0 & 7 & 15 & 6 & 0 \\ 0 & 3 & 9 & 21 & 5 \\ 0 & 0 & 0 & 0 & 2 \end{pmatrix} \quad B = \begin{pmatrix} 0.0 & 0.05 & 0.08 & 0.16 & 0.33 \\ 0.11 & 0.0 & 0.03 & 0.10 & 0.26 \\ 0.22 & 0.08 & 0.0 & 0.07 & 0.22 \\ 0.41 & 0.22 & 0.11 & 0.0 & 0.14 \\ 0.78 & 0.5 & 0.33 & 0.17 & 0.0 \end{pmatrix} \quad C = \begin{pmatrix} 1.0 & -2.8 & -1.8 & -1.6 & -2.3 \\ 0.34 & 1.0 & -0.34 & -2.6 & -4.2 \\ 1.0 & 0.8 & 1.0 & 0.26 & 1.0 \\ 1.0 & 0.7 & 0.15 & 1.0 & -6.2 \\ 1.0 & 1.0 & 1.0 & 1.0 & 1.0 \end{pmatrix}$$

$$\sum_i A_{ij} = (117 \quad 270 \quad 117 \quad 56 \quad 10)$$

The characteristic values for the assigned grades are the following :

Table 3 : Characteristic values for Example 2

Strength Class	MOR (N/mm ²)	MOE (kN/mm ²)	Density (kg/m ³)
C40	41,7	16	423
C30	31,2	13,4	406
C24	25,4	11,3	371
C18	23,1	10,2	357

These grading settings meet the requirements of both the characteristic values and cost matrix. It illustrates that a given machine can be accepted or rejected depending on the choice of grades. It can also be observed that these grade settings are safe, since the upper triangle of the cost matrix has a subsequent number of negative values.

6. Extension of the method for repeatability tests.

6.1. Principles of the method.

The problem of repeatability is slightly different, in the sense that we do not want to check if a machine grades correctly, but if it grades in the same manner a given specimen passed several times through the machine. The procedure for checking repeatability is comparable to the procedure described in chapter 5, with the following exceptions :

1) A number of pieces is passed several times through the machine (e.g. 5 times). The optimum grade is defined as the first pass grade for each piece.

2) The elementary cost matrix takes into account the grade difference from one pass to another one. If, for one piece, two passes differ from one grade, the elementary cost equals 1 for the second pass. If they differ from two grades, the elementary cost equals 2, and so on.

Therefore, the elementary cost matrix, in the case where all strength classes should be considered, is the following :

Table 4 : Elementary Cost Matrix for EN 338 strength classes

Optimum Grade	Assigned Grade									
	C40	C35	C30	C27	C24	C22	C18	C16	C14	Reject
C40	0	1	2	3	4	5	6	7	8	9
C35	1	0	1	2	3	4	5	6	7	8
C30	2	1	0	1	2	3	4	5	6	7
C27	3	2	1	0	1	2	3	4	5	6
C24	4	3	2	1	0	1	2	3	4	5
C22	5	4	3	2	1	0	1	2	3	4
C18	6	5	4	3	2	1	0	1	2	3
C16	7	6	5	4	3	2	1	0	1	2
C14	8	7	6	5	4	3	2	1	0	1
Reject	9	8	7	6	5	4	3	2	1	0

In the cases where only specific grades are selected, one should apply the same principle.

2) If we consider 5 passes, the first pass corresponds to the optimum grade and the other ones correspond to assigned grades. One can construct a size matrix in the same way than described in chapter 5. The global cost matrix (C) is then constructed according to the following equation, which applies on each cell of the matrix :

$$C_{ij} = \frac{A_{ij} B_{ij}}{\sum_i A_{ij}} \quad (5.3)$$

where C is the global cost matrix,
A is the size matrix ,
B is a sub-matrix of the elementary cost matrix (see Table 4)

6.2. Requirements for checking repeatability

Once the procedure is applied, one requirement must be fulfilled :

- the global cost matrix should be such that no cells should exceed $\beta = 0.1$ (β is a value that will need further adjustments)

6.3. Examples.

Example 1 : Machine A, strength classes = (C22, C16, Reject)

$$A = \begin{pmatrix} 109 & 6 & 0 \\ 1 & 219 & 5 \\ 0 & 4 & 156 \end{pmatrix} \quad B = \begin{pmatrix} 0.0 & 1.0 & 2.0 \\ 1.0 & 0.0 & 1.0 \\ 2.0 & 1.0 & 0.0 \end{pmatrix} \quad C = \begin{pmatrix} 0.0 & 0.026 & 0.0 \\ 0.009 & 0.0 & 0.03 \\ 0.0 & 0.0175 & 0.0 \end{pmatrix}$$

$$\sum_i A_{ij} = (110 \quad 229 \quad 161)$$

This example meets the requirements for repeatability tests.

Example 2 : Machine A, strength classes = (C24, C22, C18, C16, C14, Reject)

$$A = \begin{pmatrix} 8 & 2 & 0 & 0 & 0 & 0 \\ 3 & 96 & 6 & 0 & 0 & 0 \\ 0 & 1 & 106 & 18 & 0 & 0 \\ 0 & 0 & 16 & 79 & 3 & 2 \\ 0 & 0 & 0 & 4 & 56 & 5 \\ 0 & 0 & 0 & 0 & 5 & 90 \end{pmatrix} \quad B = \begin{pmatrix} 0 & 1 & 2 & 3 & 4 & 5 \\ 1 & 0 & 1 & 2 & 3 & 4 \\ 2 & 1 & 0 & 1 & 2 & 3 \\ 3 & 2 & 1 & 0 & 1 & 2 \\ 4 & 3 & 2 & 1 & 0 & 1 \\ 5 & 4 & 3 & 2 & 1 & 0 \end{pmatrix} \quad C = \begin{pmatrix} 0 & 0.02 & 0 & 0 & 0 & 0 \\ 0.27 & 0 & 0.05 & 0 & 0 & 0 \\ 0 & 0.01 & 0 & 0.18 & 0 & 0 \\ 0 & 0 & 0.12 & 0 & 0.05 & 0.04 \\ 0 & 0 & 0 & 0.04 & 0 & 0.05 \\ 0 & 0 & 0 & 0 & 0.08 & 0 \end{pmatrix}$$

$$\sum_i A_{ij} = (11 \quad 99 \quad 128 \quad 101 \quad 64 \quad 97)$$

This example does not meet the requirements for repeatability tests, because of C_{21} , C_{43} , C_{34} . It illustrates that a machine could be very repeatable for a small number of grades, but very unstable for a high number of grades.

7. Conclusions.

The method described in this paper presents two innovative aspects. Firstly, an estimate for the errors of classification has been formulated, based on safety and economic considerations. Secondly, a procedure for checking machine settings and repeatability has been proposed. This method presents the main advantage of replacing experimental work by computing work, which is more affordable. The limiting values corresponding to the requirements are still under investigation, but should be incorporated into a new version of EN 519 [3] in a close future.

8. Acknowledgements

The author would like to thank Yves GRANDVALLET and Stephane CANUS from University of Technology of Compiègne who, while working on a cooperative project on machine grading with neural networks, originated the questions leading to this method. He would also like to thank the members of CEN TC 124, Working Group 2, Ad'Hoc Group 2, who did trial investigations of the method on their own data. The examples given in this paper come from their contribution. Jean-Luc GUILLOT, from CTBA, did similar work on our data and should also be congratulated for his contribution.

9. References.

- [1] ROUGER F. - Application of a modified statistical segmentation method to timber machine strength grading. Wood & Fiber Science, 28(4), 1996
- [2] EN 338 - Structural Timber - Strength classes
- [3] EN 519 - Structural timber - Grading - Requirements for machine strength graded timber and grading machines

Annexe 1 : Optimal grading procedure

1. Read Data File and Make a matrix in which each line contains E , σ , and ρ , plus a specimen identification and an initial grade assignment to 0

```

ORIGIN:=1
M := LIREPRN(Data)
N := dernier(M<1>)
E := sousmatrice(M, 1, N, 2, 2)
σ := sousmatrice(M, 1, N, 1, 1)
ρ := sousmatrice(M, 1, N, 3, 3)
M := augment(augment(E, σ), ρ)
i := 1..N
Ai := i
Bi := 0
M := augment(augment(M, A), B)
    
```

2. The fractile function gives the value in V having the cumulative frequency of n_{target}

```

fractile(V, ntarget) :=
| X ← tri(V)
| freq ← 0
| i ← 0
| while freq ≤ ntarget
|   i ← i + 1
|   freq ←  $\frac{i}{\text{dernier}(X)}$ 
| Xi
    
```

3. The nfractile function gives the cumulative frequency of the value f_{target} in V

```

nfractile(V, ftarget) :=
| X ← tri(V)
| i ← 1
| α ← 0 if X1 > ftarget
| α ← 1 if Xdernier(X) < ftarget
| while Xi ≤ ftarget otherwise
|   i ← i + 1
|   α ←  $\frac{i}{\text{dernier}(X)}$ 
| α
    
```

4. The Extract function extracts from a matrix M the lines for which the 5th column meets the condition c

$c(x, a) := x = a$

$\text{Extract}(M, c, a) :=$

```

i ← 1
for j ∈ 1..lignes(M<5>)
  if c(M<j,5>, a) = 1
    for k ∈ 1..5
      U<i,k> ← M<j,k>
    i ← i + 1
U<1,1> ← 0 if i = 1
U

```

5. The class function extracts from matrix B the elements which have not yet been graded (i.e. $B_{j,5} = 0$) and which, together, constitute the optimum grade having $\sigma_{05} = \sigma_0$, $E_{50} = E_0$ and $\rho_{05} = \rho_0$, unless the yield is lower than r_0

```

classe (B, E_0, sigma_0, rho_0, r_0) := A ← Extract(B, c, 0)
n ← dernier(A<1>)
while n > 0
  f_E ← nfractile(sousmatrice(A, 1, dernier(A<1>), 1, 1), E_0)
  n_E ← partentière(⌊  $\frac{\text{dernier}(A<1>)}{1 - 0.5} \cdot (f_E - 0.5)$  ⌋)
  f_sigma ← nfractile(sousmatrice(A, 1, dernier(A<1>), 2, 2), sigma_0)
  n_sigma ← partentière(⌊  $\frac{\text{dernier}(A<1>)}{1 - 0.05} \cdot (f_{\sigma} - 0.05)$  ⌋)
  f_rho ← nfractile(sousmatrice(A, 1, dernier(A<1>), 3, 3), rho_0)
  n_rho ← partentière(⌊  $\frac{\text{dernier}(A<1>)}{1 - 0.05} \cdot (f_{\rho} - 0.05)$  ⌋)

  N ←  $\begin{bmatrix} n_E \\ n_{\sigma} \\ n_{\rho} \end{bmatrix}$ 
  n ← max(N)
  n ← 0 if n < 0
  n_0 ← r_0 · dernier(B<1>)
  if (dernier(A<1>) - n) < n_0
    A_{1,1} ← ∞
    break
  if n = n_E
    A ← tricol(A, 1)
    A ← sousmatrice(A, n_E + 1, dernier(A<1>), 1, 5) if n < dernier(A<1>)
    otherwise
      A_{1,1} ← ∞
      break
  if n = n_sigma
    A ← tricol(A, 2)
    A ← sousmatrice(A, n_sigma + 1, dernier(A<1>), 1, 5) if n < dernier(A<1>)
    otherwise
      A_{1,1} ← ∞
      break
  if n = n_rho
    A ← tricol(A, 3)
    A ← sousmatrice(A, n_rho + 1, dernier(A<1>), 1, 5) if n < dernier(A<1>)
    otherwise
      A_{1,1} ← ∞
      break

```

6. The intersect function calculates the intersection between two vectors v and w

$$\text{in}(v, x) := \begin{cases} t \leftarrow 0 \\ \text{for } y \in v \\ t \leftarrow 1 \text{ if } x=y \\ t \end{cases} \quad \text{intersect}(v, w) := \begin{cases} u \leftarrow 0 \\ i \leftarrow 1 \\ \text{for } x \hat{=} v \\ \left(\begin{array}{l} u_i \leftarrow x \\ i \leftarrow i+1 \end{array} \right) \text{ if } \text{in}(w, x) \\ u \end{cases}$$

7. The Affect function assigns n to the lines of A optimally graded according the requirements a, b, c, and r

$$\text{affecte}(A, a, b, c, r, n) := \begin{cases} X \leftarrow \text{classe}(A, a, b, c, r) \\ I \leftarrow \text{intersect}(A^{<4>}, X^{<4>}) \\ \text{for } i \hat{=} 1.. \text{dernier}(I) \\ A_{(i),5} \leftarrow n \text{ if } (X_{1,1} \neq) \cdot [A_{(i),5} = 0] \\ A \end{cases}$$

8. The Optimal function performs the optimal grading of matrix M for each column of C

$$\text{optimal}(M, C, r) := \begin{cases} \text{for } i \hat{=} 1.. \text{cols}(C) \\ M \leftarrow \text{affecte}(M, C_{1,i}, C_{2,i}, C_{3,i}, r, i) \\ M \end{cases}$$

9. The Check function checks the fractiles (E_{50} , E_{mean} , σ_{05} , ρ_{05}) for each optimum grade and gives its yield, after having performed the optimal grading. The last column contains similar values for the reject. In the case where a grade cannot be found, the corresponding column is set to zero.

```

check(M,C,r) := A ← optimal(M,C,r)
                for i ∈ 1..cols(C)
                  if max(Extract(A,c,i)) ≠ 0
                    U1,i ← fractile(Extract(A,c,i)<1>,0.5)
                    U2,i ← moyenne(Extract(A,c,i)<1>)
                    U3,i ← fractile(Extract(A,c,i)<2>,0.05)
                    U4,i ← fractile(Extract(A,c,i)<3>,0.05)
                    U5,i ←  $\frac{\text{dernier}(\text{Extract}(A,c,i)^{\langle 3 \rangle})}{\text{dernier}(M^{\langle 1 \rangle})}$ 
                  otherwise
                    U1,i ← 0
                    U2,i ← 0
                    U3,i ← 0
                    U4,i ← 0
                    U5,i ← 0
                U1,i+1 ← fractile(Extract(A,c,0)<1>,0.5)
                U2,i+1 ← moyenne(Extract(A,c,0)<1>)
                U3,i+1 ← fractile(Extract(A,c,0)<2>,0.05)
                U4,i+1 ← fractile(Extract(A,c,0)<3>,0.05)
                U5,i+1 ←  $\frac{\text{dernier}(\text{Extract}(A,c,0)^{\langle 3 \rangle})}{\text{dernier}(M^{\langle 1 \rangle})}$ 
                U

```

EXAMPLE OF CALCULATION with C30, C24 and C18

$$C := \begin{pmatrix} 12 & 11 & 9 \\ 30 & 24 & 18 \\ 380 & 350 & 320 \end{pmatrix} \quad \text{check}(M,C,0.10) = \begin{pmatrix} 12.431 & 0 & 9.017 & 7.523 \\ 12.871 & 0 & 9.354 & 7.636 \\ 30.1 & 0 & 18.1 & 8.7 \\ 485 & 0 & 464 & 452 \\ 0.754 & 0 & 0.205 & 0.041 \end{pmatrix}$$

INTERNATIONAL COUNCIL FOR BUILDING RESEARCH STUDIES AND DOCUMENTATION

WORKING COMMISSION W18 - TIMBER STRUCTURES

FAILURE ANALYSIS OF SINGLE-BOLT JOINTS

by

L Daudeville

L Davenne

Laboratoire de Mécanique et Technologie

Cachan

France

M Yasumura

Department of Forest Resources Science

Shizuoka University

Japan

MEETING THIRTY

VANCOUVER

CANADA

AUGUST 1997

Failure analysis of single-bolt joints

Laurent Daudeville, Luc Davenne

Laboratoire de Mécanique et Technologie, ENS Cachan/ CNRS / Univ. Paris 6

61, avenue du Président Wilson, F- 94235 Cachan, France

E-mail. daudevil@lmt.ens-cachan.fr

Motoï Yasumura

Department of Forest Resources Science, Faculty of Agriculture, Shizuoka University

836 Ohya, Shizuoka 422, Japan

1. Introduction

An experimental and numerical analysis of failure of timber joints with one dowel under static loading is presented. Glued laminated members are chosen thin enough to avoid the fastener from presenting plastic hinges. The influences of different structural parameters such as the dowel diameter, the edge- and end- distances are investigated. Joint failure is due to fracture of wood parallel to the grain.

The joint failure may be due to splitting. The purpose is then to show that Linear Elastic Fracture Mechanics (LEFM) may provide a tool for the prediction of the load carrying capacity of timber mechanical joints and complete the present design approach of Eurocode 5 (EC5, 1993) that is based upon the Johansen's yield model (1949) and on a requirement on the shear stress in the case of a load perpendicular to the grain.

Three kinds of loading are considered, tension perpendicular and parallel to the grain (Fig. 1a and 1b), and bending (Fig. 1c).

A simplified analysis is proposed, plasticity phenomena are not considered in this study.

The crack propagation is analyzed by use of LEFM and with the Finite Element (FE) code CASTEM 2000 under the assumptions of elastic bodies and of a plane stress state. The influence of friction was investigated: The friction has essentially an influence on the

location of the crack initiation, it seems possible to neglect it at the steel and wood contacts in the analysis of propagation. The presented results are based on this assumption.

In the case of bending or tension parallel to the grain, the stress state is a combination of shear and of a tensile stress perpendicular to the grain. Thus a possible mixed mode of fracture (mode I and II) is investigated.

A Wu's criterion (1967) based on G_{Ic} is used for the propagation analysis. The critical energy release rate value is chosen in order to obtain the best comparison between results of tests performed on joints and numerical results.

The load-bearing capacity of joints was computed for each tested configuration. Comparisons between experimental, numerical and EC5 design loads for studied single bolt joints are presented. A part of the results presented in this paper have already been shown in the previous CIB-W18 meetings (Davenne et al., 1996). We add new results and comparisons with the EC5 recommendations.

2. Experiment

Tests were conducted at LMT Cachan, France (perpendicular tension, Fig. 1a) and BRI Tsukuba, Japan (parallel tension, Fig. 1b and bending, Fig. 1c). Specimens consisted of glued laminated spruce. Two steel plates connected with steel dowels of diameter d (from 8 to 20 mm) load the wood member. There was no allowance between the dowel and the wood. No knots were present around the bolt holes. Specimens were tested to failure in stroke displacement control. No plasticity in steel elements is observed.

Table 1, 2 and 3 present the ultimate load and the coefficient of variation of each configuration.

3. Eurocode 5 recommendations

According to EC5 (EC5 - 6.2.2.h, 6.1), the design load on the dowel per unit thickness is for the three studied problems (Fig. 1):

$$P_{EC5} = \min \begin{cases} (k_{mod} / \gamma_M) f_{h,\alpha,k} d \rho_k & (1) \\ 2/3 f_{v,k} a_{4,t} & (2) \end{cases}$$

$f_{h,\alpha,k}$ is the characteristic embedding strength for a load at an angle α with the grain, d is the bolt diameter. k_{mod} takes into account the variation of the loading with time (EC5 - 3.1.7), it is chosen: $k_{mod} = 1$ and $\gamma_M = 1$.

The characteristic strength $f_{h,\alpha,k}$ is defined as the five percentile value. Because of the low number of experimental results, it is not possible to obtain $f_{h,0,k}$ and $f_{h,90,k}$ from tests (EC5 - Annex A). Thus, it is recommended to use (EC5 - 6.5.1.4):

$$f_{h,0,k} = 0.082 (1 - 0.01 d) \rho_k \quad (3)$$

$$f_{h,90,k} = f_{h,0,k} / k_{90} = f_{h,0,k} / (1.35 + 0.015 d) \quad (4)$$

d is in mm, ρ_k is the density (kg/m^3). It is chosen to use the density ($\rho_k = 400 \text{ kg/m}^3$) rather than the actual one for the comparison with numerical results that do not depend on density. $f_{v,k}$ is the characteristic shear strength is chosen equal to $f_{v,k} = 3.4 \text{ N/mm}^2$ according to EN338 with $\rho_k = 400 \text{ kg/m}^3$.

Tables 1, 2 and 3 give the EC5 maximum loads according to (1)-(4).

EC5 recommends to use an end-distance greater than $7d$ and an edge distance greater than $4d$ (load perpendicular to the grain) and $2d$ (load parallel to the grain). Note that the design load-carrying capacity does not depend on the end-distance. The edge-distance is taken into account in (2).

4. Modeling

The modeling assumptions are:

H1: Plane stress state (because the bolt does not bend)

H2: Wood is linear-elastic to failure

H3: The bolt is a rigid body

H4: There is no allowance between the bolt and the wood (like tests)

H5: The transverse T and radial R directions are not distinguished.

H6 : Friction at the wood and bolt contact is neglected.

The assumption H6 is valid for propagation analyzes (Talland, 1996) but friction is important for the determination of the cracking initiation location.

In a plane stress problem, the radial R and transverse T directions cannot be distinguished so a mean behavior is considered . The elastic moduli were chosen by extrapolation of results (Guitard, 1987) with respect to the mean density. x direction corresponds to the L direction.

$$\begin{cases} E_x = E_L = 15000\text{MPa} ; E_y = \frac{E_T + E_R}{2} = 600\text{MPa} \\ G_{xy} = \frac{G_{TL} + G_{RL}}{2} = 700\text{MPa}; \nu_{xy} = 0.5 \end{cases} \quad (5)$$

4.1 Fracture initiation

Experimentally, the initiation of the crack was always observed at $\theta=0^\circ$ (Fig. 2) for a perpendicular tension or bending. In the case of a tension parallel to the grain, θ was in general equal to zero but it was sometimes observed an initiation at an angle θ between 0° and 45° . Larsen (1997) observed a propagation at $\theta=30^\circ$.

The following stress function was used for a qualitative analysis of the initiation location. The exponents of each term are chosen from the Wu's criterion (1967) (see eq. (9)):

$$f(\sigma) = \frac{\sigma_{yy}}{f_t} + \left(\frac{\sigma_{xy}}{f_v} \right)^2 \quad \text{with } \sigma_{yy} > 0 \quad (6)$$

The material constants are $f_t = 5 \text{ MPa}$ and $f_v = 8 \text{ MPa}$ (C.T.B.A., 1995).

For a tension perpendicular to the grain, the function is maximum for $\theta=0^\circ$. Under bending, the initiation angle is the same but the way of propagation (from the dowel to the edge or from the dowel to the applied central load) depends on the edge distance (see Table 3).

For a tension parallel to the grain, θ is close to zero for a friction coefficient equal to zero. The higher the friction coefficient, the higher θ .

This qualitative analysis confirms the experimental observations.

4.2 Crack propagation analysis

The existence of a crack is assumed. The propagation analysis is carried out by use of classical LEFM i.e. all damage phenomena are assumed to be concentrated at the crack tip. The energy release rate is:

$$G(P,a) = G_I + G_{II} = - \frac{1}{t_2} \frac{\partial W}{\partial a} \quad (7)$$

P is the applied load to the structure, W is the potential energy, a is the crack length, t_2 is the specimen thickness.

The computation of the global energy release rate can be carried out by means of two FE calculations 1 and 2. The crack propagation is modeled by separating two connected lines:

$$G = \frac{P^2}{2t_2(a_2 - a_1)} \left(\frac{1}{k_2} - \frac{1}{k_1} \right) \quad (8)$$

With $\Delta a = a_2 - a_1 \ll a$; k stiffness

(8) is obtained under the assumption the applied load P does not vary during the elementary crack increment. A similar relation can be obtained with displacement. Both methods lead to very similar results (Laflotte, 1997).

(8) can be used only in the case of a pure mode of fracture in association with a Griffith's criterion (1920). Because of the orthotropic feature of wood, a partition of modes is necessary in order to use the following criterion issued from the Wu's one (1967) that was originally based on stress intensity factors:

$$\sqrt{\left(\frac{G_I}{G_{Ic}} \right)} + \left(\frac{G_{II}}{G_{IIc}} \right) = 1 \quad (9)$$

The previous criterion is the Griffith's one in the case of a pure mode I or II. G_I and G_{II} are obtained separately with a local method, the crack closure technique that is based on the necessary work to close the crack during a propagation Δa :

$$G_I = \frac{1}{2t_2} \frac{Y \cdot \Delta v}{\Delta a}; G_{II} = \frac{1}{2t_2} \frac{X \cdot \Delta u}{\Delta a} \quad (10)$$

Where X and Y are the nodal forces in the grain (x) and perpendicular to the grain (y) directions (obtained in the first FE computation). Δu and Δv are the relative displacements of the released node in the x and y directions (second FE computation) (Fig. 3).

In the both local and global method, the mesh refinement at the crack tip is constant during the crack propagation.

According to Valentin et al. (1991), Mansfield-Williams (1995) and Petersson (1995) a good approximation is:

$$G_{IIc} = 3.5 G_{Ic} \quad (11)$$

The load P that leads to a crack propagation of a joint is computed for different crack lengths with (9)-(11) and for a given G_{Ic} . The maximum load gives the calculated load carrying capacity P_{cal} of the joint and the critical crack length. Fig. 4 shows the computed load with respect to the crack length of a joint loaded perpendicular to the grain.

5. Results and comparisons with EC5 recommendations

The only unknown material parameter G_{Ic} is identified in order to obtain the best comparison between experimental and numerical results. Note that the G_{Ic} value is based on assumptions concerning the fracture modes. Tables 1, 2 and 3 give the calculated load-carrying capacities of joints with:

$$G_{Ic} = 100 \text{ Nm/m}^2 \quad (12)$$

Fig. 5-8 show the comparisons between the experimental, numerical and EC5 loads per unit thickness. LEFM allows correct predictions and gives the good trends.

In the case of a perpendicular to the grain tension and with an end-distance of $7d$, accepted by the EC5, the experimental loads are under the EC5 limit, that is unsafe (Fig. 5).

For parallel tension, table 2 gives results of a propagation at an angle $\theta=0^\circ$ and no friction. The friction is not very influent in the propagation analysis (Talland, 1996).

A propagation at an angle $\theta=30^\circ$ was also studied. It gives results a little bit lower. The experimental observations confirm a more probable propagation at an angle $\theta=0^\circ$.

Fig. 6 and 7 show the influences of the bolt diameter and of the end-distance under tension parallel to the grain. As before, LEFM gives the correct trends for every end-distances.

Fig 8 shows the numerical, experimental (Yasumura et al., 1987) and EC5 maximum loads applied to the dowel under bending (Fig. 1c). On table 3 is given the way of propagation (from the bolt to the edge or from the bolt to the central load). Once again, LEFM gives the good influence of the edge-distance that is not correctly taken into account in the present code.

6. Conclusion

LEFM is a simplified approach consisting in the comparison of the energy release rate with a critical value. This method has been applied for the determination of the load carrying-capacity of mechanical joints with a single bolt. This approach can be considered as a possible tool to complement the present codes.

In particular, the influences of structural parameters that are not taken into account in the present codes may be considered.

The comparisons between the EC5 recommendations and the experimental results seem to show that the present code may be unsafe for a loading perpendicular to the grain. That can be explained by the fact that in such a case the limit load is essentially due to splitting rather than yielding.

7. References

- C.T.B.A. 1995: Étude des caractéristiques mécaniques du sapin et de l'épicéa - France entière, Rapport interne, C.T.B.A. Paris, France.
- Davenne L., Daudeville L. and Yasumura M. 1996: Failure of bolted joints loaded parallel to the grain : Experiment and Simulation, Proceedings of the 29th CIB-W18 Meeting, Bordeaux, France, paper 29-7-8.
- EC5 (Eurocode 5). 1993: Design of timber structures - Part 1-1: General rules and rules for buildings, ENV 1995-1-1, CEN, Brussels, Belgium.
- Griffith A. 1920: The phenomena of rupture and flow in solids, Philosophical Transactions of the Royal Society of London, Series A, 221: 163-198.
- Guitard D. 1987: Mécanique du matériau bois et composites. Cépadués-Editions, Toulouse, France.
- Johansen K.W. 1949: Theory of timber connections, Inter. Assoc. of Bridge and Structural Engineering, Bern, Switzerland, Publ. 9: 249-262
- Laflotte J. 1997: Méthodes simplifiées de calcul des structures en bois, Master thesis, CUST Clermont-Ferrand.
- Larsen H.J. 1996: Discussion of the paper 29-7-8, Proceedings of the 29th CIB-W18 Meeting; Bordeaux, France.
- Mansfield-Williams H.D. 1995: A new method for determining fracture energy forward shear along the grain, Proceedings of the 28th CIB-W18 Meeting, Copenhagen, Denmark, paper 28-19-2.
- Petersson H. 1995: Fracture design analysis of wooden beams with holes and notches, Proceedings of the 28th CIB-W18 Meeting, Copenhagen, Denmark, paper 28-19-3.
- Talland O. 1996: Simulation de la rupture d'un assemblage en bois boulonné, Master thesis, ENS Cachan.

Valentin G. Boström L. Gustafsson P.J. Ranta-Maunus A. Gowda S. 1991: Application of fracture mechanics to timber structures. RILEM state-of-art Report, Technical Research Centre of Finland, Espoo, Finland, Research Notes 1262.

Wu E.M. 1967: Application of fracture mechanics to anisotropic plates, Journal of Applied Mechanics, Series E, 34 (4): 967-974.

Yasumura M., Murota T. and Sakai H. 1987: Ultimate properties of bolted joints in glued laminated timber, Proceedings of the 20th CIB-W18 Meeting, paper 20-7-3.

TABLES AND FIGURES

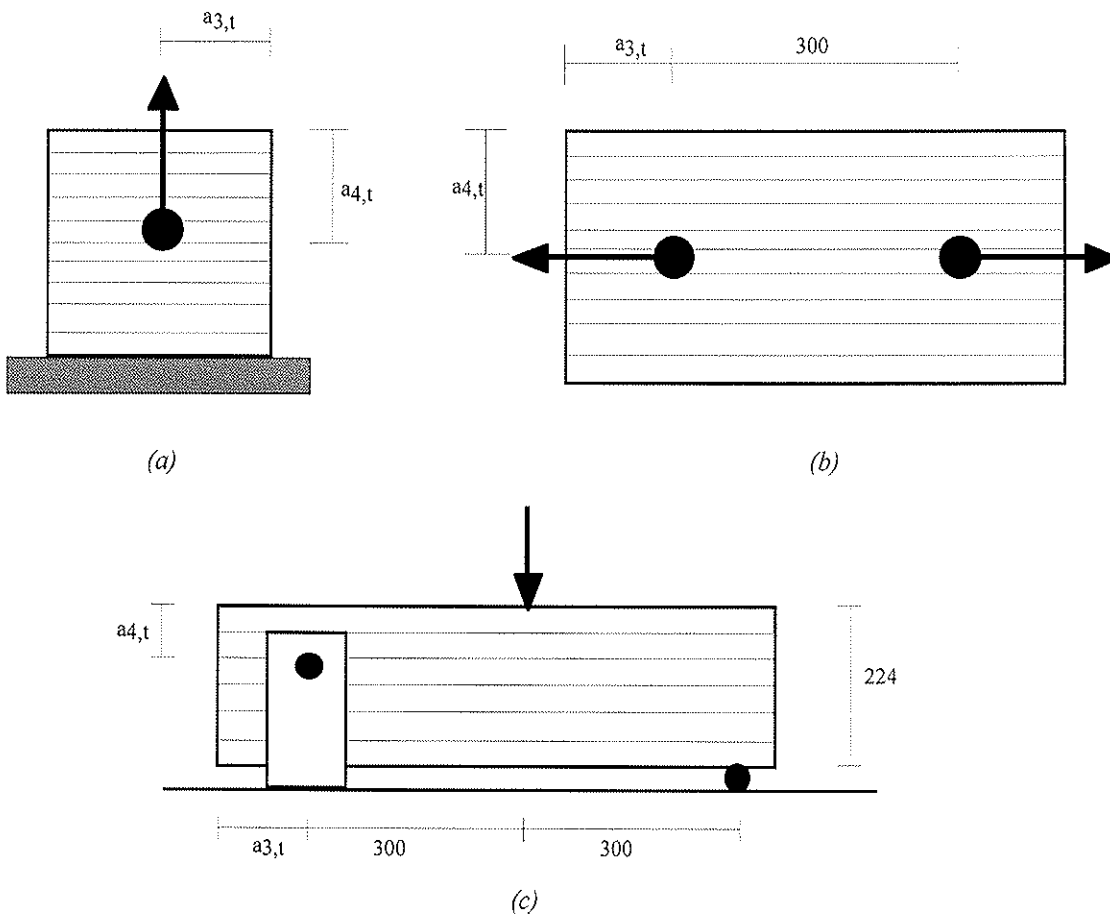


Fig. 1. Experimental program : (a) tension perpendicular to the grain, (b) tension parallel to the grain, (c) bending ; $a_{3,t}$ = end-distance, $a_{4,t}$ = edge distance

Table 1 - Specimen configurations and ultimate loads in tension perpendicular to the grain (Fig. 1a). The wood member thickness is equal to three bolt diameters ($b=3d$).

d (mm)	$a_{3,t}/d$	$a_{4,t}/d$	P_{exp} (kN/m)	COV (%)	P_{EC5} (kN/m)	P_{cal} (kN/m)
12	7	4	140	3	109	155
		8	148	10	218	163
		12	143	5	226	163
12	25	4	173	10	109	181
		8	223	1	218	242
		12	264	12	226	278
16	7	4	204	12	145	179
20	7	4	230	9	181	200

Table 2 - Specimen configurations and ultimate loads in tension parallel to the grain (Fig. 1b). The wood member thickness is equal to two bolt diameters ($b=2d$; $a_{4,t}=3d$).

d (mm)	$a_{3,t}/d$	P_{exp} (kN/m)	COV (%)	P_{EC5} (kN/m)	P_{cal} (kN/m)
8	2.5	266	4	241*	209
	4	324	10	241*	291
	7	312	15	241	418
	10	336	13	241	460
12	2.5	332	41	346*	257
	4	382	30	346*	357
	7	421	19	346	512
	10	422	12	346	560
16	2.5	307	25	441*	297
	4	550	11	441*	412
	7	599	1	441	595
	10	715	8	441	653
20	2.5	459	14	525*	334
	4	541	23	525*	464
	7	681	28	525	666
	10	751	9	525	732

Table 3 - Specimen configurations and ultimate loads on the dowel in bending (Fig. 1c). The experimental load is the average of results obtained with $b=4d$ and $b=8d$; $d=16$ mm.

$a_{3,t}/d$	$a_{4,t}/d$	P_{exp} (kN/m)	COV (%)	P_{EC5} (kN/m)	P_{cal} (kN/m)	prop.
4	4	186	11	145*	160	edge
	7	257	5	254*	238	edge
7	4	218	26	145	219	edge
	7	321	13	254	357	edge
	10	444	12	277	476	load

* Not permitted by the EC5

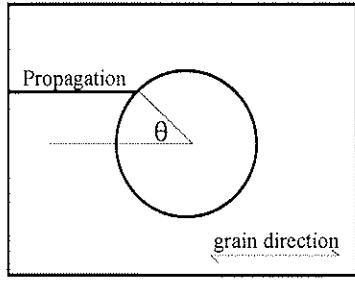


Fig. 2. Initiation of cracking

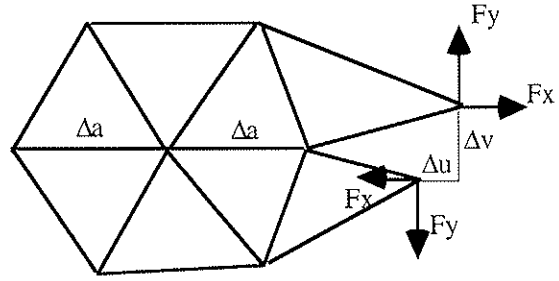


Fig. 3. Crack closure technique

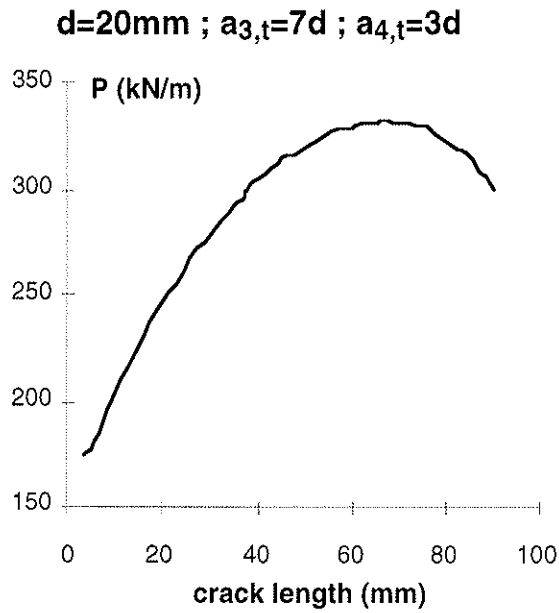


Fig. 4. Load versus crack length in tension perpendicular to grain

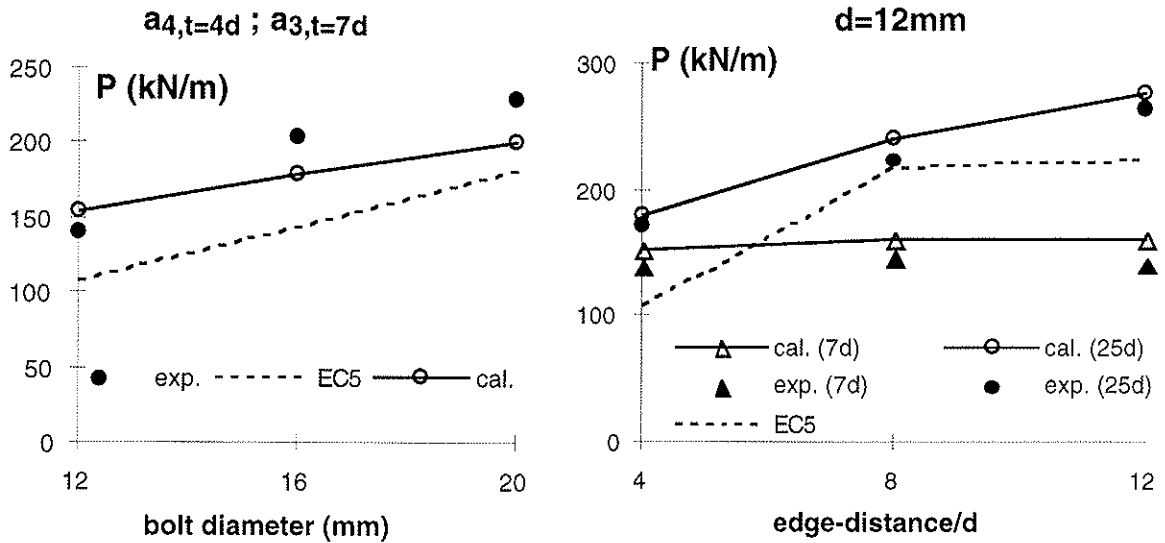


Fig. 5. Tension perpendicular to the grain

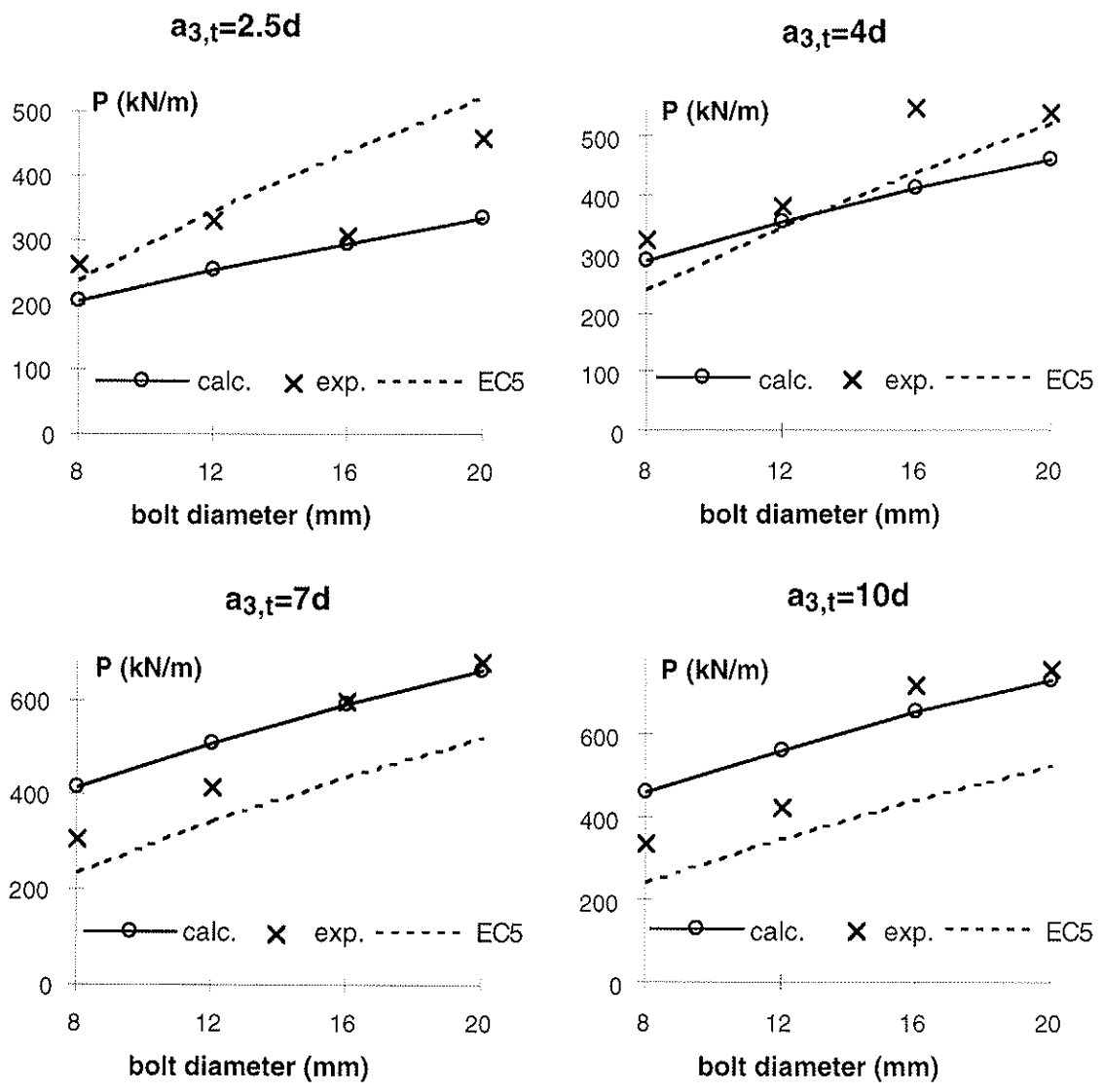


Fig. 6. Tension parallel to the grain - Influence of bolt diameter

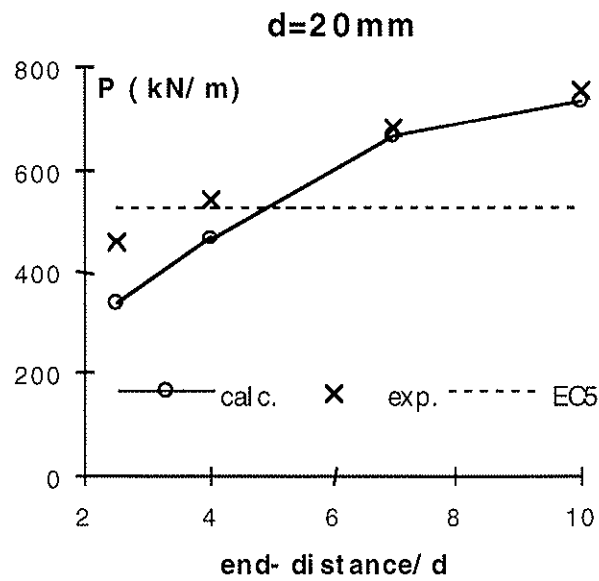


Fig. 7. Tension parallel to the grain - Influence of the end-distance

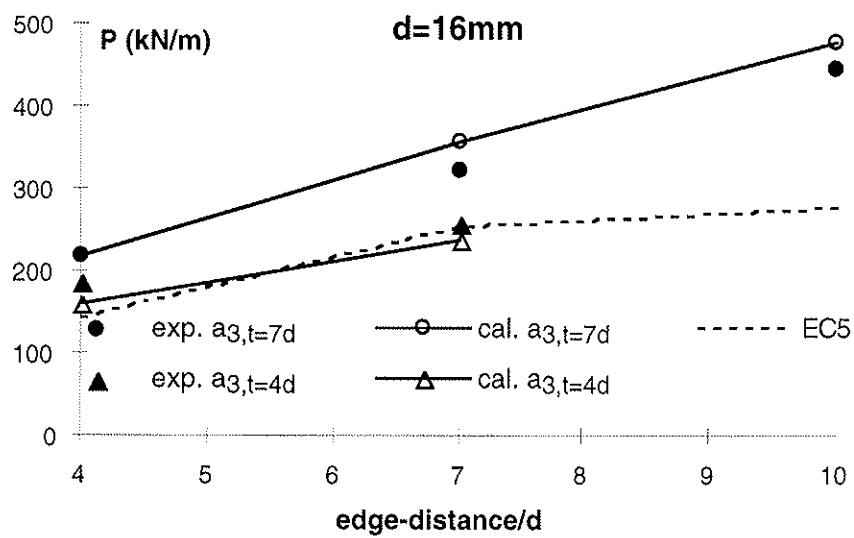


Fig. 8. Bending - Influence of the end- and edge-distances

INTERNATIONAL COUNCIL FOR BUILDING RESEARCH STUDIES AND DOCUMENTATION
WORKING COMMISSION W18 - TIMBER STRUCTURES

DESIGN PRINCIPLES FOR TIMBER IN COMPRESSION
PERPENDICULAR TO GRAIN

by

S Thelandersson
A Mårtensson
Department of Structural Engineering
Lund University
Sweden

MEETING THIRTY

VANCOUVER

CANADA

AUGUST 1997

Design principles for timber in compression perpendicular to grain

Sven Thelandersson
Annika Mårtensson

Department of Structural Engineering, Lund University, Sweden

1 Introduction

In timber frame buildings the structural system is usually designed in such a way that load is transferred perpendicular to grain in joints between walls and floors. These joints are very important elements in timber frame building systems and their design is governed by a number of technical requirements beside the structural ones, such as fire safety, sound insulation, thermal insulation and airtightness. On top of that it is necessary that the joint is designed with respect to ease of assembly and economy. It is therefore a challenge to find an optimum solution, since this detail is one of the most important factors for the competitiveness of a particular timber frame system concept.

From a structural point of view, the joint shall usually transfer vertical loads, and often also shear forces related to the horizontal stabilisation of the building. It is theoretically possible to design the joint so that load transfer perpendicular to the grain in wood elements is entirely avoided, but this is not feasible considering all other aspects of the design. The question therefore arises what kind of philosophy should be applied with respect to load transfer perpendicular to grain both from the point of view of structural safety and from the point of view of limiting the short and long term deformations in the joint. Deformations perpendicular to grain are crucial in such joints especially for multi-storey timber frame buildings, where deformations at each level can add up to substantial movements over the building height.

The adverse consequences of deformations in a structural system are obvious. For example, non-structural elements, such as windows, doors and partitions could become inoperable or damaged if primary structural elements deflect to a point where the non-structural element is part of the load path. Excessive deformations in the primary structural system may lead to damage to services and to costly deficiency corrections like e.g. repair of dry-wall cracks, floor and wall tile cracks, adjusting doors and paint touch ups. Another example is connections between timber frame and an exterior brick cladding, where excessive deformations in the timber structure may cause damage. Uneven settlements of load-bearing walls in a system may cause sloping floors, which can be very expensive to correct.

In current practice, load transfer perpendicular to grain is mostly handled by limiting the bearing stress. In most codes, stresses perpendicular to grain are checked in the ultimate limit state against a design bearing strength. This is a simple approach which works well in many cases:

- It gives a reasonable reduction of the risk that transversal crushing of a wood member will lead to loss of stability of the structural system.

- It will give an indirect limitation of deformations by limiting bearing stress along the load path.

It should be noted, however, that the deformation depends on several other factors than the bearing stress level, such as geometry along the load path, moisture changes and duration of the load.

In some situations, e.g. in timber framed structural systems, as described above, a more sophisticated philosophy is needed for the design of wood loaded perpendicular to grain.

The following issues must be addressed:

- Identification of those situations where design in the ultimate limit state is necessary.
- Formulation of design principles in the serviceability limit state for loading perpendicular to grain.
- Methods to estimate deformations under loading perpendicular to grain, including long term and moisture effects.

In this paper, design principles for compression perpendicular to grain in the ultimate as well as in the serviceability limit state are discussed. A general method to predict deformations in joints where wood is stressed perpendicular to grain is proposed. The method considers deformations induced by load as well as deformations induced by moisture variations.

2 Design in the ultimate limit state

It is clear that a possible “failure” in bearing in many practical cases will not be of serious nature. Quite frequently, it will only lead to excessive local deformation with no consequences for the overall stability of the structural system, and with no relevance for the safety of the occupants. This is valid e.g. when the “bearing strength” is exceeded in the contact area between a stud and a bottom plate which is solidly supported on some other structure which can transfer the load without problems. Figure 1 shows some examples where bearing failure may be disregarded, and consequently design with respect to bearing in the ultimate limit state is unnecessary. Design in the serviceability limit state may, however, be relevant in such cases.

On the other hand, there are situations when bearing failure may have more serious consequences. An example is when the load is transferred perpendicularly through a joist which is simultaneously loaded in bending. Local crushing of the girder may reduce the bending and shear capacity of the joist. This situation may occur in traditional platform frame construction, where vertical loads usually are transferred through the floor joists in each floor. Figure 2 shows examples where bearing stress should be considered in the ultimate limit state.

Thus, design in the ultimate limit state should only be applied in cases where “bearing failure” may reduce the capacity of structural members or otherwise affect the safety of the structural system. In other cases, design in the serviceability limit state is sufficient. The difference between designs in the ultimate limit state and the serviceability limit state is often significant. A stud at the end of a stabilising wall may for instance be subjected to

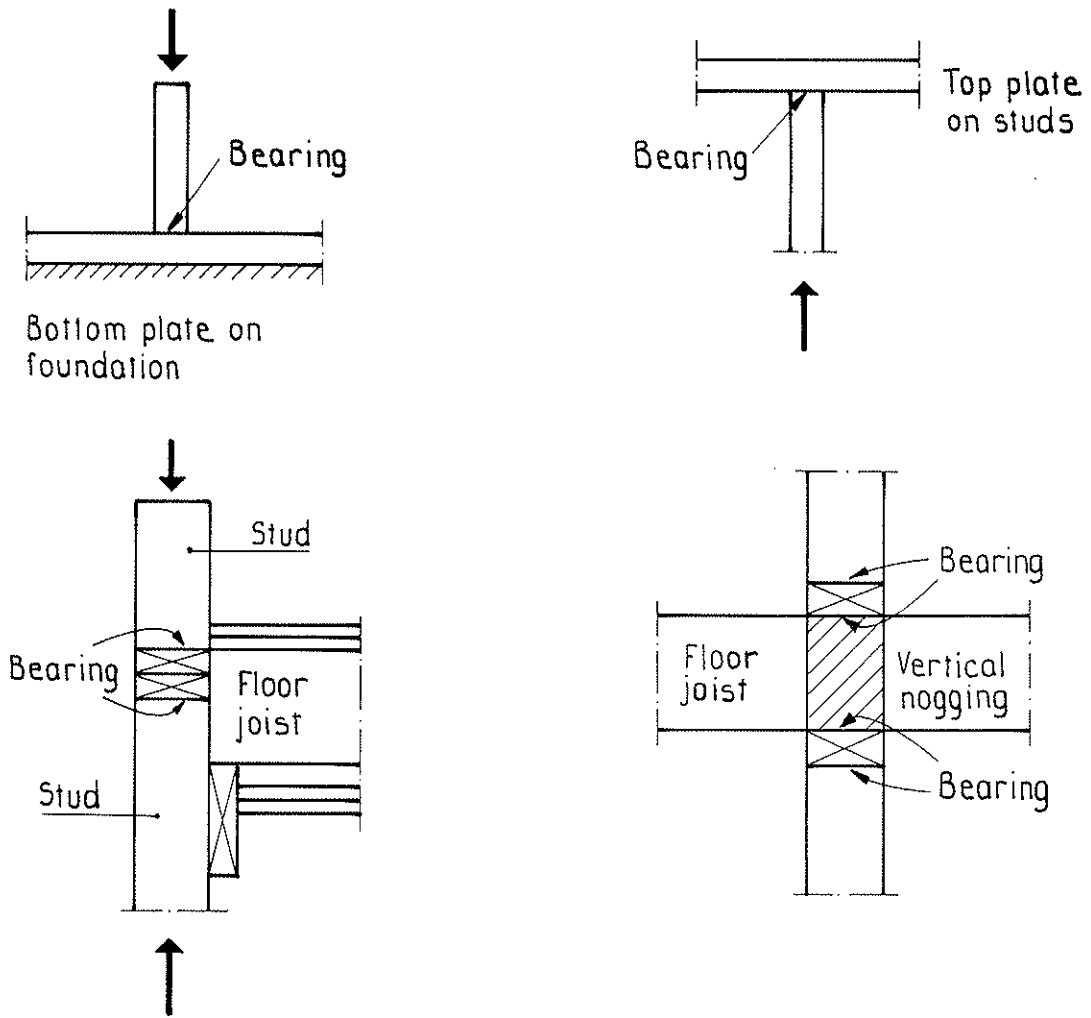


Fig 1. Joint design examples where bearing failure may be disregarded from safety point of view.

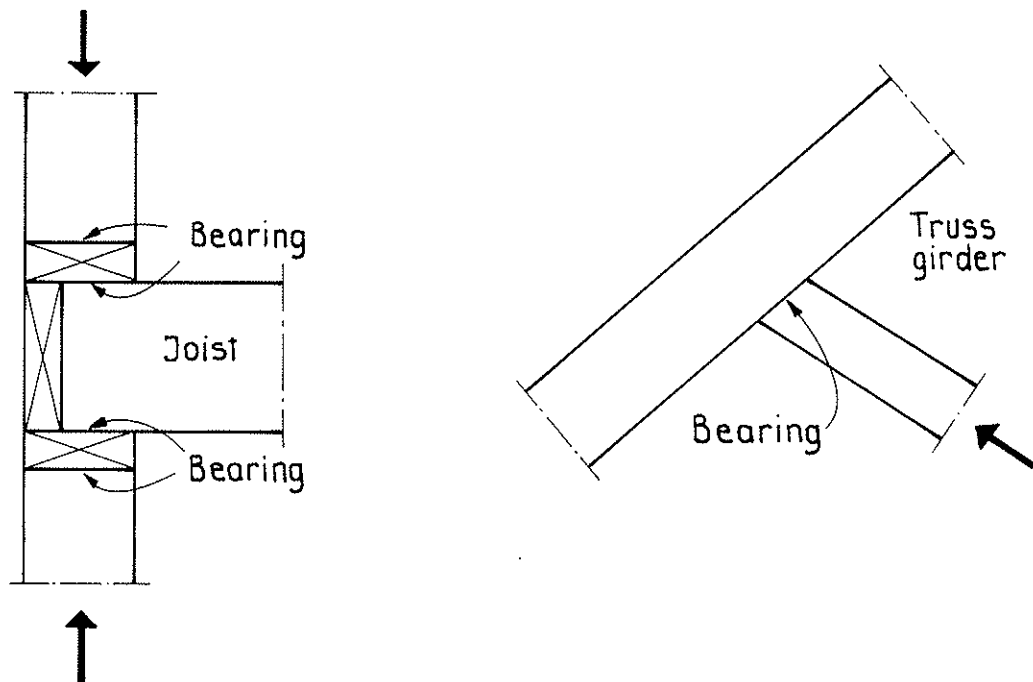


Fig 2. Design examples where bearing stress should be considered in the ultimate limit state

high compressive force with short duration due to extreme wind load in the ultimate limit state, while the corresponding force is much smaller in the serviceability limit state.

Design in the ultimate limit state can be made with the methods given in most codes. As mentioned before the principle of design is to assure that the bearing stress does not exceed the bearing strength in bearing areas along the loading path. The bearing strength, given in typical codes, is not very well defined. The relation between load and deformation in bearing is bilinear and there is no evident value of the ultimate load, as shown in Figure 3, from Backsell (1966). Table 1 shows the stress at the proportional limit obtained in tests by Frater & Thelandersson (1996) of "joints" with different designs, compared with the characteristic bearing strength f_{cbk} determined from the rules in Eurocode 5. The code values are corrected with the bearing length factor $k_{c,90}$ for each type of joint, and the load duration factor $k_{mod} = 0.9$ for short term load in service class 1 or 2. The base value of compression strength perpendicular to grain $f_{c,90,k}$ is taken to 7.0 MPa, valid for Norway spruce, in the current Swedish code, BKR 94, (1994). The values given in Table 1 are averages of six tests for each type of joint. The joint designs tested are shown in Fig. 4.

Table 1. Bearing stress at the proportional limit compared with characteristic bearing strength determined according to Eurocode 5, Frater & Thelandersson (1996)

Test specimen design, see Fig. 4	Stress at prop. limit σ_{pl} (MPa)	Bearing length (mm)	Bearing length factor $k_{c,90}$	Char. Strength $f_{cbk} = k_{mod} k_{c,90} f_{c,90,k}$ (MPa)	Ratio f_{cbk}/σ_{pl}	Deformation at stress f_{cbk} (mm)
SPP	5.14	44.5	1.62	10.2	2.0	10.5
SSPP	3.07	88.4	1.32	8.6	2.8	*
SP	4.27	44.3	1.62	10.2	2.4	8.5
SSP	4.06	88.2	1.36	8.6	2.1	*
JPP	3.45	88.4	1.32	8.6	2.5	*
JP	3.50	88.2	1.36	8.6	2.5	12.5
P	2.58	-	-	6.3	2.4	*
J	1.99	-	-	6.3	3.2	*

* The maximum stress reached when the test was terminated was lower than the characteristic strength value f_{cbk} in all or most of the tests in the series.

It is seen that the characteristic bearing strength is 2-3 times higher than the stress at proportional limit determined in the tests. There is no doubt that the wood can transfer this stress in compression perpendicular to grain, but the deformations will be quite large. The deformations observed in the tests are very variable. In some cases deformations up to 20-30 mm can be expected at a stress corresponding to the characteristic strength defined by the Swedish code. This means that the geometric configuration in a joint can be changed in a significant manner. The largest deformations tend to occur for longer bearing lengths, and in cases where both members are compressed perpendicular to grain (tests JPP and JP). The results indicate that the bearing strengths used in present Swedish practice may be too high in cases where bearing failure is of importance for the overall performance of the structural system. The main reason for this is that the characteristic base value of compression perpendicular to grain may be too high, tests J and P in Table 1. The values given in EN 338 "Structural timber - Strength classes" are significantly lower, 4.3-5.7 MPa for strength classes C14-C30. The present investigation shows that this is highly motivated.

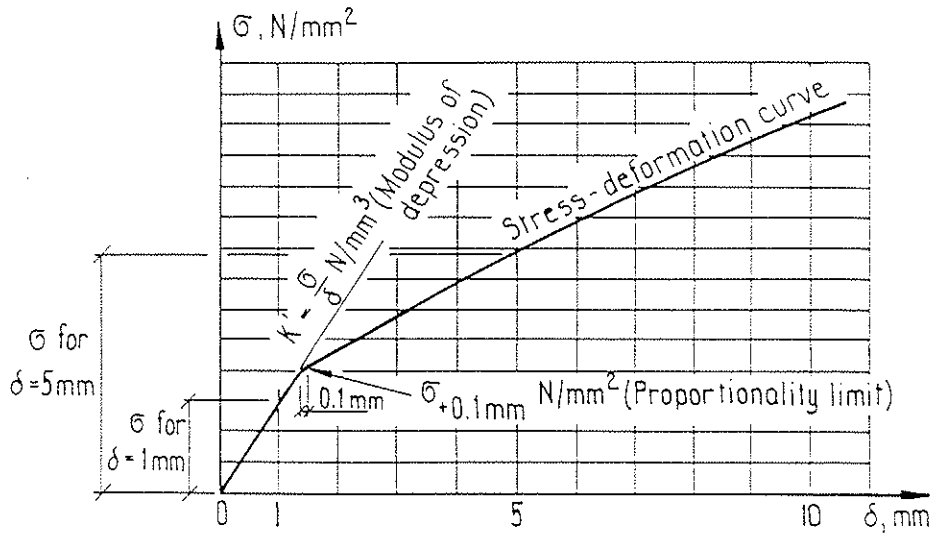


Fig 3. Stress deformation curve in bearing according to Backsell (1966)

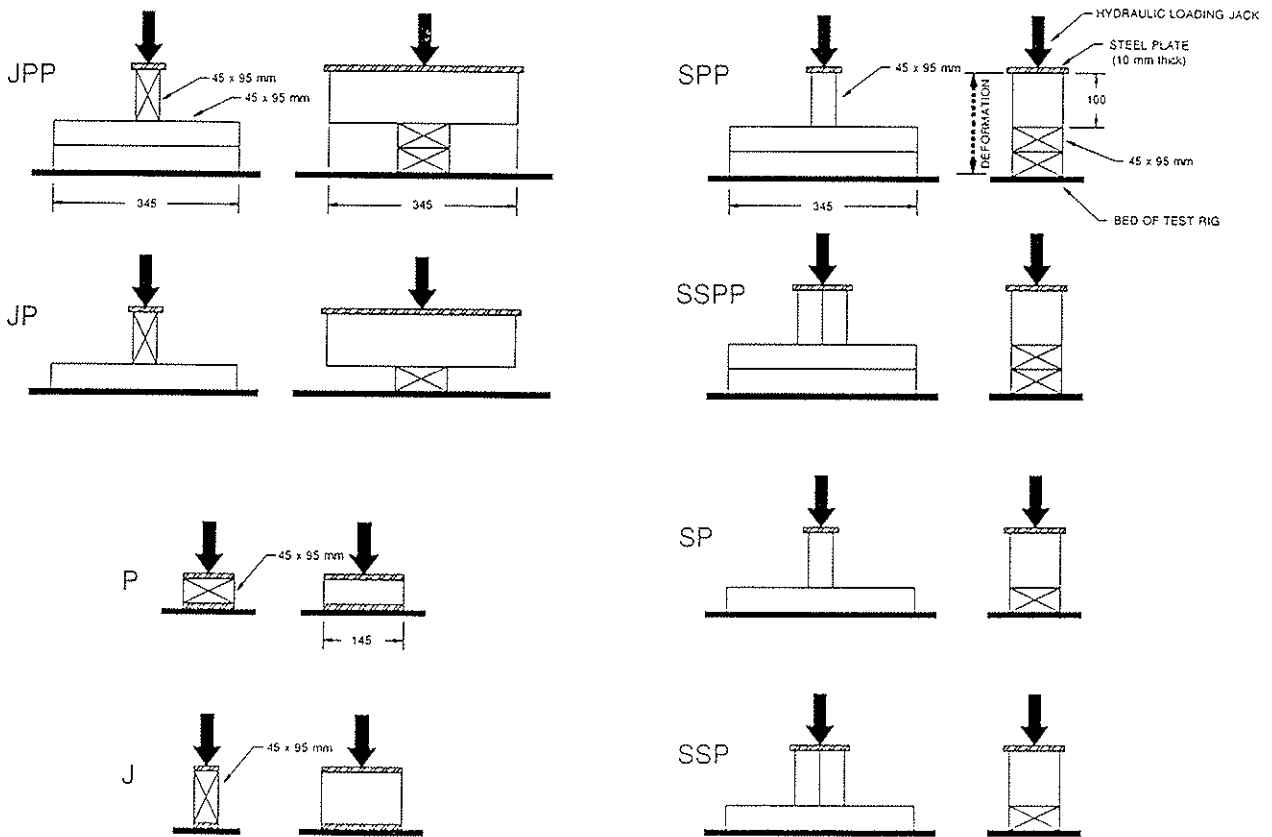


Fig 4. Joint designs used in tests by Frater & Thelandersson (1996)

3 Design in the serviceability limit state

3.1 General

In the serviceability limit state the magnitude of the bearing deformations is the main problem to the designer. It is then important to have both a method to predict the deformations and criteria to determine whether the anticipated deformations can be accepted.

Experience from USA and Canada, with a long tradition of multi-storey timber buildings, indicates that a deformation at about 8 mm per joint should be expected in a wall-floor joint in typical platform frame construction, Thorson (1989). The magnitude of the deformation depends on load level and the shrinkage in the wood. The shrinkage depends on the difference between the moisture content at the time when the wood is built in to the moisture content attained in the finished building. Kiln dried timber will typically have an initial moisture content around 18% when delivered to the building site. Up to the time when the building is erected and finished the timber will dry to a moisture content around 10-12% for indoor climate. As an example such a decrease in moisture content would lead to approximately 4-5 mm shrinkage over a joint height of 300 mm. Depending on the service conditions, the moisture will to some extent vary in the wood during the lifetime of the building. Furthermore the deformation under load increases with time (creep) and this additional deformation is also affected by moisture variations in the wood.

3.2 Long term tests of joints

To find a method that could be used to predict the magnitude of the deformation for a specific joint geometry and load case it is necessary to know the influence of different variables. Fig. 5 shows long term deformations for two types of tests, one where the bearing stress level was chosen to be 2.6 MPa with a loading period of two weeks (type a) and the other with bearing stress 2.0 MPa, with a two month duration of loading (type b). The test design was either SP or SPP as defined in Fig 4. The specimens SPa and SPPa had a moisture content (MC) of 18% when loaded and were then exposed to lower humidity so that MC after two weeks was approximately 12%. The free shrinkage for these two tests is approximately 0.5 mm for SPa and twice as much for the SPPa test. For the specimens type b tested for a longer period, MC was initially approximately 11% and the variation in moisture content was thereafter rather small ($\pm 1\%$). The difference between the deformations after two weeks for the two different cases (type b versus type a) is therefore mainly explained by the difference in shrinkage. These tests also show that there is a significant additional deformation taking place apart from pure shrinkage. The time dependent deformation after two months is 1.3-1.5 times the initial elastic deformation (after one minute) in spite of the fact that the moisture variations are very moderate in tests SPb and SPPb.

To find a simple prediction method, it is rational to define three different deformation components, namely the initial elastic, the shrinkage and the time and moisture dependent deformation. The first two are relatively easy to determine if reasonable assumptions can be made about the load level and the moisture conditions before, under and after erection of the building.

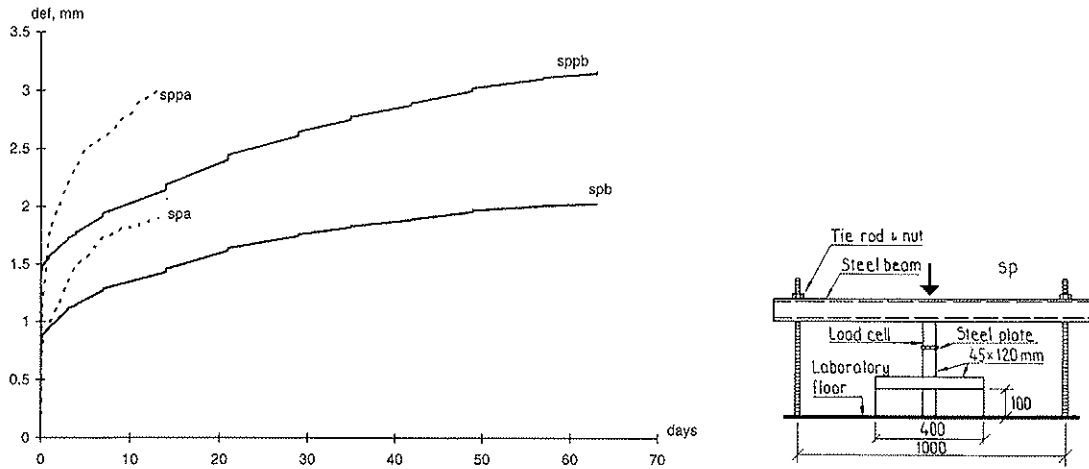


Fig 5. Results from compression tests. Two different test conditions were used: one where the wood had a moisture content of 18% initially and then dried to 12%, (sppa, spa) and one where the wood had a moisture content of 11% initially and with very small subsequent moisture variations (sppb, spb).

The bearing stress to be used in design calculations should be based on a serviceability load combination. Since the elastic deformations have been shown to be only a minor part of the deformation in most cases, this means that short term higher load levels will not affect the magnitude of the deformation significantly. The deformations depends to a great extent on the long term behaviour and it is therefore reasonable to base the calculation on a quasi-permanent load combination, i.e. an average in load over time.

3.3 Initial elastic deformation

A simple way to determine the elastic deformation Δ_e would be to use the relation

$$\Delta_e = \frac{Q}{AE_{90}}d \quad (1)$$

where Q is the quasi-permanent load, A is the bearing area and d is the height of the wood subjected to compression perpendicular to grain. Tests have, however, indicated that the deformation obtained according to these principles is far too high for this loading mode. The deformations observed in tests for moderate stresses are generally significantly lower than those predicted from Eq.(1) (Backsell, 1966, Madsen et al, 1982, Frater & Thelandersson, 1996, Jordow & Enockson 1996).

The actual deformation in bearing depends in a more complicated manner on the geometrical factors. The above mentioned tests show that the deformation decreases with decreasing bearing length for the same nominal stress. There is also a non-linearity in the dependence of height, i.e. if the height d is doubled the deformation will not be doubled, see also Fig. 5.

These effects can be accounted for approximately by replacing A in Eq. (1) with an effective area A^* which is greater than the actual bearing area A . The following relation has been proposed for A^* (Madsen et al, 1982, Enockson & Mårtensson, 1996)

$$A^* = A(1 + \mu \frac{d}{L}) \quad L_c \geq L_{c1} \quad (2)$$

where L is the bearing length, $A = bL$, see Fig. 6. Eq. (2) implies that the effective area over which the load is assumed to be distributed increases with the ratio d/L . The relation is valid for cases where the end distance L_e is greater than a certain limit L_{e1} .

Based on finite element analysis and modelling of the bearing as a beam on elastic foundation Madsen et al (1982) derived Eq. (2) with $\mu=1.06$. Enockson & Mårtensson (1996) suggests the value $\mu \approx 0.5$ based on tests of the type shown in Fig 4. Madsen et al (1982) suggest $L_{e1} = 1.6 d$. L_{e1} could also be defined as a fixed distance in mm.

In the absence of experimental results for loading near the end ($L_e < L_{e1}$) the value $A^* = A(1 + \frac{1}{2}\mu\frac{d}{L})$ could be used for $L_e = 0$. For intermediate values ($0 < L_e < L_{e1}$) linear interpolation could be used. Madsen et al (1982) suggests another - but not so simple - method to deal with bearing near the ends of the member.

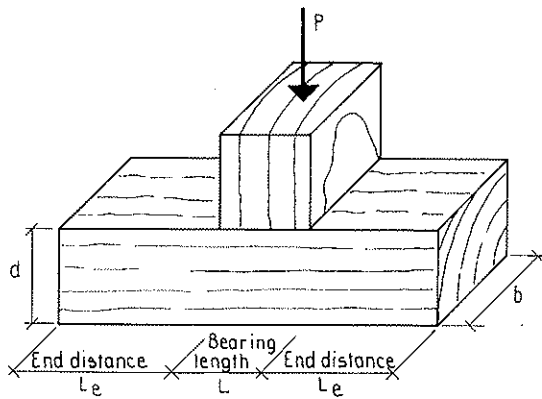


Fig 6. Simplified joint geometry.

Thus, the bearing deformation can be calculated from

$$\Delta_e = \frac{Q}{A^* E_{90}} d \quad (3)$$

The elastic modulus E_{90} in compression perpendicular to grain used in this relation can be determined in direct compression tests, corresponding to tests type P or J, shown in Fig. 4. E_{90} used in Eq. (3) should be the mean value given by codes for serviceability design. Tests performed by Frater & Thelandersson (1996) as well by Jordow & Enockson (1996) indicated however that the value of E_{90} given in EN 338 "Structural timber - Strength classes" is far too high when compared to tests of type P and J in Fig. 4. The values of the elastic modulus evaluated from these tests are only about 50-70 % of the values given in EN 338.

3.4 Shrinkage

The shrinkage can be calculated from the relation

$$\Delta_s = \alpha \cdot \Delta u \cdot d \quad (4)$$

where α is the shrinkage coefficient perpendicular to grain and Δu is the change in moisture content. The initial moisture content should correspond to the moisture content in the timber when it is delivered to the building site, provided that the timber thereafter is pro-

tected from direct water exposure. The final in-service moisture content of protected timber elements in indoor environment is usually between 8 and 12 % in most structures. For a rough estimate an in-service value of 10 % may be used. The shrinkage coefficient is of the order 0.002 per 1 % change of MC.

3.5 Time-dependent deformation

The time-dependent deformation depends on the load level, time passed from loading and the moisture variations during this time. Lack of reliable data for creep especially concerning the effects of moisture variations makes it difficult to predict the long term behaviour. It is reasonable to assume that the time-dependent deformation should relate to the initial elastic deformation, i.e.,

$$\Delta_c = k_c \cdot \Delta_e \quad (5)$$

where k_c is a function of the time elapsed from erection and also depends the moisture variations assumed to have occurred in the timber during that time. k_c may be described by the formula

$$k_c = at^c \quad (6)$$

where a and c are empirical parameters. Based on available tests of the type shown in Fig. 5 the values $a=3.0$ and $c= 0.3$ is suggested when t is inserted in years, Enockson & Mårtensson (1996).

This formulation for the creep factor is based on a limited test material from tests performed during rather short periods, up to 2 months. There is also a significant uncertainty about the effect of moisture variations over long time periods. The reliability in the prediction is generally lower for longer time periods.

3.6 Design examples

In table 2 examples of deformations calculated for two different joint geometries (see Fig. 7) are presented. It was assumed that the initial moisture content is 18% and that the timber had a moisture content of 10% in the completed building. The load used in the calculation is a quasi-permanent load with load values taken from the Swedish code. The values of the deformation are given for one joint, with loads from three storeys in a typical residential building (gravity, floor and snow loads). The elastic modulus E_{90} was taken to 150 MPa based on testing, see section 3.3. This value is significantly lower than the EN 338 values ranging from 240 to 400 MPa for strength classes C14 to C30. As can be seen in the table the deformation is significantly lower for joint type A than for type B, but this is mainly due to shrinkage. The load induced deformations are only moderately larger in joint B. For this practically realistic load level the elastic deformation is only a small part of the total deformation. If the moisture content can be reduced in the timber before and during the erection of the building the shrinkage can be reduced and the total deformation will be significantly reduced. As earlier stated the values of the additional long term deformation should be considered as tentative values since the basis for the creep factor k_c used here is rather uncertain. It can, however, be noted that the values of the deformations given for one year agrees with values observed in field measurements for multi-storey buildings in Sweden, Enockson & Mårtensson (1996).

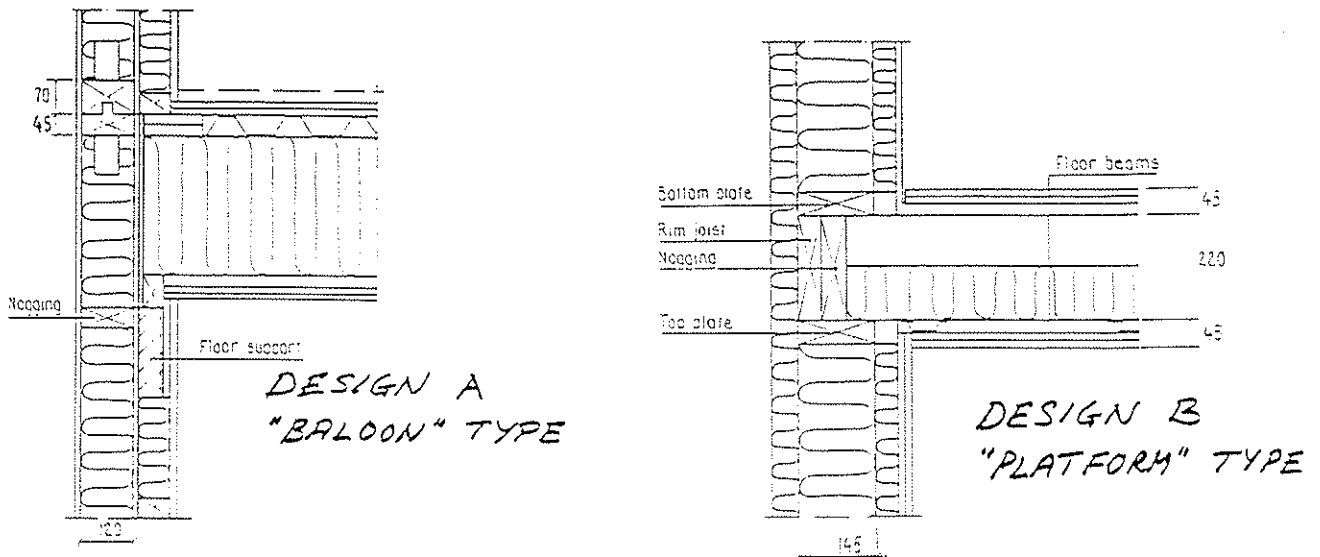


Fig 7 Joint type A and joint type B used in calculations.

Table 2. Predicted deformation in joints type A and B, see Fig. 7. $Q=5.8$ kN, $E_{90} = 150$ MPa, $\mu = 0.5$, $a=3.0$, $c=0.3$.

Time, year	deformation joint A (mm)	deformation joint B (mm)
elastic deformation	0.35	0.42
shrinkage	1.84	5.00
1	3.24	6.68
10	4.29	7.94

3.7 Acceptable deformations

In the example given in section 3.6, Table 2, the bearing deformation was predicted from the starting time when the member is built in, up to 1 year and 10 years after. The initial elastic deformation, part of the shrinkage and part of the long-term deformation will take place during the construction period before the building is painted and finished. Under normal circumstances, a very rough estimate could be that about 50 % of the 1 year deformation will take place before the building is completed, i.e. ≈ 1.5 mm for joint A and ≈ 3 mm for joint B. This is an important consideration when considering the level of acceptable deformation in each particular case.

The designer has to consider if the deformations for a particular design are acceptable or if any means have to be taken to reduce them. It is not feasible to give any general figures for acceptable deformations. The acceptance of a certain deformation depends on the structural system, the construction methods and a number of other factors. An analysis should be made to assure that the deformations are of the same order of magnitude in all vertical load bearing elements of the building to avoid slopes of horizontal structures. A special investigation should also be made to assure that non-bearing elements, services, anchorage to brick cladding etc. can survive the anticipated deformations. Two different types of design philosophy can be identified.

1. The bearing deformations are minimised by appropriate joint design, by using dry timber and controlling moisture during construction. This may however give significant constraints in the development of efficient joints for cost-effective and rational building systems.
2. Significant deformations are accepted in the joints which gives more freedom in design. The condition for this is that the design and construction of the building as a whole is made in such a way that movements can take place without damage and inconveniences.

4 Conclusions

The current practice for design of timber in compression perpendicular to grain is not sufficient for some situations in practice, such as multi-storey timber framed buildings. The present investigation has lead to the following conclusions:

- Design with respect to bearing in the ultimate limit state (ULS) need only be made when bearing failure. may reduce the structural capacity of structural members or otherwise affect the safety of the structural system.
- The present design methods for bearing can be used in ULS, and the strength values $f_{c,90}$ for compression perpendicular to grain given in EN338 seem to be properly defined.
- In all cases where design in ULS is unnecessary, design should be made in the serviceability limit state.
- Estimates of deformations can be made by considering initial elastic, shrinkage and time-dependent deformation components in a rather simple manner. It is proposed that calculation of deformation should be based on permanent and time averaged variable loads (quasi-permanent load combination).
- The EN 338 value for modulus of elasticity E_{90} in compression perpendicular to grain seems to be too high. There can be reason to adjust those values.

References

Backsell, G. 1966. Experimental Investigations into Deformations Resulting from Stresses Perpendicular to Grain in Swedish Whitewood and Redwood in Respect of the Dimensioning of Concrete Formwork, Byggforskningen, Report 12:1966, Stockholm, Sweden.

BKR 94, 1994. Boverkets konstruktionsregler. BFS 1993:58. Boverket, Stockholm, Sweden.

Enockson, P.; Mårtensson, A; 1996. Deformations in timber framed buildings. Influence of load, moisture and time. Report TVBK-7054. Department of Structural Engineering, Lund University, Lund, Sweden.

Eurocode 5, 1993. Design of Timber Structures. CEN TC 250/SC5, ENV 1995-1-1.

Frater, G.S.; Thelandersson, S. 1996. Bearing Performance of Dimensioned Lumber in a Platform Frame An Experimental Study. Report TVBK-7053. Department of Structural Engineering, Lund University, Lund, Sweden.

Jordow, N.; Enockson, P. 1996. Moisture Movements and Deformations in Timber Framed Buildings (in Swedish). Report TVBK-5079. Department of Structural Engineering, Lund University, Lund, Sweden.

Madsen, B.; Hooley, R.F.; Hall, C.P. 1982. A Design Method for Bearing Stresses in Wood. Canadian Journal of Civil Engineering, Vol. 9, pp. 338-349.

Thorson, B.R. 1989. Structural Design of Multi-storey Timber Buildings in Canada. Proceedings, Pacific Timber Engineering Conference, 105-108. New Zealand.

INTERNATIONAL COUNCIL FOR BUILDING RESEARCH STUDIES AND DOCUMENTATION

WORKING COMMISSION W18 - TIMBER STRUCTURES

SERVICEABILITY PERFORMANCE OF TIMBER FLOORS

- EUROCODE 5 AND FULL SCALE TESTING

by

R J Bainbridge

C J Mettem

TRADA Technology Ltd

United Kingdom

MEETING THIRTY

VANCOUVER

CANADA

AUGUST 1997

Serviceability Performance of Timber Floors - Eurocode 5 and Full Scale Testing

By R.J. Bainbridge, TRADA Technology Ltd, UK
C.J. Mettem, TRADA Technology Ltd, UK

Abstract

This paper describes recent research relating to the Serviceability Limit State (SLS) performance of timber floors.

The findings of full scale tests are summarised and related to Eurocode 5 based design of one-way spanning timber floor constructions.

1 Background

All of the structural Eurocodes, including Eurocode 5: Part 1.1 [1], are limit state design codes. This means that the overall performance of structures should satisfy two basic requirements. The first is the Ultimate Limit State (ULS) relating to safety, usually expressed in terms of load-bearing capacity, and the second is Serviceability Limit State (SLS) performance, which refers to the ability of the structural system and its elements to function satisfactorily in normal use.

It is generally understood that violation of safety criteria may cause substantial damage and risk to human life, whereas exceeding the serviceability limits rarely leads to such severe consequences. However, whilst this statement may suggest that serviceability is relatively unimportant, in practice it is often the key element to ensuring an economical and trouble-free structure.

Ideally, serviceability requirements should be determined in contracts, and by the design team, rather than being rigidly prescribed by codes. In small projects however, it is impractical to determine serviceability requirements from first principles each time. Furthermore, codes and supporting Guidance Documents are expected to state the general principles for load combination values, material parameters, and calculation procedures, which are appropriate for serviceability limit states.[2]

Section 3.3 of Eurocode 1: Part 1 [3] identifies the main criteria groups for consideration under SLS design, which can be translated to general serviceability requirements as follows:

- *Functioning of buildings or parts of the same.* This term encompasses irreversible limit states, e.g. avoiding damage to finishes and fixtures. The functioning of non-structural parts, plant and equipment is included here too, although strictly these conditions may be related to reversible or irreversible limit states;

- *Comfort of building users*, generally avoiding reversible effects, which may be a nuisance or affect comfort, such as vibration;
- *Appearance*, generally avoiding reversible effects, such as visible sag of floors and ceilings.

Although serviceability performance is of importance in all parts of a structure, there are a number of situations where its significance is paramount. Floors are an example of such an instance.

2 Eurocode 5 Method for Timber Floor Design

The methodology for design of timber floors under Serviceability Limit States can be subdivided thus:

- static structural considerations - e.g. deflection under load;
- dynamic structural considerations - e.g. vibration response to actions of occupancy;
- other comfort considerations - e.g. acoustic separation, thermal performance, etc.

The focus of this paper is upon recent work carried out relating to the first two items identified above.

Use of the SLS design methodology for floors in EC5 calls for the following items to be considered:

- deflection in response to an instantaneous imposed load
- deflection in response to final imposed load
- deflection in response to final total load
- vibrational performance

The limits suggested in EC5 with respect to each of these criteria are summarised in Table 1.

Parameter		Limit Suggested in EC5	
Static Deflection	instantaneous imposed load	$u_{2, inst} \leq \frac{span}{300}$	eq. 4.3.2
	final imposed load	$u_{2, fin} \leq \frac{span}{200}$	eq. 4.3.3
	final total load	$u_{net, fin} \leq \frac{span}{200}$	eq. 4.3.4
Vibration	UK NAD vibration method	$u_{net, inst} \leq \frac{span}{333}$ or 14 mm	UK NAD Cl 6.4 f)
	unit deflection	$u/F \leq 1.5 \text{ mm/kN}$	eq. 4.4.3a
	velocity response	$v \leq 100^{(11\zeta-1)} \text{ m/(Ns}^2)$	eq. 4.4.3b
	natural frequency (scope of EC5 method)	8 Hz < f1 < 40 Hz	Cl.4.4.3.(1) Cl.4.4.3.(2)

Table 1 Summary of EC5 Floor Design Limits [1]

The current method of floor design using Eurocode 5 and the UK National Application Document (NAD) is shown in outline form in Figure 1.

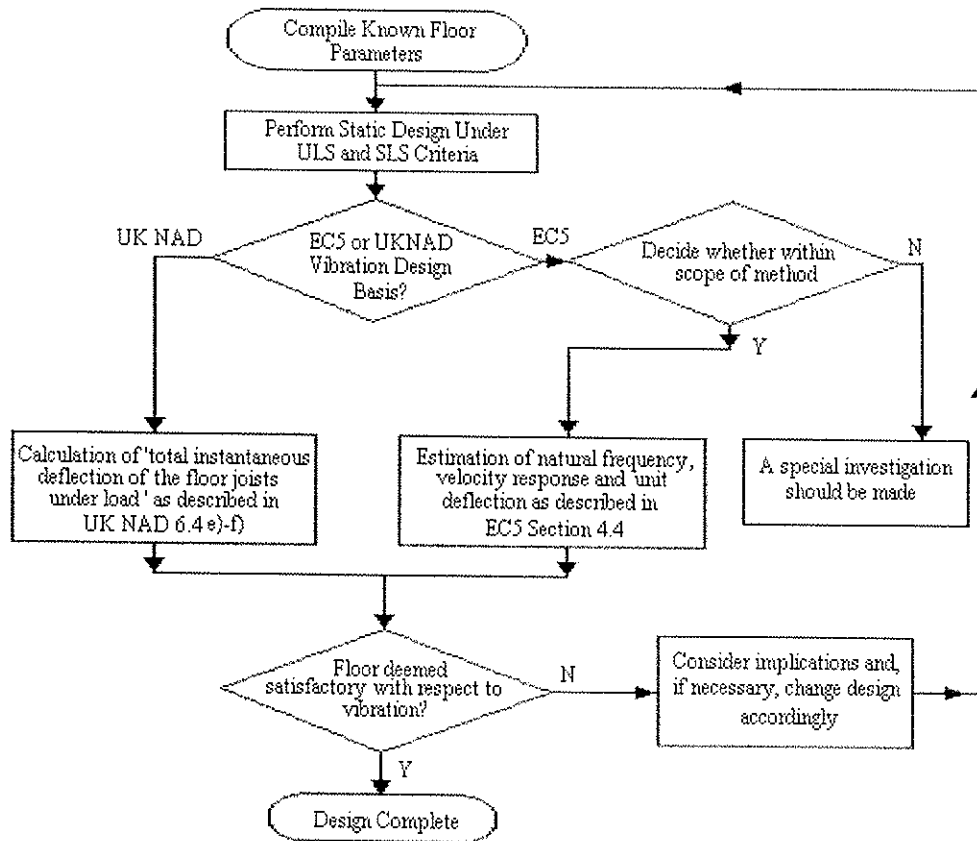


Figure 1 Overview of the EC5/UK NAD Floor Design Method.

3 Test Programmes

Recent research carried out by TTL in relation to SLS performance of Timber Floors has had a strong experimental element and has focused on the following:

- ceiling tests to investigate acceptable deflection levels;
- large domestic and non-domestic scale timber floor deflection tests;
- large domestic and non-domestic scale timber floor vibration response tests.

3.1 Ceiling Tests

Ceiling Tests were carried out to investigate deflection criteria for a range of building types which employ timber as a major material and to develop suitable design recommendations.

Full scale static load tests were carried out on an arrangement of floor joists lined with plasterboard ceilings to investigate cracking (as shown in Figure 2a). Three types of ceiling finish were tested:

- 12.5 mm plasterboard, tapered-edged, with taped and filled joints
- 12.5 mm plasterboard, square-edged, with 2-3 mm plaster skim coat
- 12.5 mm plasterboard, square-edged, with 'Artex' finish

Load tests were also carried out on the ceiling of a test room measuring 4.8m x 3.6m on plan. The visual perceptions of occupants of the room were recorded by survey, relating to a range of induced ceiling deflections. The ceiling was finished with plaster skim coat and the room was furnished with carpet, living room furniture and domestic lighting accessories. Six teams of observers, each team comprising four individuals from a mixture of technical and non-technical backgrounds, were asked to enter the room on six occasions. On each occasion a deflection (L/667, L/333 or L/222) was induced in the ceiling prior to entry, the sequence of deflections being randomly ordered.

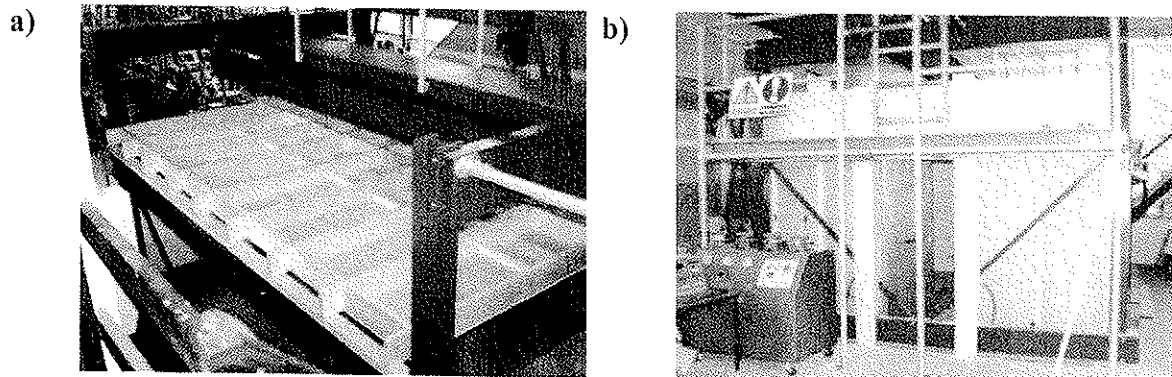


Figure 2 *Ceiling Tests*
a) Ceiling Panel Test
b) Exterior of Test Room - Perceptions of Ceiling Deflection

3.2 Floor Vibration Tests

A series of vibration tests were carried out on a range of timber test floors. The tests consisted of soft body impact tests and heel drop tests. The floor construction was varied in an attempt to reflect a range of floors suitable for different building applications, in terms of design load carrying capacity and span. Variations were also made with respect to aspects of the overall floor construction such as decking materials and the type and placement of strutting. Figure 3 shows some of the largest test floors during testing.

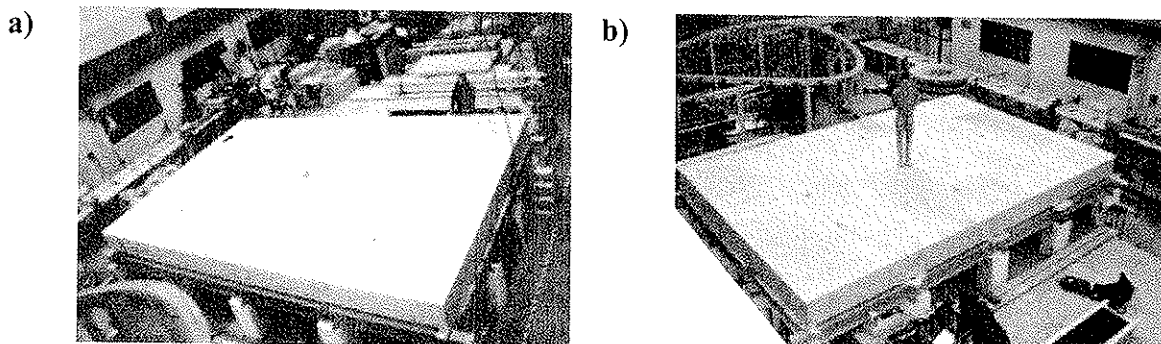


Figure 3 *Full Scale Floor Tests*
a) Vibration Test on 7.2m Span Non-Domestic Timber Floor
b) Heel Drop Vibration Test

Vertical vibrations were recorded on the decking surface of all the test floors and horizontal components of vibration in the joist members were also investigated in a number of cases.

3.3 Static Load Floor Tests

A series of static load tests were also carried out on the test floors used for the vibrational testing described in section 3.2. In addition tests were carried out on a large domestic type floor of 4.8m span, to investigate the behaviour of floors with different strutting arrangements and different decking materials as compared to a floor consisting only of joists and strutting (as shown in Figure 4).

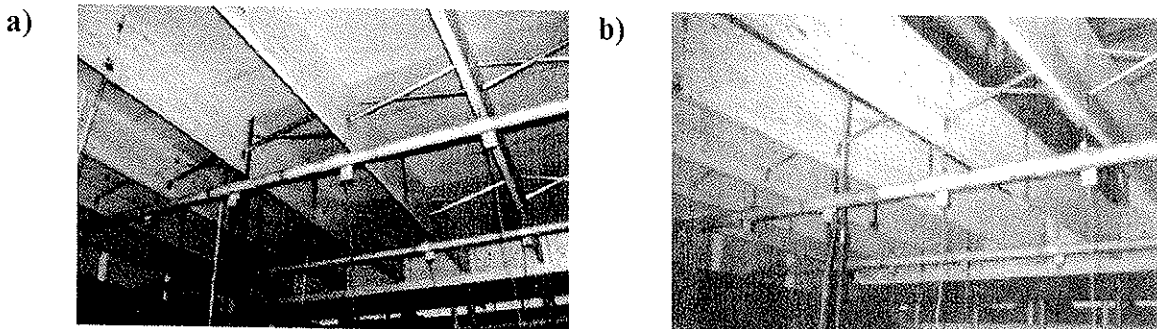


Figure 4 Full Scale Static Deflection Tests
a) Struted Floor With Chipboard Deck
b) Struted Floor With No Decking

4. Overview and Discussion Of Results

4.1 Ceiling Tests [4,5]

4.1.1 Ceiling Panel Tests

The results of the full scale ceiling tests showed that excessive deflections of joists cause significant, irreversible and visually unacceptable damage to the attached plasterboard ceilings, confirming that the limitation of deflection to prevent such damage is a realistic serviceability consideration.

The tests on plasterboard ceiling panels with a plaster skim coat or textured finished showed that cracks in the ceiling surface became visible at deflections in the range of span/116 ($8.62 \times 10^{-3} L$) to span/337 ($2.97 \times 10^{-3} L$), depending on the ceiling construction and finish. The majority of the specimens were found to remain acceptable in terms of damage up to deflections of span/150.

It was found that cracking in plasterboard can be attributed principally to curvature developed after fixing and finishing takes place, hence it should be unnecessary to include components of deflection caused by self weight of the floor structure in deflection calculations relating to this aspect of serviceability.

It was also found that the interaction of ceiling and plasterboard as an inverted 'T-beam' is significant when compared with theoretical calculations based upon the stiffness of bare joists.

4.1.2 Human Perception Tests in Furnished Test Room

In the test room, it was found that, in general, people were unconcerned by ceiling deflections up to 50% greater than the allowable value of span/333 ($3.00 \times 10^{-3} L$) in BS 5268: Part 2 [6], i.e. total deflections of span / 222 ($4.50 \times 10^{-3} L$).

The tests suggested that the human perception of structural deflections in a furnished, dry lined room is not markedly acute or critical. Subjective appraisal however, depends on the type of ceiling, the area of it that is visible, its height and its relationship to other elements of the construction (particularly elements that are horizontal or in a horizontal plane) and the lighting conditions.

These results reinforce the cited limit of L/200 presented in EC5 in the case of Reversible Final deflection, '*unless special conditions call for other requirements*'.

4.2 Floor Vibration Tests

4.2.1 Vertical Vibrations

Variations in the decking type were found to change the fundamental natural frequency only marginally. This is due to the fact that the frequency of vibration is related to both stiffness and self weight;

$$f_1 \propto \sqrt{\frac{EI}{m}}$$

where: f_1 = fundamental natural frequency
 EI = effective stiffness
 m = mass

The variations in both the effective stiffness and the overall mass of the floor, resulting from the use of the differing decking materials, were in such a ratio as to lead to only a small overall increase in fundamental frequency in cases with substantial increases in the bulk and mechanical properties of the decking material [7].

The provision of strutting did not affect the fundamental frequency or damping of vertical vibration to any appreciable degree [7,8]. Increases in the number of rows of strutting did, however, raise the frequency of higher order modes and promoted separation of adjacent vibration modes. These are both recognised benefits in the performance of the floor and affect the more complex aspects of the vibration response. Different strutting types (herringbone, solid blocking, proprietary steel systems) were found to display negligible difference in terms of effectiveness with respect to these tests [9].

It is also of note that in all the tests the measured damping was greater than the default value of 1% suggested in EC5.

7.2.2 Horizontal Vibrations

The provision of strutting does not affect the fundamental frequency or damping of horizontal vibration in joist members to any appreciable degree. The strutting does act locally to stabilise the joists, resulting in a very slight reduction in maximum recorded velocity response and a change in the pattern of recorded velocity across the floor span [9].

The influence on the transverse stability of joists can also be linked to the higher modes of vibration. In timber floors, these higher modes have a deflected modal shape linked to the transverse direction (i.e. 90° to span) as illustrated in the example mode shapes shown in Figure 5. An increase in the stability of joists will promote stiffness in this direction and thus will tend to raise the frequencies of these components of vibration. This is in line with the findings of the vertical vibration tests.

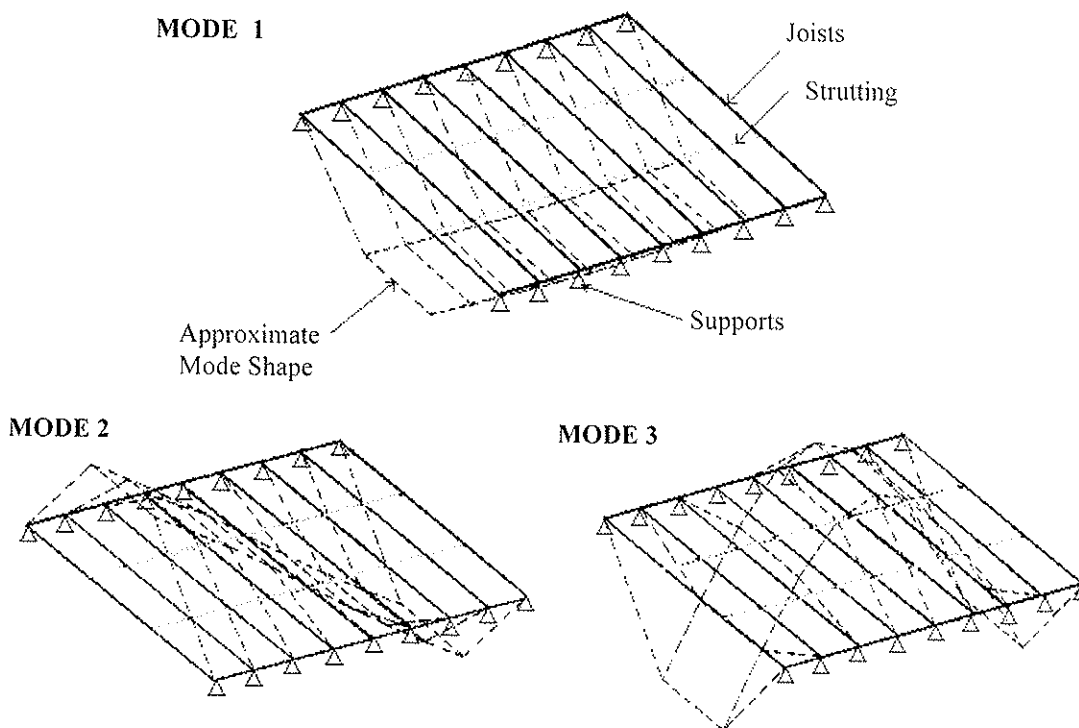


Figure 5 Example Mode Shapes (1-3) for a One Way Spanning Timber Floor Structure (Not to Scale).

4.3 Static Floor Tests

These tests have shown that the major influence on deflection is decking type, such that the effect of strutting is minimal compared with the semi-composite interaction of joists and decking [7]. Where a concentrated load is of major significance, the position of the rows relative to the load position is of greater significance than the total number of rows of strutting.

5 Comparison of Results with Eurocode 5

5.1 Static Deflections

The individual components of deflection which combine to determine the total deflection in a structural member are illustrated in Figure 6.

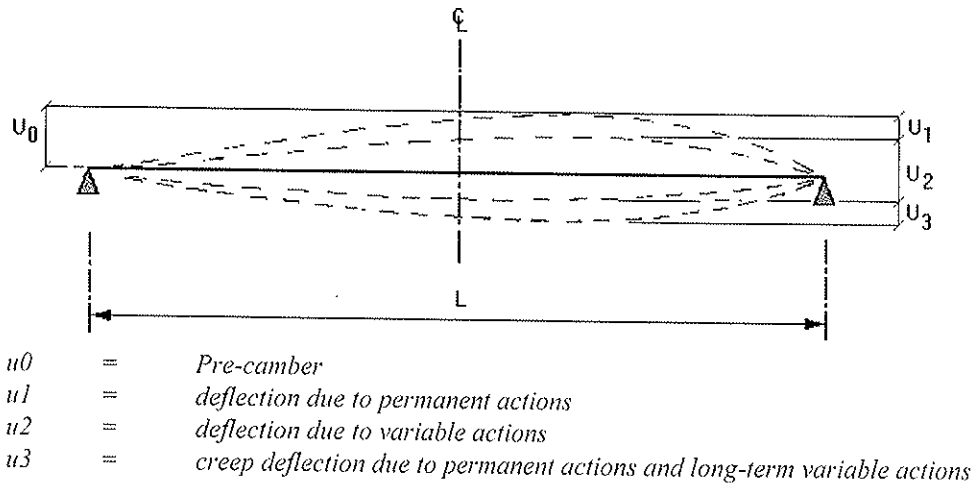


Figure 6 Components of Deflection For a Simply Supported Joist or Beam

The actual deflections at which the various limit states are reached depend on the particular limit state, the materials involved, and the purpose of the building. No specific limits are provided or required by EC1, but EC5 suggests limits for certain cases, as described previously. From the investigations detailed previously, new deflection limits have been derived for use in the UK. These are believed to be representative of a reasonable limit in each of the instantaneous and final, reversible and irreversible cases[2,10]. These are compared to the limits suggested in EC5 and the UK NAD in Table 2 and Figure 7.

Limit state	Example of use	Recommended limits	EC5 Limits
Irreversible Instantaneous	Cracking of plasterboard following installation	$u_{2,d} \leq \frac{L}{350}$	$\frac{L}{300}$
Irreversible Final	Cracking of plasterboard at end of design life	$u_{2,d} + u_{creep} \leq \frac{L}{250}$	$\frac{L}{200}$
Reversible Instantaneous	Vibration performance of domestic timber joisted floors (as in UK NAD)	$u_{1,d} + u_{2,d} \leq \min.\text{of} \left\{ \begin{array}{l} 14 \text{ mm} \\ L / 333 \end{array} \right.$	$\min.\text{of} \left\{ \begin{array}{l} 14 \text{ mm} \\ L / 333 \end{array} \right.$
Reversible Final ¹	Appearance of roofs and ceilings or serviceability of floors at end of design life	$u_{1,d} + u_{2,d} + u_{creep} \leq \frac{L}{200}$	$\frac{L}{200}$

¹ This check is unlikely to be critical for a floor or ceiling with attached plasterboard.

$u_{1,d}$ = design value of instantaneous (elastic) deformation caused by permanent actions
 $u_{2,d}$ = design value of instantaneous (elastic) deformation caused by variable actions
 u_{creep} = creep deformation caused by permanent and variable actions.
 L = structural span of beam

Table 2 Recommended Vertical Deflection Limits [1,10]

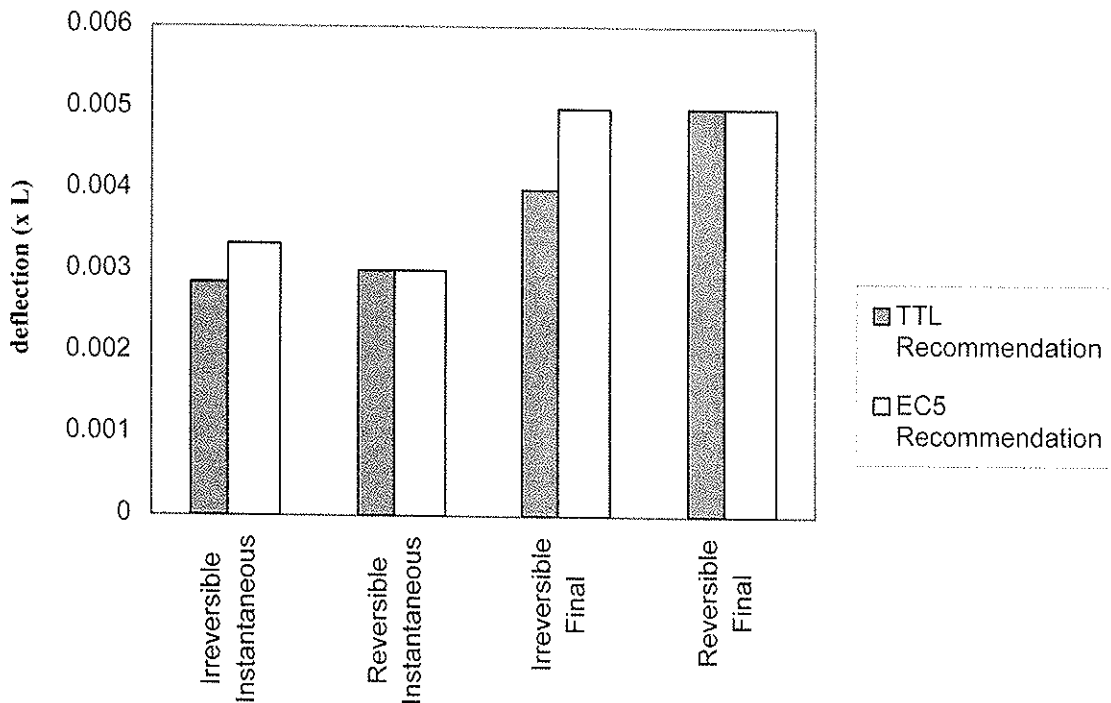


Figure 7 Comparison of Recommendations With EC5 Deflection Limits.

The changes in suggested deflection limit can be seen to be restricted to the irreversible cases, where a somewhat more strict limit is suggested. It is obviously more important not to exceed an irreversible limit state than a reversible one. The reversible instantaneous limit recommended in the current UK NAD to Eurocode 5 is supported by this research.

From the static floor tests, the predicted unit deflections for the floor joists using a calculation method based on Eurocode 5 were generally in good agreement with the deflections achieved by the floor joists with no decking and 2 rows of strutting attached. This is of note since the calculation model for static deflection does not currently include decking contribution to the stiffness of a floor and current design guidance [11] at the time of testing would lead to specification of strutting in two rows equally spaced along length of the joists.

5.2 Vibrations

Cl.4.4.1 (4) of EC5 states that “Unless other values are proved to be more appropriate, a modal damping ratio of $\zeta = 0.01$ (i.e. 1%) should be assumed.” The recorded magnitude of damping recorded in the tests, and also reported in a selection of other research papers on the subject [12-18], are plotted against floor span in Figure 8. As can be seen, the bulk of the results lie within the 1-5% range, with a few instances of higher damping value being recorded. This supports the use of 1% as a worst case value (i.e. damping taken as a reasonable minimum) in the absence of any more appropriate value, but suggests that damping may be significantly greater.

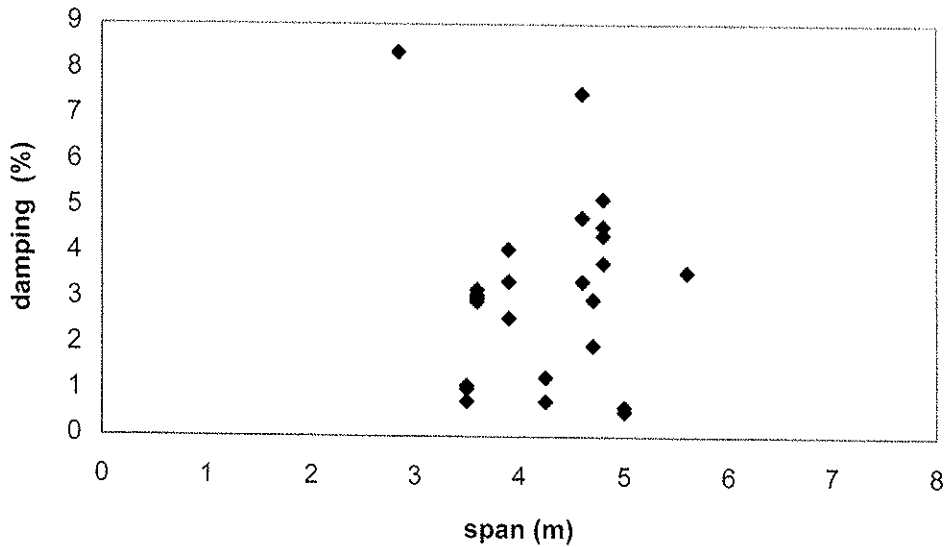


Figure 8. Summary Of ζ Values From Tests Performed At TTL And Reported In Cited Literature

The scope of the EC5 method is defined thus: “For residential floors with a fundamental frequency ≤ 8 Hz ($f_1 \leq 8$ Hz) a special investigation should be made (Cl.4.4.3 (1))”. The recorded values of fundamental frequency from the tests, together with a selection of values reported in other research papers on the subject [12-18], are plotted against floor span in Figure 9. As can be seen, the results of the tests show that fundamental frequency will tend to lie within the 10 - 30 Hz range.

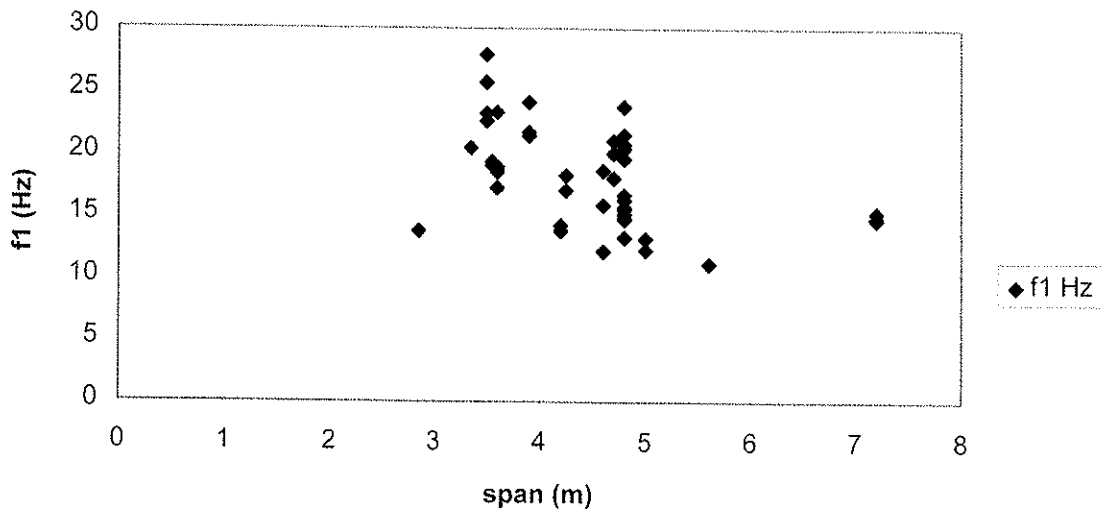


Figure 9. Summary Of f_1 Values From Tests Performed At TTL And Reported In Cited Literature

As has been reported previously [19], it has been found that the use of equation 4.4.3c produces low approximations of f_1 and that a closer approximation may be obtained for UK type timber floors with one way spanning joists, through use of the following equation:

$$f_1 = \frac{3\pi}{4l^2} \sqrt{\frac{(EI)_l}{m}}$$

where: $(EI)_l = 1.2 E_j I_j \times 1000/s$

and: $m =$ mass per unit area (kg/m^2)
 $(EI)_l =$ stiffness in direction of span, per metre width of floor
 $l =$ joist span (m)
 $E_j, I_j =$ joist properties
 $s =$ joist spacing, centre to centre (mm)

This is believed to be due to the fact that the floor behaviour is somewhere between that of a beam, as modelled in equation (4.4.3c), and a plate.

The velocity response of a floor when subjected to an impact is addressed in EC5, Cl.4.4.3 (5), as follows:

“The value of v may as an approximation be taken as

$$v = 4 (0.4 + 0.6 n_{40}) / (mbl + 200) \quad \text{m/Ns}^2 \quad (4.4.3d)$$

where $n_{40} = \left\{ \left[\left(\frac{40}{f_1} \right)^2 - 1 \right] \left(\frac{b}{l} \right)^4 \frac{(EI)_l}{(EI)_b} \right\}^{0.25} \quad (4.4.3e)''$

For a one-way spanning floor it is very difficult to calculate correctly the ratio of $(EI)_l / (EI)_b$. It has been found that for the test floors, where no ceiling was attached, a reasonable approximation of v may be derived using this formula and a factor of 540 for the ratio of $(EI)_l / (EI)_b$.

It is believed that the limits provided for domestic timber floors could be modified for use in certain non-domestic situations through application of the principles, base curves and multipliers for human exposure to vibration as set down in documents such as ISO 2631 [19,20] and BS 6472 [21], the basis of which is summarised in diagrammatic form in Figure 10.

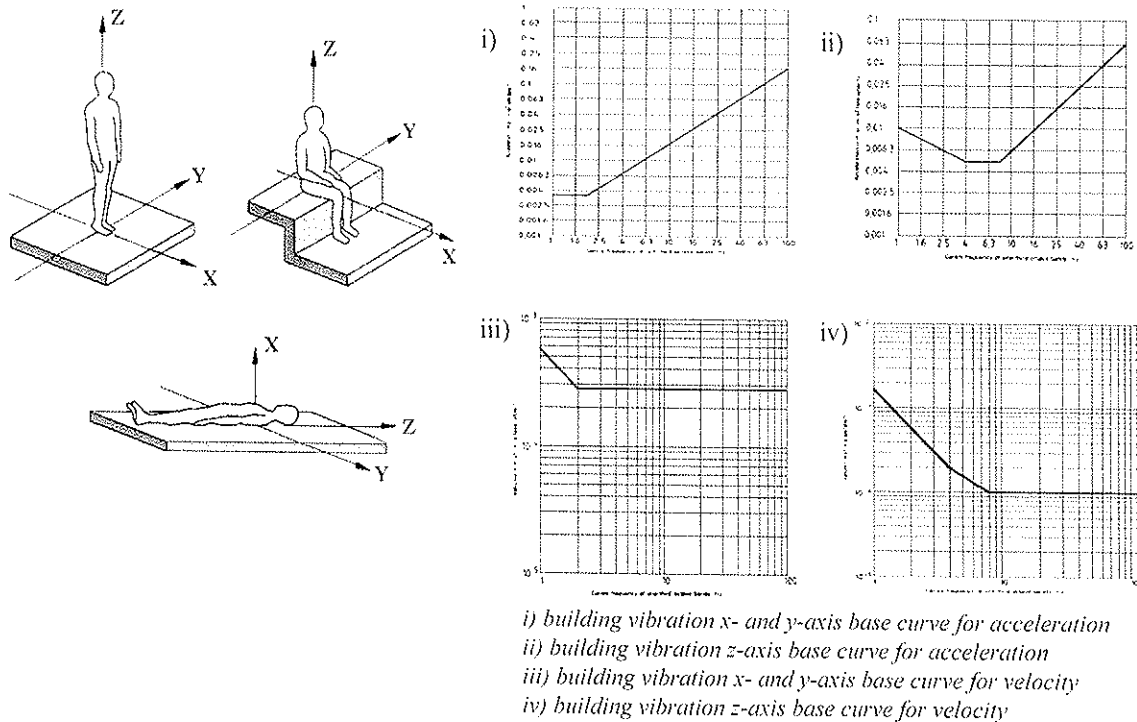


Figure 10. Summary of ISO 2631 and BS 6472 Human Exposure Limit Basis for Vibration in Buildings.

5 Conclusions

SLS criteria related to deflections and vibration frequently govern the design of horizontal timber elements, hence it is necessary to ensure that design procedures are not unduly conservative, in order to promote efficient design and material usage.

The reasons for limiting deflections must be understood and defined by the designer, who, through modern code approaches, has greater discretion when considering serviceability. This requires consideration of the action combinations and expected resultant consequences in terms of functionality, comfort and appearance.

It has been found that the floor design methods relating to SLS in timber floors presented in EC5 can be applied to predict test floor behaviours to a reasonable degree of accuracy, provided certain factors are known or can be approximated for inclusion in the formulae.

Since strutting provides stability to joists and enhances overall serviceability performance, both in terms of static stiffness and influence upon the complex aspects of the dynamic vibration performance, its provision as directed by current guidance should be regarded as a minimum.

It is also clear that the contribution of decking and plasterboard ceilings to the behaviour of the floor should be considered in the design process, since it is currently ignored. Whilst it is accepted that ultimate limit state design should be based on the primary structural system (i.e. the joists alone), this has implications relating to design under both static and dynamic aspects of serviceability.

6 Forward Look

The findings of this research are to be incorporated in EC5 design guidance documentation.

Since the current vibration assessment method in EC5 section 4.4 is difficult to apply fully to typical UK timber floor construction types, as recognised in the UK NAD , a modified method has been developed based on the EC5 method. This is to be incorporated in future design guidance related to EC5 . It should be noted that the method incorporates a number of factors based on test observations, the validity of which are not fully known in the context of floors in the complete range and variety that might be experienced in real buildings. It should therefore be viewed as a tool for prediction of likely performance and not a definitive design methodology.

This also should be put in the context of the design case considered in all dynamic assessment methods concerning floors: a floor of simplified geometry and, perhaps more importantly, with no imposed loads. Should the design be deemed to warrant a more precise assessment of dynamic performance, then special investigations should be carried out. This might be achieved through use of commercial structural engineering software packages, many of which offer dynamic modelling facilities

Acknowledgements

This paper is the result of work sponsored jointly by the Department of the Environment and the Timber Research and Development Association. TTL gratefully acknowledges their sponsorship and thanks them for their support.

References

- [1] BSI, (1994). DD ENV 1995-1-1:1994, EUROCODE 5: Design of Timber Structures Part 1.1: General Rules and Rules for Buildings. British Standards Institution, London.
- [2] TRADA, (1995). Serviceability Limit States for Timber in Buildings. WIS 4/24, TRADA, High Wycombe.
- [3] BSI, (1994). ENV 1991-1-1:1994 Eurocode 1 - Basis of Design and Actions on Structures - Part 1 : Basis of Design. British Standards Institution, London.
- [4] DAVIS, G. and METTEM, C.J., (1995). A Reappraisal of Permissible Deflection in Timber Structures - Cracking in Plasterboard Ceilings. Report PIF 106/09 , TRADA Technology Ltd, High Wycombe.
- [5] METTEM, C.J., (1995). A Reappraisal of Permissible Deflection in Timber Structures - Final Report. Report PIF 106/10, TRADA Technology Ltd, High Wycombe.
- [6] BSI, (1996). BS 5268: PART 2: 1996. Structural Use of Timber: Part 2. Code of Practice for Permissible Stress Design, Materials and Workmanship. British Standards Institution, London.
- [7] BAINBRIDGE, R.J. and METTEM, C.J., (1997). The Influence of Strutting and Decking Variations on Serviceability Limit State Performance of Timber Floors. International Conference of IUFRO S5.02 Timber Engineering, Copenhagen, Denmark.
- [8] BAINBRIDGE, R.J., (1997). The Effectiveness Of Strutting In Timber Joisted Floors :Test Report on The Influence of Strutting Variations on Serviceability Limit State Performance. Report REP 140/09, TRADA Technology Ltd, High Wycombe.
- [9] BAINBRIDGE, R.J. and METTEM, C.J., (1996). The Effectiveness Of Strutting In Timber Joisted Floors : Report On Test Programme. Report PIF 140/02, TRADA Technology Ltd, High Wycombe.

- [10] TRADA TECHNOLOGY LTD., (1997). Eurocode 5 Guidance Document 5 - How to Calculate Deformations Using Eurocode 1. GD5, TRADA Technology Ltd., High Wycombe.
- [11] TRADA, (1992). Timber Intermediate Floors For Dwellings. Approved Document to the Building Regulations 1991. TRADA, High Wycombe.
- [12] OHLSSON, S.V., (1982). Floor Vibrations and Human Discomfort. MSc Thesis, Chalmers University.
- [13] STARK, J. W., (1993). The Effect of Lateral Bracing on the Dynamic Response of Wood Floor Systems MSc Thesis, Virginia Polytechnic Institute and State University.
- [14] RUNTE, D., (1993). Fundamental Frequencies of I-Joist, Solid-Sawn Joist and Truss Floors based on Tee-Beam Modelling. Research Report, Virginia Polytechnic Institute and State University.
- [15] SMITH, I. and CHUI, Y. H., (1992). Construction Methods for Minimising Vibration Levels in Floors with Lumber Joists. Canadian Journal of Civil Engineering, Volume 19, No.5, pp 833-841.
- [16] HOMB, A., HVEEM, S. and GULBRANDSEN, O., (1988). Oscillations in Light-Weight Joist Floors. Norwegian Building Research Institute.
- [17] THURSTON, S. J., (1993). Walking Induced Vibrations of Light Timber Floors. Unpublished report U.P.306, BRANZ, New Zealand.
- [18] CHUI, Y. H., (1986). Vibrational Performance of Timber Floors and the Related Human Discomfort Criteria. TRADA, UK.
- [19] BAINBRIDGE, R.J. and METTEM, C.J., (1996). Natural Frequency Prediction For Timber Floors. CIB-W18/29-15-5, Proceedings of International Council For Building Research Studies and Documentation Working Commission W18 - Timber Structures, Meeting Twenty-Nine, Bordeaux, France.
- [20] ISO, (1985). ISO 2631/1 Evaluation of Human Exposure to Whole Body Vibration: General Requirements.
- [21] ISO, (1989). ISO 2631/2 Evaluation of Human Exposure to Whole Body Vibration: Continuous and Shock-induced Vibration in Buildings (1 to 80 Hz).
- [22] BSI, (1992). BS 6472:1992 Guide to Evaluation of Human Exposure to Vibration in Buildings (1 Hz to 80 Hz). British Standards Institution, London.

**INTERNATIONAL COUNCIL FOR BUILDING RESEARCH STUDIES AND DOCUMENTATION
WORKING COMMISSION W18 - TIMBER STRUCTURES**

**CONCEPTS FOR DRAFTING INTERNATIONAL CODES AND
STANDARDS FOR TIMBER CONSTRUCTIONS**

by

R H Leicester
CSIRO Building
Australia

**MEETING THIRTY
VANCOUVER
CANADA
AUGUST 1997**

CONCEPTS FOR DRAFTING INTERNATIONAL CODES AND STANDARDS FOR TIMBER CONSTRUCTION

R.H. Leicester
CSIRO, Australia

1. INTRODUCTION

Advances in the development of national product standards and design codes tends to be influenced by a variety of subjective and industrial matters, the availability and experience of technologists involved and to an increasing extent, by trade and international trends. However, in the development of international design codes and product standards, a more rational basis for action needs to be considered so as to make best use of the limited available drafting resource; for this purpose it is useful to discuss criteria in the form of checklists and thereby minimise the influence of subjective opinions.

Table 1 shows the basic categories of codes and standards that are applicable to the structural use of timber. Generally there has been an emphasis on the development of product standards and design codes. A list of typical products that are covered by codes and standards are given in Table 2.

Table 1.
Types of building codes and standards
for structural timber

FOR PRODUCERS
• product standards
• quality control procedures
FOR USERS
• design codes
• maintenance standards

Table 2.
List of timber based products

<ul style="list-style-type: none">• wood • reconstituted wood • mechanical fasteners • glued joints • composite construction<ul style="list-style-type: none">– wood/reconstituted wood– wood/steel • building elements<ul style="list-style-type: none">– floor systems– roof systems– shear walls

Design codes are required to cover both collapse limit states and serviceability limit states. For collapse limit states, design codes are based on specified 5-percentile values; it should be noted that to measure 5-percentile values for a product associated with a high degree of variability, such as structural timber, large sample sizes must be tested. However for serviceability limit states, such as deflection, design is based on mean values and hence only limited samples need be used to measure specified design properties such as the modulus of elasticity.

2. IDEAL ISO CODES AND STANDARDS

2.1 General Principles

Ideally an ISO standard should be applicable globally. This is easier said than done. However, if it is not done, then some countries will be disadvantaged. In particular, it should be borne in mind that most concepts currently used for structural timber codes and standards have been developed in Europe and North America and often these do not take into consideration the range of timber species, climate, biological hazards and limited technology infrastructure to be found in many tropical countries.

A set of criteria for an ideal international standard are given in Table 3. Some possible procedures for achieving these criteria are given in Table 4. Examples of the application of these procedures will be given in the following Sections.

Table 3.
Globalisation criteria for
ideal ISO Codes and Standards

- | |
|---|
| <p>Codes and standards should be applicable to:</p> <ul style="list-style-type: none"> • all species • all constructions • all countries <ul style="list-style-type: none"> – loads – climate – biological hazards – environmental hazards – existing data – existing technology – existing infrastructure – existing culture |
|---|

Table 4.
Some possible procedures to assist in the globalisation
of international codes and standards

- | |
|---|
| <ul style="list-style-type: none"> • use performance-based criteria • establish equivalence with national product standards • accept trade-off between efficiency and quality control • draft tiered design codes • define multiple quality levels • use grouping methods for <ul style="list-style-type: none"> – timber species – loads – member sizes – building elements |
|---|

The drafting of *tiered design codes* refers to design codes which contain both simple and complex design procedures; the simple procedures would not be efficient but would be suitable for use by developing countries. The specification to *multiple quality levels* is to address the issue that acceptable levels of safety and serviceability may vary from country to country for historical, social or cost-optimisation reasons; an example of this would be specified performance levels for the dynamic

characteristics of floors; the important matter is to carefully define the meaning of performance targets and to present methods for measuring and for obtaining them. Finally, some mention should be made of *grouping procedures*. As an example, tropical countries that utilise thousands of species, frequently use grouping methodology for defining timber properties, both structural and non-structural; without the use of this methodology it would not be possible to market more than a few dozen species.

It would be worth considering the application of grouping methodology to all structural parameters not only to timber properties but also to loads, member sizes and building elements. In addition to simplifying the design and marketing, the technique of grouping (if correctly done) would serve to provide a transparent indicator of the uncertainties associated with existing design technology.

2.2 Product Standards

Difficulties in the globalisation of product standards are well illustrated by considering the case of the assessment of timber for the purpose of assigning structural design properties.

Table 5 compares the cost, time and outcome of structural evaluations based on structural size testing and evaluations made on the basis of small clear specimen testing. It is seen that the former is about 1000 times as expensive and time consuming as the latter. The procedure based on structural size testing is favoured in the countries of Europe and North America because of its high accuracy and hence efficiency. However, it should be realised that these countries have extensive testing facilities and are concerned only with a dozen or so commercial species. On the other hand, many tropical countries are concerned with thousands of species and limited laboratory facilities; for these countries the small clears approach is obviously highly attractive. In addition, the loss of accuracy is not a problem because the hardwoods of these countries are 2–4 times as strong as the softwoods of Europe and North America; it is quite acceptable for these countries to take a penalty of 30% in assessed design strength to cover the inaccuracies arising from the use of the small clears assessment procedure. Hence an ideal standard should accept the possibility of using either procedure.

Another matter worth mentioning is the choice of standard test conditions. The specification of a test environment of around 23°C suits the laboratories of Europe and North America; but this specification leads to an unnecessary (and sometimes prohibitive) expense for air-conditioning for countries in tropical regions.

Table 5.
Comparison of two methods for evaluating the design properties of structural timber

Evaluation method	Cost for evaluating one species	Laboratory time	Typical error in 5-percentile strength estimate
structural size timber	\$1000 000	1 year	±5%
small clears	\$ 1000	1 week	±30%

In Table 3, mention was made that international standards should take into account existing data, because of the considerable expense and time invested in earlier evaluations. An important example is again the assessment of structural properties. As illustrated in Table 6, because of the heterogenous nature of timber, the derived design properties can be significantly different depending on the evaluation method used, different enough in fact that it may be uneconomic or unsafe to ignore the differences. At a cost of about \$1 million and one year of testing per species for an evaluation using structural size timber, it is obviously a very expensive exercise to undertake a fresh reassessment of all previous evaluations. Hence, the only sensible way out of this dilemma is for an international standard to accept and where possible to provide a method of equivalencing the evaluations of national standards with that of the international standard.

Table 6.
Evaluation of 90 x 35 mm F5 machine stress graded Radiata pine

Evaluation standard	5-percentile bending strength (MPa)	Mean modulus of elasticity (GPa)
EN: 384/408(1)	13.6	7.8
AS/NZS: 4063(2)	17.0	9.4

(1) Worst defect in a piece located at midspan of test specimen

(2) Test specimen selected from random location along a piece of timber

As mentioned in Table 4, the use of performance-based criteria is essential to the removal of unnecessary restrictions from international standards. The use of performance-based criteria assists rapid innovation of new technologies, leads to

increased efficiencies in building design and (most importantly here) facilitates the establishment of equivalences between various product standards.

Table 7 gives concepts for drafting ideal performance-based criteria for product standards. The essential characteristic of a good test procedure for a performance-based standard is that the procedure should simulate in-service use conditions as closely as possible. For example, to test a shear wall to resist cyclonic wind forces (a) the shear wall should be constructed and supported as closely as possible to the in-service application configuration; and (b) a loading typical of that expected during a cyclonic wind lasting several hours should be applied. If for testing expediency the wind load is simplified (for example by reducing the number of loading cycles from 10,000 cycles to 10 cycles) then the range of shear walls to which the test may be applied (without undue conservatism) will be reduced accordingly. In practice one can only fulfil the conditions shown in Table 7 in a very rough sense; not every in-service condition or loading can be tested, and a complete simulation of an applied load is, in general, prohibitively expensive. However, the closer the ideal is approached, the more the advantages of the use of performance-based criteria will be realised.

Table 7.
Ideal concepts for performance-based
criteria for product standards

- in-service configuration of structural element
- in-service loading simulation
 - human forces
 - floor loads
 - thunderstorm winds
 - cyclone winds
 - earthquake forces

The acceptance of performance-based criteria is particularly important for countries where timber species and biological hazards can have characteristics that are quite different from those of Europe and North America. Since the rationale for the procedures of product standards and assessment protocols developed in Europe and North America are often not applicable for these countries.

On the basis of the above, the ideal format for an ISO product standard is that shown in Table 8. In general, the normative section containing the performance requirements will be relatively brief. The current best practices will be placed in an

informative section as a non-mandatory examples of compliance; this leaves the door open for the development of more cost-effective methods of compliance for reasons discussed previously. The informative section should also contain procedures for equivalencing ISO and existing national standards.

Table 8.
Proposed format for an ideal ISO product standard

Normative <ul style="list-style-type: none"> • Performance requirements
Informative <ul style="list-style-type: none"> • examples of compliance • equivalencing procedures

2.3 Design Codes

Table 9 lists some of the characteristics to be expected in an ideal ISO design code. The topic coverage is quite daunting but nevertheless essential for an ideal international standard.

As an example of the necessity to cover all failure modes, consider the matter of creep buckling. Since 1972 the Australian timber engineering design code, formerly CA 65 (Standards Association of Australia 1972), has taken into account the possibility of structural failure by creep buckling. This is because in Australia creep buckling represents a potential mode of failure for compression members of unseasoned hardwoods under long duration dead loads. However, for Canada and many other countries of North America and Europe the critical loading is often a short duration snow load acting on softwood members; hence if compression members in Canada and these countries are sized to cope with this snow loading, then the ignoring of creep-buckling effects would not increase the risk of failure significantly. Thus, while it would be possible to ignore creep buckling within a Canadian design code, it would be essential to include it in an ISO design code intended for global application.

One aspect of an ISO design code is that it should be applicable, ideally equally applicable, to all species utilised for structural purposes. Some of the earlier European and North American design codes were applicable only to a narrow range of softwood species. As a result, some factors in these codes were related to timber strength, whereas it would be more appropriate to relate these factors to relative

strength; an example of a factor that is suitable for normalising quality could be a grade ratio factor defined as follows,

$$\text{grade ratio} = \frac{\text{5-percentile bending strength}}{\text{mean small clear wood bending strength}} \quad (1)$$

Examples of data described according to this grade ratio factor are given in Figures 1 and 2; this Figure shows data on Southern Pine, based on the information given by Doyle and Markwardt (1966, 1967) and extend to estimates for pole properties based on data for radiata pine by Boyd (1964).

For the purposes of specifying design properties based on clear wood strength, it would be useful to normalise the test data by defining relative strength and stiffness as follows,

$$\text{relative strength} = \frac{\text{strength}}{\text{mean small clear wood bending strength}} \quad (2)$$

$$\text{relative modulus of elasticity} = \frac{\text{modulus of elasticity}}{\text{mean small clear wood modulus of elasticity}} \quad (3)$$

The data for Southern Pine normalised in this way are shown in Figures 3 and 4. It would be expected that the effects of grade ratio would be similar for all species that are similar in a botanical sense.

Table 9.
Characteristics of ideal ISO design codes

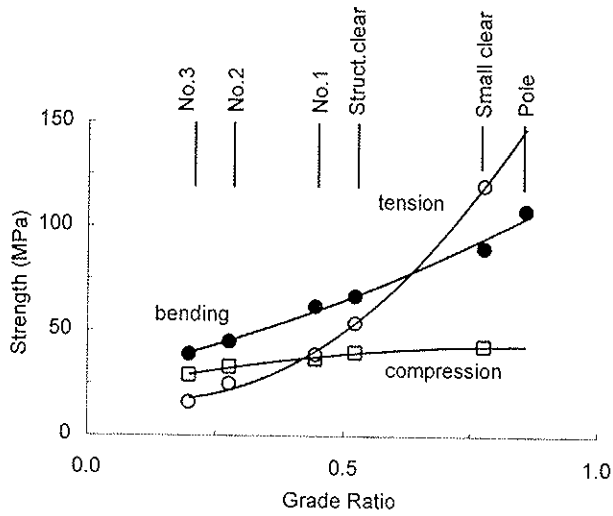
<p>Design code should be applicable to</p> <ul style="list-style-type: none"> - all species - all elements - all constructions - all climates - all biological hazards - all loadings - all failure modes
--

There are other more subtle aspects related to species. In the European and ASTM product standards there is considerable emphasis on standardising the size effect. For example, if timber of size 140 x 35 mm has a 5-percentile bending strength of 18.5 (MPa), then according to ASTM D-1990 (ASTM 1994), 240 x 45 mm timber of the same grade should be weaker in terms of ultimate stress and, in fact, the bending strength should be exactly 15.8 MPa. However, as shown in Table 10, it is possible for the larger sizes to have a stronger unit strength. This is because in addition to the effects related to the nature of timber, there are also other industry specific factors such as the relationship between log size and cutting pattern that affect strength. An ISO design code should accept the full range of international possibilities arising from international practices and should make it quite transparent as to when design rules reflect the nature of timber and when they reflect specific industry practice.

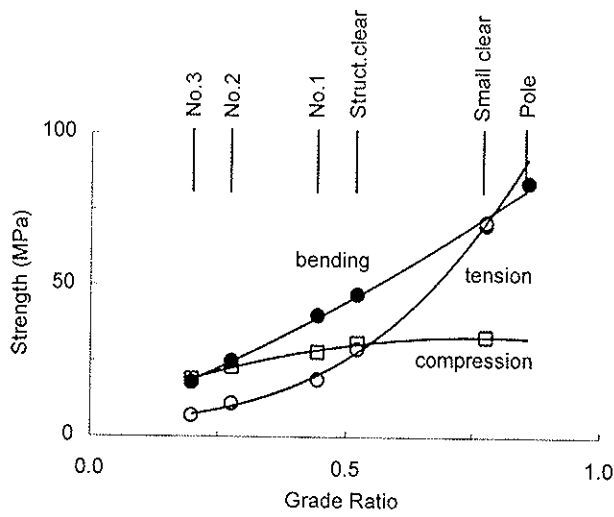
Table 10.
Size effect of Hoop pine, visually graded
to VSG No. 4

Basis of evaluation	5-percentile bending strength (MPa)	
	140 x 35 mm	240 x 45 mm
Measured values (N = 170)	18.5	20.1
ASTM D-1990	18.5	15.8*

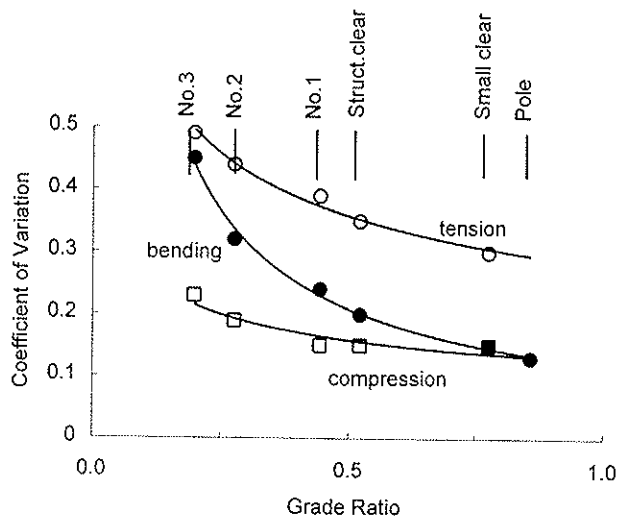
* expected value based on ASTM D-1990.



(a) mean strength

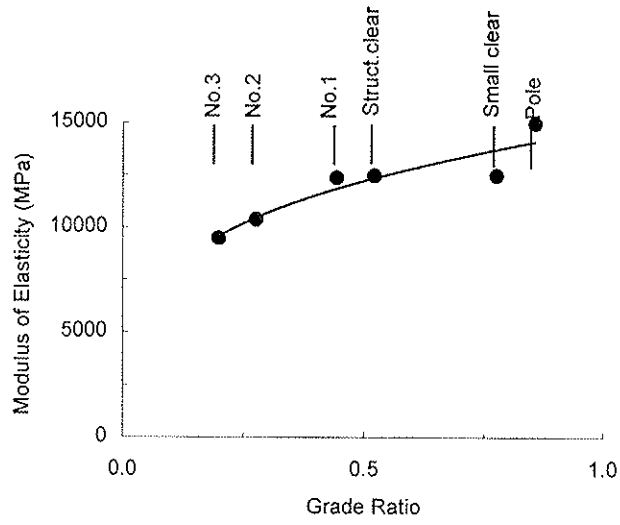


(b) 5-percentile strength

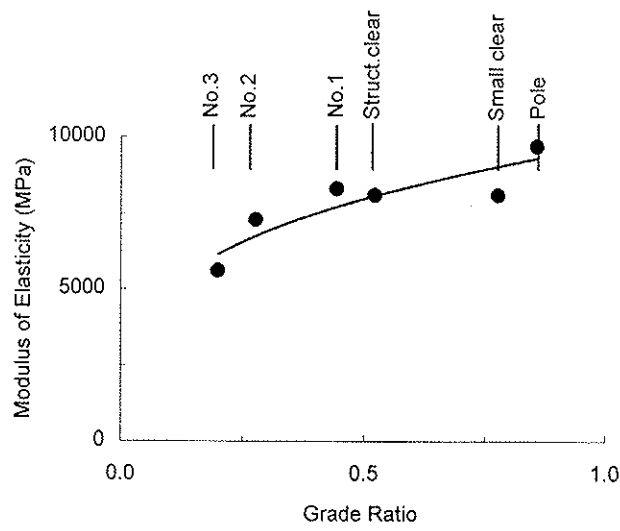


(c) coefficient of variation of strength

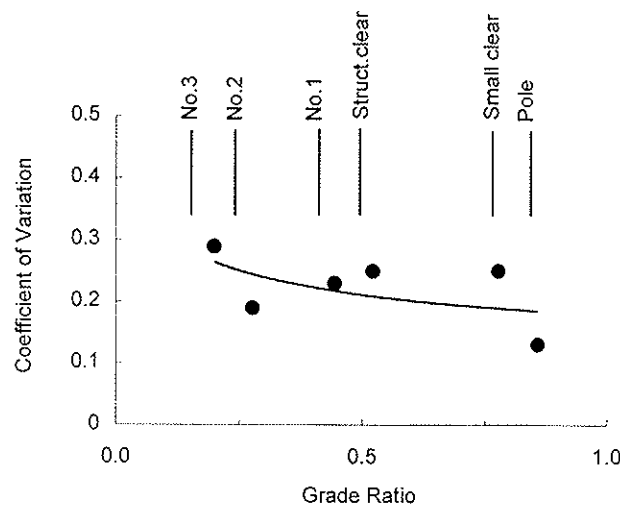
Figure 1. Effect of grade ratio on strength properties of Southern Pine.



(a) mean modulus of elasticity

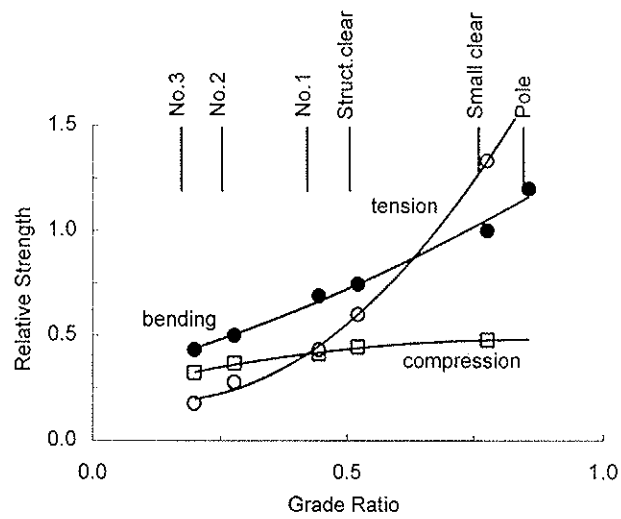


(b) 5-percentile modulus of elasticity

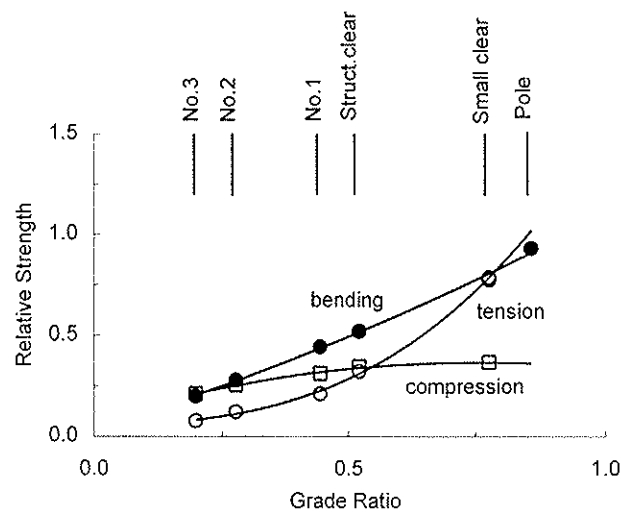


(c) coefficient of variation of modulus of elasticity

Figure 2. Effect of grade ratio on the modulus of elasticity of Southern Pine.

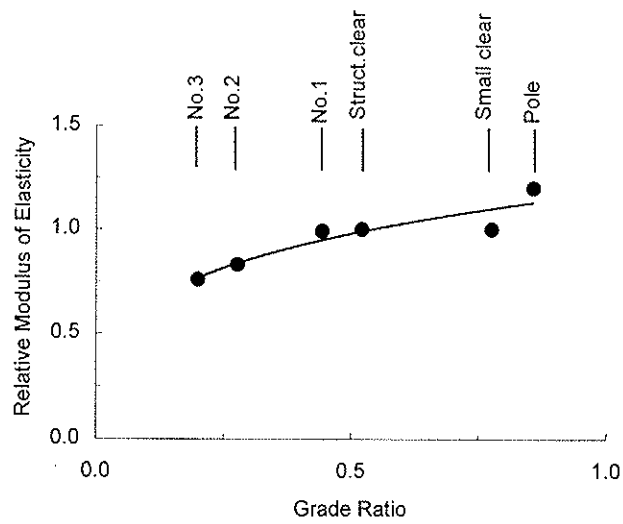


(a) mean relative strength

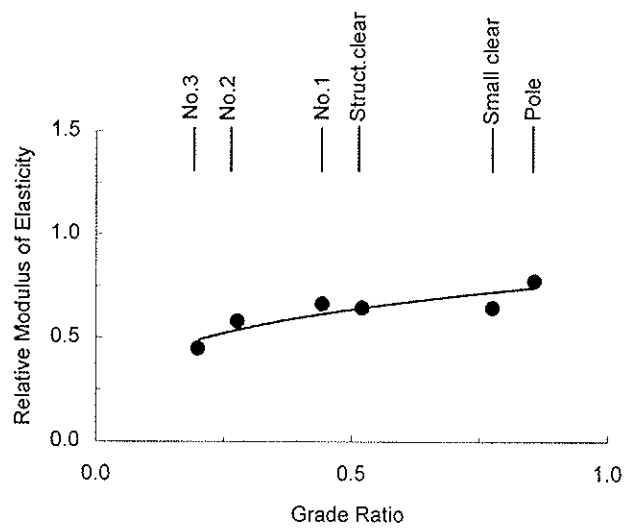


(b) 5-percentile relative strength

Figure 3. Effect of grade ratio on the relative strength properties of Southern Pine.



(a) mean relative modulus of elasticity



(b) 5-percentile relative modulus of elasticity

Figure 4 Effect of grade ratio on the relative modulus of elasticity of Southern Pine.

3. OTHER DIFFICULTIES

The previous Sections have dealt with the problem of drafting ISO codes and standards that have formats and contents that are suitable for application internationally. However, even if there were to be universal good will and cooperation in the drafting of such standards, some difficulties would still remain.

The first would be to obtain agreement on accepting a international set of limited preferred sizes and configurations for sawn wood, reconstituted board products, connectors etc. Such an agreement would not only assist international trade in these products but also in technology transfer between countries; technology could be developed in terms of load capacity rather than stress capacity; framing systems would be simpler to define and assess. Unfortunately all previous attempts to establish a set of preferred sizes, even within a single country, have foundered; possibly this is due to the fact that existing sizes are the result of strongly entrenched local industry practices, often shaped by competitive consideration.

Second, there is the matter of quality control, certification and legal liability, all of which varies tremendously from country to country. Even if ISO product standards were to avoid the aspect of certification and were to be limited to quality control procedures, there would still remain difficulties in obtaining international agreement on a technical linkage between quality control and design properties.

Finally, there is the difficulty of drafting product standards where the performance requirement relates to strength under long duration loads. Ideally, the standard could be based on an accelerated test, and this can be done if the strength loss mechanism is understood. Unfortunately the relevant mechanisms are often only poorly understood, particularly in the case of reconstituted wood and glued products. It is worth mentioning that in January 1993, a three day international meeting convened by the Structural Board Association of Canada was held at Toronto, to attempt to get agreement on a test method to assess the long duration strength of oriented strand board; the meeting concluded without agreement among the participants on the degradation mechanism even of this one board product.

4. CONCLUDING COMMENT

Within this discussion paper it has been demonstrated that there are difficulties in the drafting of international codes and standards that are internationally beneficial and do not disadvantage specific countries and/or regions. This is because there is a great difference in timber species, biological hazards, climates and technology infrastructure to be found around the world. A set of guidelines has been given which may assist in overcoming some of these difficulties.

5. REFERENCES

ASTM (1994). D-1990 – Standard Practice for Establishing Allowable Properties for Visually-graded Dimension Lumber from In-grade Tests of Full-size Specimens. In *1994 Annual Book of ASTM Standards*, Philadelphia, USA, 299–323.

Boyd, J.D. (1964). The Strength of Australian Pole Timbers – IV: Radiata Pine Poles. CSIRO Division of Forest Products Technological Paper No. 32, Australia, 35 pages.

Doyle, D.V. and Markwardt, L.J. (1966). Properties of Southern Pine in Relation to Strength of Dimension Lumber. Research paper FPL64, Forest Products Laboratory, USDA Forest Service, Madison, USA, July.

Doyle, D.V. and Markwardt, L.J. (1967). Tension Parallel-to-Grain Properties of Southern Pine Dimension Lumber. Research paper FPL84, Forest Products Laboratory, USDA Forest Service, Madison, USA, December.

Standards Association of Australia (1972). CA 65–SAA Timber Engineering Code. Sydney, Australia, 125 pages.